Rythmes cérébraux et codage neural de la mémoire

Michaël Zugaro

Mémoire

présenté à l'UPMC

par

Michaël Zugaro

pour l'obtention d'une

Habilitation à Diriger des Recherches

Laboratoire de Physiologie de la Perception et de l'Action (UMR7152)
CNRS – Collège de France, 11 place M. Berthelot, 75005 Paris
Directeur : Dr. Sidney Wiener, Chaire : Pr. Alain Berthoz

2009

Travaux scientifiques

Ma thématique de recherche est l'étude des mécanismes neurophysiologiques qui sous-tendent les fonctions cognitives, et j'ai choisi la cognition spatiale chez le rat comme domaine expérimental.

Mes travaux combinent plusieurs approches complémentaires : comportement animal, électrophysiologie, traîtement du signal et analyses de données.

Dans la première partie de ce chapitre, je présenterai les grands systèmes neuraux sur lesquels portent mes travaux et je définirai un certain nombre de notions nécessaires à l'étude de la cognition spatiale. La deuxième partie sera consacrée à la présentation de l'essentiel de mes travaux, en rappelant au fur et à mesure le contexte théorique et expérimental dans lequel chaque étude s'est inscrite. Enfin, dans une dernière section, je présenterai en détail quelques résultats plus complexes, dont l'exposé me permettra d'illustrer certaines méthodes avancées de traîtement du signal et d'analyse de données que j'ai mises en œuvre pour l'étude de mes données expérimentales. Cet aspect fondamental mais plus technique de mon travail sera présenté à part afin de faciliter la lecture de ce document et de faire ainsi mieux ressortir la pertinence de mes différents résultats.

Pour mener à bien les études présentées dans ce mémoire, dans la plupart des cas j'ai été amené à former et encadrer des pré-doctorants, doctorants ou post-doctorants. Le cas échéant, ces expériences de formation et d'encadrement sont signalées par un triangle noir (►).

1 Introduction

1.1 Bases neurales des représentations spatiales

Pour se déplacer efficacement dans leur environnement, les hommes et les animaux ont recours à diverses stratégies plus ou moins complexes, depuis la répétition d'actes moteurs stéréotypés, jusqu'à l'utilisation de représentations spatiales flexibles et robustes. Chez le rat, ces représentations sont sous-tendues par au moins trois grands systèmes neuraux complémentaires : les *cellules de lieu* de l'hippocampe (O'Keefe et Nadel, 1978) et les *cellules de grille* du cortex entorhinal (Hafting et coll., 2005), qui codent la position de l'animal dans son environnement, ainsi que les *cellules de direction de la tête* (DT) du système limbique (Ranck, 1984), qui codent son orientation (Figure 1).

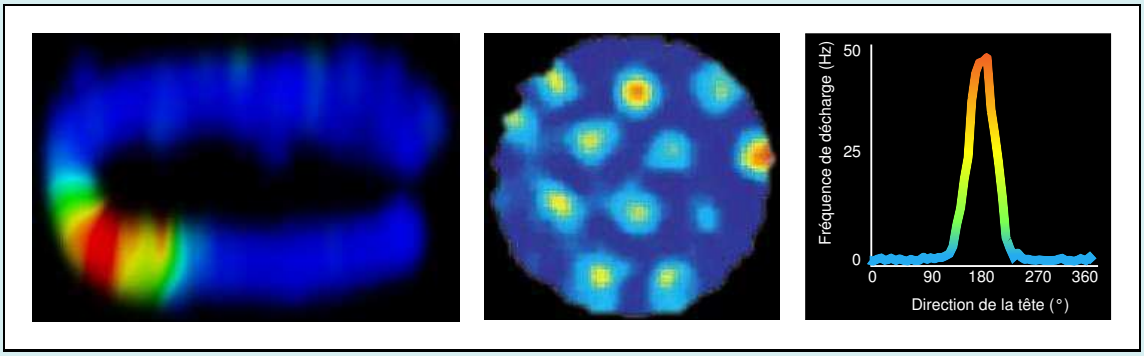

Fig. 1 – Les cellules de lieu, les cellules de grille et les cellules DT codent la position et l'orientation de l'animal dans son environnement. *À gauche.* Les réponses d'une cellule de lieu sont enregistées tandis qu'un rat explore librement un petit labyrinthe en forme de « C ». La fréquence de décharge de cette cellule varie en fonction de la position du rat dans le labyrinthe : elle est maximale lorsque le rat occupe le coin inférieur gauche, et nulle partout ailleurs. La position codée par une cellule de lieu est appelée son *champ d'activité*. Sur cette image, le labyrinthe est vu du dessus et la couleur représente la fréquence de décharge de la cellule de lieu en chaque point du labyrinthe (bleu = 0 Hz, vert = 15 Hz, rouge = 30 Hz). Celle-ci est estimée selon la formule $f(x)dt = \sum n_t w(|x_t - x|) / \sum w(|x_t - x|)$, où x_t est la position du rat à l'instant t, n_t est le nombre de potentiels d'action émis à l'instant t, et w est une gaussienne d'écart type ∼3cm (en simplifiant, la fréquence de décharge en un point donné du labyrinthe est estimée en comptant sur toute la durée de l'enregistrement tous les potentiels d'action émis lorsque le rat se trouve en ce point, et en divisant ce nombre par le temps total que le rat a passé en ce point). *Au centre.* Les réponses d'une cellule de grille sont enregistrées tandis qu'un rat se déplace librement dans une enceinte cylindrique. Comme précédemment, la couleur code la fréquence de décharge du neurone. Les cellules de grille ont des champs d'activité multiples dont les centres sont situés aux croisements d'une grille hexagonale. *À droite.* Les réponses d'une cellule DT sont enregistées tandis qu'un rat explore librement une enceinte cylidrique (non représentée ici). Sur cette courbe, la fréquence de décharge de la cellule DT est représentée en fonction de la direction de la tête du rat dans l'enceinte. Cette courbe est déterminée selon le même principe que pour les cellules de lieu. Le maximum est atteint lorsque la tête du rat est orientée à 180°. L'orientation codée par une cellule DT est appelée sa *direction préférée*.

L'étude de ces grands systèmes neuraux chez le rat est susceptible de nous renseigner sur les mécanismes qui sous-tendent la cognition spatiale chez l'homme. En effet, les cellules de lieu et les cellules DT ont été identifiées non seulement chez le rat et la souris (Rotenberg et coll., 1996 ; McHugh et coll., 1996 ; Khabbaz et coll., 2000), mais également chez le singe (Ono et coll., 1991 ;

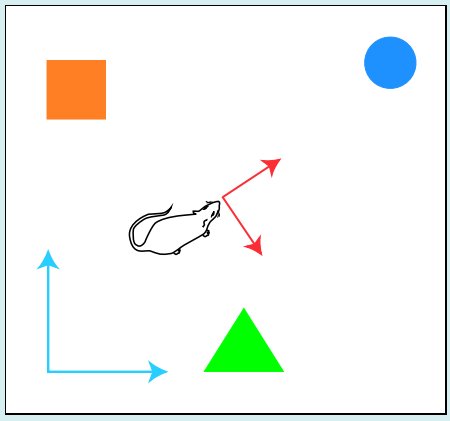

Fig. 2 – Référentiels égocentriques et allocentriques. Un rat est vu ici entouré de trois objets. Si l'on décrit la position des objets par rapport au rat, on utilise un référentiel égocentrique (*flèches rouges*). En revanche, si l'on décrit la position des objets ou du rat par rapport à la pièce, on utilise un référentiel allocentrique (*flèches bleues*).

Rolls et O'Mara, 1995 ; Robertson et coll., 1999). Chez l'homme, le gyrus parahippocampique et l'hippocampe jouent un rôle critique dans la cognition spatiale (Berthoz, 1997 ; Aguirre et coll., 1998 ; O'Keefe et coll., 1998 ; Maguire et coll., 1999), et des travaux récents montrent que certains neurones hippocampiques se comportent également comme des cellules de lieu (Ekstrom et coll., 2001). Les structures cérébrales impliquées dans l'élaboration de représentations spatiales sont donc relativement conservées au fil de l'échelle phylogénétique.

1.2 Concepts théoriques

1.2.1 *Référentiels égocentriques et allocentriques*

Un référentiel est un système de référence dans lequel s'expriment des relations spatiales. Par exemple, dans une pièce contenant tout un ensemble d'objets, les positions des objets peuvent être décrites par rapport à la pièce, auquel cas la pièce sert de référentiel. Mais les positions des objets peuvent également être décrites par rapport à un sujet qui se trouve dans la pièce, et dans ce cas c'est le sujet qui constitue le référentiel. Dans les études portant sur la cognition spatiale, les référentiels centrés sur le sujet sont généralement nommés référentiels *égocentriques*, et les référentiels centrés sur l'extérieur sont nommés référentiels *allocentriques* (Figure 2).

Les cellules de lieu et les cellules DT, qui codent la position et l'orientation de la tête de l'animal par rapport à son environnement (et non pas, par exemple, par rapport à son corps), sous-tendent des représentations spatiales allocentriques.

1.2.2 *Navigation grâce aux repères et intégration de trajet*

Comment un sujet peut-il se localiser et s'orienter dans son environnement ? Comme le montre la Figure 3, il peut utiliser au moins deux types de stratégies complémentaires : il peut naviguer grâce aux *repères* qui l'entourent, ou par *intégration de trajet* (Mittelstaedt et Mittelstaedt, 1980).

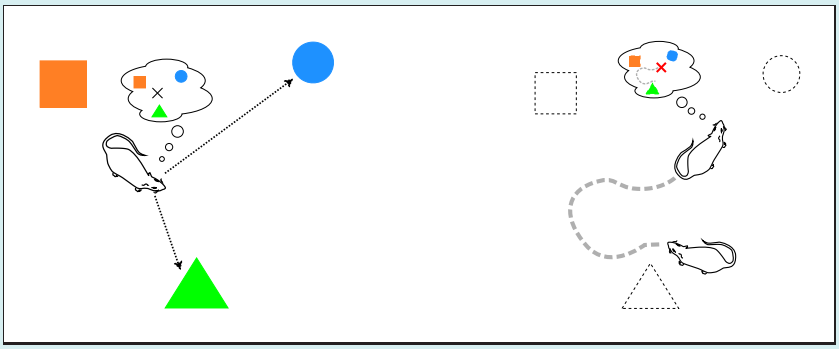

Fig. 3 – Navigation grâce aux repères et intégration de trajet. *À gauche*. Le rat perçoit un ensemble d'objets familiers autour de lui, dont la configuration le renseigne directement sur sa position et sur son orientation dans l'environnement : il se localise et s'oriente grâce à des repères. *À droite*. Le rat est maintenant dans l'obscurité. Bien qu'il ne perçoive plus les objets qui l'entourent, pour peu qu'il connaisse sa position de départ, il peut continuer à estimer sa position et son orientation au fil de ses déplacements : il navigue par intégration de trajet.

Ces deux modes de navigation sont rendus possibles par différents types de signaux sensoriels et moteurs. Les repères peuvent en effet être perçus via différentes modalités sensorielles relevant de l'extéroception : vision, olfaction, toucher, etc. Quant à l'intégration de trajet, elle repose sur de nombreux signaux sensoriels et moteurs qui renseignent le sujet sur ses déplacements : par exemple les signaux vestibulaires, qui codent les accélérations de sa tête, les signaux proprioceptifs et kinesthésiques, qui signalent les positions et les mouvements de ses articulations et de ses muscles, etc. On remarquera que certaines modalités sensorielles entrent en jeu dans les deux formes de navigation : ainsi, la vision permet-elle non seulement de connaître la position des repères dans l'environnement, mais elle permet également au sujet de calculer sa vitesse de déplacement à partir du mouvement de la scène visuelle sur ses rétines.

On peut cependant séparer expérimentalement ces différentes composantes sensori-motrices, ou les mettre en conflit, pour comprendre comment les représentations spatiales sont élaborées par le système nerveux central : c'est la démarche que j'ai adoptée dans mes travaux sur les cellules DT.

2 Intégration des signaux sensori-moteurs par les cellules DT

Les travaux que je présenterai dans cette section ont été effectués au cours de ma thèse, co-dirigée par Alain Berthoz et Sidney Wiener, et de mon premier post-doctorat (LPPA, CNRS–Collège de France, Paris). Afin de mettre en évidence la démarche expérimentale et le type de connaissances apportées par mes travaux, je présenterai ici en détail certaines des études que j'ai effectuées ; les autres études seront résumées à leurs résultats principaux.

2.1 Repères de l'environnement

Parmi tous les éléments de l'environnement, lesquels sont susceptibles de servir de repères pour les cellules DT, c'est-à-dire d'en contrôler les directions préférées, et comment les cellules DT les « sélectionnent »-elles ? Une fois les repères sélectionnés, quelle est la dynamique de la mise à jour

des directions préférées qui en résulte ? C'est à ces questions que tentent de répondre les trois études qui sont présentées dans cette section.

2.1.1 *Repères du premier plan et de l'arrière-plan*

Zugaro, Berthoz et Wiener (2001). Background, but not foreground, spatial cues are taken as references for head direction responses by rat anterodorsal thalamus neurons. *J. Neurosci.* 21, 1–5.

Dans un grand nombre de travaux portant sur les cellules de lieu et la vaste majorité des travaux concernant les cellules DT, l'environnement est délibérément réduit à une simple enceinte cylindrique dont la paroi porte une grande carte contrastée. Dans un tel environnement, la carte est le repère principal pour les champs d'activité des cellules de lieu et les directions préférées des cellules DT : en effet, si la carte est tournée le long de la paroi de l'enceinte, en général les champs d'activité et les directions préférées la suivent (ils tournent du même angle) (Muller et Kubie, 1987 ; Taube et coll., 1990 ; Poucet et coll., 1994 ; Knierim et coll., 1995).

Pour mieux caractériser les éléments de l'environnement qui sont susceptibles de servir de repères, Cressant et coll. (1997) ont utilisé un environnement plus riche, comportant diverses configurations d'objets tridimensionnels placés tour à tour au centre de l'enceinte ou contre sa paroi. Ils ont montré que les champs d'activité des cellules de lieu n'étaient contrôlés par ces objets que lorsque ceux-ci étaient placés contre la paroi de l'enceinte expérimentale – ce qui mettait en évidence une dichotomie entre les objets centraux et les objets périphériques.

Pour déterminer si cette dichotomie existait également dans le cas des cellules DT, j'ai testé les réponses de cellules DT du noyau antérodorsal du thalamus (AD) dans des conditions similaires. Mon hypothèse était que les objets, même périphériques, ne serviraient de repères que s'ils faisaient partie de l'arrière-plan. Pour tester cette hypothèse, j'ai comparé deux conditions expérimentales, dans lesquelles l'arrière plan se trouvait soit juste derrière les objets, soit bien plus loin – les objets étant toujours placés à la périphérie dans les deux conditions expérimentales.

Trente cellules DT ont été enregistrées chez trois rats. Les résultats montrent une différence très nette entre les deux conditions (Figure 4) :

- Objets à l'arrière-plan : Dans tous les cas, **les directions préférées étaient ancrées sur les objets** : après rotation de 120° des objets, les directions préférées les suivaient (rotation moyenne : 115±10°, plage : 99∼134°).
- Objets au premier plan : Dans tous les cas, **les directions préférées sont restées stables malgré la rotation des objets** : en moyenne, les directions préférées ne tournaient que de 6±7° (plage : 0∼28°).

Ainsi les objets ne contrôlent-ils les directions préférées des cellules DT que lorsqu'ils se trouvent à l'arrière-plan. Ces résultats montrent donc que les repères sont sélectionnés parmi les éléments de l'arrière-plan. Reste à déterminer grâce à quels mécanismes s'opère cette sélection. L'expérience suivante a été conçue pour répondre à cette question.

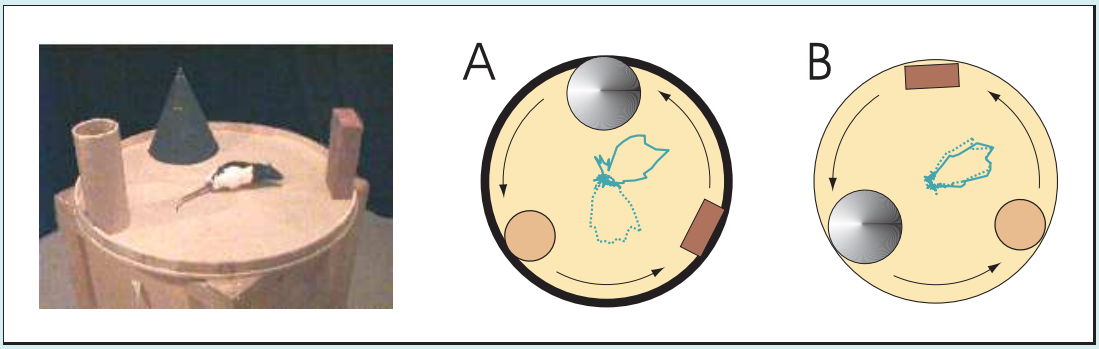

Fig. 4 – Les directions préférées des cellules DT sont ancrées sur les repères de l'arrière-plan. Les rats se déplaçaient librement sur une plate-forme surélevée comportant trois objets. Dans la première condition, une enceinte circulaire empêchait les rats de voir au-delà des objets. Dans la seconde condition (*à gauche*), l'enceinte était retirée, et les rats pouvaient voir, en arrière-plan distant, les rideaux qui tendaient la pièce. Dans chaque condition, les courbes de réponses des cellules DT étaient comparées avant (*courbes en pointillés*) et après (*courbes en trait continu*) rotation des objets d'un angle de 120°. Les rotations avaient lieu en l'absence du rat, qui était désorienté dans l'obscurité entre deux enregistrements. Les directions préférées des cellules DT suivaient les objets lorsque l'enceinte était présente (A), mais pas lorsqu'elle était retirée (B) – c'est-à-dire seulement lorsque les objets se trouvaient à l'arrière-plan dans la scène visuelle.

2.1.2 *Sélection des repères de l'arrière-plan*

Zugaro, Arleo, Déjean, Burguière, Khamassi et Wiener (2004). Rat anterodorsal thalamic head direction neurons depend upon dynamic visual signals to select anchoring landmark cues. *Eur. J. Neurosci.* 20, 530–6.

▶ Dans le cadre de cette étude, j'ai formé et travaillé en collaboration avec un post-doctorant, Angelo Arleo, roboticien de formation, docteur de l'École Polytechnique Fédérale de Lausanne (EPFL), et j'ai co-encadré trois étudiants, Cyril Déjean, Éric Burguière et Mehdi Khamassi – ce dernier a obtenu en 2007 une thèse de l'Université Paris VI dans notre équipe de recherche, en co-direction avec l'Animatlab du LIP6 (Jussieu).

Lorsqu'un sujet se déplace dans son environnement, la scène visuelle se déplace en sens inverse sur ses rétines. Ces mouvements de la scène visuelle sur les rétines sont appelés *flux optique*. Tous les éléments de la scène visuelle ne se déplacent cependant pas à la même vitesse : les images des objets de l'arrière-plan se déplacent plus lentement que celles des objets du premier plan – c'est la *parallaxe de mouvement*. Par conséquent, ces signaux visuels dynamiques permettent en théorie de distinguer les objets les plus proches des objets les plus distants. Ils pourraient donc constituer le mécanisme de sélection des repères de l'arrière-plan par les cellules DT.

Pour tester cette hypothèse, j'ai perturbé le traitement de ces signaux en utilisant un éclairage stroboscopique. Dans de telles conditions, les directions préférées des cellules DT étaient contrôlées tour à tour et de façon aléatoire soit par les repères du premier plan (27%), soit par ceux de l'arrière plan (33%), soit encore par les deux à la fois, menant alors à un « compromis » (33%). Autrement dit, les directions préférées n'étaient plus ancrées sur les repères distants comme en lumière continue (test V, $p < 0,01$), car elles ne distinguaient plus entre premier plan et arrière-plan (test U_n^2, $p > 0,1$). Ces résultats mettent donc en évidence que **les signaux visuels dynamiques exercent bien une influence critique dans la sélection des repères par le système des cellules DT**.

Comment ce mécanisme intervient-il quand le rat explore son environnement ? Lorsque le rat perçoit un changement dans la configuration des repères qui l'entourent, par exemple au moment où il pénètre dans un environnement familier, ses déplacements produisent un flux optique qui permet aux cellules DT de sélectionner les repères de l'arrière-plan ; les directions préférées sont alors mises à jour grâce à ces repères.

Mais combien de temps faut-il pour que s'opère cette mise à jour ? C'est la question qui a motivé l'expérience suivante.

2.1.3 *Délais de mise à jour grâce aux repères*

Zugaro, Arleo, Berthoz et Wiener (2003). Rapid spatial reorientation and head direction cells. *J. Neurosci.* 23, 3478–82.

▶ Pour mener à bien ce travail, j'ai formé et collaboré avec un post-doctorant, Angelo Arleo, roboticien de formation, docteur de l'École Polytechnique Fédérale de Lausanne (EPFL).

Des simulations numériques (Zhang, 1996 ; Redish, 1999) prédisaient qu'il pourrait suffire de 200∼400 ms pour que les directions préférées des cellules DT soient mises à jour après une rotation soudaine de l'environnement visuel. Mais aucun protocole expérimental utilisé jusqu'alors ne permettait de mesurer des délais aussi brefs.

J'ai donc mis au point un nouveau protocole permettant d'obtenir cette précision temporelle. Les rats devaient rester immobiles pour recevoir des gouttes d'eau dans un petit réservoir. Une carte repère était déplacée dans l'environnement de façon à induire la mise à jour des directions préférées des cellules DT : lorsque la carte était dans l'une des deux positions choisies, les cellules DT ne déchargeaient presque pas, mais lorsque la carte était dans l'autre position, leurs fréquences de décharge étaient maximales. Comme la carte était déplacée dans l'obscurité, lorsque la lumière était rallumée le déplacement semblait se produire instantanément, ce qui permettait de mesurer précisément les délais de mise à jour des directions préférées (Figure 5). En cumulant les réponses de cellules DT enregistrées au moment où la lumière était allumée (de 0,5 s avant à 0,5 s après l'allumage, $N = 129$ essais), j'ai mis en évidence des changements extrêmement rapides des fréquences de décharge : lorsque la carte repère était dans son orientation initiale, **il fallait seulement 80±10 ms pour que les réponses des cellules DT augmentent de leur niveau de base à leur niveau maximal** ; et lorsque la carte était tournée, il leur fallait 140±10 ms pour diminuer de leur niveau maximal à leur niveau de base.

La rapidité surprenante avec laquelle les directions préférées sont mises à jour indique que les cellules DT bénéficient d'un traitement visuel extrêmement rapide.

Ces résultats ont mis en évidence les limites des modèles des cellules DT développés jusqu'alors (McNaughton et coll., 1991 ; Skaggs et coll., 1995 ; Blair, 1996 ; Redish et coll., 1996 ; Zhang, 1996 ; Goodridge et Touretzky, 2000 ; Arleo et Gerstner, 2000). En effet, ces modèles utilisaient tous des neurones formels à fréquence de décharge continue, et ne permettaient pas de modéliser des transitions aussi rapides. Inspirées par mes travaux, deux nouvelles études computationnelles ont depuis été publiées (Degris et coll., 2003, 2004) : en remplaçant les neurones formels à fréquence continue par des neurones formels « intègre-et-décharge », ces nouveaux modèles ont pu répliquer mes résultats expérimentaux.

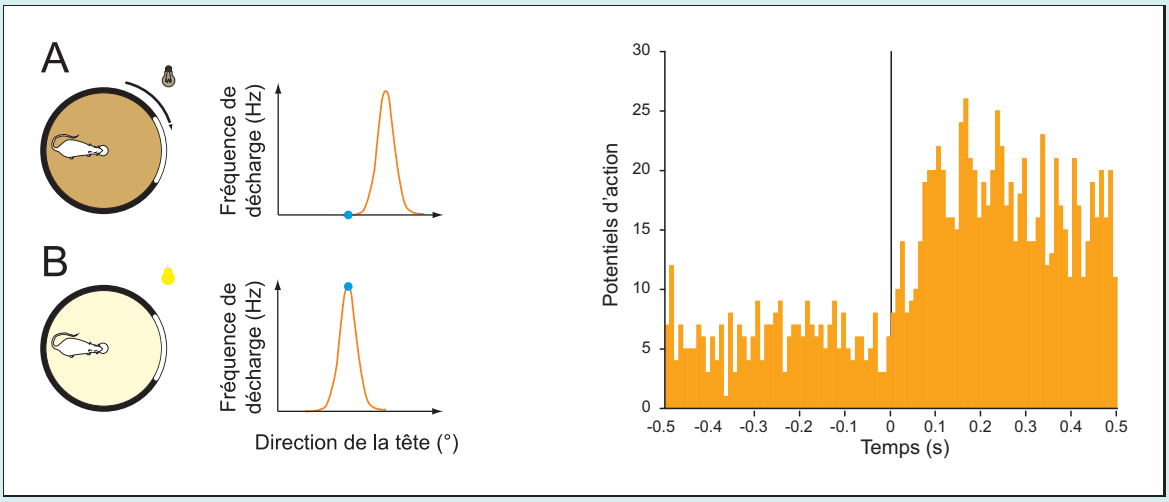

Fig. 5 – Réorientation rapide et cellules DT. Le rat immobile reçoit des gouttes d'eau dans un petit réservoir central. Avant l'extinction de la lumière (*non représentée ici*), la carte repère est placée de telle façon que la fréquence de décharge de la cellule DT enregistrée soit minimale compte tenu de l'orientation du rat. Dans l'obscurité, la carte repère est tournée de -90° le long de la paroi du cylindre (A). La fréquence de réponse est toujours minimale (A, *point bleu sur la courbe de réponse*). Mais lorsque la lumière est rallumée (B), le rat voit soudain la carte dans sa nouvelle orientation, ce qui a pour effet de remettre à jour la direction préférée de la cellule DT (la *courbe de réponse* en B se déplace de -90°). La fréquence de décharge de la cellule DT devient maximale (B, *point bleu sur la courbe de réponse*). Les données montrent que cette mise à jour s'effectue en moyenne en 80 ms (*histogramme péri-événement, à droite* ; lumière allumée à $t = 0$).

2.2 Mouvements propres

La section précédente a été consacrée contrôle des directions préférées des cellules DT par les repères environnementaux. J'en viens maintenant au second type d'informations spatiales qui permettent l'élaboration des réponses des cellules DT : les signaux de mouvement propre, qui sous-tendent l'intégration de trajet (cf. page 3). Parmi ces signaux, certains sont générés quelle que soit l'origine des mouvements propres, qu'ils soient actifs ou passifs : il s'agit de signaux *sensoriels* (c'est le cas par exemple des signaux vestibulaires). D'autres au contraire ne sont présents que si les mouvements sont générés par l'animal lui-même : ce sont des signaux de *type moteur*. En effet, lorsqu'un rat se déplace activement, les commandes motrices qui génèrent ses mouvements sont également transmises en parallèle à diverses structures cérébrales, sous forme de copies motrices efférentes ou de décharges collatérales.

Les travaux qui sont présentés dans cette section concernent l'influence des signaux de mouvement propres, sensoriels et de type moteur, sur les réponses des cellules DT.

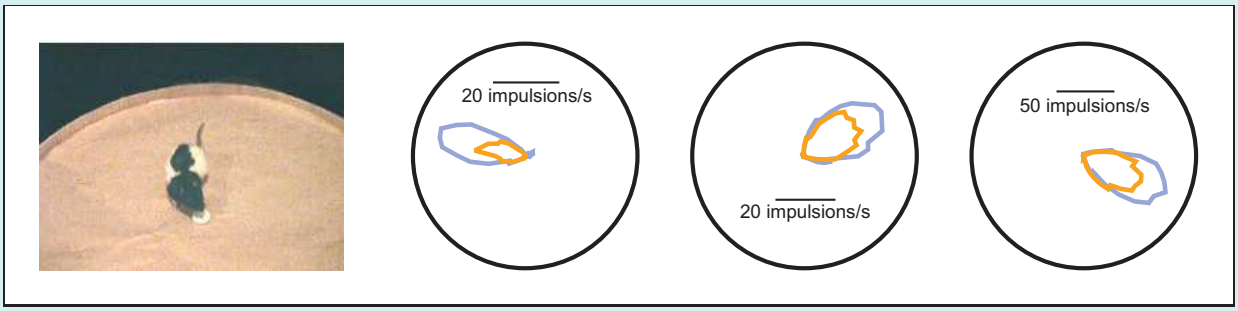

Fig. 6 – Diminution de la fréquence maximale de décharge des cellules DT en l'absence de signaux de type moteur. Pour pouvoir enregistrer les réponses des cellules DT pendant des rotations passives *sans contention*, les rats étaient entraînés à boire de l'eau dans un petit réservoir (*à gauche*) et à rester immobiles pendant que la plate-forme était tournée de gauche à droite et de droite à gauche. Lors des rotations passives (*courbes de réponse orange*), les cellules DT maintenaient leurs directions préférées et leur précision (largeur des courbes de réponse), mais leur fréquence maximale de décharge diminuait de 27% en moyenne par rapport aux déplacements actifs (*courbes de réponse bleues*).

2.2.1 *Modulation par les signaux de type moteur*

Zugaro, Tabuchi, Fouquier, Berthoz et Wiener (2001). Active locomotion increases peak firing rates of anterodorsal thalamic head direction cells. *J. Neurophysiol.* 86, 692–702.

▶ Pour réaliser cette étude, j'ai co-encadré une étudiante de DEA, Céline Fouquier.

Pour déterminer la contribution spécifique des signaux de type moteur au signal de direction de la tête, j'ai comparé les réponses des cellules DT lorsque des rats parcouraient librement une enceinte expérimentale cylindrique, et lorsqu'ils étaient soumis à des rotations passives *sans contention* (Figure 6), car la contention altère fortement les réponses des cellules DT (Taube et coll., 1990 ; Taube et Burton, 1995). J'ai montré que les directions préférées et les largeurs des courbes de réponse étaient inchangées pendant les rotations passives (tests de Wilcoxon, NS), mais qu'en revanche **les fréquences maximales de décharge diminuaient de 27% en moyenne** (régression linéaire, $r^2 = 0,73$, $p < 0,001$).

Ces résultats sont compatibles avec l'hypothèse que les copies motrices efférentes et les décharges collatérales modulent les signaux de direction de la tête. Ainsi, le signal DT pourrait-il être augmenté pour transmettre plus d'information directionnelle (Brunel et Nadal, 1998) lorsque le rat explore activement son environnement. A contrario, le signal DT serait réduit durant les comportements non spatiaux (par exemple, quand l'animal mange ou se repose).

2.2.2 *Signaux de type moteur et réponses anticipées*

Le travail qui est décrit dans cette section a été effectué dans le cadre d'une collaboration entre le CNRS et la *National Science Foundation* américaine avec Jeffrey Taube (Dartmouth College, Hanover NH, USA), Robert Muller (New York University, Brooklyn, USA) et Patricia Sharp (University of Illinois, Urbana-Champaign IL, USA).

Bassett, **Zugaro**, Muir, Golob, Muller et Taube (2005). Passive movements of the head do not abolish anticipatory firing properties of head direction cells. *J. Neurophysiol.* 93, 1304–1316.

Une particularité des cellules DT du noyau antérodorsal du thalamus (AD) est que leurs réponses anticipent la direction future de la tête : en effet, lorsque le rat tourne la tête, la fréquence de décharge d'une cellule DT du AD atteint son maximum en moyenne 25 ms avant que la direction préférée ne soit atteinte (Blair et Sharp, 1995 ; Blair et coll., 1997 ; Taube et Muller, 1998 ; Blair et coll., 1999). Taube et Muller (1998) ont proposé l'hypothèse que cette anticipation résultait de la prise en compte de signaux de type moteur (copies motrices efférentes ou décharges collatérales) qui, en « renseignant » les cellules DT sur les mouvements à venir, permettraient d'en prédire les conséquences – à savoir la direction future de la tête.

Une conséquence directe de cette hypothèse est que les réponses des cellules DT du AD doivent cesser d'anticiper la direction future de la tête en l'absence de ces signaux de type moteur, c'est-à-dire si les mouvements du rat ne sont pas générés par le rat lui-même, par exemple lors de rotations passives. Nous avons montré que contrairement à cette prédiction, **l'anticipation des cellules DT du AD n'est pas annulée si les rats sont tournés passivement**. Cette anticipation ne dépend donc pas de façon critique de signaux de type moteur.

2.2.3 *Modulation par les signaux vestibulaires*

Zugaro, Berthoz et Wiener (2002). Peak firing rates of rat anterodorsal thalamic head direction cells are higher during faster passive rotations. *Hippocampus* 12, 481–486.

Les signaux vestibulaires semblent jouer un rôle fondamental dans l'élaboration du signal DT : on sait en effet qu'après lésion du système vestibulaire, les réponses des cellules DT perdent toute spécificité directionnelle (Stackman et Taube, 1997). Les signaux vestibulaires pourraient contribuer à maintenir la direction représentée par les cellules DT en phase avec la direction réelle de la tête au fil des mouvements. En effet, lorsque le rat tourne la tête, l'activité doit se « déplacer » au sein du réseau des cellules DT pour refléter ce changement d'orientation, et ce déplacement d'activité doit se faire à une vitesse proportionnelle à la vitesse de rotation de la tête. Ceci serait rendu possible par le signal de vitesse angulaire[1] d'origine vestibulaire. Plusieurs modèles computationnels qui implémentent cette idée prédisent que les fréquences de décharge des cellules DT du AD doivent être modulées par la vitesse angulaire de la tête (Blair et Sharp, 1996 ; Redish et coll., 1996).

En comparant les réponses de cellules DT chez des rats soumis à des rotations passives lentes (38±15°/s) ou rapides (153±27°/s), j'ai montré qu'effectivement **les fréquences maximales de décharge augmentaient en moyenne de 36±6%** (ESM, plage : +11∼+100%) pendant les rotations rapides.

Ces résultats sont donc compatibles avec les prédictions théoriques des modèles postulant que le signal de vitesse angulaire d'origine vestibulaire sert à mettre à jour la représentation de la direction de la tête du rat au fil de ses mouvements. Ils indiquent également que les cellules DT du AD pourraient véhiculer des informations non seulement sur la direction de la tête, mais également sur sa vitesse angulaire. De nouvelles expériences seront cependant nécessaires pour déterminer si cette composante de vitesse est effectivement utilisée par les structures cérébrales en aval.

[1] Une première intégration (au sens mathématique) de l'accélération de la tête est effectuée au niveau-même du système vestibulaire, et le signal qui en résulte code la vitesse de la tête.

2.3 Intégration multisensorielle par les cellules DT

Zugaro, Tabuchi et Wiener (2000). Influence of conflicting visual, inertial and substratal cues on head direction cell activity. *Exp. Brain Res.* 133, 198–208.

Les résultats précédents ont été obtenus en séparant expérimentalement les contributions des différents signaux sensori-moteurs, en particulier ceux générés par la perception des repères environnementaux de ceux générés par les mouvements propres du rat. Cette dernière expérience a pour but de mieux comprendre comment ces différents signaux sont combinés dans l'élaboration des réponses des cellules DT.

Pour comparer les influences des repères et des mouvements propres sur les directions préférées de cellules DT corticales et thalamiques, j'ai soumis des rats à des conflits visio-vestibulaires dans un cylindre dont la paroi et le sol pouvaient être tournés indépendemment l'un de l'autre. J'ai ainsi montré que **les repères visuels exerçaient une influence dominante (∼90%), mais incomplète, tandis que les signaux inertiels avaient une influence plus faible (∼10%), mais néanmoins significative**.

Ces résultats sont compatibles avec la proposition que les repères visuels peuvent servir à recalibrer sur l'environnement des représentations directionnelles mises à jour par intégration de trajet.

3 Propriétés de réseau de l'hippocampe

3.1 Mécanismes de la précession de phase hippocampique

Les travaux que je présenterai dans cette section ont été menés dans le cadre de mon second post-doctorat, dans le laboratoire de György Buzsáki au Center for Molecular and Behavioral Neuroscience (Rutgers, Newark, USA) dont la thématique est l'étude des propriétés des réseaux neuraux qui sous-tendent les fonctions cognitives. Ce laboratoire s'intéresse tout particulièrement aux mécanismes physiologiques des oscillations dans les réseaux neuraux (rythme thêta, rythme gamma, « ripples », etc.), dont une fonction majeure est d'organiser en séquences temporelles l'activité d'ensembles de neurones anatomiquement distribués. À cette fin, il regroupe des mathématiciens, des physiciens, des ingénieurs et des biologistes, et a développé des technologies d'enregistrement électrophysiologique de pointe et des méthodes d'analyse avancées permettant d'étudier les réponses de plusieurs dizaines de neurones enregistrés simultanément chez l'animal libre de ses mouvements, ainsi que les champs de potentiel locaux échantillonnés en une centaine de points distincts dans l'hippocampe ou le néocortex. En outre, ce laboratoire mène également des études anatomiques, et physiologiques en intracellulaire (enregistrements aigus), et constituait donc un cadre idéal pour me permettre d'enrichir ma formation scientifique, et d'apprendre de nouveaux outils d'analyse complétant ceux que j'avais acquis au cours de ma formation initiale d'ingénieur.

Après avoir étudié l'intégration de différents signaux sensori-moteurs par les cellules DT pendant ma thèse et mon premier post-doctorat, mon sujet de recherche dans le laboratoire de György Buzsáki consistait à comparer au niveau de l'hippocampe les influences des diverses afférences

sensori-motrices à la dynamique propre du réseau, afin de déterminer comment signaux intrinsèques et extrinsèques sont combinés dans l'élaboration des réponses des cellules de lieu.

Pour mener à bien les travaux présentés ici, j'ai obtenu un *Long Term Fellowship* (LTF) de l'*International Human Frontiers Program Organization* (HFSP), financement de post-doctorat d'une durée de trois ans qui soutient des projets internationaux innovants aux frontières des disciplines scientifiques traditionnelles.

Jusqu'ici, j'ai présenté le codage de l'espace par les cellules de lieu ou les cellules DT comme un codage *fréquentiel*. De ce point de vue en effet, l'information spatiale fournie par exemple par une cellule de lieu est contenue dans sa fréquence de décharge instantanée : c'est ainsi que les cellules de lieu ont été initialement décrites lorsqu'elles ont été découvertes (O'Keefe et Dostrovsky, 1971), et c'est également ainsi qu'elles sont décrites depuis dans la vaste majorité des travaux concernant l'hippocampe. Mais une découverte majeure, dont l'importance a longtemps été sous-estimée, a ouvert une nouvelle voie d'exploration théorique et expérientale : le décours temporel des potentiels d'action émis par les cellules de lieu contient au moins autant d'information spatiale que la fréquence de décharge (O'Keefe et Recce, 1993). Autrement dit, les cellules de lieu codent également l'espace selon un codage *temporel*. La première question qui se pose est évidemment celle-ci : ces deux formes de codage sont-elles équivalentes, ou peut-on les dissocier ? Cette question a reçu des réponses contradictoires (Hirase et coll., 1999 ; Harris et coll., 2002 ; Mehta et coll., 2002 ; Huxter et coll., 2003). Il s'avère donc nécessaire de mieux comprendre les mécanismes physiologiques qui sous-tendent le codage temporel par les cellules de lieu. Le but de mon travail était de confronter expérimentalement les différents modèles théoriques qui avaient été proposés comme bases de ce codage.

Quelle est la nature du codage temporel hippocampique ? Lorsqu'un rat se déplace, le potentiel de champ local[2] enregistré dans l'hippocampe oscille à 7∼10 Hz. Cette oscillation est connue sous le nom de *rythme thêta*. Or il se trouve que les potentiels d'action émis par les cellules de lieu sont précisément organisés au sein de chaque cycle thêta : à mesure que le rat traverse le champ d'activité d'une cellule de lieu, celle-ci émet des potentiels d'action de plus en plus tôt par rapport au rythme thêta (Figure 7). C'est le phénomène de précession de phase (O'Keefe et Recce, 1993). En quoi cela constitue-t-il un codage temporel ? Chaque fois que l'animal occupera la même position, les potentiels d'action seront émis environ à la même phase de thêta. La position du rat à un instant donné peut donc être estimée à l'aide de la phase de thêta à laquelle les potentiels d'action d'une cellule de lieu sont émis (Jensen et Lisman, 2000 ; Huxter et coll., 2003).

3.1.1 *Intégration des afférences sensori-motrices à la dynamique propre des assemblées de neurones hippocampiques*

Zugaro, Monconduit et Buzsáki (2005). Spike phase precession persists after transient intrahippocampal perturbation. *Nature Neurosci.* 8, 67–71.

▶ Dans le cadre de cette étude, j'ai formé et travaillé en collaboration avec une post-doctorante, Lénaïc Monconduit, docteure de l'Université de Clermont I.

[2]Similaire à l'électroencéphalogramme mais enregistré localement à l'aide de microélectrodes plutôt que sur le scalp à l'aide d'électrodes de surface, le potentiel de champ local résulte de la sommation des potentiels postsynaptiques excitateurs et inhibiteurs produits sur les dendrites et les corps cellulaires de très nombreux de neurones. Il s'agit donc d'une mesure de la quantité moyenne d'excitation ou d'inhibition reçue par une large population de neurones.

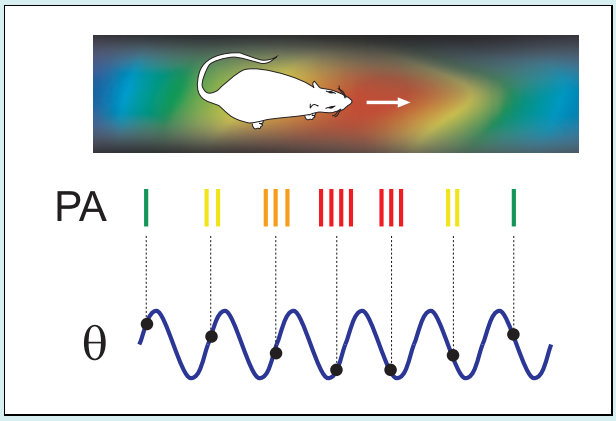

Fig. 7 – Précession de phase des réponses hippocampiques. À mesure que le rat traverse le champ d'activité d'une cellule de lieu (*en haut*), les potentiels d'action (PA) émis par cette cellule se produisent de plus en plus tôt (*disques noirs*) par rapport au rythme thêta (θ). Pour quantifier cet effet, on mesure pour chaque cycle thêta la phase moyenne des potentiels d'action. La phase diminue à mesure que le rat avance : c'est la précession de phase.

De nombreux modèles ont été proposés pour rendre compte de la précession de phase hippocampique (O'Keefe et Recce, 1993 ; Jensen et Lisman, 1996 ; Tsodyks et coll., 1996 ; Wallenstein et Hasselmo, 1997 ; Kamondi et coll., 1998 ; Bose et coll., 2000 ; Bose et Recce, 2001 ; Booth et Bose, 2001 ; Koene et coll., 2003 ; Lengyel et coll., 2003 ; Sato et Yamaguchi, 2003 ; Yamaguchi, 2003 ; Magee, 2003), mais on dispose de relativement peu de données expérimentales directes (O'Keefe et Recce, 1993 ; Skaggs et coll., 1996 ; Kamondi et coll., 1998 ; Ekstrom et coll., 2001 ; Magee, 2001 ; Harris et coll., 2002 ; Mehta et coll., 2002 ; Huxter et coll., 2003). Pour comparer les prédictions de ces différents modèles (que je décrirai plus loin), j'ai perturbé transitoirement les décharges des neurones hippocampiques et remis à zéro le rythme thêta en stimulant électriquement la commissure hippocampique ventrale chez des rats en comportement.

Dans un premier temps, je ne présenterai ici que les résultats principaux de ces travaux, afin de bien mettre l'accent sur l'essentiel. Les analyses plus avancées seront détaillées dans la section suivante (page 17).

Cinq rats ont été entraînés à effectuer des allers-retours entre deux petits réservoirs d'eau dans un labyrinthe en forme de « C ». Chaque fois qu'un rat quittait l'un des réservoirs, un photodétecteur déclenchait une stimulation intrahippocampique, qui interrompait transitoirement les réponses hippocampiques et réinitialisait le rythme thêta (Figure 8), sans pour autant affecter le comportement du rat. L'interruption des réponses peut s'expliquer par plusieurs facteurs : en activant de façon synchrone de vastes ensembles de cellules pyramidales et d'interneurones, la stimulation commissurale déclenche en effet non seulement une inhibition médiée par les récepteurs GABA, mais aussi une augmentation de la conductance potassique médiée par le calcium, et enfin une disfacilitation (Buzsáki et coll., 1981 ; Buzsáki et Czéh, 1981 ; Douglas et coll., 1983). Le protocole comportait trois conditions expérimentales : contrôle (pas de stimulation), stimulation de faible intensité (juste au-dessus du seuil pour obtenir un potentiel d'action de population[3]), et stimulation de forte intensité (amplitude du potentiel d'action de population : 50% du maximum).

[3]Sommation des potentiels d'action émis simultanément par un très grand nombre de neurones.

Malgré ces perturbations du réseau hippocampique, dès la reprise de l'activité neurale la phase des potentiels d'action émis par les cellules de lieu continuait de diminuer : **la précession de phase continuait donc normalement, aussi bien après des stimulations de faible que de forte instensité** (Figure 9).

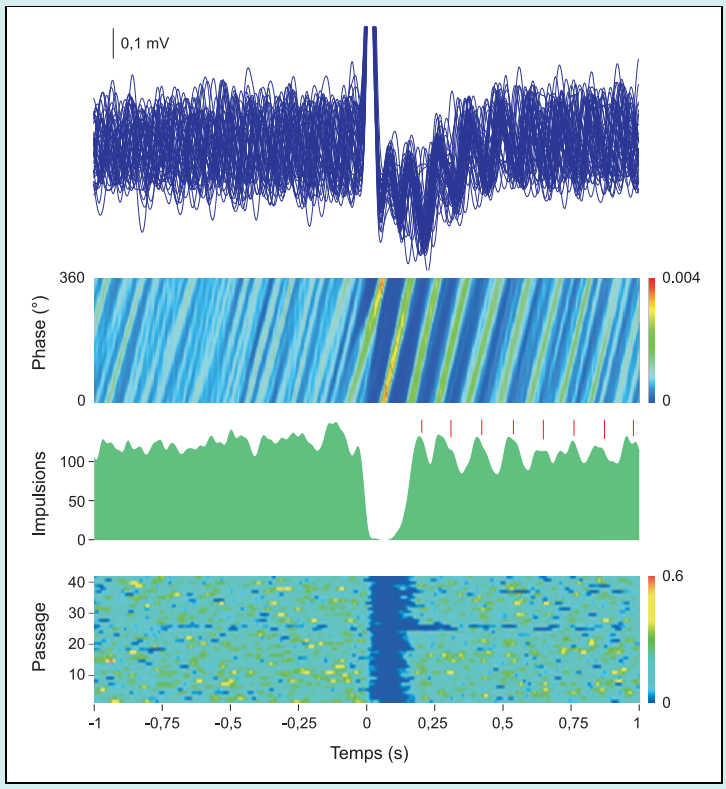

Fig. 8 – Interruption transitoire des décharges hippocampiques et réinitialisation du rythme thêta par stimulation commissurale. *En haut*. Les potentiels de champ locaux sont enregistrés à chaque passage du rat devant le photodétecteur (durée : 2 s, de 1 s avant à 1 s après la stimulation). Ils sont représentés ici superposés et synchronisés sur l'instant où a lieu la stimulation (à $t = 0$). Ce tracé fait apparaître qu'avant la stimulation la phase varie de façon aléatoire d'un passage à l'autre, alors qu'elle est bien plus cohérente après la stimulation. *Deuxième panneau*. La distribution des phases d'un passage à l'autre est représentée ici en fonction du temps (la fréquence d'observation est codée par la couleur, comme l'indique la *barre colorée* à droite). Cette image fait clairement apparaître une distribution aléatoire avant la stimulation, mais unimodale après la stimulation, avec un pic étroit observable pendant environ 1 s : la stimulation a donc bien réinitialisé le rythme thêta. *Troisième panneau*. Décharges cumulées de trois interneurones durant tous les passages. Les décharges s'interrompent juste après la stimulation, et le silence dure ∼200 ms (noter la modulation des décharges par le rythme thêta après le silence). *En bas*. Décharges de nombreuses cellules pyramidales ($N > 20$) et des trois interneurones combinées. Pour chaque passage, la fréquence de décharge moyenne instantanée est représentée par la couleur (*barre colorée* à droite). Tous les neurones cessent de décharger juste après la stimulation : la stimulation a donc bien interrompu transitoirement toutes les réponses hippocampiques.

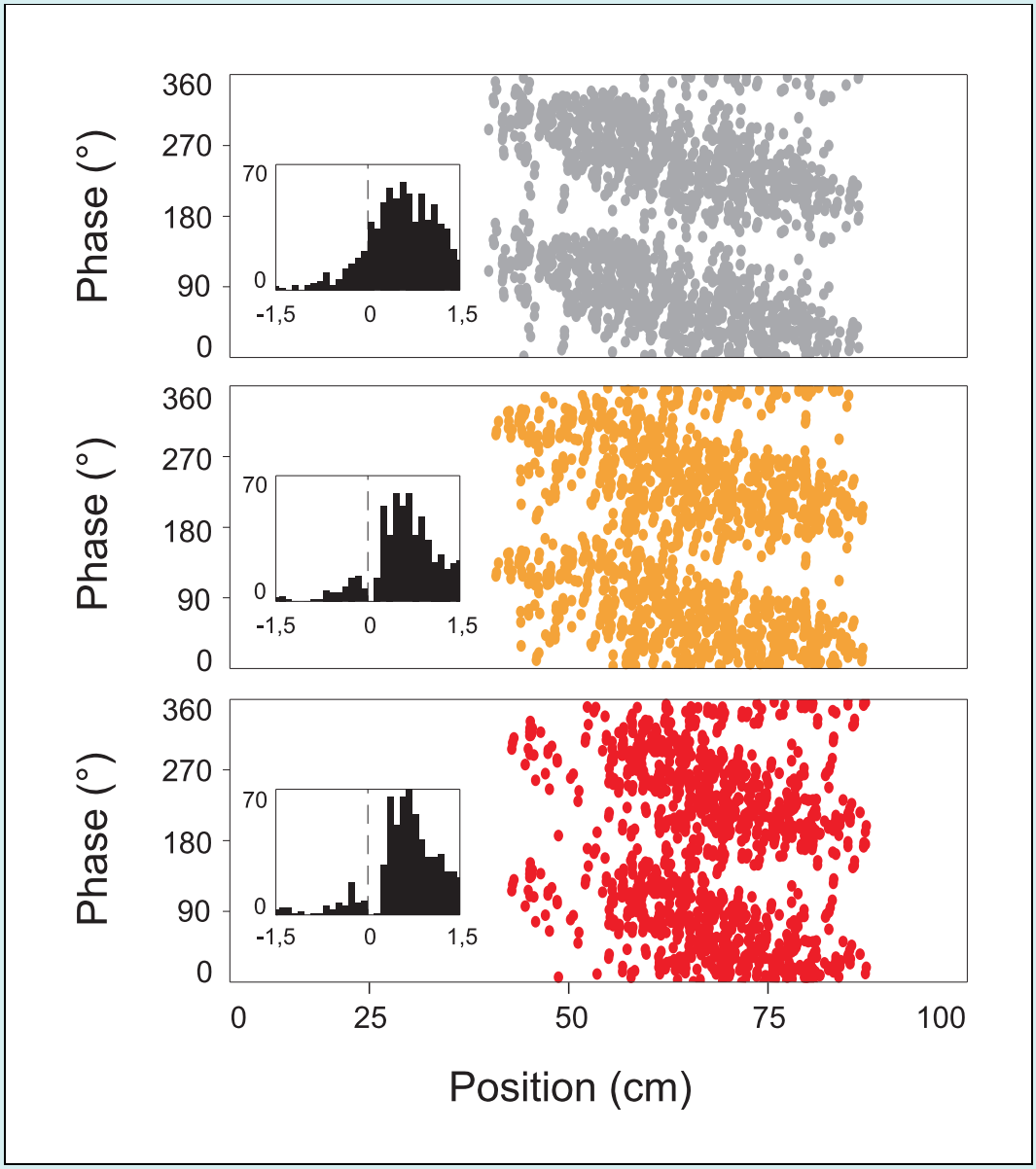

Fig. 9 – Le précession de phase continue malgré la perturbation du réseau hippocampique. *En haut*, condition de contrôle. Les réponses d'une cellule de lieu sont échantillonnées à chaque passage devant le photodétecteur. Pour chaque potentiel d'action (*disques gris*), la phase de thêta est représentée en fonction de la position du rat. Le nuage de points a une « pente » décroissante, qui correspond à la précession de phase. *Au milieu* et *en bas*, stimulation de faible et de forte intensité (resp.) Juste après la stimulation, la cellule de lieu cesse de décharger (*histogrammes péri-événement* en encart ; abscisses : temps en secondes), mais la précession de phase reprend normalement dès la remise en route du réseau hippocampique.

Que nous apprennent ces résultats ?

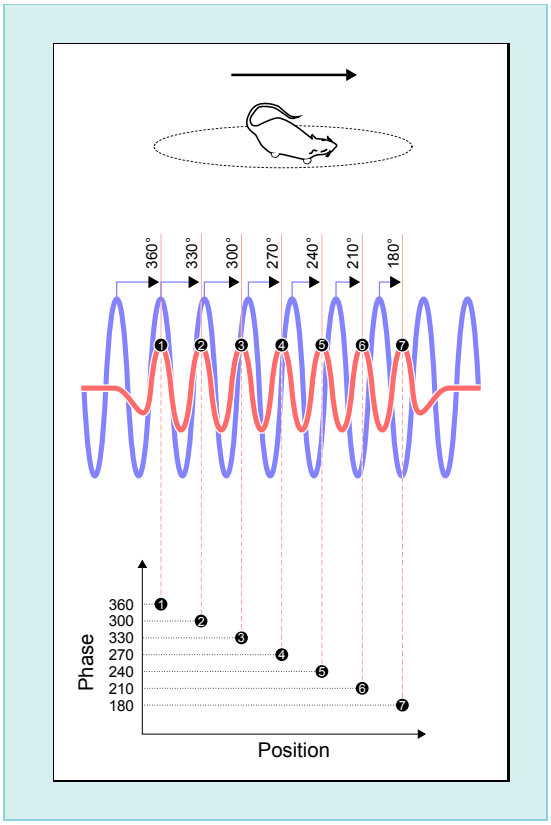

Une première catégorie de modèles de la précession de phase est basée sur une idée initialement proposée par O'Keefe et Recce (1993), qui ont postulé l'existence de deux oscillateurs ayant des fréquences légèrement différentes (par exemple, comme de nombreux auteurs l'ont suggéré plus tard, le rythme thêta et le potentiel de membrane dendritique de la cellule de lieu). Lorsque le rat traverse le champ d'activité d'une cellule de lieu (*ellipse en pointillés*), le potentiel de membrane de cette cellule (*courbe rouge*) se met à osciller à une fréquence légèrement supérieure à celle du rythme thêta (*courbe bleue*). La cellule de lieu décharge chaque fois que son potentiel de membrane est maximal (*points noirs*), ce qui se produit de plus en plus tôt (*lignes verticales rouges* successives) par rapport au début de chaque cycle thêta (*flèches bleues*) : la phase diminue, passant de 360° au début du champ d'activité (*point noir 1*) à 180° en fin de champ d'activité (*point noir 7*). Ces modèles prédisent que si au moins l'un des deux oscillateurs est remis à zéro, la précession de phase doit être fortement altérée. Par conséquent, aucun des modèles pour lesquels au moins l'un des deux oscillateurs est dans l'hippocampe (Bose et coll., 2000 ; Bose et Recce, 2001 ; Booth et Bose, 2001 ; Lengyel et coll., 2003) ne peut rendre compte de mes résultats. Les modèles qui postulent que les deux oscillateurs sont dans le cortex entorhinal (Sato et Yamaguchi, 2003 ; Yamaguchi, 2003) prédisent correctement que la précession de phase doit se poursuivre normalement après la perturbation, mais ne peuvent expliquer la réinitialisation du rythme thêta par la stimulation.

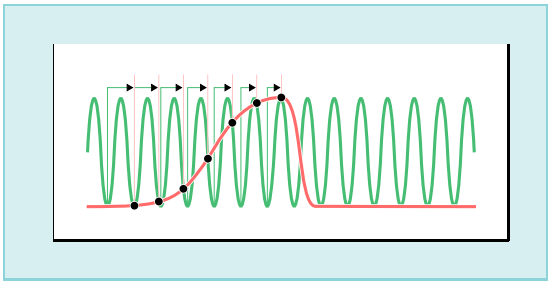

Une seconde catégorie de modèles propose que la précession de phase résulte des propriétés membranaires des cellules de lieu (Kamondi et coll., 1998 ; Magee, 2001 ; Harris et coll., 2002 ; Mehta et coll., 2002 ; Magee, 2003). Dans cette optique, c'est le niveau d'excitation postsynaptique total qui détermine à quelle phase la cellule de lieu décharge : plus la membrane est dépolarisée, plus la cellule décharge tôt par rapport au rythme thêta. Lorsque l'animal traverse le champ d'activité, la cellule de lieu reçoit un niveau d'excitation croissant à chaque cycle thêta (*courbe rouge*), et sous l'action combinée de l'excitation dendritique et de l'inhibition somatique (*courbe verte*), la membrane atteint le seuil de décharge de plus en plus tôt (*points noirs*) – ce qui produit la précession de phase. Ces modèles prédisent que l'interruption transitoire des réponses hippocampiques doit être suivie d'une reprise de la précession de phase, en repartant d'une phase déterminée par le niveau d'excitation. En principe, ces modèles peuvent donc rendre compte de mes résultats pour peu que cette excitation soit fournie par des entrées extrahippocampiques.

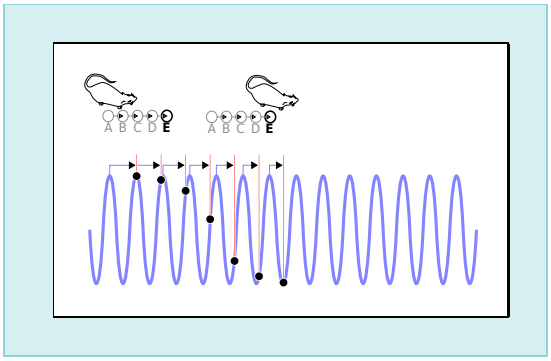

Une troisième catégorie de modèles explique la précession de phase par des proriétés de réseau de l'hippocampe (Jensen et Lisman, 1996 ; Tsodyks et coll., 1996 ; Wallenstein et Hasselmo, 1997). Selon ces modèles, l'assemblée de neurones qui code la position du rat à un instant donné décharge fortement au moment du creux du cycle thêta. Dans le réseau récurrent du champ CA3 de l'hippocampe, ce groupe excite via des connexions unidirectionnelles l'assemblée qui représente la position suivante du rat le long de la trajectoire prévue (les *cercles* sous le rat représentent les assemblées de cellules de lieu, et les *flèches* représentent les connexions unidirectionnelles). À cause des délais de conduction et de transmission synaptique, les cellules dont le champ d'activité apparaît plus loin dans la trajectoire déchargent plus tard dans le cycle thêta. Par conséquent, à mesure que le rat s'approche du champ d'activité d'une cellule de lieu, celle-ci décharge de plus en plus tôt par rapport au rythme thêta : elle manifeste une précession de phase. Cette propagation est interrompue par l'inhibition rythmique due aux interneurones hippocampiques. L'activation de la séquence suivante d'assemblées de neurones est initiée au cycle thêta suivant par des entrées extrahippocampiques : ce mécanisme prédit donc correctement que la précession de phase ne doit être que transitoirement interrompue par la perturbation du réseau hippocampique.

Mes résultats suggèrent donc que les assemblées de neurones hippocampiques auto-organisent leurs séquences d'activation, tout en intégrant à chaque nouveau cycle thêta des informations extrahippocampiques provenant de l'environnement ou des mouvements propres. L'organisation temporelle des assemblées de neurones hippocampiques résulte donc d'une intéraction entre la dynamique propre de l'hippocampe et les entrées extrahippocampiques.

3.1.2 *Acquisition, prétraitement et analyse de données*

Analyser de grandes quantités de données électrophysiologiques enregitrées chez un animal libre de ses mouvements requiert des outils mathématiques et statistiques appropriés. Afin de faciliter la lecture de la section précédente et ainsi de mieux mettre l'accent sur mes résultats scientifiques, j'ai volontairement reporté la présentation de certains aspects plus complexes de ce travail. Dans cette section, je me propose d'expliciter certaines des méthodes d'analyse auxquelles j'ai eu recours pour analyser ces données.

Mais avant d'en venir à l'analyse des données, une première étape est évidemment de pouvoir acquérir des données.

Pour pouvoir étudier l'impact des perturbations intrahippocampiques sur la précession de phase, j'ai dû réaliser sur mesure un système d'acquisition de données électrophysiologiques et comportementales. Tandis qu'un premier système d'acquisition enregistrait les signaux électrophysiologiques, une caméra vidéo filmait le rat, et un second système d'acquisition gérait automatiquement le fonctionnement du labyrinthe. J'ai entièrement réalisé et développé l'équippement comportemental : construction du labyrinthe, réalisation des composants électroniques nécessaires, combinaison de systèmes d'acquisition existants, synchronisation des données, et développement d'un programme de pilotage d'expérience (détection par les photodétecteurs, stimulation intrahippocampique, distribution d'eau, enregistrement sur disque, etc.)

Une fois les données enregistrées sur disque, elles doivent encore faire l'objet de plusieurs prétraitements avant de pouvoir être analysées.

Hazan* & **Zugaro*** [premiers auteurs équivalents] et Buzsáki (2006). Klusters, NeuroScope, NDManager : a free software suite for neurophysiological data processing and visualization. *J. Neurosci. Methods* 155, 207–216.

En effet, un premier problème auquel est confronté le neurophysiologiste quand il enregistre les réponses de plusieurs dizaines de neurones simultanément, est de pouvoir attribuer chaque potentiel d'action enregistré au neurone qui l'a émis. Cette tâche complexe est décrite par la Figure 10. Elle inclut essentiellement deux étapes : la classification se fait d'abord de façon semi-automatique, puis la première version ainsi obtenue est corrigée manuellement. J'ai contribué au développement de `Klusters`, une application graphique qui permet d'effectuer cette étape manuelle. Ce logiciel libre peut être téléchargé à `http://klusters.sourceforge.net` (j'ai également contribué au développement de deux autres applications, NeuroScope et NDManager, qui sont aujourd'hui utilisées par de nombreux laboratoires aussi bien aux États-Unis qu'en Europe ou au Japon, et je participe depuis 2004 à un Projet Européen (§ 1.3, page 30) ayant entre autres pour but de compléter les outils de traitement informatique existants et de développer des techniques plus avancées pour améliorer l'étape semi-automatique).

Dans le laboratoire de György Buzsáki, j'ai ainsi pu isoler 162 cellules de lieu chez 5 rats, en utilisant un microdescendeur d'électrodes équippé de 8 tétrodes - microdescendeur que j'ai conçu et réalisé.

Une fois ces divers prétraîtements effectués, commence l'analyse de données proprement dite.

La Figure 8 montre un exemple de réinitialisation du rythme thêta, pour un rat au cours d'une séance d'enregistrement typique. Pour quantifier cet effet sur l'ensemble des données, les potentiels de champ locaux ont tout d'abord été filtrés (bande passante : 7∼20 Hz), puis les instants où apparaissaient les dix premiers pics du rythme thêta après la stimulation ont été relevés (les pics étant définis comme les points à mi-chemin entre les zéros de l'onde pseudo-sinusoïdale). Pour chaque passage, une série de 10 valeurs a ainsi été obtenue. La variance de ces valeurs sur l'ensemble des passages a été choisie comme mesure de la dispersion de thêta en fonction du temps après la stimulation. Les tests statistiques (F-tests) montrent que thêta est resynchronisé pendant environ une seconde par la stimulation, et que l'efficacité de cette resynchronisation augmente avec l'intensité de la stimulation (Figure 11).

Comme le suggère la Figure 9, les tracés de phases sont très similaires dans les trois conditions expérimentales. Pour détecter d'éventuelles différences sur l'ensemble des données, le champ d'activité de chaque cellule de lieu a été subdivisé en trois zones : initiale, médiane, et finale. La comparaison de la phase moyenne dans chaque zone entre les trois conditions expérimentales n'a révélé aucune différence significative (analyse de variance circulaire, NS). Pour cette analyse, deux approches complémentaires ont été utilisées : tout d'abord, parce que la précession de phase des différents neurones ne parcourt pas la même plage de valeurs, chaque mesure a été recentrée sur la phase moyenne du neurone correspondant (en prenant chaque condition expérimentale séparément). Une première analyse de variance circulaire a alors été effectuée (Figure 12). Parce que cette analyse ne pourrait pas détecter un changement de plage de précession de phase (translation verticale des nuages de points) entre conditions expérimentales, les données ont été transformées une deuxième fois : chaque mesure a été recentrée sur la phase moyenne pour les trois conditions expérimentales, en prenant chaque zone séparément. Une seconde analyse de variance circulaire confirmait qu'il n'y avait pas de différence significative entre les trois conditions expérimentales.

Pour autant, l'analyse précédente ne nous permet pas de savoir si la précession de phase s'est interrompue pendant la période de silence, ou plutôt si elle a continué en dépit de l'absence d'activité au sein de l'hippocampe. Pour répondre à cette question, l'évolution de la phase des potentiels

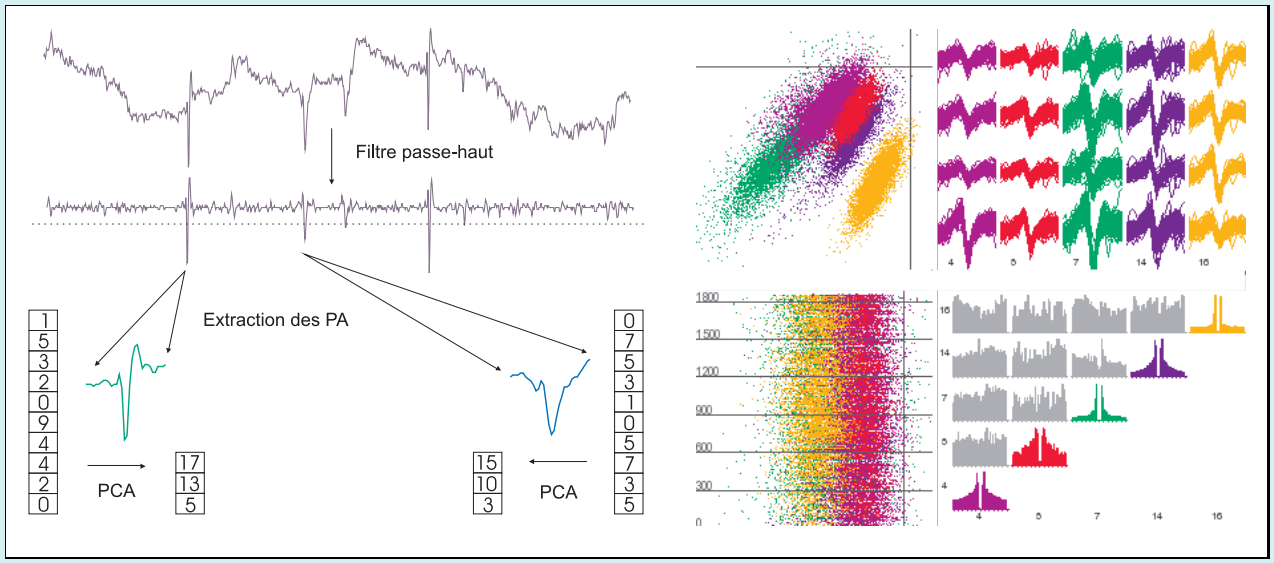

Fig. 10 – Tri des potentiels d'action. Cette tâche est rendue possible par l'utilisation d'électrodes multiples comme la *tétrode*, un groupe de quatre électrodes de 12 µm de diamètre torsadées (donc très proches les unes des autres). Les mêmes potentiels d'action sont enregistrés sur les quatre électrodes, avec toutefois des amplitudes différentes, qui dépendent de la position des neurones par rapport à chaque électrode. On peut donc trier les potentiels d'action en prenant en compte d'une part leur forme et d'autre part leurs amplitudes relatives sur les différentes électrodes. *À gauche*. Cette figure représente les données enregistrées par l'une de ces électrodes et les différentes transformations précédant le tri proprement dit. Une fois la trace filtrée (l'enregistrement se fait initialement en bande passante large, 1 Hz∼9 kHz), les potentiels d'action qui dépassent un seuil calculé automatiquement sont « extraits » : pour chaque potentiel d'action, on relève les 32 échantillons de mesure du potentiel extracellulaire enregistrés pendant un intervalle de temps de 1,6 ms autour du pic ; le potentiel d'action est alors représenté par un vecteur à 32 composantes (par électrode). Une analyse en composantes principales permet de réduire la dimensionnalité de ce vecteur en ne conservant que les 3 premières composantes par électrode. *À droite*. Le tri des potentiels d'action commence par l'utilisation d'un programme de classification semi-automatique implémentant l'alghrithme CEM. Il faut ensuite corriger manuellement cette première version en utilisant des informations supplémentaires comme le temps (pour prendre en compte la dérive des électrodes) et les corrélogrammes croisés (pour identifier des groupes correspondant à un même neurone). Cette figure montre cinq groupes de potentiels d'action, correspondant à cinq neurones : les nuages de points sont les projections bidimensionnelles des potentiels d'action sur deux composantes principales (*en haut à gauche*), et sur une composante principale et le temps (*en bas à gauche*), ainsi que les potentiels d'action enregistrés sur chacune des électrodes (*en haut à droite*) et les autocorrélogrammes et corrélogrammes croisés des neurones (*en bas à droite*). Ces figures ont été obtenues avec notre logiciel `Klusters`.

d'action a été mesurée pour chaque passage pris séparément : la phase juste après l'interruption des décharges est-elle différente de la phase juste avant la stimulation ? La Figure 13 (panneaux A et B) illustre cette question. La différence de phase entre ces deux instants a été mesurée pour chaque passage. La moyenne et l'intervalle de confiance à 95% pour chaque condition expérimentale sont représentés sur la Figure 13C. Aucun intervalle de confiance ne contient la valeur nulle, ce qui montre que la phase lorsque les décharges reprennent est significativement inférieure à la phase avant la stimulation ($P < 0,05$) : la précession de phase continue donc pendant que l'hippocampe est inactivé, ce qui indique qu'elle dépend également de signaux extrahippocampiques.

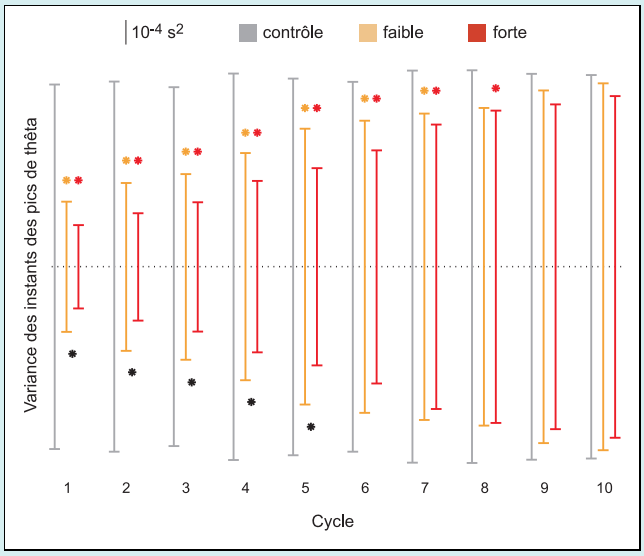

Fig. 11 – Resynchronisation de thêta par la stimulation intrahippocampique. Variance des instants des pics de thêta (*barres verticales*) au cours des cycles suivant la stimulation, comparée aux cycles suivant le passage devant le photodétecteur dans la condition de contrôle. Plus les barres sont petites, plus la variance est faible et plus les phases sont cohérentes ($* : P < 0,01$, F-test). Les *astérisques colorées* indiquent des différences significatives avec la condition de contrôle, et les *astérisques noires* indiquent des différences significatives entre niveaux de stimulation.

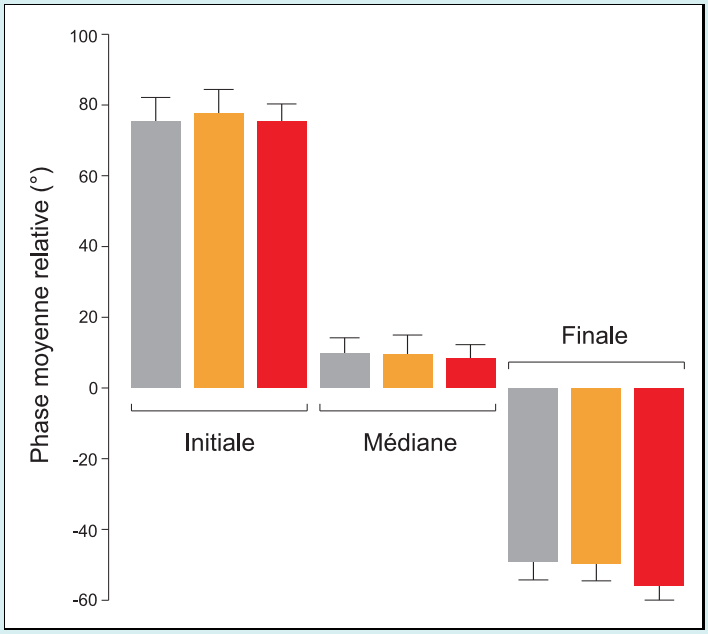

Fig. 12 – La précession de phase continue après la stimulation intrahippocampique. Les champs d'activité des cellules de lieu sont subdivisés en trois zones (*initiale*, *médiane*, et *finale*). La phase moyenne pour chaque zone et chaque condition (mesurée par rapport à la phase moyenne pour l'ensemble du champ d'activité) est représentée par les *barres colorées* (*barres verticales*, intervalles de confiance à 95%). Les analyses de variance circulaire montrent qu'il n'y a pas de différence significative entre les trois conditions expérimentales.

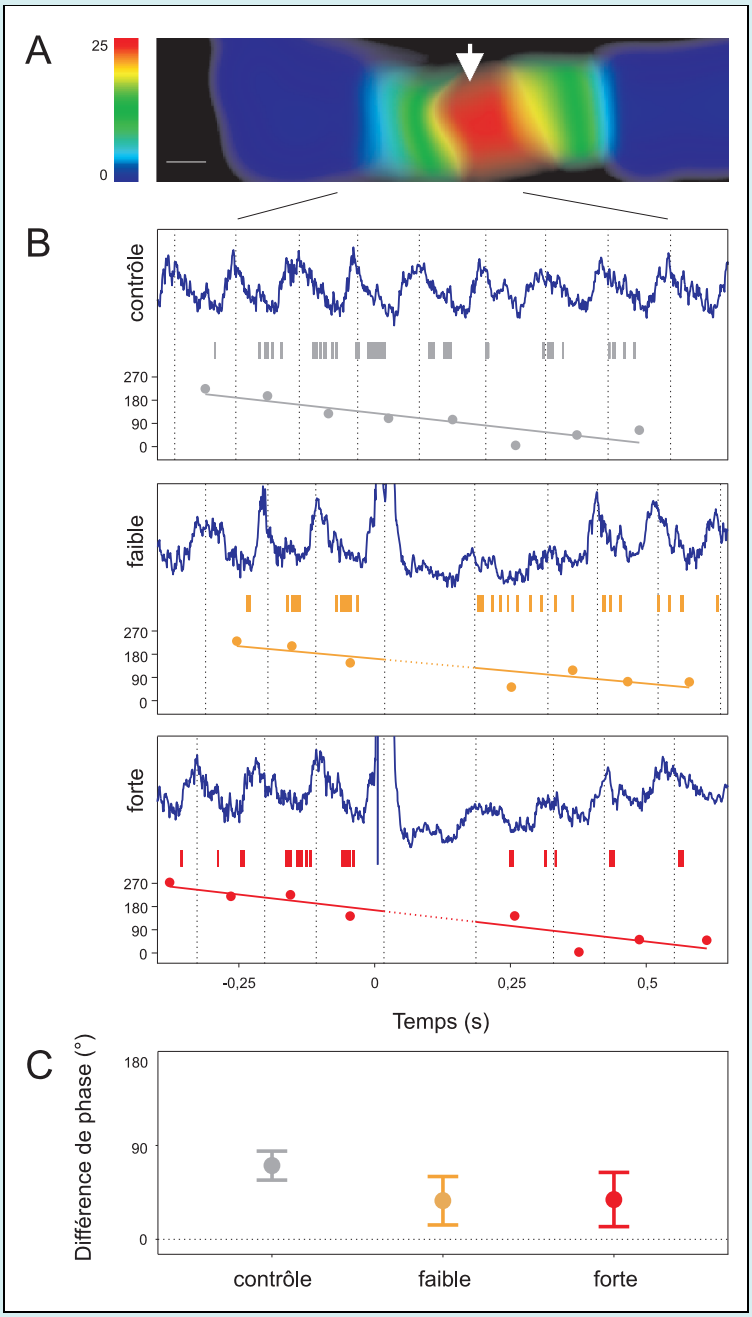

Fig. 13 – La précession de phase continue pendant l'inactivation du réseau hippocampique. A. Le rat traverse le champ d'activité d'une cellule de lieu (photodétecteur indiqué par la *flèche blanche*). B. Les potentiels de champ locaux (*traces bleues*) et les potentiels d'action (*petites barres verticales*) sont enregistés, et la phase instantanée est calculée pour chaque cycle thêta (*disques colorés*), dans chacune des conditions expérimentales. La pente descendante (*droites colorées*, regression linéaire) correspond à la précession de phase, vue ici sur un seul passage à travers le champ d'activité. Noter l'interruption transitoire des décharges et la remise à zéro du rythme thêta juste après la stimulation (à $t = 0$). C. Différence moyenne entre la phase à la reprise des décharges et la phase juste avant la stimulation (hauteur de la *barre verticale* : intervalles de confiance à 95%). La précession de phase continue pendant la perturbation, ce qui met en évidence le rôle de signaux extrahippocampiques.

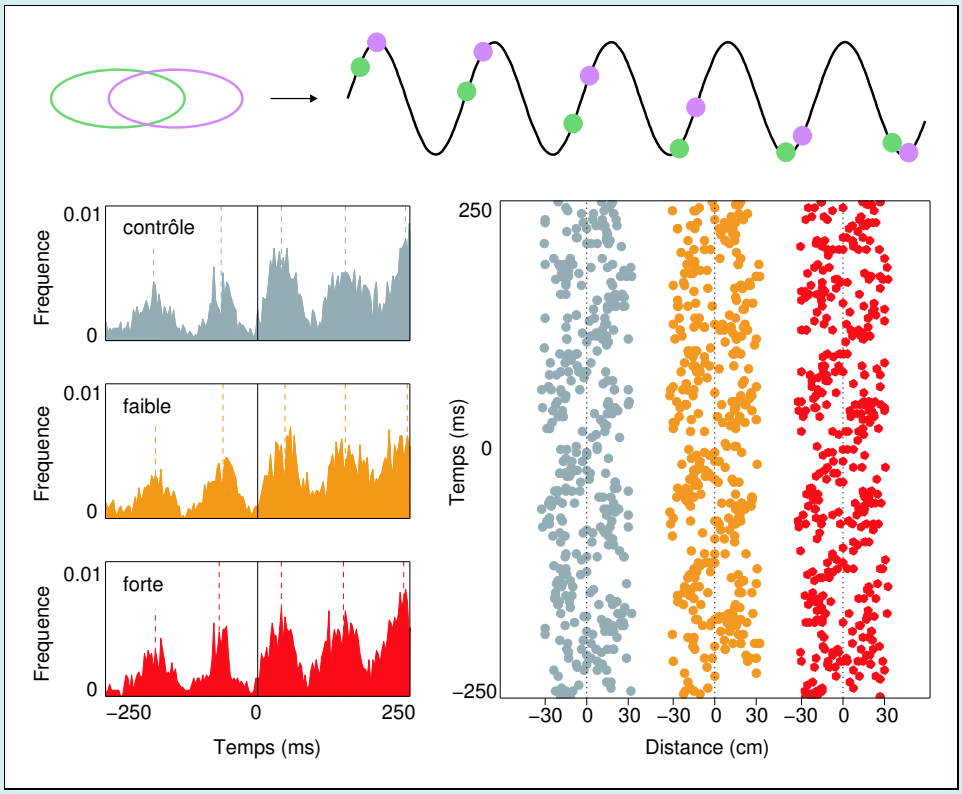

Fig. 14 – Préservation des séquences d'activation malgré la perturbation du réseau hippocampique. *En haut*. Représentation schématique de la compression temporelle des séquences comportementales. Deux cellules de lieu dont les champs d'activité se chevauchent (*ellipses bleue et verte*) émettent au sein de chaque cycle thêta (*sinusoïde*) des potentiels d'action (*disques colorés*) dont la séquence reflète l'ordre de passage par les champs d'activité. *À gauche*. Corrélogrammes croisés de deux cellules de lieu dont l'une a un champ d'activité à hauteur d'un photodétecteur. Noter la modulation par le rythme thêta. *À droite*. La compression temporelle des séquences comportementales est similaire dans les trois conditions expérimentales. Dans chaque cas, les cinq ellipsoïdes obliques correspondent à cinq cycles thêta successifs (pics détectés comme indiqué *à gauche*).

Une dernière question importante concerne l'organisation séquentielle des assemblées de neurones. Lorsqu'un rat parcourt une trajectoire donnée, un certain nombre de cellules de lieu sont activées au fur et à mesure que le rat se déplace. À la traversée successive des champs d'activité (séquence comportementale qui peut prendre plusieurs secondes) correspond une activation successive des cellules de lieu *dans le même ordre* au sein même de chaque cycle thêta (séquence physiologique qui ne dure que quelques dizaines de millisecondes). Cette compression temporelle des séquences comportementales (Skaggs et coll., 1996) pourrait avoir d'importantes conséquences fonctionnelles, comme la potentialisation à long terme des connexions synaptiques entre les cellules de lieu impliquées (Bliss et Lomo, 1973). Pour tester si cette propriété était perturbée par la stimulation, j'ai tout d'abord sélectionné toutes les paires de cellules de lieu dont l'une au moins avait un champ d'activité à hauteur d'un photodétecteur. J'ai ensuite calculé les corrélogrammes croisés de chaque paire, et déterminé les instants où apparaissaient les pics (Figure 14, à gauche). Enfin, j'ai représenté la distance entre les centres des champs d'activité en fonction des instants où apparaissaient les pics (Figure 14, à droite). La très grande similitude entre les trois nuages de points indique que l'organisation fine des séquences d'activation est préservée malgré la perturbation du réseau hippocampique.

3.2 Modulation des oscillateurs neuronaux hippocampiques par la vitesse de déplacement du rat

Cette section et la suivante présentent succinctement des travaux que j'ai menés en partie durant mon post-doctorat chez György Buzsáki, et en partie depuis ma nomination comme Chargé de Recherche de Niveau 1 (CR1) du CNRS au LPPA, dans l'équipe de Sidney Wiener.

Geisler, Robbe, **Zugaro**, Sirota et Buzsáki (2007). Hippocampal place cell assemblies are speed-controlled oscillators. *PNAS* 109, 8149–54.

Dans les modèles computationnels de la précession de phase faisant intervenir au moins un oscillateur (cf. § 3.1.1, page 16), les intervalles successifs entre deux bouffées de potentiels d'action émises par une cellule de lieu sont en grande partie déterminés par la fréquence instantanée de l'oscillateur. Or les données expérimentales montrent que l'instant auquel une cellule de lieu décharge au sein d'un cycle thêta dépend de la position du rat – c'est la précession de phase. Il faut donc que la fréquence de l'oscillateur dépende des variations de position du rat, c'est-à-dire de la vitesse instantanée de l'animal.

Pour tester cette hypothèse, nous avons enregistré des cellules de lieu chez des rats entraînés à effectuer des allers-retours entre deux réservoirs d'eau, et nous avons comparé les autocorrélogrammes de leurs décharges lorsque les rats se déplaçaient à haute et à basse vitesse (respectivement, en utilisant les données correspondant aux 50% les plus rapides et les plus lents des trajets).

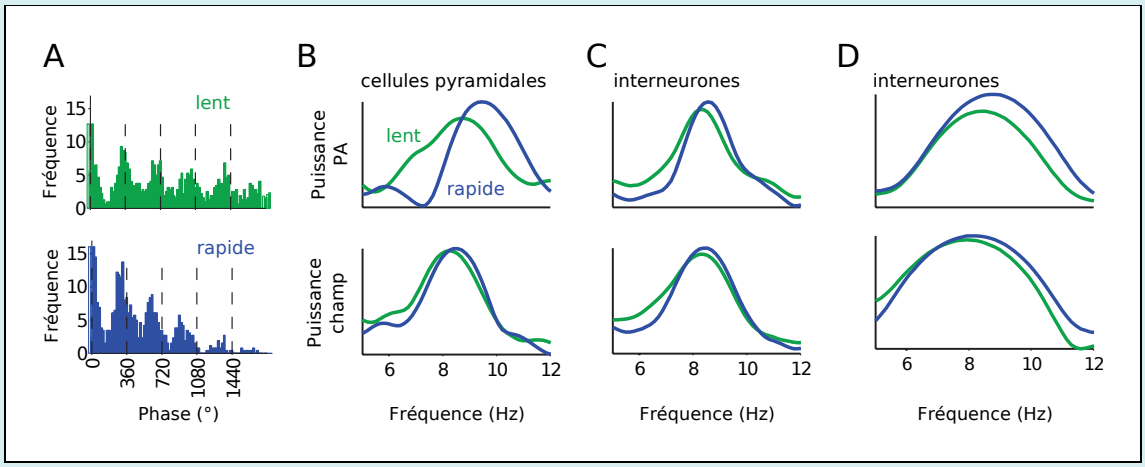

Fig. 15 – La fréquence d'oscillation des neurones hippocampiques est modulée par la vitesse de déplacement du rat. A. Autocorrélogrammes des décharges d'une cellule de lieu, analysées séparément lors de déplacements lents (*en vert*) et rapides (*en bleu*). La fréquence d'oscillation (*pics successifs des autocorrélogrammes*) est plus basse lors des déplacements lents (*lignes verticales en pointillés*). B. Spectres de puissance des décharges des neurones hippocampiques (*en haut*) et des champs de potentiel locaux (*en bas*). La fréquence d'oscillation est plus élevée lors des déplacements rapides pour les cellules pyramidales (*à gauche*), mais pas pour les interneurones (*au milieu*) – sauf si l'on restreint l'analyse aux zones où les interneurones manifestent de la précession de phase (*à droite*), ce qui indique qu'ils participent alors à des assemblées de neurones codant la zone correspondante de l'environnement.

Nous avons observé que **la fréquence d'oscillation des décharges des cellules de lieu était plus élevée lors des trajets rapides, et que cette augmentation était plus importante que celle des potentiels de champ locaux** (test de Wilcoxon, $p \ll 0.001$; Figure 15). En revanche, la fréquence d'oscillation des décharges des interneurones n'augmentait pas davantage que celle des potentiels de champ locaux avec la vitesse de déplacement du rat (test de Wilcoxon, NS). Les interneurones ayant des champs d'activité bien plus diffus que les cellules pyramidales, on considère généralement qu'ils ne participent pas au codage de la position du rat. Or nos données ont montré que certains interneurones pouvaient manifester une précession de phase, du moins dans certaines zones restreintes de leur champ d'activité. Ceci semble indiquer qu'ils sont alors contrôlés par des cellules de lieu présynaptiques avec lesquelles ils forment des assemblées de neurones. Cette interprétation est corroborée par le fait qu'en analysant les potentiels d'action émis uniquement dans les zones où les interneurones manifestent de la précession de phase, nous avons observé que **les interneurones augmentaient leur fréquence d'oscillation davantage que les potentiels de champ locaux**, et de manière comparable aux cellules de lieu (Figure 15).

Ces résultats sont compatibles avec l'hypothèse que la précession de phase résulte d'une modulation par la vitesse de déplacement de la fréquence d'oscillation d'assemblées de neurones.

3.3 Entraînement des décharges neuronales et des oscillations gamma corticales par le rythme thêta hippocampique

Sirota, Montgomery, Fujisawa, Isomura, **Zugaro** et Buzsáki (2007). Entrainment of Neocortical Neurons and Gamma Oscillations by the Hippocampal Theta Rhythm. *Neuron* 60, 683-697.

L'influence des oscillations hippocampiques sur les réseaux corticaux est encore mal comprise. Cette étude a mis en évidence une modulation par le rythme thêta hippocampique des décharges de cellules pyramidales et d'interneurones corticaux, ainsi que d'oscillations gamma localisées. Ces oscillations gamma provenaient d'oscillateurs multiples ayant des fréquences et des localisations précises distinctes.

Plus précisément, nous avons trouvé qu'**un grand nombre de neurones néocorticaux étaient modulés par le rythme thêta hippocampique**. La proportion d'interneurones modulés par thêta (32% dans le pariétal, 46% dans le préfrontal) était plus élevée que celle des cellules pyramidales (11% et 28%, respectivement). La plupart de ces neurones déchargeaient lors du front descendant du cycle thêta enregistré dans CA1 (Figure 16A). Étudier les générateurs de gamma présente une difficulté technique liée à la conduction volumique des potentiels de champ locaux. En effet, plusieurs générateurs de fréquence et de localisation spécifiques peuvent être présents simultanément et fausser l'analyse spectrale. Pour identifier les générateurs, une nouvelle mesure a donc dû être développée : les spectrogrammes de chaque voie d'enregistrement sont combinés en une matrice de dimensions $(n_F.n_V) \times n_T$ (où n_F est le nombre de classes de fréquence, n_V est le nombre de voies, et n_T est le nombre de classes de temps, c'est-à-dire d'échantillons) sur laquelle sont appliquées tour à tour une analyse en composantes principale puis une rotation orthogonale selon la méthode *varimax*, pour obtenir des facteurs dont seuls quelques coefficients sont élevés (les autres étant presque nuls). Cette méthode nous a permis d'identifier des générateurs de gamma localisés et de fréquences spécifiques ; en particulier, certains générateurs avaient des fréquences semblables mais étaient situés dans des zones corticales distinctes, alors que d'autres avaient des fréquences différentes mais se chevauchaient spatialement (Figure 16B). **La magnitude des oscillateurs gamma était modulée par le rythme thêta hippocampique** (Figure 16C). **De plus, la probabilité d'ocurrence de certaines « bouffées » de gamma était biaisée par la phase de thêta**.

Ces résultats indiquent que le rythme thêta hippocampique peut influencer le décours temporel des computations néocorticales. Ceci pourrait permettre de coordonner l'activité d'ensembles de neurones distribués dans de vastes zones hippocampiques et corticales.

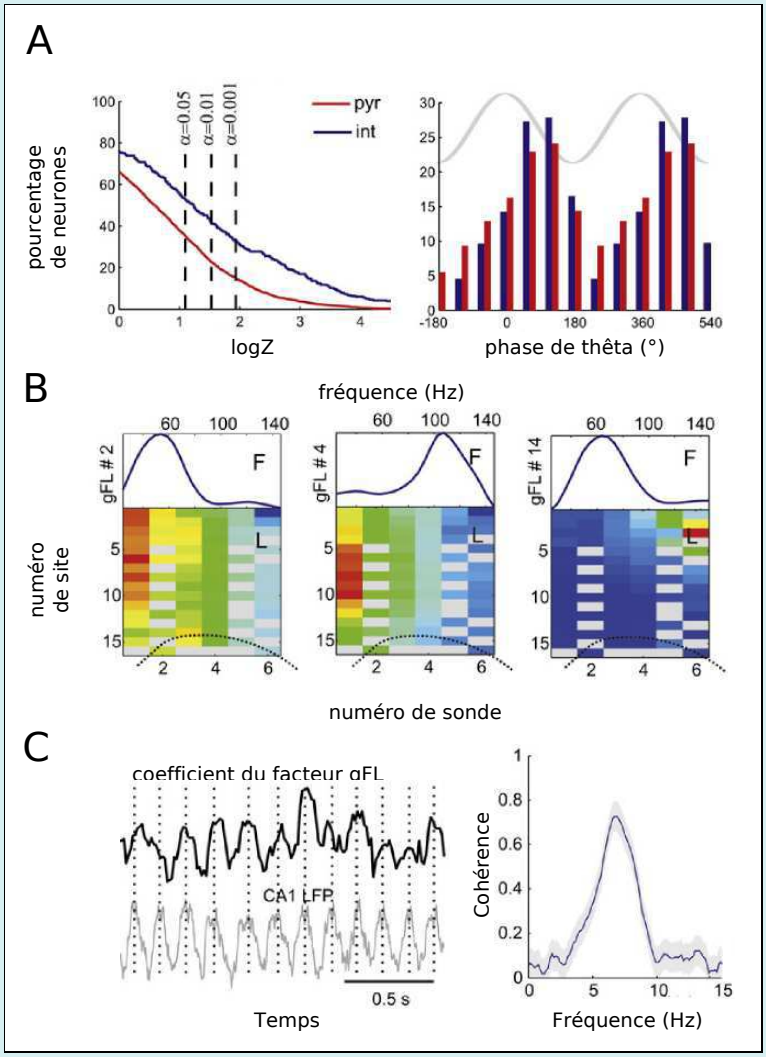

Fig. 16 – Les décharges neuronales et les oscillateurs gamma corticaux sont modulés par le rythme thêta hippocampique. A. *À gauche*. Pourcentage de neurones préfrontaux (*en rouge*, neurones pyramidaux ; *en bleu*, interneurones) modulés par le rythme thêta hippocampique. *Abscisse*, statistique de Rayleigh (test d'uniformité de la distribution circulaire des phases de décharge). *À droite*. Distribution des phases préférées pour les neurones préfrontaux significativement modulés par le rythme thêta hippocampique. B. Exemples de coefficients des facteurs gamma (*gFL*) pour un même enregistement, représentés en termes de fréquences (*F*, *courbes bleues*) et de localisation dans le cortex (*L*, *cartes colorées*). Des oscillateurs gamma peuvent avoir des fréquences similaires mais des localisations distinctes (*à gauche* et *à droite*), ou des fréquences différentes mais des localisations en grande partie communes (*à gauche* et *au centre*). C. *À gauche*. Décours temporel du coefficient d'un facteur gamma (magnitude instantanée de l'oscillateur gamma correspondant) et oscillation du potentiel de champ local hippocampique. La cohérence entre ces deux séries temporelles est représentée *à droite* : elle est maximale pour des fréquences correspondant à thêta.

Projets scientifiques

1 Vue d'ensemble

1.1 Thématique de recherche

Ma thématique de recherche en Neurosciences Intégratives est l'étude des mécanismes neurophysiologiques qui sous-tendent les fonctions cognitives, et j'ai choisi la cognition spatiale chez le rat comme domaine expérimental.

Comment de vastes ensembles de neurones anatomiquement distribués organisent-ils leur activité en séquences temporelles pour former les « assemblées de neurones » (Hebb, 1949) qui pourraient sous-tendre la cognition ? Les oscillations des potentiels de champ locaux semblent fournir la base temporelle neurophysiologique nécessaire (Varela et coll., 2001) : différents rythmes (thêta, gamma, oscillations rapides, etc.) permettent en effet d'organiser des assemblées de neurones à différentes échelles spatio-temporelles, impliquant aussi bien des réseaux locaux que plusieurs structures distantes – comme par exemple dans le cas du liage perceptif étudié chez les mammifères supérieurs (Engel et coll., 2001). Pour mieux comprendre les bases neurales des fonctions cognitives, je me propose d'étudier les réponses de dizaines de neurones enregistrés simultanément au sein d'une ou plusieurs structures cérébrales, et leur organisation temporelle par rapport aux potentiels de champ locaux de ces structures.

Mon travail expérimental est centré sur l'étude des propriétés de réseau des cellules de lieu, des cellules de grille, et des cellules DT. Au sein de l'équipe de Sidney Wiener, je participe également

à l'étude des interactions entre ces deux systèmes neuraux et des structures cérébrales impliquées dans des fonctions complémentaires comme la planification et la prise de décision (par exemple, le striatum).

Un tel projet nécessite de pouvoir enregistrer des dizaines de neurones simultanément chez l'animal en comportement, ce qui est maintenant possible grâce aux trois dispositifs d'enregistrement multiélectrodes que j'ai mis en place en tirant parti de mes compétences d'ingénieur : systèmes d'acquisition de signaux électrophysiologiques à 64 voies avec capture vidéo, descendeurs conçus et réalisés sur mesure pour 16 tétrodes[1] indépendantes ou pour électrodes multisites en silicium[2], et labyrinthes informatisés. Pour analyser les données complexes que fournissent de tels enregistrements, je tire profit des méthodes statistiques et de traitement du signal que j'ai acquises aussi bien durant ma formation initiale d'ingénieur que lors de mon post-doctorat dans le laboratoire de György Buzsáki (Rutgers University, Newark NJ, USA).

1.2 Projets, encadrement et collaborations

Pour mener à bien les projets présentés dans cette section, j'encadre actuellement deux étudiantes de troisième cycle, Gabrielle Girardeau (doctorante en Neurosciences à l'Université Paris VI) et Anne Larrieu (master 2 « Biologie Intégrative et Physiologie » (BIP) à l'Université Paris VI), ainsi qu'un post-doctorant, Karim Benchenane (docteur de l'Université de Caen).

À court et moyen terme, nous étudierons les questions suivantes :

– *Rôle des ripples hippocampiques dans la consolidation mnésique* (§ 2.1, page 31). Ce projet constitue le travail de master 2 et de thèse de Gabrielle Girardeau. Gabrielle a intégré notre équipe en 2006 dans le cadre de son cursus à l'ENS-Paris, pour suivre le master 2 BIP (Université Paris VI), au terme duquel elle a obtenu une allocation du Ministère de la Recherche. Elle est maintenant en deuxième année de doctorat à l'Université Paris VI.

  Ce projet comporte plusieurs volets. Le premier (§ 2.1.1, page 31) teste directement l'hypothèse théorique que le renforcement des traces mnésiques pendant le sommeil à ondes lentes est sous-tendu par la réactivation de séquences d'assemblées de neurones lors des oscillations rapides (∼200 Hz, *ripples*) du potentiel de champ local hippocampique. C'est une étude pour laquelle j'ai obtenu le prix *Career Development Award* de la fondation *Human Frontiers Science Program* (HFSP), et que nous menons en collaboration avec György Buzsáki (Rutgers University, Newark NJ, USA). Deux études prolongeront ce travail : nous caractériserons les mécanismes homéostatiques qui semblent réguler l'apparition des *ripples* (§ 2.1.2, page 37) et nous produirons des *ripples* artificielles pour tenter d'augmenter les performances mnésiques des rats (§ 2.1.3, page 38). Enfin, le dernier volet de ce projet testera l'influence de la valence hédonique (stimuli appétitifs et aversifs) sur les réactivations des traces mnésiques pendant le sommeil (§ 2.1.4, page 39). Cette dernière étude constitue la partie expérimentale d'un projet scientifique que j'ai soumis à l'Agence Nationale pour la Recherche (ANR), dans le

[1] Une tétrode est un groupe de 4 électrodes filaires torsadées, qui permet de discriminer les réponses de 5∼10 neurones différents.

[2] Projet européen NeuroProbes et sondes NeuroNexus.

cadre du programme « Domaines Émergents ». Il s'agit d'une collaboration avec Nicolas Brunel (DR2, CNRS – UMR 8119, Laboratoire de Neurophysique et Physiologie), qui abordera la question d'un point de vue théorique et computationnel.

– *Mémoire épisodique et codage hippocampique de séquences spatio-temporelles* (§ 2.2, page 40). Il s'agit du projet de master 2 et de thèse d'Anne Larrieu. Anne a effectué un stage de recherche dans notre équipe en 2006 dans le cadre de sa licence 3 à l'ENS-Lyon : elle a alors participé aux expériences pilotes de l'étude du rôle des oscillations hippocampiques dans la consolidation mnésique (§ 2.1.1, page 31). Je l'ai ensuite envoyée effectuer son stage de master 1 (5 mois) dans le laboratoire de György Buzsáki (Rutgers University, Newark NJ, USA). Elle est maintenant de retour dans notre équipe pour son master 2 BIP à l'Université Paris VI.

  Ce projet a pour but de poursuivre l'étude du codage hippocampique des séquences spatio-temporelles (cf. § 3.1, page 11), qui pourrait sous-tendre la formation de certaines formes de mémoire épisodique. Dans une première étude, nous perturberons le système hippocampe-cortex entorhinal en déplaçant passivement des rats en marche arrière (§ 2.2.1, page 40), et nous confronterons nos résultats expérimentaux aux prédictions des différents modèles computationnels : certains modèles prédisent que dans ces conditions la relation entre phase et position sera inchangée, alors que d'autres modèles prédisent qu'elle sera inversée. Dans un second temps, nous étudierons les relations fonctionnelles entre les précessions de phase hippocampique et entorhinale (§ 2.2.2, page 42). Enfin, nous testerons le rôle des séquences d'activité dans certaines formes de mémoire (§ 2.2.3, page 44).

Karim Benchenane contribue à deux projets : l'étude des déficits mnésiques causés par la suppression des oscillations hippocampiques (§ 2.1.1, page 31) en collaboration avec Gabrielle Girardeau, et la caractérisation du couplage dynamique hippocampo-préfrontal au cours d'un apprentissage nécessitant un changement de stratégie (Projet Intégré Européen ICEA, cf. § 1.3, page 30).

À plus long terme, j'envisage d'aborder également les questions suivantes :

– *Intégration du signal DT dans l'élaboration des réponses des cellules de grille* (§ 2.3.1, page 45). Les modèles computationnels attribuent aux cellules DT un rôle critique dans la détermination des axes d'orientation des grilles. En collaboration avec Daniel Bennequin (mathématicien, Professeur de l'Université Paris VII), nous testerons cette hypothèse théorique.
– *Intégration des signaux DT à la dynamique hippocampique* (§ 2.3.2, page 45). Cellules de lieu et cellules DT sont anatomiquement et fonctionnellement liées, mais on ignore tout des mécanismes qui sous-tendent les coopérations entre ces deux systèmes. Je compte étudier les couplages entre l'hippocampe et les structures contenant des cellules DT, en analysant le décours temporel de leurs réponses et de leurs potentiels de champ locaux.
– *Mécanismes de mise à jour des cellules DT* (§ 2.3.3, page 46, et § 2.3.4, page 46). Je souhaite tester les prédictions de modèles computationnels des cellules DT en déterminant comment l'activité se réorganise dynamiquement au sein des réseaux de cellules DT suite à des modifications de l'environnement, et en étudiant les mécanismes (intégration du flux optique) qui permettent à l'activité de se déplacer au sein du réseau lorsque le rat tourne la tête, pour que la direction représentée soit mise à jour en conséquence.
– *Représentations spatiales et planification de comportements orientés vers des buts.* Le striatum, impliqué dans la planification, reçoit des projections hippocampiques directes.

Pour déterminer comment ces deux structures interagissent, je participerai au projet de l'équipe de Sidney Wiener visant à étudier les changements dynamiques de leur couplage lorsque la tâche comportementale exige un changement de stratégie de navigation. Il s'agit d'un prolongement du Projet Intégré Européen ICEA (cf. ci-dessous).

1.3 Projets Intégrés Européens (FP6)

Mes projets scientifiques s'intègrent dans la dynamique de recherche de l'équipe de Sidney Wiener, qui participe à trois grands Projets Intégrés dans le cadre du 6e Programme-Cadre (FP6) de la Commission Européenne :

- Le projet `ICEA` (*Integrating Cognition, Emotion and Autonomy*) fait suite au projet `Psikharpax`, et regroupe huit laboratoires et deux industriels. Il a pour objectif de concevoir des robots autonomes capables de développer des représentations de leur environnement en termes spatiaux, émotionnels[3] et comportementaux, et d'utiliser cette connaissance pour anticiper, planifier, et décider. Dans ce cadre, l'étude du cerveau et du comportement du rat sert de source d'inspiration pour de nouveaux algorithmes pour le robot. Les travaux de notre équipe concernant les interactions entre l'hippocampe et le cortex préfrontal, ainsi qu'entre l'hippocampe et les ganglions de la base, servent de base pour la mise au point d'un système biomimétique de prise de décision et de planification de stratégies.
- Le projet `BACS` (*Bayesian Approach to Cognitive Systems*) fait suite au projet `BIBA` (*Bayesian Inspired Brain and Artefacts*) et regroupe huit laboratoires et trois industriels. Son but est de tester l'hypothèse que les neurones individuels et les réseaux neuronaux sont des processeurs bayésiens, ainsi que d'étendre la modélisation bayésienne de la cognition naturelle et de développer des systèmes cognitifs artificiels capables d'évoluer dans des environnements réels complexes. La modélisation de la cognition naturelle est effectuée à différents niveaux d'intégration (du neurone au comportement), et est validée par un ensemble de données neurophysiologiques et psychophysiques. L'implémentation neurobiologique des calculs probabilistes est l'un des principaux problèmes scientifiques que ce programme se propose d'aborder. Nos enregistrements de neurones permettent de tester la nature bayésienne du traitement des signaux au niveau de neurones individuels et d'ensembles de neurones.
- Le projet `NeuroProbes` regroupe neuf laboratoires et cinq industriels. Il vise à développer de nouvelles matrices d'électrodes en silicium qui permettent d'enregistrer de vastes ensembles de neurones (davantage que les électrodes conventionnelles, notamment en provoquant des dommages encore plus limités), ainsi que les potentiels de champs locaux en une centaine de points anatomiquement bien définis, ce qui permettra d'analyser les densités de sources de courant de plusieurs structures cérébrales simultanément. Ces nouvelles électrodes permettront également d'infuser localement des substances pharmacologiques et d'inactiver temporairement (par voie chimique ou calorique) des zones restreintes du cerveau. Nous testons la biocompatibilité des ces électrodes, aidons à développer de nouvelles configurations tridimensionnelles (cubiques) de sites d'enregistrement, effectuons des enregistrements chez l'animal libre de ses mouvements, et

[3] L'émotion est ici comprise dans le sens restrictif suivant : les stimulti environnementaux et les actions motrices sont codés en termes d'effets anticipés sur le bien-être de l'organisme ou du robot.

développons des logiciels d'analyse de données multi-voies qui sont mis librement à la disposition de la communauté scientifique.

Les deux premiers projets ont une composante centrale computationnelle, à la fois théorique et appliquée, à laquelle nous apportons un volet expérimental. En ce qui concerne le projet `Neuro-Probes`, j'aide à définir les caractéristiques requises pour ces nouvelles électrodes, en tirant parti de mon expérience acquise dans le laboratoire de György Buzsáki où des systèmes semblables (*Michigan Probes*) sont déjà utilisés. Je participe également au développement des solutions logicielles nécessaires au traitement et à l'analyse des données recueillies grâce à ces électrodes.

2 Études expérimentales

2.1 Ripples hippocampiques et consolidation mnésique

2.1.1 *Déficits mnésiques causés par la suppression des ripples*

Je présenterai ici un projet que je mène depuis 2006 dans le cadre d'une collaboration avec György Buzsáki, et pour lequel j'ai obtenu le prix *Career Development Award* de la fondation *Human Frontiers Science Program* (HFSP), financement d'une durée de trois ans qui vise à soutenir le développement de jeunes équipes de recherche au niveau international.

▶ Ce projet constitue la première partie de la thèse de Gabrielle Girardeau, et implique également Karim Benchenane [Anne Larrieu a participé aux expériences pilotes au cours de son stage de licence 3 en 2006].

De nombreuses études comportementales menées aussi bien chez l'homme que chez le rat montrent que le sommeil contribue à consolider certaines formes de mémoire (cf. les revues récentes de Peigneux et coll. (2001) ; Smith (2001) ; Walker et Stickgold (2004) ; Stickgold (2005) ; mais aussi la position contraire exprimée par Vertes et coll. (2004)). Compte tenu de son rôle central dans de nombreux processus mnésiques, il est vraisemblable que l'hippocampe intervienne ici encore de façon critique. On sait que pendant le sommeil à ondes lentes, la dynamique du réseau hippocampique change radicalement : elle est alors caractérisée par une activité irrégulière et par l'apparition périodique dans le champ CA1 de potentiels de population (*sharp waves*) et d'oscillations transitoires de haute fréquence (*ripples* ; Buzsáki et coll. (1992)), pendant lesquelles de vastes ensembles de neurones déchargent de façon synchrone, activité qui se propage du champ CA3 au champ CA1, puis du champ CA1 au subiculum et au cortex entorhinal (Buzsáki et coll., 1992 ; Ylinen et coll., 1995 ; Chrobak et Buzsáki, 1996 ; Penttonen et coll., 1997 ; Csicsvari et coll., 1998, 1999b,a, 2000). Or si cette activité des neurones hippocampiques est endogène, elle n'en est pas pour autant aléatoire : elle reproduit en effet de manière frappante celle qui a été observée pendant la période de veille précédant le sommeil (Pavlides et Winson, 1989 ; Wilson et McNaughton, 1994 ; Skaggs et McNaughton, 1996 ; Nádasdy et coll., 1999 ; Kudrimoti et coll., 1999 ; Lee et Wilson, 2002 ; Foster et Wilson, 2006 ; Diba et Buzsáki, 2007). Ainsi, des séquences entières d'activation d'assemblées de neurones sont-elles « réactivées » pendant le sommeil - comme si, en quelque sorte, après avoir exploré son environnement, le rat parcourait à nouveau les mêmes trajectoires dans son sommeil (Figure 1). Fait remarquable, ces séquences sont reproduites à des échelles de temps beaucoup plus courtes et à des fréquences beaucoup plus élevées (∼200 Hz), comparables aux stimulations utilisées dans les protocoles expérimentaux d'induction de potentialisation à long terme

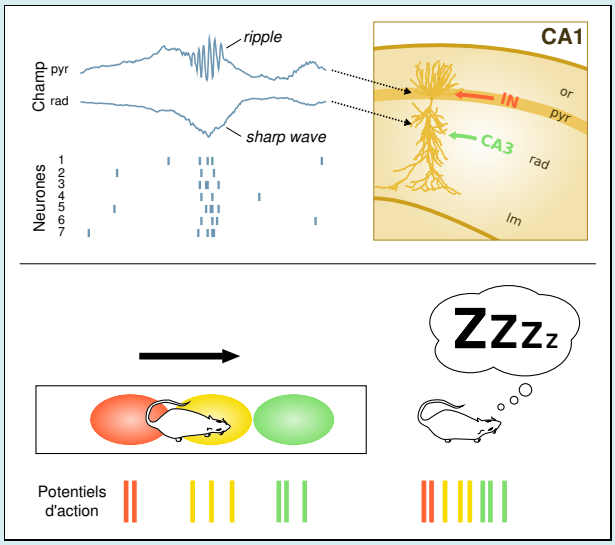

Fig. 1 – Réactivations de séquences d'assemblées de neurones hippocampiques pendant le sommeil à ondes lentes. *En haut*. Pendant le sommeil à ondes lentes, de vastes ensembles de neurones du champ CA3 se réactivent spontanément en émettant périodiquement des bouffées de potentiels d'action synchrones. Ceci provoque une puissante excitation des dendrites distales des cellules pyramidales du champ CA1 (*flèche verte*), qui se traduit dans les enregistrements de potentiels de champ locaux (*à gauche, courbes bleues*) par un potentiel de population (*sharp wave*) au niveau du *stratum radiatum* (*rad*). Simultanément, l'inhibition rythmique des corps cellulaires et des dendrites proximales de ces mêmes cellules pyramidales par les interneurones de CA1 (*IN, flèche rouge*) se traduit par des oscillations rapides (*ripples*) au niveau du *stratum pyramidale* (*pyr*). Sous l'influence combinée de ces excitations et inhibitions, de nombreuses cellules pyramidales de CA1 se mettent à décharger à leur tour de façon synchrone (*à gauche*, à titre d'illustration, les décharges de sept cellules pyramidales sont représentées schématiquement : chaque *barre verticale bleue* représente un potentiel d'action). L'activité se propage ensuite au cortex entorhinal (5 à 30 ms plus tard), où des événements de champ similaires sont également observés. Parce que cette réactivation spontanée implique de très nombreux neurones hippocampiques (jusqu'à 10% des neurones de CA1 simultanément) qui déchargent à des fréquences globales très élevées (∼200 Hz), elle pourrait induire des phénomènes de plasticité synaptique dans les structures corticales situées en aval de l'hippocampe. Autres abréviations : *so = stratum oriens, lr = stratum lacunosum moleculare*. *En bas, à gauche*. Lorsqu'un rat parcourt un couloir, ses cellules de lieu sont activées l'une après l'autre en séquence (*rouge*, puis *jaune*, puis *verte*). Par la suite, lors du sommeil à ondes lentes, les mêmes cellules se réactivent spontanément, dans le même ordre, pendant les *ripples*.

(Bliss et Collingridge, 1993) - le mécanisme cellulaire et moléculaire qui sous-tend certaines formes de mémoire à long terme (Whitlock et coll., 2006 ; Pastalkova et coll., 2006).

Pourtant, même si ces diverses études mettent en évidence un lien de corrélation entre les complexes *sharp wave-ripples* (SPW-R) hippocampiques et la consolidation mnésique, une relation causale reste à démontrer. Pour montrer que les complexes SPW-R jouent un rôle critique dans la consolidation mnésique, nous les avons sélectivement supprimés en stimulant très brièvement (impulsions simples de 0,5 ms) la voie commissurale hippocampique ventrale chaque fois qu'une *ripple* était détectée pendant le sommeil qui suivait un entraînement à réaliser une tâche de mémoire spatiale à long terme mettant en jeu l'hippocampe (Figure 2).

Dix-sept rats ont été équipés d'électrodes bilatérales implantées dans la couche CA1 de l'hippocampe dorsal, où des *ripples* ont été enregistrées. La fréquence de décharge des neurones augmentait

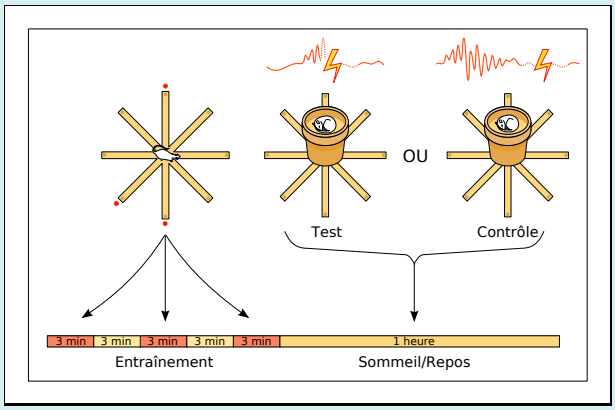

Fig. 2 – Protocole expérimental. Chaque jour, le rat effectue trois essais dans le labyrinthe radial où les trois mêmes bras sont appâtés une fois par essai (*à gauche, points rouges*). Le rat est retiré du labyrinthe dès qu'il a trouvé les trois récompenses (ou après un maximum de 3 min). Des périodes de repos de 3 min sont intercalées entre les essais, pendant lesquelles le rat est maintenu dans un pot de fleurs au centre du labyrinthe. Après le troisième essai, le rat peut dormir ou se reposer dans le pot de fleurs pendant une heure, pendant laquelle les stimulations sont déclenchées soit pendant les *ripples* (rats de test, *au milieu*), soit en dehors des *ripples* (rats de contrôle stimulés, *à droite*).

durant les SPW-R ; l'augmentation était plus forte pour les cellules pyramidales que pour les interneurones, ce qui correspondait à un gain d'excitabilité. Les décharges des cellules pyramidales et des interneurones étaient verrouillées en phase par rapport aux *ripples* (Figure 3a,b). Pour bloquer les *ripples*, nous avons mis au point un nouveau protocole de détection-stimulation. Des électrodes bipolaires sont implantées dans la commissure hippocampique ventrale. De brèves stimulations (impulsions simples) déclenchaient des potentiels de champ présentant un profil caractéristique de densité de courant, avec un puits dans la couche *radiatum* et une source dans la couche pyramidale (Figure 3d). La stimulation commissurale était automatiquement déclenchée dès le début des *ripples*. Cela empêchait que l'oscillation se développe davantage et interrompait transitoirement les réponses des neurones hippocampiques (Figure 3c,e), ce qui bloquait la réactivation de séquences de cellules de lieu activées lors de l'exploration du labyrinthe. Contrairement aux neurones hippocampiques, les cellules néocorticales n'étaient pas affectées (Figure 3c,e). Du fait que pour les intensités de stimulation les plus faibles, l'interruption de l'activité hippocampique durait moins de 100 ms (Figure 3c), nous avons utilisé des stimulations de basse intensité pendant les expériences comportementales pour pouvoir perturber sélectivement et transitoirement le réseau hippocampique.

Nous avons ensuite testé le rôle des *ripples* dans la consolidation mnésique chez des rats entraînés à effectuer une tâche comportementale mettant en jeu l'hippocampe. Trois groupes de rats (rats de test : $n = 7$, rats de contrôle stimulés : $n = 7$, rats de contrôle non implantés : $n = 12$) ont été entraînés à trouver des récompenses alimentaires sur un labyrinthe radial à 8 bras où trois bras, toujours les mêmes, étaient appâtés (Figure 2). Les rats effectuaient trois essais par jour, après quoi ils pouvaient dormir pendant une heure. Pendant cette période de sommeil, toutes les *ripples* détectées automatiquement ont été supprimées par la stimulation chez les rats de test (Figure 4a,b ; pourcentage de détection automatique : $86,0 \pm 1,3\%$ des *ripples* détectées a postériori par des algorithmes plus sensibles). Les rats de contrôle stimulés étaient soumis au même protocole, mais un délai aléatoire était introduit entre la détection des *ripples* et la stimulation, pour assurer que la stimulation se produise essentiellement en dehors des *ripples* (Figure 4b). Ces rats de contrôles

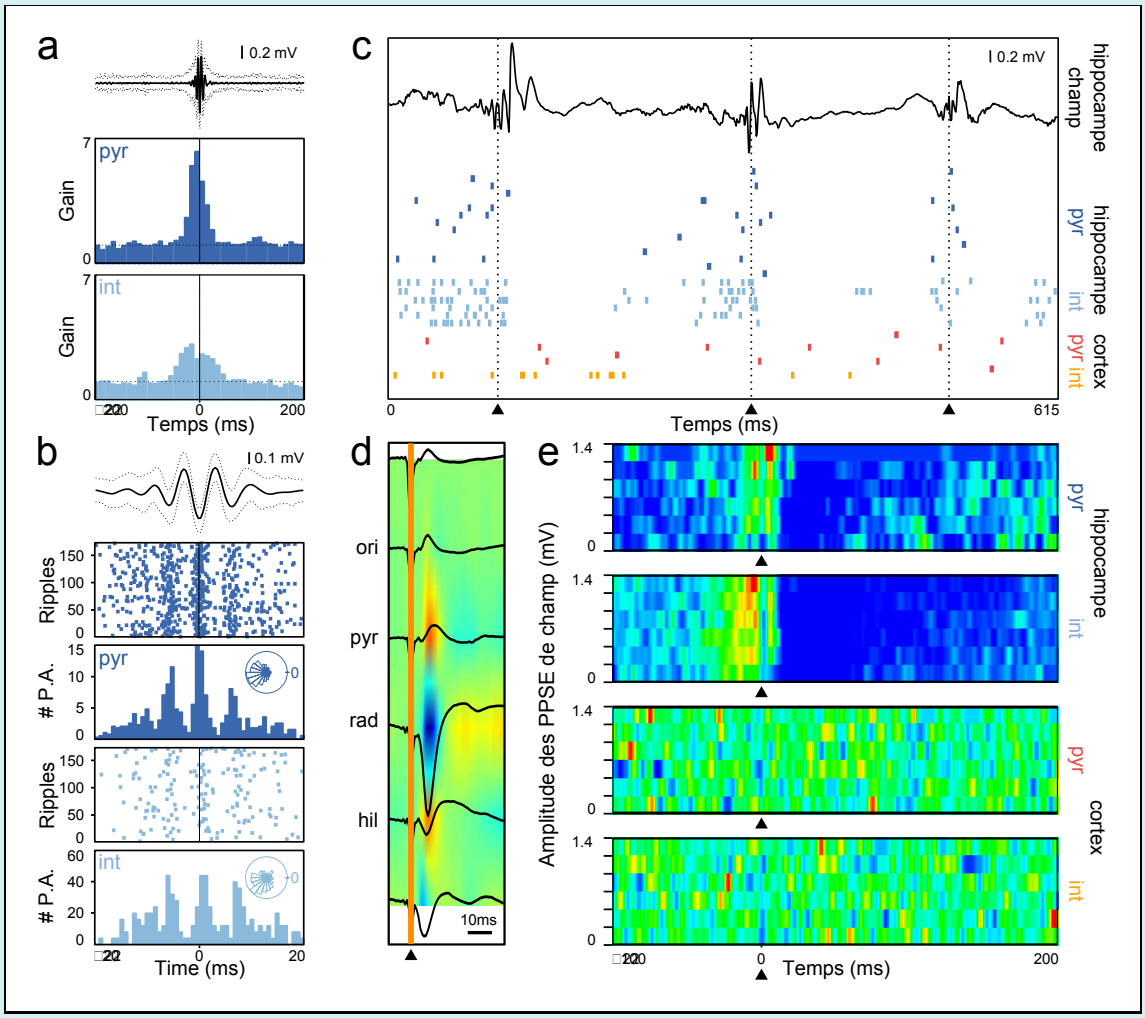

Fig. 3 – La stimulation de la voie commissurale hippocampique ventrale interrompt les *ripples* et les réponses des neurones hippocampiques. *A*. La fréquence de décharge des neurones hippocampiques augmente sensiblement pendant les *ripples*. Tracé moyen (*en haut*, les *lignes en pointillés* représentant les intervalles de confiance à 95%) et gain de la fréquence de décharge des cellules pyramidales (*bleu foncé*) et des interneurones (*bleu clair*). *B*. Décharge verrouillée en phase des cellules pyramidales hippocampiques (*bleu foncé*) et des interneurones (*bleu clair*) durant les *ripples*. En encadré : distribution de la phase des potentiels d'action (en coordonnées polaires). *C*. Interruption des *ripples* et des réponses hippocampiques. Potentiels de champ locaux (*courbes noires*) dans l'hippocampe et réponses (*traits verticaux*) des cellules pyramidales (*pyr* ; hippocampe, *bleu foncé* ; cortex sensorimoteur, *rouge*) et des interneurones (*int* ; hippocampe, *bleu clair* ; cortex sensorimoteur, *orange*). *Lignes verticales en pointillés* et *têtes de flèches* : stimulations. *D*. Densité de courant moyenne des réponses évoquées (*courbes noires*) à plusieurs profondeurs ($n = 500$). Remarquer un puits important dans la couche *radiatum* (*rad* ; *bleu*) et une source dans la couche pyramidale (*pyr* ; *rouge*). Échelle : 10 ms, *hil* : hilus, *ori* : stratum oriens. *E*. Durée d'interruption de l'activité en fonction de l'amplitude de la réponse évoquée. Les z-scores de la fréquence de décharge instantanée sont représentés en couleur en fonction du niveau de stimulation. L'interruption de l'activité dans l'hippocampe dépend de l'amplitude de la réponse évoquée (pour les cellules pyramidales comme pour les interneurones), mais n'est pas modifiée dans le néocortex. L'augmentation précédant la stimulation est due au recrutement progressif des neurones au début des *ripples*.

subissaient donc le même nombre de stimulations que les rats de test (test de Student, NS), mais leurs *ripples* n'étaient pas affectées. L'architecture globale du sommeil n'était pas modifiée par la suppression des *ripples* (Figure 4c-e). La puissance spectrale des rythmes liés au sommeil comme thêta (pendant le sommeil paradoxal) et delta (pendant le sommeil à ondes lentes) n'était pas différente chez les rats de tests et les rats de contrôle stimulés (Figure 4d). Qui plus est, le rapport sommeil paradoxal/sommeil à ondes lentes était inchangé (Figure 4e). Par conséquent, notre protocole de stimulation nous assurait que tout déficit de performance éventuellement observé chez les rats de test pourrait être spécifiquement attribué à la suppression sélective des *ripples* et non à des effets non spécifiques de la stimulation hippocampique.

Comme les réactivations d'assemblées de neurones se produisent surtout pendant la première demi-heure de sommeil suivant l'exploration, notre raisonnement était que bloquer les *ripples* pendant une heure suffirait à interférer avec le mécanisme supposé de transfert et de consolidation hippocampo-cortical. Nous avons mesuré la performance comportementale au fil des jours en nous basant sur le rapport du nombre de récompenses trouvées et du nombre total de visites. La stimulation en dehors des *ripples* n'a pas affecté l'apprentissage, comme l'a montré l'absence de différence significative entre les rats de contrôle stimulés et non implantés (ANOVA à deux facteurs, groupe $\times$ jour, NS). Les données des deux groupes ont donc été groupées et comparées aux rats de test. Une ANOVA à deux facteurs (groupe $\times$ jour) a montré que les performances des rats de test étaient significativement diminuées par rapport à celle des rats de contrôle (facteurs principaux, $p < 0,001$; interaction, $p < 0,01$; Figure 5). Chez les rats de contrôle, la performance dépassait le niveau aléatoire dès le 5^{e} jour d'entraînement, alors que les rats de contrôle avaient une performance aléatoire jusqu'au 8^{e} jour (tests de Student, $p < 0,05$).

La suppression des SPW-R et des décharges neuronales associées a donc perturbé la consolidation mnésique. Le déficit comportemental observé était spécifiquement causé par la suppression des SPW-R, et non par des effets non spécifiques de la stimulation, puisque la stimulation des rats de contrôle n'a eu aucun impact comportemental détectable. Ce déficit est d'autant plus frappant que nous n'avons supprimé les SPW-R que durant une heure. L'ampleur du déficit est comparable à celui observé chez des rats ayant subi une lésion hippocampique (Jarrard, 1995). La légère amélioration des performances des rats de test peut être due aux SPW-R de plus faible amplitude qui n'auraient pas été automatiquement détectées (et donc supprimées), aux SPW-R après la période de stimulation, ou à d'autres mécanismes d'apprentissage non hippocampiques, comme cela a été observé chez des rats ayant subi une lésion hippocampique. Nos résultats montrent donc que les SPW-R jouent un rôle critique dans la consolidation mnésique, probablement parce qu'ils permettent la compression temporelle des réactivations de séquences observées pendant le comportement (Pavlides et Winson, 1989 ; Wilson et McNaughton, 1994 ; Skaggs et McNaughton, 1996 ; Nádasdy et coll., 1999 ; Kudrimoti et coll., 1999 ; Lee et Wilson, 2002 ; Foster et Wilson, 2006 ; Diba et Buzsáki, 2007), de façon à les reproduire dans des fenêtres temporelles compatibles avec la plasticité synaptique, et parce que, en synchronisant l'activité neuronale, ils permettent aux ensembles neuraux réactivés d'exercer une influence importante sur les structures en aval (Chrobak et Buzsáki, 1996). De plus, les SPW-R hippocampiques sont coordonnées avec les décharges néocorticales, les oscillations lentes et les fuseaux thalamo-corticaux (Siapas et Wilson, 1998 ; Sirota et coll., 2003 ; Battaglia et coll., 2004), ce qui suggère qu'ils pourraient exercer une influence distribuée sur les fonctions corticales sous-tendant la consolidation mnésique.

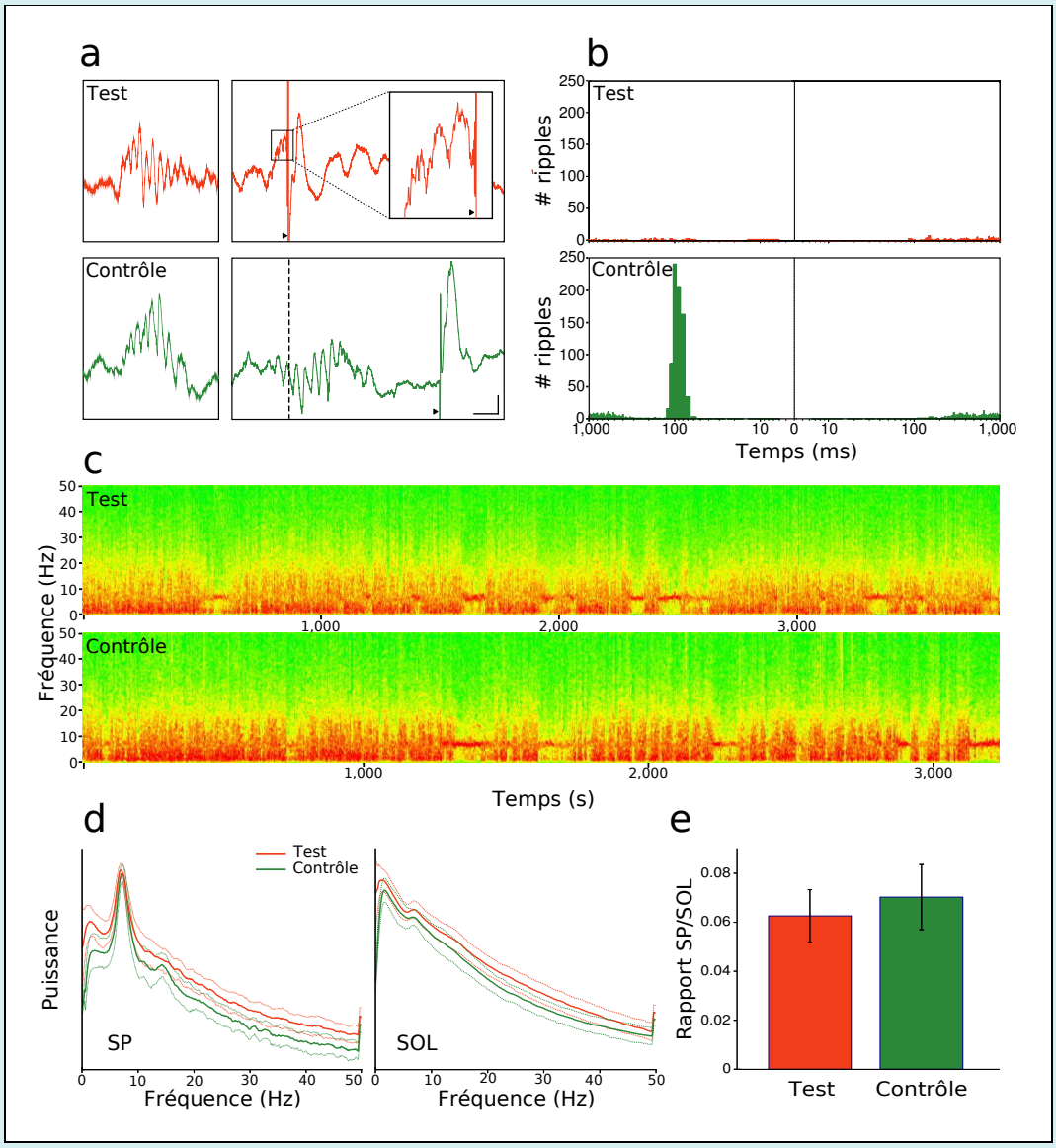

Fig. 4 – Les stimulations déclenchées par détection des SPW-R interrompent les *ripples* sans affecter la structure globale du sommeil. *A*. Exemples de *ripples* chez un rat de test et un rat de contrôle enregistrées pendant une période de sommeil précédant l'exploration du labyrinthe (*à gauche*). Au cours de la période de sommeil suivant l'exploration, les *ripples* étaient bloquées après quelques cycles chez le rat de test (*en haut, à droite*), alors que la stimulation (*tête de flèche*) était déclenchée après un délai aléatoire (80∼120 ms) après les *ripples* chez le rat de contrôle (*en bas, à droite*). Pour cette illustration, le seuil de détection était légèrement plus élevé que dans les sessions d'enregistrement typiques (*en encadré*). Échelle : 20 ms, 0,2 mV. *B*. Corrélogrammes croisés des stimulations et des *ripples* intactes détectées à posteriori chez les rats de test et de contrôle. Pratiquement toutes les *ripples* ont été supprimées chez les rats de test. *C*. Exemples de spectrogrammes du champ de potentiel local hippocampique enregistrés pendant une session de sommeil chez un rat de test et un rat de contrôle. *D*. Spectres moyens pendant le sommeil paradoxal (SP) et le sommeil à ondes lentes (SOL) (mêmes rats qu'en *c* ; *courbes en pointillés*, écarts types). La puissance était élevée dans la bande thêta (7∼12 Hz) pendant le SP et dans la bande delta (1∼4 Hz) pendant le SOL. *E*. Rapport moyen SP/SOL dans un sous-ensemble aléatoire de sessions de test et de contrôle ($n = 24$ et $n = 27$, respectivement ; test de Student, NS).

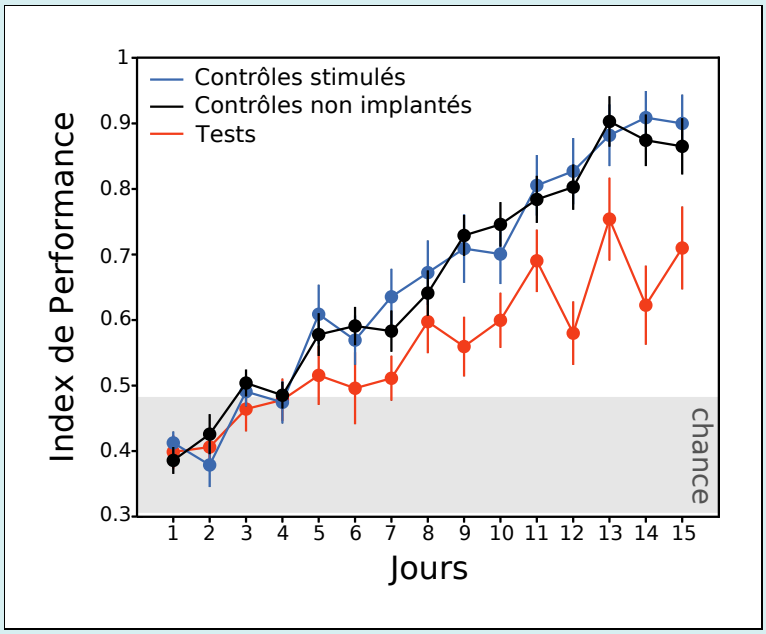

Fig. 5 – La suppression des *ripples* hippocampiques interfère avec la consolidation mnésique. Les rats de test (*en rouge*, $n = 7$) ont une performance significativement diminuée par rapport aux rats de contrôle (*en bleu*, $n = 7$ contrôles stimulés, et *en noir*, $n = 12$ contrôles non implantés) dans la tâche spatiale du labyrinthe radial, tâche qui implique l'hippocampe. *Zone grisée*, zone de performance aléatoire. Bien que la performance s'améliore pour tous les rats, les rats sans *ripples* mettent plus de jours à dépasser le niveau de performance aléatoire (tests de Student, $p < 0,05$) et leur performance reste systématiquement en dessous de celle des rats de contrôle (ANOVA : groupe, $p < 0,001$; jour, $p < 0,001$; interaction groupe $\times$ jour, $p < 0,01$).

2.1.2 *Homéostasie des réactivations hippocampiques*

▶ Ce prolongement du projet de suppression des *ripples* fera partie de la thèse de Gabrielle Girardeau, qui travaillera en collaboration avec Anne Larrieu.

Nos données préliminaires indiquent que des mécanismes homéostatiques pourraient être déclenchés par la suppression expérimentale des *ripples*. Il s'agirait vraisemblablement de mécanismes à court terme. En effet, alors que le nombre de *ripples* enregistrées pendant l'heure qui suit les sessions de stimulation n'est pas significativement différent chez les rats de test et chez les rats de contrôle stimulés, en revanche, pendant les sessions de stimulation le nombre de *ripples* chez un même rat semble être plus élevé lorsque les stimulations ont lieu pendant les *ripples* qu'en dehors des *ripples*. Plus intéressant, cette différence n'apparaîtrait que lorsque le rat est soumis à une tâche d'apprentissage avant l'enregistement. Nous allons donc poursuivre ces expériences pilotes, et si ce résultat se confirme, nous caractériserons les mécanismes homéostatiques qui sous-tendent cette augmentation sélective de l'incidence des *ripples*.

Le protocole sera similaire à celui de la suppression des *ripples*. Dans une première condition (apprentissage), des rats seront entraînés à parcourir un labyrinthe radial à huit bras pour y trouver des récompenses alimentaires situées à emplacements fixes. Dans une deuxième condition (contrôle), ils exploreront une enceinte circulaire pour obtenir des récompenses alimentaires dispersées aléatoirement. Juste après la phase d'exploration (apprentissage ou contrôle), les rats seront placés dans un pot de fleurs où ils pourront dormir pendant une heure, et nous stimulerons la

commissure hippocampique ventrale chaque fois qu'une *ripple* sera détectée, soit immédiatement (suppression) soit après un délai aléatoire (délai). Nous aurons donc quatre conditions expérimentales pour chaque rat (apprentissage ou contrôle, et suppression ou délai). Notre hypothèse est que le nombre de *ripples* sera plus élevé dans la condition apprentissage-suppression que dans les trois autres conditions.

Pour confirmer le rôle de la plasticité synaptique induite par l'apprentissage (Behrens et coll., 2005) dans cette augmentation sélective, nous effectuerons les mêmes tests chez des rats chez lesquels nous aurons préalablement saturé la potentialisation à long terme (Moser et Moser, 1998) ou bloqué les récepteurs NMDA impliqués dans la potentialisation à long terme : nous ne devrions alors plus voir d'augmentation sélective du nombre de *ripples* dans la condition apprentissage-suppression.

Nous enregistrerons simultanément les potentiels de champ locaux et l'activité multi-unitaire dans CA1 et CA3. Nous caractériserons l'activité multi-unitaire et les potentiels de champ (gain d'excitabilité, patterns spatiaux-temporels, cohérence) précédant le développement des *ripples* de CA1, et nous testerons s'ils présentent des propriétés spécifiques dans la condition apprentissage-suppression. Cette étude neurophysiologique pourra être complétée par une approche pharmacologique en collaboration avec Susan Sara (CNRS, DR émérite dans l'équipe de Sidney Wiener).

2.1.3 *Oscillations imposées et augmentation des performances mnésiques*

▶ Cette étude, qui constitue un second prolongement du projet de suppression des *ripples*, fera partie de la thèse de Gabrielle Girardeau, qui travaillera en collaboration avec Anne Larrieu.

Puisque la suppression des *ripples* induit une diminution de performance dans une tâche de mémoire spatiale, on peut se demander si a contrario une augmentation du nombre de *ripples* pourrait induire une amélioration de la performance. Pour tester cette hypothèse, nous développerons un protocole de microstimulation sinusoïdale locale, ayant une durée, une fréquence et une amplitude semblable à celles des *ripples*. Nous formulons quatre hypothèses :

1. En produisant des *ripples* artificielles pendant le sommeil à ondes lentes, entre les *ripples* naturelles (par exemple, après un délai de 500 ms après chaque *ripple*), nous recruterons préférentiellement les mêmes cellules de lieu que celles activées pendant le comportement exploratoire précédant le sommeil.
2. Ces cellules de lieu formeront des séquences semblables à celles observées pendant l'exploration.
3. En produisant des *ripples* artificielles *juste après* (quelques millisecondes) des *ripples* naturelles, les séquences initiées pendant les *ripples* naturelles seront prolongées pendant les *ripples* artificielles.
4. Si les hypothèses 2 ou 3 sont vérifiées, les performances des rats seront améliorées ; si seule l'hypothèse 1 est vérifiée, il n'y aura pas d'amélioration.

Cette étude nécessitera d'enregistrer de vastes ensembles de neurones hippocampiques pendant le comportement, puis pendant le sommeil.

2.1.4 *Modulation hédonique des réactivations hippocampiques*

Cette étude constitue le volet expérimental d'un projet scientifique que j'ai soumis à l'Agence Nationale pour la Recherche (ANR), dans le cadre du programme « Domaines Émergents ». Il s'agit d'une collaboration avec Nicolas Brunel (DR2, CNRS – UMR 8119, Laboratoire de Neurophysique et Physiologie), qui abordera la question d'un point de vue théorique et computationnel. En cas d'acceptation du projet par l'ANR, j'en assurerais la coordination.

▶ Ce travail sera mené en parallèle avec l'étude de la précession de phase (cf. § 2.2, page 40), et fera partie de la thèse de Gabrielle Girardeau, qui travaillera en collaboration avec Anne Larrieu.

Bien que la mémoire spatiale ait fait l'objet de très nombreuses études théoriques et expérimentales, peu de travaux concernent l'influence de la pertinence de certains endroits spécifiques (ex : sources de nourriture, par rapport à des endroits « neutres ») sur leur codage et leur stockage à long terme (cf. par exemple Hollup et coll. (2001) ; Rivard et coll. (2004)). Des données récentes obtenues chez le rat indiquent que les neurones qui subissent le plus de plasticité durant la phase de codage de l'information interviennent ensuite davantage pendant le sommeil pour la stabilisation à long terme des traces mnésiques (consolidation mnésique) (O'Neill et coll., 2008). Sachant que des signaux neuromodulateurs liés à la récompense, comme la dopamine (Schultz, 2007), peuvent altérer la plasticité synaptique (Otmakhova et Lisman, 1996 ; Li et coll., 2003), nous proposons que cela permettrait un renforcement de la consolidation des endroits pertinents pour l'animal.

Pour tester cette hypothèse, nous combinerons deux approches complémentaires : modélisation théorique et computationnelle de l'hippocampe (CA1 et CA3), incluant la neuromodulation par des signaux liés à la récompense, et investigation expérimentale de l'influence des valeurs hédoniques (récompenses) sur les mécanismes sous-tendant le stockage à long terme des items mnésiques dans l'hippocampe. Des résultats expérimentaux préliminaires et les données de la littérature nous aideront à concervoir le modèle, puis les prédictions théoriques et computationnelles seront confrontées à nos résultats expérimentaux finals, à la fois pour tester notre modèle et pous nous aider à interpréter nos découvertes expérimentales.

Du point de vue expérimental, il est difficile de tester cette hypothèse avec un protocole comportemental classique : en effet, lorsque le rat reçoit une récompense alimentaire, il doit s'arrêter pour la consommer, si bien qu'il passe davantage de temps dans le champ d'activité des cellules de lieu codant l'emplacement de la récompense que dans celui d'autres cellules de lieu. De plus, sa vitesse est bien moins élevée à l'emplacement de la récompense qu'ailleurs ; or la vitesse affecte la fréquence de décharge des cellules de lieu (McNaughton et coll., 1983 ; Czurkó et coll., 1999 ; Hirase et coll., 1999 ; Huxter et coll., 2003) – et à vitesse nulle, le rythme thêta s'arrête (Buzsáki et coll., 2002).

En déplaçant passivement des rats sur un train électrique, nous pourrons leur distribuer des récompenses (eau sucrée) et des stimuli aversifs (bouffées d'air) à emplacements fixes dans la pièce, sans modifier leur vitesse instantanée, ni la proportion de temps qu'ils passeront dans le champ d'activité des cellules de lieu concernées. Nous comparerons ensuite pendant le sommeil les nombres de réactivations qui correspondent aux emplacements à valence positive, négative et neutre. Nous pourrons ainsi mieux comprendre les mécanismes neurophysiologiques de l'influence de la valence hédonique sur la consolidation mnésique.

Incidemment, nous pourrons également répondre à deux questions complémentaires :

– Les réactivations sont-elles altérées lorsque l'animal explore passivement l'environnement ?

– On sait que les champs d'activité des cellules de lieu ont tendance à être plus nombreux aux endroits où sont situées des récompenses ou qui peuvent être considérés comme des buts à atteindre (Hollup et coll., 2001), mais on ignore si cette hétérogénéité est liée à des différences de comportement spatial lors de l'exploration, quand s'établissent les champs d'activité. Si nous observons une accumulation des champs d'activité à proximité de l'emplacement des récompenses avec notre protocole de déplacement passif, nous pourrons exclure l'influence d'un comportement exploratoire spécifique.

2.2 Mémoire épisodique et codage de séquences spatio-temporelles

2.2.1 *Perturbation de la précession de phase dans le système hippocampique*

▶ Cette étude constitue le projet de master 2 et de début de thèse d'Anne Larrieu, qui travaillera en collaboration avec Gabrielle Girardeau.

La mémoire *épisodique* est souvent définie comme la mémoire des événements placés dans leur contexte spatio-temporel. Elle met en jeu l'hippocampe, du moins dans les phases initiales de formation des traces mnésiques. Les oscillations thêta (7∼12 Hz) et gamma (30∼80 Hz) hippocampiques pourraient jouer un rôle important dans ce processus : en effet, la structuration temporelle des décharges des neurones hippocampiques par ces rythmes pourrait permettre à la fois de former des assemblées de neurones correspondant à différents items mnésiques (Lisman et Idiart, 1995 ; Harris et coll., 2003) dans leur contexte spatial (O'Keefe et Conway, 1978), et de les organiser en séquences temporelles (Lisman et Buzsáki, 2008 ; Pastalkova et coll., 2008). Le mécanisme neurophysiologique qui sous-tend cette structuration temporelle est la précession de phase, déjà présentée au § 3.1, page 11. Bien que mon travail de post-doctorat (Zugaro et coll., 2005) ait permis de tester les différents modèles théoriques et computationnels de la précession de phase et de restreindre le nombre de modèles acceptables, plusieurs questions fondamentales restent encore ouvertes. En particulier, certains modèles peuvent être reformulés pour ajuster leurs prédictions et échapper à l'invalidation expérimentale, alors que d'autres modèles ne peuvent pas être départagés car leurs prédictions sont identiques. De plus, la perturbation de la dynamique hippocampique induite par le protocole expérimental que j'ai développé était volontairement restreinte à l'hippocampe et n'affectait pas le cortex entorhinal. Le but de ce projet est donc de poursuivre la confrontation des modèles de la précession de phase, en étudiant les modifications de la dynamique hippocampique à la suite de perturbations affectant l'ensemble du système hippocampo-entorhinal.

Trois grandes classes de modèles de la précession de phase hippocampique ont été proposés :

– *Modèle à deux oscillateurs.* La précession de phase résulte de l'interférence entre deux oscillateurs de fréquences différentes (Figure 6A) : le rythme thêta, et le potentiel de membrane de la cellule de lieu qui oscille à une fréquence légèrement supérieure à thêta. La cellule de lieu décharge au pic de son oscillation propre, et comme celle-ci est plus rapide que thêta, cela se traduit par un décalage progressif de la phase de décharge par rapport à thêta (Bose et coll., 2000 ; Bose et Recce, 2001 ; Booth et Bose, 2001 ; Lengyel et coll., 2003 ; Sato et Yamaguchi, 2003 ; Yamaguchi, 2003).
– *Modèles du niveau d'excitation.* La précession de phase est due à l'interférence entre un niveau d'excitation croissant au niveau des dendrites distales, et une inhibition rythmique modulée par thêta au niveau du soma et des dendrites proximales (Figure 6B). Le neurone décharge dès que l'excitation dépasse l'inhibition, ce qui se produit de plus

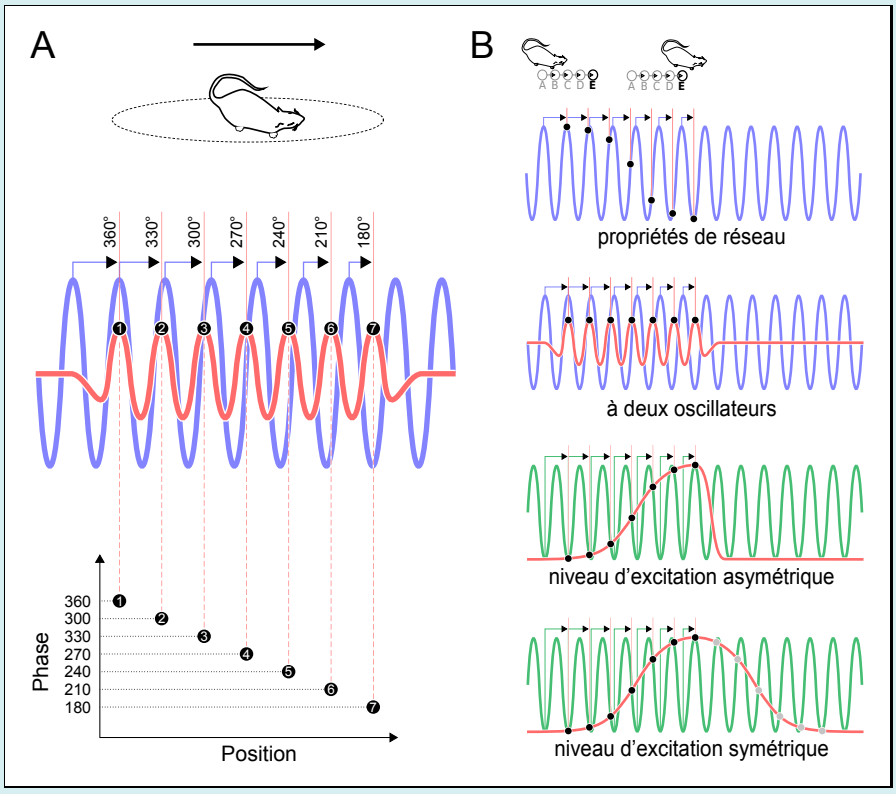

Fig. 6 – Modèles théoriques et computationnels de la précession de phase hippocampique. *A*. Modèle à deux oscillateurs. Lorsque le rat traverse le champ d'activité d'une cellule de lieu (*ellipse en pointillés*), le potentiel de membrane de cette cellule (*courbe rouge*) se met à osciller à une fréquence légèrement supérieure à celle du rythme thêta (*courbe bleue*). La cellule de lieu décharge chaque fois que son potentiel de membrane est maximal (*points noirs*), ce qui se produit de plus en plus tôt (*lignes verticales rouges* successives) par rapport au début de chaque cycle thêta (*flèches bleues*) : la phase diminue, passant de 360° au début du champ d'activité (*point noir 1*) à 180° en fin de champ d'activité (*point noir 7*). *En bas*, la phase est représentée en fonction de la position. *B*. Classification des modèles de la précession de phase (cf. explication détaillée, page 40). Pour les modèles du niveau d'excitation, la *courbe rouge* représente l'excitation, et la *courbe verte* représente l'inhibition rythmique.

en plus tôt dans le cycle au fur à mesure que l'excitation augmente (Kamondi et coll., 1998 ; Magee, 2001 ; Harris et coll., 2002 ; Mehta et coll., 2002 ; Magee, 2003). Si ce modèle rend bien compte de la précession de phase, en revanche il prédit qu'à mesure que l'excitation décroît (lorsque le rat quitte le champ d'activité de la cellule de lieu), on devrait observer une *récession* de phase, ce qui est contredit par les données expérimentales. Deux solutions ont été proposées : soit l'onde de dépolarisation est *asymétrique* (Figure 6B, *3e ligne*), et la diminution rapide de l'excitation interrompt l'interférence avec l'inhibition (Mehta et coll., 2002), soit l'onde est *symétrique* (Figure 6B, *en bas*), mais un phénomène d'adaptation empêche le neurone de décharger lors de la repolarisation (Harris et coll., 2002).

– *Modèles des propriétés de réseau.* La précession de phase résulte des délais de transmission de l'activité entre cellules de lieu. Le rat traverse successivement les champs d'activité d'un certain nombre de cellules de lieu le long de son parcours, par exemple $A \rightarrow B \rightarrow C \rightarrow D \rightarrow E$ (Figure 6B, *en haut*). Initialement, quand le rat est au centre du champ d'activité de la cellule A, celle-ci décharge maximalement et l'excitation se

propage successivement aux neurones B, C, D, et enfin E : le neurone E ne décharge donc qu'après un délai relativement long, en fin de cycle thêta. Mais par la suite, lorsque le rat parvient par exemple au centre du champ d'activité de la cellule C, celle-ci va faire décharger la cellule D qui va faire décharger la cellule E avec un délai inférieur au délai initial, donc à une phase plus précoce du cycle thêta. Ainsi, à mesure que le rat avance, la phase des potentiels d'action diminue (Jensen et Lisman, 1996 ; Tsodyks et coll., 1996 ; Wallenstein et Hasselmo, 1997).

Pour comparer ces différents modèles théoriques, une méthode efficace consiste à étudier leur comportement lorsqu'ils sont soumis à des perturbations (Zugaro et coll., 2005). Nous allons donc confronter les prédictions de ces modèles aux réponses des cellules de lieu hippocampiques et aux cellules de grille entorhinales lorsqu'un rat parcourt leurs champs d'activité *en marche arrière*. Pour ce faire, des rats seront transportés passivement dans un train électrique, d'abord en marche avant (condition de contrôle), puis en marche arrière (condition de test).

Dans ces conditions expérimentales, certains modèles prédisent que la relation entre la position du rat et la phase des potentiels d'action des cellules de lieu et de grille sera inversée, tandis que d'autres modèles ne prédisent aucun changement :

- *Modèle à deux oscillateurs.* Le phénomène d'interférence entre les deux oscillateurs se met en place dès que le rat entre dans le champ d'activité, le décalage de phase augmentant à mesure que le rat recule : la relation entre la position et la phase est donc inversée (Figure 7A).
- *Modèles du niveau d'excitation.* Dans le cas *asymétrique* (Figure 7B, *3e ligne*, à lire de droite à gauche), l'excitation augmente brusquement puis diminue progressivement. La cellule de lieu ne décharge pas (ou très brièvement) durant la première phase, puis à mesure que l'excitation diminue, elle décharge chaque fois que l'excitation dépasse l'inhibition, ce qui se fait de plus en plus tard dans le cycle thêta. La phase de décharge augmente donc à mesure que le rat recule : la relation entre la position du rat et la phase des potentiels d'action est inchangée. En revanche, dans le cas du modèle *symétrique* (Figure 7B, *en bas*), l'excitation augmente progressivement, si bien que la cellule de lieu décharge pendant la phase ascendante, chaque fois que l'excitation dépasse l'inhibition, ce qui se fait de plus en plus tôt dans le cycle thêta. La phase de décharge diminue donc à mesure que le rat recule : la relation entre la position du rat et la phase des potentiels d'action est inversée (comme en marche avant, un mécanisme d'adaptation empêche la cellule de décharger pendant la phase de repolarisation).
- *Modèles des propriétés de réseau.* La précession de phase dépend des délais de transmission de l'activité entre cellules de lieu, qui sont indépendants du sens de déplacement. La relation entre la position du rat et la phase des potentiels d'action est donc inchangée.

2.2.2 *Relations entre les précessions de phase hippocampique et entorhinale*

▶ Ce projet sera mené dans le cadre de la thèse d'Anne Larrieu, qui travaillera en collaboration avec Gabrielle Girardeau.

Des travaux récents ont mis en évidence une précession de phase des décharges des cellules de grille de la couche II du cortex entorhinal (Hafting et coll., 2008). Quelles relations y a-t-il entre la précession de phase hippocampique et la précession de phase entorhinale ? Sachant que la précession de phase entorhinale persiste après inactivation de l'hippocampe par infusion de muscimol (agoniste

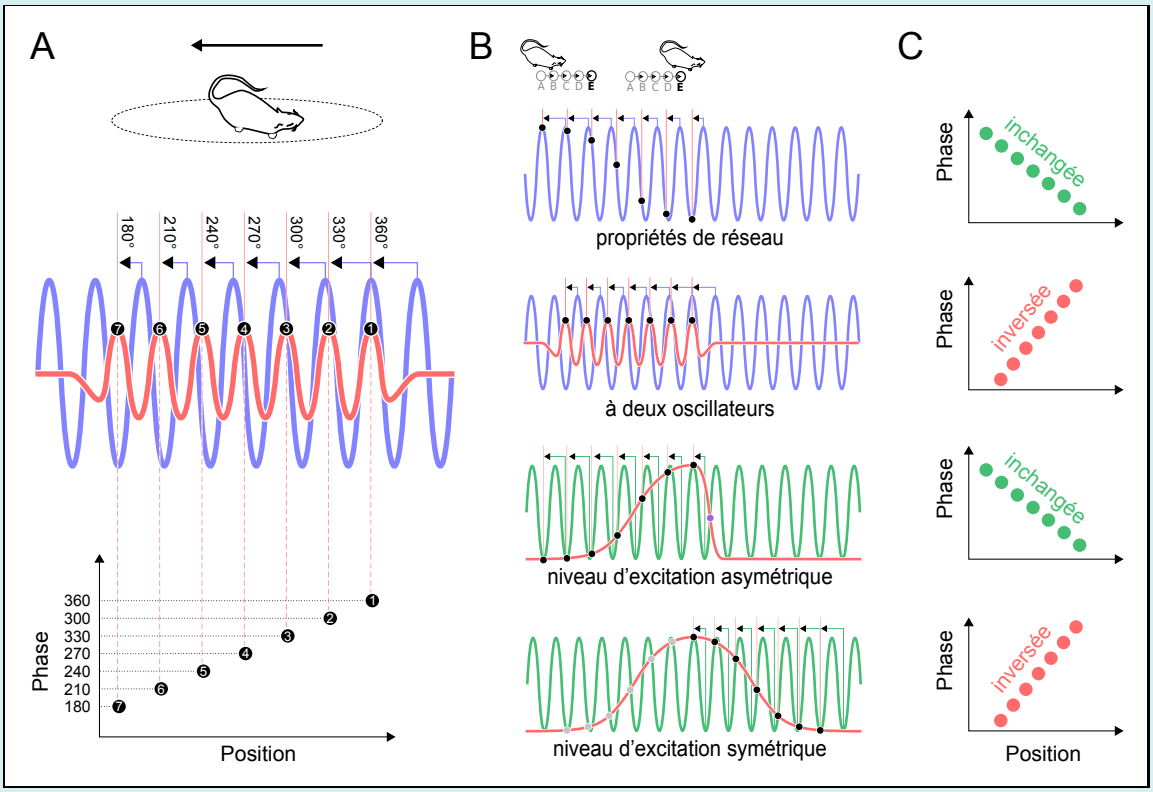

Fig. 7 – Prédictions des modèles de la précession de phase hippocampique. *A*. Cas du modèle à deux oscillateurs. Le rat traverse le champ d'activité d'une cellule de lieu (*ellipse en pointillés*) en marche arrière (*flèche noire*). Comme dans le cas de la marche avant (Figure 6), le potentiel de membrane de cette cellule (*courbe rouge*) se met à osciller à une fréquence légèrement supérieure à celle du rythme thêta (*courbe bleue*). Attention : sur cette figure, le temps s'écoule maintenant *de droite à gauche*, et la première bouffée de potentiels d'action (*point noir 1*) est émise lorsque le rat se trouve en fin de champ d'activité. Les potentiels d'action (*points noirs 1 à 7*) sont émis de plus en plus tôt (*lignes verticales rouges* successives) par rapport au début de chaque cycle thêta (*flèches bleues*) : la phase passe de 360° en fin de champ d'activité (*point noir 1*) à 180° au début du champ d'activité (*point noir 7*). La relation entre la position et la phase est donc inversée (*en bas*). *B,C*. Prédictions des différents modèles de la précession de phase (cf. explication détaillée, page 42). Remarque : en *B*, le temps s'écoule de droite à gauche. *C*. Le modèle à deux oscillateurs et le modèle du niveau d'excitation symétrique prédisent une inversion de la relation entre la position et la phase des potentiels d'action par rapport à thêta.

du $GABA_A$), elle est vraisemblablement générée par des mécanismes indépendants de l'hippocampe (Hafting et coll., 2008). A contrario, la précession de phase hippocampique semble bénéficier de mises à jour extrahippocampiques périodiques, probablement d'origine entorhinale (Zugaro et coll., 2005). On peut donc se demander si la précession de phase émerge localement dans le cortex entorhinal, pour être ensuite simplement transmise passivement à l'hippocampe (via la connexion directe de la couche II à CA3).

Un tel modèle est cependant difficilement conciliable avec l'observation que les cellules étoilées du cortex entorhinal et les cellules pyramidales de l'hippocampe déchargent avec un décalage de phase moyen d'environ 90° (Stewart et coll., 1992), trop important pour résulter d'une simple transmission monosynaptique. L'intéraction entre ces deux structures est donc probablement plus complexe qu'un simple transfert passif, et pourrait impliquer plusieurs générateurs couplés. De même, les relations entre CA3 et CA1 ne sont peut-être pas univoques non plus. En effet, bien

que l'avance de phase moyenne ($\sim 30°$) de CA3 sur CA1 (Harris et coll., 2002) soit compatible avec une transmission passive de la précession de phase entre ces deux champs hippocampiques, au sein de chaque cycle gamma, les cellules pyramidales de CA1 déchargent en moyenne 2,5 ms (20°) avant celles de CA3 (Csicsvari et coll., 2003), c'est-à-dire dans l'ordre inverse de celui attendu. Les mécanismes qui sous-tendent la précession de phase dans chaque aire du système hippocampique sont donc encore assez mal compris.

Pour étudier les interactions entre les précessions de phase hippocampique et entorhinale, nous enregistrerons de vastes ensembles de neurones simultanément dans ces deux structures, et nous déterminerons leurs dépendances fonctionnelles en perturbant tour à tour l'hippocampe (par stimulation de la commissure hippocampique ventrale) et le cortex entorhinal (par stimulation du *psalterium dorsale*).

2.2.3 *Rôle causal de la précession de phase dans la mémoire*

▶ Ce projet fera partie de la thèse d'Anne Larrieu, qui travaillera en collaboration avec Gabrielle Girardeau.

Lorsque des rats sont entraînés à effectuer une tâche d'alternance spatiale avec un délai entre les essais, leur hippocampe génère de manière endogène de longues séquences d'activation d'assemblées de neurones pendant le délai, en l'absence de changements sensoriels ou moteurs. Fait remarquable, ces séquences permettent de prédire les choix des rats à l'essai suivant, y compris leurs erreurs (Pastalkova et coll., 2008). Ceci a été interprété comme une indication que le mécanisme d'élaboration de séquences d'activation hippocampiques, qui aurait évolué pour permettre le codage de trajectoires et de représentations spatiales, pourrait également intervenir dans certaines formes de mémoire épisodique et de planification - ce qui constituerait une sythèse théorique entre les résultats obtenus chez le rat, qui assignent à l'hippocampe une fonction essentiellement spatiale (O'Keefe et Nadel, 1978), et ceux obtenus chez l'homme, qui mettent en exergue son rôle central dans la mémoire (Scoville et Milner, 1957).

Ici encore, la précession de phase hippocampique pourrait sous-tendre l'élaboration des séquences d'activité hippocampiques : en effet, non seulement les neurones participant à ces séquences manifestent une précession de phase, mais de surcroît, dans une tâche de contrôle ne mettant en jeu aucune forme de mémoire, les neurones ne manifestent pas de précession de phase, et ne s'organisent pas en séquences caractéristiques (Pastalkova et coll., 2008).

Pour démontrer un lien de causalité entre les séquences d'activité, la précession de phase et le comportement des rats, nous interromprons transitoirement les décharges hippocampiques et nous réinitialiserons le rythme thêta par brève stimulation commissurale (Zugaro et coll., 2005) pendant le délai entre deux essais. Nous prédisons qu'à la suite de cette perturbation, les séquences d'activité générées de manière endogène par l'hippocampe seront interrompues. Si ces séquences jouent effectivement un rôle critique dans le maintien en mémoire d'informations permettant aux rats de réussir la tâche d'alternance spatiale, ceci devrait avoir pour conséquence de diminuer drastiquement leurs performances.

2.3 Cellules de lieu, de grille et de direction de la tête

Les cellules DT ont fait l'objet de nombreuses études depuis une vingtaine d'années (Wiener et Taube, 2005), études qui ont permis de décrire l'anatomie générale de ce système (en termes de structures impliquées), de caractériser les influences des différents signaux sensoriels et moteurs

dans l'élaboration et la mise à jour des réponses directionnelles, et de mieux comprendre les relations entre ces réponses directionnelles et le comportement spatial de l'animal. Cependant, on dispose encore de très peu de données concernant l'anatomie fine et la physiologie des cellules DT (connectivité du réseau, types de neurones impliqués, propriétés membranaires, constitution des éventuelles assemblées de neurones, organisation temporelle des réponses par rapport aux différents rythmes cérébraux, etc.) Un frein à l'exploration de certaines de ces questions scientifiques a longtemps été l'impossibilité d'enregistrer les réponses de plus de deux ou trois neurones simultanément. Grâce aux nouvelles technologies d'acquisition massivement parallèle que j'ai mises en place, je souhaite caractériser les propriétés de réseau des cellules DT, notamment en testant directement certaines hypothèses formulées dans le cadre d'études théoriques et computationnelles (McNaughton et coll., 1991 ; Skaggs et coll., 1995 ; Blair et Sharp, 1996 ; Zhang, 1996 ; Redish et coll., 1996 ; Brunel et Nadal, 1998 ; Goodridge et Touretzky, 2000 ; Baird et coll., 2001 ; Degris et coll., 2004 ; Boucheny et coll., 2005 ; Burgess et coll., 2007).

2.3.1 *Orientation des grilles par les cellules DT*

Lors d'une déformation globale de l'environnement, le pas des cellules de grille peut subir des transformations anisotropes : par exemple, lorsqu'on raccourcit dans une direction donnée l'enceinte carrée dans laquelle les rats sont placés, les grilles sont compressées dans la même direction (Barry et coll., 2007). Cette propriété peut difficilement être expliquée par les modèles pour lesquels les réponses des cellules de grilles résultent de la topologie des connexions au sein du cortex entorhinal (Fuhs et Touretzky, 2006 ; McNaughton et coll., 2006) : en effet, la compression des grilles correspondrait alors à une réorganisation instantanée et cohérente des poids synaptiques de l'ensemble du réseau. Un autre modèle propose au contraire que les réponses des cellules de grille résultent de l'interférence de plusieurs oscillations de leur potentiel de membrane, chacune dans une dendrite différente, et dont les amplitudes respectives dépendent de la direction de la tête du rat (Burgess et coll., 2007). Dans ce modèle, la compression des grilles pourrait s'expliquer par des rotations anisotropes des directions préférées des cellules DT.

En collaboration avec Daniel Bennequin (mathématicien, Professeur de l'Université Paris VII), nous testerons cette hypothèse en enregistrant des cellules de grille et des cellules de direction de la tête chez des rats qui explorent une enceinte carrée. Après une période de contrôle, une paroi de l'enceinte sera déplacée de manière à obtenir une enceinte rectangulaire. Nous déterminerons alors si les directions préférées des cellules de direction de la tête subissent les transformations prédites par la théorie.

2.3.2 *Intégration des signaux DT à la dynamique hippocampique*

L'hippocampe et les structures contenant des cellules DT sont anatomiquement et fonctionnellement couplés (Knierim et coll., 1995 ; Cacucci et coll., 2004 ; Sargolini et coll., 2006), mais on ignore comment s'opèrent les transferts d'information entre ces systèmes. Plusieurs auteurs ont proposé l'hypothèse que le signal DT permet d'orienter la « carte » hippocampique par rapport à l'environnement (McNaughton et coll., 1996 ; Touretzky et Redish, 1996 ; Sharp, 1999), mais on dispose de très peu de données expérimentales sur la question (Calton et coll., 2003). Si les cellules DT fournissent effectivement une information directionnelle à l'hippocampe, on peut s'attendre que les réponses des cellules DT soient organisées temporellement par rapport au rythme thêta hippocampique. En effet, le rythme thêta semble constituer une « horloge » de référence pour l'hippocampe et pour les structures qui communiquent avec lui (Colom et coll., 1988 ; Pedemonte et coll., 1996 ; Csicsvari et coll., 1999a ; Gambini et coll., 2002 ; Buzsáki et coll., 2002). Qui

plus est, en combinant des analyses de données expérimentales et des modèles computationnels de l'hippocampe, plusieurs auteurs ont proposé l'hypothèse que parmi les différents signaux que reçoit une cellule de lieu, ce sont les entrées extrahippocampiques qui dominent au début du cycle thêta, tandis qu'en fin de cycle ce sont les signaux intrahippocampiques récurrents qui dominent (Tsodyks et coll., 1996 ; Wallenstein et Hasselmo, 1997 ; Yamaguchi et coll., 2002).

Je me propose de tester ces hypothèses théoriques. Plusieurs dizaines de cellules DT seront donc enregistrées en même temps que les potentiels de champ locaux hippocampiques chez des rats qui exploreront librement une enceinte expérimentale pour obtenir de petites récompenses alimentaires. L'analyse des corrélations croisées entre décharges des cellules DT et rythme thêta permettra de déterminer si les cellules DT déchargent préférentiellement à certaines phases du cycle comme le suggèrent les modèles computationnels – ce qui renforcerait la proposition que thêta se comporte comme une « horloge » dont les cycles déterminent les fenêtres temporelles pendant lesquelles le réseau hippocampique est susceptible d'intégrer des signaux extrinsèques.

2.3.3 *Dynamiques des mises à jour par les repères environnementaux*

Comment l'activité se réorganise-t-elle au sein d'un réseau de cellules DT lors d'une mise à jour des directions préférées par les repères environnementaux ? La dynamique de cette réorganisation est susceptible de nous renseigner sur la structure du réseau. En effet, de nombreux théoriciens ont proposé l'hypothèse que les cellules DT forment un réseau d'attracteurs continus[4] (Skaggs et coll., 1995 ; Zhang, 1996 ; Redish et coll., 1996 ; Goodridge et Touretzky, 2000). Il est intéressant de noter que cette hypothèse a également été formulée pour l'hippocampe (Tsodyks et Sejnowski, 1995 ; McNaughton et coll., 1996 ; Samsonovich et McNaughton, 1997 ; Redish et Touretzky, 1998) et qu'elle a récemment été confirmée expérimentalement (Wills et coll., 2005 ; Leutgeb et coll., 2005). Si cette hypothèse se confirme également pour les cellules DT, une telle architecture impose des contraintes sur les dynamiques de mise à jour de leur activité, qui ne peuvent prendre que deux formes qualitativement distinctes, selon la distance angulaire entre les pics d'activité avant et après la mise à jour (Figure 8).

Pour tester cette prédiction théorique, je reprendrai le protocole qui m'a permis de mesurer les délais de mise à jour des directions préférées (« Travaux Scientifiques », page 7) en faisant varier l'angle de rotation de la carte, et j'échantillonnerai les réponses d'un grand nombre de cellules DT en même temps.

Si les cellules DT forment effectivement un réseau d'attracteurs continus, elles doivent manifester les dynamiques illustrées sur la Figure 8, avec un changement qualitatif à ∼90°. Dans le cas contraire, les modèles computationnels actuels seront invalidés, ce qui nécessitera d'envisager d'autres architectures neurales possibles pour rendre compte des propriétés des cellules DT.

2.3.4 *Déplacement du pic d'activité par le flux optique*

Il s'agit de tester l'hypothèse théorique que le système des cellules DT contient un intégrateur neural, c'est-à-dire que la direction représentée par les cellules DT est déterminée par intégration

[4]Un attracteur est un état d'activation `A` du réseau qui vérifie les deux propriétés suivantes : 1) lorsque le réseau se trouve dans l'état `A`, il s'y maintient indéfiniment en l'absence de perturbations, et 2) lorsque le réseau se trouve dans un état voisin de `A`, il est attiré vers `A`. Dans un réseau d'attracteurs continus, de faibles perturbations de l'activité du réseau suffisent à faire passer le réseau d'un attracteur à un attracteur voisin.

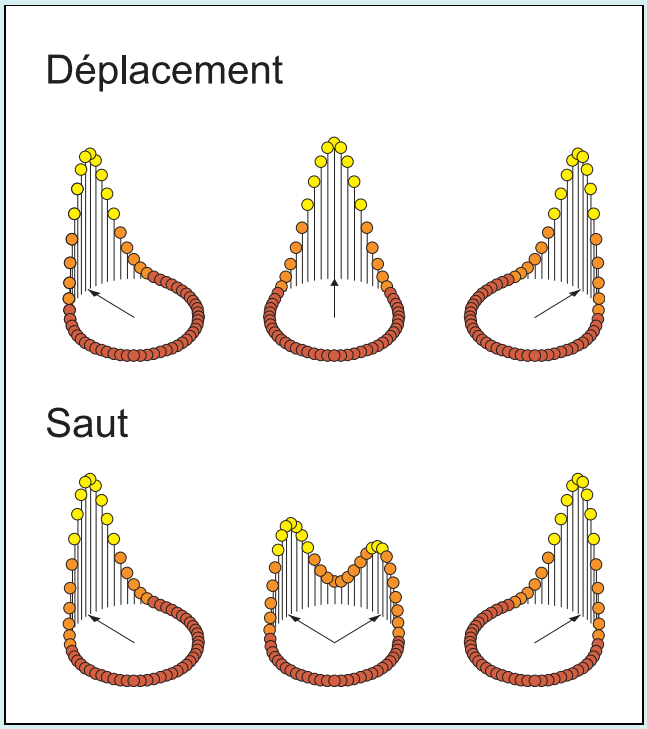

Fig. 8 – Dynamique des mises à jour dans un réseau des cellules DT, prévues par les modèles à base de réseaux d'attracteurs continus. A chaque instant, seules sont actives les cellules DT dont la direction préférée est voisine de la direction de la tête du rat : cette activité forme un « pic » qui se déplace au fil des mouvements de l'animal. Lors d'une mise à jour des directions préférées, par exemple suite à une rotation des repères visuels dans l'environnement, comment le pic d'activité passe-t-il d'une sous-populations de cellules DT à une autre ? Les modèles prédisent que la dynamique de cette transition dépend de l'angle de rotation des repères : pour des angles inférieurs à $\sim$90°, le pic d'activité se déplacerait progressivement vers la nouvelle sous-population de cellules DT (*en haut*), mais pour des angles supérieurs, il « sauterait » d'une sous-population à l'autre (*en bas*).

mathématique d'un signal de vitesse angulaire (Skaggs et coll., 1995 ; Blair et Sharp, 1996 ; Zhang, 1996 ; Redish et coll., 1996 ; Arleo et Gerstner, 2000 ; Goodridge et Touretzky, 2000). En particulier, le flux optique, qui est généré par les mouvements propres de l'animal, déplace-t-il effectivement de façon cohérente l'activité au sein du réseau de cellules DT lorsque le rat tourne la tête, pour que la direction représentée soit mise à jour en conséquence ? Bien que cette proposition théorique soit compatible avec plusieurs résultats expérimentaux (Taube et Burton, 1995 ; Blair et Sharp, 1995 ; Blair et coll., 1997 ; Stackman et Taube, 1997 ; Blair et coll., 1998 ; Zugaro et coll., 2002), elle n'a jamais été étudiée directement, excepté par Blair et Sharp (1996). Mais leurs résultats doivent être considérés avec circonspection, parce que les stimulimulations visuelles employées n'étaient pas appropriées (trop peu de contrastes, durées trop courtes), et parce que les déplacements de directions préférées que ces stimulations auraient pu induire auraient en tout état de cause été annulées par la présence de repères visuels (certes rendus volontairement ambigus, mais néanmoins présents).

Nous avons donc entrepris de réexaminer le rôle du flux optique en utilisant comme stimulus une constellation de points lumineux en rotation pendant des durées prolongées (Hess et coll., 1985). Des rats ont été placés sur une petite plate-forme au centre d'un vaste rideau cylindrique noir. Un planétarium simplifié (une petite sphère opaque percée de nombreux orifices) fournissait

la stimulation nécessaire. Ce travail est encore en cours, mais les résultats montrent clairement que les directions préférées des cellules DT dévient pendant la rotation du planétarium, ce qui est compatible avec l'hypothèse que l'activité a bien été déplacée dans le réseau par le flux optique. Une analyse plus fine des réponses des cellules DT, que nous menons actuellement en collaboration avec Angelo Arleo (CR1, CNRS – UMR 7102, Neurobiologie des Processus Adaptatifs), révélera si l'activité neurale se « déplace » effectivement au sein des cellules DT pendant les stimulations.

3 Développements technologiques

Afin de pouvoir étudier les mécanismes neurophysiologiques de coopération ou de compétition entre de larges ensembles de neurones distribués sur plusieurs structures anatomiques, il sera nécessaire de mettre en œuvre des technologies d'enregistrement et d'analyse de pointe. Je compte notamment :

- développer des microdescendeurs d'électrodes de dimensions encore plus réduites que ceux que j'utilise actuellement (Figure 9A) : cela permettra non seulement d'augmenter le nombre de sites d'enregistrements chez le rat adulte, mais également de mieux adapter les microdescendeurs actuels à l'enregistrement chez le petit rongeur (jeunes rats, souris), ce qui ouvrira des perspectives scientifiques nouvelles, comme l'étude du développement des mécanismes neurophysiologiques sous-tendant les fonctions cognitives, et l'intégration des approches génétique, moléculaire et physiologique, grâce à des enregistrements effectués chez des souris *knock-out*, en collaboration avec Karim Benchenane (postdoctorant dans l'équipe de Sidney Wiener, docteur de l'Université de Caen) ;
- mettre en œuvre pour la première fois en France les nouvelles électrodes en silicium (Figure 9B), grâce auxquelles on peut enregistrer des dizaines de neurones simultanément, ainsi que les potentiels de champs locaux en une centaine de points anatomiquement bien définis, ce qui permet d'analyser les densités de sources de courant de plusieurs structures cérébrales simultanément ;
- implémenter de nouveaux algorithmes de classification semi-automatique des potentiels d'action émis par différents neurones enregistrés sur un même groupe d'électrodes (par exemple, réduction dimensionnelle par ondelettes ou par analyse en composantes indépendantes, classification super-paramagnétique, etc.), ce qui permettra d'identifier davantage de neurones, mais aussi de pouvoir isoler des neurones plus petits, comme ceux du gyrus denté ;
- poursuivre le développement d'outils de classification manuelle et de visualisation des données (Figure 10), et les intégrer au sein d'une suite logicielle mise librement à la disposition de la communauté scientifique ;
- concevoir de nouveaux outils d'analyse pour étudier l'activité simultanée d'une centaine de neurones individuels, pour déterminer comment cette activité est organisée en séquences temporelles par les oscillations des potentiels de champ locaux, et pour comprendre comment cette organisation est modifiée par les différents états cérébraux (vigilance, inactivité, sommeil à ondes lentes, sommeil paradoxal, anesthésie, etc.)

Il s'agit de développements technologiques que j'ai déjà commencé à mettre en place dans le cadre du projet européen `NeuroProbes` (§ 1.3, page 30).

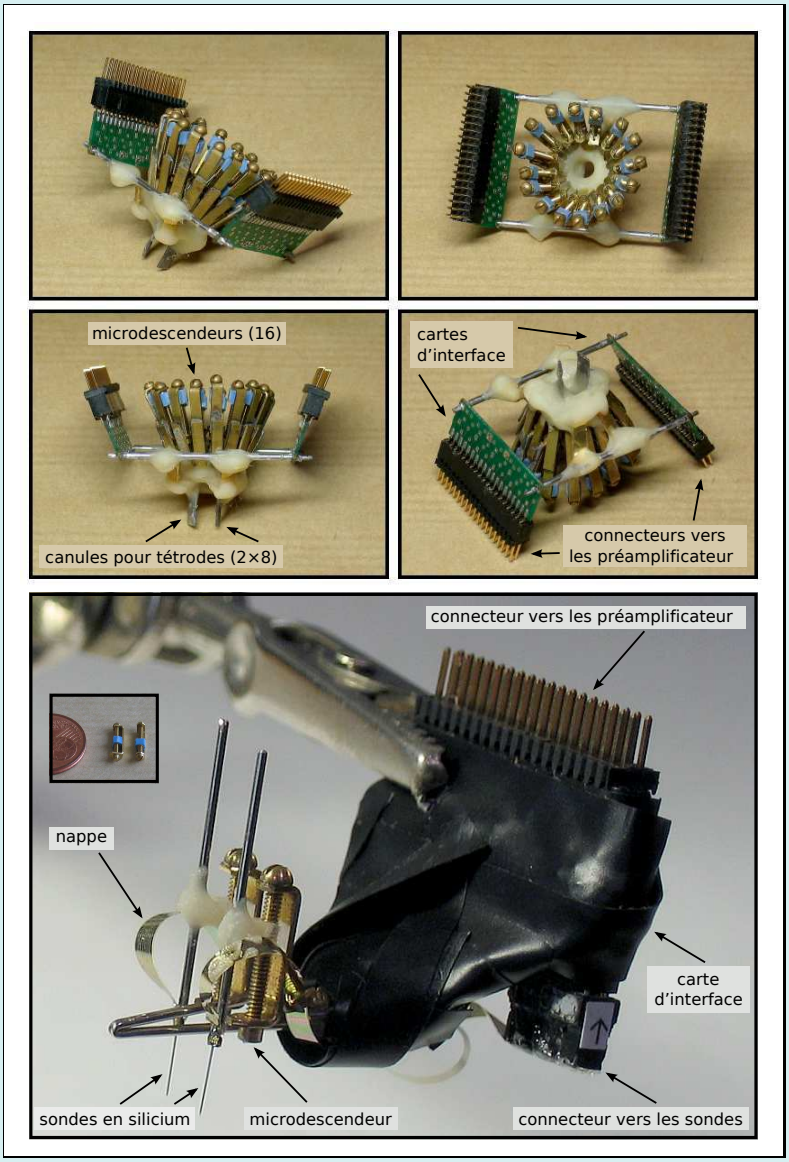

Fig. 9 – Descendeurs pour tétrodes et sondes en silicium. *En haut*. Descendeur pour 16 tetrodes (64 voies) que Gabrielle Girardeau et moi avons réalisé sur mesure pour enregistrer bilatéralement dans l'hippocampe chez des rats libres de leurs mouvements. Chacune des 16 tétrodes peut être déplacée individuellement par pas de 15∼20 µm. Ce système sera adapté pour les enregistrements chez le jeune rat ou la souris. *En bas*. Descendeur pour deux sondes en silicium (que j'ai conçu et réalisé). Chaque sonde comporte 16 sites d'enregistrement (projet européen `NeuroProbes`, page 30), et peut être déplacée individuellement. Selon l'écartement des sites, ces sondes permettent d'enregistrer simultanément dans le néocortex et l'hippocampe (espacement de 200 µm), ou dans une seule de ces structures mais avec une résolution plus fine (espacement de 100 µm).
Encart. Microdescendeurs individuels utilisés dans les deux types de descendeurs.

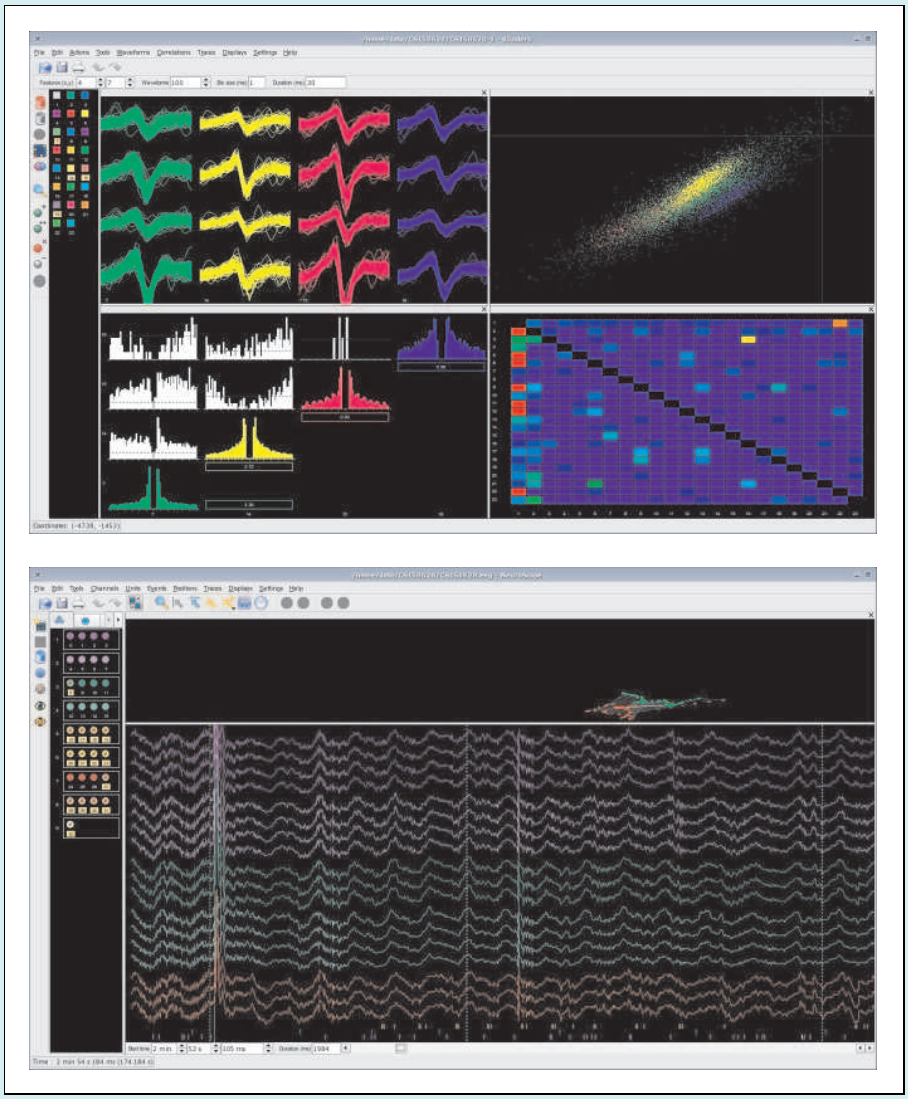

Fig. 10 – Outils informatiques pour le dépouillement et l'analyse de données électrophysiologiques et comportementales. *En haut*. Le logiciel de classification manuelle de potentiels d'action `Klusters`. Les potentiels d'action (*en haut à gauche*) sont représentés dans l'espace réduit des composantes principales (*en haut à droite*). Les autocorrélogrammes et corrélogrammes croisés (*en bas à gauche*) aident à corriger les erreurs de classification automatique. Une « matrice d'erreur » (*en bas à droite*) permet de repérer les neurones dont les potentiels d'action ont indûment été attribués à plusieurs unités. *En bas*. Le logiciel de visualisation de données expérimentales `NeuroScope`. L'écran principal montre les potentiels de champ locaux (*traces colorées*, 18 voies affichées), les potentiels d'action (*petites barres verticales colorées*, 3 neurones affichés) et les événements comportementaux (*grandes lignes pointillées colorées*) en fonction du temps. Les positions de l'animal sont également indiquées (les *points rouges et verts* successifs correspondent respectivement à la diode placée au-dessus de la tête du rat et à la diode placée 10 cm en arrière, au fil du temps).

Bibliographie

G. K. Aguirre, E. Zarahn, et M. D'Esposito. Neural components of topographical representation. *Proc Natl Acad Sci U S A*, 95(3):839–46, 1998.

S. V. Albertin, A. B. Mulder, E. Tabuchi, M. B. Zugaro, et S. I. Wiener. Lesions of the medial shell of the nucleus accumbens impair rats in finding larger rewards, but spare reward-seeking behavior. *Behav Brain Res*, 117(1-2):173–83, 2000.

A. Arleo et W. Gerstner. Spatial cognition and neuro-mimetic navigation: a model of hippocampal place cell activity. *Biol Cybern*, 83(3):287–99, 9 2000.

J. C. Baird, J. S. Taube, et D. V. Peterson. Statistical and information properties of head direction cells. *Percept Psychophys*, 63(6):1026–37, 2001.

C. Barry, R. Hayman, N. Burgess, et K. J. Jeffery. Experience-dependent rescaling of entorhinal grids. *Nat Neurosci*, 10(6):682–684, 6 2007.

P. Barthó, H. Hirase, L. Monconduit, M. Zugaro, K. D. Harris, et G. Buzsáki. Characterization of neocortical principal cells and interneurons by network interactions and extracellular features. *J Neurophysiol*, 92(1):600–8, 2004.

J.P. Bassett, M.B. Zugaro, G.M. Muir, E.J. Golob, R.U. Muller, et J.S. Taube. Passive movements of the head do not abolish anticipatory firing properties of head direction cells. *J Neurophysiol.*, 93(3): 1304–16, 2005. sous presse.

F. P. Battaglia, G. R. Sutherland, et B. L. McNaughton. Local sensory cues and place cell directionality: additional evidence of prospective coding in the hippocampus. *J Neurosci*, 24(19):4541–50, 2004.

C. J. Behrens, L. P. van den Boom, L. de Hoz, A. Friedman, et U. Heinemann. Induction of sharp wave-ripple complexes in vitro and reorganization of hippocampal networks. *Nat Neurosci*, 8(11): 1560–7, 11 2005.

A. Berthoz. Parietal and hippocampal contribution to topokinetic and topographic memory. *Philos Trans R Soc Lond B Biol Sci*, 352(1360):1437–48, 1997.

H. T. Blair et P. E. Sharp. Anticipatory head direction signals in anterior thalamus: evidence for a thalamocortical circuit that integrates angular head motion to compute head direction. *J Neurosci*, 15(9):6260–70, 1995.

H. T. Blair et P. E. Sharp. Visual and vestibular influences on head-direction cells in the anterior thalamus of the rat. *Behav Neurosci*, 110(4):643–60, 1996.

H. T. Blair, B. W. Lipscomb, et P. E. Sharp. Anticipatory time intervals of head-direction cells in the anterior thalamus of the rat: implications for path integration in the head-direction circuit. *J Neurophysiol*, 78(1):145–59, 1997.

H. T. Blair, J. Cho, et P. E. Sharp. Role of the lateral mammillary nucleus in the rat head direction circuit: a combined single unit recording and lesion study. *Neuron*, 21(6):1387–97, 1998.

H. T. Blair, J. Cho, et P. E. Sharp. The anterior thalamic head-direction signal is abolished by bilateral but not unilateral lesions of the lateral mammillary nucleus. *J Neurosci*, 19(15):6673–83, 1999.

H.T. Blair. *A thalamocortical circuit for computing directional heading in the rat*, pages 152–158. MIT Press, Cambridge, MA, 1996.

T V Bliss et G L Collingridge. A synaptic model of memory: long-term potentiation in the hippocampus. *Nature*, 361(6407):31–9, 1 1993.

T. V. Bliss et T. Lomo. Long-lasting potentiation of synaptic transmission in the dentate area of the anaesthetized rabbit following stimulation of the perforant path. *J Physiol*, 232(2):331–56, 1973.

V. Booth et A. Bose. Neural mechanisms for generating rate and temporal codes in model ca3 pyramidal cells. *J Neurophysiol*, 85(6):2432–45, 2001.

A. Bose et M. Recce. Phase precession and phase-locking of hippocampal pyramidal cells. *Hippocampus*, 11(3):204–15, 2001.

A. Bose, V. Booth, et M. Recce. A temporal mechanism for generating the phase precession of hippocampal place cells. *J Comput Neurosci*, 9(1): 5–30, 2000.

C. Boucheny, N. Brunel, et A. Arleo. A continuous attractor network model without recurrent excitation: maintenance and integration in the head direction cell system. *Journal of Computational Neuroscience*, 18(2):205–227, 2005.

N. Brunel et J. P. Nadal. Mutual information, fisher information, and population coding. *Neural Comput*, 10(7):1731–57, 10 1998.

Neil Burgess, Caswell Barry, et John O'Keefe. An oscillatory interference model of grid cell firing. *Hippocampus*, 17(9):801–12, 2007.

G. Buzsáki et G. Czéh. Commissural and perforant path interactions in the rat hippocampus. field potentials and unitary activity. *Exp Brain Res*, 43 (3-4):429–38, 1981.

G. Buzsáki, E. Grastyàn, J. Czopf, L. Kellènyi, et O. Prohaska. Changes in neuronal transmission in the rat hippocampus during behavior. *Brain Res*, 225(2):235–47, 1981.

G. Buzsáki, Z. Horváth, R. Urioste, J. Hetke, et K. Wise. High-frequency network oscillation in the hippocampus. *Science*, 256(5059):1025–7, 1992.

G. Buzsáki, J. Csicsvari, G. Dragoi, K. Harris, D. Henze, et H. Hirase. Homeostatic maintenance of neuronal excitability by burst discharges in vivo. *Cereb Cortex*, 12(9):893–9, 2002.

F. Cacucci, C. Lever, T. J. Wills, N. Burgess, et J. O'Keefe. Theta-modulated place-by-direction cells in the hippocampal formation in the rat. *J Neurosci*, 24(38):8265–77, 2004.

J. L. Calton, R. W. Stackman, J. P. Goodridge, W. B. Archey, P. A. Dudchenko, et J. S. Taube. Hippocampal place cell instability after lesions of the head direction cell network. *J Neurosci*, 23(30): 9719–31, 2003.

J. J. Chrobak et G. Buzsáki. High-frequency oscillations in the output networks of the hippocampal-entorhinal axis of the freely behaving rat. *J Neurosci*, 16(9):3056–66, 1996.

L. V. Colom, B. R. Christie, et B. H. Bland. Cingulate cell discharge patterns related to hippocampal eeg and their modulation by muscarinic and nicotinic agents. *Brain Res*, 460(2):329–38, 1988.

A. Cressant, R. U. Muller, et B. Poucet. Failure of centrally placed objects to control the firing fields of hippocampal place cells. *J Neurosci*, 17(7):2531–42, 1997.

J. Csicsvari, H. Hirase, A. Czurko, et G. Buzsáki. Reliability and state dependence of pyramidal cell-interneuron synapses in the hippocampus: an ensemble approach in the behaving rat. *Neuron*, 21 (1):179–89, 1998.

J. Csicsvari, H. Hirase, A. Czurkó, A. Mamiya, et G. Buzsáki. Oscillatory coupling of hippocampal pyramidal cells and interneurons in the behaving rat. *J Neurosci*, 19(1):274–87, 1999a.

J. Csicsvari, H. Hirase, A. Czurkó, A. Mamiya, et G. Buzsáki. Fast network oscillations in the hippocampal ca1 region of the behaving rat. *J Neurosci*, 19(16):RC20, 1999b.

J. Csicsvari, H. Hirase, A. Mamiya, et G. Buzsáki. Ensemble patterns of hippocampal ca3-ca1 neurons during sharp wave-associated population events. *Neuron*, 28(2):585–94, 2000.

J. Csicsvari, B. Jamieson, K. D. Wise, et G. Buzsáki. Mechanisms of gamma oscillations in the hippocampus of the behaving rat. *Neuron*, 37 (2):311–22, 2003.

A. Czurkó, H. Hirase, J. Csicsvari, et G. Buzsáki. Sustained activation of hippocampal pyramidal cells by 'space clamping' in a running wheel. *Eur J Neurosci*, 11(1):344–52, 1999.

T. Degris, N. Brunel, et A. Arleo. Rapid response of head direction cells to reorienting visual cues: A computational model. In *Proceedings of the Computational Neuroscience Meeting (CNS2003)*, 2003.

T. Degris, O. Sigaud, S. I. Wiener, et A. Arleo. Rapid response of head direction cells to reorienting visual cues: A computational model. *Neurocomputing*, 58(60C):675–682, 2004.

K. Diba et G. Buzsáki. Forward and reverse hippocampal place-cell sequences during ripples. *Nat Neurosci*, 9 2007.

R. M. Douglas, B. L. McNaughton, et G. V. Goddard. Commissural inhibition and facilitation of granule cell discharge in fascia dentata. *J Comp Neurol*, 219(3):285–94, 1983.

A. D. Ekstrom, J. Meltzer, B. L. McNaughton, et C. A. Barnes. Nmda receptor antagonism blocks experience-dependent expansion of hippocampal "place fields". *Neuron*, 31(4):631–8, 2001.

A. K. Engel, P. Fries, et W. Singer. Dynamic predictions: oscillations and synchrony in top-down processing. *Nat Rev Neurosci*, 2(10):704–16, 10 2001.

D. J. Foster et M. A. Wilson. Reverse replay of behavioural sequences in hippocampal place cells during the awake state. *Nature*, 440(7084):680–3, 3 2006.

M. C. Fuhs et D. S. Touretzky. A spin glass model of path integration in rat medial entorhinal cortex. *J Neurosci*, 26(16):4266–76, 4 2006.

J. P. Gambini, R. A. Velluti, et M. Pedemonte. Hippocampal theta rhythm synchronizes visual neurons in sleep and waking. *Brain Res*, 926(1-2): 137–41, 2002.

J. P. Goodridge et D. S. Touretzky. Modeling attractor deformation in the rodent head-direction system. *J Neurophysiol*, 83(6):3402–10, 2000.

T. Hafting, M. Fyhn, S. Molden, M. B. Moser, et E. I. Moser. Microstructure of a spatial map in the entorhinal cortex. *Nature*, 2005.

Torkel Hafting, Marianne Fyhn, Tora Bonnevie, May-Britt Moser, et Edvard I Moser. Hippocampus-independent phase precession in entorhinal grid cells. *Nature*, 5 2008.

K. D. Harris, D. A. Henze, H. Hirase, X. Leinekugel, G. Dragoi, A. Czurkó, et G. Buzsáki. Spike train dynamics predicts theta-related phase precession in hippocampal pyramidal cells. *Nature*, 417 (6890):738–41, 2002.

K. D. Harris, J. Csicsvari, H. Hirase, G. Dragoi, et G. Buzsáki. Organization of cell assemblies in the hippocampus. *Nature*, 424(6948):552–6, 2003.

D.O. Hebb. *The organization of behavior*. John Wiley, New York, 1949.

B. J. Hess, W. Precht, A. Reber, et L. Cazin. Horizontal optokinetic ocular nystagmus in the pigmented rat. *Neuroscience*, 15(1):97–107, 5 1985.

H. Hirase, Czurkó HH7, J. Csicsvari, et G. Buzsáki. Firing rate and theta-phase coding by hippocampal pyramidal neurons during 'space clamping'. *Eur J Neurosci*, 11(12):4373–80, 1999.

S. A. Hollup, S. Molden, J. G. Donnett, M. B. Moser, et E. I. Moser. Accumulation of hippocampal place fields at the goal location in an annular watermaze task. *J Neurosci*, 21(5):1635–44, 2001.

J. Huxter, N. Burgess, et J. O'Keefe. Independent rate and temporal coding in hippocampal pyramidal cells. *Nature*, 425(6960):828–32, 2003.

L E Jarrard. What does the hippocampus really do? *Behavioural Brain Research*, 71(1-2):1–10, 11 1995.

O. Jensen et J. E. Lisman. Theta/gamma networks with slow nmda channels learn sequences and encode episodic memory: role of nmda channels in recall. *Learn Mem*, 3(2-3):264–78, 1996.

O. Jensen et J. E. Lisman. Position reconstruction from an ensemble of hippocampal place cells: contribution of theta phase coding. *J Neurophysiol*, 83(5):2602–9, 2000.

A. Kamondi, L. Acsády, X. J. Wang, et G. Buzsáki. Theta oscillations in somata and dendrites of hippocampal pyramidal cells in vivo: activity-dependent phase-precession of action potentials. *Hippocampus*, 8(3):244–61, 1998.

A. Khabbaz, M.S. Fee, J.Z. Tsien, et D.W. Tank. A compact converging-electrode microdrive for recording head direction cells in mice. *Soc. Neurosci. Abstcts.*, 26(1):984, 2000.

J. J. Knierim, H. S. Kudrimoti, et B. L. McNaughton. Place cells, head direction cells, and the learning of landmark stability. *J Neurosci*, 15(3 Pt 1): 1648–59, 1995.

R. A. Koene, A. Gorchetchnikov, R. C. Cannon, et M. E. Hasselmo. Modeling goal-directed spatial navigation in the rat based on physiological data from the hippocampal formation. *Neural Netw*, 16 (5-6):577–84, 2003.

H. S. Kudrimoti, C. A. Barnes, et B. L. McNaughton. Reactivation of hippocampal cell assemblies: effects of behavioral state, experience, and eeg dynamics. *J Neurosci*, 19(10):4090–101, 1999.

A. K. Lee et M. A. Wilson. Memory of sequential experience in the hippocampus during slow wave sleep. *Neuron*, 36(6):1183–94, 2002.

M. Lengyel, Z. Szatmáry, et P. Erdi. Dynamically detuned oscillations account for the coupled rate and temporal code of place cell firing. *Hippocampus*, 13(6):700–14, 2003.

J. K. Leutgeb, S. Leutgeb, A. Treves, R. Meyer, C. A. Barnes, B. L. McNaughton, M. B. Moser, et E. I. Moser. Progressive transformation of hippocampal neuronal representations in "morphed" environments. *Neuron*, 48(2):345–58, 10 2005.

Shaomin Li, William K Cullen, Roger Anwyl, et Michael J Rowan. Dopamine-dependent facilitation of ltp induction in hippocampal ca1 by exposure to spatial novelty. *Nature neuroscience*, 6(5): 526–31, 5 2003.

J. E. Lisman et M. A. Idiart. Storage of 7 +/- 2 short-term memories in oscillatory subcycles. *Science*, 267(5203):1512–5, 1995.

John Lisman et György Buzsáki. A neural coding scheme formed by the combined function of gamma and theta oscillations. *Schizophrenia bulletin*, 34 (5):974–80, 9 2008.

J. C. Magee. Dendritic mechanisms of phase precession in hippocampal ca1 pyramidal neurons. *J Neurophysiol*, 86(1):528–32, 2001.

J. C. Magee. A prominent role for intrinsic neuronal properties in temporal coding. *Trends Neurosci*, 26(1):14–6, 2003.

E. A. Maguire, N. Burgess, et J. O'Keefe. Human spatial navigation: cognitive maps, sexual dimorphism, and neural substrates. *Curr Opin Neurobiol*, 9(2):171–7, 1999.

T. J. McHugh, K. I. Blum, J. Z. Tsien, S. Tonegawa, et M. A. Wilson. Impaired hippocampal representation of space in ca1-specific nmdar1 knockout mice. *Cell*, 87(7):1339–49, 1996.

B. L. McNaughton, C. A. Barnes, et J. O'Keefe. The contributions of position, direction, and velocity to single unit activity in the hippocampus of freely-moving rats. *Exp Brain Res*, 52(1):41–9, 1983.

B. L. McNaughton, C. A. Barnes, J. L. Gerrard, K. Gothard, M. W. Jung, J. J. Knierim, H. Kudrimoti, Y. Qin, W. E. Skaggs, M. Suster, et K. L. Weaver. Deciphering the hippocampal polyglot: the hippocampus as a path integration system. *J Exp Biol*, 199(Pt 1):173–85, 1996.

B. L. McNaughton, F. P. Battaglia, O. Jensen, E. I. Moser, et M. B. Moser. Path integration and the neural basis of the 'cognitive map'. *Nat Rev Neurosci*, 7(8):663–678, 8 2006.

B.L. McNaughton, L.L. Chen, et E.J. Markus. "dead reckoning," landmark learning, and the sense of direction: A neurophysiological and computational hypothesis. *J. Cogn. Neurosci.*, 3:190–201, 1991.

M. R. Mehta, A. K. Lee, et M. A. Wilson. Role of experience and oscillations in transforming a rate code into a temporal code. *Nature*, 417(6890):741–6, 2002.

M. Mittelstaedt et H. Mittelstaedt. Homing by path integration in a mammal. *Naturwiss.*, 67:566, 1980.

M. B. Moser et E. I. Moser. Functional differentiation in the hippocampus. *Hippocampus*, 8(6): 608–19, 1998.

R. U. Muller et J. L. Kubie. The effects of changes in the environment on the spatial firing of hippocampal complex-spike cells. *J Neurosci*, 7(7):1951–68, 1987.

Z. Nádasdy, H. Hirase, A. Czurkó, J. Csicsvari, et G. Buzsáki. Replay and time compression of recurring spike sequences in the hippocampus. *J Neurosci*, 19(21):9497–507, 1999.

J. O'Keefe et D. H. Conway. Hippocampal place units in the freely moving rat: why they fire where they fire. *Exp Brain Res*, 31(4):573–90, 1978.

J. O'Keefe et J. Dostrovsky. The hippocampus as a spatial map. preliminary evidence from unit activity in the freely-moving rat. *Brain Res*, 34(1): 171–5, 1971.

J. O'Keefe et L. Nadel. *The hippocampus as a cognitive map*. Clarendon Press, Oxford, 1978.

J. O'Keefe et M. L. Recce. Phase relationship between hippocampal place units and the eeg theta rhythm. *Hippocampus*, 3(3):317–30, 1993.

J. O'Keefe, N. Burgess, J. G. Donnett, K. J. Jeffery, et E. A. Maguire. Place cells, navigational accuracy, and the human hippocampus. *Philos Trans R Soc Lond B Biol Sci*, 353(1373):1333–40, 1998.

Joseph O'Neill, Timothy J Senior, Kevin Allen, John R Huxter, et Jozsef Csicsvari. Reactivation of experience-dependent cell assembly patterns in the hippocampus. *Nature neuroscience*, 11(2):209–15, 2 2008.

T. Ono, R. Tamura, et K. Nakamura. The hippocampus and space: are there "place neurons" in the monkey hippocampus? *Hippocampus*, 1(3):253–7, 1991.

N A Otmakhova et J E Lisman. D1/d5 dopamine receptor activation increases the magnitude of early long-term potentiation at ca1 hippocampal synapses. *The Journal of neuroscience : the official journal of the Society for Neuroscience*, 16 (23):7478–86, 12 1996.

E. Pastalkova, P. Serrano, D. Pinkhasova, E. Wallace, A. A. Fenton, et T. C. Sacktor. Storage of spatial information by the maintenance mechanism of ltp. *Science*, 313(5790):1141–4, 8 2006.

Eva Pastalkova, Vladimir Itskov, Asohan Amarasingham, et György Buzsáki. Internally generated cell assembly sequences in the rat hippocampus. *Science (New York, N.Y.)*, 321(5894):1322–7, 9 2008.

C. Pavlides et J. Winson. Influences of hippocampal place cell firing in the awake state on the activity of these cells during subsequent sleep episodes. *J Neurosci*, 9(8):2907–18, 8 1989.

M. Pedemonte, J. L. Peña, et R. A. Velluti. Firing of inferior colliculus auditory neurons is phase-locked to the hippocampus theta rhythm during paradoxical sleep and waking. *Exp Brain Res*, 112 (1):41–6, 1996.

P. Peigneux, S. Laureys, X. Delbeuck, et P. Maquet. Sleeping brain, learning brain. the role of sleep for memory systems. *Neuroreport*, 12(18): A111–24, 12 2001.

M. Penttonen, A. Kamondi, A. Sik, L. Acsády, et G. Buzsáki. Feed-forward and feed-back activation of the dentate gyrus in vivo during dentate spikes and sharp wave bursts. *Hippocampus*, 7(4):437–50, 1997.

B. Poucet, C. Thinus-Blanc, et R. U. Muller. Place cells in the ventral hippocampus of rats. *Neuroreport*, 5(16):2045–8, 1994.

J.B.Jr Ranck. Head-direction cells in the deep cell layers of dorsal presubiculum in freely moving rats. *Soc. Neurosci. Abstcts.*, 10:599, 1984.

A. D. Redish et D. S. Touretzky. The role of the hippocampus in solving the morris water maze. *Neural Comput*, 10(1):73–111, 1998.

A.D. Redish. *Beyond the Cognitive Map: From Place Cells to Episodic Memory*. MIT Press, 1999.

A.D. Redish, A.N. Elga, et D.S. Touretzky. A coupled attractor model of the rodent head direction system. *Network*, 7:671–685, 1996.

B. Rivard, Y. Li, P. P. Lenck-Santini, B. Poucet, et R. U. Muller. Representation of objects in space by two classes of hippocampal pyramidal cells. *J Gen Physiol*, 124(1):9–25, 7 2004.

R. G. Robertson, E. T. Rolls, P. Georges-François, et S. Panzeri. Head direction cells in the primate pre-subiculum. *Hippocampus*, 9(3):206–19, 1999.

E. T. Rolls et S. M. O'Mara. View-responsive neurons in the primate hippocampal complex. *Hippocampus*, 5(5):409–24, 1995.

A. Rotenberg, M. Mayford, R. D. Hawkins, E. R. Kandel, et R. U. Muller. Mice expressing activated camkii lack low frequency ltp and do not form stable place cells in the ca1 region of the hippocampus. *Cell*, 87(7):1351–61, 1996.

A. Samsonovich et B. L. McNaughton. Path integration and cognitive mapping in a continuous attractor neural network model. *J Neurosci*, 17 (15):5900–20, 1997.

F. Sargolini, M. Fyhn, T. Hafting, B. L. McNaughton, M. P. Witter, M. B. Moser, et E. I. Moser. Conjunctive representation of position, direction, and velocity in entorhinal cortex. *Science*, 312 (5774):758–62, 5 2006.

N. Sato et Y. Yamaguchi. Memory encoding by theta phase precession in the hippocampal network. *Neural Comput*, 15(10):2379–97, 2003.

Wolfram Schultz. Behavioral dopamine signals. *Trends in neurosciences*, 30(5):203–10, 5 2007.

W. B. Scoville et B. Milner. Loss of recent memory after bilateral hippocampal lesions. *J Neurol Neurosurg Psychiatry*, 20(1):11–21, 2 1957.

P. E. Sharp. Complimentary roles for hippocampal versus subicular/entorhinal place cells in coding place, context, and events. *Hippocampus*, 9 (4):432–43, 1999.

A. G. Siapas et M. A. Wilson. Coordinated interactions between hippocampal ripples and cortical spindles during slow-wave sleep. *Neuron*, 21(5): 1123–8, 1998.

A. Sirota, J. Csicsvari, D. Buhl, et G. Buzsáki. Communication between neocortex and hippocampus during sleep in rodents. *Proc Natl Acad Sci U S A*, 100(4):2065–9, 2003.

W. E. Skaggs et B. L. McNaughton. Replay of neuronal firing sequences in rat hippocampus during sleep following spatial experience. *Science*, 271 (5257):1870–3, 1996.

W. E. Skaggs, J. J. Knierim, H. S. Kudrimoti, et B. L. McNaughton. A model of the neural basis of the rat's sense of direction. *Adv Neural Inf Process Syst*, 7:173–80, 1995.

W. E. Skaggs, B. L. McNaughton, M. A. Wilson, et C. A. Barnes. Theta phase precession in hippocampal neuronal populations and the compression of temporal sequences. *Hippocampus*, 6(2):149–72, 1996.

C. Smith. Sleep states and memory processes in humans: procedural versus declarative memory systems. *Sleep Med Rev*, 5(6):491–506, 12 2001.

R. W. Stackman et J. S. Taube. Firing properties of head direction cells in the rat anterior thalamic nucleus: dependence on vestibular input. *J Neurosci*, 17(11):4349–58, 1997.

M Stewart, G J Quirk, M Barry, et S E Fox. Firing relations of medial entorhinal neurons to the hippocampal theta rhythm in urethane anesthetized and walking rats. *Experimental brain research. Experimentelle Hirnforschung. Expérimentation cérébrale*, 90(1):21–8, 1992.

R. Stickgold. Sleep-dependent memory consolidation. *Nature*, 437(7063):1272–8, 10 2005.

J. S. Taube et H. L. Burton. Head direction cell activity monitored in a novel environment and during a cue conflict situation. *J Neurophysiol*, 74(5): 1953–71, 1995.

J. S. Taube et R. U. Muller. Comparisons of head direction cell activity in the postsubiculum and anterior thalamus of freely moving rats. *Hippocampus*, 8(2):87–108, 1998.

J. S. Taube, R. U. Muller, et J. B. Ranck. Head-direction cells recorded from the postsubiculum in freely moving rats. ii. effects of environmental manipulations. *J Neurosci*, 10(2):436–47, 1990.

D. S. Touretzky et A. D. Redish. Theory of rodent navigation based on interacting representations of space. *Hippocampus*, 6(3):247–70, 1996.

M. V. Tsodyks, W. E. Skaggs, T. J. Sejnowski, et B. L. McNaughton. Population dynamics and theta rhythm phase precession of hippocampal place cell firing: a spiking neuron model. *Hippocampus*, 6(3):271–80, 1996.

M.V. Tsodyks et T.J. Sejnowski. Associative memory and hippocampal place cells. *Int J Neural Sys*, 6:81–86, 1995.

F. Varela, J. P. Lachaux, E. Rodriguez, et J. Martinerie. The brainweb: phase synchronization and large-scale integration. *Nat Rev Neurosci*, 2(4): 229–39, 2001.

R. P. Vertes, W. B. Hoover, et G. V. Di Prisco. Theta rhythm of the hippocampus: subcortical control and functional significance. *Behav Cogn Neurosci Rev*, 3(3):173–200, 2004.

M. P. Walker et R. Stickgold. Sleep-dependent learning and memory consolidation. *Neuron*, 44 (1):121–33, 9 2004.

G. V. Wallenstein et M. E. Hasselmo. Gabaergic modulation of hippocampal population activity: sequence learning, place field development, and the phase precession effect. *J Neurophysiol*, 78(1):393–408, 1997.

J. R. Whitlock, A. J. Heynen, M. G. Shuler, et M. F. Bear. Learning induces long-term potentiation in the hippocampus. *Science*, 313(5790): 1093–7, 8 2006.

S. I. Wiener et J. S. Taube. *Head direction cells and the neural mechanisms of spatial orientation*. MIT Press, 2005.

S. I. Wiener, A. Berthoz, et M. B. Zugaro. Multisensory processing in the elaboration of place and head direction responses by limbic system neurons. *Brain Res Cogn Brain Res*, 14(1):75–90, 2002.

T. J. Wills, C. Lever, F. Cacucci, N. Burgess, et J. O'Keefe. Attractor dynamics in the hippocampal representation of the local environment. *Science*, 308(5723):873–6, 2005.

M. A. Wilson et B. L. McNaughton. Reactivation of hippocampal ensemble memories during sleep. *Science*, 265(5172):676–9, 1994.

Y. Yamaguchi. A theory of hippocampal memory based on theta phase precession. *Biol Cybern*, 89 (1):1–9, 2003.

Y. Yamaguchi, Y. Aota, B. L. McNaughton, et P. Lipa. Bimodality of theta phase precession in hippocampal place cells in freely running rats. *J Neurophysiol*, 87(6):2629–42, 2002.

A. Ylinen, A. Bragin, Z. Nádasdy, G. Jandó, I. Szabó, A. Sik, et G. Buzsáki. Sharp wave-associated high-frequency oscillation (200 hz) in the intact hippocampus: network and intracellular mechanisms. *J Neurosci*, 15(1 Pt 1):30–46, 1995.

K. Zhang. Representation of spatial orientation by the intrinsic dynamics of the head-direction cell ensemble: a theory. *J Neurosci*, 16(6):2112–26, 1996.

M. B. Zugaro, E. Tabuchi, et S. I. Wiener. Influence of conflicting visual, inertial and substratal cues on head direction cell activity. *Exp Brain Res*, 133(2):198–208, 2000a.

M. B. Zugaro, A. Berthoz, et S. I. Wiener. Background, but not foreground, spatial cues are taken as references for head direction responses by rat anterodorsal thalamus neurons. *J Neurosci*, 21(14): RC154, 2001a.

M. B. Zugaro, E. Tabuchi, C. Fouquier, A. Berthoz, et S. I. Wiener. Active locomotion increases peak firing rates of anterodorsal thalamic head direction cells. *J Neurophysiol*, 86(2):692–702, 2001b.

M. B. Zugaro, A. Berthoz, et S. I. Wiener. Peak firing rates of rat anterodorsal thalamic head direction cells are higher during faster passive rotations. *Hippocampus*, 12(4):481–6, 2002.

M. B. Zugaro, A. Arleo, A. Berthoz, et S. I. Wiener. Rapid spatial reorientation and head direction cells. *J Neurosci*, 23(8):3478–82, 2003.

M. B. Zugaro, A. Arleo, C. Déjean, E. Burguière, M. Khamassi, et S. I. Wiener. Rat anterodorsal thalamic head direction neurons depend upon dynamic visual signals to select anchoring landmark cues. *Eur J Neurosci*, 20(2):530–6, 2004.

M. B. Zugaro, L. Monconduit, et G. Buzsáki. Spike phase precession persists after transient intrahippocampal perturbation. *Nat Neurosci*, 8(1):67–71, 2005.

M.B. Zugaro, E. Tabuchi, A. Berthoz, et S.I. Wiener. *Interplay of externally and internally generated self-movement signals in updating neurons sensitive to heading direction in behaving rats*, pages 121–128. International Society for Adaptive Behavior, Honolulu, 2000b.

Neuron
Article

Entrainment of Neocortical Neurons and Gamma Oscillations by the Hippocampal Theta Rhythm

Anton Sirota,[1] Sean Montgomery,[1] Shigeyoshi Fujisawa,[1] Yoshikazu Isomura,[1,2] Michael Zugaro,[1,3] and György Buzsáki[1,*]
[1]Center for Molecular and Behavioral Neuroscience, Rutgers, The State University of New Jersey, 197 University Avenue, Newark, NJ 07102, USA
[2]Present address: Neural Circuit Theory, RIKEN Brain Science Institute, 2-1 Hirosawa, Wako, Saitama 351-0198, Japan
[3]Present address: CNRS - Collège de France, LPPA, UMR 7152, 11, place Marcelin Berthelot, 75005 Paris, France
*Correspondence: buzsaki@axon.rutgers.edu
DOI 10.1016/j.neuron.2008.09.014

SUMMARY

Although it has been tacitly assumed that the hippocampus exerts an influence on neocortical networks, the mechanisms of this process are not well understood. We examined whether and how hippocampal theta oscillations affect neocortical assembly patterns by recording populations of single cells and transient gamma oscillations in multiple cortical regions, including the somatosensory area and prefrontal cortex in behaving rats and mice. Laminar analysis of neocortical gamma bursts revealed multiple gamma oscillators of varying frequency and location, which were spatially confined and synchronized local groups of neurons. A significant fraction of putative pyramidal cells and interneurons as well as localized gamma oscillations in all recorded neocortical areas were phase biased by the hippocampal theta rhythm. We hypothesize that temporal coordination of neocortical gamma oscillators by hippocampal theta is a mechanism by which information contained in spatially widespread neocortical assemblies can be synchronously transferred to the associative networks of the hippocampus.

INTRODUCTION

An essential aspect of cortical operation is that the results of local computations are integrated globally. Although the mechanisms of such local-global interactions are not well understood (Buzsáki, 2006; Dehaene et al., 2003; Engel et al., 2001; Varela et al., 2001), network oscillations have been assumed to play a critical role (Destexhe and Sejnowski, 2001; Engel et al., 2001). A general feature of cortical oscillations is that slow rhythms engage large areas and effectively modulate the more localized and shorter-lived fast oscillations (Bragin et al., 1995; Chrobak and Buzsáki, 1998a; Lakatos et al., 2005). Integration of information between different structures, such as the hippocampus and neocortex, is a special case of global coordination.

In waking cortical networks, local cell assembly organization is reflected in the occurrence of gamma oscillations (Gray and Singer, 1989; Harris et al., 2003). In the hippocampus, "activation" state is reflected by highly synchronous theta frequency oscillations (Buzsáki, 2002; Grastyán et al., 1959; Green and Arduni, 1954; Jouvet, 1969; Vanderwolf, 1969), which has been hypothesized to serve as a temporal organizer for a variety of functions (Bland, 1986; O'Keefe and Burgess, 2005). Theta-modulated cells have been found in the entorhinal cortex (Alonso and Garcia-Austt, 1987; Chrobak and Buzsáki, 1998b), perirhinal cortex (Muir and Bilkey, 1998), cingulate cortex (Colom et al., 1988; Holsheimer, 1982; Leung and Borst, 1987), prefrontal cortex (Hyman et al., 2005; Jones and Wilson, 2005; Siapas et al., 2005), amygdala (Collins et al., 1999; Paré and Gaudreau, 1996), anterior thalamus (Vertes et al., 2001), mammillary bodies, the supramammillary nucleus (Kocsis and Vertes, 1994), and the subiculum (Anderson and O'Mara, 2003). In addition, the rhythmic synchronous output of the hippocampus has been suggested to time the initiation of voluntary movements (Berg et al., 2006; Buño and Velluti, 1977; Macrides et al., 1982; Semba and Komisaruk, 1978) and gate sensory information (cf. Bland, 1986). Mainly on the basis of these behavioral results, the influence of hippocampal theta oscillations on neurons outside the limbic areas has been repeatedly conjectured (Bland, 1986; Buño and Velluti, 1977; Miller, 1991; Semba and Komisaruk, 1978), but experimental evidence to support this function is lacking. Phase modulation is a potential mechanism by which the hippocampus can coordinate disparate neocortical cell assemblies. To test this hypothesis and expand on previous works (Hyman et al., 2005; Jones and Wilson, 2005; Siapas et al., 2005), we recorded unit activity and local field potentials (LFP) from multiple neocortical regions, including primary sensory areas and the medial prefrontal cortex (PFC), along with hippocampal activity in rats and mice. We report here that a significant fraction of neurons in all recorded neocortical areas and locally emerging gamma oscillations are phase modulated by the hippocampal theta rhythm.

RESULTS

To investigate the effect of hippocampal theta oscillations on neocortical networks we recorded multiple single units and LFP in the associative and primary somatosensory (Figure 1A,

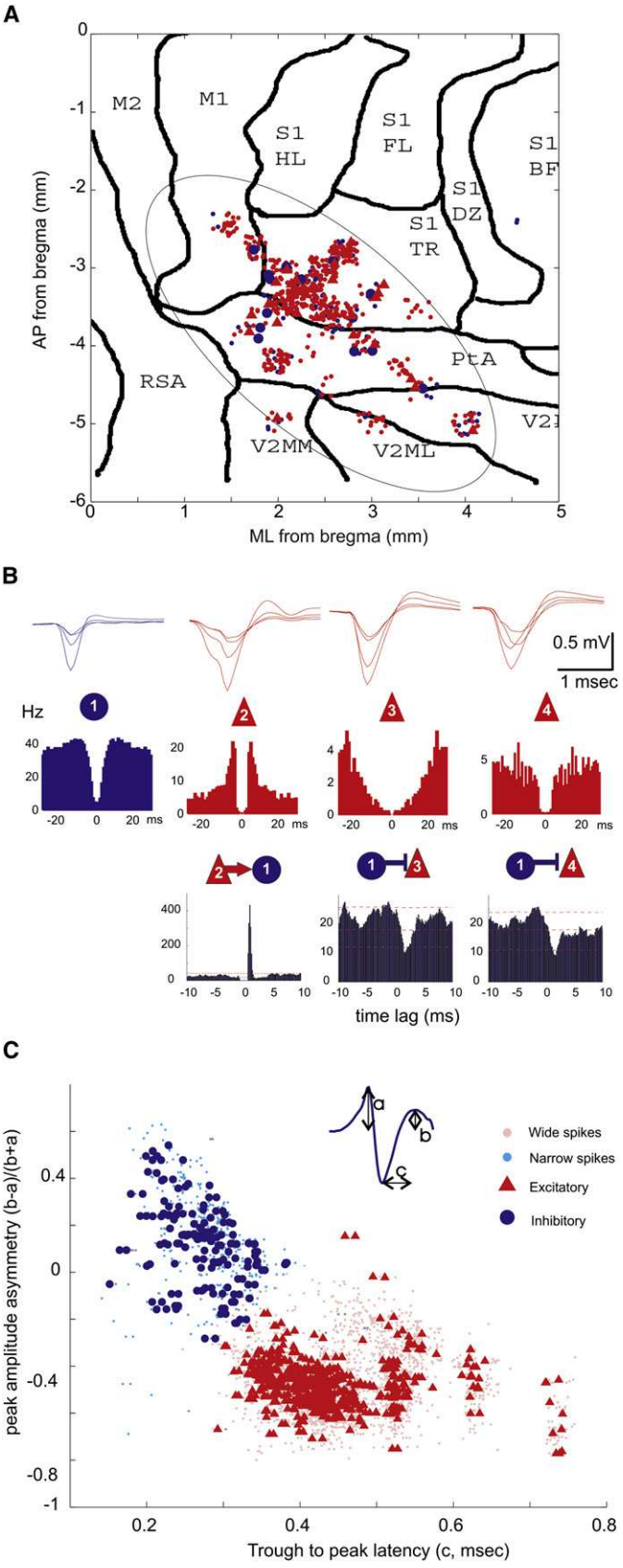

Figure 1. Separation of Putative Neocortical Interneurons and Pyramidal Cells

(A) Topographic distribution of putative pyramidal cells (red dots, triangles) and interneurons (small and larger blue dots) recorded from the parietal cortical area in all animals. Each symbol corresponds to a neuron (n = 767 from 24 rats), the position of which was inferred from implantation coordinates of the electrodes on a flattened cortical map. M1, M2, motor cortex; S1, primary somatosensory cortex; HL, hindlimb; FL, forelimb; BF, barrel field; TR, trunk; PtA, posterior associative area; V2MM, V2ML, secondary visual cortex; RSA, retrosplenial cortex.

(B) Average wide band-recorded waveforms (1 Hz-5 kHz; upper row) and autocorrelograms (middle row) of four example units. Superimposed traces were recorded by the four tetrode sites. Bottom row, short-latency monosynaptic interactions between neuron pairs, as revealed from the crosscorrelograms. Neuron 2 excites neuron 1 (recorded on the same electrode), which in turn, inhibits neurons 3 and 4 (on a different electrode). Lines indicate mean and 1% and 99% global confidence intervals.

(C) Neurons were clustered according to waveform asymmetry and mean filtered spike width (see inset; 0.8–5 kHz). Each symbol corresponds to an isolated unit (n = 2716, including neurons recorded from the medial prefrontal cortex, mPFC). Putative excitatory and inhibitory neurons form separate clusters. Circles/triangles in (A) and (C) correspond to inhibitory and excitatory neurons identified by monosynaptic interactions (as in [B]; Barthó et al., 2004).

referred to here as "parietal") areas or the anterior cingulate and prelimbic divisions of the medial prefrontal cortex (PFC) in 28 rats and 11 mice during task performance on an elevated maze and/or REM sleep. The reference theta oscillation signal was always derived from the CA1 pyramidal layer of the dorsal hippocampus (see Figure S1 available online).

Segregation of Principal Cells and Inhibitory Interneurons

Network activity in the cortex is organized by the interplay of various classes of principal cells and inhibitory interneurons (Markram, 2006; Somogyi and Klausberger, 2005). Since these two major classes of neurons have different firing rates, circuit and resonant properties and contribute differentially to cortical operations (Beierlein et al., 2000; Freund and Buzsáki, 1996; Markram, 2006), experimental identification, and separation of excitatory principal cells and inhibitory neurons are important for studying the effects of afferent signals on neocortical activity. Simultaneous recording of multiple single units in a small neocortical volume allowed us to identify putative principal cells and inhibitory interneurons (Figures 1B and 1C; Barthó et al., 2004; Constantinidis and Goldman-Rakic, 2002; Tierney et al., 2004; see Supplemental Data). The majority of the recorded neocortical units were classified as putative pyramidal cells (n = 2297, 85% in rats, n = 72, 84% mice) and the minority as putative interneurons (n = 343, 13% in rats; n = 14, 16% in mice).

Hippocampal Theta Phase-Locking of Neocortical Neurons

Several statistical methods were used to quantify the significance and magnitude of theta phase-locking of neocortical cells (Figures 2A–2D). Using Rayleigh tests (Figures 2E and 2F; α = 0.05) we found that the percentage of significantly modulated interneurons was higher than that of pyramidal cells in both parietal (32% versus 11%, respectively) and prefrontal cortices (46% versus 28%, respectively). The percentage of both cell types with significant theta phase-locking was significantly higher in PFC than in the parietal area (Figures 2E and 2F), but the fractions of significantly modulated neurons within the parietal subregions were similar (interneurons/pyramidal cells; S1: 33%/10%; posterior associative area [PtA]: 27%/11%). In contrast, the depth of theta modulation (von Mises concentration coefficient) of pyramidal cells was consistently higher than that of the interneurons (Figure S2). Additional analyses, including nonparametric tests, fit of a mixture model and spectral analysis, aimed to control for the assumptions of the Rayleigh test and gave comparable results (Supplemental Data; Figures S2 and S3). The preferred phases of significantly modulated neurons were similarly and broadly distributed for both interneurons and pyramidal cells, with highest density corresponding to the peak/descending phase of the CA1 theta cycle (Figures 2G and 2H).

Theta phase-locking of neocortical neurons occurred during both running on the track and REM sleep. Neurons could be significantly phase locked to theta in either one or both of these theta-associated states (Figures 2I–2L). In the subset of significantly modulated neurons that were recorded in both states the preferred phase of theta modulation was correlated across states (Figure 2L; $R_{circular}$ = 0.42). On average, the preferred phase of the population was significantly delayed during running compared to during REM in PFC, but not in the parietal cortex ($\sim 75^{\circ}$; circular anova, $p < 10^{-5}$ and $p > 0.3$, respectively; Figures 2K and 2L). Comparable results were obtained in mice (Figure S4). Approximately 60% of putative interneurons (of n = 14 total) and 35% of pyramidal neurons (of n = 72) were significantly (α = 0.05) modulated, with similar theta phase preferences across the population. These findings in rats and mice show that hippocampal theta oscillations impose a detectable phase-modulatory effect on the firing rate of neocortical neurons.

Locally Generated Neocortical Gamma Oscillations

Before examining the impact of theta phase on gamma oscillations, we investigated the local origin of gamma activity in the neocortex. First, we estimated the coherence between spike trains of pairs of neurons with sufficiently high firing rates (>5Hz). In a fraction of them (n = 123 pairs, 15% ± 10% of all pairs) significant coherence peaks between 30 and 140 Hz were found (Figure S5). Next, we computed the coherence between unit firing and the LFP recorded at multiple sites of the silicon probe (Figure 3A). Spikes were locked most coherently in a narrow band of a particular gamma frequency to the LFP in a localized cortical volume (Figures 3B–3D, 3F, and S6A–S6C). Spike-LFP coherence in the gamma band was in general, though not always, highest around the soma of the respective unit and decreased with distance (Figures 3D and 3E). Most neurons were phase-locked to the troughs of LFP gamma cycles (Figure 3G). In a related approach, we calculated average spectral power in short (50–100 ms) epochs temporally surrounding the action potentials of single neurons. Similar to coherence analysis, these "spike-triggered" spectra showed strong correlation between the firing of a subset of neurons and the LFP power within specific narrow ranges of gamma frequency oscillations in localized neocortical areas (Figures 3H, 3I, and S6D–S6I). Analysis of spectra at various time lags from the triggering spike showed that increases of the space-frequency localized power were transient, reaching maximum within 0–100 ms from the reference spike (Figure S6). Some data sets contained simultaneously recorded neurons that were phase-locked or correlated with gamma oscillations, which were localized at the same location (putative layer and/or column) and/or frequency (e.g., Figures 3C, 3D, 3H, and 3I), indicating that gamma oscillations with particular localization and/or frequency are associated with the activity of unique groups of neurons.

Synchronization of pools of neurons was tentatively associated with transient increases of LFP power at specific locations and narrow gamma frequency bands. Because of volume conduction and the linear summation of different transient gamma oscillations with variable amplitudes and frequencies continuous summation of spectral power in the gamma band may not yield reliable results. Therefore, we devised two alternative approaches. The first approach is based on the monotonous decay of power away from gamma sources. Exploiting our multiple site recordings, a subset of well isolated gamma bursts were detected as local maxima of the spectral power in time, space, and frequency, and the detected events tended to cluster (e.g., Figure 4). The second approach for the detection of gamma

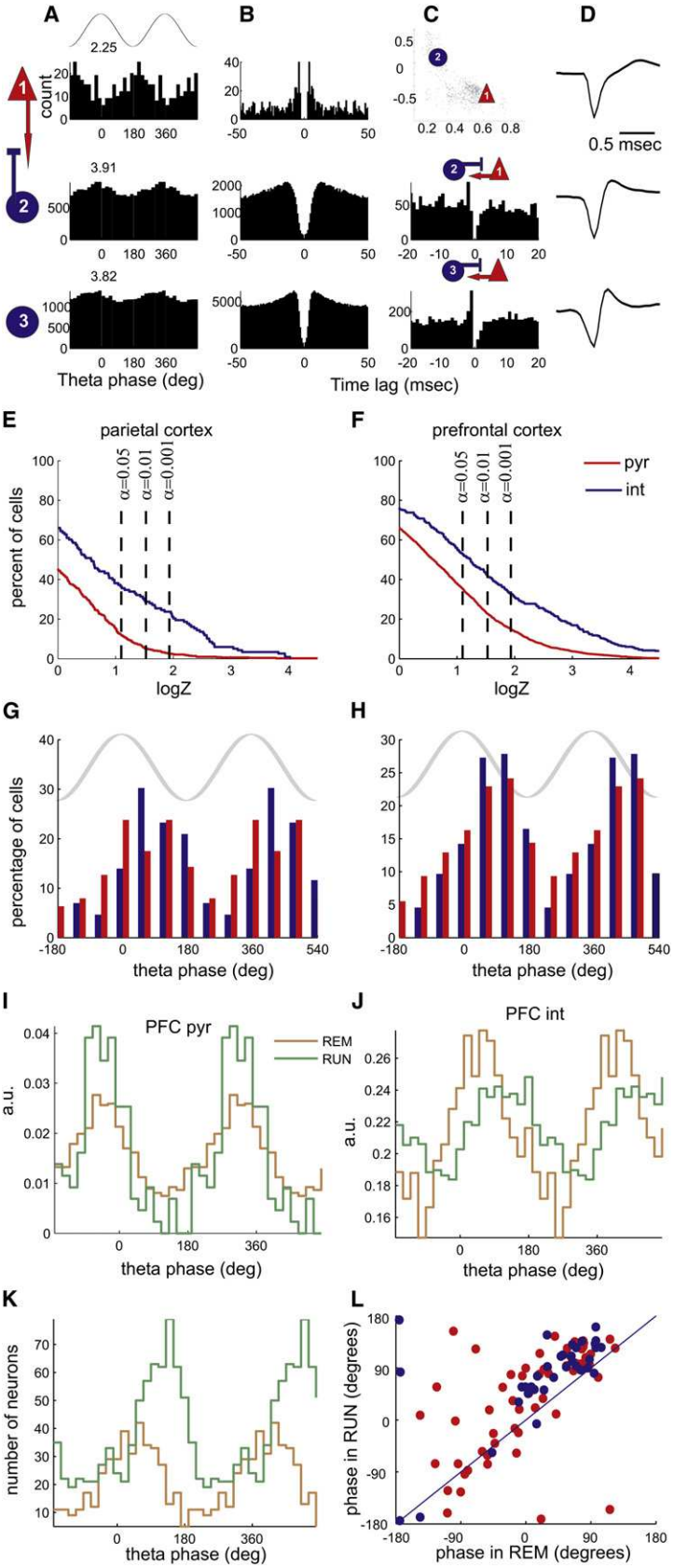

Figure 2. Hippocampal Theta Phase Modulation of Neocortical Neurons

(A–D) Each row corresponds to a single unit from the parietal-S1 area. (A) Theta phase histograms of neurons firing during REM sleep. Top, cartoon theta wave from the CA1 pyramidal layer. Numbers above, logZ statistics. Columns (B)–(D) characterize the units. (B) Autocorrelograms of the respective units. (C) Wave shape parameter scatterplot (top) and crosscorrelograms between the respective neuron and its monosynaptic partner (rows 2 and 3). (D) Average wideband-recorded (1 Hz–5 kHz) spike wave forms.

(E and F) Cumulative density function of phase modulation statistics (logZ) for putative pyramidal cells (pyr, red) and interneurons (int, blue) from the parietal (E) and mPFC (F). The plot is normalized to show the percentage of neurons (y axis) with logZ statistics greater than given value (*x* axis), y = P(X > x).

(G and H) Distribution of preferred phases for all significantly modulated ($p < 0.05$) neurons in the parietal cortex (G) and mPFC (H). Both cell types fire preferentially at around the peak/descending slope of hippocampal theta (phase 0°–90°).

(I and J), Theta phase histograms of an example pyramidal cell (I) and interneuron (J) from PFC during REM sleep and running on an elevated maze. Note that both neurons are significantly modulated in both states. Note also shift of phase preference of the interneuron.

(K) Phase histograms of preferred phases of all significantly modulated neurons during REM and awake running. Note phase shift of the population to the later theta phase during running.

(L) Scatterplot of preferred phases of neurons significantly modulated in both REM and RUN conditions (n = 98). Red, putative pyramidal cells; blue, putative inhibitory neurons.

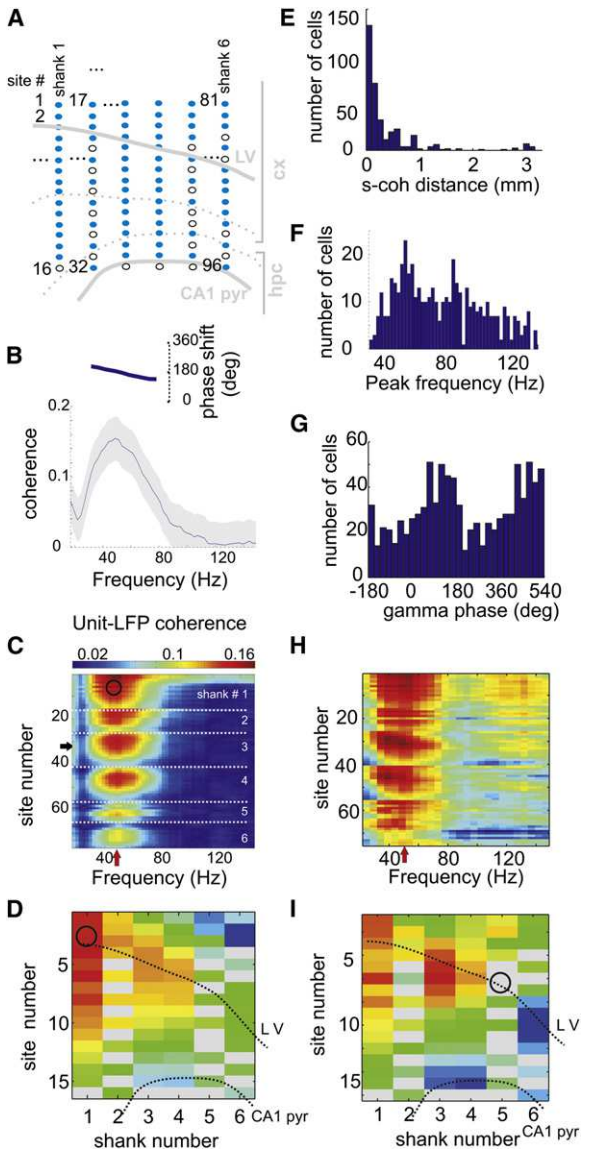

Figure 3. Gamma Frequency Band Synchronization of Neocortical Neurons

(A) Anatomical layout indicating the location of recording sites of the silicon probe used in the examples (B)–(D) and (H) and (I). Shanks are spaced by 300 μm, and each contains 16 recording sites 100 μm apart. Malfunctioning recording sites are shown as open circles and omitted from further analysis.

(B) Coherence (gray shading, 95 percentile confidence bands; inset, phase spectrum) between the spike train of a putative interneuron and the LFP at one recording site (horizontal arrow in [C]) in the parietal area.

(C) Coherence (color-coded) in the gamma range between a putative interneuron (recorded at site marked by a circle) and LFPs at all recording sites of the six shank silicon probe (y axis; 76 of 96; the remaining 20 sites with artifacts were excluded; see Supplemental Data). White dotted lines separate recording sites from adjacent shanks. Note increase of unit-LFP coherence at a preferred frequency (red vertical arrow, 40–50 Hz) and preferred depth/sites.

(D) Unfolding the unit-LFP coherence from (C) at the maximal frequency (red arrow in [C]) to a spatial map. The CA1 pyramidal layer and the approximate cortical layer 5 (dotted lines) are superimposed for spatial orientation. Circle, location of the soma of the recorded unit. Note that coherence (color) is highest locally and remains relatively high in a spatially contiguous volume up to 1 mm. Gray rectangles, sites with artifacts.

(E–G) Group statistics for all unit-LFP pairs with significant coherence (n = 456 units). (E) Distribution of the distances between the site of the recorded neuron (putative location of the soma) and the maximum unit-LFP coherence (s-coh distance). (F) Distribution of peak frequencies of unit-LFP coherence. (G) Distribution of preferred firing phases within the gamma cycle (trough, 180°).

(H and I) Example of spike triggered spectral analysis for a unit (same session as [A]–[D]). (H) Spike-triggered average power spectra (minus the power spectra calculated over the entire session; see Supplemental Data) color coded (red, relative increase of power; blue, relative decrease) for all channels (y axis). (I) Unfolding the spike-triggered power at preferred frequency from (H) to a spatial map. Circle, site of the recorded unit (putative soma location) used for triggering. Note that the power reaches maximum at a narrow "preferred" frequency band and at neighboring recording sites.

bursts is based on the covariance of spectral power in space (between different recording sites) and frequency (between different frequency bins, see Supplemental Data). Briefly, we performed factor analysis (principal component analysis followed by the Varimax rotation of the eigenvectors) of the spectral power in the gamma frequency range (30–150 Hz) seeking basis vectors that most parsimoniously captured the structure of power covariation between different frequency bins at different recording sites (Figures 3H, 3I, and 4D). The end product of this analysis was a set of factors, each of which was characterized by a vector of factor loadings reflecting the contribution of the respective frequency bins and recording sites to spectral power covariations. Projection of the spectra on these factors yielded a time series, termed factor scores, which reflect the strength of a given factor at any moment in time (Figure S7). Each of these factors could correspond to gamma oscillations with a distinct frequency and location pattern, and thus we refer to them as gamma frequency location (gFL) factors, or gFLs.

Several (from 0 to 32) gFLs were selected in each session based on explained covariance (Figure 5A). The space-frequency profiles of gFL factor loadings shared many features with those produced by unit-LFP spectral analysis and local maxima analysis. First, the gFL profiles showed a clear peak at a particular frequency and location (Figures 5B–5G). Second, some gFLs from the same recording session had similar frequencies but localized at different locations (Figures 5C, 5E, and 5G), while others displayed gamma oscillations of different frequencies at overlapping locations (Figures 5C, 5D, and 5G). Third, the spatial profiles of gFLs had elevated loading over several hundred micrometers, occasionally showing apparent localization in one cortical layer or a single cortical "column" (e.g., Figures 5C and 5E). Several location-frequency profiles of gFLs closely corresponded to those revealed by the unit-LFP spectral analysis (compare Figures 3C and 3D and Figures 5B and 5C) and local maxima analysis (Figure 4), confirming the validity of the method.

Hippocampal Theta Phase-Locking of Neocortical Gamma Oscillations

We next tested whether neocortical gamma oscillators are modulated by hippocampal theta. First, we found that the strongest theta modulation of neocortical gamma power occurred in a gamma frequency band higher than in the hippocampus (Figure 6A), eliminating volume-conduction of hippocampal gamma

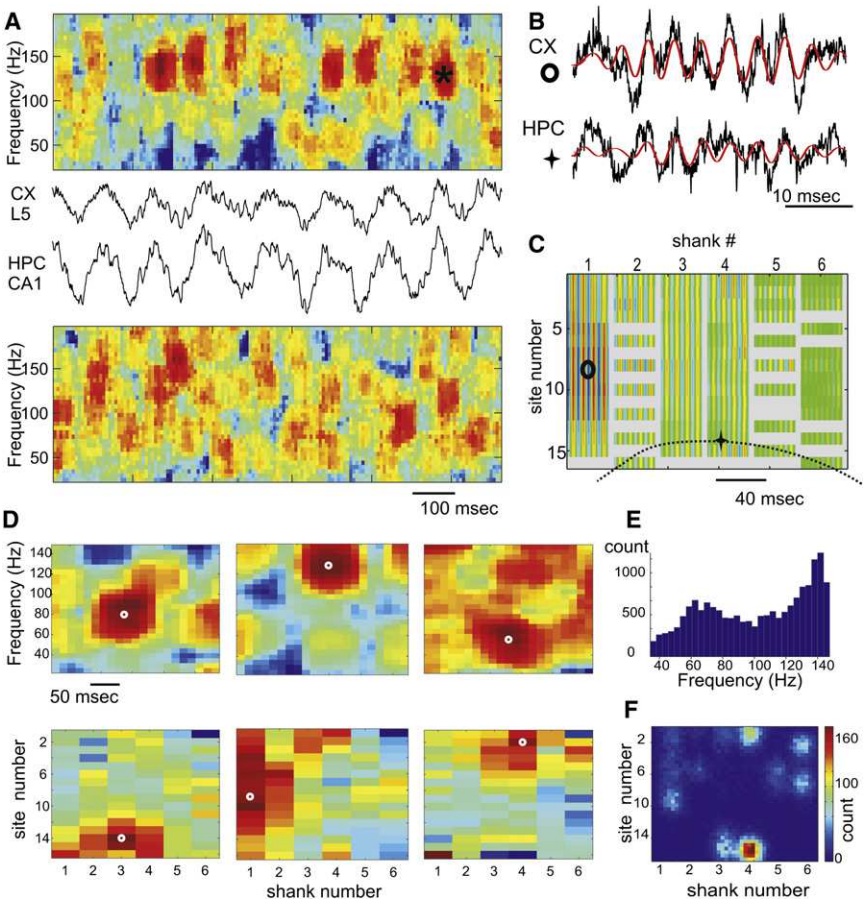

Figure 4. Temporal and Spatial Structure of Neocortical Gamma Oscillations

(A) A short epoch of neocortical (CX L5) and hippocampal (HPC CA1) LFPs and their associated "whitened" spectrograms.

(B) Gamma "burst" (red, band-pass,100–200 Hz, signal) from sites shown in (C).

(C) Color-coded spatial profile of band-pass-filtered segment in (B) at all recording sites (anatomical layout as in Figure 3A). Each column, separated by gray vertical stripes, corresponds to an electrode shank with 16 recording sites each. Malfunctioning sites are gray.

(D) Examples of isolated gamma bursts in hippocampus (left) and neocortex (middle, right). Each burst is characterized by a local maximum (white circles) of LFP spectral power (color) in both time-frequency (top) and anatomical space (bottom).

(E) Distribution of frequencies of individual local maxima. Note two modes, slow and fast gamma.

(F) Probability density of the spatial locations of local maxima of gamma power for the entire session. Note spatially segregated clusters.

to the neocortex as a potential confound. Second, in a subset of fast firing (>15 Hz) putative interneurons, we estimated the strength of unit-LFP gamma coherence at various time leads and lags from the peak of hippocampal theta (Figure 6B) and found maximum coherence on the descending slope of theta. Third, in a subset of experiments, we spatially isolated gamma bursts on the basis of power decay and clustered them in space and frequency (Figures 4D–4F). The probability of gamma bursts in some of these clusters was significantly biased by theta phase (Figure 6C). Although these separate approaches provided firm evidence for the theta phase modulation of neocortical gamma power, each of them had limitations. To overcome these limitations, we analyzed the relationship between the gFL factor score time series (which reflects the instantaneous strength of individual gamma oscillators; Figure S7) and hippocampal theta LFP (Figure 6D) and found significant coherence at theta frequency in a large fraction of the gFLs (e.g., Figure 6E). We also detected discrete times of gamma "burst" occurrence using the local maxima of the continuous gFL score time series. In a large percentage (~30%) of detected neocortical gFLs we found that gamma bursts were significantly phase modulated by hippocampal theta with the highest incidence near the peak of theta (Figures 6F–6H). High-frequency neocortical gamma bursts (>100 Hz) had stronger theta modulation and theta phase preference at a later phase (~50°; Figure 6I) than lower-frequency gamma oscillations. As expected from unit analysis, hippocampal gFL-bursts were more likely to be significantly modulated by hippocampal theta than those localized in the neocortex (60% versus 30%; Figure 6G).

Because the gFL analysis does not exploit the phase in the LFP signal, it can still be biased by the volume conduction of hippocampal gamma to the neocortex. We performed a number of analyses to rule out the contribution of the volume-conduction (see Supplemental Data). First, we estimated coherence between the gFL score and hippocampal LFP by partializing it by the hippocampal gamma power corresponding to the frequency range of the respective gFL. Approximately 90% of all gFLs (>98% for high frequency gFLs) retained a significant peak in the theta band. Second, for each gFL we computed coherence between the LFP in the center of the gFL-identified spatial gamma profile and at all other sites. The peak coherence occurred at the frequency close to the preferred frequency of the gFL (Figures S8A and S8B), with a spatial profile that matched that of the gFL (Figure 6J), providing a direct phase-synchronization measure of the local neocortical gamma. Next, we computed the integrated gamma LFP-LFP coherence within the gFL preferred frequency band in short sliding windows for the entire session and estimated the coherence between this time series and hippocampal LFP for each pair of recording sites (Figure 6K). The significant peaks at theta frequency revealed theta modulation of gamma synchronization between the LFP in the center of the gFL and spatially contiguous recording sites. If modulation of gamma power in the neocortex was a result of volume conduction of currents from the hippocampus one would expect that theta modulation of LFP-LFP coherence would increase toward hippocampus. However, in most cases the spatial profile of theta modulation of LFP-LFP gamma coherence closely matched that of the gFL and average LFP-LFP gamma

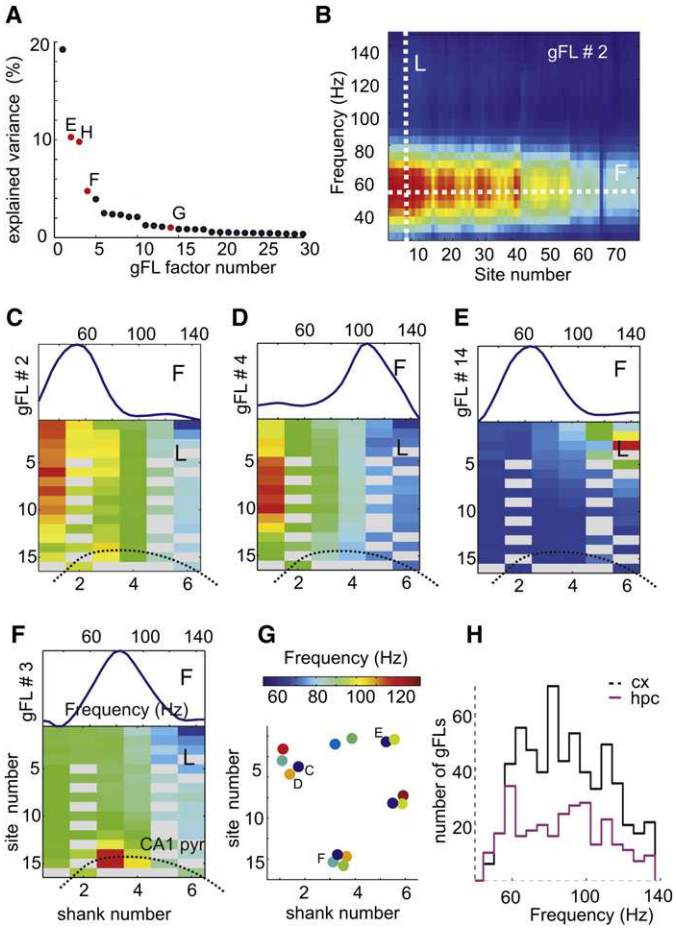

Figure 5. Spatial and Frequency Heterogeneity of Neocortical Gamma Oscillations

(A–G) Frequency-location gamma power (gFL) factor analysis (see Supplemental Data). (A) Percentage of total variance explained by the first 30 gFL factors. (B) Color-coded gFL factor loadings at 76 recording sites of the six shanks (20 malfunctioning sites removed) and gamma frequency bins (30–150 Hz). Red, positive, and blue, negative loading values. Maximal loading is localized at a given frequency (white line F) and location (white line L). (C–F) Examples of gFL factor loadings represented by frequency profile (F, top plots, loading at the maximal site across frequencies) and location profile (L, bottom, spatial maps; color indicates loading at the maximal frequency across sites) in the neocortex (C–E) and hippocampus (F). (G) Frequency (color) and spatial location of the center of mass of gFL components in a single session. Note spatial clusters of different frequency gFLs (e.g., C, D) or similar frequency preference but different locations (e.g., C, E).

(H) Distribution of the preferred frequency of cortical (n = 588, black) and hippocampal (n = 285, magenta) gFL factors.

coherence (e.g., compare Figure 5D and Figures 6J and 6K). The phase shift between gamma synchronization signal and hippocampal LFP was larger for the fast gamma, consistent with the phase preference analysis of gFL bursts (Figures S8C and S8D). Third, the spatial location of gFLs, the magnitude of theta modulation and the preferred theta phase of gFL-identified gamma bursts were similar between the first and second halves of the recording session (Figure S9), indicating that each gFL score represents the time course of an independent process. Finally, we identified a number of theta modulated gFLs in PFC, where volume-conduction of gamma is not expected due to its distance from the hippocampus. Overall, these findings indicate that hippocampal theta oscillations can exert a significant effect on local computation, represented by location and frequency-specific gamma oscillations, in wide neocortical areas.

Theta Modulation of the Membrane Potential in Neocortical Neurons

Theta phase modulation of neocortical unit discharges and gamma activity should be reflected by the membrane potential fluctuations in single neurons. To test this hypothesis, we obtained stable intracellular recordings from deep layer S1 neurons (n = 4) and biocytin-filled pyramidal cells in the mPFC (layer 2 = 1; layer 5 = 15; layer 6 = 7), together with simultaneous LFP recordings from the hippocampal CA1 pyramidal layer in an additional 27 rats anesthetized by urethane/ketamine-xylazine (Isomura et al., 2006). Hippocampal theta (3–5 Hz under anesthesia) occurred either spontaneously or was induced by tail pinching. Theta frequency oscillations of the membrane potential occurred transiently in several neocortical neurons. The intracellular voltage fluctuations occurred coherently with hippocampal theta in 16 out of 27 neurons (Figures 7A–7E). Spectral analysis of the membrane potential oscillations revealed significant power in the gamma frequency band, which fluctuated coherently with hippocampal theta (10 out of 27; Figures 7B and 7D). Both phase and strength of theta phase modulation of the membrane potential and the intracellular power of gamma were correlated with each other, although the coherence between the LFP and the membrane potential was stronger than that between the LFP and the gamma power ($p = 0.004$; Figures 7F and 7G). These analyses of intracellular data confirm that hippocampal theta oscillation can modulate the activity of neocortical neurons.

Volume Conduction of Hippocampal Theta Currents to the Neocortex

LFP theta oscillations in the parietal area were consistently present whenever hippocampal theta was observed, and the two theta signals co-varied in both frequency and magnitude. To examine whether LFP theta was generated by the neocortical circuits independent of hippocampal theta, we analyzed simultaneous LFP recordings in the hippocampus-neocortex axis, using multiple-site silicon probes (n = 21 sessions; Figures 8A1 and 8A2) and epidural grids (n = 9 sessions; Figures 8B1 and 8B2). In support of previous observations in anesthetized animals (Bland and Whishaw, 1976; Gerbrandt et al., 1978), the average magnitude of theta power monotonically decreased with distance from the hippocampus (Figure 8A3), and the distribution of theta power on the cortical surface reflected the physical layout of the underlying hippocampus (Figure 8B3). Theta power decreased, on average, 30%/mm in vertical direction and only 5%–10%/mm along the surface of the brain (Figure 8C). Both epidural and depth LFPs were strongly coherent with hippocampal LFP at theta frequency, with coherence

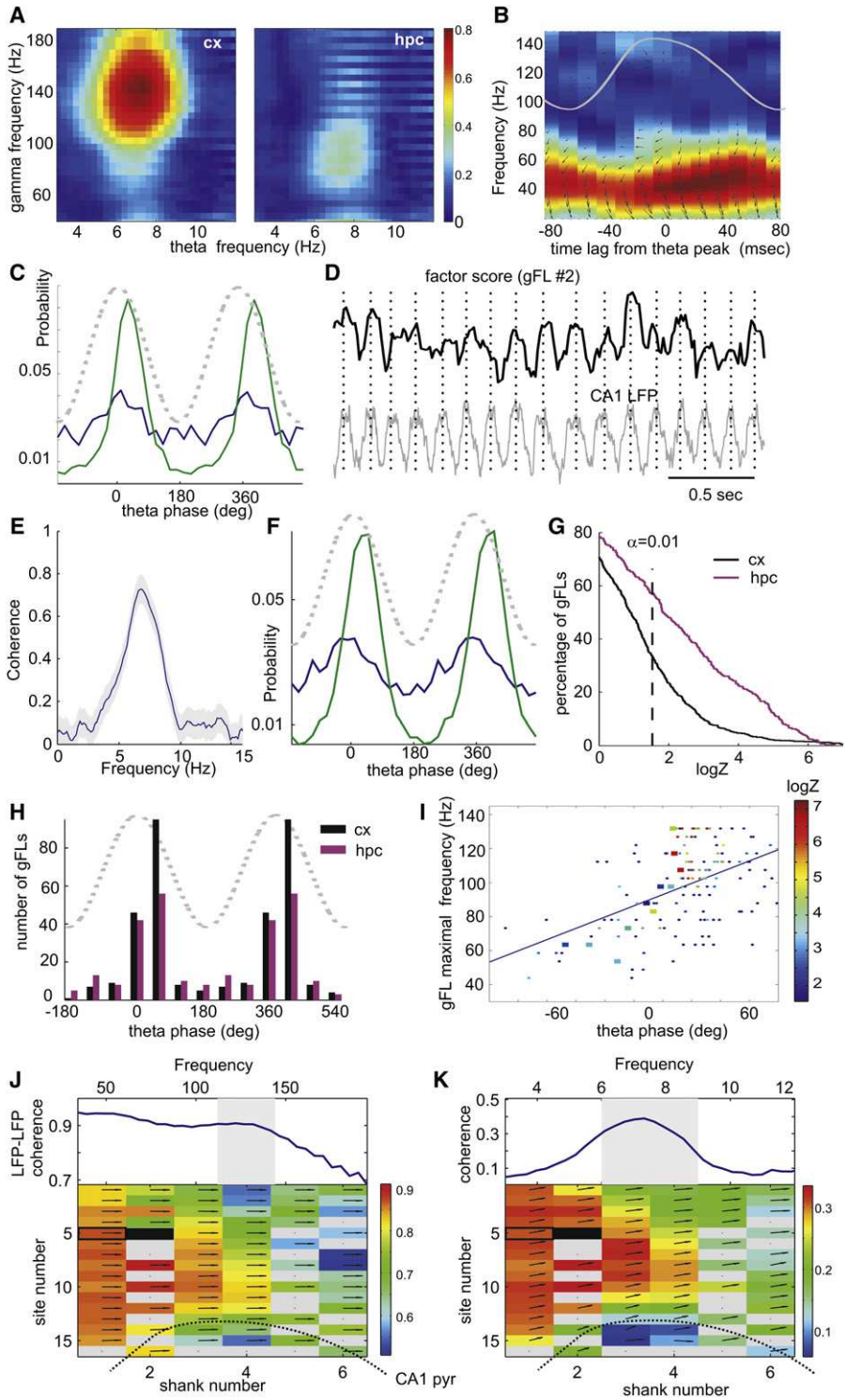

Figure 6. Hippocampal Theta Oscillations Modulate Neocortical Gamma

(A) Color-coded coherence between theta LFP in hippocampus and gamma power in different frequency bins (y axis) in the neocortex (cx) and hippocampus (hpc). Note strong modulation of higher-frequency gamma in the neocortex.

(B) Spike-LFP gamma band coherence (same unit-site pair as in Figure 3B) as a function of time lag from the peak of hippocampal theta (superimposed gray line). Small arrows, phase of spikes related to local gamma waves (zero is 3 o'clock).

(C) Theta phase histograms for two clusters of isolated gamma busts (Figures 4 E and 4F), whose spatial and frequency features correspond to those of gFL factors in Figures 5C and 5D. Dashed line, theta phase.

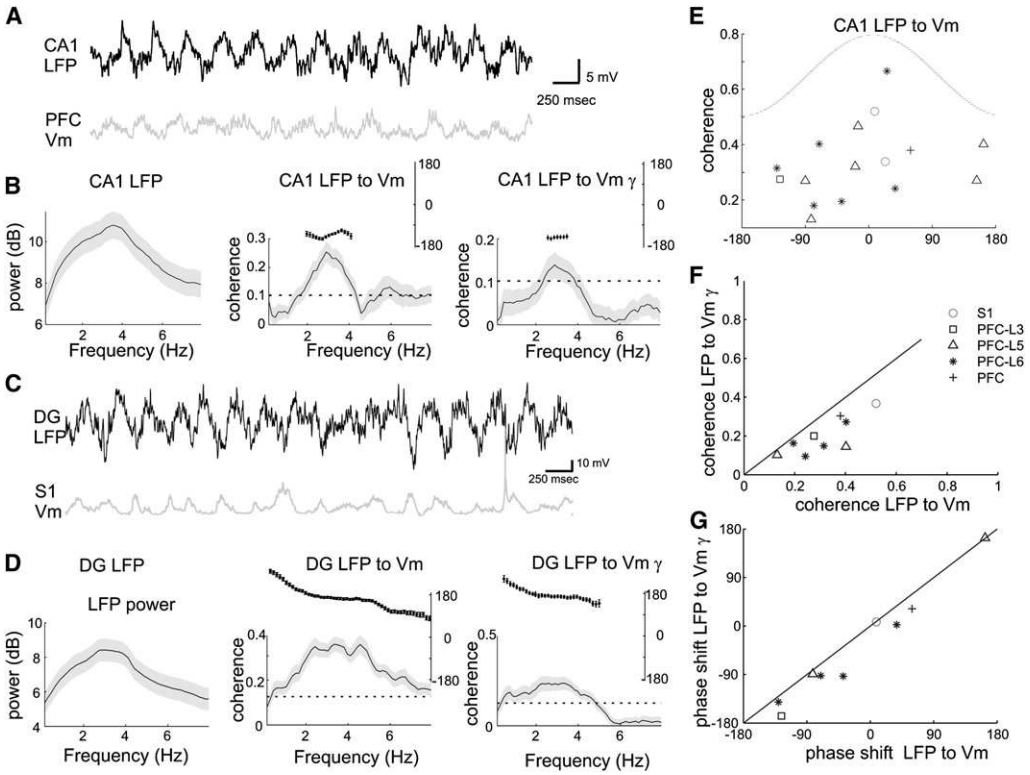

Figure 7. Theta phase Modulation of Membrane Potential in Neocortical Neurons under Anesthesia

(A) Simultaneous recording of LFP in the CA1 pyramidal layer and intracellularly recorded membrane potential in a layer 5 PFC neuron (PFC Vm).

(B) Power spectrum of the LFP (gray shading, 95 percentile confidence intervals, left); coherence between the LFP and the PFC Vm (middle); coherence between the LFP and integrated gamma power in PFC Vm (right); Inset, phase shift for the significantly coherent frequency band.

(C and D) Same display as in (A) and (B) for the simultaneous recording of LFP in the dentate gyrus (DG; theta phase ~160 degrees shifted from that in CA1) and intracellular recording from a layer 5 neuron in S1.

(E) Scatter plot of the phase shift versus the coherence value at the peak coherence frequency between CA1 LFP and Vm in cortical neurons (n = 16 significantly coherent neurons). Zero phase shift corresponds to depolarization in the Vm at the peak of hippocampal CA1 theta.

(F) Relationship between two coherence measures; coherence between the LFP and Vm versus coherence between the LFP and integrated Vm gamma power (both passed significance test).

(G) Relationship between phase shifts for cells in (F). S1, somatosensory area; PFC-L3, -L5, -L6, layers 3 to 6 of mPFC.

decaying at a rate of 5%–10%/mm (Figure 8D). Theta waves recorded between the CA1 pyramidal layer and cortical surface had approximately the same phase at all recording sites (Figure 8A4). However, the phase difference increased as a function of distance from the hippocampus in lateral and posterior directions up to 60° (e.g., Figure 8B4; n = 4 rats). Commensurate with these observations, current-source density analysis of LFP did not yield significant local sinks or sources in the theta band in the parietal area overlying the hippocampus. These findings suggest that theta measurements in the rodent neocortex are

(D) Short epoch of hippocampal theta oscillation (LFP) and factor score time series for a representative neocortical gFL (shown in Figure 5C).

(E) Coherence spectrum between the hippocampal LFP and the neocortical gFL score time series shown in (D).

(F) Theta phase histograms of neocortical "gamma bursts" (the peaks of the factor score time series) for gFLs shown in Figures 5C and 5D. Note the similarity between (C) (local maxima-based) and (F) (gFL-based) gamma burst identification.

(G) Cumulative density functions of theta phase modulation strength (logZ) for gamma bursts localized in the neocortex (black) and the hippocampus (magenta).

(H) Distribution of preferred phases of significantly ($p < 0.01$) theta-modulated gamma bursts in the neocortex (n = 280 out of 588 gFLs; black) and the hippocampus (n = 188 out of 285 gFLs; magenta).

(I) Scatterplot of the preferred theta phase of significantly modulated neocortical gamma bursts against their preferred frequency. Color indicates the strength of theta modulation statistic logZ (dots, all data; large squares, single session). Note that high-frequency gamma bursts occur at the later theta phase.

(J) Bottom, spatial map of average coherence between the LFP at the site (solid rectangle) in the center of a gFL in Figure 5D) and other sites at the gFL preferred frequency (shaded area). Top trace, example coherence for one site (open rectangle). Arrows, phase shift (zero at 3 o'clock).

(K) Top, coherence between theta LFP and gamma coherence between two neocortical sites (open rectangle and center of gFL, solid rectangle). Integrated gamma LFP-LFP coherence within the frequency band of maximum coherence (shaded range in [J]) was first computed in short sliding windows and the coherence between the resulting time series and hippocampal LFP is displayed here. Integral of this coherence in the shaded area quantifies theta modulation of gamma LFP-LFP coherence. Bottom, spatial map of theta modulation of coherence between the gFL center site (black) and other sites. See also Figure S10.

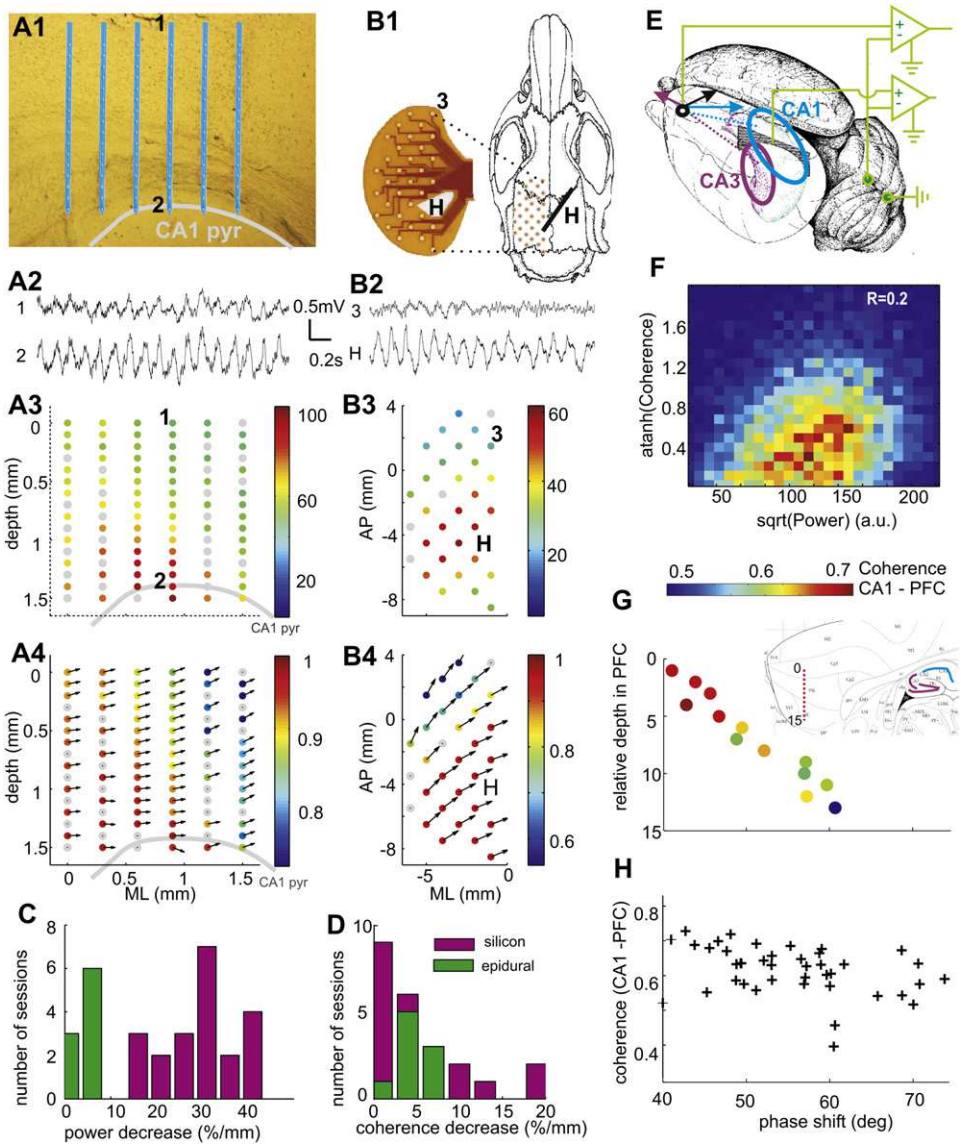

Figure 8. Volume-Conducted Hippocampal Theta Signals in the Neocortex

(A1) Position of probe shanks in the neocortex and CA1 pyramidal layer (highlighted by gray line). (A2) LFP signals from the supragranular layer of neocortex (1) and hippocampus (2). Two-dimensional map of theta power (normalized, A3) and coherence between site 2 (CA1 pyr) and other sites (A4). Theta phase shifts are indicated by arrows. Zero phase difference corresponds to 3 o'clock direction.

(B1) Layout of epidural recording of surface LFP with a flex cable (photo left). H, hippocampal depth electrode. (B2) LFP signals from site 3 of neocortex (3) and hippocampus (H). Two-dimensional map of surface theta power (B3) and coherence (B4).

(C and D) Distribution of the rate of power decrease (C) and rate coherence decrease (D) across experiments with silicon probe recordings (vertical axis, magenta) and epidural grids (horizontal axis, green).

(E) Lateral-posterior view of the left hemisphere. Arrows, hypothetical contribution of volume-conducted theta LFP vectors in PFC from the CA1 and CA3 regions (ellipsoids). The locations of ground and reference screw electrodes are also shown.

(F) Joint probability density of LFP theta power in CA1 pyr. layer and coherence between CA1 and mPFC LFP in one awake running session. Rank correlation coefficient $R = 0.2$, $p < 0.0001$.

(G) Relationship between CA1-PFC theta phase shift (coherence color-coded) and recording depth in PFC. Inset, location of the recording sites (red dots) in a sagittal section of PFC. Note monotonic phase shift and decreasing coherence with relative depth.

(H) Scatterplot of coherence between CA1 and PFC signals versus theta phase shift (n = 5 rats; REM and wake sessions combined).

dominated by the currents that are volume-conducted from the hippocampus (Bland and Whishaw, 1976; Gerbrandt et al., 1978).

LFP in the more anterior mPFC region was typically "flat" during continuous hippocampal theta oscillations (Jones and Wilson, 2005; Siapas et al., 2005) and only occasionally displayed

visible transient periods (0.5–2 s) of theta frequency oscillations (e.g., Figure 8B2). Although these intermittent theta periods were associated with increased coherence between hippocampus and PFC LFP, their occurrence was positively correlated with the power increases of hippocampal theta (Figure 8F; n = 44 sessions, rank correlation R = 0.2 ± 0.07). Moreover, LFP recorded at various depths in mPFC showed a linear phase shift and decreasing coherence referenced to the CA1 pyramidal layer (Figure 8G). Across experiments, the average CA1-mPFC coherence in the theta range was ~0.7 and the phase shift ranged from 40° to 70° (n = 25 sessions; Figure 8H). Importantly, coherence between PFC unit activity and hippocampal LFP, on average, was generally higher than the coherence between unit firing and locally recorded LFP.

Several aspects of the observations in mPFC are consistent with a volume-conductor model containing two (or more) distributed sources: e.g., CA1 and CA3/dentate regions of the hippocampus, and entorhinal cortex. Since LFP in the CA3 pyramidal layer is phase shifted (~150°) relative to CA1 pyramidal layer (cf. Buzsáki, 2002), the amplitude, phase, and coherence of theta at any location in the brain is determined by the vector summation of two (or more) volume-conducted currents (Figure 8E) and thus by the relative strength and phase of the theta generators and their relative distances from the recording site.

DISCUSSION

The major finding of the present experiments is that hippocampal theta oscillations can effectively bias the timing of local computation in the neocortex. A fraction of neurons in different neocortical areas, including the primary somatosensory area and PFC, as well as spatially localized and frequency-specific gamma oscillations were phase locked to hippocampal theta oscillations. These data suggest that theta oscillation entrainment provides a mechanism by which activity in spatially widespread neocortical and hippocampal networks can be temporally coordinated.

Hippocampal Theta Phase Locking of Neocortical Neurons

A robust finding of our experiments in both rats and mice is that 5% to 40% of neocortical neurons were significantly phase locked to hippocampal theta oscillations during either exploration or REM sleep. Importantly, theta-modulated neurons were found not only in the PFC which has massive direct afferents from the hippocampus (Swanson, 1981), but also in the primary somatosensory area, which has only multisynaptic connections with the hippocampus (Witter, 1993; Cenquizca and Swanson, 2007). The overall fraction of theta-locked units in the PFC (~35%) is comparable to that reported previously (Siapas et al., 2005), although the identity of units was not characterized in that study. These numbers should be contrasted to those in the hippocampus where, in the CA1 region, approximately 80% of the pyramidal cells and more than 90% of interneurons are significantly phase locked to theta oscillations (Figure S10; Csicsvari et al., 1999). In addition, the strength of theta modulation was considerably weaker in the neocortex, especially in the parietal cortex. These observations support the hypothesis that firing of neurons in many cortical areas is biased by the hippocampal theta oscillations (Miller, 1991).

Theta phase-locking of neocortical neurons can be brought about by multiple potential mechanisms. The simplest and oldest model assumes an independent pacemaker, residing in the septal complex (Petsche et al., 1962) and/or the supramammillary nucleus (Kocsis and Vertes, 1994), and recent studies suggest that a portion of neocortex-projecting neurons in the basal forebrain are phase-locked to hippocampal theta (Lee et al., 2005; Lin et al., 2006). An alternative mechanism of theta entrainment of distant neocortical neurons may entail the utilization of the entorhinal cortex and/or the PFC by way of their widespread, mostly reciprocal, connections with numerous neocortical regions (Groenewegen and Uylings, 2000; Swanson, 1981; Swanson and Kohler, 1986; Thierry et al., 2000; Witter, 1993). A final possibility is that hippocampo-neocortical coordination is brought about by the class of sparse long-range hippocampal projections to distant neocortical regions (Cenquizca and Swanson, 2007; Jinno et al., 2007). Any of these pathways alone or in combination may impose the hippocampal rhythmic output on their targets. The selective entrainment of a subset of neocortical neurons may be explained by either stronger synaptic connectivity between the hippocampus and selected target neocortical neurons or by the intrinsic properties of neuronal subgroups (Beierlein et al., 2000; Blatow et al., 2003; Gutfreund et al., 1995; Ulrich, 2002). Furthermore, various pharmacological manipulations can evoke theta-frequency oscillations in neocortical slices (Bao and Wu, 2003; Flint and Connors, 1996; Silva et al., 1991). Thus, theta oscillations in neocortical structures may emerge locally or/and phase-synchronize with the hippocampus via the above conduits.

The stronger entrainment of interneurons by hippocampal theta may also contribute to the enhancement of gamma oscillations (Beierlein et al., 2000; Csicsvari et al., 2003; Gibson et al., 1999; Hasenstaub et al., 2005). The similar theta phase preference of pyramidal cells and interneurons can be explained by either assuming that rhythmic afferents activated the two populations in a feed-forward manner or that local circuits are also involved in the generation of theta activity, similar to that in the CA3 hippocampal region (Buzsáki, 2002; Konopacki et al., 1987).

Locally Generated Neocortical Gamma Oscillations

Previous work has established that engagement of local circuits is reflected by the transient emergence of local gamma frequency oscillations (Bragin et al., 1995; Engel et al., 2001; Gray and Singer, 1989). We used several methods to explore neocortical gamma oscillations and demonstrated their local origin. In contrast to the hippocampus (Bragin et al., 1995; Csicsvari et al., 2003), gamma oscillations in the neocortex were transient and highly localized, confirming similar observations made with subdural grid recordings in humans (Canolty et al., 2006; Edwards et al., 2005; Howard et al., 2003; Menon et al., 1996; Sederberg et al., 2003). The amplitude of gamma oscillations decreased rapidly with distance. Gamma oscillators were often localized to either a single cortical layer and/or a putative column, consistent with previous reports (Gray and Singer, 1989; Steriade and Amzica, 1996; Sukov and Barth, 1998). Emergence of these transient fast rhythms faithfully reflects behaviorally relevant specific

computation in small networks (e.g., Gray and Singer, 1989; Montgomery and Buzsáki, 2007; Pesaran et al., 2002; Schoffelen et al., 2005; Sederberg et al., 2003). Our findings demonstrate that hippocampal theta oscillations can effectively link these sporadic and spatially distinct local gamma oscillations.

Hippocampal Theta Phase Locking of Neocortical Gamma Oscillations

Previous work has shown crossfrequency coupling between theta and gamma rhythms in the hippocampus (Bragin et al., 1995) and entorhinal cortex (Chrobak and Buzsáki, 1998a; Mormann et al., 2005). Recently, theta-gamma coupling was reported in the temporoparietal lobe of epileptic patients as well (Canolty et al., 2006). Intracranial recordings in patients also showed coupling between single unit activity and oscillations of various frequencies in the theta-gamma range (Jacobs et al., 2007). Furthermore, ''midline theta oscillations'' in human scalp recordings (Gevins et al., 1979) as well as isolated, transient neocortical theta oscillations in subdural and intracranial recordings during performance in various cognitive tasks have also been described (Caplan et al., 2003; Kahana et al., 1999; Raghavachari et al., 2001; Rizzuto et al., 2003), However, neither the mechanisms nor the origin of theta signals could be demonstrated in these clinical studies. Simultaneous recordings from the hippocampus and neocortex in our studies established that hippocampal theta oscillations exert an effect on local neocortical computation by rhythmically biasing synchrony of local gamma oscillations. We also found that neocortical fast gamma oscillations (80–150 Hz) were more strongly modulated by theta and occurred at a later phase (~50 degrees). This observation suggests that at least two distinguishable mechanisms can generate gamma oscillations in the neocortex with the higher frequency mechanism more responsive to hippocampal output (Wyart and Tallon-Baudry, 2008). The effect of theta phase-locked output on neocortical network dynamics may be analogous to that of a sensory stimulus (Engel et al., 2001; Gray and Singer, 1989; Sukov and Barth, 1998) since both effects can induce localized gamma oscillations. The widespread synchronization of neocortical neuronal assemblies by the hippocampal theta rhythm might provide a mechanism for ''gating'' of sensory information and temporally biasing movement initiation by the hippocampal theta rhythm (Bland, 1986).

Volume Conduction of Hippocampal Theta to the Neocortex

Using a combination of approaches, including epidural grid and silicon probe recordings of LFP, our findings support previous suggestions that theta signals in a large expanse of the rat neocortex and other proximal structures are largely volume conducted from the hippocampus and/or entorhinal cortex (Bland and Whishaw, 1976; Gerbrandt et al., 1978). Coherence of theta signals was attenuated monotonically as a function of both vertical and horizontal distance from the hippocampus, with a predictable phase shift between hippocampal and neocortical recording sites. If theta signal represented a single periodic dipole and originated from a point source, its attenuation and phase could be calculated from the biophysical features of the conducting brain tissue (Logothetis et al., 2007). However, theta is a consortium of several oscillators generated by multiple hippocampal-entorhinal regions and mechanisms, and both the power and phase relation of the generators vary as a function of behavior (Buzsáki, 2002). The important consequence of this complex relationship is that LFP signals recorded from cortical or subcortical sites in the rodent may reflect superposition of volume-conducted currents from two or more spatially distributed current sources in the hippocampus (Figure 8E) and the entorhinal cortex. The implication of the multiple-source volume-conductor model is that the amplitude, phase, and degree of coherence to hippocampal theta of extrahippocampally recorded theta signals may show systematic variations with behavior, yet such changes may arise entirely from intrahippocampal mechanisms.

These observations and considerations, of course, do not exclude neocortical generation of theta oscillations (Caplan et al., 2003; Ishii et al., 1999; Kahana et al., 1999; Raghavachari et al., 2001; Rizzuto et al., 2003). Importantly, we found that a small portion of PFC theta bursts was different in frequency from hippocampal theta (not shown), indicating that PFC circuits can generate LFP in the theta frequency band (Siapas et al., 2005; Jones and Wilson, 2005). However, when such transient epochs are of the *same* frequency as hippocampal theta, disambiguating locally generated currents and volume-conducted currents becomes difficult with currently available LFP recording methods.

Reciprocal Information Transfer by Theta Oscillations

Transfer of information in the brain from source (sender) to target (receiver) is usually considered unidirectional: the source network sends the information to a recipient network (Abeles, 1991). Oscillatory entrainment, however, allows for a different mechanism of information exchange, which we refer to as ''reciprocal information transfer.'' In this hypothetical mechanism, we assume that the recipient structure plays an initiating role by temporally biasing activity in the source structure, creating time windows within which the recipient structure can most effectively receive information (Fries, 2005; Isomura et al., 2006; Sirota et al., 2003; Sirota and Buzsáki, 2007; Womelsdorf et al., 2007). For example, experiments suggest that during slow wave sleep transfer of hippocampal information to the neocortex is initiated by the down-up transition of neocortical slow oscillation (Isomura et al., 2006; Sirota et al., 2003; Sirota and Buzsáki, 2007). In a similar manner, we suggest that transfer of neocortical information to the hippocampus is actively initiated by the hippocampus via theta-phase biasing of neocortical network dynamics. As a result, self-organized gamma oscillations at multiple cortical locations is temporally biased so that the information contained in the gamma bursts would arrive at the hippocampus at the phase of the theta cycle when the network can be perturbed maximally and when it is most plastic (Holscher et al., 1997; Huerta and Lisman, 1996; Hyman et al., 2003), which, in the case of CA1 pyramidal cells, corresponds to the positive (least active) phase of the theta cycle (Csicsvari et al., 1999). In this context, it is noteworthy that hippocampal neurons begin to discharge at this late (positive) phase when the rat enters the place field of the neuron (O'Keefe and Recce, 1993), likely triggered by the cooperative action of neocortical assemblies.

The postulated model of reciprocal information transfer can ensure that information from wide areas of the neocortex can be presented to the hippocampus in a temporally synchronous manner and integrated into its associative networks.

EXPERIMENTAL PROCEDURES

Animals and Recording

Chronic recordings in the neocortex and hippocampus using silicon probes, tetrodes, or epidural electrodes were performed in rats (n = 28) and mice (n = 11) during sleep and waking behavior. Acute extracellular recordings in the hippocampus and intracellular recordings in the neocortex were performed in anesthetized rats (n = 27; Isomura et al., 2006).

Data Analysis

All analysis was performed using custom-written tools in Matlab (Mathworks). For detailed description, see Supplemental Data.

SUPPLEMENTAL DATA

The Supplemental Data include Ten Figures and Supplemental Experimental Procedures and can be found with this article online at http://www.neuron.org/supplemental/S0896-6273(08)00762-9.

ACKNOWLEDGMENTS

We thank Asohan Amarasigham, Carina Curto, Kamran Diba, Caroline Geisler, Kenji Mizuseki, Simal Ozen, Lucas Parra, and Alfonso Renart for useful discussions and comments on the manuscript; Derek Buhl and Dirk Isbrandt for providing recordings in mice; Alexei Ponomarenko and Matthew Guilfoyle for assisting with recordings; Darrell A. Henze for intracellular recordings from somatosensory cortex; and John Bentley and Michael Stephens for help with statistical analysis of the mixture model. Supported by National Institutes of Health (NS034994; MH54671), National Science Foundation (SBE0542013), the J.D. McDonnell Foundation, Uehara Memorial Foundation, and the Japan Society of Promotion for Sciences.

Accepted: September 4, 2008
Published: November 25, 2008

REFERENCES

Abeles, M. (1991). Corticonics: Neural Circuits of the Cerebral Cortex (Cambridge: Cambridge University Press).

Alonso, A., and Garcia-Austt, E. (1987). Neuronal sources of theta rhythm in the entorhinal cortex of the rat. II. Phase relations between unit discharges and theta field potentials. Exp. Brain Res. *67*, 502–509.

Anderson, M.I., and O'Mara, S.M. (2003). Analysis of recordings of single-unit firing and population activity in the dorsal subiculum of unrestrained freely moving rats. J. Neurophysiol. *90*, 655–665.

Bao, W., and Wu, J.Y. (2003). Propagating wave and irregular dynamics: spatiotemporal patterns of cholinergic theta oscillations in neocortex in vitro. J. Neurophysiol. *90*, 333–341.

Barthó, P., Hirase, H., Monconduit, L., Zugaro, M., Harris, K.D., and Buzsáki, G. (2004). Characterization of neocortical principal cells and interneurons by network interactions and extracellular features. J. Neurophysiol. *92*, 600–608.

Beierlein, M., Gibson, J.R., and Connors, B.W. (2000). A network of electrically coupled interneurons drives synchronized inhibition in neocortex. Nat. Neurosci. *3*, 904–910.

Berg, R.W., Whitmer, D., and Kleinfeld, D. (2006). Exploratory whisking by rat is not phase locked to the hippocampal theta rhythm. J. Neurosci. *26*, 6518–6522.

Bland, B.H. (1986). The physiology and pharmacology of hippocampal formation theta rhythms. Prog. Neurobiol. *26*, 1–54.

Bland, B.H., and Whishaw, I.Q. (1976). Generators and topography of hippocampal theta (RSA) in the anaesthetized and freely moving rat. Brain Res. *118*, 259–280.

Blatow, M., Rozov, A., Katona, I., Hormuzdi, S.G., Meyer, A.H., Whittington, M.A., Caputi, A., and Monyer, H. (2003). A novel network of multipolar bursting interneurons generates theta frequency oscillations in neocortex. Neuron *38*, 805–817.

Bragin, A., Jando, G., Nadasdy, Z., Hetke, J., Wise, K., and Buzsáki, G. (1995). Gamma (40–100 Hz) oscillation in the hippocampus of the behaving rat. J. Neurosci. *15*, 47–60.

Buño, W., Jr., and Velluti, J.C. (1977). Relationships of hippocampal theta cycles with bar pressing during self-stimulation. Physiol. Behav. *19*, 615–621.

Buzsáki, G. (2002). Theta oscillations in the hippocampus. Neuron *33*, 325–340.

Buzsáki, G. (2006). Rhythms of the Brain (New York: Oxford University Press).

Canolty, R.T., Edwards, E., Dalal, S.S., Soltani, M., Nagarajan, S.S., Kirsch, H.E., Berger, M.S., Barbaro, N.M., and Knight, R.T. (2006). High gamma power is phase-locked to theta oscillations in human neocortex. Science *313*, 1626–1628.

Caplan, J.B., Madsen, J.R., Schulze-Bonhage, A., Aschenbrenner-Scheibe, R., Newman, E.L., and Kahana, M.J. (2003). Human theta oscillations related to sensorimotor integration and spatial learning. J. Neurosci. *23*, 4726–4736.

Cenquizca, L.A., and Swanson, L.W. (2007). Spatial organization of direct hippocampal field CA1 axonal projections to the rest of the cerebral cortex. Brain Res. Brain Res. Rev. *56*, 1–26.

Chrobak, J.J., and Buzsáki, G. (1998a). Gamma oscillations in the entorhinal cortex of the freely behaving rat. J. Neurosci. *18*, 388–398.

Chrobak, J.J., and Buzsáki, G. (1998b). Operational dynamics in the hippocampal-entorhinal axis. Neurosci. Biobehav. Rev. *22*, 303–310.

Collins, D.R., Lang, E.J., and Paré, D. (1999). Spontaneous activity of the perirhinal cortex in behaving cats. Neuroscience *89*, 1025–1039.

Colom, L.V., Christie, B.R., and Bland, B.H. (1988). Cingulate cell discharge patterns related to hippocampal EEG and their modulation by muscarinic and nicotinic agents. Brain Res. *460*, 329–338.

Constantinidis, C., and Goldman-Rakic, P.S. (2002). Correlated discharges among putative pyramidal neurons and interneurons in the primate prefrontal cortex. J. Neurophysiol. *88*, 3487–3497.

Csicsvari, J., Hirase, H., Czurko, A., Mamiya, A., and Buzsáki, G. (1999). Oscillatory coupling of hippocampal pyramidal cells and interneurons in the behaving rat. J. Neurosci. *19*, 274–287.

Csicsvari, J., Jamieson, B., Wise, K.D., and Buzsáki, G. (2003). Mechanisms of gamma oscillations in the hippocampus of the behaving rat. Neuron *37*, 311–322.

Dehaene, S., Sergent, C., and Changeux, J.P. (2003). A neuronal network model linking subjective reports and objective physiological data during conscious perception. Proc. Natl. Acad. Sci. USA *100*, 8520–8525.

Destexhe, A., and Sejnowski, T. (2001). Thalamocortical Assemblies—How Ion Channels, Single Neurons and Large-Scale Networks Organize Sleep Oscillations (Oxford: Oxford University Press).

Edwards, E., Soltani, M., Deouell, L.Y., Berger, M.S., and Knight, R.T. (2005). High gamma activity in response to deviant auditory stimuli recorded directly from human cortex. J. Neurophysiol. *94*, 4269–4280.

Engel, A.K., Fries, P., and Singer, W. (2001). Dynamic predictions: oscillations and synchrony in top-down processing. Nat. Rev. Neurosci. *2*, 704–716.

Flint, A.C., and Connors, B.W. (1996). Two types of network oscillations in neocortex mediated by distinct glutamate receptor subtypes and neuronal populations. J. Neurophysiol. *75*, 951–957.

Freund, T.F., and Buzsáki, G. (1996). Interneurons of the hippocampus. Hippocampus *6*, 347–470.

Fries, P. (2005). A mechanism for cognitive dynamics. Neuronal communication through neuronal coherence. Trends Cogn Sci. *9*, 474–480.

Gerbrandt, L.K., Lawrence, J.C., Eckardt, M.J., and Lloyd, R.L. (1978). Origin of the neocortically monitored theta rhythm in the curarized rat. Electroencephalogr. Clin. Neurophysiol. *45*, 454–467.

Gevins, A.S., Zeitlin, G.M., Doyle, J.C., Yingling, C.D., Schaffer, R.E., Callaway, E., and Yeager, C.L. (1979). Electroencephalogram correlates of higher cortical functions. Science *203*, 665–668.

Gibson, J.R., Beierlein, M., and Connors, B.W. (1999). Two networks of electrically coupled inhibitory neurons in neocortex. Nature *402*, 75–79.

Grastyán, E., Lissák, K., Madarász, I., and Donhoffer, H. (1959). The hippocampal electrical activity during the development of conditioned reflexes. Electroencephalogr. Clin. Neurophysiol. *11*, 409–430.

Gray, C.M., and Singer, W. (1989). Stimulus-specific neuronal oscillations in orientation columns of cat visual cortex. Proc. Natl. Acad. Sci. USA *86*, 1698–1702.

Green, J.D., and Arduni, A.A. (1954). Hippocampal electrical activity in arousal. J. Neurophysiol. *17*, 533–557.

Groenewegen, H.J., and Uylings, H.B. (2000). The prefrontal cortex and the integration of sensory, limbic and autonomic information. Prog. Brain Res. *126*, 3–28.

Gutfreund, Y., Yarom, Y., and Segev, I. (1995). Subthreshold oscillations and resonant frequency in guinea-pig cortical neurons: physiology and modelling. J. Physiol. *483*, 621–640.

Harris, K.D., Csicsvari, J., Hirase, H., Dragoi, G., and Buzsáki, G. (2003). Organization of cell assemblies in the hippocampus. Nature *424*, 552–556.

Hasenstaub, A., Shu, Y., Haider, B., Kraushaar, U., Duque, A., and Mccormick, D.A. (2005). Inhibitory postsynaptic potentials carry synchronized frequency information in active cortical networks. Neuron *47*, 423–435.

Holscher, C., Anwyl, R., and Rowan, M.J. (1997). Stimulation on the positive phase of hippocampal theta rhythm induces long-term potentiation that can be depotentiated by stimulation on the negative phase in area CA1 in vivo. J. Neurosci. *17*, 6470–6477.

Holsheimer, J. (1982). Generation of theta activity (RSA) in the cingulate cortex of the rat. Exp. Brain Res. *47*, 309–312.

Howard, M.W., Rizzuto, D.S., Caplan, J.B., Madsen, J.R., Lisman, J., Aschenbrenner-Scheibe, R., Schulze-Bonhage, A., and Kahana, M.J. (2003). Gamma oscillations correlate with working memory load in humans. Cereb. Cortex *13*, 1369–1374.

Huerta, P.T., and Lisman, J.E. (1996). Low-frequency stimulation at the troughs of theta-oscillation induces long-term depression of previously potentiated CA1 synapses. J. Neurophysiol. *75*, 877–884.

Hyman, J.M., Wyble, B.P., Goyal, V., Rossi, C.A., and Hasselmo, M.E. (2003). Stimulation in hippocampal region CA1 in behaving rats yields long-term potentiation when delivered to the peak of theta and long-term depression when delivered to the trough. J. Neurosci. *23*, 11725–11731.

Hyman, J.M., Zilli, E.A., Paley, A.M., and Hasselmo, M.E. (2005). Medial prefrontal cortex cells show dynamic modulation with the hippocampal theta rhythm dependent on behavior. Hippocampus *15*, 739–749.

Ishii, R., Shinosaki, K., Ukai, S., Inouye, T., Ishihara, T., Yoshimine, T., Hirabuki, N., Asada, H., Kihara, T., Robinson, S.E., and Takeda, M. (1999). Medial prefrontal cortex generates frontal midline theta rhythm. Neuroreport *10*, 675–679.

Isomura, Y., Sirota, A., Ozen, S., Montgomery, S., Mizuseki, K., Henze, D.A., and Buzsáki, G. (2006). Integration and segregation of activity in entorhinal-hippocampal subregions by neocortical slow oscillations. Neuron *52*, 871–882.

Jacobs, J., Kahana, M.J., Ekstrom, A.D., and Fried, I. (2007). Brain oscillations control timing of single-neuron activity in humans. J. Neurosci. *27*, 3839–3844.

Jinno, S., Klausberger, T., Marton, L.F., Dalezios, Y., Roberts, J.D., Fuentealba, P., Bushong, E.A., Henze, D., Buzsáki, G., and Somogyi, P. (2007). Neuronal diversity in gabaergic long-range projections from the hippocampus. J. Neurosci. *27*, 8790–8804.

Jones, M.W., and Wilson, M.A. (2005). Theta rhythms coordinate hippocampal-prefrontal interactions in a spatial memory task. PLoS Biol. *3*, e402. 10.1371/journal.pbio.0030402.

Jouvet, M. (1969). Biogenic amines and the states of sleep. Science *163*, 32–41.

Kahana, M.J., Sekuler, R., Caplan, J.B., Kirschen, M., and Madsen, J.R. (1999). Human theta oscillations exhibit task dependence during virtual maze navigation. Nature *399*, 781–784.

Kocsis, B., and Vertes, R.P. (1994). Characterization of neurons of the supramammillary nucleus and mammillary body that discharge rhythmically with the hippocampal theta rhythm in the rat. J. Neurosci. *14*, 7040–7052.

Konopacki, J., Bland, B.H., Maciver, M.B., and Roth, S.H. (1987). Cholinergic theta rhythm in transected hippocampal slices: independent CA1 and dentate generators. Brain Res. *436*, 217–222.

Lakatos, P., Shah, A.S., Knuth, K.H., Ulbert, I., Karmos, G., and Schroeder, C.E. (2005). An oscillatory hierarchy controlling neuronal excitability and stimulus processing in the auditory cortex. J. Neurophysiol. *94*, 1904–1911.

Lee, M.G., Hassani, O.K., Alonso, A., and Jones, B.E. (2005). Cholinergic basal forebrain neurons burst with theta during waking and paradoxical sleep. J. Neurosci. *25*, 4365–4369.

Leung, L.W., and Borst, J.G. (1987). Electrical activity of the cingulate cortex. I. Generating mechanisms and relations to behavior. Brain Res. *407*, 68–80.

Lin, S.C., Gervasoni, D., and Nicolelis, M.A. (2006). Fast modulation of prefrontal cortex activity by basal forebrain noncholinergic neuronal ensembles. J. Neurophysiol. *96*, 3209–3219.

Logothetis, N.K., Kayser, C., and Oeltermann, A. (2007). In vivo measurement of cortical impedance spectrum in monkeys: implications for signal propagation. Neuron *55*, 809–823.

Macrides, F., Eichenbaum, H.B., and Forbes, W.B. (1982). Temporal relationship between sniffing and the limbic theta rhythm during odor discrimination reversal learning. J. Neurosci. *2*, 1705–1717.

Markram, H. (2006). The blue brain project. Nat. Rev. Neurosci. *7*, 153–160.

Menon, V., Freeman, W.J., Cutillo, B.A., Desmond, J.E., Ward, M.F., Bressler, S.L., Laxer, K.D., Barbaro, N., and Gevins, A.S. (1996). Spatio-temporal correlations in human gamma band electrocorticograms. Electroencephalogr. Clin. Neurophysiol. *98*, 89–102.

Miller, R. (1991). Cortico-Hippocampal Interplay (New York: Springer-Verlag).

Montgomery, S.M., and Buzsáki, G. (2007). Gamma oscillations dynamically couple hippocampal CA3 and CA1 regions during memory task performance. Proc. Natl. Acad. Sci. USA *104*, 14495–14500.

Mormann, F., Fell, J., Axmacher, N., Weber, B., Lehnertz, K., Elger, C.E., and Fernandez, G. (2005). Phase/amplitude reset and theta-gamma interaction in the human medial temporal lobe during a continuous word recognition memory task. Hippocampus *15*, 890–900.

Muir, G.M., and Bilkey, D.K. (1998). Synchronous modulation of perirhinal cortex neuronal activity during cholinergically mediated (type II) hippocampal theta. Hippocampus *8*, 526–532.

O'Keefe, J., and Burgess, N. (2005). Dual phase and rate coding in hippocampal place cells: theoretical significance and relationship to entorhinal grid cells. Hippocampus *15*, 853–866.

O'Keefe, J., and Recce, M.L. (1993). Phase relationship between hippocampal place units and the EEG theta rhythm. Hippocampus *3*, 317–330.

Paré, D., and Gaudreau, H. (1996). Projection cells and interneurons of the lateral and basolateral amygdala. Distinct firing patterns and differential relation to theta and delta rhythms in conscious cats. J. Neurosci. *16*, 3334–3350.

Pesaran, B., Pezaris, J.S., Sahani, M., Mitra, P.P., and Andersen, R.A. (2002). Temporal structure in neuronal activity during working memory in macaque parietal cortex. Nat. Neurosci. *5*, 805–811.

Petsche, H., Stumpf, C., and Gogolak, G. (1962). The significance of the rabbit's septum as a relay station between the midbrain and the hippocampus. I. The control of hippocampus arousal activity by the septum cells. Electroencephalogr. Clin. Neurophysiol. *14*, 202–211.

Raghavachari, S., Kahana, M.J., Rizzuto, D.S., Caplan, J.B., Kirschen, M.P., Bourgeois, B., Madsen, J.R., and Lisman, J.E. (2001). Gating of human theta oscillations by a working memory task. J. Neurosci. *21*, 3175–3183.

Rizzuto, D.S., Madsen, J.R., Bromfield, E.B., Schulze-Bonhage, A., Seelig, D., Aschenbrenner-Scheibe, R., and Kahana, M.J. (2003). Reset of human neocortical oscillations during a working memory task. Proc. Natl. Acad. Sci. USA *100*, 7931–7936.

Schoffelen, J.M., Oostenveld, R., and Fries, P. (2005). Neuronal coherence as a mechanism of effective corticospinal interaction. Science *308*, 111–113.

Sederberg, P.B., Kahana, M.J., Howard, M.W., Donner, E.J., and Madsen, J.R. (2003). Theta and gamma oscillations during encoding predict subsequent recall. J. Neurosci. *23*, 10809–10814.

Semba, K., and Komisaruk, B.R. (1978). Phase of the theta wave in relation to different limb movements in awake rats. Electroencephalogr. Clin. Neurophysiol. *44*, 61–71.

Siapas, A.G., Lubenov, E.V., and Wilson, M.A. (2005). Prefrontal phase locking to hippocampal theta oscillations. Neuron *46*, 141–151.

Silva, L.R., Amitai, Y., and Connors, B.W. (1991). Intrinsic oscillations of neocortex generated by layer 5 pyramidal neurons. Science *251*, 432–435.

Sirota, A., and Buzsáki, G. (2007). Interaction between neocortical and hippocampal networks via slow oscillations. Thalamus Relat. Syst. *3*, 245–259.

Sirota, A., Csicsvari, J., Buhl, D., and Buzsáki, G. (2003). Communication between neocortex and hippocampus during sleep in rodents. Proc. Natl. Acad. Sci. USA *100*, 2065–2069.

Somogyi, P., and Klausberger, T. (2005). Defined types of cortical interneurone structure space and spike timing in the hippocampus. J. Physiol. *562*, 9–26.

Steriade, M., and Amzica, F. (1996). Intracortical and corticothalamic coherency of fast spontaneous oscillations. Proc. Natl. Acad. Sci. USA *93*, 2533–2538.

Sukov, W., and Barth, D.S. (1998). Three-dimensional analysis of spontaneous and thalamically evoked gamma oscillations in auditory cortex. J. Neurophysiol. *79*, 2875–2884.

Swanson, L.W. (1981). A direct projection from ammon's horn to prefrontal cortex in the rat. Brain Res. *217*, 150–154.

Swanson, L.W., and Kohler, C. (1986). Anatomical evidence for direct projections from the entorhinal area to the entire cortical mantle in the rat. J. Neurosci. *6*, 3010–3023.

Thierry, A.M., Gioanni, Y., Degenetais, E., and Glowinski, J. (2000). Hippocampo-prefrontal cortex pathway: anatomical and electrophysiological characteristics. Hippocampus *10*, 411–419.

Tierney, P.L., Degenetais, E., Thierry, A.M., Glowinski, J., and Gioanni, Y. (2004). Influence of the hippocampus on interneurons of the rat prefrontal cortex. Eur. J. Neurosci. *20*, 514–524.

Ulrich, D. (2002). Dendritic resonance in rat neocortical pyramidal cells. J. Neurophysiol. *87*, 2753–2759.

Vanderwolf, C.H. (1969). Hippocampal electrical activity and voluntary movement in the rat. Electroencephalogr. Clin. Neurophysiol. *26*, 407–418.

Varela, F., Lachaux, J.P., Rodriguez, E., and Martinerie, J. (2001). The brainweb: phase synchronization and large-scale integration. Nat. Rev. Neurosci. *2*, 229–239.

Vertes, R.P., Albo, Z., and Viana, D.P. (2001). Theta-rhythmically firing neurons in the anterior thalamus: implications for mnemonic functions of Papez's circuit. Neuroscience *104*, 619–625.

Witter, M.P. (1993). Organization of the entorhinal-hippocampal system: a review of current anatomical data. Hippocampus *3 Spec No*, 33–44.

Womelsdorf, T., Schoffelen, J.M., Oostenveld, R., Singer, W., Desimone, R., Engel, A.K., and Fries, P. (2007). Modulation of neuronal interactions through neuronal synchronization. Science *316*, 1609–1612.

Wyart, V., and Tallon-Baudry, C. (2008). Neural dissociation between visual awareness and spatial attention. J. Neurosci. *28*, 2667–2679.

Hippocampal place cell assemblies are speed-controlled oscillators

Caroline Geisler, David Robbe, Michaël Zugaro*, Anton Sirota, and György Buzsáki†

Center for Molecular and Behavioral Neuroscience, Rutgers, The State University of New Jersey, 197 University Avenue, Newark, NJ 07102

Edited by Nancy J. Kopell, Boston University, Boston, MA, and approved March 28, 2007 (received for review November 14, 2006)

The phase of spikes of hippocampal pyramidal cells relative to the local field θ oscillation shifts forward (''phase precession'') over a full θ cycle as the animal crosses the cell's receptive field (''place field''). The linear relationship between the phase of the spikes and the travel distance within the place field is independent of the animal's running speed. This invariance of the phase–distance relationship is likely to be important for coordinated activity of hippocampal cells and space coding, yet the mechanism responsible for it is not known. Here we show that at faster running speeds place cells are active for fewer θ cycles but oscillate at a higher frequency and emit more spikes per cycle. As a result, the phase shift of spikes from cycle to cycle (i.e., temporal precession slope) is faster, yet spatial-phase precession stays unchanged. Interneurons can also show transient-phase precession and contribute to the formation of coherently precessing assemblies. We hypothesize that the speed-correlated acceleration of place cell assembly oscillation is responsible for the phase–distance invariance of hippocampal place cells.

cell assembly | interneurons | phase locking | phase precession | θ oscillations

While animals navigate in an environment, the hippocampal local field potential (LFP) is characterized by a highly regular θ oscillation (8–10 Hz). Principal cells in the hippocampus show place-specific firing by two criteria. First, the firing is tuned to a particular location (''place field''), showing a bell-shaped tuning curve centered around its preferred location (1). Second, the timing of spikes within subsequent θ cycles systematically shifts forward (''phase precession''), ≈1 full cycle in total, as the rat runs through the place field of the neuron (2, 3) (see also Fig. 1 *A* and *B*). Both the firing rate and discharge phase within a θ cycle are correlated with the rat's position. However, how the rate change and θ-phase precession of spikes are related is poorly understood. The available experiments support both a rate-phase interdependence (4–6) and independence (7).

Several explanations for the place–phase relationship were put forward (4–6, 8–18). To confront these models, we examined the relationship among running speed, oscillation frequency of place cells and LFP θ, and timing of spikes within the θ cycle. We show that principal cells oscillate at a frequency faster than the simultaneously recorded LFP θ oscillation, and that this oscillation frequency depends on the rat's running speed. Together with the place- and speed-dependent oscillation frequencies of interneurons, the findings support the hypothesis that place coding results from coordinated network activity. We propose that the locomotion speed-dependent oscillation of place cell assemblies may underlie the mechanisms responsible for distance encoding in the hippocampus.

Results

We recorded the firing patterns of pyramidal cells, interneurons, and the LFP from the CA1 pyramidal layer of rats as they ran on a U-shaped or circular track for water reward. Fig. 1*A* shows the relationship among LFP θ oscillation, place cell firing, and the rat's position on the track in two selected trials, during which the average speed of the rat in the place field was slow (31 cm/sec) and fast (55 cm/sec), respectively. During the slow trial, it took the rat 12 θ cycles to run through the place field of the neuron. In contrast, during the fast trial, it took only seven cycles. The average number of spikes per θ cycle was higher during the faster run, but the total numbers of spikes emitted in the place field are comparable in the two trials (11 spikes during the slow trials and 12 spikes during the fast trial). This shortening of the interspike intervals during faster runs leads to a higher average firing rate within the place field [see ref. 7 and supporting information (SI) Fig. 7]. Nevertheless, the relationship between the rat's position on the track and the θ phase at which the place cell emitted spikes (''spatial-phase precession'') was very similar, as indicated by the distance–phase relationship of the 20% slowest (11 trials, average speed 24 cm/sec) and 20% fastest trials (11 trials, average speed 54 cm/sec) (Fig. 1*B*). The autocorrelogram of the spike phases relative to θ shows a strong oscillatory modulation (Fig. 1*C*). Furthermore, the phase advance of the spikes relative to θ was steeper in fast than in slow trials. Similarly, the autocorrelogram of the spike times oscillated faster in fast trials compared with slow trials and accelerated relative to the spike-triggered average of the LFP (Fig. 1*D*).

Oscillation Frequency of Place Cells Correlates with Running Speed. Running speed affected the oscillation frequency of place cells and the relationship between spikes and θ phase (Fig. 1 *C* and *D*). As illustrated in Fig. 1 *C* and *D*, speed exerted a larger effect on the oscillation frequency of place cells relative to the spike-triggered LFP so that at a faster speed the cycle-by-cycle phase advancement of spikes (temporal phase precession) was steeper.

For cell-group comparison, we computed the power spectra of the spike trains of all place cells during place field crossing, interneurons during complete trials, and the corresponding LFP segments separately for fast (upper 50%) and slow (lower 50%) speed runs (Fig. 2). The oscillation frequency of place cells increased with speed in 79 of 85 (94%) place fields, and, as evidenced, the peak in the power spectra of place cells is shifted to higher frequencies for faster runs (Fig. 2*A*). The speed-dependent frequency increase was larger for place cells than for the LFP corresponding to the segments while the rat crossed the place fields (Fig. 2*A*: place cells, 0.9 ± 0.7 Hz; LFP, 0.4 ± 0.3 Hz; $P = 4e\text{-}7$, rank-sum test; see also Fig. 2 *C* and *D*). Furthermore, the frequency shift was larger for greater speed differences between the fast and slow trials. Although interneurons also oscillated faster at faster running speeds, the speed-dependent

Author contributions: C.G. and G.B. designed research; C.G., D.R., and M.Z. performed research; C.G. and A.S. contributed new analytic tools; C.G., D.R., and M.Z. analyzed data; and C.G. and G.B. wrote the paper.

The authors declare no conflict of interest.

This article is a PNAS Direct Submission.

Abbreviations: C.I., confidence interval; LFP, local field potential.

*Present address: CNRS-Collège de France, LPPA, 11 Place Marcelin Berthelot, 75005 Paris, France.

†To whom correspondence should be addressed. E-mail: buzsaki@rutgers.edu.

This article contains supporting information online at www.pnas.org/cgi/content/full/0610121104/DC1.

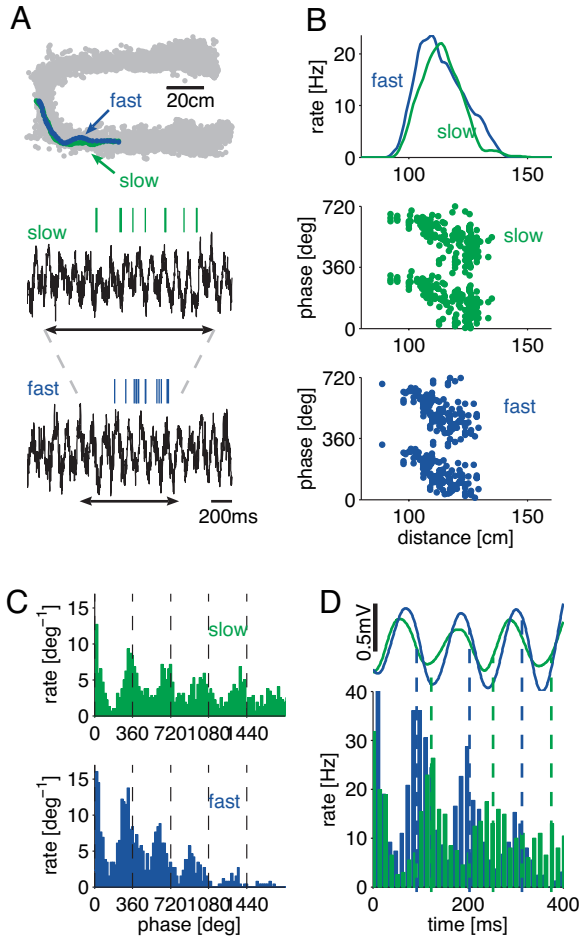

Fig. 1. Speed affects oscillation frequency of place cells. (*A*) Trajectories of the rat through a place field on two trials with different speeds [*Top*: green, slow trial (mean speed 31 cm/sec); blue, fast trial (mean speed 55 cm/sec)]. (*Middle* and *Bottom*) Spikes of one place cell and the corresponding LFP of the same two trials. The black arrows indicate the time it takes for the rat to cross the place field. (*B*) Smoothed firing rates (tuning curves) and position vs. spike phase of θ (spatial-phase precession) of the neuron (phases are plotted twice for better visibility). Trials were sorted by speed and divided into fast (upper 20%, 11 trials) and slow (lower 20%, 11 trials) trials. (*C*) Autocorrelograms of spike phases during slow (*Upper*) and fast (*Lower*) trials. (*D*) Autocorrelograms of spike times and above spike-triggered average of the LFP using all spikes in the 20% fastest and 20% slowest trials, respectively. Note the larger phase advance of place cells during fast runs.

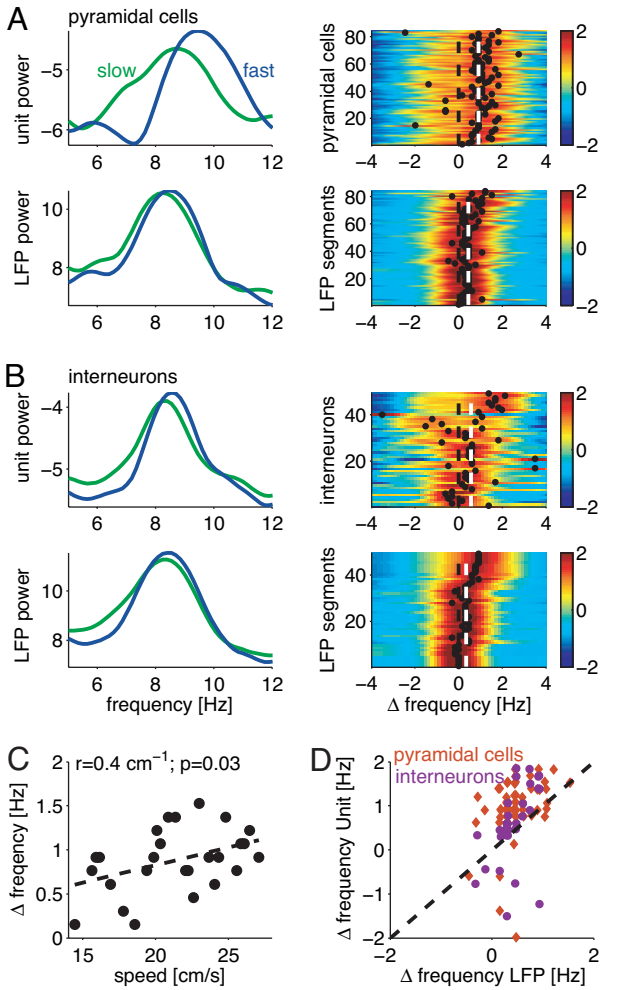

Fig. 2. Speed modulates oscillation frequency of place cells. (*A*) (*Left*) The power spectra of fast (upper 50%) and slow (lower 50%) runs of a single place cell and the LFP segments during the place field crossing. The frequency shift between these spectra was determined by computing the maximum of their cross-correlograms. (*Right*) Most place cells show a positive frequency shift between fast and slow runs. The cross-correlograms for all place cells are normalized by their SD, and their amplitude is color-coded. The black dots mark the maxima of the cross-correlograms, and the dashed line marks zero frequency lag. The place fields are sorted by the speed difference between the fast and slow trials (ranging from $\Delta f = 5$ cm/sec to $\Delta f = 25$ cm/sec). Note the larger frequency shift for a larger speed difference ($n = 84$ place fields from 48 CA1 pyramidal cells). (*B*) Same as in *A*, but for interneurons. Speed difference between the fast and slow trials ranges from $\Delta f = 4$ cm/sec to $\Delta f = 19$ cm/sec ($n = 20$ CA1 interneurons; the two running directions were treated separately). (*C*) Frequency difference between neuronal and LFP oscillations as a function of speed (dots, mean of five trials). Note the positive correlation between speed and the frequency shift. (*D*) Frequency shifts of units as a function of the associated shifts in LFP θ. Values above the dashed line indicate a larger frequency increase due to speed for units than for the corresponding LFP. Note that most of the pyramidal cells lie above the diagonal.

increase in oscillation frequency for the whole group was not significantly larger than the speed-dependent frequency increase of the corresponding LFP segments, when the spectra were computed over the entire length of the running track (Fig. 2*B*: interneurons, 0.6 ± 1.2 Hz; LFP, 0.3 ± 0.3 Hz; $P = 0.24$, rank-sum test; see also Fig. 2*D* and SI Fig. 8).

Time Compression of Place Cell Sequences Is Speed-Dependent. Previous works have shown that information about the past, present, and future positions of the animal and the distances among the respective place fields is "compressed" into time lags between spikes within a θ cycle (3, 19). The time compression is defined as a ratio of the time it takes the animal to travel between two place fields and the time lag between the spikes of the two corresponding place cells within one θ cycle (19). Because speed affected the phase vs. time slope of individual neurons, we examined whether speed also affects the temporal compression. Fig. 3*A* illustrates a pair of neurons with overlapping place fields. As expected, the time difference between the peak firing of the respective neurons varied as a function of running speed because during slower runs it took proportionally more time for the rat to traverse the same distance (Fig. 3 *B* and *C*). In contrast, the time offsets of the neuron pair at the time scale of the θ period was speed-independent for the population (Fig. 3*D*). Similarly, the phase difference of the neurons within the θ cycle remained unaffected by the speed differences (see SI Fig. 9). Because the temporal distance between place fields within the θ cycle does not depend on speed, but the travel time between place fields

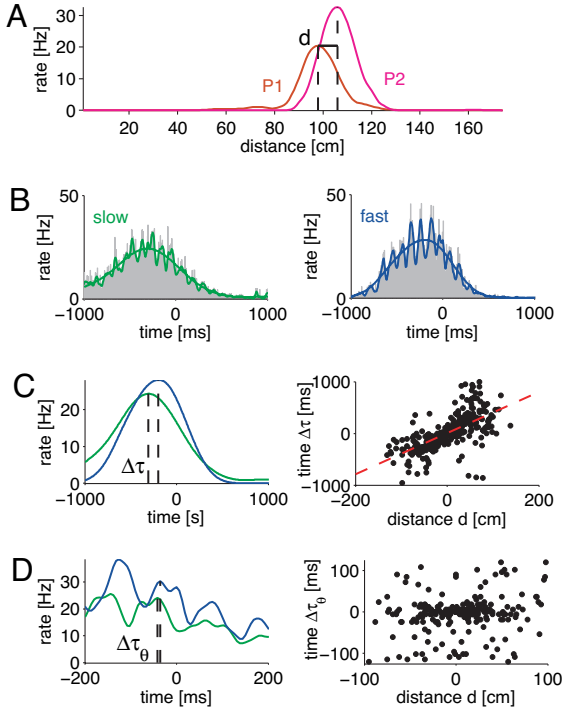

Fig. 3. Sequence compression of place cells varies as a function of speed. (*A*) Tuning curves of two place cells (P1, P2) with overlapping fields and a distance *d* between field centers. (*B*) Cross-correlograms between the two neurons for slow (*Left*, lower 50%) and fast (*Right*, upper 50%) trials, low-pass filtered at 1.5 Hz (time scale of travel time between place fields) and 40 Hz (time scale of θ). The peak of the cross-correlogram filtered at 1.5 Hz indicates the travel time between the centers of two place fields. (*C*) The cross-correlograms filtered at 1.5 Hz from *B* for fast and slow trials. (*Left*) It takes $\Delta\tau$ longer to cross between the place fields in slow runs than in fast runs. (*Right*) This travel time difference $\Delta\tau$ is linearly correlated with the distance *d* between the place fields, as shown for all cell pairs. (*D*) (*Left*) The cross-correlograms filtered at 40 Hz from *B* for fast and slow trials. (*Right*) The time difference $\Delta\tau_\theta$ between the fast and slow trials within one θ cycle does not depend on the distance *d*, as shown for all cell pairs. For all group plots, $n = 96$ place fields of 55 CA1 pyramidal cells were used, corresponding to 801 pairs.

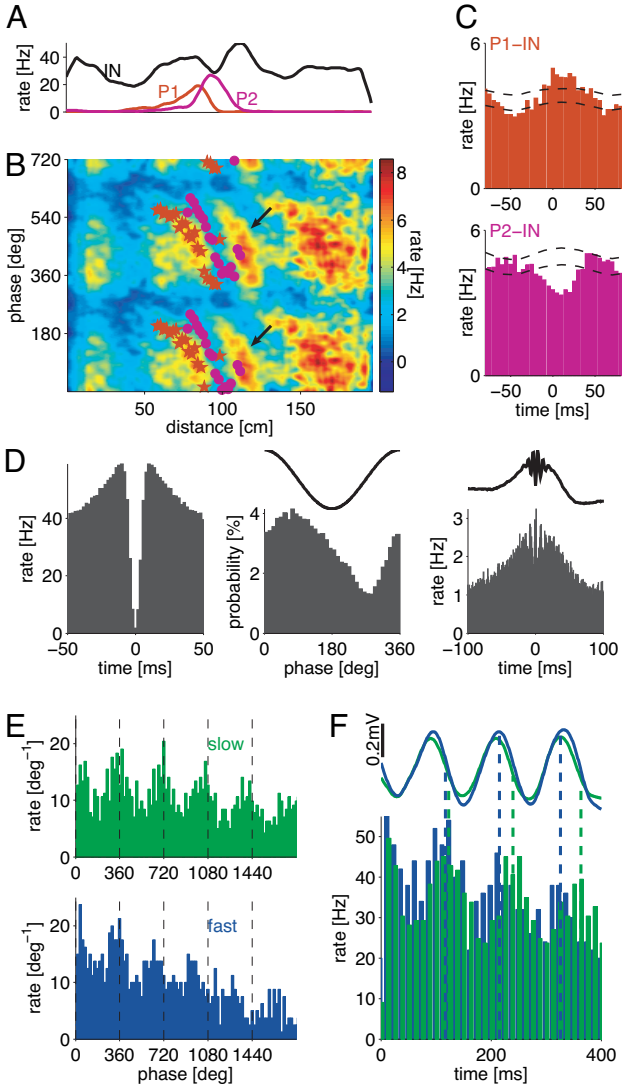

Fig. 4. Interneurons segregate place cell assemblies. (*A*) Firing rates of two pyramidal cells (red, P1; magenta, P2) and an interneuron (black, IN) as a function of distance on the running track. (*B*) Phase precession of interneuron spikes. The interneuron's color-coded smoothed density of firing is plotted as a function of θ phase and the rat's position on the track. Phase distributions are shown twice for better visibility. Stars and dots indicate the running mean phase of P1 and P2, respectively. Note the similar phase slope of P1 and the interneuron. (*C*) Temporal cross-correlation between P1 and interneuron IN and P2 and the same interneuron IN. Note the opposite phase relationship of P1 and P2. The dashed lines indicate the 95% confidence interval (C.I.) for shuffled spike trains such that the phase is conserved. Distribution that exceeds the C.I. is significantly more correlated or anticorrelated than could be expected simply by common phase locking. (*D*) Autocorrelogram, θ-spike cross-correlogram, and ripple-spike cross-correlogram of the interneuron. (*E*) Autocorrelogram of the interneuron's spike phases during 10% slowest (five trials, average speed 19 cm/sec) and 10% fastest (five trials, average speed 40 cm/sec) runs across the field marked by black arrows in *B*. (*F*) Superimposed autocorrelograms of spike times of the same trials as in *E* and the spike-triggered average (using all spikes from the slow and fast trials, respectively) of the related θ oscillation from the CA1 pyramidal layer during slow and fast runs across the field marked by black arrows in *B*. Note the steeper phase advancement of the interneuron spikes during faster speed.

does, the temporal compression of place cell sequences is interpretable only if information about speed is also available.

Interneurons Shape Cell Assemblies. Interneurons form heterogeneous groups (20), and identification of group members by physiological criteria alone is not always possible (21). Consequently, we could not rationally cluster all individual interneurons into subgroups. When viewed as a single group, the oscillation frequency of most interneurons also increased with speed (Fig. 2 *B* and *D*). However, in agreement with previous observations, several interneurons showed definable place fields, although these were typically multiple and less pronounced than those of the pyramidal cells (22, 23, 25, 59). Because spike-transmission probability between place cells and interneurons can be quite reliable (23, 26, 27), it is expected that some spikes emitted by interneurons are driven by their presynaptic place cells (59). In support of this hypothesis, we found that 8 of the 25 interneurons showed phase precession in at least one location of the track (Fig. 4).

Even interneuron–pyramidal cell pairs that were not directly monosynaptically connected (Fig. 4) showed comparable phase precession and correlated firing (cell P1 and interneuron in Fig. 4 *A–D*), suggesting that both cells belonged to the same cell assembly and their spiking was timed by some common input. In contrast, interneuron–pyramidal cell pairs with anticorrelated discharge within the θ cycle had shifted place fields (cell P2 and interneuron in Fig. 4 *A–D*) and likely belonged to different, competing assemblies. The consequence of this interaction is that an interneuron driven by a place cell can exert a precisely

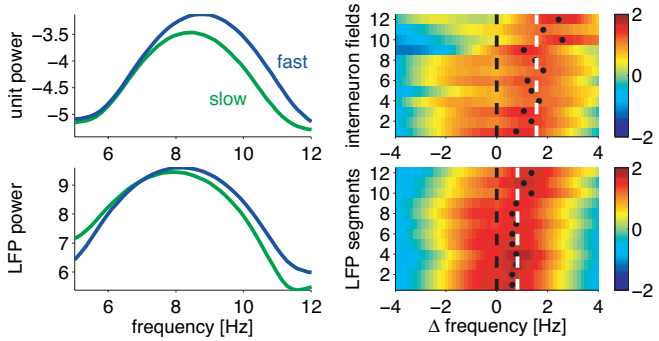

Fig. 5. Oscillation frequency of phase-precessing interneurons is speed-dependent. The power spectra are calculated only for spikes and LFP during segments when the rat crosses the interneuron's place field (compare with Fig. 2*B*). Interneurons increase their oscillation frequency significantly more with faster running speed than the LFP [interneurons, mean (Δf) = 0.8 ± 0.7; LFP, mean(Δf) = 1.5 ± 0.9; $P < 0.01$]. Fields were sorted according to the speed difference between fast and slow trials (speed differences ranged from 5 to 25 cm/sec). Spectra were computed for 12 place fields of eight interneurons.

timed inhibition on other pyramidal cells and effectively segregate the current assembly from other competing assemblies.

Interneurons that displayed phase precession showed an increased oscillation frequency beyond that of LFP, with increased running speed within their place fields similar to what was found for pyramidal cells (compare Fig. 1 *C* and *D* with Fig. 4 *E* and *F*). The overall speed-dependent frequency change of interneurons within their place fields was comparable to that of pyramidal cells (compare Fig. 2*A* with Fig. 5).

Some interneurons showed no indication of phase precession, but instead displayed a relatively fixed-phase relationship with the θ cycle (Fig. 6). The illustrated cell's preferred θ phase of discharge (circular mean phase 297°), its increased firing preceding sharp-wave ripples, and its location above the pyramidal cell layer suggest that it may correspond to an oriens lacunosum-moleculare or long-range interneuron (21). Thus, some interneuron classes may keep a fixed θ-phase relationship, whereas other types can be effectively driven by place cell assemblies.

Discussion

The main finding of these experiments is a correlation between speed and oscillation frequency of hippocampal place cells and interneurons. We hypothesize that the "gain" of the oscillation frequency of pyramidal cell–interneuron assemblies with respect to speed can account for the invariant travel distance vs. spike–phase relationship. This hypothesis offers a novel perspective on the cell assembly coordination by hippocampal θ oscillation. We hypothesize that the combination of speed and spatial inputs gives rise to a transient oscillation of sequentially activated cell assemblies. Phase precession is a consequence of this more fundamental mechanism.

Speed-Dependent Oscillation of Place Cells Can Keep the Spike Phase Versus Position Relation Invariant. Previous experiments have shown that the phase precession slope of place cells correlated with the size of its place field (7, 19, 28) so that the total phase precession is always about one full θ cycle, and that both the phase precession slope and field size increase along the septo-temporal axis of the hippocampus (29). It has been suggested that phase precession can be produced by faster oscillating pyramidal cells than the LFP, and it has been shown that the phase–space relationship is speed-independent (2), but no mechanisms were provided. Here we directly show that the temporal-phase precession slope, and therefore the oscillation frequency of place cells, is positively correlated with the locomotion speed

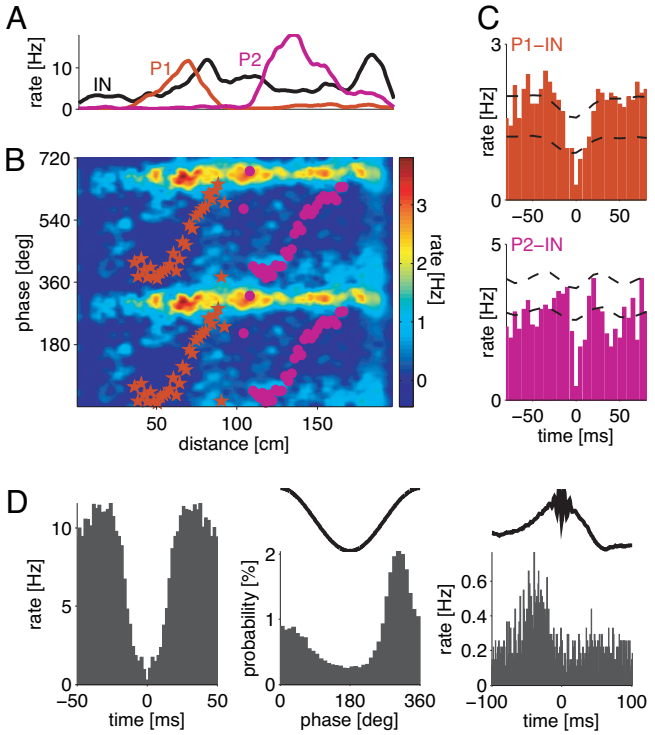

Fig. 6. Nonphase-precessing interneuron. (*A*) Firing rates of two pyramidal cells (red, P1; magenta, P2) and an interneuron (black, IN) as a function of distance on the running track. (*B*) The spikes of the interneuron are locked to a small phase range (compare Fig. 4). The circular mean phases of the two simultaneously recorded pyramidal cells are marked with red dots and magenta stars, respectively. (*C*) Temporal cross-correlograms between P1 and interneuron IN and P2 and the same interneuron IN. Note that both pyramidal cells are anticorrelated to the activity on the interneuron. The dashed lines give the 95% C.I. for phase locking; cross-correlograms exceeding this C.I. have a significant correlation beyond phase locking. (*D*) Autocorrelogram, θ-spike cross-correlogram, and ripple–spike cross-correlogram of the interneuron.

of the rat, such that the phase–distance relationship remains invariant.

One possible explanation for the speed effect on the oscillation frequency of place cells is that the frequency is controlled by the activation of voltage-dependent intrinsic mechanisms that support oscillations in single pyramidal cells (5, 8, 9, 13, 30–34). However, this individuated oscillation cannot account for several experimental observations (7, 24, 35). As an alternative, we hypothesize that simultaneously activated neurons interact and form oscillating assemblies whose oscillation frequency is controlled by afferents that correlate with the locomotion speed of the animal.

The phase of spikes within the θ cycle correlates with a number of variables, including the position of the animal, the time from the beginning of the run, the time since entering the place field, and the instantaneous firing rate of the neuron (2–4, 6, 7, 36). Because the strongest correlation occurs between position and spike phase (7), it has been suggested that the spike phase is determined by sensory inputs, and that the spike-phase precession phenomenon can be regarded as a mechanism for coding the spatial relations between environmental signals (2, 3, 7, 16, 36, 37). However, it is not clear what mechanism is responsible for aligning the environmental signals to the phase of the internally generated θ rhythm. Furthermore, the slope of the phase precession remains the same in the dark (38), eliminating the crucial role of visual cues in the spike phase.

An alternative explanation for the strong phase–position

correlation is that environmental, idiothetic, or internal cues trigger a transient oscillation in a unique cell assembly. We assume that assembly oscillation of place cells is a transient phenomenon, lasting for ≈1 sec in the dorsal hippocampus (7, 19, 39). The oscillation frequency of an active place cell assembly is under the control of speed inputs as shown here. If the running speed is constant, the cycle-by-cycle phase shift (i.e., the temporal-phase precession determined by the frequency of the oscillating assembly) and the phase–distance relationship provide the same accuracy in predicting distance (8, 13). However, because the speed variability, the temporal-phase precession, and the phase–distance relationship are out of register, it is necessary to tune the oscillation frequency of the activated cell assembly as shown here. The result of this adjustment is that the spike-phase assignment remains invariant relative to travel distance.

However, it remains unanswered what tunes the oscillation frequency precisely, such that phase precession spans ≈1 full θ cycle and starts at the same phase. One possibility is that the phase-precessing assemblies should not be viewed as independent units, but as part of the rhythm-generating mechanism. The transiently oscillating cell assemblies may be coupled through variable delays so that the successive oscillators are trailing relative to each other (40). By way of this hypothetical mechanism, place cells may play a critical role in θ-rhythm generation, although they individually oscillate faster than the θ field.

Distance Representation by Time Compression Is Speed-Dependent. In the CA1 region of the hippocampus, the ordered spatial distances between sequential locations are represented by multiple assemblies and "compressed" into the θ cycle because of the location-specific phase segregation of cells (3, 19, 36, 41). It has been suggested that the distances between place fields, represented by the respective assemblies, are encoded by the synaptic strengths between CA3-CA3 and CA3-CA1 connections (42). A prediction of this hypothesis is that the temporal intervals of assembly sequences within θ cycles should reflect distance representations, independent of other variables, such as the speed of motion. Our observations confirm this prediction. The temporal relationship of cell pairs within the θ cycle, representing distances, remained constant within the natural variability of running speed. Because the θ scale–time relationship between cell pairs is fixed, whereas the elapsed time required to run from one place field to the other depends on the speed of locomotion, the magnitude of temporal compression should vary as shown here. Thus, the magnitude of temporal compression is informative only if corrected by the speed.

Without speed information, the discharge rate of place cells alone is ambiguous for defining the animal's current location because the firing rate of hippocampal place cells is correlated with speed (25, 43, 44). Conversely, the discharge rate of pyramidal cells may not independently "code" for speed either (but see refs. 7 and 37) because the rate is a combined effect of speed and the rat's position. Instead, we hypothesize that the assemblies that receive similar information (representing the same location) will oscillate at a similar speed-adjusted frequency and synchronize with a constant phase–time relationship.

Interneurons Contribute to the Formation of Cell Assemblies. Further support for the assembly representation of external information in the hippocampus is the phase precession of interneurons. Although interneurons are usually not considered to carry specific information, several previous studies have noted that interneuron spikes are not distributed homogeneously over the visited places (22, 25), and interneuron firing rates can vary specifically with task demands (45).

A potential mechanism responsible for the place-specific firing and phase precession of some interneurons (see also ref. 59) is the firing-frequency tunability of the pyramidal cell–interneuron synapse (23, 46–48) and their low-discharge threshold (26, 27). Furthermore, soma targeting interneurons are endowed with resonant properties that allow them to respond maximally when presynaptic neurons fire in the γ-frequency range (23, 34), whereas dendrite-targeting interneurons respond best at θ frequency (49, 50). Therefore, the recruited interneurons have the ability to segregate small assemblies of principal cells by temporarily silencing competing assemblies.

We hypothesize that, within the place field, perisomatic interneurons are entrained to the fast-firing place cells, and the spikes of the formed assembly members oscillate coherently. As shown here, the magnitude of the cycle-by-cycle temporal shift of spikes is controlled by speed. Conversely, during episodes where the interneuron does not phase precess, it might receive input from many place cells equally. Because the highest firing probability of place cells is at the trough of θ, the interneuron receives the strongest input at the trough of θ during each cycle. We hypothesize that interneurons phase precess only when a particular place cell assembly dominates their drive.

The absence of phase precession in some interneurons may be explained in two different ways. First, all interneurons show phase procession when driven exclusively or predominantly by a given oscillating cell assembly. Under this hypothesis, our failure to observe phase precession in every interneuron might be explained by not testing the neuron exhaustively in multiple environments. Second, dendrite-targeting interneuron types are not effectively recruited by place cells. Our finding that some interneurons showed a very narrow phase preference of spiking is in favor of this possibility. It will be important in future research to determine the anatomical identity of such θ phase-fixed interneurons.

The speed-controlled assembly oscillator hypothesis, as opposed to the individuated cell oscillator (4–6, 8, 9, 13, 32), can explain why on individual trials with dramatically different firing rates the spatial-phase precession slope of single place cells can remain unaltered (7). Rate variability can occur because assembly oscillation is a cooperative product where timing of spikes remains robust despite the variation of individual firing rates (51–53). In addition, the oscillating cell assembly hypothesis can also account for the observation that spikes of single place cells can switch assembly membership even within a single θ cycle (24).

Methods

Experimental Procedures. Six adult male Long-Evans rats (250–300 g) were implanted with either movable tetrodes in the hippocampus (35) or silicon probes (54) following National Institutes of Health guidelines. They were trained to shuttle back and forth between two water cups on a U-shaped maze (35) or on an elevated circular maze (55). Two small light-emitting diodes (10-cm separation) mounted above the head stage were used to track the rats' positions (sampled at 40 Hz).

Data Acquisition and Analysis. Wide-band (1 Hz–5 kHz) signals were acquired at 20 kHz on a 64-channel DataMax system (RC Electronics, Santa Barbara, CA). For offline spike sorting, the wide-band signals were digitally high-pass filtered (0.8–5 kHz). Units were then identified and isolated by a semiautomatic cluster-cutting algorithm (56, 57).

Cell Identification and Place Fields. Cells were classified into putative interneurons and pyramidal cells by their firing rate, autocorrelogram, and spike-wave shape (26). Pyramidal neurons without clearly defined place fields (4) were not included. The place field was defined as the continuous area in one direction of running within which the firing rate was >0 or when the neuron would fire over large parts of the maze, $>10\%$ of the maximal firing rate (7). The place fields of interneurons that

showed clear phase precession were selected manually. A total of 96 place fields of 55 CA1 pyramidal cells were analyzed. Further, 25 interneurons were included in this study. Different directions of running were treated separately, resulting in 49 interneuron firing fields. For the analysis of interneurons in Fig. 5, episodes of phase precession were selected manually when phase precession was clearly visible. The firing within those place fields was then analyzed identically to that of pyramidal cells.

Running Speed. The instantaneous running speed was calculated offline from the rat's position on the maze. The speed was low-pass filtered to eliminate large speed changes due to the rat's head movement. Because running speed varied in different parts of the testing apparatus and the size of the place fields showed large variability, even for neurons recorded with the same electrode (19), the measurement of the rat's speed was restricted to the place field.

Speed-Dependent Trial Sorting. Trials were sorted by direction and average speed. Trials in which the rat did not complete the full path or stopped for exploration were discarded. The maze was linearized semimanually by orthogonally projecting all position points onto the averaged trajectory of the rat. To investigate the differences between fast and slow runs, the fastest 50% and slowest 50% were used unless mentioned otherwise.

Spectral Analysis and Frequency Shift. The spectra were computed by using multitaper estimators (58). The spectra were averaged across the 50% slowest and 50% fastest trials, respectively. To compute the speed-dependent frequency shift between units and LFP, we computed the cross-correlograms between the spectra and determined the frequency lag of the maximal correlation.

Distance Between Place Fields. The temporal relationship between overlapping place cells on the time scale of place field crossing and within a θ cycle was computed for fast and slow trials separately as described in ref. 19. The phase relationship between cells was determined by computing the cross-correlogram of the unwrapped θ phase of each spike.

We thank Sean Montgomery and Dr. Horacio Rotstein for comments on the manuscript, and Lénaïc Monconduit and Pavel E. Rueda-Orozco for collecting some of the data. This work was supported by National Institutes of Health Grants NS34994, NS43157, and MH54671 (to G.B.); and the Human Frontier Science Foundation (D.R. and M.Z.).

1. O'Keefe J, Nadel L (1978) *The Hippocampus as a Cognitive Map* (Oxford Univ Press, Oxford).
2. O'Keefe J, Recce ML (1993) *Hippocampus* 3:317–330.
3. Skaggs WE, McNaughton BL, Wilson MA, Barnes CA (1996) *Hippocampus* 6:149–172.
4. Harris KD, Henze DA, Hirase H, Leinekugel X, Dragoi G, Czurko A, Buzsáki G (2002) *Nature* 417:738–741.
5. Kamondi A, Acsady L, Wang XJ, Buzsáki G (1998) *Hippocampus* 8:244–261.
6. Mehta MR, Lee AK, Wilson MA (2002) *Nature* 417:741–746.
7. Huxter J, Burgess N, O'Keefe J (2003) *Nature* 425:828–832.
8. Bose A, Booth V, Recce M (2000) *J Comput Neurosci* 9:5–30.
9. Magee JC (2001) *J Neurophysiol* 86:528–532.
10. Booth V, Bose A (2001) *J Neurophysiol* 85:2432–2445.
11. Jensen O, Lisman JE (1996) *Learning and Memory* 3:264–278.
12. Koene RA, Gorchetchnikov A, Cannon RC, Hasselmo ME (2003) *Neural Netw* 16:577–584.
13. Lengyel M, Szatmary Z, Erdi P (2003) *Hippocampus* 13:700–714.
14. Magee JC (2003) *Trends Neurosci* 26:14–16.
15. Sato N, Yamaguchi Y (2003) *Neural Comput* 15:2379–2397.
16. Tsodyks MV, Skaggs WE, Sejnowski TJ, McNaughton BL (1996) *Hippocampus* 6:271–280.
17. Wallenstein GV, Hasselmo ME (1997) *Brain Res Bull* 43:485–493.
18. Yamaguchi Y (2003) *Biol Cybern* 89:1–9.
19. Dragoi G, Buzsaki G (2006) *Neuron* 50:145–157.
20. Freund TF, Buzsáki G (1996) *Hippocampus* 6:347–470.
21. Klausberger T, Magill PJ, Marton LF, Roberts JDB, Cobden PM, Buzsáki G, Somogyi P (2003) *Nature* 421:844–848.
22. Kubie JL, Muller RU, Bostock EM (1990) *J Neurosci* 10:1110–1123.
23. Marshall L, Henze DA, Hirase H, Leinekugel X, Dragoi G, Buzsáki G (2002) *J Neurosci* 22:1–5.
24. Maurer AP, Cowen SL, Burke SN, Barnes CA, McNaughton BL (2006) *Hippocampus* 16:785–794.
25. McNaughton BL, Barnes CA, O'Keefe J (1983) *Exp Brain Res* 52:41–49.
26. Csicsvari J, Hirase H, Czurko A, Buzsáki G (1998) *Neuron* 21:179–189.
27. Miles R (1990) *J Physiol* 431:659–676.
28. Terrazas A, Krause M, Lipa P, Gothard KM, Barnes CA, McNaughton BL (2005) *J Neurosci* 25:8085–8096.
29. Maurer AP, Vanrhoads SR, Sutherland GR, Lipa P, McNaughton BL (2005) *Hippocampus* 15:841–852.
30. Gillies MJ, Traub RD, LeBeau FE, Davies CH, Gloveli T, Buhl EH, Whittington MA (2002) *J Physiol* 543:779–793.
31. Hu H, Vervaeke K, Storm JF (2002) *J Physiol* 545:783–805.
32. Huhn Z, Orban G, Erdi P, Lengyel M (2005) *Hippocampus* 15:950–962.
33. Leung LS, Yu HW (1998) *J Neurophysiol* 79:1592–1596.
34. Pike FG, Goddard RS, Suckling JM, Ganter P, Kasthuri N, Paulsen O (2000) *J Physiol* 529:205–213.
35. Zugaro MB, Monconduit L, Buzsaki G (2005) *Nat Neurosci* 8:67–71.
36. Jensen O, Lisman JE (2000) *J Neurophysiol* 83:2602–2609.
37. O'Keefe J, Burgess N (2005) *Hippocampus* 15:853–866.
38. Moser EI, Moser MB, Lipa P, Newton M, Houston FP, Barnes CA, McNaughton BL (2005) *Neuroscience* 130:519–526.
39. Samsonovich A, McNaughton BL (1997) *J Neurosci* 17:5900–5920.
40. Williams TL, Sigvardt KA, Kopell N, Ermentrout GB, Remler MP (1990) *J Neurophysiol* 64:862–871.
41. Harris KD, Csicsvari J, Hirase H, Dragoi G, Buzsáki G (2003) *Nature* 424:552–556.
42. Muller RU, Stead M, Pach J (1996) *J Gen Physiol* 107:663–694.
43. Czurko A, Hirase H, Csicsvari J, Buzsaki G (1999) *Eur J Neurosci* 11:344–352.
44. Wiener SI, Paul CA, Eichenbaum H (1989) *J Neurosci* 9:2737–2763.
45. Wiebe SP, Staubli UV (2001) *J Neurosci* 21:3955–3967.
46. Abbott LF, Varela JA, Sen K, Nelson SB (1997) *Science* 275:220–224.
47. Thomson AM (2000) *Prog Neurobiol* 62:159–196.
48. Tsodyks M, Uziel A, Markram H (2000) *J Neurosci* 20:1–5.
49. Pouille F, Scanziani M (2004) *Nature* 429:717–723.
50. Whittington MA, Traub RD (2003) *Trends Neurosci* 26:676–682.
51. Scarpetta S, Marinaro M (2005) *Hippocampus* 15:979–989.
52. Wang XJ, Buzsáki G (1996) *J Neurosci* 16:6402–6413.
53. Rotstein HG, Pervouchine DD, Acker CD, Gillies MJ, White JA, Buhl EH, Whittington MA, Kopell N (2005) *J Neurophysiol* 94:1509–1518.
54. Csicsvari J, Henze DA, Jamieson B, Harris KD, Sirota A, Bartho P, Wise KD, Buzsáki G (2003) *J Neurophysiol* 90:1314–1323.
55. Robbe D, Montgomery SM, Thome A, Rueda-Orozco PE, McNaughton BL, Buzsáki G (2006) *Nat Neurosci* 9:1526–1533.
56. Harris KD, Henze DA, Csicsvari J, Hirase H, Buzsaki G (2000) *J Neurophysiol* 84:401–414.
57. Hazan L, Zugaro M, Buzsaki G (2006) *J Neurosci Methods* 155:207–216.
58. Jarvis MR, Mitra PP (2001) *Neural Comput* 13:717–749.
59. Maurer AP, Cowen SL, Burke SN, Barnes CA, McNaughton BL (2006) *J Neurosci* 26:13485–13492.

ELSEVIER

Journal of Neuroscience Methods 155 (2006) 207–216

JOURNAL OF NEUROSCIENCE METHODS

www.elsevier.com/locate/jneumeth

Klusters, NeuroScope, NDManager: A free software suite for neurophysiological data processing and visualization

Lynn Hazan [1], Michaël Zugaro [1], György Buzsáki *

Center for Molecular and Behavioral Neuroscience, Rutgers, The State University of New Jersey, Newark, NJ 07102, USA

Received 12 August 2005; received in revised form 6 January 2006; accepted 10 January 2006

Abstract

Recent technological advances now allow for simultaneous recording of large populations of anatomically distributed neurons in behaving animals. The free software package described here was designed to help neurophysiologists process and view recorded data in an efficient and user-friendly manner. This package consists of several well-integrated applications, including NeuroScope (http://neuroscope.sourceforge.net), an advanced viewer for electrophysiological and behavioral data with limited editing capabilities, Klusters (http://klusters.sourceforge.net), a graphical cluster cutting application for manual and semi-automatic spike sorting, NDManager (http://ndmanager.sourceforge.net), an experimental parameter and data processing manager. All of these programs are distributed under the GNU General Public License (GPL, see http://www.gnu.org/licenses/gpl.html), which gives its users legal permission to copy, distribute and/or modify the software. Also included are extensive user manuals and sample data, as well as source code and documentation.

Keywords: Spike sorting; Cluster cutting; Data mining; Unit activity; Local field potentials

1. Introduction

In recent years, remarkable technological advances have allowed neurophysiologists to record from large ensembles of anatomically distributed neurons in behaving rodents and primates (Buzsáki et al., 1992; Wilson and McNaughton, 1993; Wilson and McNaughton, 1994; Hampson et al., 1999; Hoffman and McNaughton, 2002; Csicsvari et al., 2003; Nicolelis et al., 2003; Buzsáki, 2004; Nicolelis, 1998; Eichenbaum and Davis, 2001). However, visualizing and processing the large amounts of data generated by modern recording systems requires efficient computer software. The free software package presented here consists of several well-integrated applications and tools designed to assist the experimenter in extracting and exploring brain signals, starting from raw (wide-band) or preprocessed (action potentials and local field potentials) signals typically recorded by hardware acquisition systems. The integrated package has been successfully used in recent studies (Khazipov et al., 2004; Zugaro et al., 2005).

The programs presented below are designed to process and explore data collected in experiments ranging from acute recordings in anesthetized animals to complex chronic recordings where brain signals are recorded from freely moving animals as they perform behavioral tasks in automated apparatuses. Thus, in the most complex cases, the data can consist of electrophysiological signals (action potentials and local field potentials), behavioral events (e.g., crossing of photodetectors, reward delivery) and video recordings (e.g., position tracking).

Of the three types of data, processing of electrophysiological signals is the most challenging. Extracellular electrodes typically record action potentials emitted by several nearby neurons, many of which are relegated as indiscrimnable 'noise', and occasionally artefacts generated by muscle activity, surrounding electrical devices and other sources.

Processing of electrophysiological data requires three steps (Fig. 1). First, putative action potentials ('spikes') must be detected and extracted from the wide-band signals in hardware or software. This is usually done first by high-pass filtering and thresholding, then by extracting an adequate number of voltage samples (e.g., corresponding to a time window of a spike) each time a predetermined threshold is crossed. Thus, each spike is described by a vector, the components

* Corresponding author. Tel.: +1 973 353 1080; fax: +1 973 353 1820.
E-mail address: buzsaki@axon.rutgers.edu (G. Buzsáki).
[1] These authors have contributed equally to the present work.

0165-0270/$ – see front matter © 2006 Elsevier B.V. All rights reserved.
doi:10.1016/j.jneumeth.2006.01.017

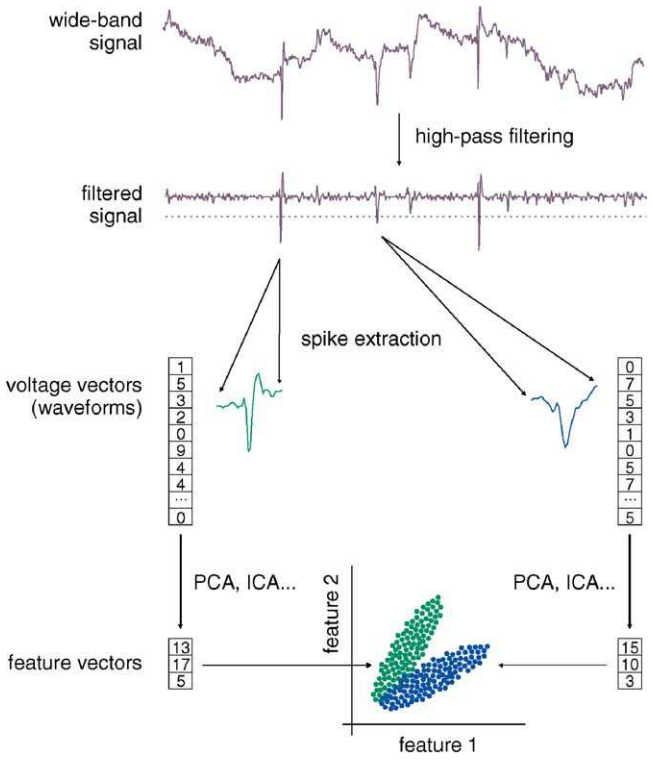

Fig. 1. Processing of electrophysiological spike data. First, wide-band continuous brain signals are high-pass filtered and thresholded to detect putative action potentials ('spikes'); waveforms are extracted around the peak of each spike. Second, the high-dimensionality of the waveforms is reduced for subsequent sorting, using e.g., principal component analysis. Finally, the resulting feature vectors are sorted. The goal of this process is to group the action potentials emitted by each single neuron into distinct clusters. Ideally, each recorded action potential is assigned to the neuron that emitted it.

of which are successive voltages in time. The second step is feature extraction. Although complete voltage vectors ('waveforms') are the most accurate description of the spikes, they are rarely appropriate for subsequent processing because of their high dimensionality. There are several methods to drastically reduce the number of components per spike while retaining most of the relevant information. These include principal component analysis (PCA, Abeles and Goldstein, 1977), independent component analysis (ICA, Jutten and Herault, 1991), factor analysis, and other related methods. The third step is 'spike sorting', where spikes are tentatively assigned to the individual neurons that have emitted them. This results in grouping spikes in different 'clusters' corresponding to different putative neurons (hence, this process is also referred to as 'cluster cutting'). Spike sorting is most efficiently performed by combining semi-automatic and manual approaches (Harris et al., 2000).

Action potentials of single cells are embedded in networks and related to behavior and the ultimate goal of spike detection is to reveal these relationships. Therefore, spikes should be displayed and compared to spikes of other neurons, local field potentials and behavioral events. To facilitate these analyses, we describe a number of computer applications and tools, which allow for processing and visual exploration of the data before subsequent quantitative analyses.

2. The software suite

What makes the package described here different from other existing offerings is threefold. First and foremost, it is free software distributed under the GNU General Public License (GPL, see http://www.gnu.org/licenses/gpl.html). With this license, our users are explicitly granted legal permission to copy and redistribute the software, as well as to modify it (or have someone modify it) using the source code. We therefore distribute the software both in binary and source forms (care was taken to develop high-quality, clear and documented code). We hope this will help form a community of interested investigators willing to contribute to the project. The second difference is that our software can be downloaded from the internet at no cost. The third difference is that because our software was developed within a neuroscience laboratory rather than by an external company, the feature set was directly chosen and defined by experimenters. This resulted in a package with numerous and relevant advanced features (such as the Error Matrix View or the Trace View in Klusters). In addition, constant and direct user feedback ensured that the programs featured easy and efficient user interfaces: intuitive and flexible layout of the graphical elements, numerous configurable keyboard shortcuts and consistent keyboard navigation, optimized display speed, highly responsive interface via multithreading, etc.

Our package runs on GNU/Linux and MacOS X and is expected to run on any Unix-like system that includes the KDE libraries and libxml2. We provide installable binary packages for Debian-based distributions (Debian, KNOPPIX, Kubuntu, etc.) and SUSE. Alternatively, the applications can be built from source (they are known to run on e.g., RedHat and MacOS X with Fink). Detailed information is available at the respective websites.

3. Data formats and preprocessing

Contrary to many data acquisition and processing programs, our software does not use a single file with a complex structure, but a collection of very simple files. This ensures that files are easy to read from and write to, and can thus be manipulated using any data analysis package without requiring complex import and export filters. There are dedicated files for continuous brain signals (wide-band .dat, local field potentials .eeg, high-pass filtered .fil, etc.), spike waveforms (.spk), feature vectors (.fet), spike clusters (.clu), behavioral events (.evt) and position tracking (data file formats are described in Supplementary Figs. 2 and 3). To reduce disk usage, potentially large files (continuous brain signals and spike waveforms) contain multiplexed binary data. All other files contain ASCII format data, making them easy to manipulate by standard Unix file utilities. Files are homogeneous and do not contain headers. All the relevant information (number of channels, sampling frequency, spike waveform length, date and comments, etc.) is stored in a common parameter file in XML format. This standard, well-supported, self-described format allows for easier extensibility for future versions of the software.

In many cases, data needs preprocessing before analyses can be performed. An example is spike extraction from continuously recorded wide-band signals. Continuous recording of wide-band signals allows for a complete post-hoc replay and exploration of the original, unprocessed brain signals recorded during the experiment. Other examples of data preprocessing include extracting from a video stream the position of the head lights carried by the animal, concatenating multiple recording files, or simply converting data files from a proprietary format to one of our open formats.

4. Klusters: a graphical spike sorting application

Klusters is a graphical application for manual spike sorting. It can be used either to improve the output of automatic clustering or to manually cluster raw data. The initial set of features was inspired by the cluster cutting program sgclust by J. Csicsvari (unpublished).

Klusters works with a spike waveform file (.spk) and a feature file (.fet), and optionnally a cluster file (.clu) produced by an automatic clustering program (Harris et al., 2000) such as KlustaKwik (K.D. Harris, http://klustakwik.sourceforge.net). For data recorded continuously, the wide-band recording file (.dat) can also be used to display raw traces. Once the clusters have been manually created or refined by the experimenter, upon saving a cluster file (.clu) is created.

After loading the files, Klusters displays an overview of the data. This includes several graphical elements referred to as 'views', namely a cluster view, a waveform view and a correlation view (described in detail below). It is possible to work with several displays in parallel, each of which can flexibly combine different numbers and types of views arranged in custom layouts and showing different subsets of the data (Fig. 2). On the left side of the main window is the palette where each cluster is represented as a colored square. Clusters selected in the palette are shown simultaneously in all the views of the currently active display. Notice that in order to ensure rapid and easy identification, individual clusters are drawn using the same customizable colors throughout the application (palette and views).

4.1. Cluster views

For viewing and editing purposes, Klusters provides cluster views displaying two-dimensional projections of the feature vectors. To help visualize the data in multiple dimensions, any number of cluster views can be combined to display different projections simultaneously (Fig. 3). Several editing tools are available. These allow for direct manipulation of whole spike clusters as well as arbitrary subsets of points enclosed within user-defined polygons.

Klusters provides several specific tools to discard 'artefacts' and biological signals designated as 'noise' (e. g., background small amplitude multiunit activity). Discarded spikes are never actually deleted from the data files; rather, by convention, artefacts and noise are assigned to clusters 0 and 1, respectively. Klusters provides additional tools to create new clusters or correct existing clusters. Although automatic spike sorting should ideally yield one distinct cluster for each neuron, in practice, two different kinds of systematic error can occur, which require manual correction: 'overclustering', where spikes emitted by a single neuron are split in multiple clusters, and 'underclustering', where individual clusters contain spikes from multiple neurons. To correct for overclustering, multiple clusters can be grouped together. A special case occurs when one or more electrodes drift during the course of the recording session. In this case automatic spike sorting typically splits the spikes in several clusters because spike amplitudes change as a function of time. Selecting time as one of the projection dimensions and carefully inspecting the resulting clusters helps correct for such errors (Fig. 4). To correct for underclustering, one can split existing clusters by manually selecting arbitrary sets of points. These are extracted from their current clusters and, depending on the tool, either grouped together in a single new cluster, or assigned to one new cluster for each original cluster.

4.2. Waveform views

Assessing whether a cluster is contaminated by action potentials of other neurons or artefacts, or determining whether two or more clusters actually correspond to a single neuron, is facilitated by inspection and comparison of spike waveforms (Supplementary Fig. 1). Klusters provides waveform views where the waveforms for the currently selected clusters are displayed as colored traces (side by side, or overlaid). Because clusters can contain hundreds of spikes, by default only a subset of the waveforms are actually displayed (in order to reduce display time and memory usage). There are two possible selection modes: the view displays either a user-defined number of waveforms evenly spaced in time, or all waveforms occurring within a customizable time frame. Waveform means and standard deviations can also be displayed.

4.3. Correlation views

Autocorrelograms and cross-correlograms plotted in correlation views (Fig. 5) provide invaluable information for assessing the success of spike clustering. For instance, well isolated clusters contain spikes emitted by a single neuron, and thus their autocorrelograms show a clear refractory period (McCormick et al., 1985; Fee et al., 1996; Csicsvari et al., 1998; Harris et al., 2000). Conversely, autocorrelograms which do not show a clear refractory period correspond to 'noisy' clusters, i.e. clusters which combine spikes emitted by multiple units. Auto- and cross-correlograms also help finding instances of single neurons erroneously split across multiple clusters (cross-correlograms resembling the respective autocorrelograms) and identifying successive spikes within complex spikes (one-sided cross-correlograms): for example, the asymmetry and common refractoriness of the crosscorrelograms between clusters 11 and 15 are strong indications that these subclusters should be combined since they represent subsequent spikes of complex spike bursts. In addition, the correlation view is also used for screening monosynaptic excitatory and/or inhibitory connections between cell pairs, characterized by short-latency, large

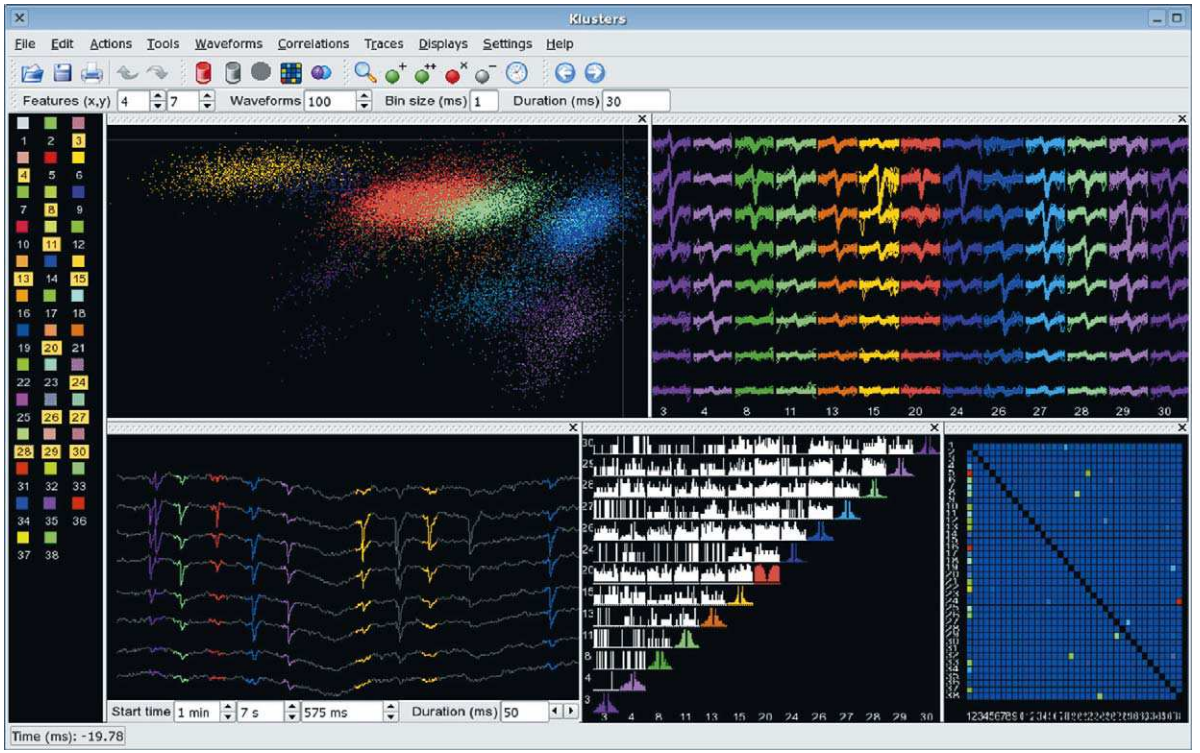

Fig. 2. Klusters. An overview, showing a cluster view (two-dimensional projection of the feature vectors, top left view), a waveform view (top right view), a trace view (spikes highlighted on wide-band brain signals, bottom left view), a correlation view (auto- and crosscorrelograms, bottom middle view), and an error matrix view (color-coded matrix of mean identification error probability, bottom right view). Individual views can be interactively moved around in the display, and more views can be added (e.g., additional cluster views using different projection features, and additional correlation views displaying different time scales). For rapid identification, data from single clusters are represented using the same color throughout the interface, including the selection palette (left panel). Several tools are shown in the tool bar (icons): delete artefact cluster(s) (red trash can), delete noise cluster(s) (grey trash can), update error matrix (colored matrix), group clusters (intersecting purple and blue spheres), zoom (magnifier lens), new cluster (green sphere with a plus sign), split clusters (green sphere with two plus signs), delete artefact spikes (red sphere with a cross sign), delete noisy spikes (grey sphere with a minus sign), select time (clock), previous and next spikes (blue arrows). Several view parameters can be adjusted in the various text fields: projection features, number of waveforms, correlogram bin size and half duration, trace start time and duration (data provided by David Robbe).

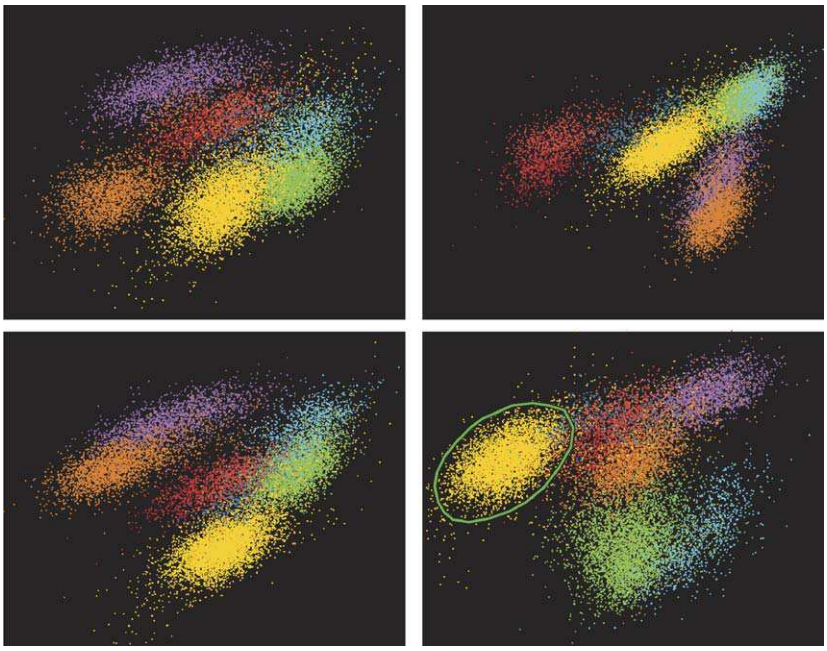

Fig. 3. Cluster views. Each view shows different two-dimensional projections of the feature vectors. Different clusters are represented by different colors. Any number of cluster views can be used simultaneously in order to display different projections of the data side-by-side. Editing tools allow for the creation of new clusters from points enclosed in user-defined polygons (green polygon in lower right panel), as well as grouping or deletion of existing clusters.

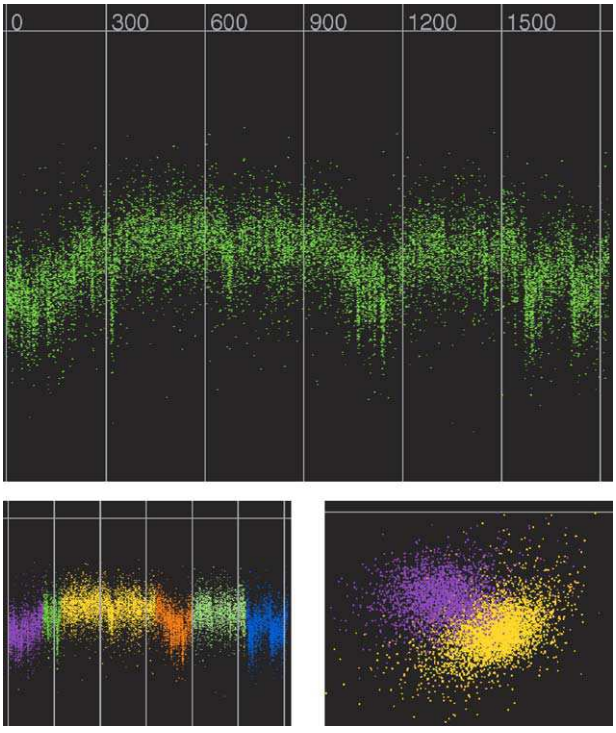

Fig. 4. Time axis in cluster views. Using time as one of the projection dimensions shows how spike features change over the course of a recording session. Top: this cluster shows evidence for electrode drift, as indicated by the magnitude shifts of the feature on the *y*-axis. Such drifts may occur when the electrode is located very close to the neuron and even relatively small relative movements can induce noticeable spike waveform changes (e.g., in amplitude). When this happens, the automatic clustering algorithms typically split the spikes across multiple clusters (bottom left), which can misleadingly appear distinct in two-dimensional projections (bottom right). Here, using time as one of the projection dimensions helps identify such misidentification.

amplitude, 1–3 ms wide bins or spike suppression (Csicsvari et al., 1998; Barthó et al., 2004).

4.4. Error matrix view

Although visual inspection of auto- and crosscorrelogram is necessary for the adjustment of clusters, quantification of such errors is advantageous when large numbers of clusters are formed. To this end, Klusters provides an error matrix view, a graphical representation of a statistical measure of cluster similarities (Fig. 2). This view indicates for each pair of clusters the mean probability that the spikes in the first cluster actually belong to the second cluster, using the same estimation method as the Classification Expectation Maximization (CEM) algorithm (Celeux and Govaert, 1992) implemented in KlustaKwik.

4.5. Trace views

Provided that continuous wide-band signals were recorded during the experiment, Klusters can use the corresponding data file (.dat) to display trace views where brain signals (spikes and local field potentials) are shown in time (Fig. 2). Exploring raw data allows for direct assessment of statistical properties evidenced e.g., in auto- and cross-correlograms, and helps detect spurious effects or confirm likely hypotheses (for instance regarding complex spike bursts). Trace views feature a reduced set of the functionalities available in NeuroScope such as spike browsing (see below).

4.6. Automatic reclustering

Although Klusters features a number of tools to correct for underclustering, in most cases manually splitting clus-

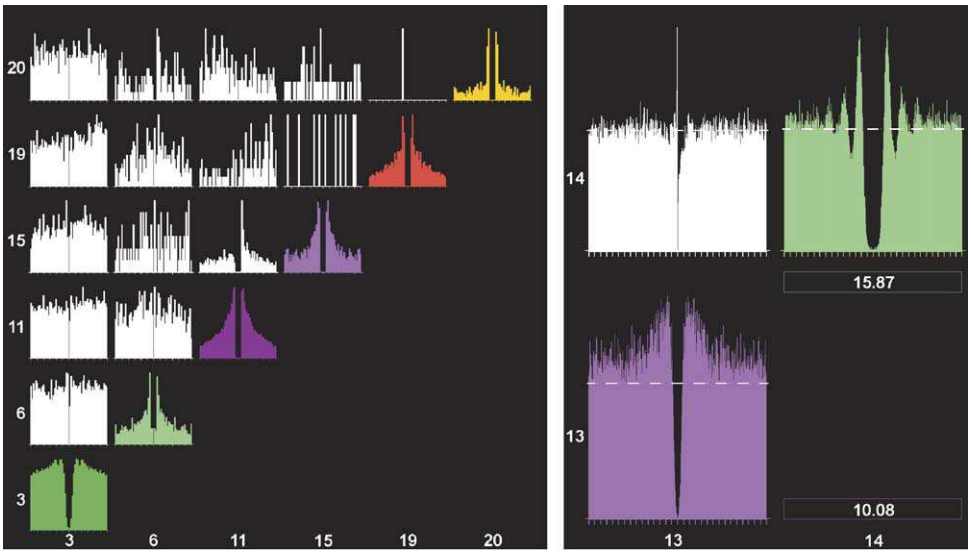

Fig. 5. Correlogram views. Autocorrelograms (colored histograms) and cross-correlograms (white histograms) help determine isolation quality. For instance, cluster 6 has a noisy refractory period, indicating poor isolation. Similar refractory periods in the auto- and the cross-correlograms together with a single-sided peak in the cross-correlograms for clusters 11 and 15 reveal splitting of spikes of bursty neurons. Autocorrelogram 3 with its broad shoulder is indicative of a putative fast spiking interneuron. The asymetric cross-correlogram for clusters 13 and 14 (right) suggests a bidirectional monosynaptic connection between excitatory and inhibitory neurons. Displaying a longer time scale (right vs. left) can reveal firing rythmicity (e.g., for cluster 14). Notice the average firing rate optionally indicated in the color boxes and as dashed horizontal lines.

ters involves arbitrary and potentially biasing choices (a typical example is cluster 'shaving', where peripheral points are removed from a cluster). To allow for unbiased reclustering of a set of existing clusters, Klusters can interactively run an automatic clustering program on a subset of the data. This is usually a computing intensive task, which can require long processing time, and should thus be performed on a reduced number of clusters. In particular, this feature should not be used as a graphical front-end to initial automatic cluster cutting over the whole data. For large files, this can run for up to several days on current computer hardware.

4.7. Exporting as vector graphics

Once optimal clusters have been determined, it is often useful to export waveform traces, spike cluster plots and cross-correlograms for presentations or manuscripts. Although this can be achieved by simply using a screen capture utility, doing so results in bitmapped images that do not scale or print well. Instead, Klusters can export high-quality graphics to PostScript (PS) or Portable Document Format (PDF) files. These standard vector graphics formats can then be imported in any drawing application for further editing.

5. Neuroscope: an electrophysiological and behavioral viewer

NeuroScope is a viewer for continuously recorded signals (e.g., wide-band or local field potentials), spiking activity, and behavioral events.

NeuroScope is not a data analysis program; rather, it allows for the easy and efficient inspection of raw data. Although statistical analyses and plots provide synthetic views of data properties, direct examination of raw data often provides invaluable insight into the fine structure underlying these properties, helps avoid spurious effects, and may generate hypotheses for subsequent quantitative analyses. NeuroScope was specifically designed to efficiently handle large amounts of data (dozens of channels recorded at high sampling rates, plus dozens of neuronal spike trains, and video tracking).

NeuroScope works with a continuous recording file (.dat, .eeg, .fil, etc.). Optionally, it can also display unit activity loaded from spike timings files (.res) and cluster files (.clu), as well as position tracking data from a position file (.whl), and behavioral events from one or more event files (.evt). Although NeuroScope is mainly a viewer application, it features limited editing capabilities allowing for modification of event files (.evt), such as adding markers to visually identified events.

NeuroScope displays the data in a trace view (electrophysiological signals) and optionally a position view (position tracking) combined in a display (Fig. 6). Similarly to Klusters, it is possible to work with several displays in parallel, each of which can show different subsets of the data. On the left side of the main window is the palette where channels, units and events are represented as colored icons in dedicated tabbed layouts. Again, rapid and easy identification is ensured by drawing individual elements using the same customizable colors throughout the application (palette and views).

5.1. Browsing continuous brain signals

Any number of continuously recorded channels can be displayed in custom colors and arrangements (Fig. 7). Data browsing combines direct access to specific points in time, and step-by-step replay of recordings across time. The duration of the data displayed in the view can be adjusted (doubled, halved,

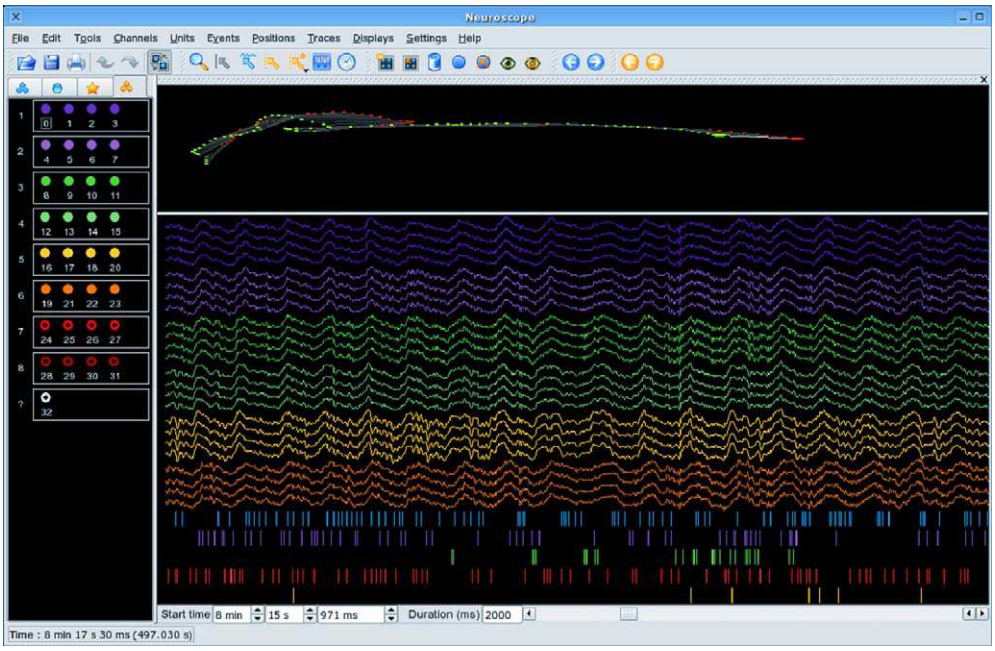

Fig. 6. NeuroScope. An overview, showing the trace view (electrophysiological signals, bottom view) and a position view (position tracking, here using two head lights, top view). For rapid identification, data from single sources (e.g., channel, cluster) are represented using the same color throughout the interface, including the selection palette (left panel). Several tools are shown in the tool bar (icons): zoom (magnifier lens), draw time line (grey arrow with vertical bar), select channels (blue arrow with horizontal trace), select event (yellow arrow with vertical dashed bar), add event (yellow arrow with vertical dashed bar and plus sign), measure (mutlimeter), select time (clock), previous and next spikes (blue arrows), previous and next events (yellow arrows), move channels to new group (square with four blue spheres and yellow star), remove channels from group (square with four blue spheres and red cross), discard channels (blue trash can), keep channels (blue sphere), skip channels (to label bad channels on silicon probes, crossed blue sphere), show channels (eye), hide channels (crossed eye). Trace start time and duration can be adjusted in the respective text fields.

set explicitly or interactively), for instance to show an overview of brain rhythms over longer periods of time, or help inspect spiking activity over shorter periods of time. A zooming tool is also provided to focus on even more restricted portions of the data (for instance, data sampled from a specific channel during a small time window).

5.2. Browsing unit activity

Unit activity can be represented as rasters below the continuous traces, vertical lines spanning the entire view, or full waveforms highlighted directly on the continuous traces (Fig. 8). Rasters allow for inspection of patterns of population activity, vertical lines emphasize relations between unit activity and local field events, and spike highlighting on the traces makes it possible to examine and compare waveforms at higher temporal resolution. For quick and convenient browsing, NeuroScope provides the possibility to directly move to the next or previous spike within a user-defined set of spike trains.

5.3. Position tracking

Provided the position of the animal was tracked during the experiment, NeuroScope can plot successive positions across time (using the same time window as for brain signals), each position being plotted as a connected set of colored points along a regular polygon, one point per head light carried by the animal (Fig. 6). By convention, the front light is plotted in red and all other lights in green. Thus, if the animal carries a single light, this will be represented as a red dot on the position tracking view, if it carries two lights (required to measure head direction), this will be represented as a segment with a red dot at the front end and a green dot at the back end, etc. To better estimate where the animal is located in the experimental apparatus, it is possible to display in the background an overhead photograph of the maze and/or the trajectory of the animal over the course of the entire experiment.

5.4. Browsing and editing events

Events can be plotted as vertical dashed lines in the trace view, and as cross marks in the position view, at the position occupied by the animal when they occurred (Fig. 6). Similar to spikes, one can directly move to the next or previous event in a user-defined set of events. Although NeuroScope is essentially a viewer, it also features a limited set of editing tools, allowing for addition, deletion and modification of events. This is particularly useful to manually indicate, or correct automatic detection of, field events such as hippocampal ripples, thalamo-cortical spindles, epileptic spikes, etc.

6. NDManager: a simple experimental parameter manager

Klusters and NeuroScope share a common parameter file (this is also used by other tools, as described in the next section). This file stores in XML format all the parameters required for data

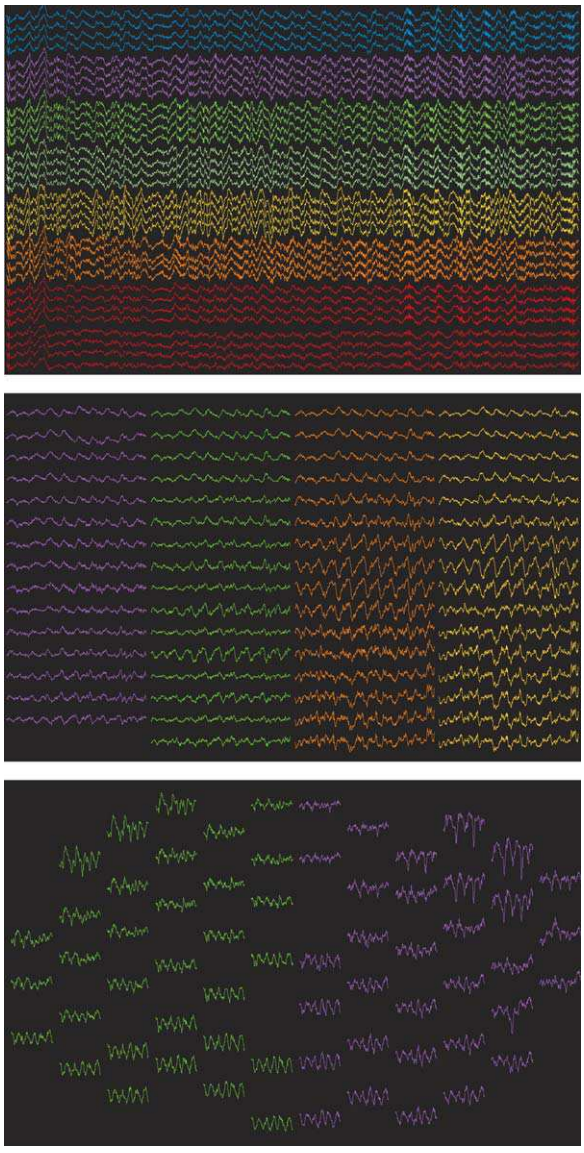

Fig. 7. Trace views: layouts. Electrode groups are displayed in different colors, either in vertical arrangements (top, tetrodes), in columnar arrangements (middle, silicon probes with regularly spaced recording sites), or in arbitrary layouts (bottom, epidural electrode array, arranged according to the topography of recording sites).

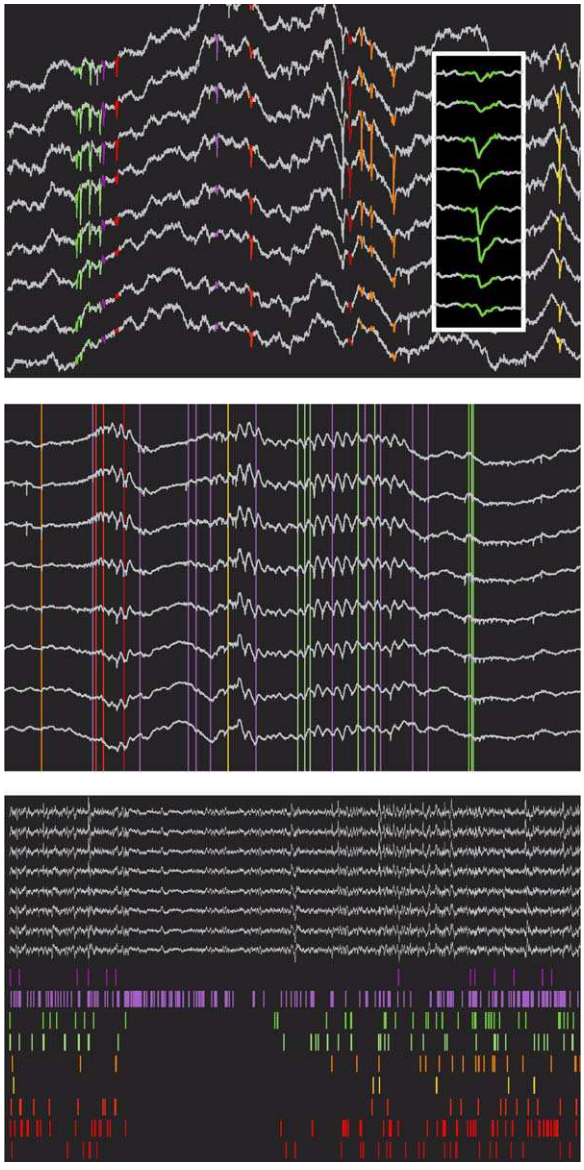

Fig. 8. Trace views: unit activity. Simultaneous display of clustered unit activity and field recordings. Unit activity can be shown as highlighted spike waveforms directly on the traces (top), emphasizing waveform shapes (inset, lower time scale), as vertical lines overlaid on the traces, emphasizing relations between unit and field activity (middle), or as rastergrams below the traces, emphasizing population firing patterns (bottom).

viewing and processing, including:

- general information: date, experimenter, description, notes;
- acquisition system: number of channels, sampling rate, resolution (in bits), offset, voltage range and amplification gain;
- video: sampling rate and frame size;
- file information: sampling rate and channel correspondence for processed files (e.g., low-pass filtered local field potentials, high-pass filtered data, average tetrode narrow-band field potentials, etc.)
- anatomical and spike groups: anatomical layout of the electrodes and groups for spike extraction and sorting;
- preprocessing parameters: software filter cutoff frequencies, spike extraction threshold, number of samples per waveform, number of principal components, etc.

All these parameters can be edited graphically using NDManager (Fig. 9). This simple application is designed to handle two related tasks: managing experimental parameters edition and data processing execution (as described below).

7. Integrated framework

Klusters, NeuroScope and NDManager are the three main components of a framework intended to provide all the necessary tools to process the data to bring it to suitable form for subsequent analysis: filtering, spike extraction and sorting, position tracking, event preprocessing, etc. Although several recording systems provide integrated tools to perform these steps, our

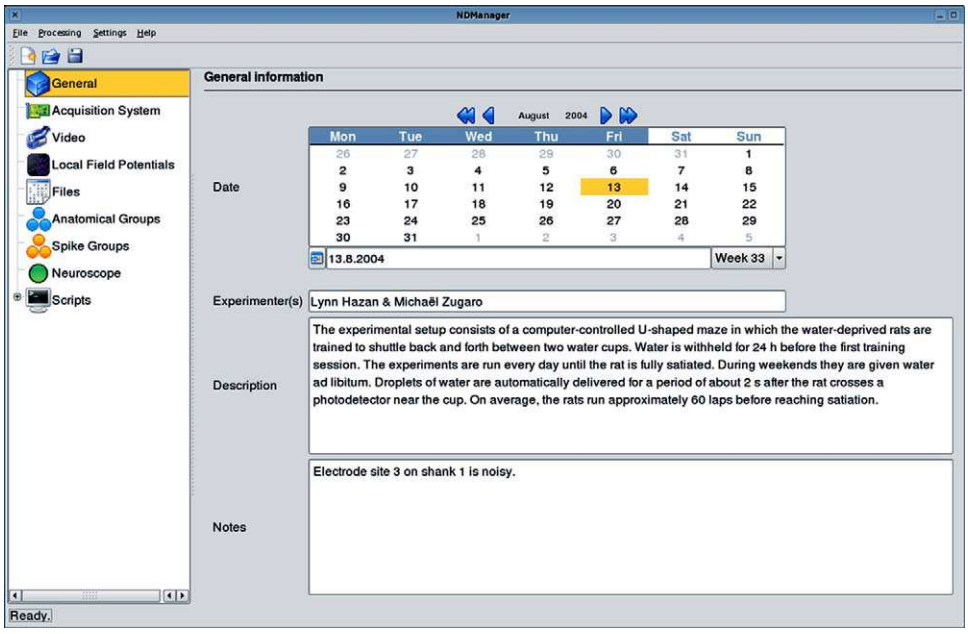

Fig. 9. NDManager. This simple application is designed to handle the parameter file used Klusters and NeuroScope, as well as processing utilities. Parameters are grouped into categories (left panel) and include general information (right panel: date, experimenters, description of the experiment, notes), information about the acquisition system, preprocessing parameters, etc. NDManager is also designed to run preprocessing utilities. Thus, it constitutes a convenient central point from where parameters can be edited, files can be processed, and Klusters and NeuroScope can be started.

package offers a number of advantages: it allows researchers to modify and redistribute it as they see fit (hopefully bringing together a community of users and developers constantly improving this common resource); it includes powerful spike sorting capabilities by combining KlustaKwik, an efficient automatic clustering program, and Klusters, an advanced manual clustering application (most other packages only offer basic capabilities); it has the capability to eventually include all processing steps in an integrated suite.

In our framework, non-interactive processing such as high-pass filtering is typically done by command-line tools, usually written in C (but any other language can be used as well to develop additional custom components). Preprocessing does not require user intervention except for the definition of initial parameters (e.g., high-pass threshold). Although for technically sophisticated users, the command-line is a satisfactory user interface, for most users a simple graphical interface may be required, if only to define these parameters and start the actual processing more easily. This functionality is provided by NDManager, which has the capability to act as a graphical 'front-end' to any processing tools. This allows researchers to easily integrate their own processing tools within our framework without code modification. Only an intermediate script is required to read the parameters from the XML file (rather than from the command-line or legacy configuration files), and pass them along to the tools.

In practice, tools are executed via simple scripts (these can be written in sh, bash, perl, python, etc.), which first test the environment to anticipate possible errors (e.g., missing data files required for a specific task), then read parameters from the XML parameter file, and finally generate a command to start the respective tools. Along with each script and tool pair, a description file in XML format describes the parameters required for the task and provides a short help text. NDManager dynamically generates a graphical interface from this file, presenting the user a list of named parameters where values can easily be edited. Once all values have been provided, NDManager can execute the script, which reads these values and starts the tool accordingly.

8. Conclusion

The applications presented here allow for advanced processing and visualization of neurophysiological data sets including brain signals (action potentials and local field potentials), behavioral events and position tracking. These applications can be downloaded from the internet (http://neuroscope.sourceforge.net, http://klusters.sourceforge.net, and http://ndmanager.sourceforge.net). All the applications and tools described here are free software distributed under the GNU General Public License (GPL, see http://www.gnu.org/licenses/gpl.html). This license grants its users legal permission to copy, distribute and/or modify the software as they see fit. To this end, the source code is distributed alongside of the executable binaries. The only restriction imposed on the users is that should they decide to redistribute the software in its original or modified form, they must in turn grant their users the same rights. This guarantees that the software or any derivative of it will always remain freely available to the neuroscience community, and avoids the risk of vendor 'lock in' associated with proprietary software. We hope to attract an active community of users who could benefit from and contribute to this project.

Acknowledgements

We wish to thank Jozsef Csisvari, Anton Sirota, Lénaïc Monconduit, Judith Creso, David Robbe, Stephan Marguet, Sean Montgomery, Derek Buhl, Kenneth Harris, Peter Barthó and Hajime Hirase who helped define the feature set of the applications. Data used in the figures were provided by M. B. Z, Lénaïc Monconduit, Anton Sirota, David Robbe, Sean Montgomery and Peter Barthó. Supported by National Institutes of Health (NS34994, NS43157, MH54671) and the Human Frontier Science Foundation (to M. B. Z).

Appendix A. Supplementary data

Supplementary data associated with this article can be found, in the online version, at doi:10.1016/j.jneumeth.2006.01.017.

References

Abeles M, Goldstein MH. Multispike train analysis. In: Proceedings of the IEEE, vol. 65; 1977. pp. 762–73.

Barthó P, Hirase H, Monconduit L, Zugaro M, Harris KD, Buzsáki G. Characterization of neocortical principal cells and interneurons by network interactions and extracellular features. J Neurophysiol 2004;92:600–8.

Buzsáki G, Horváth Z, Urioste R, Hetke J, Wise K. High-frequency network oscillation in the hippocampus. Science 1992;256:1025–7.

Buzsáki G. Large-scale recording of neuronal ensembles. Nat Neurosci 2004;7:446–51.

Celeux G, Govaert G. A classification EM algorithm for clustering and two stochastic versions. Computational Statistics Data Anal 1992;14:315–32.

Csicsvari J, Hirase H, Czurko A, Buzsáki G. Reliability and state dependence of pyramidal cell-interneuron synapses in the hippocampus: an ensemble approach in the behaving rat. Neuron 1998;21:179–89.

Csicsvari J, Henze DA, Jamieson B, Harris KD, Sirota A, Barthó P, Wise KD, Buzsáki G. Massively parallel recording of unit and local field potentials with silicon-based electrodes. J Neurophysiol 2003;90:1314–23.

Eichenbaum HB, Davis JL. Neuronal ensembles: strategies for recording and decoding. New York: Wiley-Liss; 2001.

Fee MS, Mitra PP, Kleinfeld D. Automatic sorting of multiple unit neuronal signals in the presence of anisotropic and non-Gaussian variability. J Neurosci Methods 1996;69:175–88.

Hampson RE, Simeral JD, Deadwyler SA. Distribution of spatial and nonspatial information in dorsal hippocampus. Nature 1999;402:610–4.

Harris KD, Henze DA, Csicsvari J, Hirase H, Buzsáki G. Accuracy of tetrode spike separation as determined by simultaneous intracellular and extracellular measurements. J Neurophysiol 2000;84:401–14.

Hoffman KL, McNaughton BL. Coordinated reactivation of distributed memory traces in primate neocortex. Science 2002;297:2070–3.

Jutten C, Herault J. Blind separation of sources. Part I. An adaptive algorithm based on neuromimetic architecture. Signal Process 1991;24:1–10.

Khazipov R, Sirota A, Leinekugel X, Holmes GL, Ben-Ari Y, Buzsáki G. Early motor activity drives spindle bursts in the developing somatosensory cortex. Nature 2004;432:758–61.

McCormick DA, Connors BW, Lighthall JW, Prince DA. Comparative electrophysiology of pyramidal and sparsely spiny stellate neurons of the neocortex. J Neurophysiol 1985;54:782–806.

Nicolelis MA. Methods for neural ensemble recordings. Florida: CRC-Press; 1998.

Nicolelis MA, Dimitrov D, Carmena JM, Crist R, Lehew G, Kralik JD, Wise SP. Chronic, multisite, multielectrode recordings in macaque monkeys. Proc Natl Acad Sci USA 2003;100:11041–6.

Wilson MA, McNaughton BL. Dynamics of the hippocampal ensemble code for space. Science 1993;261:1055–8.

Wilson MA, McNaughton BL. Reactivation of hippocampal ensemble memories during sleep. Science 1994;265:676–9.

Zugaro MB, Monconduit L, Buzsáki G. Spike phase precession persists after transient intrahippocampal perturbation. Nat Neurosci 2005;8:67–71.

nature neuroscience

Spike phase precession persists after transient intrahippocampal perturbation

Michaël B Zugaro, Lénaïc Monconduit & György Buzsáki

Oscillatory spike timing in the hippocampus is regarded as a temporal coding mechanism for space, but the underlying mechanisms are poorly understood. To contrast the predictions of the different models of phase precession, we transiently turned off neuronal discharges for up to 250 ms and reset the phase of theta oscillations by stimulating the commissural pathway in rats. After recovery from silence, phase precession continued. The phase of spikes for the first theta cycle after the perturbation was more advanced than the phase of spikes for the last theta cycle just before the perturbation. These findings indicate that phase advancement that emerges within hippocampal circuitry may be updated at the beginning of each theta cycle by extrahippocampal inputs.

The timing of neuronal spikes in oscillatory networks is under the combined influence of external inputs and the internal self-organizing dynamics of the network. A robust example of this is the firing patterns of hippocampal pyramidal cells. Pyramidal cells discharge selectively when the rat is in specific locations in its environment[1], yet the timing of their spikes is influenced by the endogenous theta oscillation. As the rat walks through the firing field of a place cell, which takes five to ten theta cycles, the cell fires at progressively earlier phases on successive cycles of the ongoing theta oscillation[2]. This relationship allows for the prediction of the future center of the field from the phase advancement of the action potentials across successive theta cycles[3–6]. Furthermore, neuronal assemblies that represent successive places along the trajectory of the rat have a predictable temporal relationship within each theta cycle[3,7,8]. This mechanism is potentially useful for encoding sequence information and for preparing the animal for what is to come next[9,10].

Although numerous computational models have attempted to account for the mechanisms that underlie the spike 'phase-precession' observation[2,9,11–21], direct experimental exploration of the phenomenon is limited[3–6,13,22,23]. Here we test and contrast the predictions of different classes of models by transiently perturbing firing patterns of place cells and resetting the phase of theta oscillations by stimulating the ventral hippocampal commissure. We found preservation of the spatial dependence of theta phases of individual spikes after transient perturbation, indicating that spatial information in intrahippocampal networks may be updated by cortical inputs at every theta cycle.

RESULTS

Single-pulse stimulation of the intrahippocampal pathways reset the theta phase and reliably silenced all recorded hippocampal pyramidal cells and interneurons for a period of one or two theta cycles (**Fig. 1a**). Under anesthesia, single-pulse stimulation, by synchronously discharging large ensembles of pyramidal cells and interneurons, triggers a combination of GABA receptor–mediated inhibition, Ca^{2+}-mediated K^+ conductance increase and disfacilitation. As a result, all pyramidal cells, granule cells and interneurons are silenced for 50–250 ms, depending on the strength of simulation[24–26]. In the present experiments, stronger stimulation synchronized theta more reliably ($P < 0.01$; F-test) and produced longer silent periods ($P < 0.01$; t-test). Recovery of population firing after the stimulation was fast, and after 200–250 ms, both firing rate and theta amplitude fully recovered, even after the strong stimulus. Significantly increased phase coherency of the local field potentials across individual laps could be observed for about 1 s (seven to eight theta cycles) after the stimulation (**Fig. 1b**). Single-pulse stimulation of the perforant-path input can also reset theta and transiently silence place-related activity (E.I. Moser *et al.*, *Soc. Neurosci. Abstr.* **33**, 519.12, 2003). Neurons in the entorhinal cortex, when strongly synchronized by the CA1 output, produce a detectable population spike in the granule cell layer[27]. Evoked reverberating activity was never observed here (data not shown), even at stronger stimulus intensity, indicating that the major effect of stimulation was confined to the hippocampus[28]. The stimulation produced no overt behavioral effects and did not affect the running velocity of the rat (control, 0.26 ± 0.02 m/s; weak stimulation, 0.24 ± 0.01 m/s; strong stimulation, 0.23 ± 0.02 m/s; not significant, t-test).

We recorded from 162 well-isolated CA1 place cells in five rats. Thirty-five units had firing fields in the start area of the maze where stimulation was delivered, and these units were used to examine the effects of stimulation on phase precession (number of cells/sessions for the five rats: 2/1, 3/2, 5/3, 17/3, 8/3). As expected from the suppression of population firing, single-pulse stimulation transiently silenced in-field firing for at least one or two theta cycles. During stimulation trials, despite the theta phase reset and transient interruption of firing, spike phases were still correlated with the spatial position of the animal immediately after recovery, similar to control trials (**Fig. 2a**). To quantify this effect,

Center for Molecular and Behavioral Neuroscience, Rutgers, The State University of New Jersey, Newark, New Jersey 07102, USA. Correspondence should be addressed to G.B. (buzsaki@axon.rutgers.edu).

Published online 12 December 2004; doi:10.1038/nn1369

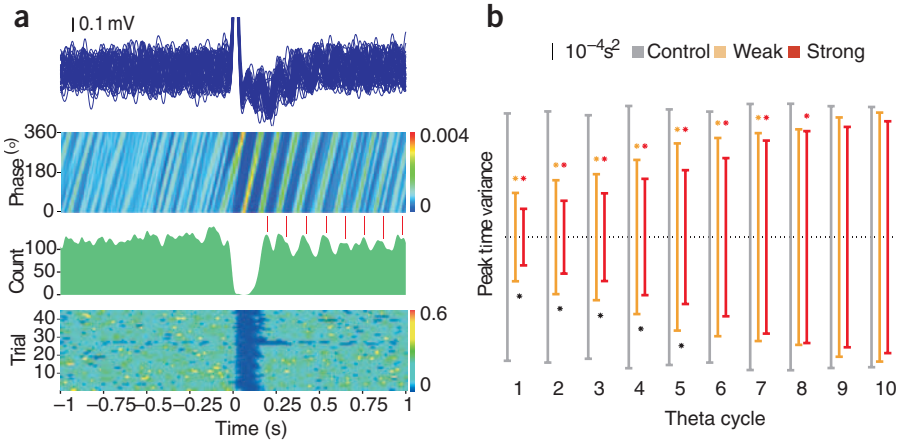

Figure 1 Single-pulse stimulation of intrahippocampal afferents resets theta and silences spiking activity. (**a**) First (upper) panel: superimposed field activity recorded during successive runs in a typical recording session, before and after weak stimulation (time zero). Second panel: instantaneous distribution of phases across successive runs as a function of time. Vertical lines indicate troughs of averaged field activity (data not shown). Third panel: peri-event histogram of three simultaneously recorded interneurons. Fourth (bottom) panel: combined peri-event spiking activity of pyramidal cells ($n = 20$) and interneurons ($n = 3$). Color calibration, spikes per bin (fourth panel), probability (second panel). Note transient silence (<200 ms) and full recovery of global firing rate after stimulation. (**b**) Theta reset after single-pulse stimulation ($n = 5$ rats). Variance of theta peak occurrence times (vertical bars) in successive cycles after stimulation compared with the control condition after crossing of the photobeam. A smaller variance corresponds to higher phase coherence: $^*P < 0.01$, *F*-test; colored asterisk indicates significant difference when compared with control; black asterisk indicates significant difference between strong and weak stimulation.

we determined the mean theta phase for the early, middle and late portions of the firing field for all neurons[6]. This analysis showed no effect of stimulation on spike phase precession (**Fig. 2b**; not significant, circular analysis of variance (ANOVA)). Furthermore, neither peak firing rate nor mean phase at the center of the field was affected by the stimulation (not significant, linear ANOVA and circular ANOVA, respectively). The small but nonsignificant decrease in peak firing rate (**Fig. 2b**) is probably due to the missing spikes after the stimulation.

To examine possible transient effects that were not detected by the previous analysis, we measured the difference between the average spike phase in the last theta cycle before stimulation and the average spike phase in the first theta cycle upon recovery for each lap. We compared this resulting phase difference to the phase advancement of similarly spaced theta cycles in control trials. Assuming an average-sized firing field, the phase of place cell spikes is expected to advance about 40–60° during the time period of two theta cycles[2]. After both weak and strong stimulation, the phase advanced by approximately 40° (**Fig. 3**), which is significantly larger than the zero change expected if phase precession resumed from the same point upon recovery (**Fig. 3c**). The mean phase shift after the perturbations was less than that during control laps (~70°), but the magnitude of the phase shift did not differ significantly across the groups (as indicated by overlapping 95% confidence intervals in **Fig. 3c**).

The final analysis examined whether single-pulse stimulation had an impact on population coding. Within each theta cycle, place cells with overlapping fields discharge in the same order as their fields are traversed; moreover, the closer their firing fields are in space, the closer their respective firings occur in time[3,7]. Thus, the behavioral sequence (traversal of the first and then the second field), which may take on the order of a second, is reflected in the fine-timescale physiological activity (activation of the first and then the second place cell within a given theta cycle), which lasts on the order of a few dozen milliseconds. This results in a time-compressed

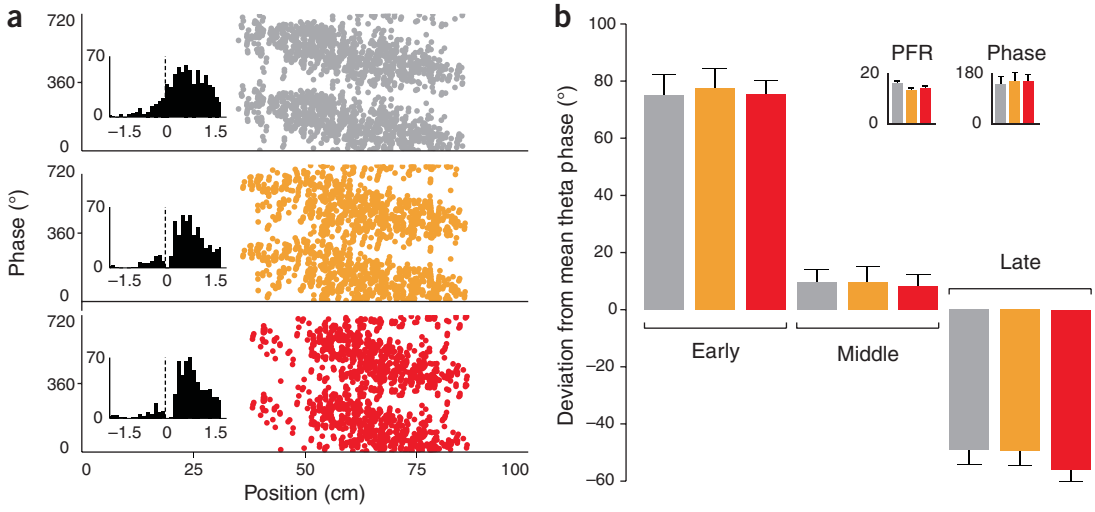

Figure 2 Phase precession is preserved after stimulation-induced perturbation. (**a**) Phase precession for a place cell during control, weak and strong stimulation runs. Note overall similarity of plots across conditions. Insets: peri-stimulus histograms of spikes (*x* axis, counts per bin; *y* axis, time in seconds). (**b**) For overall group statistics, theta phases were determined separately for each of the early, middle and late subfields and were expressed as deviations from the overall mean phase. Error bars, 95% confidence intervals. Insets: Peak firing rates (PFR) and theta phases (Phase) at peak firing rate locations. Color code for experimental conditions as in **Figure 1**.

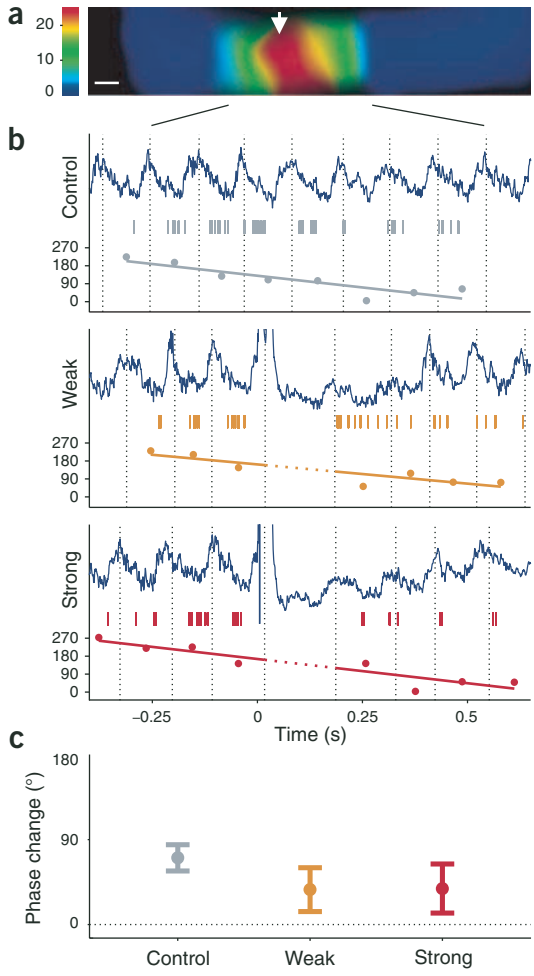

Figure 3 Phase precession is preserved after stimulation-induced perturbation. (**a**) Firing field during control trials. Color calibration, spikes per second; white bar, 5 cm; arrow, stimulation site. (**b**) Field theta rhythm, place cell firing (ticks) and average spike phase per theta cycle (in degrees; closed circles) from representative single runs under each condition. Note similar slope of phase advancement in each trial, despite transient disruption of spiking and theta oscillation after stimulation. (**c**) Group data for 35 neurons. Mean phase difference between the last theta cycle before stimulation and the first theta cycle after stimulation. For the control, the last theta cycle before crossing the photobeam and the theta cycle closest in time to the recovery cycle in stimulation trials were analyzed. Vertical bars, 95% confidence intervals. Under all three conditions, the theta phase advanced significantly ($P < 0.05$). Control and stimulation conditions did not differ significantly.

representation of spatial information. To test how this property was affected by hippocampal perturbation, we first selected all place cell pairs with overlapping fields for which at least one of the neurons overlapped with the position of stimulation ($n = 99$). We then plotted for all cell pairs the peaks of their time cross-correlograms (**Fig. 4a**) as a function of the spatial distance between the centers of their firing fields[7]. The five diagonal dot clouds (**Fig. 4b**) reflect time-compressed representation of spatial information[3,7] in five subsequent theta cycles. The great degree of similarity between the three conditions indicates that fine-timescale properties of spike sequences within place-coding cell assemblies are preserved despite perturbation of hippocampal dynamics.

DISCUSSION

Single-pulse stimulation of the intrahippocampal associational and commissural afferents reset theta phase and transiently inactivated hippocampal network activity. Despite these perturbations, the phase of the spikes after recovery was similarly correlated with the spatial position of the animal as it was in control laps. Although the behavioral variable in our experiments was the position of the rat, the physiological mechanisms that underlie phase precession are also relevant for a broad range of behaviors[4,29].

Several computational models have been proposed to account for the phase precession phenomenon. These models differ in their assumptions and predictions. One class of models assumes interactions between two oscillators with slightly different frequencies, whereby the cycles of the faster oscillator occur progressively earlier relative to those of the slower oscillator (that is, it precesses in phase). These models predict that if one or both oscillators are reset, the resuming spike-phase relationship should be strongly altered by the perturbation. Thus, a simple two-oscillator model in which at least one oscillator is within the hippocampus[2,14–16,18] (as opposed to the entorhinal cortex[17,21], for example) cannot account for the present observations. Yet our findings do not invalidate all versions of coupled oscillators. More-complex models that take into account the history-dependent activity of neuronal population activity[30] may be compatible with the present observations.

A second class of models base phase precession on single-cell membrane properties[4,5,13,19,23]. In this view, the amount of excitation determines the phase at which a cell fires: the more the membrane is depolarized, the earlier the cell discharges relative to theta. As the animal traverses the firing field of a place cell, this cell receives increasing amounts of excitation at each theta cycle; therefore, the combined dendritic excitation and somatic inhibition reach firing threshold earlier and earlier—resulting in phase precession. These models predict that transient interruption of hippocampal firings should be followed by resumption of phase precession, commensurate with the resumed level of excitation. In principle, these single-cell models can account for our findings with the additional assumption that continued excitation is provided by extrahippocampal inputs. Silencing the network should abolish spike history–dependent

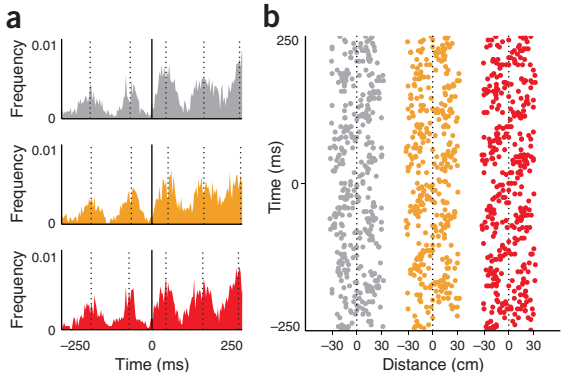

Figure 4 Assembly coding is maintained after transient perturbation. (**a**) Cross-correlograms of two place cells with partially overlapping firing fields (distance between centers, 22 cm). Notice theta rhythm modulation of cross-correlograms. Successive peak occurrence times (vertical dotted lines) were determined for all overlapping pairs ($n = 99$) for group statistics. (**b**) Cross-correlation between peak occurrence times and distance between firing fields of neuron pairs[7]. Color code for experimental conditions as in **Figure 1**.

effects in single cells[4], and thus the contribution of spiking history in place cells does not seem to be critical.

The simplest, but rather unlikely, explanation of our findings is that the timing of each spike in the CA1 hippocampal region is under the exquisite control of extrahippocampal inputs that themselves code for position. Alternatively, external inputs are combined with self-organization of hippocampal cell assemblies. Models in this group[9,11,12] assume that phase precession reflects some internally generated sequence-predicting mechanism, as is the case during hippocampal sharp waves[31–33]. In these models, the cell assembly that codes for the current position of the rat strongly discharges at the trough of the theta cycle in both CA1 and CA3 pyramidal cells. In the recurrently connected hippocampal CA3 network, this group in turn is assumed to excite (by unidirectional connections) the cell assembly that represents the next position of the animal along the predicted trajectory[34,35]. Because of synaptic and propagation delays, cells with firing fields that occur later in the sequence fire later during the theta cycle. As a result, as the rat moves toward the firing field of a cell, that cell discharges at progressively earlier phases, that is, it precesses relative to the theta 'clock' signal. This continuous propagation of activity within the CA3 network is interrupted by the next inhibitory phase of theta oscillation[36]. The initiation of assembly sequence reactivation during the next theta cycle is triggered by inputs from structures upstream of the hippocampus. In our experiments, the average spike phase during the first theta cycle on recovery was smaller than the average spike phase during the last theta cycle before commissural stimulation. This is consistent with the hypothesis that extrahippocampal inputs update the network at each theta cycle. Alternatively, other internal mechanisms, operating at a timescale that is slower than the theta cycle, may be responsible for the advancement of phase after transient silencing of the hippocampal network.

In summary, our findings indicate that intrahippocampal cell assemblies may self-organize their sequences cycle by cycle[3,7] and that extrahippocampal information, which conveys updated environmental, movement-generated feedback and other influences operating at a slower timescale, is incorporated in each new theta cycle.

METHODS

Rats and stimulation protocol. Five adult male Long-Evans rats (250–300 g) were implanted with eight independently movable tetrodes (groups of four twisted 13-μm nichrome wires) in the hippocampus (3–4 mm posterior to bregma, 1.5–3.5 mm from the midline) and with a bipolar stimulation electrode (diameter, 60 μm) in the contralateral hippocampal commissure (1.3 mm from the midline), following National Institutes of Health guidelines. The protocol was approved by the Institutional Animal Care and Use Committee of Rutgers University. After the animals had recovered, evoked responses were triggered by single-pulse (0.1 ms) stimulation at two current levels. 'Weak' and 'strong' stimuli corresponded to population spike threshold and to approximately 50% of maximal population spike, respectively.

Behavioral task. The experimental setup consisted of a computer-controlled U-shaped maze in which the water-deprived rats were trained to shuttle back and forth between two water cups. Water was withheld for 24 h before the first training session. The experiments were run every day until the rat was fully satiated. During weekends they were given water *ad libitum*. Droplets of water were automatically delivered for a period of about 2 s after the rat crossed a photodetector near the cup. For stimulation trials, the rats received single electric pulses (0.1 ms; current range, 60–400 μA; weak or strong stimulus) when crossing a photodetector as they departed from a water cup on their way to the other water cup. On average, the rats ran approximately 60 laps before reaching satiation, yielding 20 laps for each of the control, weak-stimulation and strong-stimulation conditions. A recording session typically consisted of blocks of five laps for each experimental condition, intermingled in a pseudorandom order.

Data acquisition and analysis. During the recording sessions, electrode signals were acquired at 20 kHz on a 64-channel DataMax system (16-bit resolution; RC Electronics Inc.). For offline spike sorting, the wide-band signals were digitally high-pass filtered (0.8–5 kHz). Units were then identified and isolated by a semiautomatic 'cluster cutting' algorithm[37,38], followed by computing auto- and cross-correlations. To track the position of the animals in the maze, two small light-emitting diodes (10-cm separation) mounted above the headstage were filmed by a digital video camera. Their moment-to-moment positions were later extracted and resampled (at 40 Hz) for analysis. All behavioral events (including arrival at and departure from water cups, opening and closing of a solenoid valve controlling water delivery and brain stimulation) were monitored, triggered and stored on disk by custom-written software running in LabView (National Instruments). Neurophysiological and behavioral data were explored using NeuroScope (http://neuroscope.sourceforge.net, L. Hazan, Center for Molecular and Behavioral Neuroscience, Rutgers University; G. Buzsáki *et al.*, *Soc. Neurosci. Abstr.* **33**, 768.2, 2004). Spike sorting was performed in two steps, first automatically using KlustaKwik (http://klustawik.sourceforge.net, K. Harris, Center for Molecular and Behavioral Neuroscience, Rutgers University) and then manually using Klusters (L. Hazan, http://klusters.sourceforge.net; L. Hazan *et al.*, *Soc. Neurosci. Abstr.* **33**, 768.3, 2004]). Firing maps were computed using a kernel-based method[39]. The firing rate at a point, x, was estimated by

$$f(x)dt = \frac{\sum n_t w(|x - x_t|)}{\sum w(|x - x_t|)}$$

where n_t is the number of action potentials emitted in a given time bin, x_t is the position of the rat in that time bin and dt is the time bin size. The kernel function w is a Gaussian of width 2.5 cm. Firing fields were defined as the ensemble of contiguous bins containing the location of maximal firing rate, for which the firing rates were >20% of the peak firing rate[6].

Phase reset was assessed by measuring the time stamps of successive theta peaks (defined as midpoints between zero crossings of the theta wave) after stimulation, and then comparing stimulation against control laps using F-tests.

To estimate the duration of silence induced by the stimulation, poststimulus time histograms (duration, 500 ms; bin width, 10 ms) were constructed, and the transition point was determined using a maximum likelihood estimator[40]. The two levels of stimulation were compared to the control with t-tests.

To compare phase precession plots across experimental conditions, firing fields were first divided into early (first third), middle (second third) and late (last third) subfields. Because the phase precession for different neurons spans slightly different ranges, the phase for each spike was first recentered on the overall mean phase in the firing field. The resulting relative phases in each subfield were then compared between experimental conditions using circular ANOVAs. This analysis would not, however, detect an overall shift in the phase precession plot toward higher or lower phases (a vertical translation that maintained an identical slope) in the different experimental conditions. Thus, a second approach was also used. For each subfield, the average theta phase was measured across experimental conditions (using all spikes fired in that subfield under all three conditions). Then, for each spike the angular deviation from the average phase was computed. Deviations were then compared between experimental conditions using circular ANOVAs.

Peak firing rates were compared using ANOVAs, and theta phases at peak locations were compared using circular ANOVAs. To control for different running velocities, the time taken for each rat to walk through a small area around the location of the stimulation (from 10 cm before to 20 cm after) was measured during the three experimental conditions.

ACKNOWLEDGMENTS

We thank M. Hasselmo, J. Lisman, J. Magee, M. Mehta, M. Tsodyks and Y. Yamaguchi for making the prediction of their models explicit after transient inactivation. We also thank K.D. Harris, A. Sirota and D.L. Buhl for assisting with data processing and L. Hazan, E. Pastalkova, S. Montgomery, S. Marguet and S. Royer for commenting on the manuscript. Supported by the National Institutes of Health (G.B.), the Human Frontier Science Program (M.B.Z.) and the French Defense Ministry (L.M.).

COMPETING INTERESTS STATEMENT

The authors declare that they have no competing financial interests.

Received 20 July; accepted 25 October 2004
Published online at http://www.nature.com/natureneuroscience/

1. O'Keefe, J. & Dostrovsky, J. The hippocampus as a spatial map. Preliminary evidence from unit activity in the freely-moving rat. *Brain Res.* **34**, 171–175 (1971).
2. O'Keefe, J. & Recce, M.L. Phase relationship between hippocampal place units and the EEG theta rhythm. *Hippocampus* **3**, 317–330 (1993).
3. Skaggs, W.E., McNaughton, B.L., Wilson, M.A. & Barnes, C.A. Theta phase precession in hippocampal neuronal populations and the compression of temporal sequences. *Hippocampus* **6**, 149–172 (1996).
4. Harris, K.D., Henze, D.A., Hirase, H., Leinekugel, X., Dragoi, G., Czurko, A. & Buzsáki, G. Spike train dynamics predicts theta-related phase precession in hippocampal pyramidal cells. *Nature* **417**, 738–741 (2002).
5. Mehta, M.R., Lee, A.K. & Wilson, M.A. Role of experience and oscillations in transforming a rate code into a temporal code. *Nature* **417**, 741–746 (2002).
6. Huxter, J., Burgess, N. & O'Keefe, J. Independent rate and temporal coding in hippocampal pyramidal cells. *Nature* **425**, 828–832 (2003).
7. Dragoi, G., Harris, K.D. & Buzsáki, G. Place representation within hippocampal networks is modified by long-term potentiation. *Neuron* **39**, 843–853 (2003).
8. Jensen, O. & Lisman, J.E. Position reconstruction from an ensemble of hippocampal place cells: contribution of theta phase coding. *J. Neurophysiol.* **83**, 2602–2609 (2000).
9. Jensen, O. & Lisman, J.E. Hippocampal CA3 region predicts memory sequences: accounting for the phase precession of place cells. *Learn. Mem.* **3**, 279–287 (1996).
10. Lisman, J.E. Relating hippocampal circuitry to function: recall of memory sequences by reciprocal dentate-CA3 interactions. *Neuron* **22**, 233–242 (1999).
11. Tsodyks, M.V., Skaggs, W.E., Sejnowski, T.J. & McNaughton, B.L. Population dynamics and theta rhythm phase precession of hippocampal place cell firing: a spiking neuron model. *Hippocampus* **6**, 271–280 (1996).
12. Wallenstein, G.V. & Hasselmo, M.E. GABAergic modulation of hippocampal population activity: sequence learning, place field development, and the phase precession effect. *J. Neurophysiol.* **78**, 393–408 (1997).
13. Kamondi, A., Acsady, L., Wang, X.J. & Buzsáki, G. Theta oscillations in somata and dendrites of hippocampal pyramidal cells *in vivo*: activity-dependent phase-precession of action potentials. *Hippocampus* **8**, 244–261 (1998).
14. Bose, A., Booth, V. & Recce, M. A temporal mechanism for generating the phase precession of hippocampal place cells. *J. Comput. Neurosci.* **9**, 5–30 (2000).
15. Bose, A. & Recce, M. Phase precession and phase-locking of hippocampal pyramidal cells. *Hippocampus* **11**, 204–215 (2001).
16. Booth, V. & Bose, A. Neural mechanisms for generating rate and temporal codes in model CA3 pyramidal cells. *J. Neurophysiol.* **85**, 2432–2445 (2001).
17. Yamaguchi, Y. A theory of hippocampal memory based on theta phase precession. *Biol. Cybern.* **89**, 1–9 (2003).
18. Lengyel, M., Szatmary, Z. & Erdi, P. Dynamically detuned oscillations account for the coupled rate and temporal code of place cell firing. *Hippocampus* **13**, 700–714 (2003).
19. Magee, J.C. A prominent role for intrinsic neuronal properties in temporal coding. *Trends Neurosci.* **26**, 14–16 (2003).
20. Koene, R.A., Gorchetchnikov, A., Cannon, R.C. & Hasselmo, M.E. Modeling goal-directed spatial navigation in the rat based on physiological data from the hippocampal formation. *Neural Net.* **16**, 577–584 (2003).
21. Sato, N. & Yamaguchi, Y. Memory encoding by theta phase precession in the hippocampal network. *Neural Comput.* **15**, 2379–2397 (2003).
22. Ekstrom, A.D., Meltzer, J., McNaughton, B.L. & Barnes, C.A. NMDA receptor antagonism blocks experience-dependent expansion of hippocampal "place fields". *Neuron* **30**, 631–638 (2001).
23. Magee, J.C. Dendritic mechanisms of phase precession in hippocampal CA1 pyramidal neurons. *J. Neurophysiol.* **86**, 528–532 (2001).
24. Buzsáki, G. & Czeh, G. Commissural and perforant path interactions in the rat hippocampus. Field potentials and unitary activity. *Exp. Brain Res.* **43**, 429–438 (1981).
25. Buzsáki, G., Grastyan, E., Czopf, J., Kellenyi, L. & Prohaska, O. Changes in neuronal transmission in the rat hippocampus during behavior. *Brain Res.* **225**, 235–247 (1981).
26. Douglas, R.M., McNaughton, B.L. & Goddard, G.V. Commissural inhibition and facilitation of granule cell discharge in fascia dentata. *J. Comp. Neurol.* **219**, 285–294 (1983).
27. Buzsáki, G., Chen, L.S. & Gage, F.H. Spatial organization of physiological activity in the hippocampal region: relevance to memory formation. *Prog. Brain Res.* **83**, 257–268 (1990).
28. Deadwyler, S.A., West, J.R., Cotman, C.W. & Lynch, G. Physiological studies of the reciprocal connections between the hippocampus and entorhinal cortex. *Exp. Neurol.* **49**, 35–57 (1975).
29. Lisman, J.E. & Idiart, M.A. Storage of 7±2 short-term memories in oscillatory subcycles. *Science* **267**, 1512–1515 (1995).
30. Gilden, D.L., Thornton, T. & Mallon, M.W. 1/f noise in human cognition. *Science* **267**, 1837–1839 (1995).
31. Kudrimoti, H.S., Barnes, C.A. & McNaughton, B.L. Reactivation of hippocampal cell assemblies: effects of behavioral state, experience, and EEG dynamics. *J. Neurosci.* **19**, 4090–4101 (1999).
32. Nadasdy, Z., Hirase, H., Czurkó, A., Csicsvari, J. & Buzsáki, G. Replay and time compression of recurring spike sequences in the hippocampus. *J. Neurosci.* **19**, 9497–9507 (1999).
33. Lee, A.K. & Wilson, M.A. Memory of sequential experience in the hippocampus during slow wave sleep. *Neuron* **36**, 1183–1194 (2002).
34. Blum, K.I. & Abbott, L.F. A model of spatial map formation in the hippocampus of the rat. *Neural Comput.* **8**, 85–93 (1996).
35. Mehta, M.R., Barnes, C.A. & McNaughton, B.L. Experience-dependent, asymmetric expansion of hippocampal place fields. *Proc. Natl. Acad. Sci. USA* **94**, 8918–8921 (1997).
36. Buzsáki, G. Theta oscillations in the hippocampus. *Neuron* **33**, 325–340 (2002).
37. Csicsvari, J., Hirase, H., Czurko, A. & Buzsáki, G. Reliability and state dependence of pyramidal cell-interneuron synapses in the hippocampus: an ensemble approach in the behaving rat. *Neuron* **21**, 179–189 (1998).
38. Harris, K.D., Henze, D.A., Csicsvari, J., Hirase, H. & Buzsáki, G. Accuracy of tetrode spike separation as determined by simultaneous intracellular and extracellular measurements. *J. Neurophysiol.* **84**, 401–414 (2000).
39. Harris, K.D., Hirase, H., Leinekugel, X., Henze, D.A. & Buzsáki, G. Temporal interaction between single spikes and complex spike bursts in hippocampal pyramidal cells. *Neuron* **32**, 141–149 (2001).
40. Friedman, H.S. & Priebe, C.E. Estimating stimulus response latency. *J. Neurosci. Methods* **83**, 185–194 (1998).

J Neurophysiol 92: 600–608, 2004;
10.1152/jn.01170.2003.

Characterization of Neocortical Principal Cells and Interneurons by Network Interactions and Extracellular Features

Peter Barthó, Hajime Hirase, Lenaïc Monconduit, Michael Zugaro, Kenneth D. Harris, and György Buzsáki
Center for Molecular and Behavioral Neuroscience, Rutgers, The State University of New Jersey, Newark, New Jersey 07102

Submitted 8 December 2003; accepted in final form 6 February 2004

Barthó, Peter, Hajime Hirase, Lenaïc Monconduit, Michael Zugaro, Kenneth D. Harris, and György Buzsáki. Characterization of neocortical principal cells and interneurons by network interactions and extracellular features. *J Neurophysiol* 92: 600–608, 2004; 10.1152/jn.01170.2003. Most neuronal interactions in the cortex occur within local circuits. Because principal cells and GABAergic interneurons contribute differently to cortical operations, their experimental identification and separation is of utmost important. We used 64-site two-dimensional silicon probes for high-density recording of local neurons in layer 5 of the somatosensory and prefrontal cortices of the rat. Multiple-site monitoring of units allowed for the determination of their two-dimensional spatial position in the brain. Of the ~60,000 cell pairs recorded, 0.2% showed robust short-term interactions. Units with significant, short-latency (<3 ms) peaks following their action potentials in their cross-correlograms were characterized as putative excitatory (pyramidal) cells. Units with significant suppression of spiking of their partners were regarded as putative GABAergic interneurons. A portion of the putative interneurons was reciprocally connected with pyramidal cells. Neurons physiologically identified as inhibitory and excitatory cells were used as templates for classification of all recorded neurons. Of the several parameters tested, the duration of the unfiltered (1 Hz to 5 kHz) spike provided the most reliable clustering of the population. High-density parallel recordings of neuronal activity, determination of their physical location and their classification into pyramidal and interneuron classes provide the necessary tools for local circuit analysis.

INTRODUCTION

Transformation, transmission, and storage of information in the brain are achieved by cooperative action of neuronal ensembles. A main goal of neurophysiology is to understand the rules that determine the behavior of these flexible coalitions (Chicurel 2001; Deadwyler and Hampson 1995; Eichenbaum and Davis 1998). A first step in this process is the simultaneous recording from large numbers of neurons in the behaving animal. The recent advent of multisite, closely spaced extracellular recording techniques has improved single-unit sorting by taking advantage of the temporal coherence of spikes from closely spaced recording sites (Csicsvari et al. 1999, 2003b; Drake et al. 1988; Gray et al. 1995; McNaughton et al. 1983; O'Keefe and Recce 1993; Wilson and McNaughton 1993), allowing identification and classification of multiple extracellularly recorded neurons. In the neocortex, several classes of interneurons (Somogyi et al. 1998; Swadlow 2003) provide timing, oscillatory background, and other general contexts for the computations carried out by the principal cells (Buzsáki and Chrobak 1995). Therefore experimental separation of interneurons from pyramidal cells is of utmost importance in the understanding of the operation principles of the neocortex. The last, and perhaps most difficult, task is to identify subclasses of interneurons and principal cells from their extracellular signatures (Klausberger et al. 2003).

In the hippocampus, the combination of several extracellular features, such as spike duration, firing rate, and pattern and spike waveform, reliably separates pyramidal cells from interneurons (Csicsvari et al. 1999). The validity of neuron classification on the basis of extracellular features has been supported by in vivo intra- and juxtacellular labeling as well as simultaneous extra- and intracellular recordings from the same neurons (Henze et al. 2000; Klausberger et al. 2003; Sik et al. 1995). Similar classification criteria are not available in the neocortex. Mountcastle et al. (1969) have noted that the occasionally recorded "thin spikes" in the somatosensory cortex had different response properties than the majority of units and suspected that they were interneurons. Other observations indicated that fast-spiking neurons have receptive and evoked response properties different from the majority of slower, more regular firing cells (Constantinidis and Goldman-Rakic 2002; Simons 1978; Swadlow 2003; Swadlow and Gusev 2002; Swadlow and Lukatela 1996; Swadlow et al. 1998). Intracellular recordings and labeling in cortical slices showed numerous classes of interneurons on the basis of the firing rates, spike morphology, and spike dynamics (Connors et al. 1982; Gupta et al. 2000; Kawaguchi and Kubota 1993; Somogyi et al. 1998). However, the information gathered in intracellular experiments in vitro cannot be directly applied to extracellularly recorded spikes in the intact brain. Furthermore, intra- and juxtacellular studies carried out in vivo do not directly support the suggestion that fast firing neurons unequivocally identify interneurons (Azouz et al. 1997; Degenetais et al. 2002; Douglas et al. 1995; Gray and McCormick 1996; Steriade et al. 1998).

To provide more direct classification criteria for cell identification, we took advantage of large-scale parallel recording of unit activity in a small cortical volume (Csicsvari et al. 2003a). In a large data base, we found that ~0.25% of the recorded cell pairs had short-latency (<3 ms), putative monosynaptic interactions. Units exciting other units at monosynaptic latency were regarded as pyramidal cells, whereas units suppressing discharges of target partners were regarded as GABAergic inhibitory interneurons. These physiologically identified neurons helped us assess the physiological features of the extra-

Address for reprint requests and other correspondence: G. Buzsáki, Center for Molecular and Behavioral Neuroscience, Rutgers University, 197 University Ave., Newark, NJ 07102 (E-mail: buzsaki@axon.rutgers.edu).

The costs of publication of this article were defrayed in part by the payment of page charges. The article must therefore be hereby marked "*advertisement*" in accordance with 18 U.S.C. Section 1734 solely to indicate this fact.

cellular spikes and classify the whole population into putative pyramidal and interneuron groups.

METHODS

Surgery and recording

For acute recordings, Sprague-Dawley rats (300-500 g; Hilltop Laboratories, Scottsdale, PA, or Zivic-Miller laboratories, Pittsburgh, PA) were anesthetized with urethan (1.5 g/kg) and placed in a stereotaxic frame. After preparing a 1 × 3-mm window in the skull, the dura was removed using a dissection microscope, and the probe was positioned so that the tips avoided blood vessels. The skull cavity was filled with a mixture of wax and paraffin, which decreased brain pulsation as well as provided lateral support for the probe shanks. The recording silicon probe was attached to a micromanipulator and moved gradually to its desired depth position. The probe consisted of eight shanks (200-μm shank separation), and each shank had eight recording sites (160 μm^2 each site; 1-3 MΩ impedance) with recordings sites staggered to provide a two-dimensional arrangement (20 μm vertical separation; see Fig. 3. For information on silicon probes manufactured at University of Michigan, see http://www.engin.umich.edu/center/cnct/). The middle shanks were centered at anterior-posterior, AP = −1.5 mm and mediolateral; ML = 3.5 mm position to record from the primary somatosensory cortex. After each acute experiment the probe was rinsed with de-ionized water. Probes were used repeatedly for several months without noticeable deterioration in performance. Extracellular signals were high-pass filtered (1 Hz) and amplified (1,000 times) using a 64-channel amplifier (Sensorium, Charlotte, VT). All data were digitized at 25 kHz (DataMax System, RC Electronics, Santa Barbara, CA) using 16-bit resolution and stored on a computer disk for later analysis.

The general surgical procedures for chronic recordings have been described (Csicsvari et al. 2003b). In short, rats of the Sprague-Dawley strain (400-900 g) were anesthetized with a mixture (4 ml/kg) of ketamine (25 mg/ml), xylazine (1.3 mg/ml), and acepromazine (0.25 mg/ml) and placed in the stereotaxic apparatus. Instead of silicon probes, wire tetrodes were attached to a custom-prepared microdrive. The tetrodes were implanted the same way as in the acute experiments. During implantation the tips of the tetrodes were lowered ~400 μm below the brain surface. After recovery from surgery, the probes were moved gradually, and recordings were made at several depth locations. In both acute and chronic experiments, location of layer V neurons was assessed by recording delta waves and unit activity. Delta waves reverse in polarity below layer IV, and units are silenced during positive delta waves (Buzsáki et al. 1988). The physiological data were collected during sleep and spontaneous exploration in the home cage. All procedures conformed to the National Institutes of Health Guide for the Care and Use of Laboratory Animals.

SPIKE SORTING AND CONNECTION ANALYSIS. The continuously recorded wide-band signals were high-pass filtered (0.8-5 kHz) digitally. Units were identified and isolated by a semiautomatic "cluster cutting" algorithm ("KlustaKwik"; available at: http://osiris.rutgers.edu/buzsaki/software) followed by manual clustering (Csicsvari et al. 1998). Auto- and cross-correlations were calculated to verify the clustering procedure. The quality of spike clusters was estimated by measuring the Mahalanobis distance ("isolation distance") from the cluster center within which as many points belong to other clusters as belong to the specified cluster (Harris et al. 2001). Center of mass was calculated as the mean *x-y* position of the recording sites weighted by the spike amplitude at each site. For the identification of excitatory connections, short-latency and -duration sharp peaks in the cross-correlograms were used as described by Csicsvari et al. (1998). Significant peaks (1-ms bin width) within 3 ms of the center bin were considered as putative monosynaptic connections. A peak in a cross-correlogram was defined significant when at least one of the bins exceeded 99.9th percentile of the mean. Similarly, short-latency troughs were considered to be due to inhibition when at least two neighboring 1-ms bins were <0.1th percentile of the mean (Constantinidis et al. 2002). The mean (control number of spikes) was calculated between –50 and –10 ms to control for a potential low-frequency fluctuation of firing rate. For cell pairs recorded from the same electrode, the 0- to 1-ms bin was not considered because our clustering program cannot resolve superimposed spikes. This artificial trough was excluded from the analysis.

Histological procedures

After completion of the experiments, the rats were killed and perfused through the heart first with 0.9% saline solution followed by consisting of 4% paraformaldehyde, 15% picric acid, and 0.05% glutaradehyde in 0.1 M phosphate buffer. The brains were sectioned by a Vibroslice at 60 μm in the coronal plane, washed extensively in phosphate buffer, and treated with 0.5% Triton to enhance penetration. Sections were mounted on slides, Nissl-stained, and coverslipped. The tracks of the silicon probe shanks were reconstructed from multiple sections.

RESULTS

Unit recording and clustering

Figure 1 illustrates recordings with the 64-site probe from layer V of the somatosensory cortex of the urethan-anesthetized rat. Most of the 64 recording sites yielded unit activity in every experiment ($n = 16$), and the same units were recorded by several recording sites of the same shank. The voltage profile of spikes across the recording sites provided an approximate location of the cell body of the recorded neuron. The spike amplitude from presumed perisomatic locations often exceeded 0.3 mV. The spike amplitude and waveform variability across recording sites were used for separating single units (Gray et al. 1995; Wise and Angell 1975). The eight recording sites in each shank provided a total of 28 two-dimensional views of unit clusters for each shank (Fig. 1). The reliability of spike cluster separation was quantitatively determined by the isolation distance measure of unit quality and the spike contamination of the refractory period in the auto-correlograms (Harris et al. 2000). Silicon shanks placed in layer V pyramidal layer yielded 12-18 high-quality units per shank. A total of 1,414 units were recorded from the primary somatosensory area and the prefrontal cortex (anesthetized $n = 16$ rats, freely moving $n = 7$ rats).

Monosynaptic neuronal interactions in layer V neurons

Monosynaptic connections were assessed by examining the short-latency interactions between neurons pairs as described in the hippocampus (Csicsvari et al. 1998). Paired recordings from layer V neurons in vitro showed that short onset latency monosynaptic excitatory postsynaptic potential (EPSP) responses corresponded to monosynaptic connections between pyramidal cell-interneuron pairs (Angulo et al. 2003; Gupta et al. 2000; Somogyi et al. 1998; Thomson and Deuchars 1997; Thomson et al. 1995) and pyramidal-pyramidal cells (Deuchars et al. 1994; Holmgren et al. 2003; Markram 1997). Short-latency inhibitory postsynaptic potentials (IPSPs) were also evoked by single interneuron spikes in both pyramidal and interneuron targets (Buhl et al. 1997; Maccaferri et al. 2000;

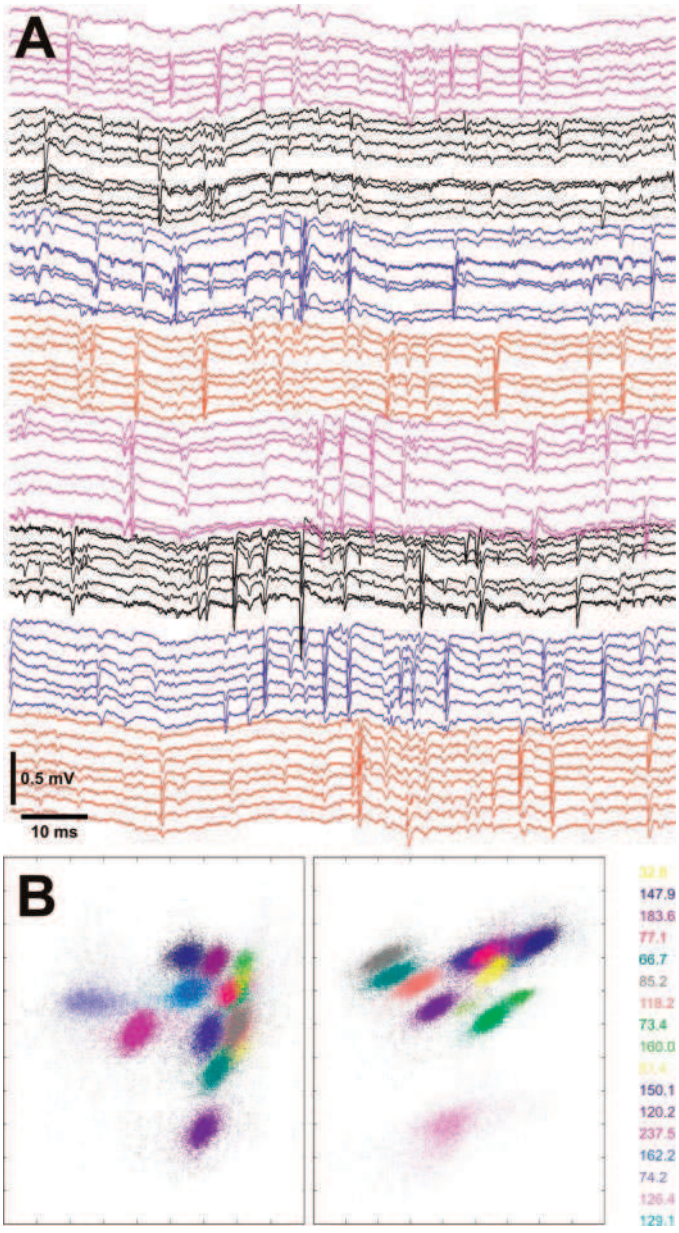

FIG. 1. Parallel recording of unit activity in layer V of the somatosensory cortex by an 8-shank probe. Each shank had 8 recording sites (for tip details Fig. 3). A short segment of wide-band signal (field and unit activity) is displayed. Recordings from the 8 parallel shanks are color-coded and plotted below each other. Note temporally coherent spikes on several sites of a given shank and lack of "cross-talk" across shanks. *Bottom*: 2 separate 2-dimensional views of unit clusters from 1 shank. The 8 recording sites provided a total of 24 2-dimensional views of unit clusters for each shank. Clusters are color-coded. Quality of clusters ("isolation distance") was estimated by measuring the Mahalanobis distance (color coded figures) from the cluster center within which as many points belong to other clusters as belong to the specified cluster (Harris et al. 2001).

Tamas et al. 1997; Thomson and Bannister 2003). Neurons with <1-Hz firing rates (n = 281) were excluded from these analyses. Of the 56,845 cross-correlograms (n = 6,754 from prefrontal cortex recordings) 107 (0.2%) had short-latency (<5 ms onset) significant peaks or troughs (Fig. 2). Of these, 58 had large and narrow peaks (Fig. 2*A*), indicating that the presynaptic neuron was an excitatory pyramidal cell. The precise short-latency drive could often be visualized by superpositioning of the spike trains (Fig. 2*B*). Another 21 pairs had significant short-latency suppression (Fig. 2*C*), indicating that the presynaptic neuron was an inhibitory interneuron. To quantitatively assess the time course of monosynaptic inhibition, an exponential curve was fit for the spike bins after the presynaptic spike (the inhibitory trough on the cross-correlogram). The mean time constant of spike suppression was 5.17 ± 3.12 ms, although with substantial variability as indicated by the large SD. Finally, 28 pairs showed both short-latency peaks and troughs, suggesting that these pairs were mutually connected pyramidal-interneuron pairs (Fig. 2*D*). As expected from anatomical connectivity, the detected physiological connections were not distributed homogenously among the population. The majority of monosynaptically connected pairs were detected from the neuronal pool recorded by the same shank (excitatory connections = 0.87%; inhibitory connections = 0.55%), although pairs were also identified between shanks as well (excitatory connections = 0.15%; inhibitory connections = 0.09%). Often a single neuron was connected to several postsynaptic targets. More than a quarter (29%) of the physiologically identified interneurons suppressed activity of two to seven target cells. Convergence of excitation is illustrated by the finding that among the excitatory connections 40% of the target cells were excited by 2–12 presynaptic neurons. Most neurons that were excited were shown to be putative inhibitory interneurons by their spike suppression effects of their targets (58%). Neurons that were classified as excitatory in one or more connections never suppressed activity of any target. Conversely, putative interneurons were never found to excite other partners. Figure 3 illustrates the circuit analysis of multiple uni- and bidirectionally connected pairs in a small neuronal pool. The largest "hub" involved interneuron 3, which was excited by 5 of the 15 neurons recorded by the same shank and 7 of the 37 neurons recorded by the surrounding shanks. In turn, it inhibited 4 of the 15 cells from the same shank and 3 of the 37 neurons recorded by the other shanks. Five connections were bidirectional. These simultaneous recordings also indicated that the magnitude and time course of the monosynaptic effects were quite heterogeneous on the postsynaptic targets.

The preceding findings in urethan-anesthetized animals were confirmed by wire tetrode recordings from the somatosensory area in drug-free, behaving rats. Of the 3,814 unit pairs, 9 putative excitatory and 2 putative inhibitory connections were identified. Reciprocal interaction was detected in one pair. The similar proportions of putative monosynaptic connections in the drug-free and anesthetized preparations indicated that urethan anesthesia did not affect the fast monosynaptic connections dramatically.

Characterization of pyramidal cells and interneurons by extracellular features

The monosynaptic interactions were used as criteria for the classification of the remaining, nonidentified units into pyramidal cell and interneuron classes. Neurons with short-latency, narrow peaks were regarded as putative excitatory (pyramidal) cells, whereas neurons with short-latency suppression of activity as putative inhibitory interneurons. In addition, units that were excited by a presynaptic pyramidal cell were also distinguished. In principle, these neurons could be other pyramidal

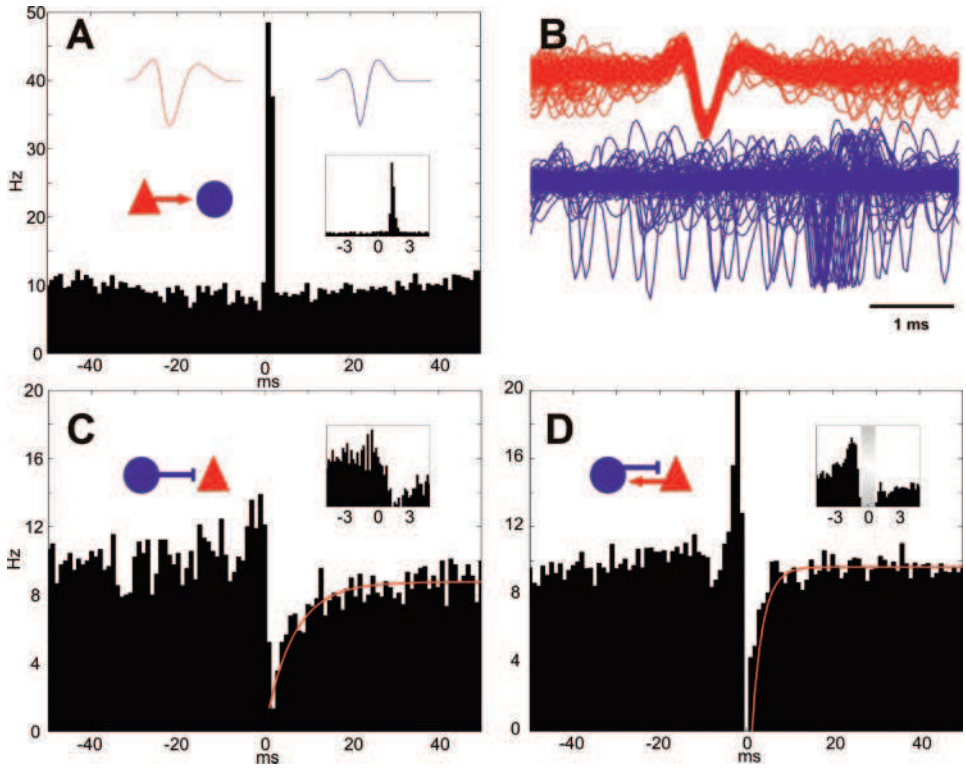

FIG. 2. Short-latency, monosynaptic interactions between neuron pairs. *A*: excitatory drive by a putative pyramidal cell (red triangle). Note large, sharp peak at ~2 ms in the cross-correlogram. Reference event is the spike of the putative pyramidal neuron (*time 0*). *Inset*: higher temporal resolution of the histogram. Averaged waveforms of the units (filtered: 600 Hz to 5 kHz) are also shown. On the bases of spike duration, the target cell was classified as a putative interneuron (blue circle; see text). *B*: superimposed traces of the neuron pair from 2 recording sites with the largest amplitude for each spike. Arrow, monosynaptically driven spikes. *C*: inhibitory suppression. Reference event: spike of the putative interneuron (blue circle). Note strong and immediate suppression of target spikes. The 2 neurons were recorded from different shanks (200-μm lateral separation). Red line indicates exponential fit of suppression time course. *D*: reciprocal monosynaptic interactions of neurons recorded from the same shank. Reference event: spike of the putative interneuron (blue circle). Note excitation of the putative interneuron and strong suppression of the pyramidal cell (red triangle) spikes by the interneuron. Shading indicates the blank period of spike sampling (see METHODS).

cells. However, single-spike discharge in the presynaptic neuron has not been shown to bring the postsynaptic pyramidal cell to threshold (Markram et al. 1997). On the other hand, several studies reported reliable spike transmission between pyramidal-interneuron pairs (Holmgren et al. 2003; Marshall et al. 2002; Swadlow 2003). Using these criteria, several features of the extracellularly recorded units, including discharge frequency, spike duration, spike asymmetry, and amplitude ratio of the negative and positive peaks, as well as features of the auto-correlogram, such as center of mass, time from zero to peak, and burstiness ratio, were examined together with the whole recorded population (Fig. 4). Of these criteria, spike duration provided the best separation. Spike duration was measured between the trough and the following peak of the unfiltered trace because these time points reflect the maximum rate of rise and the maximum rate of decay of the intracellularly recorded action potential (Henze et al. 2000). This criterion was consistently reliable for providing a bimodal distribution of units in somatosensory cortex, prefrontal cortex and in the drug-free animal (Fig. 4; 7.42 vs. 92.57%). The spike duration of putative interneurons was significantly ($P < 0.0001$; *t*-test) more narrow (0.43 ± 0.27 ms) than that of the putative pyramidal cells (0.86 ± 0.17 ms). Table 1 summarizes the distribution of the various interactions in the two groups. Approximately 40% of narrow spike neurons either inhibited target cells or were excited by a presynaptic partner. None of them were classified as excitatory. We also noted that 8 of 54 unconnected narrow spike neurons had bursty auto-correlograms (see following text), whereas none of the 40 neurons with significant interactions did. Excitatory forward connections were detected only in the wide spike group (6.9%) and nearly all of the inhibited neurons belonged to this group (Table 1).

Subclasses of cortical neurons

Following classification of the neurons on the basis of functional connectivity into putative pyramidal and interneuron classes, we searched for potential subgroups within the populations. The auto-correlograms of putative pyramidal cells showed two extreme behaviors. "Bursting" cells had large peaks at 3-6 ms followed by an exponential decay (Fig. 5*A*). Cells were classified as bursting, if the maximum peak on the auto-correlogram between 3 and 6 ms was ≥50% of the maximum bin value of the first 50 ms. The criterion for "regular spiking" (nonbursting) cells was that the mode of interspike-interval histogram was >35 ms. Regular spiking neurons rarely discharged in bursts, and the auto-correlogram showed an exponential rise from *time 0* to tens of milliseconds (Fig. 5*A*). Cells that did not match either of these criteria were labeled "unclassified." Of the putative pyramidal cell population, 53.3% were assigned to regular spiking, 18.24% bursting, and 28.45% belonged to the unclassified or intermediate group. The average firing rate was similar in these three groups (5.62 ± 3.27, 4.02 ± 3.46, and 3.42 ± 3.06 Hz, respectively). The spike duration of the wide-band recorded signal was also similar across these putative groups (0.79 ± 0.15, 0.85 ± 0.13, and 0.88 ± 0.15 ms, respectively). Neurons in each of these groups excited postsynaptic targets. Of the identified excitatory cells, 68.42% was regular spiking, 17.54% bursting, and 14.04 unclassified. Similarly, within the inhibited cell group 65.85% were regular spiking, 14.63% bursting, and 19.51% unclassified (Fig. 5*B*).

As discussed in the preceding text, neurons that were excited at monosynaptic latency could, in principle, include pyramidal cells and interneurons. This group was heterogeneous by firing frequency, spike duration, and other criteria. Nevertheless, the auto-correlograms in this group were more similar to the pu-

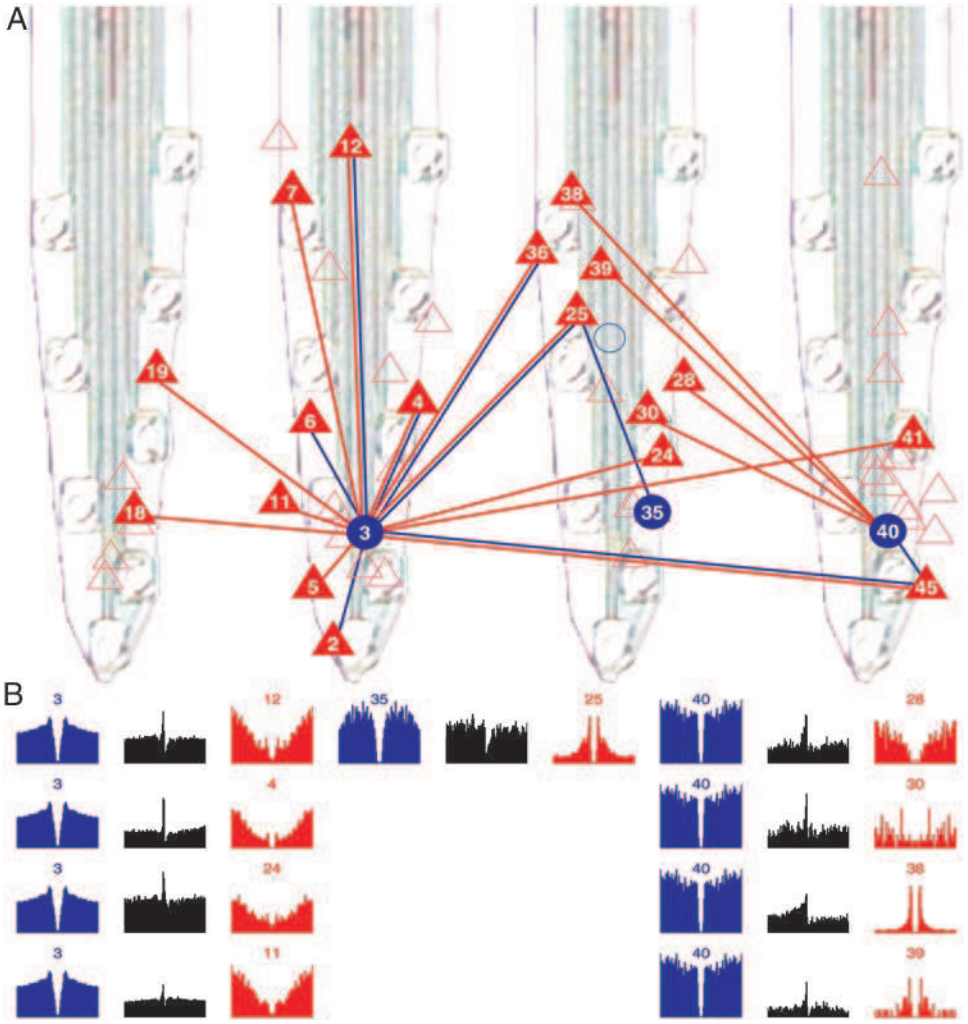

FIG. 3. Tracing of functional connections in local networks. *A*: units recorded by only 4 shanks are shown. Filled symbols, participating pyramidal cells (red triangles) and interneurons (blue circles). Empty symbols, neurons not connected functionally. Red line, monosynaptic excitation; blue line, monosynaptic inhibition. Note that a single interneuron (e.g., 3 and 40) is activated by large number pyramidal cells, and an interneuron inhibits several local and distant pyramidal cells. The relative position of the neurons was determined by calculating the "center of mass" on the basis of the spike amplitude recorded from multiple sites. Sites are spaced 20 μm vertically. The shanks were 200 μm apart but for illustration purposes they are placed closer to each other here. *B*: auto-correlograms (blue and red) and cross-correlograms of some of the pairs shown in *A*. Note short-latency interactions.

tative interneuron group, identified by their inhibitory effects and narrow spikes than to those of the pyramidal cells. No unit in this group had either a bursting or regular spiking type auto-correlogram, typical of pyramidal cells.

DISCUSSION

The main finding of the present experiments is a physiological method for the identification and separation of inhibitory interneurons and principal cells in cortical networks. Although our work was carried out in layer V of the rat, the method based on short-latency cross-correlation of spike dynamics can be used in any other layers and networks regardless of the species. The identified minority then can be used as a template for classifying the recorded population into at least two major classes (putative principal cells and interneurons) and estimate the error associated with the classification. Parallel recording of neuronal activity in the two-dimensional space also allows for the identification of anatomically functionally connected assemblies.

Identification of neuron types on the basis of synaptic interactions

The main hypothesis of the present work was that neurons with robust short-term cross-correlation reliably identify the nature of the presynaptic neuron. A prerequisite of this approach is a reliable separation of individual neurons. To date, the most widely used method for the separation of multiple neuronal activity, recorded in a small piece of tissue, is based on the temporal correlation of spikes (Drake et al. 1988; McNaughton et al. 1983; O'Keefe and Recce 1993). This can be achieved by monitoring unit activity with closely spaced multiple sensors, such as tetrodes and silicon probes (Csicsvari et al. 1999, 2003a; Gray et al. 1995; Harris et al. 2000; Quirk and Wilson 1999; Wilson and McNaughton 1993). Silicon probes with multiple, staggered recording sites used in the present study provided distinct neuronal clusters in layer 5 of the neocortex. Although the reliability of single neuron separation cannot be objectively determined without information about the intracellularly recorded action potentials (Henze et al. 2000), the Mahalanobis distance between spike clusters is a reliable indicator for the "cleanness" of the clusters (Harris et al. 2001). The geometrically precise distribution of the eight recording sites also allowed for the determination of the "center of mass", i.e., the approximate two-dimensional position of cell bodies of the putative single neurons.

One of ~400 unit pairs showed robust short-latency interactions, indicative of monosynaptic connections. Large, narrow peaks in the cross-correlograms within 3 ms were taken as

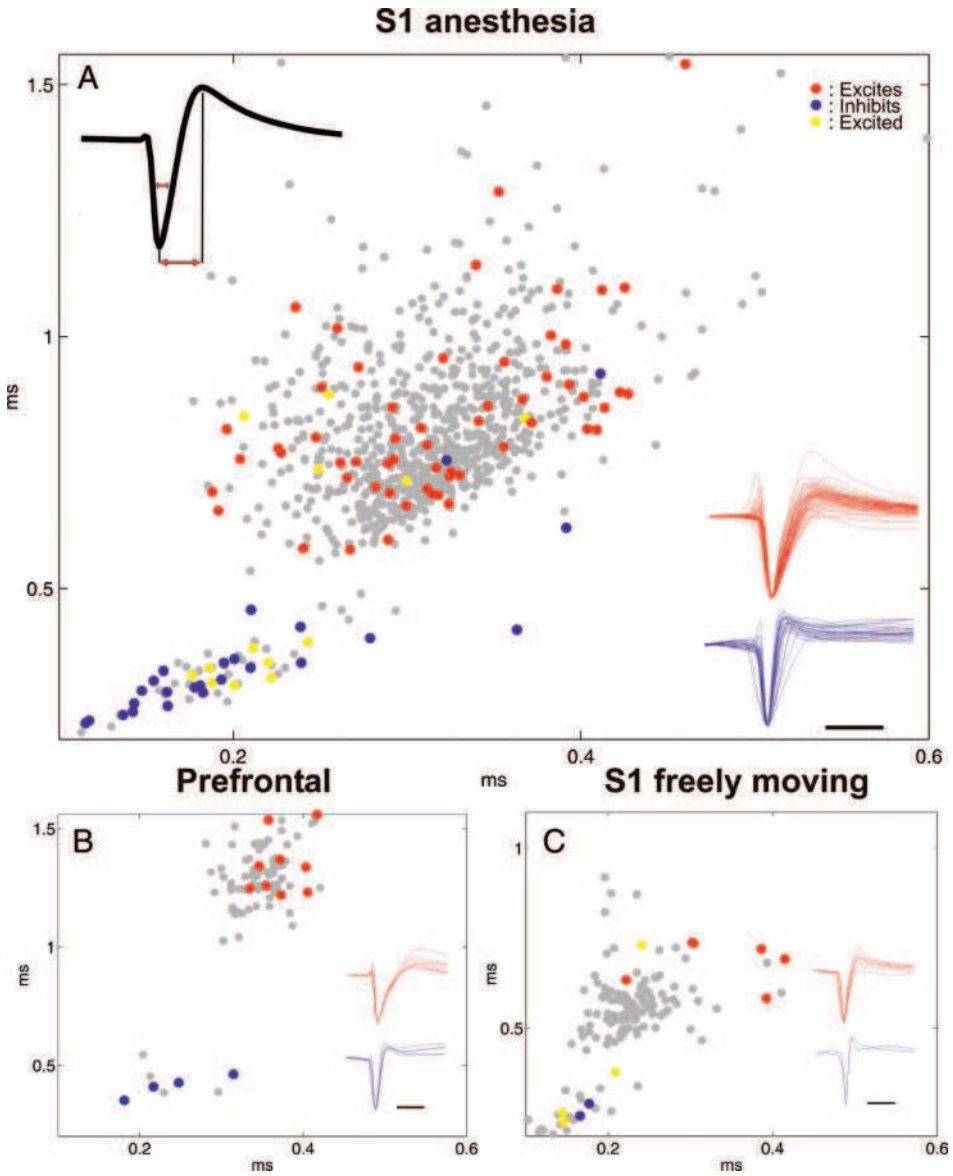

FIG. 4. Separation of putative neocortical interneurons and pyramidal cells. *A*: black trace, temporal parameters used in the clustering process (half-amplitude duration, *x* axis; trough to peak time, *y* axis). Red and blue dots: excitatory and inhibitory cells identified by monosynaptic interactions in the somatosensory cortex (S1). Green dots: neurons excited monosynaptically. Gray dots: unidentified units. *Inset*: average waveforms of identified excitatory and inhibitory units (1 Hz to 5 kHz) normalized for peak-to-peak amplitude. *B*: same as *A* but for units recorded in the prefrontal cortex (PFC). *C*: same as *A* but for units recorded by wire tetrodes in freely moving rats. Note clear separation of unit clouds in each case.

evidence that the presynaptic neuron was excitatory. Potential interactions recorded by the same recording sites within 1 ms could not be studied with the present methods because activity was ignored in this time bin by our spike-detection program. Previous studies in the hippocampus in vivo revealed high spike-transmission probabilities between pyramidal cells and interneurons either by cross-correlation or by intracellular stimulation of the presynaptic pyramidal neuron (Csicsvari et al. 1998, 1999; Marshall et al. 2002). Similarly, cross-correlation between thalamocortical and putative neocortical interneurons identified monosynaptic excitatory connections (Swadlow and Gusev 2001). Paired recordings from neocortical pyramidal cells and target interneurons also showed high reliability of synaptic transmission (Holmgren et al. 2003; Somogyi et al. 1998; Thomson and Bannister 2003), although EPSPs rather than spike transmission probabilities have been studied in those in vitro studies. It should be noted here that the cross-correlation method used here creates a bias in favor of active neurons.

TABLE 1. *Physiological interactions of neurons with wide and narrow action potentials*

Type	*n*	Exciting	Inhibiting	Excited Only	Inhibited Only	Excited and Inhibiting	Unconnected
Wide	1039	72 (6.9)	5 (0.5)	6 (0.6)	20 (1.9)	2 (0.2)*	936 (90.1)
Narrow	94	0 (0.0)	28 (29.8)	11 (11.7)	1 (1.1)	20 (21.3)*	54 (57.4)

Parentheses enclose percentages. Exciting, neurons with significant short-latency peaks in cross-correlogram (reference neuron). Inhibiting, neurons with significant short-latency suppression in cross-correlogram (reference neuron). Excited only, neurons with significant short-latency peaks in cross-correlogram (target neuron). Inhibited only, neurons with significant short-latency suppression in cross-correlogram (target neuron). Excited and inhibiting, neurons which were both excited by a reference neuron and inhibiting a target neuron. *These percentage values are excluded from the total (100%) because they reflect subgroups with dual effect.

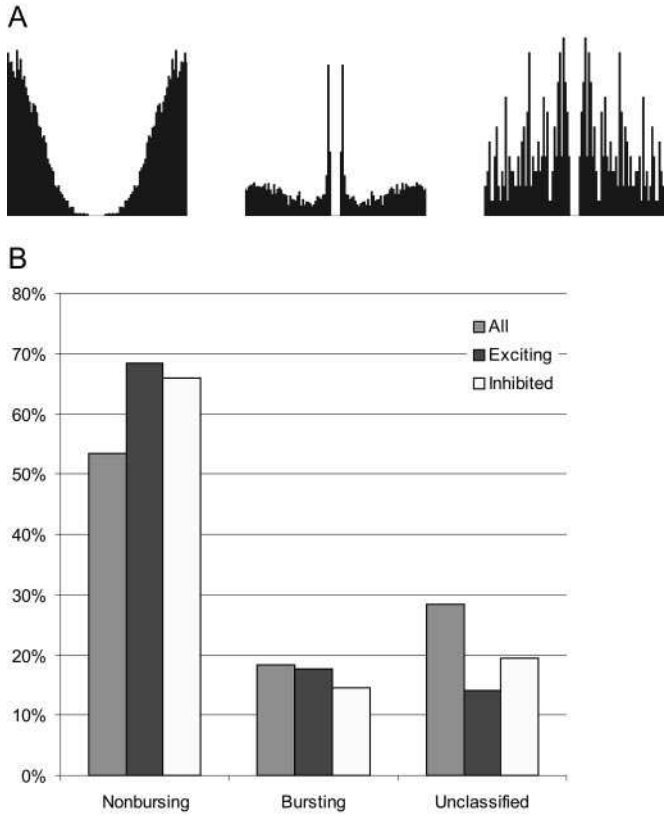

FIG. 5. Classification of putative pyramidal neurons on the basis of spike dynamics. *A*: putative pyramidal cells were classified into "nonbursting" (regular spiking; *left*), "bursting" (*middle*), and unclassified (*right*) groups on the basis of their auto-correlograms. Three examples are shown. *B*: distribution of the 3 groups. Note that the probability of monosynaptic excitation or being inhibited by an interneuron was similar in the groups.

Connected pairs with very low firing rates may have remained undetected.

Suppression of unit activity in the cross-correlogram by identified inhibitory neurons is a novel observation, although short-latency suppression in cross-correlograms has been reported earlier (Constantinidis et al. 2002). Several pairs, recorded by either the same or different shanks, displayed strong, short-latency suppression after the presynaptic spike. We regard these interactions as support for the inhibitory nature of the presynaptic neuron. In principle, a third-party bias, involving direct excitation of neuron 1 and feed-forward inhibition of neuron 2 by a third, unrecorded neuron, could also result in suppressed activity in the cross-correlogram between neurons 1 and 2. This scenario is not very likely though for the following reasons. First, in several cases we have seen strong and complete cessation of spiking in the putative postsynaptic neuron. For third-party excitation-feed-forward inhibition explanation, an additional assumption should be made that whenever neuron 1 fired, it was always discharged by the third party and not by other neurons in the network. This is unlikely given the low threshold and large convergence of excitatory inputs onto inhibitory interneurons (Somogyi et al. 1998; Swadlow 2003). Second, the spike waveform of most putative inhibitory interneurons was significantly shorter than that of the putative postsynaptic cells, indicating that they belonged to different neuron types. In support of our interpretation, paired recordings from interneurons and neocortical pyramidal cells in vitro revealed that IPSP transmission is highly reliable and effective in suppressing spiking activity brought about either by synaptic activity or intracellular depolarizing pulses (Gupta et al. 2000; Somogyi et al. 1998; Thomson and Bannister 2003). Although direct comparison of in vitro and in vivo situations is not straightforward, the temporal dynamics of in vitro measured IPSPs (Tamas et al. 1997; Thomson et al. 1996) and the time constant of spike suppression in our study (~5 ms) were similar.

A third consideration of the short-latency interactions is the nature of the postsynaptic neuron in pairs with large, short-latency peaks. Pyramidal cells excite both pyramidal cells and interneurons. Paired recordings between some layer 5 pyramidal neuron pairs by Markram et al. (1997) showed 5–15 putative release sites and relatively low probability of EPSP failures. However, spikes were never evoked in the postsynaptic neuron even by presynaptic spike bursts. Our observations indicate that at least some of the postsynaptic neurons in our pairs were interneurons. First, in the hippocampal CA1 region with very sparse local collaterals, monosynaptic peaks between neuronal pairs always involved postsynaptic interneurons (Csicsvari et al. 1998, 1999). Second, several units with a short-latency peak in our study had narrow spikes, indicating that they were interneurons (see following text). Third, some pairs had bidirectional interactions, identifying the excited postsynaptic neurons as an inhibitory cell. Fourth, none of the units with short-latency excitation had auto-correlograms that would unequivocally identified them as bursting or regular spiking, features that characterized many identified pyramidal cells. However, in several cases, the postsynaptic nature of the monosynaptically excited neuron could not be identified by the preceding criteria. Their spike width and waveform were indistinguishable from those of the pyramidal cells. It is notable though that some interneuron types in both hippocampus and neocortex have action potentials and firing rates quite similar to those of pyramidal cells (Degenetais et al. 2003; Freund and Buzsáki 1996).

Identification of small groups of neurons in the recorded population by their short-time correlations allowed us to use them as templates for the classification of the whole population. Of the several parameters tested, the duration of the wide-band recorded spike proved to be most efficient, confirming Mountcastle's original suggestion that "thin" spikes correspond to inhibitory interneurons (Mountcastle et al. 1969), at least in layer 5 of the neocortex. In the hippocampus, combination of parameters (spike duration, shape, firing rate, spike dynamics) proved more efficient for the separation of pyramidal cells and interneurons than using just a single parameter (Csicsvari et al. 1999). Previous investigators used discharge rate differences elicited by afferent stimulation to distinguish these two major categories (cf. Swadlow 2003). In our experiments, firing-rate differences did not provide reliable separation, although many inhibitory neurons and unidentified short-duration spike neurons fired at high frequency. The auto-correlograms of physiologically identified and putative interneurons were never as fast decaying or slow rising as those of pyramidal neurons. Nevertheless, there was an overlap with putative pyramidal cells in the unclassified group.

Unit classification based on spike duration resulted in a clear bimodal distribution with ~7% of units belonging to the interneuron group. Approximately 15-20% of neocortical neu-

rons are believed to be GABAergic and are equally distributed in the cell body and dendritic layers of the cortex (Beaulieu and Colonnier 1983). Although there are no separate percentage estimates for interneurons in layer 5 only, the 7% figure appears low. One potential explanation for this low number is that not all inhibitory interneurons have short-duration action potentials (Freund and Buzsáki 1996). Indeed, a minority of neurons that inhibited their target partner(s) but had wider spikes than the designated interneuron group generated most of the classification errors in the identified cell groups. Furthermore, a portion of the units that were excited at a monosynaptic latency had wide spikes. Some or all of these excited neurons with wide spikes could belong to the GABAergic interneuron group. In the hippocampus, most interneurons with cell bodies in the pyramidal layer have short-duration spikes (putative basket and chandelier cells), whereas spike duration of stratum oriens/alveus interneurons is quite heterogeneous (Csicsvari et al. 1999). A large portion of all narrow spikes cells (40%) was either inhibiting other neurons or excited by a presynaptic partner. This proportion is exceptionally high compared with very low incidence of short-latency interactions in the population as a whole (1 in 400 pairs). This finding indicates that most spike-spike interactions occur among pyramidal-interneuron pairs rather than among pyramidal-pyramidal cell pairs.

Although physiological identification of neuronal interactions support the general validity of spike duration-based classification of neurons, it involves both commission and omission errors. For example, a few units in the narrow spike group without significant interactions had bursty auto-correlograms. Because no such spike dynamics was observed in the physiologically identified group, it is possible that this subgroup corresponds to the "chattering" or fast bursting neurons described earlier (Azouz et al. 1997; Steriade et al. 1998). The ambiguity of a small portion wide spike units has been discussed in the preceding text. Another obvious caveat is that most of our results were carried out under anesthesia, which may have influenced the firing patterns of neurons. We expect therefore that firing rate differences and spike dynamics features may prove additionally useful parameters in unit classification in drug-free behaving animals (Constantinidis and Goldman-Rakic 2002). Neuron identification on the basis of short-term cross-correlations can serve as a reliable tool for further improvement of interneuron and principal cell separation.

Our identified and putative pyramidal cells showed two extreme spike dynamics: bursting with large peaks at 3-10 ms in the auto-correlogram and regular spiking corresponding to a slow slope of the auto-correlogram. In vitro investigations also described these two modes of firing patterns and attributed burst propensity to distinct dendritic morphology (Kim and Connors 1993; Mainen and Sejnowski 1996). Nevertheless, the relationship between the in vitro and in vivo groups remains to be investigated. We found no differences in their firing rates, ability to excite target neurons, or probability of being inhibited by interneurons.

Circuit analysis

Most axonal wiring in the neocortex is local (Douglas et al. 1995) and most neuronal interactions occur locally. Analysis of these local interactions requires high-density recording of unit activity. The two-dimensional silicon probes used here appear ideal for such a task because of their ability to record from large number of units and because multiple recording sites allow for the determination of the spatial layout of the recorded units (Csicsvari et al. 2003a). After identification of neuronal types, as described here, functional connectivity in local circuits can be studied (Holmgren et al. 2003) at least between pyramidal cells and interneurons. Further work in behaving animals will reveal how such local interactions are modified by state changes and experience (Constantinidis et al. 2002; Csicsvari et al. 1998).

GRANTS

This work was supported by the National Institutes of Health (NS-34994, NS-43157, MH-54671, and 1P41RR-09754).

REFERENCES

Angulo MC, Staiger JF, Rossier J, and Audinat E. Distinct local circuits between neocortical pyramidal cells and fast-spiking interneurons in young adult rats. *J Neurophysiol* 89: 943–953, 2003.

Azouz R, Gray CM, Nowak LG, and McCormick DA. Physiological properties of inhibitory interneurons in cat striate cortex. *Cereb Cortex* 7: 534–545, 1997.

Beaulieu C and Colonnier M. The number of neurons in the different laminae of the binocular and monocular regions of area 17 in the cat. *J Comp Neurol* 217: 337–344, 1983.

Buhl EH, Tamas G, Szilagyi T, Stricker C, Paulsen O, and Somogyi P. Effect, number and location of synapses made by single pyramidal cells onto aspiny interneurones of cat visual cortex. *J Physiol* 500: 689–713, 1997.

Buzsáki G, Bickford RG, Armstrong DM, Ponomareff G, Chen KS, Ruiz R, Thal LJ, and Gage FH. Electric activity in the neocortex of freely moving young and aged rats. *Neuroscience* 26: 735–744, 1988.

Buzsáki G and Chrobak JJ. Temporal structure in spatially organized neuronal ensembles: a role for interneuronal networks. *Curr Opin Neurobiol* 5: 504–510, 1995.

Chicurel M. Windows on the brain. *Nature* 412: 266–268, 2001.

Connors BW, Gutnick MJ, and Prince DA. Electrophysiological properties of neocortical neurons in vitro. *J Neurophysiol* 48: 1302–1320, 1982.

Constantinidis C and Goldman-Rakic PS. Correlated discharges among putative pyramidal neurons and interneurons in the primate prefrontal cortex. *J Neurophysiol* 88: 3487–3497, 2002.

Constantinidis C, Williams GV, and Goldman-Rakic PS. A role for inhibition in shaping the temporal flow of information in prefrontal cortex. *Nat Neurosci* 5: 175–180, 2002.

Csicsvari J, Henze DA, Jamieson B, Harris KD, Sirota A, Bartho P, Wise KD, and Buzsáki G. Massively parallel recording of unit and local field potentials with silicon-based electrodes. *J Neurophysiol* 90: 1314–1323, 2003a.

Csicsvari J, Hirase H, Czurkó A, and Buzsáki G. Reliability and state dependence of pyramidal cell-interneuron synapses in the hippocampus: an ensemble approach in the behaving rat. *Neuron* 21: 179–189, 1998.

Csicsvari J, Hirase H, Czurko A, Mamiya A and Buzsáki G. Oscillatory coupling of hippocampal pyramidal cells and interneurons in the behaving rat. *J Neurosci* 19: 274–287, 1999.

Csicsvari J, Jamieson B, Wise KD, and Buzsáki G. Mechanisms of gamma oscillations in the hippocampus of the behaving rat. *Neuron* 37: 311–322, 2003b.

Deadwyler SA and Hampson RE. Ensemble activity and behavior—what's the code. *Science* 270: 1316–1318, 1995.

Degenetais E, Thierry AM, Glowinski J, and Gioanni Y. Electrophysiological properties of pyramidal neurons in the rat prefrontal cortex: an in vivo intracellular recording study. *Cereb Cortex* 12: 1–16, 2002.

Degenetais E, Thierry AM, Glowinski J, and Gioanni Y. Synaptic influence of hippocampus on pyramidal cells of the rat prefrontal cortex: an in vivo intracellular recording study. *Cereb Cortex* 13: 782–792, 2003.

Deuchars J, West DC, and Thomson AM. Relationships between morphology and physiology of pyramid-pyramid single axon connections in rat neocortex in vitro. *J Physiol* 478: 423–435, 1994.

Douglas RJ, Koch C, Mahowald M, Martin KAC, and Suarez HH. Recurrent excitation in neocortical circuits. *Science* 269: 981–985, 1995.

Drake KL, Wise KD, Farraye J, Anderson DJ, and BeMent SL. Performance of planar multisite microprobes in recording extracellular single-unit intracortical activity. *IEEE Trans Biomed Eng* 35: 719–732, 1988.

Eichenbaum H and Davis JL. *Neuronal Ensembles: Strategies for Recording and Coding.* New York: Wiley-Liss, 1998.

Freund TF and Buzsáki G. Interneurons of the hippocampus. *Hippocampus* 6: 347–470, 1996.

Gray CM, Maldonado PE, Wilson M, and McNaughton B. Tetrodes markedly improve the reliability and yield of multiple single-unit isolation from multi-unit recordings in cat striate cortex. *J Neurosci Methods* 63: 43–54, 1995.

Gray CM and McCormick DA. Chattering cells: superficial pyramidal neurons contributing to the generation of synchronous oscillations in the visual cortex. *Science* 274: 109–113, 1996.

Gupta A, Wang Y, and Markram H. Organizing principles for a diversity of GABAergic interneurons and synapses in the neocortex. *Science* 287: 273–278, 2000.

Harris KD, Henze DA, Csicsvari J, Hirase H, and Buzsáki G. Accuracy of tetrode spike separation as determined by simultaneous intracellular and extracellular measurements. *J Neurophysiol* 84: 401–414, 2000.

Harris KD, Hirase H, Leinekugel X, Henze DA, and Buzsáki G. Temporal interaction between single spikes and complex spike bursts in hippocampal pyramidal cells. *Neuron* 32: 141–149, 2001.

Henze DA, Borhegyi Z, Csicsvari J, Mamiya A, Harris KD, and Buzsáki G. Intracellular features predicted by extracellular recordings in the hippocampus in vivo. *J Neurophysiol* 84: 390–400, 2000.

Holmgren C, Harkany T, Svennenfors B, and Zilberter Y. Pyramidal cell communication within local networks in layer 2/3 of rat neocortex. *J Physiol* 551: 139–153, 2003.

Kawaguchi Y and Kubota Y. Correlation of physiological subgroupings of nonpyramidal cells with parvalbumin- and calbindinD28k-immunoreactive neurons in layer V of rat frontal cortex. *J Neurophysiol* 70: 387–396, 1993.

Kim HG and Connors BW. Apical dendrites of the neocortex: correlation between sodium- and calcium-dependent spiking and pyramidal cell morphology. *J Neurosci* 13: 5301–5311, 1993.

Klausberger T, Magill PJ, Marton LF, Roberts JD, Cobden PM, Buzsáki G, and Somogyi P. Brain-state- and cell-type-specific firing of hippocampal interneurons in vivo. *Nature* 421: 844–848, 2003.

Maccaferri G, Roberts JD, Szucs P, Cottingham CA, and Somogyi P. Cell surface domain specific postsynaptic currents evoked by identified GABAergic neurons in rat hippocampus in vitro. *J Physiol* 524: 91–116, 2000.

Mainen ZF and Sejnowski TJ. Influence of dendritic structure on firing pattern in model neocortical neurons. *Nature* 382: 363–366, 1996.

Markram H. A network of tufted layer 5 pyramidal neurons. *Cereb Cortex* 7: 523–533, 1997.

Markram H, Lubke J, Frotscher M, Roth A, and Sakmann B. Physiology and anatomy of synaptic connections between thick tufted pyramidal neurons in the developing rat neocortex. *J Physiol* 500: 409–440, 1997.

Marshall L, Henze DA, Hirase H, Leinekugel X, Dragoi G, and Buzsáki G. Hippocampal pyramidal cell-interneuron spike transmission is frequency dependent and responsible for place modulation of interneuron discharge. *J Neurosci* 22: RC197, 2002.

McNaughton BL, O'Keefe J, and Barnes CA. The stereotrode: a new technique for simultaneous isolation of several single units in the central nervous system from multiple unit records. *J Neurosci Methods* 8: 391–397, 1983.

Mountcastle VB, Talbot WH, Sakata H, and Hyvarinen J. Cortical neuronal mechanisms in flutter-vibration studied in unanesthetized monkeys. Neuronal periodicity and frequency discrimination. *J Neurophysiol* 32: 452–484, 1969.

O'Keefe J and Recce ML. Phase relationship between hippocampal place units and the EEG theta rhythm. *Hippocampus* 3: 317–330, 1993.

Quirk MC and Wilson MA. Interaction between spike waveform classification and temporal sequence detection. *J Neurosci Methods* 94: 41–52, 1999.

Sik A, Penttonen M, Ylinen A, and Buzsáki G. Hippocampal CA1 interneurons: an in vivo intracellular labeling study. *J Neurosci* 15: 6651–6665, 1995.

Simons DJ. Response properties of vibrissa units in rat SI somatosensory neocortex. *J Neurophysiol* 41: 798–820, 1978.

Somogyi P, Tamas G, Lujan R, and Buhl EH. Salient features of synaptic organisation in the cerebral cortex. *Brain Res Brain Res Rev* 26: 113–135, 1998.

Steriade M, Timofeev I, Durmuller N, and Grenier F. Dynamic properties of corticothalamic neurons and local cortical interneurons generating fast rhythmic (30-40 Hz) spike bursts. *J Neurophysiol* 79: 483–490, 1998.

Swadlow HA. Fast-spike interneurons and feedforward inhibition in awake sensory neocortex. *Cereb Cortex* 13: 25–32, 2003.

Swadlow HA, Beloozerova IN, and Sirota MG. Sharp, local synchrony among putative feed-forward inhibitory interneurons of rabbit somatosensory cortex. *J Neurophysiol* 79: 567–582, 1998.

Swadlow HA and Gusev AG. The impact of "bursting" thalamic impulses at a neocortical synapse. *Nat Neurosci* 4: 402–408, 2001.

Swadlow HA and Gusev AG. Receptive-field construction in cortical inhibitory interneurons. *Nat Neurosci* 5: 403–404, 2002.

Swadlow HA and Lukatela K. Cross-correlation and microstimulation: complementary tools in the extracellular analysis of synaptic interactions. *J Neurosci Methods* 64: 219–225, 1996.

Tamas G, Buhl EH, and Somogyi P. Fast IPSPs elicited via multiple synaptic release sites by different types of GABAergic neuron in the cat visual cortex. *J Physiol* 500: 715–738, 1997.

Thomson AM and Bannister AP. Interlaminar connections in the neocortex. *Cereb Cortex* 13: 5–14, 2003.

Thomson AM and Deuchars J. Synaptic interactions in neocortical local circuits: dual intracellular recordings in vitro. *Cereb Cortex* 7: 510–522, 1997.

Thomson AM, West DC, and Deuchars J. Properties of single axon excitatory postsynaptic potentials elicited in spiny interneurons by action potentials in pyramidal neurons in slices of rat neocortex. *Neuroscience* 69: 727–738, 1995.

Thomson AM, West DC, Hahn J, and Deuchars J. Single axon IPSPs elicited in pyramidal cells by three classes of interneurons in slices of rat neocortex. *J Physiol* 496:81–102, 1996.

Wilson MA and McNaughton BL. Dynamics of the hippocampal ensemble code for space. *Science* 261: 1055–1058, 1993.

Wise KD and Angell JB. A low-capacitance multielectrode probe for use in extracellular neurophysiology. *IEEE Trans Biomed Eng* 22: 212–219, 1975.

J Neurophysiol 93: 1304–1316, 2005.
First published October 6, 2004; doi:10.1152/jn.00490.2004.

Passive Movements of the Head Do Not Abolish Anticipatory Firing Properties of Head Direction Cells

Joshua P. Bassett,[1] Michaël B. Zugaro,[2] Gary M. Muir,[1] Edward J. Golob,[1] Robert U. Muller,[3,4] and Jeffrey S. Taube[1]

[1]*Department of Psychological and Brain Sciences, Center for Cognitive Neuroscience, Dartmouth College, Hanover, New Hampshire;* [2]*Centre National de la Recherche Scientifique, College de France, Laboratoire de Physiologie de la Perception et de l'Action, Paris, France;* [3]*Medical Research Council Centre for Synaptic Plasticity, University of Bristol, Bristol, United Kingdom; and* [4]*Department of Physiology, State University of New York, Downstate Medical Center, Brooklyn, New York*

Submitted 19 May 2004; accepted in final form 27 September 2004

Bassett, Joshua P., Michaël B. Zugaro, Gary M. Muir, Edward J. Golob, Robert U. Muller, and Jeffrey S. Taube. Passive movements of the head do not abolish anticipatory firing properties of head direction cells. *J Neurophysiol* 93: 1304–1316, 2005. First published October 6, 2004; doi:10.1152/jn.00490.2004. Neurons in the anterior dorsal thalamic nucleus (ADN) of the rat selectively discharge in relation to the animal's head direction (HD) in the horizontal plane. Temporal analyses of cell firing properties reveal that their discharge is optimally correlated with the animal's future directional heading by ~24 ms. Among the hypotheses proposed to explain this property is that ADN HD cells are informed of future head movement via motor efference copy signals. One prediction of this hypothesis is that when the rat's head is moved passively, the anticipatory time interval (ATI) will be attenuated because the motor efference signal reflects only the active contribution to the movement. The present study tested this hypothesis by loosely restraining the animal and passively rotating it through the cell's preferred direction. Contrary to our prediction, we found that ATI values did not decrease during passive movement but in fact increased significantly. HD cells in the postsubiculum did not show the same effect, suggesting independence between the two sites with respect to anticipatory firing. We conclude that it is unlikely that a motor efference copy signal alone is responsible for generating anticipatory firing in ADN HD cells.

INTRODUCTION

Head direction (HD) cells are neurons that selectively discharge in relation to an animal's head direction in the horizontal plane. A given HD cell fires only when the animal is facing a direction that falls within a limited angular range, decreasing in rate as the head moves in either direction from a maximum in the center of its range, called the preferred firing direction. HD cells are not sensitive to the position of the head relative to the body but rather to the direction of the head with respect to the surrounding environment, and they fire independently of the animal's location within the environment. They are believed to represent the directional heading information necessary for navigational behaviors as part of a larger spatial cognition circuit involving many structures within the limbic system.

HD cells have been studied primarily in rats and have been found in several regions including the postsubiculum (PoS) (Taube et al. 1990a), anterior dorsal thalamic nucleus (ADN) (Taube 1995), lateral mammillary nuclei (LMN) (Blair et al. 1998; Stackman and Taube 1998), retrosplenial cortex (Chen et al. 1994; Cho and Sharp 2001), parts of prestriate cortex (Chen et al. 1994), and dorsal striatum (Wiener 1993). HD cells within the ADN, retrosplenial cortex, and LMN have been observed to fire in a manner that encodes the rat's *future* directional heading by an average of 24 ms in ADN (Blair and Sharp 1995; Taube and Muller 1998), 25 ms in the retrosplenial cortex (Cho and Sharp 2001), and 67 ms in LMN (Stackman and Taube 1998; cf. Blair et al. 1998), respectively. In contrast, HD cell discharge in the PoS corresponds most closely with directional heading in the present or recent past (~0 ms) (Blair and Sharp 1995; Taube and Muller 1998). The amount of time that peak firing precedes head direction is referred to as the anticipatory time interval (ATI). The observation that HD cells in some brain areas anticipate future head direction is further evidence that HD cell activity is not simply a sensory response to external cues but rather an abstract representation of spatial relationships within the local environment.

One hypothesis proposed to account for this phenomenon is that anticipatory HD cell signals combine sensory input from the recent past with motor information to predict future sensory input, thereby updating the directional representation (Taube and Muller 1998). According to this view, the anticipatory properties of ADN HD cells may arise from motor commands projected to the ADN (or elsewhere in the HD circuit) as motor efference copy signals. There is ample precedent in the study of sensorimotor integration for such a mechanism (von Holst and Mittelstaedt 1950). As a convergence point for cortical and subcortical projections from structures possibly involved in generating the HD signal, the ADN is anatomically well-situated to receive and integrate information about environmental cues and self-motion. Vestibular and possibly optokinetic cues contribute to HD signal updating based on self-motion monitoring, probably via routes from the vestibular nuclei → nucleus prepositus → dorsal tegmental nucleus → lateral mammillary nuclei → ADN (Bassett and Taube 2001a; Blair and Sharp 1996; Lannou et al. 1984; Stackman and Taube 1997; Taube 1998). Routes by which motor information could reach ADN HD cells are less clear but could involve projec-

Address for reprint requests and other correspondence: J. S. Taube, Dept. of Psychological and Brain Sciences, Dartmouth College, 6207 Moore Hall, Hanover, NH 03755 (E-mail: jeffrey.taube@dartmouth.edu).

The costs of publication of this article were defrayed in part by the payment of page charges. The article must therefore be hereby marked "*advertisement*" in accordance with 18 U.S.C. Section 1734 solely to indicate this fact.

tions from the medial frontal cortex, a motor or supplementary motor area containing putative frontal eye fields and vibrissae and forelimb representations (Neafsey et al. 1986). This area projects both to the retrospenial cortex (Vogt and Miller 1983) and directly to ADN (Guandalini 2001). Subcortical sources of motor information for ADN HD cells are currently unknown. In contrast to the ADN, HD cells in the PoS are not, on average, anticipatory, but instead correspond to current head direction or a small delay [−7 ms (Taube and Muller 1998); 2 ms (Blair and Sharp 1995)]. While it is clear that HD cell firing in PoS is dependent on an intact ADN (Goodridge and Taube 1997), how the temporal firing properties of the two areas are related is unknown.

Previous efforts to subject rats to passive movement while recording from HD cells have often involved substantial restraint of the animals, such as wrapping them in a cloth so that they cannot move either head or limbs (Golob et al. 1998; Knierim et al. 1995; Taube 1995). Under such conditions, most (but not all) HD cells undergo considerable reductions of firing rate or cease firing altogether. Here, we imposed passive movement on rats while restraining them as little as possible. There were two passive movement conditions: hand-held and cart. In the hand-held passive condition, rats were lightly restrained by an experimenter and then rotated back and forth in the horizontal plane through ~180° about the preferred firing direction. They were thus limited in their orienting movements relative to the environment but could still respond reflexively with head and postural movements. In the cart condition, rats were moved around the recording arena in a cart with clear Plexiglas walls and thus were able to move freely inside, while their vestibular and visual experiences were dominated by the imposed movement. In both cases, the animals had some freedom to move on their own onto which we imposed passive movement. The cart experiment was included as a control against the predictable movement pattern of the hand-held condition because the experimenter typically rotated the animal back and forth in a semi-regular manner. In addition, the cart experiment provided a different degree of movement restriction against which to compare the results of the passive hand-held condition. We recorded both ADN and PoS cells under the same experimental conditions to compare them and specifically to determine if changes in one corresponded with changes in the other.

The aim of the present experiments was not to restrict head movement to exclusively passive motion but rather to interfere with the normal flow of motor information and determine whether the anticipatory properties of ADN HD cell activity remained present. All movements were some combination of self-initiated and passive motion. The hand-held condition minimized (but did not eliminate) active movements, whereas the cart condition added passive movement to an unrestricted range of active movements. If anticipatory HD cell firing reflects the convergence of motor and sensory information, then one would expect an imposed mismatch between the two to alter the anticipatory property of HD cell activity. In the present experiments, rats experienced vestibular and visual cues that were imposed on it and that could not be associated with a motor efference copy signal corresponding to their head-in-space movements. We predicted that the ATI would be reduced or abolished in animals that did not actively control the movement of their head through a cell's preferred firing direction.

METHODS

Subjects and training

Subjects were 17 female Long-Evans rats, weighing 250–300 g. Rats were maintained on a food-restricted diet (15–20 g/day) and housed separately in suspended wire mesh cages. Tap water was available ad libitum except during procedures requiring water reward (see following text). All training and unit screening took place while rats foraged for food pellets in a gray cylindrical enclosure (76 cm diam, 51 cm high) with replaceable gray photographic backdrop paper covering the floor. A black curtain extending from the floor to the ceiling enclosed the training/recording environment, and lighting was provided by uniformly arranged DC lights overhead. A color video camera (model XC-711; Sony, Tokyo, Japan) was centered above the cylinder 3 m from the floor surface. The only intentionally introduced asymmetry in the environment was a white cue card that occupied 100° of arc along the wall of the cylinder. Rats were habituated to the cylinder and trained to forage for small pellets (45 mg, Bio-Serv, Frenchtown, NJ) tossed randomly into the cylinder. By the completion of training, rats engaged in nearly continuous food pellet foraging, moving over the entire floor surface of the cylinder. All procedures involving the rats were performed in compliance with institutional standards set forth by the National Institutes of Health Guide for the Care and Use of Laboratory Animals and the Society for Neuroscience.

Surgery

Electrode construction and implantation has been described in detail previously (Taube et al. 1990a). Each electrode array consisted of ten 25-μm-diam nichrome wires (California Fine Wire, Grover City, CA) insulated except at the tips. The wires were passed through a 26-gauge, ~2-cm-long stainless steel cannula, and each wire connected to a modified 10-pin Augat connector. The electrode array could be advanced in the dorsoventral plane through the use of three screws attached to an acrylic base on the electrode (Kubie 1984). After ≥1 wk of training (1 trial/day), each rat was anesthetized with a ketamine-xylazine mixture (2 ml/kg im) and stereotaxically implanted with an electrode array directed at the ADN (n = 11) or PoS (n = 6). Coordinates (in mm) were as follows, from bregma: ADN: A/P –1.4; M/L ± 1.3; D/V –4.0 from cortical surface. PoS: A/P –6.8; M/L ± 2.7; D/V –2.0 from cortical surface (Paxinos and Watson 1998). Two stainless steel screws each were placed in the skull posterior to lambda and anterior to bregma, and dental cement anchored the electrode in place. Rats were allowed ≥1 wk of postoperative recovery before single-unit screening was started.

Single-unit recording

The activity on each electrode wire was assessed during daily screening sessions while the rat foraged for food pellets in the cylinder. The electrode wires were advanced over several weeks while screening for single-unit waveforms that were sufficiently isolated from background electrical noise. Rats were transported into the screening/recording area in a covered cardboard enclosure. Each rat was momentarily restrained while a recording cable was attached to the implanted electrode and then released into the cylinder from an entry point that was varied in a pseudo-random manner.

Electrical signals from the electrode wires were passed through a field-effect transistor in a source-follower configuration through an overhead commutator (Biela Development), amplified (Grass Instruments, P5 Series), band-pass filtered (300–10,000 Hz, 3 dB/octave: Peavey Electronics, Model No. PME8), and then passed through a

series of window discriminators (BAK Electronics, Model Mo. DDIS-1). The resultant signal was then displayed on an oscilloscope (Tektronix, Model No. 2214). Electrode activity was monitored while observing the rat's behavior on a video monitor. Two light-emitting diodes (LEDs) attached to the recording cable were visible to the camera mounted overhead. The *x,y* coordinates of a red LED positioned over the rat's snout and a green LED positioned over its back were monitored at 60 Hz, the relative position of the two lights indicating the directional heading of the rat and its position in the cylinder. If no HD cell activity was found, the electrode was advanced further into the brain, and the screening process was repeated at least daily and with ≥2 h between screening sessions. When the waveform of a cell could be sufficiently isolated from background noise, the LED coordinates and neuronal discharges were sampled at 60 Hz and acquired by a data-acquisition interface board (National Instruments, Model No. DIO-96) in a personal computer (Macintosh Quadra 840AV). Data were stored for subsequent off-line analyses using LabView software programs (National Instruments). During recording sessions, white noise was played over a speaker mounted on the ceiling and centered above the cylinder to mask uncontrolled auditory cues.

Data analysis

Three methods were used to determine the temporal relationship between head direction and cell activity: time-shifted optimization of peak firing rate, time-shifted optimization of information content, and separation angle.

OPTIMIZATION FOR PEAK FIRING RATE. During the recording of HD cell activity, cell firing and head direction are monitored simultaneously; the number of spikes fired within a given directional range is then divided by the amount of time the rat's head spent pointing in that range, yielding the firing rate in each direction. Because the spike train and head direction are monitored independently of each other, each data series can be shifted in time relative to the other. Parameters such as peak firing rate and information content (discussed in the following text) are usually reported when samples of head direction and spike activity are aligned in time. These parameters can be optimized, however, by shifting the samples forward or backward in time. For example, the calculated peak firing rate will be highest when time samples containing the greatest cell activity are distributed through the smallest directional range. In the case of ADN and LMN HD cells, the peak firing rate is optimized when head direction is shifted forward in time relative to the spike train. The number of samples shifted to reach this optimized value is defined as the ATI. Positive ATI values indicate anticipatory firing, whereas negative values indicate firing that lags head direction.

The spike time series was shifted forward or backward in time in 1/60th-s intervals (16.6 ms) relative to the head direction time series. The shift that produced the highest peak firing was defined as the amount by which cell firing preceded or followed the head's passing through the preferred firing direction.

OPTIMIZATION FOR INFORMATION CONTENT. Information content estimates the amount that a cell's firing reduces the uncertainty of the rat's head direction. This measure has been discussed in detail elsewhere (Skaggs et al. 1993), but briefly, if a cell fired exclusively and reliably in only 1 of the 60 (6°) angular bins, then head direction would be known to 1 part in 60 or one part in $\sim 2^{5.9}$. Thus the information per spike would be 5.9 bits. Because HD cells have a firing range >6° and often have a small amount of background activity outside the cell's directional firing range, information content for ADN HD cells is not typically >2.8 bits (Taube and Muller 1998). Information content is given by

$$\mathrm{IC} = \sum p_i(\lambda_i/\lambda) \log_2(\lambda_i/\lambda)$$

where p_i = time spent with the head pointing in the *i*th bin divided by the total time (probability that the head pointed in the *i*th bin); λ_i = the mean firing rate of the cell in the *i*th bin; and λ = the overall firing rate of the cell for the entire recording session.

SEPARATION ANGLE. The preferred firing direction for each function was determined by calculating the mean firing direction based on weighting the firing rate for each directional bin within the directional firing range. The directional firing range was defined as the range of head directions over which elevated discharge occurred (see Taube et al. 1990a). The angular difference between the preferred firing directions of the two functions was labeled ∂ using the nomenclature of Blair and Sharp (1995). A cell whose firing anticipates or trails head direction will reach its peak firing rate at different directions; the greater the lead or lag, the greater the expected angular difference between peak firing rates for clockwise (CW) and counterclockwise (CCW) turns. Because the anticipatory firing of ADN HD cells is independent of angular head velocities (Taube and Muller 1998), the angular difference between CW and CCW tuning curves (∂) tends toward zero at very low angular head velocities. Because of this tendency, analyses using decomposed curves have typically excluded samples where instantaneous angular velocity is <90°/s. Probability distributions of angular head velocity across a session reveal a strong bias toward the lowest angular head velocities. Thus to increase the total number of samples included when plotting firing rate by head direction functions, we elected to use those samples containing an angular head velocity of >45°/s. However, selecting different cut-off values for angular head velocity, either higher or lower than 45°/s (e.g., 0 or 90°), did not significantly change the overall effects reported in the following text. Multiple curves were constructed using data series that were time-shifted forward and backward by six 1/60th-s (16.6 ms) intervals. We constructed a plot of ∂ versus time shift and defined the *x* intercept of the best-fit line as the ATI for the cell. This measure is referred to as "separation angle" and is identical to the measure described by Blair and Sharp (1995) with the exception that we did not approximate the original firing rate versus head direction functions with Gaussian distributions. ATI values are calculated for all measures as the number of video samples shifted and then reported in milliseconds (i.e., the number of samples shifted multiplied by 16.6). The dispersion of ATI values is reported with the SE. Statistical comparisons between groups were conducted using a one-way ANOVA with Tukey honestly significant difference tests (HSD) used for post hoc comparisons when the ANOVA was significant ($P < 0.05$).

To evaluate the interdependence of HD cell firing properties under different experimental conditions, we calculated the area under the curve for the firing rate by head direction functions. The area under the curve corresponds to the sum of the firing rates for each directional bin within the directional firing range. The directional firing range was defined as the set of contiguous directional bins in which neuronal firing rate exceeded the mean background firing rate and also contained the directional bin with the highest firing rate for the session.

We evaluated variability in the preferred firing direction between individual passes through the directional firing range by plotting head direction and firing rate as a function of time. Mean head direction and firing rate was calculated over 10-sample temporal bins (1 sample = 1/60th s; 1 temporal bin = 1/6th s). For each episode in which the head passed through a directional range of 24° (four 6° directional bins) on either side of the mean preferred firing direction for the overall session, we sampled the exact head direction for the temporal bin containing the highest firing rate for that episode. We refer to this head direction for individual passes through the preferred firing direction as the "instantaneous preferred firing direction," and the firing rate at this direction as the "instantaneous peak firing rate." Instantaneous preferred firing directions were sampled over the full recording session for each cell. Because differences in ATI would affect the spread between CW and CCW instantaneous preferred directions (see explanation for separation angle in the preceding text),

the SD was calculated separately for CW and CCW turns. SDs were then compared between active and passive conditions.

We show in RESULTS that there was variability in the preferred firing direction in the passive conditions. This variability could affect the ATI. We therefore modeled the effects of passive movement on the directional tuning function by adding directional noise according to a pseudo-Gaussian probability function and determined whether this effect altered the ATI. As described in the preceding text, each recorded spike is assigned to a 6° directional bin according to the position of the LEDs on the rat's head during the time interval in which the spike was sampled. When noise was added, each such assignment was made with some probability that the directional sample for that spike would be altered by addition or subtraction of a variable amount, thereby potentially changing the bin assignment. For example, if 6° of noise was added, each spike sample during that session would have a 0.4 probability of being assigned to its true directional bin, a 0.4 probability of having 3° added or subtracted before its bin assignment, and a 0.2 probability of being shifted 6° in either direction. If 12° of noise was added, there would again be 0.4 probability of no change, 0.4 probability of a shift by 6° in either direction, and 0.2 probability of a 12° shift in either direction. This method of adding directional noise was intended to model the effects of increased uncertainty of head direction at a given moment that would occur due to decreased information to the HD cell system during passive movements.

All mean values are reported ±SE.

Experimental conditions

Rats were recorded under three conditions: active movements, passive movements while loosely restrained, and passive movements in a cart.

ACTIVE. Active sessions consisted of 8 min of sampling during free foraging behavior under conditions identical to screening sessions as described in the preceding text.

PASSIVE. Following an active session, the experimenter held the rat while supporting its feet, in a manner that restricted movement as little as possible while keeping the rat in place and under control of the experimenter. Unlike hand-held passive motion conditions in previous studies, rats were not bound or restrained in a towel. Rats had full freedom of movement of the head and neck and were able to make limited limb movements and postural adjustments. Rats were rotated at ~180–270°/s, through a range of ~180°, resulting in peak head velocities (imposed plus self-initiated head movement) of 837.3°/s and mean head velocities of 96.5°/s on average (see Fig. 6). Rotations of the rat were centered around the preferred firing direction of the recorded HD cell as determined from the standard session. Each hand-held session consisted of 2 min of sampling, representing one-quarter of the normal sampling time. During the last 20 s of this recording, the rat was rotated through the entire 360° to sample all directions. Because of the difficulty of controlling a loosely restrained animal, passive sessions generally consisted of two combined 1-min sessions. After passive sessions, the rats were again recorded for 8 min during free foraging so that firing parameters from before and after the passive session could be compared. Figure 1 shows the characteristic movement patterns of each condition.

CART. To achieve the desired uncoupling of sensory and motor feedback in a manner that did not require restraining or touching the rat, we used an additional condition. The rat was placed on a cart with a 22 × 22 cm square wood floor on which rested a clear Plexiglas enclosure, 20 × 20 × 14 cm high. The platform and enclosure rested on four swiveling wheels that held the platform 4 cm off the ground. The cart was then rotated at a rate, and over a range, similar to the passive sessions in rate and range, but the rat was free to move within the clear enclosure. In this way, the rat's freedom to move was completely unrestrained by the experimenter, but its vestibular and visual feedback were affected by the imposed movement. Thus in the hand-held condition, motor commands initiated by the rat were entirely disconnected from passes through the preferred firing direction. By contrast, in the cart condition, the rat's self-initiated movements could lead to turns through the preferred firing direction, albeit with passive motion added to its active movements. Each cart session consisted of 4 min of sampling. Cart sessions were also bracketed by freely moving standard sessions in the cylinder.

At the completion of the experiments, animals were killed, their brains perfused with 10% formalin, soaked in 20% sucrose, frozen, and then sectioned (40 μm) on a cryostat (see Taube 1995; for details on histology). Sections were examined under a microscope and electrode tracks were reconstructed. All HD cells were found to be in the intended target sites of ADN or PoS.

RESULTS

ADN HD cells

HAND-HELD PASSIVE CONDITION. We recorded 21 HD cells from the ADN in 11 rats. Results for all conditions are summarized in Table 1. For each measure of ATI, we performed a one-way ANOVA for repeated measures (correlated samples), comparing passive sessions to the preceding and following active sessions. By all measures, ATI values were reliably higher during the hand-held passive session than during the preceding or subsequent active session (peak firing rate $F(2,21) = 8.41$; $P < 0.001$, $HSD_{0.05} = 1.42$; information content: $F(2,21) = 28.16$, $P < 0.0001$, $HSD_{0.01} = 1.20$; separation angle $F(2,21) = 24.21$, $P < 0.0001$, $HSD_{0.01} = 1.27$). Post hoc comparisons showed no difference between the two active sessions. Thus contrary to our prediction, anticipatory firing was not abolished, but instead showed a significant increase during the hand-held passive condition.

Not every cell in every recording session conformed to this pattern. When the 21 sessions were compared based on optimized peak firing rate, 14 sessions (66.7%) showed an increase in ATI during the passive condition relative to the first active condition, 6 sessions (28.6%) showed a decrease, and 1 session (4.8%) showed no change. The outcome was less varied when data were time-shifted to optimize information content (increase: 95.2%, decrease: 0%, no change: 4.8%) or minimize separation angle (increase: 80.9%, decrease: 19.1%, no change: 0%). Figure 2 shows a representative tuning function of an ADN HD cell that exhibited an increased ATI during hand-held passive rotations.

We also compared other parameters of HD firing across conditions to determine whether these other parameters changed and were related to the changes observed in the ATI. There was a significant effect of condition on both the observed peak firing rate and the directional firing range. Mean observed peak firing rates were lower by ~23% during passive rotation [$F(2,20) = 8.81$, $P < 0.001$], decreasing from 61.9 ± 8.9 spikes/s in the first active session to 47.1 ± 5.6 spikes/s during the passive condition, and returning to 60.8 ± 8.9 spikes/s in the second active session. Mean directional firing range increased significantly from 97.1 ± 3.2 to 113.5 ± 5.1° during the passive session [$F(2,21) = 8.95$, $P < 0.001$].

This result appears to contradict the results of Zugaro et al. (2002), who reported that peak firing rates were not significantly different during active locomotion and fast (at least ~150°/s) passive rotations. However, the lower peak firing

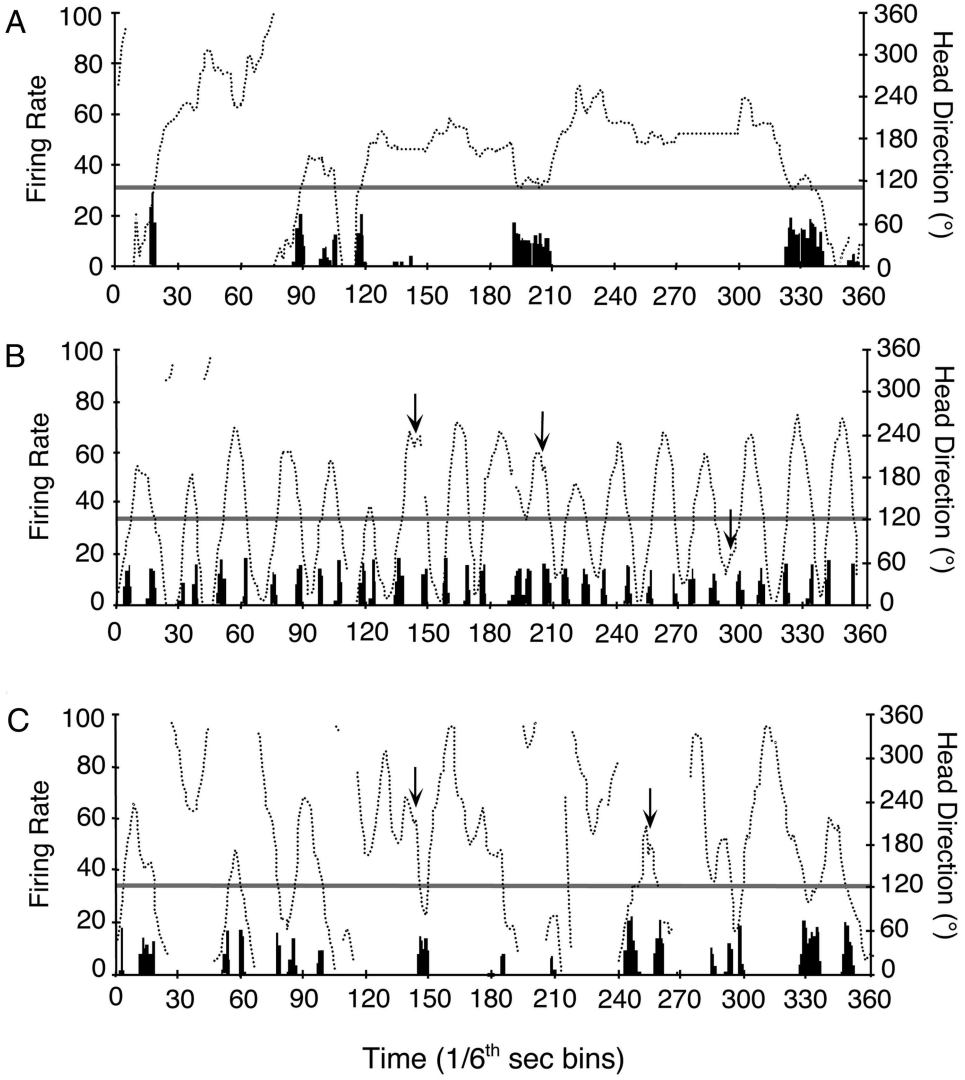

FIG. 1. Head direction and spikes fired as a function of time during active (*A*), hand-held (*B*), and cart conditions (*C*). Head direction across time (dotted line) is shown for 1 min of recording in the same cell from each condition. Each temporal bin on the horizontal axis is 10 1/60th-s samples or 1/6th s. Head direction represents the average 6° directional bin for these 10 samples. Neuronal spiking (vertical black bars) occurs when the rat's head passes through or near the mean preferred firing direction determined for the entire session (gray horizontal bar). Each bar represents the sum of spikes fired within the temporal bin. Instantaneous preferred firing directions are not identical for each pass (see also Fig. 3). Arrows in *B* and *C* indicate examples of head movement initiated by the rat on top of experimenter-imposed movement.

rates observed here during passive rotations could have resulted from some instability in the preferred directions over time, rather than from an actual decrease in peak firing rate. To distinguish between these possibilities, we performed three different analyses: area under the tuning curve, variability of the head direction at times of peak firing, and peak firing rate during individual passes through the directional firing range.

If a cell fired at its maximum rate at slightly different directional headings over time, its HD tuning curve would have a lower peak and a wider directional firing range because the same number of spikes would be averaged over a greater number of directional firing bins. However, if the firing rate for each individual pass of the head through the preferred firing direction was lower, then the total number of spikes would be

TABLE 1. *Anticipatory time intervals compared across conditions*

		ADN				PoS		
	n	Active	Hand-held/Cart	Active	*n*	Active	Hand-held/Cart	Active
Hand-held								
Firing rate	21	45.8 ± 9.9	75.1 ± 10.6**	37.1 ± 11.3	20	−9.1 ± 15.6	6.6 ± 10.4	−24.0 ± 13.6
Information content		48.2 ± 5.9	88.5 ± 5.9**	45.1 ± 7.8		−0.8 ± 9.0	1.7 ± 9.1	−9.1 ± 10.0
Separation angle		45.0 ± 8.3	88.5 ± 7.3**	50.4 ± 9.4		−11.2 ± 8.4	16.4 ± 17.0*	−13.2 ± 12.5
Cart								
Firing rate	10	28.2 ± 11.0	26.6 ± 27.2	28.2 ± 11.1	16	−12.4 ± 14.04	6.2 ± 17.9	−1.0 ± 31.3
Information content		33.2 ± 7.4	44.8 ± 13.6	33.2 ± 7.4		0.0 ± 10.2	0.0 ± 15.4	−7.3 ± 10.9
Separation angle		45.1 ± 15.3	39.9 ± 14.5	52.4 ± 13.4		1.4 ± 6.4	−9.2 ± 20.7	−8.4 ± 17.1

All values are means ± SE and are reported in milliseconds. ADN, anterior dorsal thalamic nucleus; PoS, postsubiculum. *Significantly different from Active, $P < 0.05$; **significantly different from Active, $P < 0.01$.

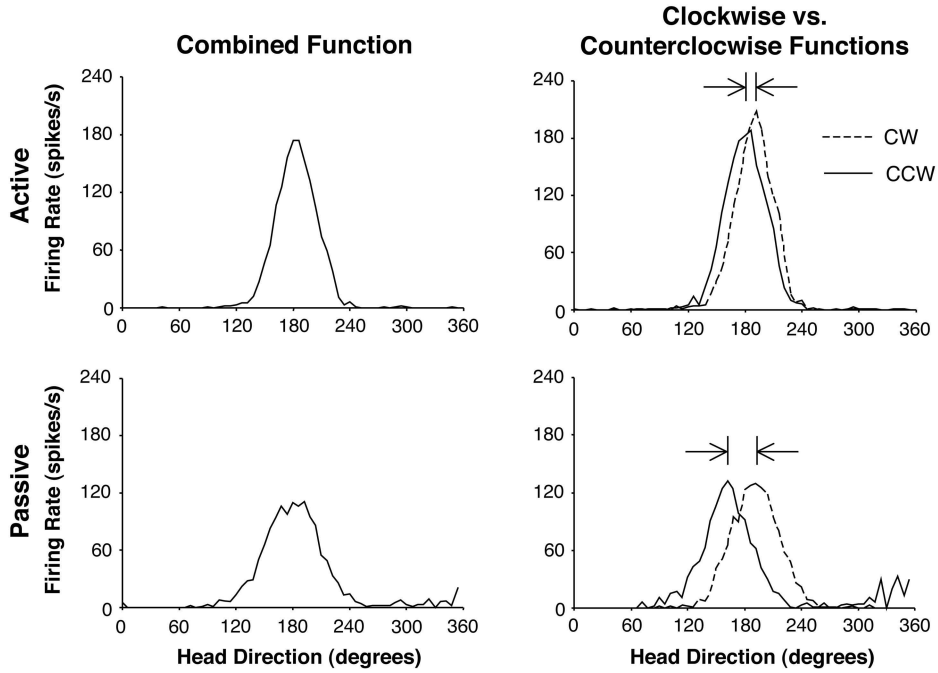

FIG. 2. Examples of changes in the tuning curves from anterior dorsal thalamic nucleus (ADN) head direction (HD) cells between active and hand-held passive conditions. Firing rate as a function of head direction was plotted for a representative cell during the first active session (*top*) and the hand-held passive session (*bottom*). *Left*: head turns in both directions; *right*: data from the same sessions decomposed into clockwise (CW) and counter clockwise (CCW) functions. A lower peak firing rate and broader directional firing range is evident in both cases. CW functions that occur to the right of CCW functions indicate anticipatory firing. *Right*: an increased ATI during the passive session is inferable from the greater separation angle between CW and CCW functions (represented by the space between the two arrows). ATI values, as determined by separation angle, are 58.3 and 109.6 ms for the active and passive sessions, respectively.

averaged over the same directional range. Given no other changes in HD cell properties besides error in the preferred firing direction, this difference should be reflected in the area under the directional tuning curve between active and passive sessions. If the firing rate was decreased and the directional range remained the same, then the area under the curve would decrease. If the firing rate was the same, but spread out over a wider directional range, then the area under the curve would remain constant.

When we compared the area under the curve for the initial active session and the passive session with a paired *t*-test, we observed no significant difference (mean area for active sessions: 2,948 ± 475 spike degrees/s; for passive sessions: 2,667 ± 403 spike degrees/s; $t = 1.79$, $P > 0.05$). If the area under the curve is the same, then the decreased firing rate and increased directional range must either be the result of greater variability in the preferred firing direction or a change in the two parameters (peak firing rate and directional range width) in proportion to one another but in opposite directions. The variability in preferred firing direction during a passive session might arise because the available sensory and motor information is insufficient to accurately track current directional heading compared with when the animal is actively moving. If peak firing rate and directional firing range changed in exact proportion but in opposite directions, it would be evidence of a dependence between the two parameters that has not been demonstrated previously.

To evaluate the variability of each cell's preferred firing direction, we determined the preferred firing direction for individual passes of the head through the directional firing range. By plotting firing rate and head direction as a function of time, we sampled the instantaneous preferred firing direction and peak firing rate during each pass of the head through the directional firing range. We first examined whether the peak firing rates for individual passes were similar between active and passive sessions. As in the case of mean peak firing rate determined for a full session, instantaneous peak firing rates were significantly higher during active than passive conditions (mean instantaneous peak firing rate for active sessions: 74.7 ± 9.7 spikes/s; passive sessions: 57.1 ± 6.2 spikes/s; $t = 4.25$, $P > 0.0005$). This result is consistent with previous studies in which restraint reduced peak firing rates (Golob et al. 1998; Taube 1995; Taube et al. 1990b). We next compared the variability in the instantaneous preferred firing direction between active and passive conditions. A paired *t*-test of SDs for the instantaneous preferred firing direction during individual passes through the directional firing range showed a significant difference between active and passive conditions with passive conditions showing greater variability on average (mean SD for active sessions: 13.8 ± 4.4°; passive sessions: 18.2 ± 10.1°; $t = 2.02$, $P < 0.01$). Increased variability in the instantaneous preferred firing direction would lead to spikes being distributed over a greater number of directional bins over the course of a recording session, resulting in both a lower peak firing rate and greater directional firing range for the overall session. Figure 3 depicts the variability observed in the preferred firing direction from one representative HD cell during an active and passive session. Note that the passive session contained greater variability in preferred firing direction. Taken together, the area-under-the-curve analysis and the variability in preferred direction for individual passes analysis suggest that the changes we observed in the peak firing rate and directional firing range in the passive sessions may be due both to a reduction in peak firing rate and increased variation in the head direction at maximal firing.

We then determined if this increased variability in the preferred firing direction during passive sessions could contribute to the changes in the ATI. We first looked at passive sessions for correlations between changes in either peak firing rate or directional firing range and the ATI. The uniformly low correlation values suggest that the increased ATI has a different basis than variation in preferred firing direction (see Table 2). Interestingly, we found a reasonably good correlation between the different measures of ATI where all *r* values were

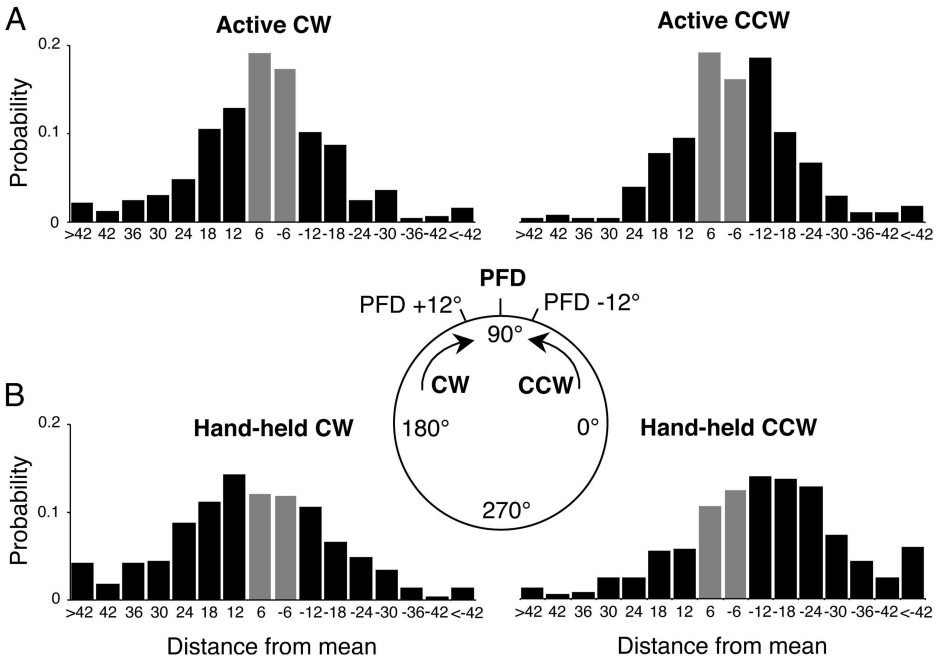

FIG. 3. Variance in the instantaneous preferred firing direction during active (*A*) and hand-held (*B*) conditions. Instantaneous preferred directions were determined for cells during active and hand-held conditions and sorted by turn direction (CW vs. CCW) and deviation from the cell's mean preferred firing direction for both turn directions. For example, if a cell's preferred firing direction was 90°, an instantaneous preferred direction of 83° would fall into the −12° bin (*inset*). For a cell exhibiting anticipatory firing, instantaneous preferred directions tend to fall to the left of the preferred firing direction during CW head turns and to the right of the preferred firing direction during CCW head turns. Compared with active foraging conditions, the instantaneous preferred directions during hand-held rotations were shifted away from the preferred firing direction, indicating greater anticipation, and distributions were flatter, indicating greater variance. Bins surrounding 0 (±6°) are highlighted in gray to illustrate movement of the distributions' centers.

>0.65 for the active condition and >0.50 for the passive condition. These result differ from those reported previously by Taube and Muller (1998) who reported that all *r* values <0.25. The reason for this difference is unclear.

To further test the independence of ATI changes from changes in peak firing rate and directional firing range, we modeled the effect of imposing passive movements by adding "directional noise" to the spike time series in active sessions. We assumed, in other words, that noise simulates smearing of the preferred direction over time (see Fig. 4*A*). As expected, directional noise increased the directional range width and lowered peak firing rates. We added noise in increasing 6° increments to find the amount of noise necessary to model the effect of the passive condition (Fig. 4*B*). To maximize the correlation between the active and passive conditions for both peak firing rate and directional firing range across the entire cell population, it was necessary to add ±18° of noise to the active session spike time series, although some cells required more or less than 18° of noise. The fact that the highest correlation for both directional range width and peak firing rate was achieved with the same level of added noise is further evidence that increased uncertainty about current direction during passive rotations reduces mean peak firing rate independent of the reduction of instantaneous peak firing rate that we also observed (see preceding text).

Adding this level of noise (18°) to active sessions, we then recalculated ATI values and compared them to the ATIs in passive sessions. For all measures of ATI, values for the passive sessions were still significantly higher than active sessions with noise added [peak firing rate: $F(2,21) = 8.30$, $P < 0.001$; information content: $F(2,21) = 32.02$, $P < 0.0001$; separation angle: $F(2,21) = 26.65$, $P < 0.0001$]. This result

TABLE 2. *Correlation between HD cell firing parameters*

Active	ATI (Firing Rate)	ATI (Information Content)	ATI (Separation Angle)	Peak Firing Rate
Active				
ATI (firing rate)	1.00			
ATI (information content)	0.68	1.00		
ATI (separation angle)	0.77	0.86	1.00	
Peak firing rate	0.07	−0.01	0.07	1.00
Directional range width	0.21	−0.01	0.14	0.48
Passive				
ATI (firing rate)	1.00			
ATI (information content)	0.51	1.00		
ATI (separation angle)	0.56	0.74	1.00	
Peak firing rate	−0.30	−0.24	−0.06	1.00
Directional range width	−0.10	0.20	0.32	0.48
Change (passive-active)				
ATI (firing rate)	1.00			
ATI (information content)	0.46	1.00		
ATI (separation angle)	0.57	0.75	1.00	
Peak firing rate	−0.07	−0.03	−0.11	1.00
Directional range width	−0.28	−0.26	−0.05	−0.18

HD, had direction; ATI, anticipatory time interval.

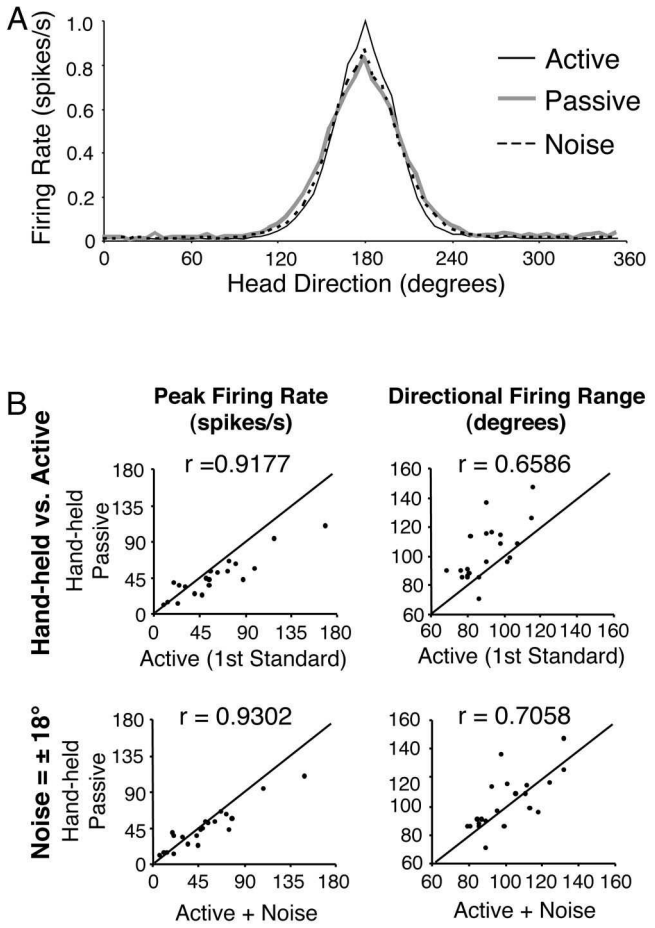

FIG. 4. Effects of directional noise on HD cell firing parameters. *A*: firing rate × HD tuning curves from all ADN cells in the hand-held passive condition were normalized to the peak firing rate in the first active session of each cell. Each tuning curve was then shifted horizontally along the HD axis such that the cell's peak firing rate was aligned to a HD of 180°. Mean normalized firing rate as a function of HD for all cells is shown for active and passive sessions and for active sessions with 18° of directional noise added (see text for details). Peak firing rate is lower and directional firing range is wider for passive and noise trials. *B*: peak firing rate (*left*) and directional firing range (*right*) data are plotted between conditions. In the *first row,* data for active sessions are plotted against their corresponding data in hand-held passive sessions. In the *second row,* data for hand-held passive sessions are plotted against active data with ±18° of directional noise added (see text for details).

indicates that the increased ATI during passive sessions is independent of the increased variability of preferred firing direction and reduced peak firing rate.

CART CONDITION. In the cart condition, the rat was moved passively in a Plexiglas-walled cart that allowed it to move freely relative to the cart floor, but imposed movement on it relative to the spatial cues within the local environment. We tested 10 cells in six rats. Because the rats could move freely in the cart, directional sampling was similar across all directions. To control for differences in sampling time that might affect variability, we compared the 4-min cart sessions with the first 4 min of each active session. Unlike the hand-held passive session, there was no apparent effect of condition on ATI in the cart sessions [peak firing rate: $F(2,10) = 0.29$, $P > 0.05$; information content: $F(2,10) = 0.81$, $P > 0.05$; separation angle: $F(2,10) = 0.48$, $P > 0.05$]. Furthermore, there was no effect of condition on peak firing rate [$F(2,10) = 0.78$, $P > 0.05$] or directional range width [$F(2,10) = 1.53$, $P > 0.05$]. Figure 5 shows representative CW and CCW tuning functions from a cart session compared with the preceding active control.

ANGULAR HEAD VELOCITY. During passive conditions, the animals' head velocity was the sum of self-determined and imposed velocity. Taube and Muller (1998) showed that ATIs increased in a near-linear manner with angular head velocity for ADN HD cells. Thus conditions or sessions that contained high angular head velocities would be expected to have higher ATI values compared with conditions with low angular head velocities. To determine whether differences in the distribution of different angular head velocities could account for any observed changes in ATI, we examined the distribution of angular head velocities over the course of a recording session for each condition. Figure 6 shows probability distributions for all conditions compared with their respective preceding control sessions. Mean instantaneous angular head velocities were lower during control sessions (active foraging) than during experimental conditions for hand-held and cart trials (active: 57.92 ± 3.16°/s, passive: 96.47 ± 4.68°/s, cart: 93.30 ± 4.15°/s). Thus this result raises the possibility that velocity is the variable affecting ATI. Three considerations, however, argue against this interpretation. First, there was a poor (and sometimes moderate negative) correlation among cells between mean angular head velocity and ATI ($r = -0.19$, -0.42, and -0.53 for active, passive, and cart sessions, respectively); thus sessions in which angular head velocity was higher did not tend to produce higher ATI values. Second, angular head velocities in the cart condition were higher than in active conditions and similar to hand-held conditions, but did not lead

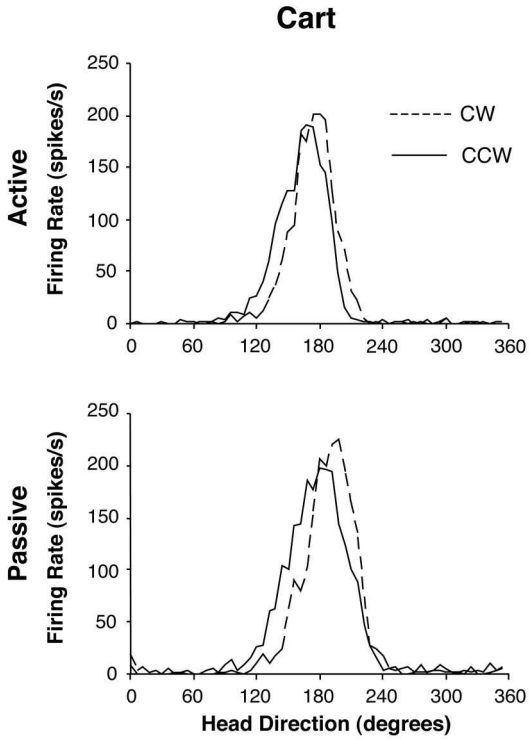

FIG. 5. Examples of changes in the CW and CCW tuning curves from HD cells between active and cart conditions. Firing rate as a function of head direction was plotted for a representative cell during the first active session (*top*) and the cart condition (*bottom*). The ATI is not significantly changed, as is evident from the proximity of the CW and CCW functions.

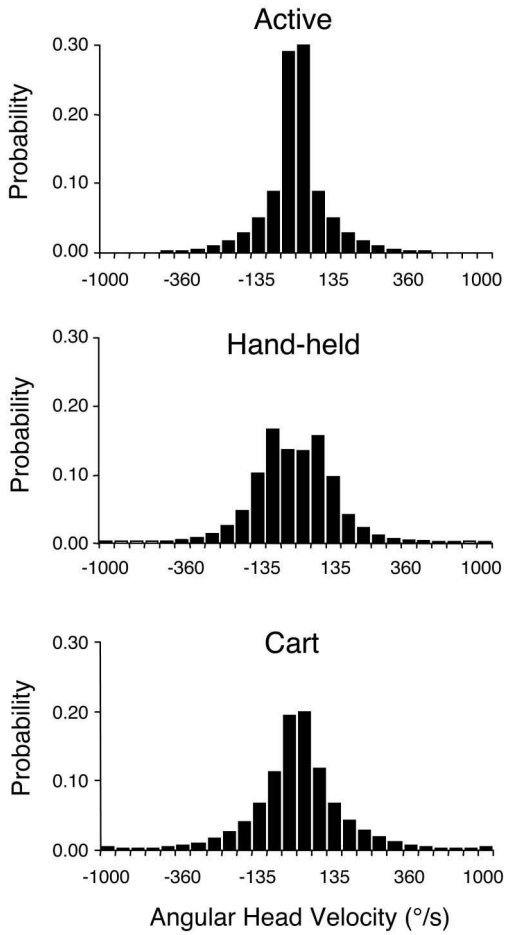

FIG. 6. Changes in angular head velocity (AHV) between conditions. For each probability distribution, instantaneous AHV values for each 1/60th-s sample are grouped in 45°/s bins according to probability across the recording session and averaged across all cells within the experimental group. Distributions from active conditions (*top*) are taken from sessions immediately preceding the hand-held and cart sessions (*bottom*).

to higher ATIs in the cart conditions. Finally, the separation angle measure excludes samples in which angular head velocity <45°/s. Excluding these samples, the mean angular head velocity for each condition was active: 121.83 ± 2.29°/s, passive: 123.74 ± 6.15°/s, and cart: 143.86 ± 7.37°/s. Thus for this measure the mean angular head velocity for active and passive conditions were similar, and yet this measure did not lead to lower ATIs compared with the two other measures, i.e., optimization of peak firing rate and information content (see Table 1). Taken together, we consider it unlikely that changes in ATI values between conditions correspond to differences in the angular head-velocity profiles during those sessions. If the higher ATI values in the hand-held condition were indeed the result of higher angular head velocities, this finding would suggest that ATI is more velocity-dependent than previously evident (Taube and Muller 1998).

PoS HD cells

Because we found that the ATI increased for passive rotations in ADN HD cells, we recorded HD cells in the PoS under the same conditions to determine if similar effects would also be evident in PoS. ATI values in PoS HD cells are typically near zero, and we were thus interested in determining whether ATI values would become more positive during passive sessions as they did for ADN cells. We recorded 20 PoS HD cells in six rats in the hand-held passive condition. There was a trend toward higher ATI values during the hand-held condition, but this trend reached significance for only one measure—separation angle [$F(2,20) = 3.79$, $P < 0.032$]; it was not significant for peak firing rate [$F(2,20) = 1.92$, $P < 0.160$] or information content [$F(2,20) = 0.90$, $P < 0.415$]. A Tukey post hoc comparison revealed the difference to be between the hand-held condition and the second active control trial ($HSD_{0.05} = 1.77$).

In the Cart condition, we recorded from 16 HD cells from five rats. As in the case for ADN cells, PoS cells showed no significant change across condition for any measure {peak firing rate: [$F(2,16) = 0.21$, $P > 0.05$]; information content: [$F(2,16) = 0.17$, $P > 0.05$]; separation angle: [$F(2,16) = 0.19$, $P > 0.05$]}. The results from PoS HD cells are summarized in Table 1.

DISCUSSION

We expected that subjecting a rat to passive movement would abolish or reduce the ATI in ADN HD cells. We found no such result, and in at least one type of passive manipulation, we found that there was an increase in the time by which cell firing anticipated HD. Thus our notion of *how* a motor efference copy signal would drive anticipatory firing is not able to account for this result and requires revision.

Reafference and efference copy

Since its articulation by Von Holst and Mittelstaedt (1950), the idea of a motor efference copy signal has been associated with comparisons made between afferent input resulting from self-initiated movements (reafference) and the motor signals driving those movements. Such a comparison would reduce ambiguity in situations where changes in afferent stimuli could be the result of either environmental or self-initiated motion. Classic examples involve visual/oculomotor interaction, in which motor information is used to differentiate between eye movements and independent movements of the visual scene in the external environment. In the case of directional orientation, predictable changes in the visual scene and vestibular input should result from angular head movement of a given magnitude. Proprioceptive feedback, related to stretch in the neck, back, and limb muscles, is also available and would modulate ongoing movement planning. Maintaining a correct relationship between movement and reafferent feedback would be fundamental to keeping an accurate sense of orientation. Such a comparison could utilize a model of the expected reafference for error correction, and it was our hypothesis that the anticipatory firing properties of ADN HD cells represent this kind of predictive model. Removing or altering motor information such that it was not consistent with movement of the body/head would therefore impoverish the model and preclude error correction. The finding that anticipatory firing continues under passive conditions indicates that either it is not related to the hypothesized predictive model or that the model is not dependent on motor input.

Our results strengthen previous conclusions (Taube and Muller 1998) that the anticipatory firing characteristics of ADN

HD cells are independent of other firing parameters, most notably peak firing rate and directional firing range. Although firing rate was reduced under the same conditions that ATI values increased, there was no linear relationship between the two parameters within a condition, nor between the degree of change in firing rate values and in ATI values from the active to the passive condition. Furthermore, we were able to produce distortion of the tuning curves by adding spatial noise in a manner that modeled changes in peak firing rate and directional range width without producing any change in ATI values. This finding may be significant in light of other observed effects of movement on peak firing rate.

Zugaro et al. (2002) reported that during passive rotations in unrestrained rats, peak firing rate decreased significantly at low angular head velocities, but there was no difference between passive and active groups at high angular head velocities. In contrast, earlier investigations of HD cell characteristics observed dramatically decreased firing rates in restrained animals at both low and high angular head velocities (Golob et al. 1998; Knierim et al. 1995; Taube 1995; Taube et al. 1990b). In these studies, animals were immobile, but sometimes struggled against the restraint and consequently generated motor commands. This result suggests that motor efference copy signals modulate the cell's firing rate rather than influence the ATI. During passive movement, angular head velocity may modulate peak firing rate to the degree it does because there is no motor efference copy signal to cancel the vestibular input. Restraint would represent a mixed case: motor signals arising from struggling movements may be sufficient to cancel vestibular modulation of firing rate but not to support motor-driven firing rate modulation. According to this view, the HD signal is a summation of sensory and motor signals.

Such a scenario seems plausible in light of research in monkeys that suggests just this type of vestibular-motor integration. Neuronal firing in many vestibular nucleus neurons in monkeys was modulated by angular head velocity only when the head was turned passively and not when the monkey made active head turns (McCrea et al. 1999; Roy and Cullen 2001). One type of neuron [position-vestibular-pause (PVP)] showed suppression of vestibular modulation during gaze redirection (i.e., combined head and eye movement) that ended once the eye-in-space position was stable, showing angular head-velocity modulation only while the head was still turning to bring the head in line with the eyes. Another type of neuron [velocity only (VO)] showed suppression of vestibular modulation through the entire head movement regardless of eye movement. Both types were velocity modulated during passive rotations in the dark. Furthermore, the suppression of modulation only occurred when the monkey turned its head relative to its trunk, thereby activating neck motoneurons and not when the monkey "steered" the apparatus to turn the head and body together (Roy and Cullen 2001). The authors concluded that an efference copy of the neck motor command, rather than higher-order motor commands planning head-in-space position, was responsible for influencing vestibular firing patterns. Similarly, if motor efference copy commands do contribute to the HD cell signal, such commands are likely to originate elsewhere than sites of executive motor planning like the motor cortex. Roy and Cullen's manipulation preserved intention (steering) and movement reafference (vestibular sensation) while removing motor input (head-on-body movements). Our passive manipulations preserved movement reafference (vestibular sensation) and motor input (head-on-body movements) while decoupling this information from intention (imposition of passive movement). The results in both cases argue that the kind of mismatches between intended head-in-space movements and sensory feedback that we sought to create would be independent of an efference copy-reafference loop situated between the vestibular nuclei and lower motor centers. During passive conditions, vestibular and visual reafference information would be consistent with one another and correspond normally to the head-on-body component of movements controlled by the spinal motoneurons, even while they deviate from the intended head-in-space movement controlled at the level of motor planning. Indeed, Roy and Cullen (2001) found that the passive and active components of a combined voluntary and imposed movement were differentiated at the neural level in vestibular neurons that fired only in proportion to the passive component. The protocol of Zugaro et al. (2001), in whose study rats were passively rotated while standing at a water spout, would tend to elicit no gaze redirection because the behavioral goal was stationary. Thus the rats would be in a gaze stabilization mode, and in the schema of Cullen and Roy (2004), pure vestibular modulation would be operational in the vestibular nuclei. The hand-held passive condition in our experiments would be comparable to the "reduced vestibular" condition of Roy and Cullen (2004) in which combined passive and active movements in opposite directions resulted in a lower vestibular firing rate in VO cells. This attenuated firing was putatively suppressed by motor efference copy signals. If the vestibular signals believed to drive HD cell firing interact with motor efference signals in a comparable way, then this situation may explain the different affects on firing rate seen in different passive conditions.

Previous studies that manipulated visual cues or information from motor efference copy/proprioceptive systems have shown that these systems play major roles in controlling a HD cell's preferred firing direction (Stackman et al. 2003; Taube 1995). In contrast, manipulation of vestibular cues, either through transient or permanent lesions of the vestibular labyrinth, has shown that an intact vestibular system is required to generate direction-specific activity (Stackman and Taube 1997; Stackman et al. 2002). While the attenuation of firing that occurred during active head movements in monkeys was obtained from the medial vestibular nuclei, how and where vestibular, motor, visual, and proprioceptive information might be integrated in the HD cell circuit is poorly understood. The ADN receives HD cell information from the lateral mammillary nuclei (LMN) (Blair et al. 1998; Stackman and Taube 1998), which in turn receives its primary inputs from the dorsal tegmental nucleus (DTN) (Allen and Hopkins 1989; Hayakawa and Zho 1989). ADN HD cell activity is dependent on an intact DTN (Bassett and Taube 2001b), and the majority of cells within the DTN encode angular head velocity (Bassett and Taube 2001a; Sharp et al. 2001). The DTN receives one of its major projections from the nucleus prepositus hypoglossi, which is usually thought of as part of the neural integrator for the vestibulooocular-reflex (VOR) and eccentric gaze-holding (Fukushima et al. 1992). While neurons in this structure are typically associated with eye velocity and position correlates, at least some cells were identified in primates (McFarland and Fuchs 1992), rats (Lannou et al. 1984), and gerbils (Kaufman et al. 2000) that

were sensitive to angular head velocity independent of eye movements. Taken together with the anatomy, these findings suggest that the NPH may be the principal conduit of vestibular-originating head-velocity information to the HD cell system. Its place in the HD cell circuit is intriguing, though, in light of several observations. First is the organization of motor/vestibular interaction as discussed above with regard to studies in the monkey. At a stage of processing as early as secondary vestibular neurons, cell activity reflects the complex combined head-eye interaction in gaze redirection (Cullen and Roy 2004). Second is the interconnectivity of the NPH not only with the oculomotor complex (particularly the abducens nucleus and medial rectus subdivision of the oculomotor nucleus, subserving horizontal eye movements [McCrea and Baker 1985]) but also with the superior colliculus, a midbrain structure strongly implicated in voluntary gaze direction (Hardy and Corvisier 1996). Finally, there is the observation that rats redirect their gaze primarily through head (rather than eye) movements (Meier and Dieringer 1993), leading to the possibility that HD cell activity incorporates the direction of gaze. Taken together, these observations offer a possible explanation for the shifts we found in ATI during the hand-held passive condition, which we discuss in the next section.

Numerous studies have demonstrated the tendency, in humans and other animals, for the direction of the head to anticipate the trajectory of the body during changes in heading (Grasso et al. 1998). In animals with binocular vision, these head movements are always accompanied by saccades to effect overall gaze (eyes + head) shifts in the direction of anticipated motion. Even in afoveate animals with side-set eyes, however, eye movements are involved in this gaze shift in the sense that the range of motion of reflexive eye movements (nystagmus) is shifted in the direction of movement. Several investigators have thus proposed that aligning the gaze with desired direction of motion—whether the eye-movement portion is voluntary or reflexive—provides the brain with an allocentric reference frame that can be used to guide the whole body along the intended path (Chun and Robinson 1978; Crommelinck et al. 1982). Siegler et al. (1998) have even presented evidence that reflexive gaze shifts are related to the spatial relationships of the remembered features in the surrounding environment. They assessed shifts in the eyes' range of motion during nystagmus (nystagmic "beat-fields") in human subjects exposed to identical vestibular stimulation in the dark, before and after having seen the surrounding room. In each case, they were asked to make judgments about their angular displacement. Beat-field shifts were greater and judgments were more accurate after viewing the surrounding room. Siegler et al. (1998) argued that subjects were orienting to remembered features of the room.

In light of these data, we can imagine how a HD signal could be anticipatory without necessarily relying on a motor-efference copy signal. If vestibular input alone can change the orientation of reflexive eye movements to anticipate the allocentric reference frame, as Siegler et al. argued, then it could change the neural activity underlying the representation of allocentric space. Because this reflexive gaze shift is ultimately a vestibular reflex, the reference frame anticipation need not rely on motor signals any more than anticipation in the VOR does. Instead, anticipation of future head direction could be derived simply from velocity and head-turn direction information, where a current angular head-velocity signal is fed forward and integrated into the HD cell circuit to anticipate where the animal's head will be pointing in the immediate future, given the preceding sensory information. A number of predictions arise from this hypothesis. One is that anticipatory firing would remain present even during completely passive rotations because no motor efference signal would be involved. Another is that the ATI would show a linear dependence on angular head velocity. Both of these predictions are consistent with the present results. Another interesting prediction, though more difficult to test, is that the anticipatory mechanism would function poorly at the initiation of a head turn. Little anticipation could occur at the start of a head turn because there would be no previous velocity signal to inform a prediction of future head direction.

The implication of this last prediction is that anticipation would be more robust during movements that contain fewer starts or changes of direction. Accordingly, the relatively long-duration head sweeps (i.e., low frequencies) that are evident in the HD profile of the hand-held condition (Fig. 1) may be the key to explaining the increased ATI values in this condition relative to others and suggests another similarity to the nystagmic beat-field shift phenomenon. First, nystagmic beat-field shifts, like the anticipatory firing in HD cells, are velocity dependent. Second, the beat-field shifts typically conform to a temporal profile in which they first increase in amplitude over time and then gradually subside during extended rotations (Meier and Dieringer 1993). Thus as we would predict for anticipatory HD cell firing, beat field shifts are less robust in the highest-frequency range of movement. The relatively low-frequency movements in the hand-held conditions may allow large shifts of the beat-field to develop, without being so long in duration as to allow the shifts to subside. If anticipatory firing occurs in parallel to nystagmic beat-field shifts, it may follow a similar temporal profile, such that low-frequency/long-duration turns elicit larger ATIs just as they elicit greater beat-field shifts. Although this parallel is speculative, by recording a rat's eye movements along with its directional heading under experimental conditions that lead to a beat-field shift we may be able to test this hypothesis.

Despite this possibility, current evidence does not allow us to confidently attribute any behavioral or functional role to anticipatory firing. Some models of HD cell activity posit anticipatory firing as an emergent property of the network (Goodridge and Touretzky 2000; Hahnloser 2003; Redish et al. 1996; Xie et al. 2002; Zhang 1996). In these models, anticipatory firing arises from offset connections between a double ring attractor network. For example, for CW turns, a HD cell in one layer that is tuned to 50° is connected to a 45° tuned HD cell in the second layer; for CCW turns, a different 50° tuned HD cell in the first layer would be connected to a 55° tuned HD cell in the second layer. Thus turns in one direction excite cells in the second layer that are slightly offset from cells in the first layer. The result is directional firing in the two rings that is slightly out of register in time, such that one leads the other, with no specified behavioral significance. Furthermore, because these models do not distinguish between vestibular, sensory feedback, or motor inputs into the networks, the models make no predictions about how these networks might respond differently in passive versus active conditions.

Two other cases have been reported in which the anticipatory time interval in ADN HD cells has increased after exper-

imental manipulations: after bilateral PoS lesions (Goodridge and Taube 1997) and after unilateral LMN lesions (Blair et al. 1999). In each case, structures projecting to ADN were removed from the circuit, and the ATI increased rather than decreased in the absence of input from these sources. These two findings suggest that a network functioning without experimental interventions limits the degree of anticipation rather than maximizes it and may indicate that our experimental manipulations did succeed in reducing the amount of information available to the system in our hand-held passive conditions. According to this view, our experimental conditions reduced the limiting effects the network imposes on the ATI, and allowed the ATI to tend toward unconstrained values.

For this reason, it is notable that while there was some trend toward increased ATI in the PoS, the effect was significant for only one of the three measures. Therefore while the PoS might reflect some influence of HD cell activity in the ADN, it does not seem to be merely a passive receiver. Instead, at least some influences on the temporal characteristics of PoS HD cell firing may be independent of the ADN. Given that there are reciprocal connections between the PoS and ADN (van Groen and Wyss 1990), the present results along with those from the PoS lesion experiments (Goodridge and Taube 1997), suggest a two-way flow of temporal influence between the PoS and ADN.

Summary

Although the results reported here leave uncertain the mechanisms responsible for the ATI, they add to our understanding of the ADN HD signal by showing the independence of anticipatory firing from self-initiated movement. Anticipatory firing was present in both mobile and immobile animals in which we created motor/reafference mismatches through passive movement.

ACKNOWLEDGMENTS

The authors thank J. Marcroft for technical assistance and S. Wiener for helpful comments on the manuscript.

Present addresses: M. B. Zugaro, Center for Molecular and Behavioral Neuroscience, Rutgers University, 197 University Ave., Newark, NJ 07102; E. J. Golob, Dept. of Psychology, Tulane University, 6823 St. Charles Ave., New Orleans, LA 70118; and G. M. Muir, Psychology Department, St. Olaf College, Northfield, MN 55057–1098.

GRANTS

This research was supported by grants from the National Science Foundation (INT-9726719), from the National Institute of Mental Health (MH-48924, MH-01286), and in France from the Centre National d'Etudes Spatiales, Cogniseine, Groupement d'Intérêts Scientifiques.

REFERENCES

Allen GV and Hopkins DA. Mamillary body in the rat: topography and synaptology of projections from the subicular complex, prefrontal cortex, and midbrain tegmentum. *J Comp Neurol* 286: 311–336, 1989.

Bassett JP and Taube JS. Neural correlates for angular head velocity in the rat dorsal tegmental nucleus. *J Neurosci* 21: 5740–5751, 2001a.

Bassett JP and Taube JS. Lesions of the dorsal tegmental nucleus of the rat disrupt head direction cell activity in the anterior thalamus. *Soc Neurosci Abstr* 27: 852.29, 2001b.

Blair HT, Cho J, and Sharp PE. Role of the lateral mammillary nucleus in the rat head direction circuit: a combined single unit recording and lesion study. *Neuron* 21: 1387–1397, 1998.

Blair HT and Sharp PE. Anticipatory head direction signals in anterior thalamus: evidence for a thalamocortical circuit that integrates angular head motion to compute head direction. *J Neurosci* 15: 6260–6270, 1995.

Blair HT and Sharp PE. Visual and vestibular influences on head-direction cells in the anterior thalamus of the rat. *Behav Neurosci* 110: 643–660, 1996.

Blair HT, Cho J, and Sharp PE. The anterior thalamic head-direction signal is abolished by bilateral but not unilateral lesions of the lateral mammillary nucleus. *J Neurosci* 19: 6673–6683, 1999.

Chen LL, Lin LH, Green EJ, Barnes CA, and McNaughton BL. Head-direction cells in the rat posterior cortex. I. Anatomical distribution and behavioral modulation. *Exp Brain Res* 101: 8–23, 1994.

Chun KS and Robinson DA. A model of quick phase generation in the vestibulo-ocular reflex. *Biol Cybern* 28: 209–221, 1978.

Cho J and Sharp PE. Head direction, place, and movement correlates for cells in the rat retrosplenial cortex. *Behav Neurosci* 115: 3–25, 2001.

Crommelinck M, Roucoux A, and Veraart C. The relation of neck muscles activity to horizontal eye position in the alert cat. II. Head free. In: *Physiological and Pathological Aspects of Eye Movements*, edited by A. Roucoux and M. Crommeleinck. The Hague: Junk, p. 379–398, 1982.

Cullen KE and Roy JE. Signal processing in the vestibular system during active versus passive head movements. *J Neurophsyiol* 91: 1919–1933, 2004.

Fukushima K, Kaneko CR, and Fuchs AF. The neuronal substrate of integration in the oculomotor system. *Prog Neurobiol* 39: 609–639, 1992.

Gavrilov V, Wiener SI, and Berthoz A. Discharge correlates of hippocampal complex spike neurons in behaving rats passively displaced on a mobile robot. *Hippocampus* 8: 475–490, 1998.

Golob EJ, Wolk DA, and Taube JS. Recordings of postsubicular head direction cells following lesions of the lateral dorsal thalamic nucleus. *Brain Res* 780: 9–19, 1998.

Goodridge JP and Taube JS. Interaction between postsubiculum and anterior thalamus in the generation of head direction cell activity. *J Neurosci* 17: 9315–9330, 1997.

Goodridge JP and Touretzky DS. Modeling attractor deformation in the rodent head-direction system. *J Neurophysiol* 83: 3402–3410, 2000.

Grasso R, Prevost P, Ivanenko YP, and Berthoz A. Eye-head coordination for the steering of locomotion in humans: an anticipatory synergy. *Neurosci Lett* 253: 115–118, 1998.

Groenewegen HJ, Ahlenius S, Haber SN, Kowall NW, and Nauta WJH. Cytoarchitecture, fiber connections, and some histochemical aspects of the interpeduncular nucleus in the rat. *J Comp Neurol* 249: 65–102, 1986.

Guandalini P. The efferent connections to the thalamus and brainstem of the physiologically defined eye field in the rat medial frontal cortex. *Brain Res Bull* 54: 175–186, 2001.

Hahnloser RHR. Emergence of neural integration in the head-direction system by visual supervision. *Neurosci* 120: 877–891, 2003.

Hardy O and Corvisier J. Firing properties of preposito-collicular neurones related to horizontal eye movements in the alert cat. *Exp Brain Res* 110: 413–424, 1996.

Hayakawa T and Zyo K. Retrograde double-labeling study of the mammillothalamic and the mammillotegmental projections in the rat. *J Comp Neurol* 284: 1–11, 1989.

Kaufman GD, Shinder ME, and Perachio AA. Convergent properties of vestibular-related brain stem neurons in the gerbil. *J Neurophysiol* 83: 1958–1971, 2000.

Knierim JJ, Kudrimoti HS, and McNaughton BL. Place cells, head direction cells, and the learning of landmark stability. *J Neurosci* 15: 1648–1659, 1995.

Kubie JL. A driveable bundle of microwires for collecting single-unit data from freely-moving rats. *Physiol Behav* 32: 115–118, 1984.

Lannou J, Cazin L, Precht W, and Le Taillanter M. Responses of prepositus hypoglossi neurons to optokinetic and vestibular stimulations in the rat. *Brain Res* 301: 39–45, 1984.

McCrea RA and Baker R. Anatomical connections of the nucleus prepositus of the cat. *J Comp Neurol* 237: 377–407, 1985.

McCrea RA, Gdowski GT, Boyle R, and Belton T. Firing behavior of vestibular neurons during active and passive head movements: vestibulospinal and other non-eye-movement related neurons. *J Neurophysiol* 82: 416–428, 1999.

McFarland JL and Fuchs AF. Discharge patterns in nucleus prepositus hypoglossi and adjacent medial vestibular nuclei during horizontal eye movement in behaving macaques. *J Neurophysiol* 68: 319–332, 1992.

Meier RK and Dieringer N. The role of compensatory eye and head movements in the rat for image stabilization and gaze orientation. *Exp Brain Res* 96: 54–64, 1993.

Neafsey EJ, Bold EL, Haas G, Hurley-Gius KM, Quirk G, Sievert CF, and Terreberry RR. The organization of the rat motor cortex: a microstimulation mapping study. *Brain Res* 396: 77–96, 1986.

Paxinos G and Watson C. *The Rat Brain in Stereotaxic Coordinates* (4th ed.). New York: Academic, 1998.

Redish AD, Elga AN, and Touretzky DS. A coupled attractor model of the rodent head direction system. *Network Comput Neural Syst* 7: 671–685, 1996.

Roy JE and Cullen KE. Selective processing of vestibular reafference during self-generated head motion. *J Neurosci* 21: 2131–2142, 2001.

Roy JE and Cullen KE. Dissociating self-generated from passively applied head motion: neural mechanisms in the vestibular nuclei. *J Neurosci* 24: 2102–2111, 2004.

Sharp PE, Tinkelman A, and Cho J. Angular velocity and head direction signals recorded from the dorsal tegmental nucleus of Gudden in the rat: implications for path integration in the head direction cell circuit. *Behav Neurosci* 115: 571–588, 2001.

Siegler I, Israël I, and Berthoz A. Shift of the beating field of vestibular nystagmus: an orientation strategy? *Neurosci Lett* 243: 93–96, 1998.

Skaggs WE, McNaugton BL, Gothard KM, and Markus EJ. An information theoretic approach to deciphering the hippocampal code. In: *Advances in Neural Information Processing Systems. Vol.* 5, edited by Hanson SJ, Cowan JD, and Giles CL. San Mateo, CA: Morgan Kaufmann, 1993, vol. 5, p. 1030–1037.

Stackman RW, Clark AS, and Taube JS. Hippocampal spatial representations require vestibular input. *Hippocampus* 12: 291–303, 2002.

Stackman RW, Golob EJ, Bassett JP, and Taube JS. Passive transport disrupts directional path integration by rat head direction cells. *J Neurophysiol* 90: 2862–2874, 2003.

Stackman RW and Taube JS. Firing properties of head direction cells in rat anterior thalamic neurons: dependence upon vestibular input. *J Neurosci* 17: 4349–4358, 1997.

Stackman RW and Taube JS. Firing properties of rat lateral mammillary single units: head direction, head pitch, and angular head velocity. *J Neurosci* 18: 9020–9037, 1998.

Taube JS. Head direction cells recorded in the anterior thalamic nuclei of freely moving rats. *J Neurosci* 15: 70–86, 1995.

Taube JS. Head direction cells and the neurophysiological basis for a sense of direction. *Prog Neurobiol* 55: 225–256, 1998.

Taube JS and Muller RU. Comparisons of head direction cell activity in the postsubiculum and anterior thalamus of freely moving rats. *Hippocampus* 8: 87–108, 1998.

Taube JS, Muller RU, and Ranck JB Jr. Head-direction cells recorded from the postsubiculum in freely moving rats. I. Description and quantitative analysis. *J Neurosci* 10: 420–435, 1990a.

Taube JS, Muller RU, and Ranck JB Jr. Head-direction cells recorded from the postsubiculum in freely moving rats. II. Effects of environmental manipulations. *J Neurosci* 10: 436–447, 1990b.

van Groen T and Wyss JM. The postsubicular cortex in the rat: characterization of the fourth region of the subicular cortex and its connections. *Brain Res* 529: 165–177, 1990.

Vogt BA and Miller MW. Cortical connections between rat cingulate cortex and visual, motor, and postsubicular cortices. *J Comp Neurol* 216: 192–210, 1983.

von Holst E and Mittelstaedt H. Das Reafferenzprinzip. Wechselwirkung zwischen Zentralnervensystem and Peripherie. *Naturwissenschaften* 37: 464–476, 1950.

Wiener SI. Spatial and behavioral correlates of striatal neurons in rats performing a self-initiated navigation task. *J Neurosci* 13: 3802–3817, 1993.

Xie X, Hahnloser RHR, and Seung HS. Double-ring network model of the head direction system. *Phys Rev E* 66: 041902, 2002.

Zhang K. Representation of spatial orientation by the intrinsic dynamics of the head direction cell ensemble. *J Neurosci* 16: 2112–2126, 1996.

Zugaro MB, Berthoz A, and Wiener SI. Peak firing rates of rat anterodorsal thalamic head direction cells are higher during faster passive rotations. *Hippocampus* 12: 481–486, 2002.

Zugaro MB, Tabuchi E, Fouquier C, Berthoz A, and Wiener SI. Active locomotion increases peak firing rates of anterodorsal thalamic head direction cells. *J Neurophysiol* 86: 692–702, 2001.

European Journal of Neuroscience, Vol. 20, pp. 530–536, 2004

Rat anterodorsal thalamic head direction neurons depend upon dynamic visual signals to select anchoring landmark cues

Michaël B. Zugaro,* Angelo Arleo,* Cyril Déjean, Eric Burguière, Mehdi Khamassi and Sidney I. Wiener
CNRS-Collège de France, Laboratoire de Physiologie de la Perception et de l'Action, 11 place Marcelin Berthelot, 75231 Paris CEDEX 05, France

Keywords: cue control, dynamic motion parallax, hippocampus, limbic system, single unit recordings, spatial orientation

Abstract

Head direction cells, which are functionally coupled to 'place' cells of the hippocampus, a structure critically involved in spatial cognition, are likely neural substrates for the sense of direction. Here we studied the mechanism by which head direction cells are principally anchored to background visual cues [M.B. Zugaro *et al.* (2001) *J. Neurosci.*, **21,** RC154,1–5]. Anterodorsal thalamic head direction cells were recorded while the rat foraged on a small elevated platform in a 3-m diameter cylindrical enclosure. A large card was placed in the background, near the curtain, and a smaller card was placed in the foreground, near the platform. The cards were identically marked, proportionally dimensioned, subtended the same visual angles from the central vantage point and separated by 90°. The rat was then disoriented in darkness, the cards were rotated by 90° in opposite directions about the center and the rat was returned. Preferred directions followed either the background card, foreground card or midpoint between the two cards. In continuous lighting, preferred directions shifted to follow the background cue in most cases (30 of the 53 experiments, Batschelet *V*-test, $P < 0.01$). Stroboscopic illumination, which perturbs dynamic visual signals (e.g. motion parallax), blocked this selectivity. Head direction cells remained equally anchored to the background card, foreground card or configuration of the two cards (Watson test, $P > 0.1$). This shows that dynamic visual signals are critical in distinguishing typically more stable background cues which govern spatial neuronal responses and orientation behaviors.

Introduction

Head direction (HD) neurons discharge selectively as the head is oriented in cell-specific preferred directions in the horizontal plane (Ranck, 1984; Taube *et al.*, 1990; Robertson *et al.*, 1999). They are found in an interconnected network of brain structures which is functionally coupled (Knierim *et al.*, 1998) to place-responsive cells of the hippocampal system (O'Keefe & Dostrovsky, 1971). Spatial responses of HD cells are anchored to visual cues but only when these are in the background (Zugaro *et al.*, 2001a). Background cues can also prevail over foreground cues for controlling hippocampal place responses (Cressant *et al.*, 1997). But how do HD cells select background cues? The psychophysical literature shows that relative depth in the visual field can be detected on the basis of several different stimulus attributes, including accommodation, occlusion (objects blocked by others are more distant), texture contrast, shadows, vergence and mechanisms like dynamic motion parallax (during displacements more distant objects appear to move less rapidly). Known brain systems specialized for detecting optic field flow could automatically confer the latter sensitivity on the HD system; for example, the optokinetic system is more sensitive to optic flow at low, rather than high, velocities (Hess *et al.*, 1989). The present experiments were designed to test the hypothesis that anterodorsal thalamic HD cells distinguish anchoring background cues on the basis of dynamic visual processes like motion parallax and optic field flow detection.

Correspondence: Dr Sidney I. Wiener, as above.
E-mail: sidney.wiener@college-de-france.fr

*M.B.Z. and A.A. contributed equally to this work.

Received 14 October 2003, revised 4 May 2004, accepted 26 May 2004

doi:10.1111/j.1460-9568.2004.03512.x

Materials and methods

Experimental subjects

Seven male Long-Evans (pigmented) rats (250–300 g; Centre d'Elèvage René Janvier, Le Genest-St-Isle, France) were put on a restricted food schedule to avoid excessive weight gain (about 14 g of rat chow per day). The animals were maintained on a 12 h light : 12 h dark cycle in an approved animal facility. All animal care and experimental protocols were in accord with institutional (CNRS Comité Opérationnel pour l'Ethique dans les Sciences de la Vie) and international (NIH guidelines) standards and legal regulations (Certificat no. 7186, Ministère de l'Agriculture et de la Pêche) regarding the use and care of animals.

Electrode implantation

The rats were implanted with electrodes in the anterodorsal nucleus of the (right or left) thalamus. (No differences were noted between left

and right recordings.) Electrode bundles consisted of eight formvar-coated nichrome wires (diameter 25 μm). Each bundle of wires was inserted in a 30-gauge stainless steel cannula and mounted on one of two independently advanceable connector assemblies on a single headstage (Wiener, 1993). Before surgery, the animals were tranquillized with xylazine and then deeply anesthetized with pentobarbital (40 mg/kg). The electrodes were implanted above the antero-dorsal thalamic nucleus (antero-posterior −1.4 to −2.0 mm and medio-lateral ±1.1 to ±1.4 mm relative to bregma, 4.2 mm ventral to brain surface) using conventional surgical techniques. The electrode descender assembly was permanently fixed to the skull with dental acrylic and seven tiny screws. A ground screw connector assembly was implanted in the cranial bone.

Signal processing

During the recording sessions, electrode signals passed through FETs were differentially amplified (10 000 ×) and filtered (300–5 kHz, notch at 50 Hz). The signal was then passed to a computer for automatic data collection. The acquisition software (DataWave® Discovery) digitized and collected 32 data points (at 20 kHz) for each signal that crossed a user-set threshold. Single unit activity was discriminated post-hoc using this system's spike-sorting techniques based on a maximum of eight different waveform parameters.

When a well-isolated neuron was successfully recorded, the electrodes were not advanced at the end of the session, in order to permit further recordings from the same neuron. The rationale for this was that existing studies are remarkably consistent in showing that, in simultaneous recordings of HD cells, all neurons respond coherently to cue manipulations (also see Results and Discussion). Thus, the responses would be the same in the well-isolated neuron as in its neighbor, which might prove difficult or impossible to isolate. A neuron was assumed to be recorded again in a subsequent session on the basis of the appearance of a similar waveform on the same electrode and this was supported by similar initial directional preferences and peak firing rates in the recordings. Prior to recordings, a support with two small lamps (10 cm separation) was mounted above the headstage. The (sagittally oriented) positions of the two lamps were detected by a video camera mounted above the platform (using the DataWave® video tracking system) and sampled at a rate of 60 Hz. The heading direction of the animal was later computed using the positions of the two lamps. Inversions of the lamps due to tracking errors were corrected with our own interactive software. Counterclockwise rotations are considered positive here.

Recording protocol

Anterodorsal thalamic HD cells were recorded while the rat was on a small (22-cm diameter) elevated platform in a 3-m diameter cylindrical enclosure. The experimental cues were two freely standing cards, a small one in the foreground (height 60 cm, width 11 cm, distance 36 cm) and a larger one in the background (height 240 cm, width 44 cm, distance 144 cm) (Fig. 1a). The cards were identically marked, proportionally dimensioned and subtended identical (non-overlapping) visual angles from the central viewpoint. The equivalence of the intensity of reflected light from the two cards was controlled regularly with a luminance meter (LS-100; Minolta). The goal here was to make the relative distances of the cards constitute their major distinguishing difference rather than, for example, salience or apparent size. Initially the cards were separated by 90° from the viewpoint of the central platform. (The field of vision of rats is 270°.) The preferred directions

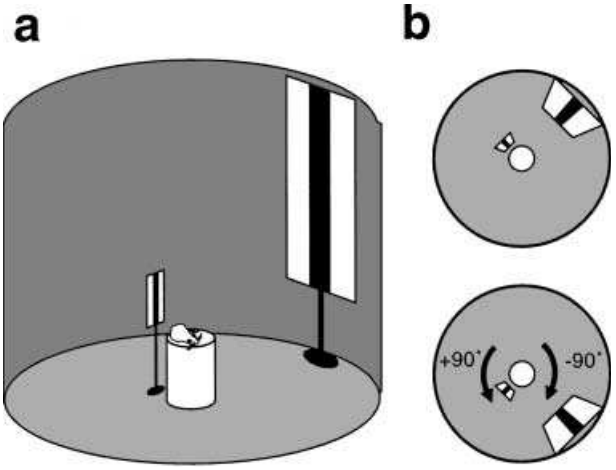

FIG. 1. Experimental protocol. (a) The rats freely foraged for food pellets on an elevated platform (diameter 22 cm) located in the center of a cylindrical black curtain (diameter 3 m). A foreground card (height 60 cm, distance 36 cm) and a background card (height 240 cm, distance 144 cm), bearing two vertical white stripes, served as principal orienting cues. The cards' respective sizes and distances to the platform center were proportioned so that they occupied the same visual angles. They were separated by 90°. (b) After an initial recording (top panel), the animal was removed from the platform and the two cards were rotated in opposite directions (bottom panel). The rat was then disoriented in complete darkness and returned to the platform as the light was turned back on and a second recording began. Recording sessions including baseline and double cue rotations were conducted in continuous or stroboscopic light (flashes at 1.5 Hz).

of HD cells were compared before and after we rotated the background card by 90° in one direction and the foreground card by 90° in the other direction around the platform (Fig. 1), thus providing conflicting orienting cues. After this rotation the cards were again separated by 90° but inverted in their left–right relation. The rats were removed from the apparatus prior to each recording, including during cue rotations, and were disoriented in a completely dark container as the experimenter rotated it erratically while walking about the room. After the disorientation procedure, the experimenter held the animal with its head oriented toward the midpoint between the two cards. The experimenter then asked a colleague to switch on the room light and placed the animal on the platform in a forward linear translation. In this way the animal was immediately exposed to both cues simultaneously while it was in motion (providing dynamic visual information). The difference in apparent angular velocity of the two cards is estimated as between 5 and 10°/s. This procedure was first carried out under continuous lighting to permit normal visual processing. It was then repeated under stroboscopic lighting at 1.5 Hz to disturb neural processing of image velocity (Wells *et al.*, 2001), which we hypothesized would provide cues for distinguishing background from foreground.

The results were interpreted as follows. If the preferred directions were anchored: (i) to the background card, they would rotate by 90° in the same direction as the card; (ii) to the foreground card, they would rotate by the 90° in the other direction, following that card; (iii) to the configuration of both cards, they would rotate by 180° (following the midpoint between the cards) and (iv) to uncontrolled room cues, they would remain unchanged. Finally, should no environmental cue exert control over the preferred directions, the latter would rotate by a random angle (as the rats were disoriented between successive recordings). The initial positions and directions of rotations of the foreground and background cards were varied among sessions. In

order to test for possible effects of the order that the manipulations were executed, in nine sessions, the protocol was repeated again immediately without unplugging the headstage or removing the animal from the experimental room (in one of these cases the protocol was repeated twice and in another three times). In two sessions the stroboscopic condition was presented first, in three others only the stroboscopic condition was tested and in one session, only the continuous light condition was presented four times.

Analyses

Methods for computing tuning curves for the HD cells are detailed in Zugaro *et al.* (2001b). Briefly, the software counted the number of spikes for each position sampling interval (16.6 ms) and associated the resulting frequency with the corresponding head angle. This was used to compute a histogram, for which each bin height was the average of all the frequencies associated with head angles within the range of the bin. To calculate preferred direction, we used a discretized adaptation of the Gaussian fit. A best-fit approximation to this curve was obtained via Matlab® (The MathWorks, Natick, MA, USA) software. Circular statistics are from Batschelet (1981). Although, for clarity, the data are shown as histograms in Fig. 4, none of the statistical tests actually relies on these binned values; instead, they use continuous random variables and thus our results are completely independent of the histogram bin sizes.

Histology

At the end of the experiments, a small electrolytic lesion was made by passing a small cathodal DC current (20 μA, 10 s) through one of the recording electrodes to mark the location of its tip. The rats were then deeply anesthetized with pentobarbital. Intracardial perfusion with saline was followed by 10% formalin–saline. Histological sections were stained with cresyl violet. Recording sites were reconstructed by detecting the small lesion and the track of the 30-gauge cannula, taking into account the distance that the microelectrode driver had been advanced from the point of stereotaxic placement of the electrodes. The recording sites were calculated by interpolation along the electrode track between the lesion site and the implantation site. Two HD cells from a fifth animal were excluded from analyses because the recording site was in the hippocampus.

Results

Seventeen anterodorsal thalamic HD cells were recorded in seven rats in 34 sessions which included 53 experiments in continuous light and 51 under stroboscopic lighting (an experiment is considered a comparison of directional responses prior to and after cue rotation.) In six sessions, multiple HD cells with different preferred directions were recorded simultaneously (two cells in three of the sessions, three cells in two sessions and four cells in the other session). In each of these cases, all of the neurons had the same responses to cue shifts in the continuous light and stroboscopic conditions (see, for example, Fig. 2). This indicates that the results from individual neurons are representative of all of the neurons of the anterodorsal nucleus of the thalamus in each of these sessions.

As shown by the typical examples in Fig. 3, in the majority (57%, i.e. 30 of 53) of the recording experiments the preferred directions of the HD cells stayed anchored to the background card after card rotations when recorded in continuous light (Fig. 3, left column). This disproportionately outnumbers the experiments where preferred

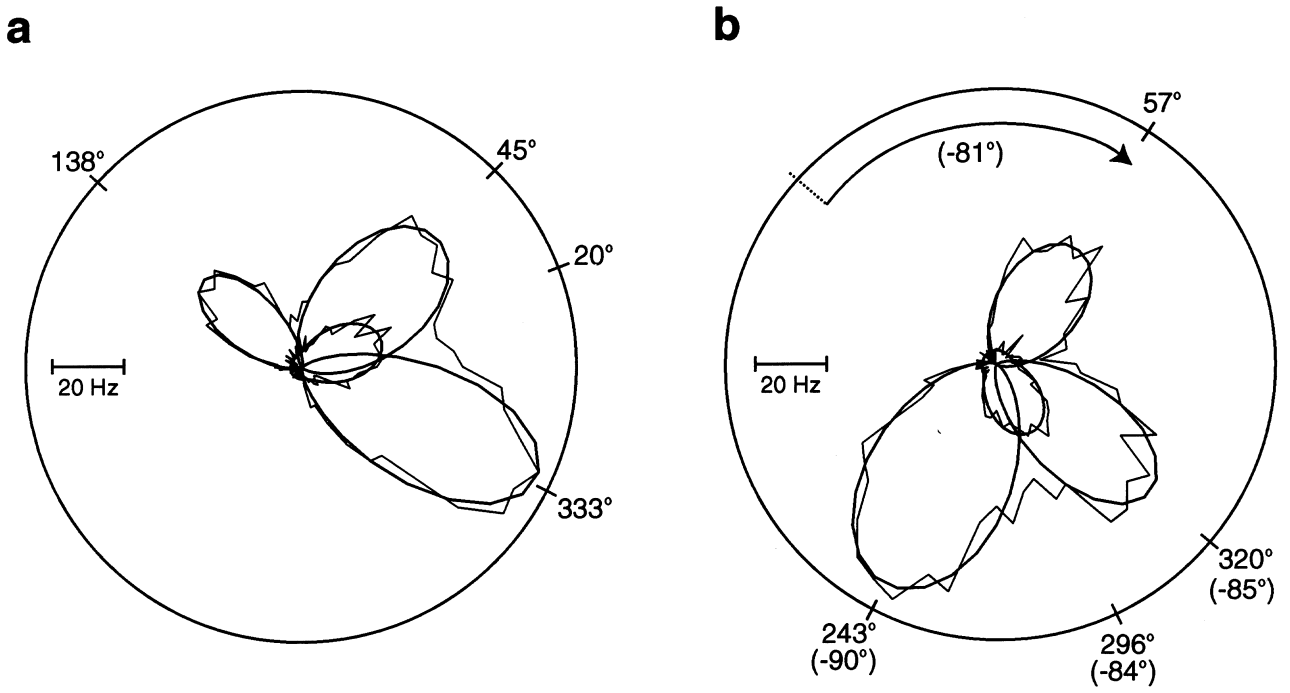

FIG. 2. Polar plots of directional responses of four anterodorsal thalamic neurons recorded simultaneously in continuous light conditions. Three were recorded simultaneously on the same electrode while the fourth (with the lowest peak firing rate) was recorded from another electrode. The thin jagged traces are the actual firing rate histograms (binwidth 6°, calibration bar to left). The thicker lines are Gaussian best-fit approximations of the individual response curves. (a) Responses prior to cue rotation. (b) Responses after cue rotation show a coherent shift of all of the preferred directions by about the same angles (−81, −85, −84 and −90°).

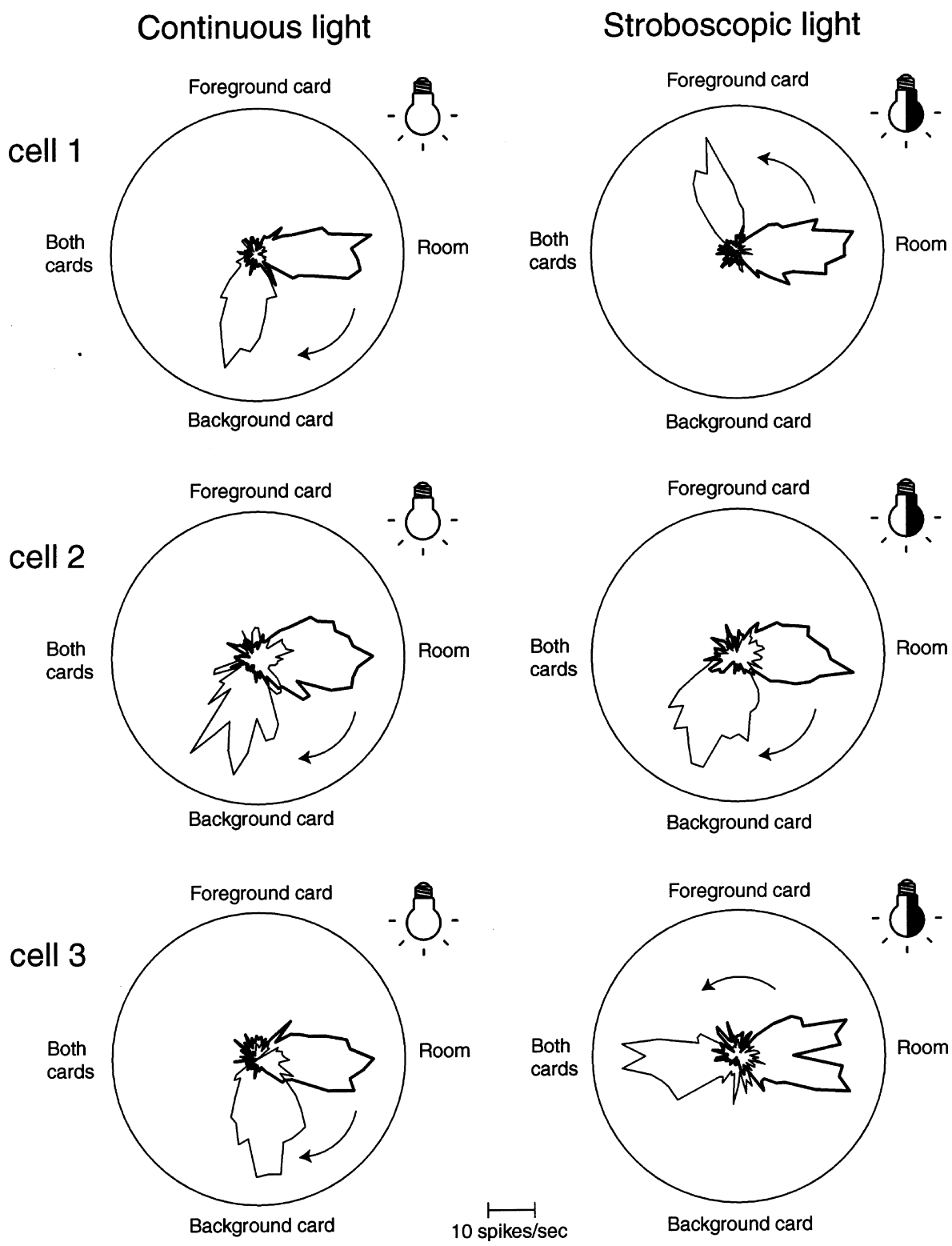

FIG. 3. Typical shifts in preferred directions after card rotations. The response curves of these head direction (HD) cells (recorded during three different sessions) were sampled during the recording preceding (thick curves) and following (thin curves) the rotation of the background card by −90° and the foreground card by +90° around the platform. The polar plots show the firing rate as distance of the trace from the central point (calibration bar at bottom center). The initial directional response curve has been oriented to point to the right (3 o'clock position) to facilitate comparisons. (a) Under continuous light conditions, the preferred directions of the HD cells always shifted by approximately 90° clockwise, following the card in the background. (b) Under stroboscopic light conditions, the preferred directions of the HD cells could shift 90° counterclockwise, following the foreground card (cell 1 in row 1), follow the background card (cell 2 in row 2) or shift by 180°, following the midpoint between the two cards (cell 3 in row 3). The labels 'Foreground card', 'Background card' and 'Both cards' show the predicted angle of rotation of the preferred direction if the respective cues had dominantly influenced the anchoring of the preferred direction. Data have been rectified to compensate for the fact that background and foreground cards were rotated in different directions among sessions.

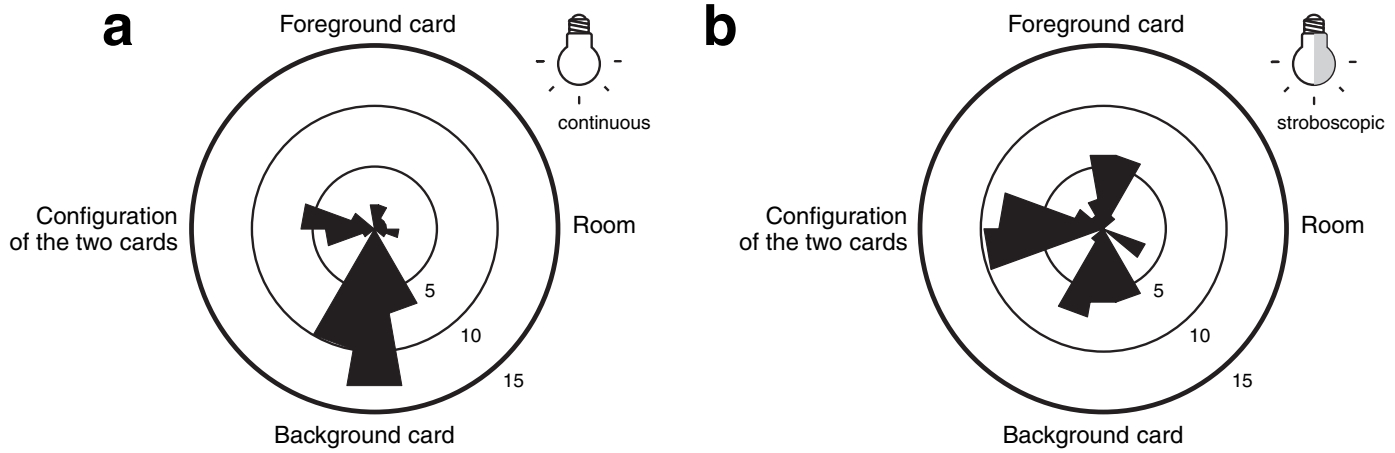

FIG. 4. Incidence of preferred direction shifts after foreground and background card rotations in (a) continuous and (b) stroboscopic light. The data are shown in the form of a circular histogram (bin size 20°) where the number of sessions corresponding to the respective shifts in preferred direction is indicated by the radius of the concentric circles that serve as calibration bars. The preferred directions after cue rotations are presented according to the same formalism as in Fig. 3 to facilitate comparisons: no shift (equivalent to dominance of room cues) is indicated at the 3 o'clock position ('Room') and shifts following the background cue are at 9 o'clock, etc. (a) Under continuous light conditions, the preferred directions of the head direction cells followed the background card in the majority of the recording sessions. (b) Under stroboscopic light conditions, the preferred directions were equally likely to follow the background card, foreground card or the configuration of both. Data have been rectified to compensate for the fact that background and foreground cards were rotated in different directions among sessions.

directions followed the foreground card in continuous light (9% of the cases, i.e. five of 53; Fig. 4a). The remaining experiments are inconclusive as the preferred directions followed the configuration of the two cards (25% of the cases, i.e. 13 of 53; as if the two cards were but a single cue) or did not shift (9% of the cases, i.e. five of 53). A *V*-test (Batschelet, 1981) showed that the data were clustered around the background cue orientation (6 o'clock position in Fig. 4a) under continuous illumination ($n = 53$, $V = 4.6521$, $P < 0.01$).

To test whether the selection of anchoring cues depends upon dynamic visual cues (such as motion parallax or optic field flow), we then repeated these experiments in stroboscopic light (flashes at 1.5 Hz). This was intended to disrupt continuous visual inputs and block the processing of fine time-scale spatial changes in retinal stimulation triggered by self motion, such as the relative shifts of images of the respective cards. Thus, under these conditions, if dynamic visual cues were of critical importance, the preferred directions of the HD cells would no longer be controlled by the background card.

Consistent with this prediction, Fig. 3 right column shows the response curves of three typical HD cells (recorded during three different sessions) before and after rotation of the cards under stroboscopic lighting. Each of the three principal responses was observed. Over all recording sessions (Fig. 4b), the preferred directions followed the background card in 33% (17 of 51), the foreground card in 27% (14 of 51) and the configuration of both in 33% (17 of 51) of the recording experiments. In three experiments the preferred directions did not shift. Thus, the preferred directions were equally likely to follow the background card, the foreground card or the configuration of both (Watson U^2n test against the normalized sum of three Gaussians centred at 90, 180 and 270° with SDs of 10°, $U^2n = 0.11703$, $n = 51$, $P > 0.1$). The distributions of responses in the continuous and stroboscopic lighting condition (shown in Fig. 4a and b) were compared and proved to be significantly different (Watson U^2 test, $U^2 = 0.2151$, $n = 104$, $P < 0.05$).

To avoid possible interference of attentional processes with the results, the rats were introduced to the environment in a special manner described in Materials and methods. In those sessions where a continuous light condition session immediately followed a recording under stroboscopic light, the results were similar to those that occurred at the beginning of the session (the background card was selected in 10 of 16 experiments while the foreground card was followed only twice; for both cards $n = 2$ and for the room cues, $n = 2$). Thus, there is little support for the different distribution of responses under stroboscopic lighting being due to its novelty or generalized disorienting effects as no systematic differences were found between responses in early versus late sessions within series in individual animals.

Discussion

The principal result is that stroboscopic lighting at a frequency disturbing certain dynamic visual processes interferes with the preferential anchoring of HD responses by background cues. This is consistent with the hypothesis that, under continuous lighting, this anchoring would occur by neural processing of fine time-scale spatial changes in retinal stimulation triggered by self motion, specifically the shifts of images of the respective cards. The relative velocities of retinal slip of the two cards would be detected during head movements. The image of the more distant card would shift more slowly and this would anchor the HD system by mechanisms as yet unknown (although anatomical pathways have been demonstrated that link these neural systems, rendering this interpretation parsimonious). Note that this requires estimation only of relative, not absolute, distance. This is supported by the absence of preferential anchoring by the background cue in stroboscopic lighting, which disrupts continuous visual inputs and blocks the use of visual motion signals (such as motion parallax) from helping to distinguish background from foreground cues. This also confirms and extends our previous findings showing that updates of the preferred directions of HD cells are dominated by background, rather than foreground, visual cues (Zugaro *et al.*, 2001a).

Although the background cue significantly dominated in the continuous light condition, the results varied from one experimental session to the next, even with repeated recording of the same individual neuron or same animal. This may be because the actual available dynamic visual cues for detecting relative distance consisted of low magnitude differences in relative velocity (estimated at 5–10°/s). As preferred directions can be reset very rapidly in the HD cell network (Zugaro *et al.*, 2003), it is not surprising that this automatic

mechanism would show variability as relative distance information was sparse and liminal. This is supported by the substantial numbers of sessions in both conditions where the preferred direction followed the midpoint between the two cues, indicating that they were not easily distinguishable. In any case, the suppression of this significant bias toward the background cue under stroboscopic lighting argues for the vital role of dynamic visual cues under continuous light, as the stroboscopic lighting deters velocity detection while not affecting other possible relative distance cues.

There are several arguments against other relative depth cues influencing the HD cells here. The experimental design and poor visual discrimination capacities of rats (Hughes, 1977; Hughes & Wässle, 1979) eliminated or dramatically reduced the risk of interference from certain other possible cues, like relative size, luminance, occlusion and texture. The two cues were positioned at the limits of the binocular viewing field of the rat visual system (Lashley, 1932), thus making vergence unlikely. Accommodation (which remains to be demonstrated in the rat) is also considered unlikely as HD cell responses are set within 80 ms while accommodation requires at least twice that time in humans (e.g. Kasthurirangan *et al.*, 2003). Nevertheless, it remains possible that under, other experimental conditions, HD cells could also be demonstrated to engage some of these other mechanisms in order to select anchoring background cues.

Each of the individual responses is considered to represent the activity of all of the neurons in the anterodorsal thalamus within that session. This is supported by our present results in four sessions with multiple cell recordings and by virtually all published reports of simultaneous recordings of HD cells (e.g. Taube *et al.*, 1990; Chen *et al.*, 1994; Goodridge & Taube, 1995; Dudchenko *et al.*, 1997; Knierim *et al.*, 1998; Zugaro *et al.*, 2001a) which consistently observe that these neurons respond coherently to changes of the orientation of the environmental cues. This binding is also a vital property permitting all existing computational models of HD cells to successfully replicate the properties of the actual neurons (Skaggs *et al.*, 1995; Blair, 1996; Redish *et al.*, 1996; Zhang, 1996; Goodridge & Touretzky, 2000; Sharp *et al.*, 2001; Xie *et al.*, 2002). This contrasts with some studies of hippocampal place responses where disparate responses among simultaneously recorded cells have been reported.

As HD cell responses varied across experiments rather than among individual cells, the relevant parameter for evaluating the results is the number of experiments (53 in continuous light and 51 in stroboscopic light) and data have been grouped together for multiple cells recorded within a single session. The absence of any apparent patterns in the session-to-session variations in the responses of individual neurons argues against any dependence of successive measures within individual animals and the same pattern of results is apparent for each animal.

In summary, dynamic visual signals play a critical role in selection of anchoring cues by HD cells. Such inputs could include dynamic motion parallax-related signals. These would permit background visual cues to be discriminated from those in the foreground during head translation movements as more distant objects appear to move at lower velocities. Alternatively, HD cells could receive critical information for this from the visual pathways specialized for detecting optic field flow; these are most sensitive to slow movements of large areas of the visual field, as provided by the image of background cues on the retina.

There is a clear adaptive advantage to selecting background cues as they are often more stable and reliable as the animal moves about. This complements the well-known role of optic flow information for updating heading information during movements (Lappe, 2000). While the latter concerns situations where the initial heading direction has already been established, the present work shows that dynamic visual cues are also important in the elaboration of these initial settings.

Acknowledgements

Thanks to Professor A. Berthoz for support and discussions, Dr J. Droulez for discussions, F. Maloumian for illustrations and M.-A. Thomas and S. Doutremer for histology. This work was supported by CNES, ACI du Ministère de la Recherche. M.B.Z. received a grant from the Fondation pour la Recherche Médicale and A.A. received a grant from the EU Marie Curie Programme.

Abbreviations

HD, head direction.

References

Batschelet, E. (1981) *Circular Statistics in Biology.* Academic Press, London.

Blair, H.T. (1996) Simulation of a thalamocortical circuit for computing directional heading in the rat. In Touretzky, D.S., Mozer, M.C. & Hasselmo, M.E. (Eds), *Advances in Neural Information Processing Systems.* MIT Press, Cambridge, MA. pp. 152–158.

Chen, L.L., Lin, L.-H., Green, E.J., Barnes, C.A. & McNaughton, B.L. (1994) Head-direction cells in the rat posterior cortex. I. Anatomical distribution and behavioral modulation. *Exp. Brain Res.*, **101**, 8–23.

Cressant, A., Muller, R.U. & Poucet, B. (1997) Failure of centrally placed objects to control the firing fields of hippocampal place cells. *J. Neurosci.*, **17**, 2531–2542.

Dudchenko, P.A., Goodridge, J.P. & Taube, J.S. (1997) The effects of disorientation on visual landmark control of head direction cell orientation. *Exp. Brain Res.*, **115**, 375–380.

Goodridge, J.P. & Taube, J.S. (1995) Preferential use of the landmark navigational system by head direction cells in rats. *Behav. Neurosci.*, **109**, 1–12.

Goodridge, J.P. & Touretzky, D.S. (2000) Modeling attractor deformation in the rodent head-direction system. *J. Neurophysiol.*, **83**, 3402–3410.

Hess, B.J.M., Blanks, R.H.I., Lannou, J. & Precht, W. (1989) Effects of kainic acid lesions of the nucleus reticularis tegmenti pontis on fast and slow phases of vestibulo-ocular and optokinetic reflexes in the pigmented rat. *Exp. Brain Res.*, **74**, 63–80.

Hughes, A. (1977) The refractive state of the rat eye. *Vis. Res.*, **17**, 927–939.

Hughes, A. & Wässle, H. (1979) An estimate of image quality in the rat eye. *Invest. Ophthalm. Vis. Sci.*, **18**, 878–881.

Kasthurirangan, S., Vilupuru, A.S. & Glasser, A. (2003) Amplitude dependent accommodative dynamics in humans. *Vis. Res.*, **43**, 2945–2956.

Knierim, J.J., Kudrimoti, H. & McNaughton, B.L. (1998) Interaction between idiothetic cues and external landmarks in the control of place cells and head direction cells. *J. Neurophys.*, **80**, 425–446.

Lappe, M. (Ed.) (2000) *Neuronal Processing of Optic Flow.* Academic Press, San Diego.

Lashley, K.S. (1932) The mechanism of vision. V. The structure and image-forming power of the rat's eye. *J. Comp. Psych.*, **13**, 173–200.

O'Keefe, J. & Dostrovsky, J. (1971) The hippocampus as a spatial map: Preliminary evidence from unit activity in the freely-moving rat. *Brain Res.*, **34**, 171–175.

Ranck, J.B. Jr (1984) Head-direction cells in the deep cell layers of dorsal presubiculum in freely moving rats. *Soc. Neurosci. Abstr.*, **10**, 599.

Redish, A.D., Elga, A.N. & Touretzky, D.S. (1996) A coupled attractor model of the rodent head direction system. *Network*, **7**, 671–685.

Robertson, R.G., Rolls, E.T., Georges-Francois, P. & Panzeri, S. (1999) Head direction cells in the primate pre-subiculum. *Hippocampus*, **9**, 206–219.

Sharp, P.E., Blair, H.T. & Cho, J. (2001) The anatomical and computational basis of the rat head-direction signal. *TINS*, **24**, 289–294.

Skaggs, W.E., Knierim, J.J., Kudrimoti, H.S. & McNaughton, B.L. (1995) A model of the neural basis of the rat's sense of direction. In Tesauro, G., Touretzky, D.S. & Leen, T.K. (Eds), *Advances in Neural Information Processing Systems*. MIT Press, Cambridge, MA. pp. 173–180.

Taube, J.S., Muller, R.U. & Ranck, J.B. Jr (1990) Head-direction cells recorded from the postsubiculum in freely moving rats. II. Effects of environmental manipulations. *J. Neurosci.*, **10**, 436–447.

Wells, E.F., Bernstein, G.M., Scott, B.W., Bennett, P.J. & Mendelson, J.R. (2001) Critical flicker frequency responses in visual cortex. *Exp. Brain Res.*, **139**, 106–110.

Wiener, S.I. (1993) Spatial and behavioral correlates of striatal neurons in rats performing a self-initiated navigation task. *J. Neurosci.*, **13**, 3802–3817.

Xie, X., Hahnloser, R.H.R. & Seung, H.S. (2002) Double-ring network model of the head direction system. *Phys. Rev. E*, **66**, 041902.

Zhang, K. (1996) Representation of spatial orientation by the intrinsic dynamics of the head-direction ensemble: a theory. *J. Neurosci.*, **16**, 2112–2126.

Zugaro, M.B., Berthoz, A. & Wiener, S.I. (2001a) Background, but not foreground, spatial cues are taken as references for head direction responses by rat anterodorsal thalamus neurons. *J. Neurosci.*, **21**, RC154, 1–5.

Zugaro, M.B., Tabuchi, E., Fouquier, C., Berthoz, A. & Wiener, S.I. (2001b) Active locomotion increases peak firing rates of anterodorsal thalamic head direction cells. *J. Neurophysiol.*, **86**, 692–702.

Zugaro, M.B., Arleo, A., Berthoz, A. & Wiener, S.I. (2003) Rapid spatial reorientation and head direction cells. *J. Neurosci.*, **23**, 3478–3482.

Rapid Spatial Reorientation and Head Direction Cells

Michaël B. Zugaro, Angelo Arleo, Alain Berthoz, and Sidney I. Wiener
Centre National de la Recherche Scientifique–Collège de France, Laboratoire de Physiologie de la Perception et de l'Action, 75231 Paris Cedex 05, France

It is surprising how quickly we can find our bearings when suddenly confronted with a familiar environment, for instance when the lights are turned on in a dark room. Subjectively, this appears to occur almost instantaneously, yet the neural processes permitting this rapid reorientation are unknown. A likely candidate is the head direction (HD) cell system. These limbic neurons found in several brain regions, including the thalamus and the hippocampus, discharge selectively when the head of an animal is oriented in a particular ("preferred") direction. This neuronal activity is independent of position and ongoing behavior and is thus likely to constitute a physiological basis for the sense of direction. Remarkably, although the HD cell system has properties resembling those of a compass, it is independent of geomagnetic fields. Rather, the preferred directions of the HD cells are strongly anchored to visual cues in the environment. Here, we bring evidence for the first time that a fundamental component of the capacity to rapidly reorient in a familiar environment may be brought about by updating of HD cell responses as rapidly as 80 msec after changes in the visual scene. Continuous attractor networks have been used successfully to model HD cell ensemble dynamics. The present results suggest that after large rotations of the surrounding landmarks, activity in such networks may be propagated in abrupt jumps rather than in a gradually progressive manner.

Key words: **anterodorsal thalamic nucleus; update latency; spatial memory; landmark; visual orientation; attractor network**

Introduction

Head direction (HD) cells discharge selectively when the head of a monkey, rat, mouse, or chinchilla is oriented in a particular direction of the environment, which is referred to as the preferred direction (Ranck, 1984; Knierim et al., 1998; Taube, 1998; Blair et al., 1999; Robertson et al., 1999; Khabbaz et al., 2000; Muir and Taube, 2002). Although HD cell responses can be influenced by various multisensory and motor signals (Blair and Sharp, 1996; Stackman and Taube, 1997; Goodridge et al., 1998; Zugaro et al., 2001b), the preferred directions are primarily updated on the basis of visual landmarks (Taube, 1995; Zugaro et al., 2001a). But how rapidly are preferred directions updated after rotation of visual landmarks? Although this question was addressed briefly in previous studies (Knierim et al., 1998; Zugaro et al., 2000), the experimental protocols could not measure updates occurring faster than 15 sec, because those procedures required recordings while the head of the animal was reoriented in many different directions. However, neural network simulations predict that preferred direction updates could be as rapid as a few hundred milliseconds (Zhang, 1996; Redish, 1999). The experimental protocol described here was developed to test this prediction.

Materials and Methods

Electrode implantation. Four adult male Long–Evans rats (200~250 gm; CERJ, Le Genest-St-Isle, France) were tranquilized with xylazine, deeply anesthetized with pentobarbital (40 mg/kg), and then surgically implanted with electrodes in the anterodorsal nucleus of the thalamus (anteroposterior, approximately −1.6–2.0 mm; mediolateral, ±1.2 mm relative to bregma; 3.8 mm ventral to brain surface). The electrode assembly consisted of bundles of eight, single wire electrodes (Formvar-coated nichrome wires: diameter, 25 μm; impedance, 200–800 kΩ) inserted in a 30 gauge stainless steel cannula and mounted on an advanceable connector assembly (Wiener, 1993). The headstage was permanently fixed to the skull with dental acrylic and tiny screws. All animal care and experimental protocols were in accord with institutional and international standards and legal regulations (Certificate 7186, Ministère de l'Agriculture et de la Pêche).

Data acquisition. During the recording sessions, electrode signals passed through field effect transistors and were differentially amplified (10,000×) and filtered (300 Hz to 5 kHz, notch at 50 Hz). The signals were acquired on a DataWave Discovery system (Longmont, CO). Two small infrared light-emitting diodes (10 cm separation) mounted above the headstage were detected by a video camera, and their moment-to-moment positions were stored by the data acquisition system for off-line analyses [for details, see Zugaro et al. (2001b)].

Apparatus. The experimental setup consisted of a black cylinder (diameter, 76 cm; height, 50 cm) with a white card attached to its inner wall. This subtended 90° and served as the principal visual cue. Water could be delivered to a small reservoir at the center of the cylinder to keep the lightly water-deprived rats immobile without applying physical restraint (Zugaro et al., 2001b), which is known to depress directional responses (Taube, 1995). The 3 × 3 × 3 m recording chamber was surrounded by black curtains suspended from the ceiling along the four walls. Illumination was provided by a 40 W overhead lamp on the ceiling that diffused light evenly within the cylinder. All electronic instruments and computers were situated outside of the curtains, and the entire experimental room was phonically isolated from the rest of the building.

Behavioral task. At the beginning of each recording session, the preferred directions of the HD cells were determined as the rat foraged for small food pellets distributed sparsely onto an elevated circular platform over a 5 min period. Then, the unrestrained rat remained immobile with its head oriented in the preferred direction while receiving small drops (~30 μl) of water at 0.5–1 sec intervals from the reservoir at the center of the platform. The rats had previously been trained to remain immobile at the water spout with a behavioral shaping procedure: water delivery was triggered only when the rat was positioned at the reservoir at the appro-

Received Sept. 17, 2002; revised Jan. 28, 2003; accepted Jan. 28, 2003.

This work was supported by the Centre National de la Recherche Scientifique-National Science Foundation cooperation program, Centre National d'Etudes Spatiales, Action Concertée Incitative du Ministère de la Recherche, Cogniseine, Groupement d'Intérêts Scientifique. M.B.Z. received a grant from the Fondation pour la Recherche Médicale. We thank N. Brunel for comments on this text, F. Maloumian for illustrations, M.-A. Thomas and S. Doutremer for histology, and L. Hazan for help with experiments.

Correspondence should be addressed to S. I. Wiener, CNRS–Collège de France LPPA, 11 place Marcelin Berthelot, 75231 Paris Cedex 05, France. E-mail: sidney.wiener@college-de-france.fr.

 0270-6474/03/233478-05$15.00/0

priate orientation, and water was ceased as soon as it moved away from the preferred direction. (The solenoid valve that released the water made a distinct clicking sound that likely served as a cue.) After a stable recording of the directional response had been established (Fig. 1A), the room light was turned off and the card was manually rotated along the cylinder wall by 90° to a new orientation (Fig. 1*B*). This was done as rapidly and silently as possible to keep the rat from detecting the rotations. The light was then turned back on (Fig. 1*C*). This was intended to trigger an update in the HD system. Because the preferred directions of the HD cells are anchored to visual cues (Taube, 1998), the previously active cells would stop firing, whereas others would become active. After a short delay, the light was turned off again, and the card was rotated back to the initial position (Fig. 1*D*). The light was then turned back on (Fig. 1*E*) to retrigger the initial cell responses. We measured the latencies of the cell responses to the light onset with the card in each position (referred to as a "reorientation event").

Data analysis. For each reorientation event, the response of each HD cell was compared 0.5 sec before and 0.5 sec after the light was turned on (referred to as a "trial"). Two criteria were used to select trials suitable for analysis: (1) the head of the rat had to remain close to the preferred direction (i.e., within two SDs of the Gaussian fit of the response curve around the preferred direction), and (2) the head direction had to remain stable throughout the whole trial, i.e., remain within ±15° around its mean value. Two methods were used to measure latencies of updating of directional responses. We first pooled all analyzable trials recorded from all cells and computed a cumulative response histogram. In the cumulative response histogram, the change point in firing rate was determined by computing the best fit slopes before and after each 10 msec bin within 250 msec after light onset. The bin corresponding to the smallest square error was then selected as the estimated update latency (Friedman and Priebe, 1998). The second method examined firing rate changes on a trial by trial basis. Only trials with a minimum of 10 action potentials were selected for this analysis. The mean interspike intervals were compared for 500 msec intervals before and after each spike occurring within 250 msec after light onset. A maximum likelihood estimator was then used to determine the transition point.

Results

Twenty-three HD cells were recorded in 15 sessions (including 7 sessions in which two or more cells were recorded simultaneously). Turning the light off did not appear to alter the cell responses. The head of the rat remained stable in 261 of 496 (53%) trials. Perhaps because of drift or attentional factors, the preferred directions of the HD cells were not always updated after the light was turned on. Trials were rejected as unusable if the number of spikes emitted was unchanged in the 500 msec before versus 500 msec after light onset [the criterion was $|spikes_{before} - spikes_{after}| / (spikes_{before} + spikes_{after}) \leq 0.2$)], or if the total number of spikes in these periods was <5. With these additional criteria, 129 of 496 (26%) trials were retained. In 51 trials, perhaps because of drift or updating of the preferred directions, the cells started firing when the light went on with the card in its rotated position or stopped firing when the light went on with the card in its initial position.

Figure 2 shows raster plots of the HD cell responses to the light going on with the cue card in the new orientation. The corresponding peri-event histograms and cumulative spike count histograms are also shown. The figure includes the plots of the best fit models of the latter histograms used to compute response latencies (Friedman and Priebe, 1998). The new preferred directions were established at a latency of 80 ± 10 msec, when the newly activated HD cells arrived at their maximum firing rate (Fig. 2*A*). However, the cessation of activity after the cue card was shifted away from its original orientation occurred at a slower rate: the return to baseline occurred only after 140 ± 10 msec (Fig. 2*B*).

We then examined the time course of firing rate changes on a trial by trial basis, using the maximum likelihood estimator of Seal et al. (1983). As shown in the example in Figure 3, there was moderate variability across trials within the same session. No systematic trend was evident, indicating that it is unlikely that learning occurred during the course of the experiment. Also, update latencies appeared reproducible across sessions and animals

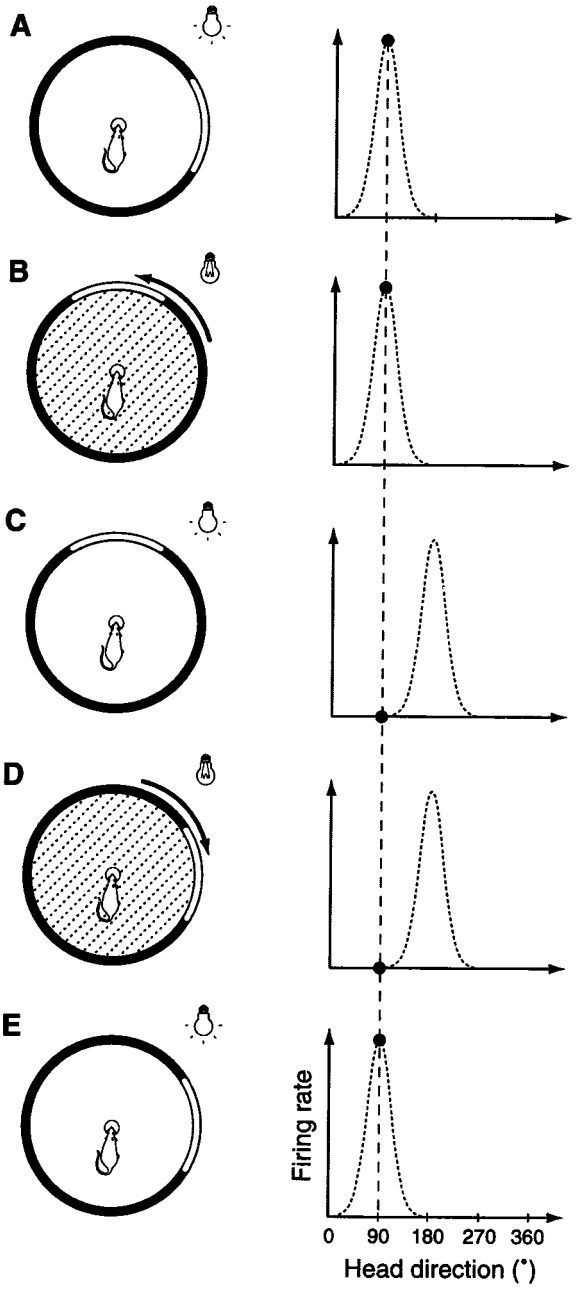

Figure 1. Experimental procedure. *A*, Because the rat remains immobile oriented in the (previously determined) preferred direction while drinking water from the reservoir (left), full response curves cannot be sampled. Rather, only the cell responses corresponding to this particular head direction can now be recorded (black circle in right panel). *B*, The light is turned off, and the card is rotated by 90° along the cylinder wall. *C*, The light is turned back on. This triggers a shift in the directional response curve of the neuron because this activity is anchored to visual cues (right panel). Accordingly there should be a marked decrease in firing rate (compare the filled circles in *B* and *C*, right panels). *D*, The light is turned off again, and the card is returned to the standard position. *E*, The light is turned back on. The preferred direction shifts back to its initial orientation (right panel). This corresponds to a marked increase in discharge frequency (compare the filled circles in *D* and *E*, right panels). Steps *B* through *E* are repeated until the rat is satiated and no longer remains immobile at the center.

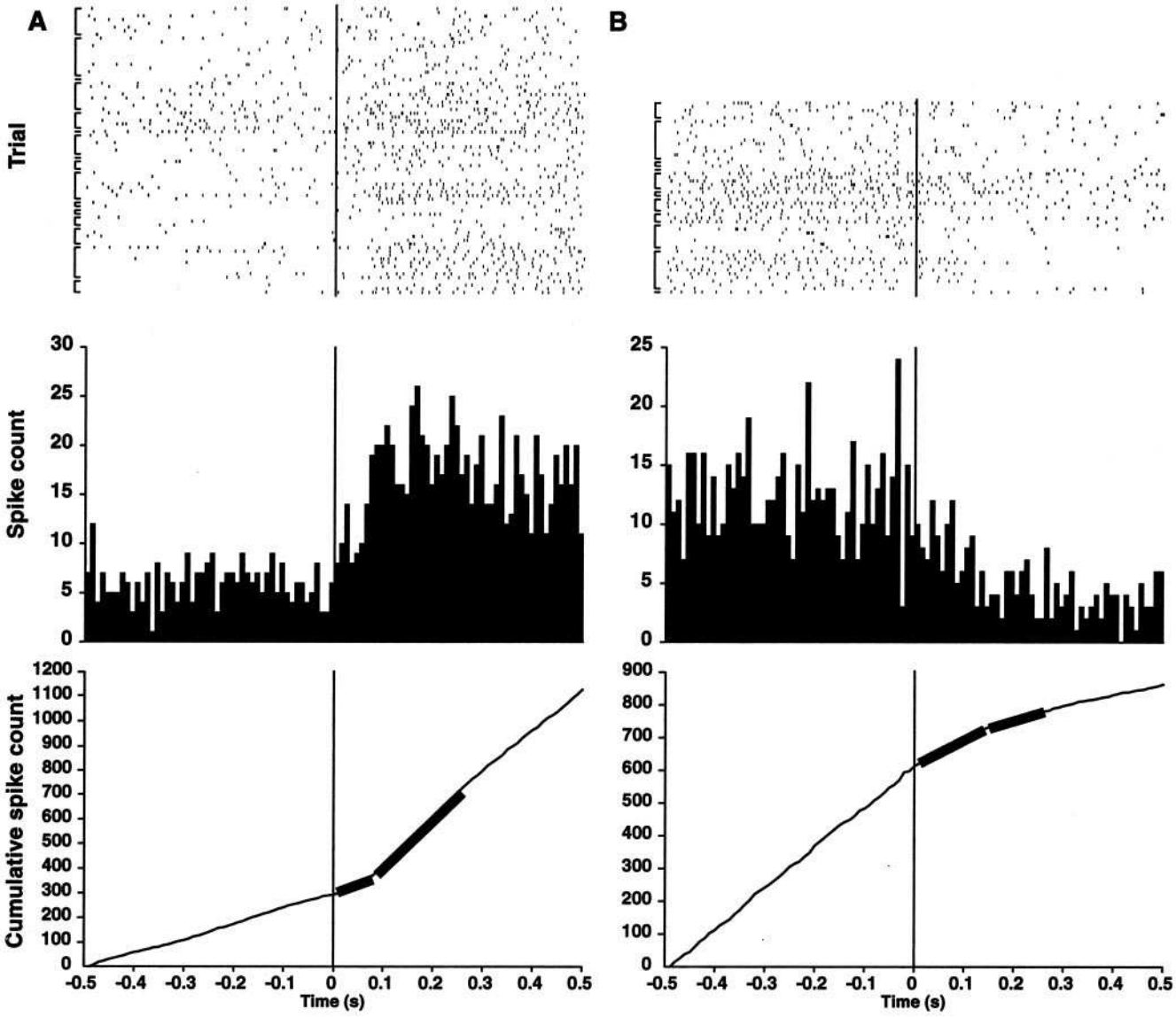

Figure 2. Latency of preferred direction updates in HD cells. Raster plots (above), peri-event histograms (middle), and cumulative histograms (below) (bin width = 10 msec) of action potentials recorded from all of the HD cells analyzed. Time 0 indicates when the lights were turned on again. After light onset, the preferred directions return to their initial orientations (*A*) or shift to the rotated (nonpreferred) orientations (*B*). To determine the average latency of the preferred direction update, least-squares estimates were computed from the cumulative histograms using the first 250 msec of data after light onset (thick curves) (Friedman and Priebe, 1998). Transition points are at 80 ± 10 msec (*A*) for returns to the preferred orientation and 140 ± 10 msec (*B*) for shifts to the nonpreferred orientation. Brackets indicate trials from the same cell within a given session; the variations in spike density among the rows of rasters reflect differences in peak and background firing rates among the neurons.

in the total of 75 trials used for this analysis (Table 1). This was tested with separate ANOVAs for the increasing and decreasing firing rate conditions. For trials in which the firing rates increased after light onset, there were no significant differences among animals ($F = 0.09$; df = 2; NS) or sessions ($F = 0.07$; df = 4; NS). One outlier was removed from these analyses. For this session, the average estimated latency was 167 msec (Table 1) (the least-square estimator described above yielded an update latency of only 70 msec). Similarly, for trials in which the firing rates decreased after the light was turned on, no significant differences were found among animals ($F = 1.18$; df = 2; NS) or sessions ($F = 0.53$; df = 4; NS).

Discussion

These results show that in HD cells of the anterodorsal thalamic nucleus, preferred direction updates, a likely basis for reorientation processes, benefit from very rapid processing of visual signals. Neural network simulations (Zhang, 1996) predict that after changes in the visual scene, the firing rates of the newly activated cells reach their maximum at latencies on the order of several hundreds of milliseconds. The present results reveal markedly briefer delays. However, all existing models of HD cells use rate code neurons rather than spiking neurons which would provide more veridical models of the dynamical properties of biological neural circuits. In neural networks with spiking neurons, state transitions can occur almost instantaneously (Brunel et al., 2001), consistent with the present results.

Our work sheds light on the nature of the dynamics of the ensemble response of HD cells to reorienting stimuli. Neural network models have described the ensemble activity profile of HD cells as a "hill" of excitation (attractor state) encoding the

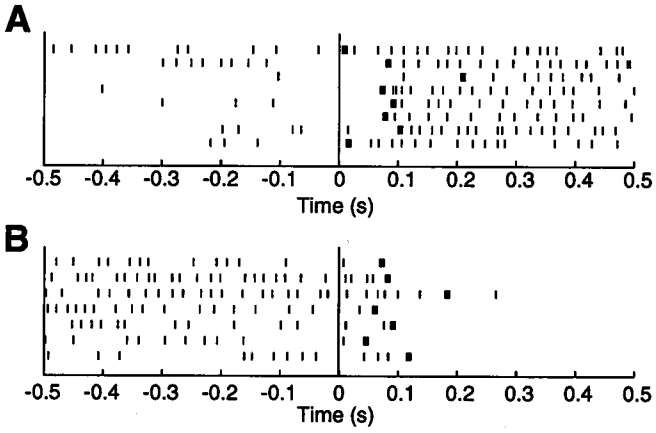

Figure 3. A typical analysis of update latency on a trial by trial basis with the method of Seal et al. (1983). Raster plots show action potentials recorded from a single HD cell during a single session, when the firing rate increases (*A*) or decreases (*B*) after card rotation. Light onset occurs at time 0. For each trial, the update latency is computed as the maximum likelihood estimator of the change point in the mean interspike interval (thick vertical bars).

Table 1. Update latencies in individual recording sessions

	Rat	Delay (msec)	Trials
Firing rate increase	1	83 ± 22	8
	1	74 ± 5	5
	1	75 ± 21	5
	3	70 ± 21	5
	3	167 ± 20	8
	4	86 ± 51	4
	(All	92 ± 64	44)
Firing rate decrease	1	90 ± 17	7
	1	141 ± 41	4
	3	142 ± 34	5
	4	100 ± 13	3
	4	96 ± 38	4
	(All	117 ± 80	31)

HD cells providing data suitable for analyses (as described in Materials and Methods) recorded during three or more trials within the same session were selected for each rat. Single-trial estimates of update latencies were then computed. Average latencies (±SEM) are displayed for each rat and each session. Average latencies computed over all trials are also shown for reference (including trials from sessions in which only one or two trials were analyzable; two outliers were removed). These were consistent with estimates obtained from cumulative response histograms.

current directional heading (Redish et al., 1996; Zhang, 1996; Goodridge and Touretzky, 2000) (cf. Droulez and Berthoz, 1991). Whether this activity profile responds to rapid visual reorientation by traveling toward a new preferred direction (Fig. 4*B*) or by jumping abruptly to it (Fig. 4*C*) has been unresolved until now (Taube, 1998). The rapid transient response (80 ± 10 msec for a 90° reorienting signal, including retinothalamic transmission time) observed in our experiment appears to support the abrupt shift model rather than the hypothesis of a pulse of activity moving to the new distal state by passing through all cells selective for the intermediate heading angles. However, it is likely that the state transition dynamics depend more generally on the magnitude of the angle of rotation (Zhang, 1996), as well as on other factors such as the efficacy of the orienting cue or the complexity of the visual scene. The longer latency observed here when the directional firing rates returned to baseline (140 msec) is consistent with the notion that recurrent inhibition triggering this decrease in firing rates would occur after the increase in overall activity within the HD cell network (illustrated in Fig. 4*C* where the left hill decreases more slowly than the right hill increases).

Previous neurophysiological studies addressing this question failed to reveal the striking rapidity reported here because the experimental protocols did not permit measures of dynamic changes of <1 sec (Knierim et al., 1998; Zugaro et al., 2000). The very short latencies observed are consistent with the fact that anterodorsal thalamic nucleus receives direct projections from the retina (Itaya et al., 1981; Ahmed et al., 1996) as well as indirect projections from the visual cortex via the postsubiculum (Vogt and Miller, 1983) and the retrosplenial cortex (Reep et al., 1994), and that visual stimulation of the retina evokes field potentials in the primary visual cortex with delays as brief as 40 msec (Galambos et al., 2000).

These experimental observations and theoretical considerations provide a plausible mechanism underlying the capacity to rapidly reorient in a familiar environment. They may also provide a new paradigm to study the deficits of this capacity in aging or in a number of neurological disorders.

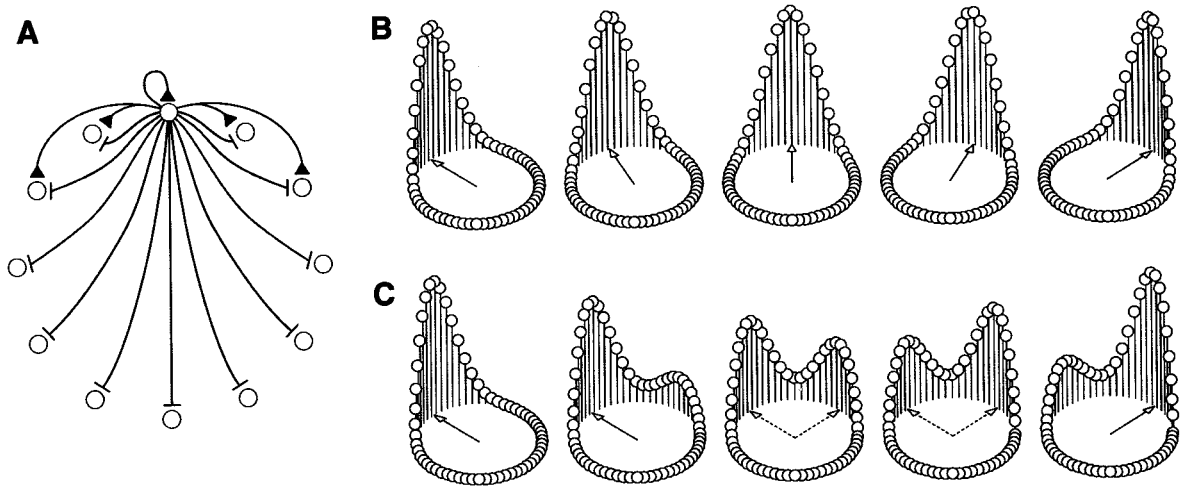

Figure 4. Two possible mechanisms for dynamic updating in continuous attractor networks. *A*, Network connectivity. Each cell (circle) sends excitatory signals (triangles) to its neighbors and inhibitory signals (bars) to all of the cells in the network (for clarity, only the connections from one prototypic cell are shown). *B*, Progressive updating of the ensemble response of the HD system. The firing rate of each formal cell is proportional to the height of the vertical bar. The hill of activity migrates progressively to the target population. *C*, Abrupt updating of the ensemble response. The hill of activity jumps to the target firing pattern without activation of intermediate neurons.

References

Ahmed AK, Guison NG, Yamadori T (1996) A retrograde fluorescent-labeling study of direct relationship between the limbic (anterodorsal and anteroventral thalamic nuclei) and the visual system in the albino rat. Brain Res 729:119–123.

Blair HT, Sharp PE (1996) Visual and vestibular influences on head-direction cells in the anterior thalamus of the rat. Behav Neurosci 110:643–660.

Blair HT, Cho J, Sharp PE (1999) The anterior thalamic head-direction signal is abolished by bilateral but not unilateral lesions of the lateral mammillary nucleus. J Neurosci 19:6673–6683.

Brunel N, Chance FS, Fourcaud N, Abbott LF (2001) Effects of synaptic noise and filtering on the frequency response of spiking neurons. Phys Rev Lett 86:2186–2189.

Droulez J, Berthoz A (1991) A neural network model of sensoritopic maps with predictive short-term memory properties. Proc Natl Acad Sci USA 88:9653–9657.

Friedman HS, Priebe CE (1998) Estimating stimulus response latency. J Neurosci Methods 83:185–194.

Galambos R, Szabo-Salfay O, Barabas P, Palhalmi J, Szilagyi N, Juhasz G (2000) Temporal distribution of the ganglion cell volleys in the normal rat optic nerve. Proc Natl Acad Sci USA 97:13454–13459.

Goodridge JP, Touretzky DS (2000) Modeling attractor deformation in the rodent head-direction system. J Neurophysiol 83:3402–3410.

Goodridge JP, Dudchenko PA, Worboys KA, Golob EJ, Taube JS (1998) Cue control and head direction cells. Behav Neurosci 112:749–761.

Itaya SK, Van Hoesen GW, Jenq CB (1981) Direct retinal input to the limbic system of the rat. Brain Res 226:33–42.

Khabbaz A, Fee MS, Tsien JZ, Tank DW (2000) A compact converging-electrode microdrive for recording head direction cells in mice. Soc Neurosci Abstr 26:984.

Knierim JJ, Kudrimoti H, McNaughton BL (1998) Interaction between idiothetic cues and external landmarks in the control of place cells and head direction cells. J Neurosci 18:425–446.

Muir GM, Taube JS (2002) Firing properties of head direction cells, place cells, and theta cells in the freely moving chinchilla. Soc Neurosci Abstr 32:584.4.

Ranck Jr JB (1984) Head-direction cells in the deep cell layers of dorsal presubiculum in freely moving rats. Soc Neurosci Abstr 10:599.

Redish AD (1999) Beyond the cognitive map: from place cells to episodic memory. Cambridge, MA: MIT.

Redish AD, Elga AN, Touretzky DS (1996) A coupled attractor model of the rodent head direction system. Network 7:671–685.

Reep RL, Chandler HC, King V, Corwin JV (1994) Rat posterior parietal cortex: topography of corticocortical and thalamic connections. Exp Brain Res 100:67–84.

Robertson RG, Rolls ET, Georges-Francois P, Panzeri S (1999) Head direction cells in the primate pre-subiculum. Hippocampus 9:206–219.

Seal J, Commenges D, Salamon R, Bioulac B (1983) A statistical method for the estimation of neuronal response latency and its functional interpretation. Brain Res 278:382–386.

Stackman RW, Taube JS (1997) Firing properties of head direction cells in the rat anterior thalamic nucleus: dependence on vestibular input. J Neurosci 17:4349–4358.

Taube JS (1995) Head direction cells recorded in the anterior thalamic nuclei of freely moving rats. J Neurosci 15:70–86.

Taube JS (1998) Head direction cells and the neurophysiological basis for a sense of direction. Prog Neurobiol 55:1–32.

Vogt BA, Miller MW (1983) Cortical connections between rat cingulate cortex and visual, motor, and postsubicular cortices. J Comp Neurol 216:192–210.

Wiener SI (1993) Spatial and behavioral correlates of striatal neurons in rats performing a self-initiated navigation task. J Neurosci 13:3802–3817.

Zhang K (1996) Representation of spatial orientation by the intrinsic dynamics of the head-direction ensemble: a theory. J Neurosci 16:2112–2126.

Zugaro MB, Tabuchi E, Wiener SI (2000) Influence of conflicting visual, inertial and substriatal cues on head direction cell activity. Exp Brain Res 133:198–208.

Zugaro MB, Berthoz A, Wiener SI (2001a) Background, but not foreground, spatial cues are taken as references for head direction responses by rat anterodorsal thalamus neurons. J Neurosci 21:RC154(1–5).

Zugaro MB, Tabuchi E, Fouquier C, Berthoz A, Wiener SI (2001b) Active locomotion increases peak firing rates of anterodorsal thalamic head direction cells. J Neurophysiol 86:692–702.

HIPPOCAMPUS 12:481–486 (2002)

Peak Firing Rates of Rat Anterodorsal Thalamic Head Direction Cells Are Higher During Faster Passive Rotations

Michaël B. Zugaro* Alain Berthoz and Sidney I. Wiener

CNRS-Collège de France, Laboratoire de Physiologie de la Perception et de l'Action, Paris, France

ABSTRACT: Head direction cells discharge selectively when the head of the animal is oriented in a specific direction. The goal of this study was to determine how sensory signals arising from passive rotations (e.g., triggered by vestibular stimulation and dynamic visual inputs) influence the responses of anterodorsal thalamic head direction cells in the absence of voluntary movement cues (e.g., motor command, efference copy, and associated kinesthetic signals). Three unrestrained rats consumed water from a reservoir at the center of a circular platform while passively subjected to sinusoidal rotatory oscillations at fast (153 ± 27°/s, sd) and slow (38 ± 15°/s) peak velocities. In 14 anterodorsal thalamic head direction cells, the preferred directions, angular response ranges and baseline firing rates remained stable, but the peak firing rates were, on average, 36% higher during the fast rotations (Wilcoxon matched-pairs test, $p < 0.001$; variation range: +11%~+100%). No cell changed its peak firing rate by less than 10%, while three cells (21%) increased their peak firing rates by more than 50%. The velocity-dependent increase in peak firing rates was similar for left and right rotations, and the skewness of the directional response curves were not significantly different between left and right turns (Wilcoxon matched-pairs tests, n = 14, ns). These results show that sensory signals concerning self-movements modulate the responses of the head direction cells in the absence of active locomotion. ***Hippocampus 2002;12:481–486.*** **© 2002 Wiley-Liss, Inc.**

KEY WORDS: spatial orientation; heading; passive rotations; idiothetic; angular velocity

INTRODUCTION

Head direction (HD) neurons discharge selectively when a monkey, rat or mouse orients its head in a specific, "preferred" direction, independently of location or ongoing behavior (Ranck, 1984; Taube, 1998; Robertson et al., 1999; Khabbaz et al., 2000). Although salient visual cues exert a dominant influence in updating the preferred directions of HD cells (Taube, 1995; Goodridge and Taube, 1995; Zugaro et al., 2001a), several lines of evidence indicate that sensory signals evoked during displacements also contribute to updating the HD signal. When rats are passively rotated in darkness at accelerations exceeding the vestibular system threshold, the preferred directions remain stable relative to the environment, but the preferred directions shift when accelerations are below threshold (Blair and Sharp, 1996). Vestibular lesions suppress directionally selective responses in rat anterodorsal nucleus of the thalamus (AD) neurons (Stackman and Taube, 1997). In intact animals, when the visual cues and the animal are displaced independently in order to provide conflicting cues, a small but significant influence of self-movement signals can be detected (Zugaro et al., 2000).

Discharge rates of HD cells in the AD are reportedly slightly higher during faster head turns (Taube, 1995; Blair and Sharp, 1995; Blair et al., 1997; Stackman and Taube, 1997; Blair et al., 1998). However, because these results were obtained in freely behaving animals, it is not known whether this effect is mediated by sensory signals (e.g., triggered by vestibular stimulation and dynamic visual inputs), or by motor-related signals (e.g., motor efferent copy or corollary discharge). Furthermore, the literature remains controversial regarding this velocity dependence (compare the latter references with Taube and Muller, 1998), perhaps because none of the experiments to date was explicitly designed to address this issue. In all previous studies, the rats performed a random foraging task and data analyses extracted brief discontinuous episodes from the recording sessions according to instantaneous head velocities. This is problematic because the ensemble of self-movement signals may not have been comparable across such episodes.

In the present study, we studied the influence of sensory signals of self-movement on the discharge rates of AD HD cells in the absence of active locomotor signals. For this, cells were recorded as immobile unrestrained rats were passively rotated in clockwise/counterclockwise oscillations at two different velocities in successive sessions. The rats were not restrained because tight restraint suppresses the discharges of AD HD cells (Taube, 1995).

Grant sponsor: CNRS-NSF; Grant sponsor: CNES; Grant sponsor: Cogniseine; Grant sponsor: Groupement d'Intérêt Scientifique; Grant sponsor: Fondation pour la Recherche Médicale.
*Correspondence to: M.B. Zugaro, CNRS-Collège de France LPPA, 11 Place Marcelin Berthelot, 75231 Paris CEDEX 05, France.
E-mail: michael.zugaro@college-de-france.fr
Accepted for publication 10 September 2001
DOI 10.1002/hipo.10022

Hence the rats were trained to remain immobile and drink water from a central reservoir on a round elevated platform that was rotated (Zugaro et al., 2001b). The regular pace of the passive rotations provided smooth head rotations through the preferred directions. This ensured that self-movement signals were similar during successive turns, in contrast with the erratic movements rats tend to make while performing the foraging task (cf. Fig. 1B in Zugaro et al., 2001b).

MATERIALS AND METHODS

Electrode Implantation

Three male Long-Evans rats (200–250 g; CERJ, Le Genest-St-Isle, France) were implanted with bundles of eight Formvar-coated nichrome wire electrodes (diameter 25 μm, impedance 200–800 kΩ). Each bundle was inserted in a 30-gauge stainless steel cannula, and mounted on an advanceable connector assembly (Wiener, 1993). Before surgery, the animals were tranquilized with xylazine (0.1 ml IM) and then deeply anesthetized with pentobarbital (40 mg/kg IP). The electrodes were implanted above the AD (AP −1.6 mm, ML ±1.2 mm relative to the bregma, 3.8 mm ventral to brain surface), and the descender assembly was permanently fixed with dental acrylic and tiny skull screws (for details, see Zugaro et al., 2000). Electrode placements were verified histologically.

Data Acquisition

During the recording sessions, electrode signals passed through FETs, were differentially amplified (10,000×) and filtered (300 Hz to 5 kHz, notch at 50 Hz). A computer automatically collected the data at a rate between 20 and 30 kHz for post hoc discrimination (DataWave, Longmont, USA). Two small lamps (10 cm separation) mounted above the headstage were sampled by a video camera at 60 Hz. The rostral lamp was identified offline on the basis of movement patterns, first automatically by a custom program written by M.B.Z, and then by manual corrections of remaining errors. To determine the response properties of the HD cells, head angles and angular velocities were computed according to the methods presented in detail in Zugaro et al., (2001b). Briefly, head angles were computed from smoothed position samples and directional response curves were fit with a pseudo-Gaussian formula

$$f(\theta) = A + B \cdot e^{K\cos(\theta - \theta_0)} \quad (1)$$

where f(θ) is the firing rate, θ_0 is the preferred direction, $B \cdot e^K$ is the peak firing rate, $230°/\sqrt{K}$ the angular range, and A is the baseline firing rate. To avoid discontinuities between 0 and 360°, angular head velocities were computed as

$$\dot{\Theta}(t) = X(t) \wedge X'(t) \quad (2)$$

This formula describes the instantaneous angular velocity of a unit-length vector X(t) as its vectorial product with its derivative vector.

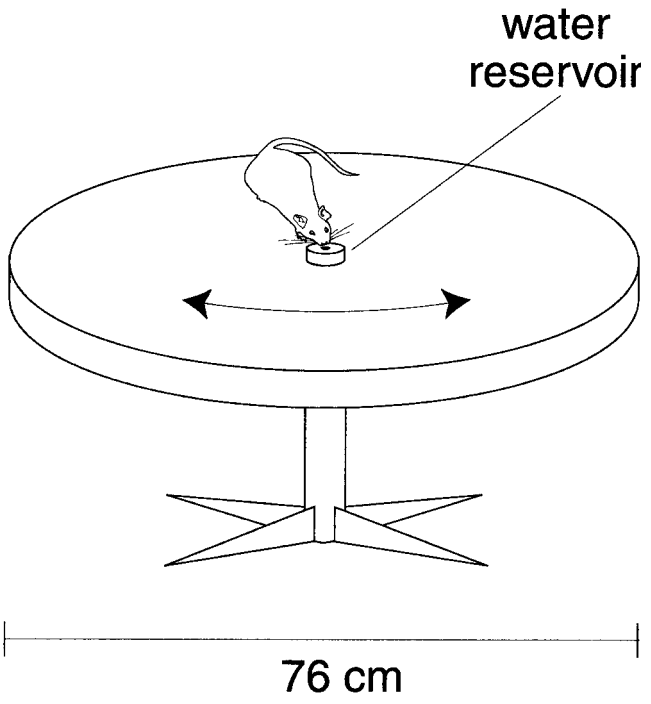

FIGURE 1. Experimental setup. The small elevated platform could be rotated around a central axis. A potentiometer sampled the azimuthal angle of the arena.

Thus, the vector series defined by the positions of the two lamps across time was smoothed (Gaussian filtering) and normalized as $X(t_i)$. Approximation of $X'(t_i)$ was obtained by filtering $X(t_i)$ with a Gaussian-derivative function. Angular head velocity was then computed as the vectorial product of $X(t_i)$ with $X'(t_i)$.

Behavioral Task

The 3-m × 3-m square recording chamber was enclosed by black curtains suspended from the ceiling along three of the walls. On the fourth side, computers and electronic devices were visible and provided stable landmark cues. The rats were placed on an elevated circular platform (76-cm diameter; Fig. 1). The HD cells were recorded in three conditions. During a control phase (active displacements), the rat moved freely within the arena for at least 5 min, foraging for small food pellets (5-mg chocolate sprinkles) that were thrown onto the platform at pseudorandom locations (Muller et al., 1987). The experimenter kept moving about the room while distributing the food pellets in order not to provide a stable spatial reference. The next two phases of the experiment consisted of fast and slow passive rotations (Fig. 2). To rotate the rats passively without applying physical restraint, they were trained to remain immobile while receiving droplets of water (≈30 μl) distributed at brief intervals (0.5–1.5 s) from the water reservoir at the center of the arena (Fig. 1). For training, mildly water-deprived rats were first placed on the platform with water already present in the reservoir. These rats rapidly learned to drink from the reservoir and were shaped behaviorally to remain immobile as water droplets were distributed at

gradually longer intervals. An experimenter stood behind the rat and manually rotated the platform with clockwise/counterclockwise oscillations (approximating sinusoidal profiles) centered on the preferred direction of the cell. A potentiometer sampled platform angular rotations at 100 Hz. This session continued for 5 min, or until the rat was satiated. To motivate the rats to perform the task, water rations were restricted to 10–15 ml/day. Body weight was maintained at ≥85% of normal values. Rats were completely rehydrated before each weekend. All protocols were in accord with institutional, national (Ministère de l'Agriculture et de la Pêche, with approval No. 7186) and international (NIH) standards.

RESULTS

Behavior

Figure 2 shows the time course of changes in the head direction of the rat as well as the platform orientation during the slow (A) and fast (B) rotations. This demonstrates that the rats remained rather immobile during the passive rotations. The average peak velocity over sessions was 153 ± 27°/s (SD; range: 110–200°/s) during fast rotations, and 38 ± 15°/s (range: 20–70°/s) during slow rotations. This corresponded to sinusoidal oscillations at 0.20 ± 0.04 Hz, with an average magnitude of 209 ± 72°, and at 0.08 ± 0.02 Hz, with a magnitude of 190 ± 55°, respectively. Throughout both passive rotations conditions, data were recorded as the rats were stationary and drinking the water droplets from the reservoir.

Cell Responses

Peak firing rates are modulated by angular velocity during passive rotations

Fourteen AD HD cells were recorded from 3 rats in 20 recording sessions. Six cells were recorded in more than one session (one cell in five sessions, and five cells in two sessions), yielding a total of 23 recordings; in six sessions, more than one cell were recorded simultaneously. Identification of the same neuron in repeated recordings was based on identification of the same waveform and on directional responses from a given electrode. In the following analyses, repeated measures obtained from the same cell were replaced by their mean.

Figure 3 shows the angular response curves of a typical HD cell with a greater peak firing rate during fast (140°/s, continuous curve) than during slow (30°/s, dashed curve) passive rotations. The peak firing rates computed from the analytically fit curves (dotted curves) were 81 impulses per second and 53 impulses per second, respectively. This corresponds to a 53% increase during fast rotations for this neuron.

For each HD cell, the peak firing rate was compared between slow and fast passive rotation conditions (Fig. 4). Overall, the peak firing rates of the HD cells were significantly higher during faster than during slower rotations (Wilcoxon matched-pairs test, $P < 0.001$, N = 14). No cell changed its peak firing rate by less than 10%, while 6 cells

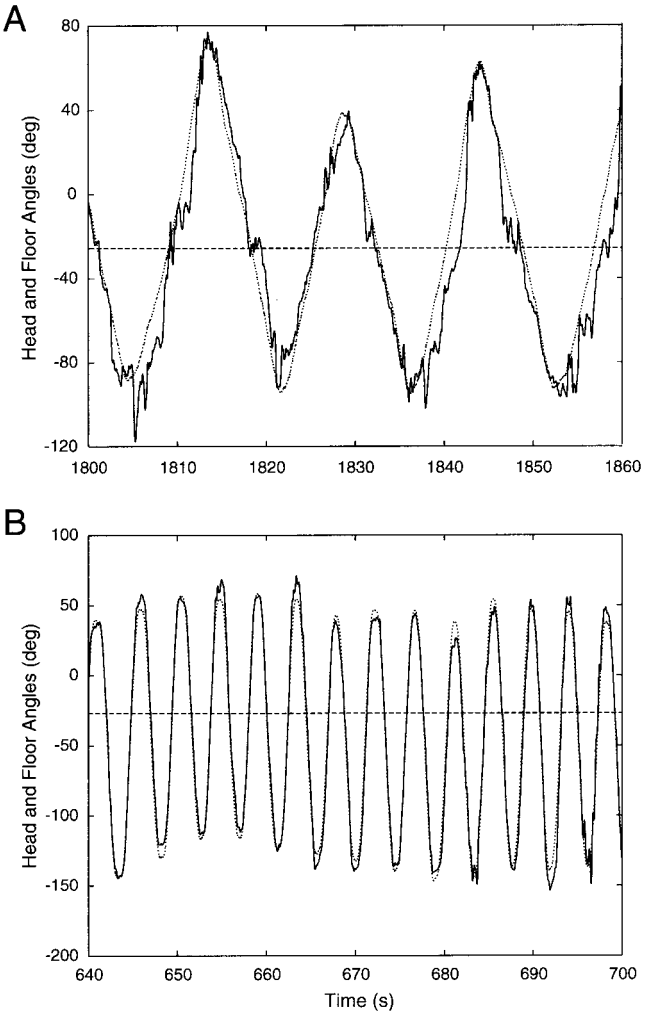

FIGURE 2. Instantaneous floor angle (dotted curves) and head orientation of the rat (continuous curves), during slow (A) and fast (B) rotations. The preferred direction of the head direction (HD) cell recorded in this session was −27° (dashed lines). A: During slow rotations, the maximum head angular velocity was 30°/s (reached each time the rat was oriented in the preferred direction). B: During fast rotations, the maximum head angular velocity was 140°/s.

(43%) increased their peak firing rates by more than one-third–and in three cases by more than 50%. On average, the peak firing rates increased by 36±6% (SEM; range: +11%~+100%) from the slow to fast passive rotations (Fig. 5, continuous line).

This did not depend on turning direction: the ratios of peak firing rates during the fast versus slow passive rotations were not significantly different between clockwise (CW) and counterclockwise (CCW) turns (Wilcoxon matched-pairs test, N = 14, NS).

In cells recorded in two or more sessions, the increase of the peak firing rate during faster passive rotations did not vary significantly between the successive sessions (Wilcoxon matched-pairs test, N = 9, NS). In the few sessions where more than one HD cell were recorded simultaneously, the changes in peak firing rates between slow and fast rotations were not significantly different in the respective neurons (Wilcoxon matched-pairs test, N = 4, NS).

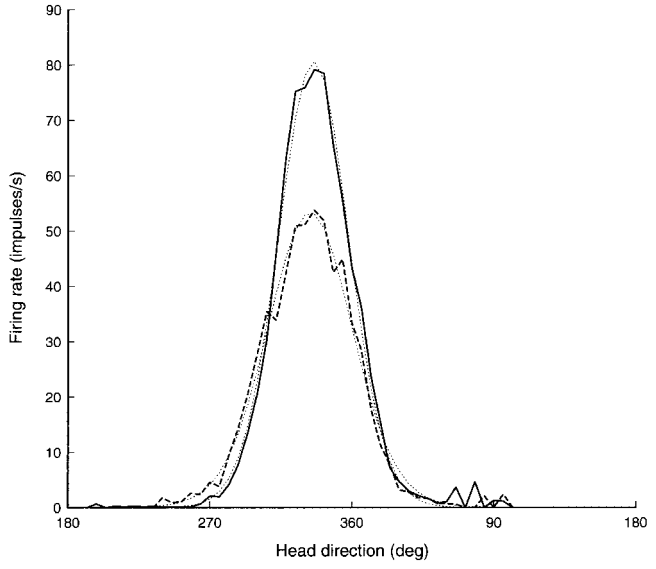

FIGURE 3. Response curves of a typical head direction (HD) cell, recorded during slow (dashed curve) and fast rotations (continuous curve). Analytical fits are represented as dotted curves.

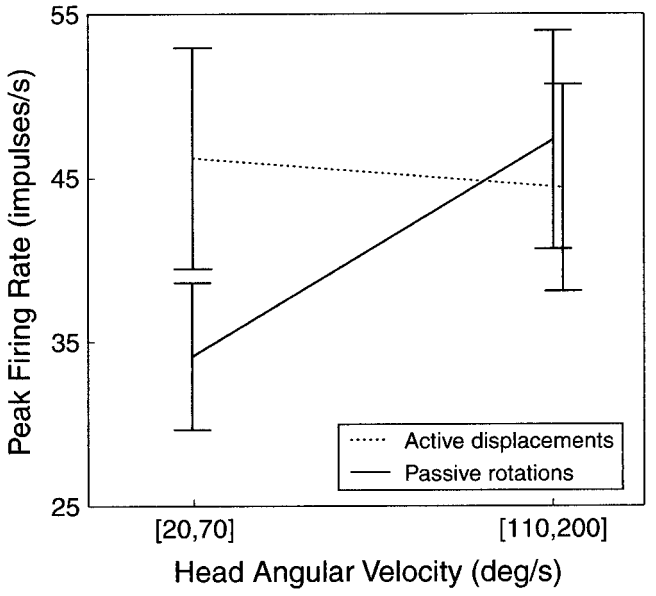

FIGURE 5. Mean peak firing rates (± SEM) during passive rotations (continuous line) and active displacements (dotted line) at slower and faster head angular velocities.

Velocity independence of preferred directions, angular response ranges, and baseline firing rates

The preferred directions remained stable between slow and fast rotations (mean shift: 5 ± 7°, SD; see also Fig. 3). The ranges of the angular responses were 115 ± 11° (SEM, range: 70–193°) during the slow passive rotations, and 100 ± 7° (range: 74–169°) during the fast passive rotations. These values were not significantly different (Wilcoxon matched-pairs test, NS, N = 14). The baseline firing rates were 0.4 ± 0.3 impulses per second (range: 0–3.1 impulses per second) during the slow passive rotations, and 0.7 ± 0.4 impulses per second (range: 0–6.2 impulses per second) during the fast passive rotations. These values were not significantly different (Wilcoxon matched-pairs test, N = 14, NS).

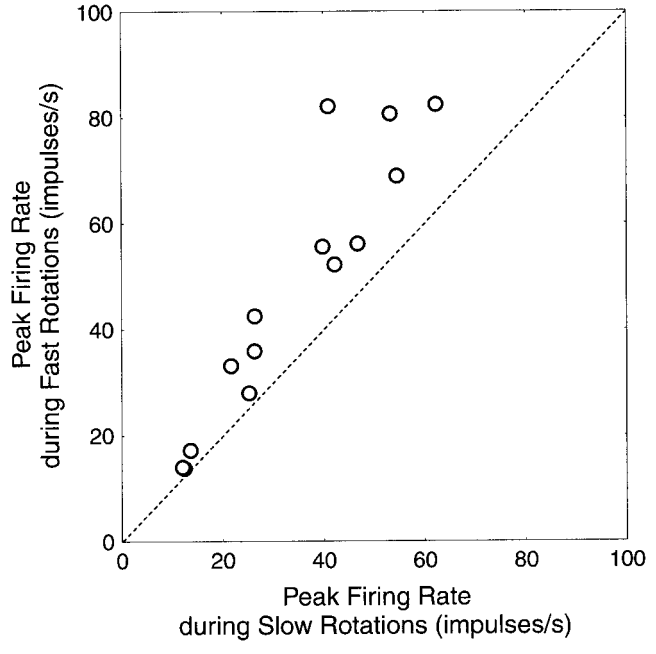

FIGURE 4. Peak firing rates during fast versus slow passive rotations for all neurons. Because unchanged peak firing rates would fall on the dashed line, virtually all neurons showed an increase in peak firing rates during rapid passive rotations.

The skewness of the angular response curve is unchanged between CW and CCW turns

One possible factor contributing to increased peak firing rates during fast rotations could be deformation of the response curve. There is controversy concerning the changes in the shapes of the angular response curves of AD HD cells during CW versus CCW head turns. Blair et al. (1997) suggested that the response curves of AD HD cells were distorted during head turns. This was inferred from the finding that the preferred directions of the CW and CCW response curves were shifted relative to one another, but that their angular ranges were not significantly different from that of the overall response curve (combining all head turns). To test this, Taube and Muller (1998) measured the ratios of the slopes of the left and right edges of the response curves. This direct comparison of CW and CCW response curves failed to demonstrate a significant difference. Here, the asymmetry of the response curves (measured as skewness) was compared in CW versus CCW response curves from fast passive rotations. This failed to show significant differences (Wilcoxon matched-pairs test, N = 14, NS). For comparison purposes, this analysis was also repeated for data recorded during the active displacements phase, and again no significant difference in skewness was found (Wilcoxon matched-pairs test, N = 14, NS).

Are peak firing rates also modulated by angular velocity during active displacements?

As mentioned in the Introduction, it remains unclear whether (and to what extent) peak firing rates of AD HD cells are modulated by angular velocity during active head turns. Although this was not the principal focus of the present study, this data analysis was made for comparison purposes. The peak firing rates of the cells were not significantly different between slow (20–70°/s) and fast (110–200°/s) active head turns (Wilcoxon matched-pairs test, $N = 14$, NS). This is shown in Figure 5 (dashed line). However, peak firing rates varied from −16% to +33% (mean: $-2 \pm 3\%$) in the two conditions. This raises the question whether there are two subpopulations of AD HD cells, which are or are not modulated by sensory signals of self-motion during both passive and active rotations. To test for this, fast/slow ratios of peak firing rates were computed for each cell in the two conditions. The pairs of ratios for each cell were then sorted in two clusters using a K-means clustering procedure. This procedure is analogous to an analysis of variance (ANOVA) "in reverse": starting with two random clusters, pairs of ratios are moved between the clusters in order to minimize variability within clusters and maximize variability between clusters. This yielded two subgroups, with significantly different ratios for passive rotations ($F(12,1) = 24.66$, $P < 0.001$), but not for active movements ($F(12,1) = 1.21$, NS). Thus, the data provide no evidence that AD HD cells can be divided into two groups based upon the presence or absence of modulation by head angular velocity during both active and passive rotations.

DISCUSSION

The principal result here is that when rats are passively rotated, the peak firing rates of the AD HD cells are greater at higher angular velocities. This was not due to variations in responses of the cells related to turning direction, as the velocity-dependent increase in peak firing rates was similar for left and right rotations, and CW and CCW response curves had indistinguishable skewness.

This experiment was designed to test the influences of sensory signals arising from self-movements in the absence of locomotor signals. Because the rats were rather immobile during the rotations, it is unlikely that the responses of the cells were due to differences in motor efferent copy or corollary discharge signals. Thus, the peak firing rate increase observed during faster rotations was more likely due to velocity signals of sensory, rather than motor origin. These would include vestibular, somatosensory, and dynamic visual inputs. Because the rats were stationary and drinking in both conditions, neck and limb proprioceptors would not have provided accurate information about the velocity of ongoing rotations. Somatosensory signals are thus unlikely to underlie the velocity-dependence of the peak firing rates of the HD cells. In contrast, both the vestibular and the dynamic visual signals provide precise information useful for computing head angular velocity. These signals are likely candidates to mediate the increase in peak firing rate of the HD cells during faster rotations.

One possible alternative explanation of the increase in peak firing rates during the faster passive rotations is that the rats may have been more attentive or aroused than during the slower passive rotations. However, this seems unlikely, in particular because one would expect that changes in attention or arousal would also correspond to variations in the baseline firing rate of the cells, which was not observed here. Also, the rats were involved in the same attentive drinking behavior during slow and fast passive rotations, suggesting that their level of attention and arousal was comparable in the two conditions.

The increase in peak firing rates during faster rotations could be related to the finding that the power of hippocampal rhythmic slow activity (RSA) at θ frequencies (~8 Hz) increases with angular velocity in passively rotated rats (Gavrilov et al., 1996). However, enhanced θ RSA is unlikely to directly mediate the increase in the peak firing rates of the AD HD cells during faster passive rotations, because there is little evidence of θ-rhythmic activity in AD (Wertes et al., 2001). Nonetheless, sensory signals arising during self-movement could independently influence both the amplitude of θ RSA as well as HD cell discharge rates.

Variability in the velocity dependence among individual neurons indicates that different cells may receive different levels of modulation by the sensory signals arising during passive rotations. However, there was no evidence that a subpopulation of AD HD cells is particularly sensitive to angular velocity during both active and passive rotations while another population is less responsive.

Consistent with the recent report that discharge rates of AD HD cells are, at best, weakly correlated with head angular velocity in freely moving rats (Taube and Muller, 1998), here in the active displacements condition, the peak firing rates of the cells were not higher during faster head turns. While this appears to contradict other reports (Taube, 1995; Blair and Sharp, 1995; Blair et al., 1997; Stackman and Taube, 1997; Blair et al., 1998), it must be emphasized that in those studies where peak firing rates, rather than mean firing rates, were compared (Blair et al., 1997; Blair et al., 1998), the increase during faster head turns was only on the order of 5–10%. Besides, as mentioned in the Introduction, the responses of the HD cells may not be directly comparable between active head turns at high versus low velocities when rats are engaged in the foraging task. Future studies should examine in a more appropriate manner whether the peak firing rates of AD HD cells increase with angular head velocity during active locomotion. This could be achieved by recording HD responses during well controlled active head turns at different velocities.

In summary, the peak firing rates of the AD HD cells were modulated by angular velocity when the rats were passively rotated (but not while they actively moved on the same platform). This is likely due to sensory signals arising during self-motion, such as vestibular and dynamic visual signals. Higher firing rates would transmit more information (Brunel and Nadal, 1998) during faster movements to downstream structures, such as the hippocampus.

Acknowledgments

The authors thank P. Bernard, E. Camand, and A. Durand for help in data collection and analysis; F. Maloumian for illustrations; M.-A. Thomas and S. Doutremer for histology; and A. Treffel and M. Ehrette for mechanical engineering. This work was supported by a program of cooperation between the CNRS and the NSF, CNES, Cogniseine, and GIS. M.B. Zugaro received support from the Fondation pour la Recherche Médicale.

REFERENCES

Blair HT, Sharp PE. 1995. Anticipatory head direction signals in anterior thalamus: evidence for a thalamocortical circuit that integrates angular head motion to compute head direction. J Neurosci 15:6260–6270.

Blair HT, Sharp PE. 1996. Visual and vestibular influences on head-direction cells in the anterior thalamus of the rat. Behav Neurosci 110:643–660.

Blair HT, Lipscomb BW, Sharp PE. 1997. Anticipatory time intervals of head-direction cells in the anterior thalamus of the rat: implications for path integration in the head-direction circuit. J Neurophysiol 78:145–159.

Blair HT, Cho J, Sharp PE. 1998. Role of the lateral mammillary nucleus in the rat head direction circuit: a combined single unit recording and lesion study. Neuron 21:1387–1397.

Brunel N, Nadal JP. 1998. Mutual information, Fisher information, and population coding. Neural Comp 10:1731–1757.

Gavrilov V, Wiener SI, Berthoz A. 1996. Whole-body rotations enhance hippocampal theta rhythmic slow activity in awake rats passively transported on a mobile robot. Ann NY Acad Sci 781:385–398.

Goodridge JP, Taube JS. 1995. Preferential use of the landmark navigational system by head direction cells in rats. Behav Neurosci 109:1–12.

Khabbaz A, Fee MS, Tsien JZ, Tank DW. 2000. A compact converging-electrode microdrive for recording head direction cells in mice. Soc Neurosci Abs 26:984.

Muller RU, Kubie JL, Ranck JB Jr. 1987. Spatial firing patterns of hippocampal complex-spike cells in a fixed environment. J Neurosci 7:1935–1950.

Ranck JB Jr. 1984. Head-direction cells in the deep cell layers of dorsal presubiculum in freely moving rats. Soc Neurosci Abs 10:599.

Robertson RG, Rolls ET, Georges-François P, Panzeri S. 1999. Head direction cells in the primate pre-subiculum. Hippocampus 9:206–219.

Stackman RW, Taube JS. 1997. Firing properties of head direction cells in the rat anterior thalamic nucleus: dependence on vestibular input. J Neurosci 17:4349–4358.

Taube JS. 1995. Head direction cells recorded in the anterior thalamic nuclei of freely moving rats. J Neurosci 15:70–86.

Taube JS. 1998. Head direction cells and the neurophysiological basis for a sense of direction. Prog Neurobiol 55:1–32.

Taube JS, Muller RU. 1998. Comparisons of head direction cell activity in the postsubiculum and anterior thalamus of freely moving rats. Hippocampus 8:87–108.

Vertes RP, Albo Z, Viana di Prisco G. 2001. Theta-rhythmically firing neurons in the anterior thalamus: implications for mnemonic functions of Papez's circuit. Neurosciece 104:619–625.

Wiener SI. 1993. Spatial and behavioral correlates of striatal neurons in rats performing a self-initiated navigation task. J Neurosci 13:3802–3817.

Zugaro MB, Tabuchi E, Wiener SI. 2000. Influence of conflicting visual, inertial and substratal cues on head direction cell activity. Exp Brain Res 133:198–208.

Zugaro MB, Berthoz A, Wiener SI. 2001a. Background, but not foreground, spatial cues are taken as references for head direction responses by rat anterodorsal thalamus neurons. J Neurosci 21(RC154):1–5.

Zugaro MB, Tabuchi E, Fouquier C, Berthoz A, Wiener SI. 2001b. Active locomotion increases peak firing rates of anterodorsal thalamic head direction cells. J Neurophysiol 86:692–702

Background, But Not Foreground, Spatial Cues Are Taken as References for Head Direction Responses by Rat Anterodorsal Thalamus Neurons

Michaël B. Zugaro, Alain Berthoz, and Sidney I. Wiener

Centre National de la Recherche Scientifique, Collège de France, Laboratoire de Physiologie de la Perception et de l'Action, 75231 Paris CEDEX 05, France

Two populations of limbic neurons are likely neurophysiological substrates for cognitive operations required for spatial orientation and navigation: hippocampal pyramidal cells discharge selectively when the animal is in a certain place (the "firing field") in the environment, whereas head direction cells discharge when the animal orients its head in a specific, "preferred" direction. Cressant et al. (1997) showed that the firing fields of hippocampal place cells reorient relative to a group of three-dimensional objects only if these are at the periphery, but not the center of an enclosed platform. To test for corresponding responses in head direction cells, three objects were equally spaced along the periphery of a circular platform. Preferred directions were measured before and after the group of objects was rotated. (The rat was disoriented in total darkness between sessions). This was repeated in the presence or absence of a cylinder enclosing the platform. When the enclosure was present, the preferred directions of all 30 cells recorded shifted by the same angle as the objects. In the absence of the enclosure, the preferred directions did not follow the objects, remaining fixed relative to the room. These results provide a possible neurophysiological basis for observations from psychophysical experiments in humans that background, rather than foreground, cues are preferentially used for spatial orientation.

Key words: foreground; background; landmark; spatial orientation; place cells; navigation

In monkeys, rats, and mice, two types of limbic system neurons have been observed that may function as neurophysiological substrates for spatial orientation. Hippocampal neurons discharge selectively when the animal is at a certain location in the environment (the firing field of the "place" cell; O'Keefe and Conway, 1978; Ono et al., 1991; Rotenberg et al., 1996; McHugh et al., 1996), whereas head direction (HD) cells discharge only when the animal orients its head in a specific direction (the preferred direction of the cell; Ranck, 1984; Taube, 1998; Robertson et al., 1999; Khabbaz et al., 2000). The head direction signal is found in an ascending series of nuclei known as the "Papez circuit", projecting to the hippocampus. A yet unsolved problem concerns the mechanisms by which these neurons select visual reference cues to anchor the head direction signals in relation to the environment.

The spatially selective responses of both hippocampal cells and HD cells are strongly influenced by landmark cues. In recordings in which rats forage for food in cylindrical enclosures, rotation of a contrasted card along the wall induces similar rotations of firing fields and of preferred directions (Muller et al., 1987; Taube et al., 1990; Taube, 1995; Zugaro et al., 2000). In simultaneous recordings, both types of cells respond coherently (Knierim et al., 1995). However, in experiments in which proximal and distal cues are displaced independently to present conflicting referents, place cells show a variety of responses: their firing fields stay fixed relative to either the distal cues, or the proximal cues, or the room, whereas other cells simply stop discharging (O'Keefe and Speakman, 1987; Wiener et al., 1995; Gothard et al., 1996; Tanila et al., 1997).

Cressant et al. (1997) compared the responses of hippocampal place cells before and after rotation of a group of objects that were always maintained in the same relative configuration. The firing fields rotated together with the objects when these were positioned in front of the wall of the enclosure. However, when the group of objects was placed near the center of the enclosure, then rotated, the firing fields did not follow. To account for this difference, the authors proposed that the centrally placed objects are ignored because the views of the configuration change too dramatically as the rat moves around in the cylinder. For example, an object can be seen either to the right or to the left of another object, depending on the position of the rat. This unreliability

Received Feb. 15, 2001; revised April 19, 2001; accepted April 23, 2001.

This work was supported by the Centre National de la Recherche Scientifique–National Science Foundation cooperation program, Centre National d'Etudes Spatiales, Cogniseine, Groupement d'Intérêt Scientifique. M.B.Z. received a grant from the Fondation pour la Recherche Médicale. We thank F. Maloumian for illustrations, P. Bernard, E. Camand, and A. Durand for help with experiments and data analysis, M.-A. Thomas and S. Doutremer for histology, and A. Treffel and M. Ehrette for the construction of the behavioral apparatus.

Correspondence should be addressed to S. I. Wiener, CNRS, Collège de France LPPA, 11 place Marcelin Berthelot, 75231 Paris CEDEX 05, France. E-mail: sidney.wiener@college-de-france.fr.

This article is published in *The Journal of Neuroscience*, Rapid Communications Section, which publishes brief, peer-reviewed papers online, not in print. Rapid Communications are posted online approximately one month earlier than they would appear if printed. They are listed in the Table of Contents of the next open issue of JNeurosci. Cite this article as: JNeurosci, 2001, 21:RC154 (1–5). The publication date is the date of posting online at www.jneurosci.org.

http://www.jneurosci.org/cgi/content/full/5390

would render the cue configuration too complex to serve as a landmark.

To further characterize the respective roles of foreground and background visual cues for spatial orientation, here we examined head direction cell responses to rotations of a configuration of objects. However, instead of changing the eccentricity of the objects on the platform, we changed their relative depth with respect to the background, by testing the responses of the HD cells in the presence and absence of a cylindrical enclosure.

MATERIALS AND METHODS

The recording and analysis protocols are described in detail in Zugaro et al. (2000) and are summarized briefly here.

Electrode implantation. Three male Long-Evans rats (200–250 gm; CERJ, Le Genest-St-Isle, France) were tranquilized with xylazine, then deeply anesthetized with pentobarbital (40 mg/kg). The electrode bundles of eight formvar-coated nichrome wire electrodes (diameter, 25 μm; impedance, 200–800 kΩ) were implanted above the anterodorsal nucleus of the thalamus (anteroposterior, −1.6 mm; mediolateral, ±1.2 mm relative to bregma, 3.8 mm ventral to brain surface). Each bundle had been inserted in a 30 gauge stainless steel cannula and mounted on an advanceable connector assembly (Wiener, 1993). The descender assembly was permanently fixed with dental acrylic and tiny skull screws. Electrodes were gradually lowered until discriminable single-unit activity was detected. All protocols were in accord with institutional, national, and international standards and regulations.

Data acquisition. During the recording sessions, electrode signals passed through field effect transistors and were differentially amplified (10,000×) and filtered (300 Hz to 5 kHz, notch at 50 Hz). The signal was then acquired on a DataWave Discovery system (Longmont, CO). Two small infrared light-emitting diodes (10 cm separation) mounted above the headstage were detected by a video camera. To determine the preferred direction of an HD cell, head angles were computed from smoothed corrected position samples, and directional response curves were fit with a pseudo-Gaussian function according to the method of Zugaro et al. (2000).

Experimental setup. The 3 × 3 × 3 m square recording chamber was surrounded by black curtains (3 m high) suspended from the ceiling along the four walls. The folds of the curtains were rather irregular (15–30 cm wide). The ceiling was also covered by a black curtain. Illumination was provided by a 40 W overhead lamp on the ceiling that diffused light evenly within the cylinder. All electronic instruments and computers were situated outside of the curtains, and the entire experimental room was phonically isolated from the rest of the building (Fig. 1).

During the experiments the rats moved freely on an elevated platform (75 cm above the floor), measuring 90 × 90 cm in earlier experiments and 76 cm diameter in later experiments. Each cell was recorded under two experimental conditions.

Proximal background condition. Here, a black cylindrical enclosure (60 cm high, 76 cm in diameter) was placed on the platform (Fig. 1*A*). This prevented the rat from viewing the curtains along the walls of the room. Three objects were placed in a triangular spatial configuration along the inner wall of the enclosure: a black cone (26 cm high, 22 cm in diameter), a cylinder covered with light brown paper (26 cm high, 10 cm in diameter), and a building brick (22 × 11 × 5 cm). The spatial configuration of the objects relative to one another never changed in the experiments, and each experiment started with the objects in the same configuration relative to the room.

Distal background condition. Here, the black cylindrical enclosure was absent, and the more distant surrounding curtains provided a background for the objects (Fig. 1*B*). The objects occupied the same placements as in the proximal background condition. The displacements of the rats were restricted to the platform area because this was elevated above the floor.

Behavioral task. The proximal background condition was always tested first. The experimental procedure was similar in both conditions. First, to determine the preferred direction of the cells, the rat was allowed to move freely within the arena for at least 5 min, foraging for small food pellets (5 mg chocolate sprinkles) thrown onto the platform at pseudorandom locations (Muller et al., 1987). The rat was then removed from the arena and secluded in a small opaque container. The objects were rotated by 120° clockwise or counterclockwise (Fig. 2*A,B*), and the floor paper was changed. To disorient the rat, all lights were turned off (including the instrument lamps), and an experimenter rotated the opaque container in an erratic manner while wandering around the room for 1 or 2 min. The rat was then replaced in the arena from a pseudorandomly selected orientation, the lights were turned back on, and a second 5 min recording session was started. This manipulation was performed for both the proximal and distal background conditions. In the distal background condition, when the enclosure was absent, an experimenter remained in the room with the rat, to throw food pellets onto the platform. As during the proximal background condition, the experimenter kept moving around the room to provide no stable reference information.

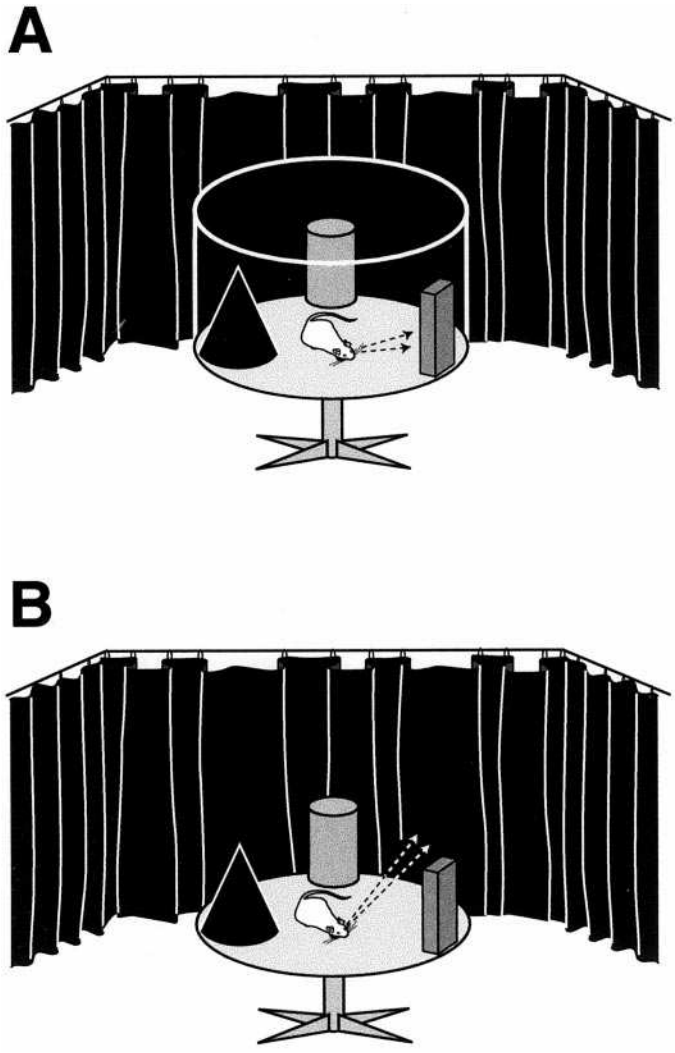

Figure 1. The experimental setup. The elevated platform was surrounded by black curtains hanging along the four walls. A cone, a cylinder, and a building brick placed on the platform served as orienting cues. *A,* In the proximal background condition, a black cylindrical enclosure was placed on the platform, restricting view and movements of the rats. *B,* In the distal background condition, the enclosure was absent. Thus, the surrounding black curtains were a more distal backdrop for the three-dimensional objects.

Histology. At the end of the experiments, the recording sites were marked by passing a small cathodal DC current (30 μA, 10 sec) through one of the recording electrodes. The rat was then anesthetized with a lethal dose of pentobarbital. Intracardial perfusion with saline was followed by 10% formalin-saline. Histological sections were stained with cresyl violet. Recording sites were determined by detecting the small lesion and the track created by the cannula. In all cases, analyses of these data indicated that the recording sites were indeed in the anterodorsal nucleus of the thalamus.

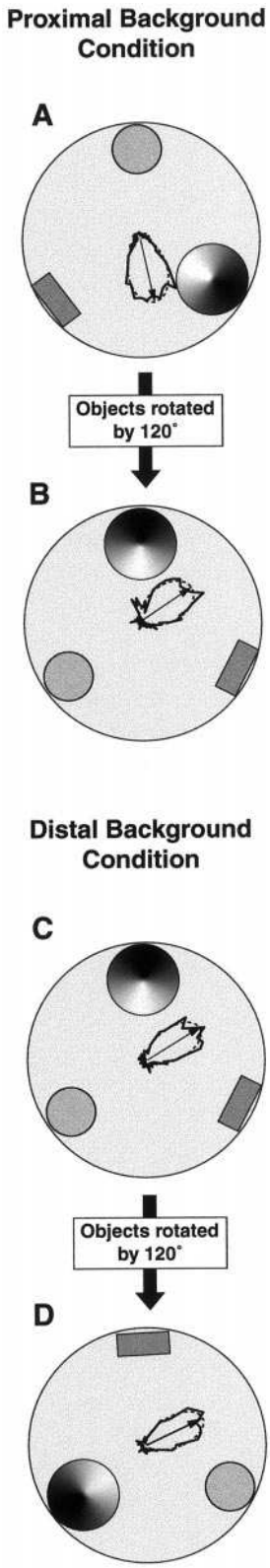

Figure 2. Directional response curves of a typical HD cell recorded while the objects were at their initial positions (*A, C*) and after they were rotated by 120° (*B, D*) while the rat was secluded in darkness. The directional response curves (*continuous curves*) are plotted along with their Gaussian-like fits (*dashed curves*). *A*, *B,* In the presence of the enclosure, the preferred direction of this neuron shifted by 112°. *C, D*, When the enclosure was absent, the preferred direction of the cell remained virtually unchanged after the objects were rotated by 120°.

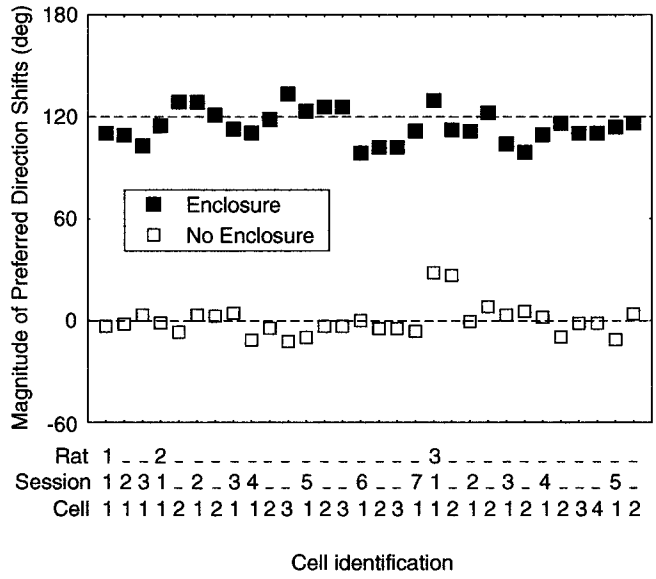

Figure 3. Responses of the cells after rotation of the objects by 120°. *Dashed lines* indicate responses anchored to the objects (120°) or to the room (0°) (shifts in preferred directions are measured relative to the room). In the presence of the enclosure, the preferred directions followed the objects (*filled squares*). When the enclosure was absent, the preferred directions remained fixed relative to the room (*open squares*). All object rotations were counterclockwise, except for rat 1–session 2 and rat 2–session 1. On the *x*-axis, repeated recordings from the same rat or session are indicated by *dashes*.

RESULTS

Proximal background condition

Figure 2 shows the typical response of an anterodorsal thalamic HD cell recorded before (*A*) and after (*B*) the objects were rotated 120° while the cylindrical enclosure was present, providing a proximal background. The preferred direction of this cell shifted (relative to the room) 109° from the first to the second trial, anchored to the 120° rotation of the objects. Similarly, in all 30 of the HD cells recorded in the three rats, the preferred directions shifted by the same angle as the objects (Fig. 3, *filled squares*). The average magnitude of the shift was 115 ± 10° (SD; range, 99–134°).

Distal background condition

Figure 2 shows the responses of the same HD cell recorded before (*C*) and after (*D*) the objects were rotated by 120° in the absence of the proximal background provided by the cylindrical enclosure. The preferred direction of this cell shifted by only −6° between the two trials, despite the rotation of the objects. Similarly, negligible shifts in preferred directions were observed in the population of HD cells recorded in the three rats (Fig. 3, *open squares*). The average magnitude of the shifts was only 6 ± 7° (SD; range, 0–28°).

One possible explanation for the lack of influence of the objects on the preferred directions in the distal background condition was that they may have no longer been salient. For example, the four curtains may have distracted the rats from attending to the objects. The curtains could have been salient because of contrasts in the folds. To test for evidence of this, the time that the rats spent near the objects after object rotations was compared between the proximal and distal background conditions. This was measured as the time spent in the vicinity (≤6 cm) of the objects. On average,

the rats spent 21 ± 6% (SD; range, 15–32%) of the time near the objects when the enclosure was present and 20 ± 4% (range, 13–30%) when the enclosure was absent. There was no significant difference in the two conditions (Wilcoxon matched pairs test, $N = 15$; NS) Thus, the objects maintained their saliency in the distal background condition.

Other response properties of the HD cells were unaffected by the removal of the enclosure: comparisons between the sessions preceding and after removal of the enclosure showed no significant difference in peak firing rates or angular response ranges (Wilcoxon matched pairs tests, $N = 30$; NS)

DISCUSSION

The preferred directions of the HD cells reoriented after rotations of a group of objects, but only when the objects were close to the visual background, the cylindrical enclosure. There are several possible explanations for the reduced efficacy of the objects when the cylindrical enclosure was absent and the distant curtains were then in the background: (1) as suggested by Cressant et al. (1997), the configuration of the objects was rejected as an unreliable reference because the rat could view them from different perspectives, (2) in the distal background condition, the curtains proved to be a larger and more salient reference landmark than the objects, (3) in the distal background condition, the geometric characteristics of the square room influenced the responses of the cells, and (4) in both conditions the most distal cues were used as reference landmarks for the head direction cells; these corresponded to the objects in the proximal background condition and to the curtains in the distal background condition. These will be discussed in the following sections.

Was the object configuration rejected as an unreliable reference in the distal background condition because it provided ambiguous orienting information?

In our proximal background condition [and the experiment with the objects placed next to the wall of the enclosure of Cressant et al. (1997)], the rats explored the narrow space between the objects and the cylindrical enclosure. This could also have provided an ambiguous view of the spatial configuration of the objects but did not reduce the influence of the objects. Furthermore, in our experiments when the cylindrical enclosure was absent, the limits of the platform prevented the rats from having access to mirror image views of the relative positions of the objects, as was the case for the centrally placed objects of Cressant et al. (1997). Nonetheless the objects no longer influenced the preferred directions of the head direction cells. In addition, the preferred directions appeared to be established within seconds after the rat is placed on the platform (our unpublished observations; also see Zugaro et al., 2000), before it explored a substantial part of the arena. Finally, in the Cressant et al. (1997) study, the firing fields often rotated by arbitrary angles after the centrally placed objects were rotated. This indicates that the firing fields were not anchored to any particular cue in the environment. In contrast, here the preferred directions were always maintained fixed relative to the room after rotations of the objects in the distal background condition. Thus, it appears that the preferred directions not only were independent from the orientation of the group of objects but were controlled by other cues in the more distant background (possibly contrasts in the curtains).

Were the objects too small and insufficiently salient in the distal background condition?

After the cylindrical enclosure was removed, the curtains provided a large and contrasted background. But the cylindrical enclosure, because of its height and proximity, subtended a larger visual angle than the curtains did in the distal background condition. The curtains, with their contrasted folds, were likely to have been salient. However, as shown above, the rats frequented the rotated objects equally in the presence and absence of the cylindrical enclosure. Thus, the objects were likely to have remained salient even when they were no longer effective in controlling the preferred directions.

Did the geometry of the square room control the preferred directions in the distal background condition?

Although rats can ignore landmark cues and instead navigate based on the geometry of the environment (Cheng, 1986; Margules and Gallistel, 1988), it is unlikely that the preferred directions of the HD cells were influenced by the geometry of the square room when the cylindrical enclosure was absent. First, the room geometry has been shown to influence orienting behavior in asymmetric (rectangular) environments. Here, there were no evident differences in the metrics of the four corners or the four walls. If the geometry of the square room was a controlling factor, one would predict that the preferred directions would have rotated by multiples of 90° because of its symmetry. However, in the distal background condition, the HD cells always retained the same preferred directions after the objects were rotated.

Were the most distal cues used as reference landmarks for anchoring preferred directions in both conditions?

Another possible explanation for the difference in efficacy of the very same objects in the two experimental conditions is that their relative distance to the background changed. Relative depth in the visual field could be detected on the basis of several different stimulus attributes including occlusion (objects blocked by others are more distant), parallax (during active displacements more distant objects appear to move less), texture contrast, shadows, vergence, etc. This criterion would be functionally relevant because stimuli that are furthest in the background remain more stable as the animal moves around and thus would be more reliable as landmarks.

Brain systems for detecting optic field flow could provide this sensitivity to the head direction system because, for example, the optokinetic system is more sensitive to optic flow at low, rather than high velocities (Hess et al., 1985). An anatomical pathway that could convey optokinetic information to head direction cells passes via the vestibular nuclei to the dorsal lateral tegmental nucleus of Güddens, then the lateral mammillary nuclei before arriving at the anterodorsal thalamic nucleus. As the rat makes displacements, the more distant objects provide the slowest optic field flow velocities. This would help the head direction system select those parts of the visual field providing the most stable reference points and also help update preferred directions after self-movements.

The hypothesis that the objects no longer controlled the preferred directions of the HD cells because they no longer were background cues is coherent with the conclusions of a psychophysical study comparing the relative importance of visual cues in the foreground versus the background in controlling vection (the visu-

ally induced sensation of motion) in human subjects. Brandt et al. (1975) showed that the apparent self motion produced by moving contrasts was strongly reduced when stationary contrasts were present in the background. The authors concluded that ". . . spatial orientation relies mainly on the information from the seen periphery . . .".

It remains to be determined precisely what stimulus attributes of background cues are most effective at driving head direction cells. Nonetheless, our proposed explanation is also applicable to the results from place cell recordings (Cressant et al., 1997). This is consistent with the notion that the head direction signal feeds into the hippocampus and that hippocampal firing fields and HD cell preferred directions are updated in a coherent manner (Knierim et al., 1995).

REFERENCES

Brandt T, Wist ER, Dichgans J (1975) Foreground and background in dynamic spatial orientation. Percept Psychophys 17:497–503.

Cheng K (1986) A purely geometric module in the rat's spatial representation. Cognition 23:149–178.

Cressant A, Muller RU, Poucet B (1997) Failure of centrally placed objects to control the firing fields of hippocampal place cells. J Neurosci 17:2531–2542.

Gothard KM, Skaggs WE, McNaughton BL (1996) Binding of hippocampal CA1 neural activity to multiple reference frames in a landmark-based navigation task. J Neurosci 16:823–835.

Hess BJ, Precht W, Reber A, Cazin L (1985) Horizontal optokinetic ocular nystagmus in the pigmented rat. Neuroscience 15:97–107.

Khabbaz A, Fee MS, Tsien JZ, Tank DW (2000) A compact converging-electrode microdrive for recording head direction cells in mice. Soc Neurosci Abstr 26:984.

Knierim JJ, Kudrimoti H, McNaughton BL (1995) Hippocampal place fields, the internal compass, and the learning of landmark stability. J Neurosci 15:1648–1659.

Margules J, Gallistel CR (1988) Heading in the rat: determination by environmental shape. Anim Learn Behav 16:404–410.

McHugh TJ, Blum KI, Tsien JZ, Tonegawa S, Wilson MA (1996) Impaired hippocampal representation of space in CA1-specific NMDAR1 knockout mice. Cell 87:1339–1349.

Muller RU, Kubie JL, Ranck Jr JB (1987) Spatial firing patterns of hippocampal complex-spike cells in a fixed environment. J Neurosci 7:1935–1950.

O'Keefe J, Conway DH (1978) Hippocampal place units in the freely moving rat: why they fire where they fire. Exp Brain Res 31:573–590.

O'Keefe J, Speakman A (1987) Single unit activity in the rat hippocampus during a spatial memory task. Exp Brain Res 68:1–27.

Ono T, Tamura R, Nakamura K (1991) The hippocampus and space: are there "place neurons" in the monkey hippocampus? Hippocampus 1:253–257.

Ranck Jr JB (1984) Head-direction cells in the deep cell layers of dorsal presubiculum in freely moving rats. Soc Neurosci Abstr 10:599.

Robertson RG, Rolls ET, Georges-François P, Panzeri S (1999) Head direction cells in the primate pre-subiculum. Hippocampus 9:206–219.

Rotenberg A, Mayford M, Hawkins RD, Kandel ER, Muller RU (1996) Mice expressing activated CaMKII lack low frequency LTP and do not form stable place cells in the CA1 region of the hippocampus. Cell 87:1351–1361.

Tanila H, Shapiro M, Gallagher M, Eichenbaum H (1997) Brain aging: changes in the nature of information coding by the hippocampus. J Neurosci 17:5155–5166.

Taube JS (1995) Head direction cells recorded in the anterior thalamic nuclei of freely moving rats. J Neurosci 15:70–86.

Taube JS (1998) Head direction cells and the neurophysiological basis for a sense of direction. Prog Neurobiol 55:1–32.

Taube JS, Muller RU, Ranck Jr JB (1990) Head-direction cells recorded from the postsubiculum in freely moving rats. I. Description and quantitative analysis. J Neurosci 10:420–435.

Wiener SI (1993) Spatial and behavioral correlates of striatal neurons in rats performing a self-initiated navigation task. J Neurosci 13:3802–3817.

Wiener SI, Korshunov VA, Garcia R, Berthoz A (1995) Inertial, substratal and landmark cue control of hippocampal CA1 place cell activity. Eur J Neurosci 7:2206–2219.

Zugaro MB, Tabuchi E, Wiener SI (2000) Influence of conflicting visual, inertial and substratal cues on head direction cell activity. Exp Brain Res 133:198–208.

Active Locomotion Increases Peak Firing Rates of Anterodorsal Thalamic Head Direction Cells

MICHAËL B. ZUGARO, EIICHI TABUCHI, CÉLINE FOUQUIER, ALAIN BERTHOZ, AND SIDNEY I. WIENER
Centre National de la Recherche Scientifique-Collège de France, Laboratoire de Physiologie de la Perception et de l'Action, 75231 Paris Cedex 05, France

Received 13 December 2000; accepted in final form 13 April 2001

Zugaro, Michaël B., Eiichi Tabuchi, Céline Fouquier, Alain Berthoz, and Sidney I. Wiener. Active locomotion increases peak firing rates of anterodorsal thalamic head direction cells. *J Neurophysiol* 86: 692–702, 2001. Head direction (HD) cells discharge selectively in macaques, rats, and mice when they orient their head in a specific ("preferred") direction. Preferred directions are influenced by visual cues as well as idiothetic self-motion cues derived from vestibular, proprioceptive, motor efferent copy, and command signals. To distinguish the relative importance of active locomotor signals, we compared HD cell response properties in 49 anterodorsal thalamic HD cells of six male Long-Evans rats during active displacements in a foraging task as well as during passive rotations. Since thalamic HD cells typically stop firing if the animals are tightly restrained, the rats were trained to remain immobile while drinking water distributed at intervals from a small reservoir at the center of a rotatable platform. The platform was rotated in a clockwise/counterclockwise oscillation to record directional responses in the stationary animals while the surrounding environmental cues remained stable. The peak rate of directional firing decreased by 27% on average during passive rotations ($r^2 = 0.73$, $P < 0.001$). Individual cells recorded in sequential sessions ($n = 8$) reliably showed comparable reductions in peak firing, but simultaneously recorded cells did not necessarily produce identical responses. All of the HD cells maintained the same preferred directions during passive rotations. These results are consistent with the hypothesis that the level of locomotor activity provides a state-dependent modulation of the response magnitude of AD HD cells. This could result from diffusely projecting neuromodulatory systems associated with motor state.

INTRODUCTION

Head direction (HD) cells discharge selectively when the head of the macaque, rat, or mouse is oriented in a specific direction in the horizontal plane, independent from location or ongoing behavior (Khabbaz et al. 2000; Ranck 1984; Robertson et al. 1999; reviews: Taube 1998; Taube et al. 1996). In rats, these neurons have been identified in the postsubiculum (PoS) (Taube et al. 1990a), the anterodorsal thalamic nucleus (AD) (Taube 1995), the dorsal striatum (Wiener 1993), the lateral dorsal thalamic nucleus (Mizumori and Williams 1993), the lateral mammillary nucleus (LMN) (Blair et al. 1998; Stackman and Taube 1998), and certain areas of parietal and retrosplenial cerebral cortices (Chen et al. 1994). The direction of maximal firing ("preferred direction") of the HD cells is strongly influenced by visual cues on the periphery (Goodridge and Taube 1995; Taube et al. 1990b; Zugaro et al. 2001). However, other sensory cues signaling changes in HD are also important since directional selectivity persists in total darkness (Blair and Sharp 1996; Chen et al. 1994; Mizumori and Williams 1993) and is abolished after lesions of the vestibular apparatus, even when visual cues are available (Stackman and Taube 1997). In experiments where visual landmarks and inertial signals provide conflicting information, preferred directions tend to recalibrate on visual cues, although inertial signals exert a small but significant influence (Knierim et al. 1998; Zugaro et al. 2000b). Altogether, the results indicate that both visual and self-motion cues are integrated in the elaboration of HD signals.

Several different sensory systems such as optokinetic, vestibular, visceral somatosensory, and proprioceptive can provide self-motion signals regardless of whether movements are active or passive, but locomotor command signals and motor efferent collateral information (combined with the proprioceptive feedback resulting from contact with the substrate) are absent in the case of passive displacements. How these respective signals are integrated in the HD system is not well understood. If rats are tightly wrapped in a towel and held firmly then rotated, the firing rates of the AD HD cells decrease to baseline firing levels (9 of 10 cells tested) (Taube 1995), while PoS HD cell firing rates decrease by 30% (7 of 9 cells tested) (Taube et al. 1990b). However, it is unclear whether this is due to the absence of active movement initiation cues or other factors related to restraint.

To better understand the influence of self-initiated motion cues on directional responses in AD HD cells, we recorded in unrestrained rats during both active displacements and passive rotations. The experiment was designed to avoid possible effects of stress or somatosensory stimulation due to restraining forces on the rats during passive rotations. For this the animals were trained to remain stationary with the muzzle above a reservoir (located in the center of the platform) that periodically delivered droplets of water. To sample a sufficient number of cell responses to generate directional response curves, the platform was rotated in clockwise/counterclockwise oscillations while the rat remained in place at the center and the cylinder on the periphery (Fig. 1) was maintained stable with

Address for reprint requests: S. I. Wiener, CNRS-Collège de France LPPA, 11 place Marcelin Berthelot, 75231 Paris Cedex 05, France (E-mail: sidney.wiener@college-de-france.fr).

The costs of publication of this article were defrayed in part by the payment of page charges. The article must therefore be hereby marked "*advertisement*" in accordance with 18 U.S.C. Section 1734 solely to indicate this fact.

respect to the experimental room (this was also repeated in the absence of the cylinder). These directional responses were then compared with those recorded from the same neurons during active foraging behavior.

Some of these data have been presented previously in abstract form (Zugaro et al. 2000a).

METHODS

Experimental subjects

Six male Long-Evans rats (200–250 g; CERJ, Le Genest-St-Isle, France) were water deprived and maintained at not <85% of normal body weight. This level of dehydration was necessary to motivate performance in the behavioral tasks, and the rats showed no obvious signs of distress (excessive grooming, hyper- or hypo-activity, aggressiveness). Animals were handled, weighed, and examined daily and, in case of the slightest indication of health problems, returned to ad libitum water and given veterinary treatment. In training and recording sessions, the rats were permitted to consume water until satiation and supplemental water was then provided ad libitum depending on body weight. Rats were permitted to rehydrate completely prior to each weekend. The animals were maintained on a 12 h light/12 h dark cycle in an approved animal facility. All animal care and experimental protocols were in accord with institutional and international standards, legal regulations (Certificat No. 7186, Ministère de l'Agriculture et de la Pêche) and the American Physiological Society policy regarding the use and care of animals.

Electrode implantation

The rats were implanted bilaterally with electrodes for recording in the AD. For four animals, the electrode bundles consisted of eight Formvar-coated nichrome wires (25 μm diam), while the other two received two tetrodes on each side (groups of 4 twisted nichrome wires insulated with polyethylene, 13 μm diam) (Recce and O'Keefe 1989). All electrode tips were gold-plated (200–800 kΩ impedance). Each pair of tetrodes or bundle of wires was inserted in a 30-gauge stainless steel cannula and mounted on one of two independently advanceable connector assemblies on a single headstage (Wiener 1993). Before surgery, the animals were tranquilized with xylazine, then deeply anesthetized with pentobarbital (40 mg/kg). The electrodes were implanted above the AD (AP -1.4 mm to -2.0 mm, ML ±1.1 mm to ±1.4 mm relative to Bregma, 4.2 mm ventral to brain surface) using conventional surgical techniques. The electrode descender assembly was permanently fixed to the skull with dental acrylic and seven tiny screws.

Behavioral apparatus

The 3×3 m square recording chamber was enclosed by a black canopy and black curtains suspended along four walls. The experimental apparatus (Fig. 1*A*) consisted of a black cylinder (60 cm high, 76 cm diam) with a white card (50 cm wide, covering 75° of arc) attached on the inner wall. This served as a salient visual landmark. The cylinder was placed on top of a platform with a small water reservoir located in the center. The water reservoir was a short (1 cm high) cylindrical block. This delivered drops of water from a slight conical depression at the top. A reserve of water was stored in an elevated bottle. A siphon tube transported the water to a computer-controlled solenoid valve outside the apparatus, then beneath the platform to the reservoir. The timing of the opening of the solenoid valves was directed and recorded by the data-acquisition system. The platform could be rotated independently while the cylinder was held fixed relative to the experimental room. Illumination was provided by a 40-W overhead lamp that diffused light evenly within the cylinder. The bright contrast of the lamp was intended to prevent the rats from viewing outside of the cylinder. All electronic instruments and computers were situated outside of the curtains, and the entire experimental room was phonically isolated from the rest of the building.

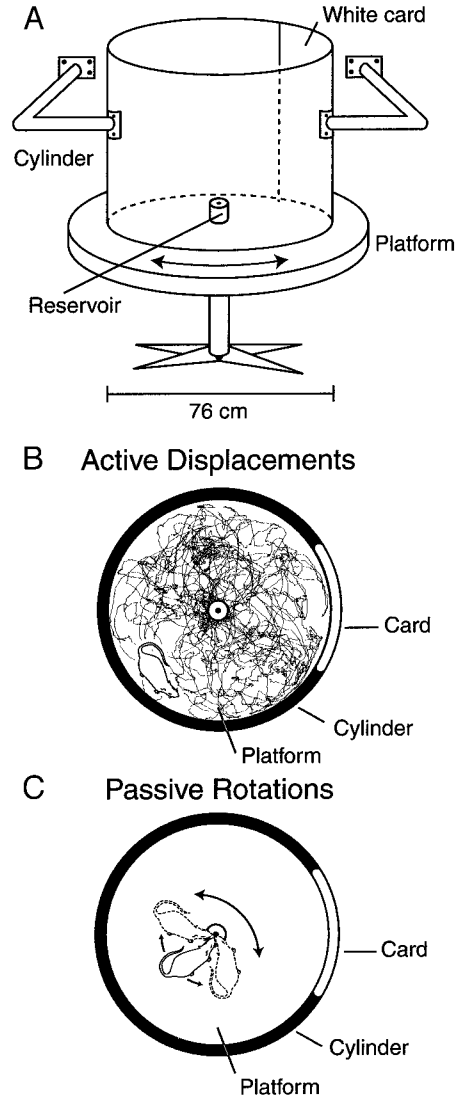

FIG. 1. *A*: the experimental apparatus. The cylinder was maintained stationary while the platform was rotated. The braces on the wall are schematic—actually an experimenter grasped the cylinder by a handle. During the active displacement phase (*B*, top view), the rat searched for food pellets (gray dotted line, trajectory). In the subsequent passive rotation phase (*C*, top view), the rat remained immobile while consuming water delivered at intervals at the center reservoir. In this phase the platform was rotated but the cylinder was maintained fixed relative to the room.

Behavioral tasks

Before the recording session was started, the experimenters estimated the preferred direction of the HD cell(s) by comparing the orientation of the freely moving rat (transmitted by an overhead camera and displayed on a monitor) with the amplified cell discharge signals from a loudspeaker. This was confirmed with the corresponding signals on an oscilloscope.

The recording sessions consisted in two phases. There was no interruption between the two phases, and thus the rat was not removed from the cylinder at any time during the experiment. In the baseline condition (*active displacements*), the rat moved freely within the arena for ≥5 min, foraging for and eating small food pellets (5 mg chocolate

sprinkles) thrown into the cylinder at pseudorandom locations by an experimenter (Muller et al. 1987); this task has also been previously used in studies of AD HD cells (Taube 1995). In this paradigm, well-trained rats visit most of the floor surface and show a fairly uniform distribution of head orientations over time (Fig. 1*B*).

The test phase (*passive rotations*) was conducted immediately before or after the active displacements phase. To motivate the rats to remain immobile at the center without physical restraint, they were trained to receive single drops of water (≈30 μl) at brief intervals (1–3 s) from the water reservoir (Fig. 1*C*). Water delivery was triggered manually either by keyboard presses that directed the computer to trigger opening of the solenoid valve or via the manual trigger of a signal generator. The transistor-transistor logic (TTL) signals were converted to 24 V to drive the solenoid valves. The only cues signaling the beginning of the passive rotations phase were the cessation of food distribution and the clicks of the solenoid valves. Water delivery was selectively timed to gently coax the rat to point its head in the preferred direction of the HD cell. While the rat was at the center, an experimenter manually rotated the platform in a clockwise/counterclockwise oscillation. Another experimenter held the cylinder stationary to keep the principal visual cues stationary relative to the experimental room. In this way, the head of the rat was passively rotated in and out of the preferred direction(s) that had been determined earlier. The amplitudes of the rotations were approximately 180°. In general the profiles were sinusoidal, and the maximum velocity ranged from 5 to 70°/s in different sessions. The central position of the reservoir ensured that the axis of rotation was centered on the head of the rat to minimize translational forces on the vestibular apparatus. The passive rotation phase of the recording session lasted from 5 to 15 min and was terminated when the rat was satiated and moved away from the reservoir.

In 8 sessions of 37 (in 3 of the 6 rats), the environmental setup was slightly different. The cylinder was absent during both the active displacements and passive rotations, and the rat could see the surrounding curtains along three walls as well as the electronic equipment along the fourth wall. In these experiments, the experimenter stood behind the rat while rotating the platform. These results were similar to those with the cylinder, and thus the data are considered together.

Data collection and unit isolation

Animals were brought into the recording room in a transparent plastic cage in the presence of orienting cues. Because the first recording session was conducted after the rats had experience within the cylinder for 6–18 days, the rats were familiar with the environment. The electrode channels were screened for HD cell activity while the rat explored freely and then performed the foraging task in the cylinder. If no supra-threshold HD cell activity was detectable, the electrodes were advanced slightly (25–50 μm). The electrode signals were checked again ≥4 h later. If HD cells were present, the platform was cleaned (if necessary) and the recording session began. Screening was conducted every working day.

During the recording sessions, electrode signals passed through field-effect transistors (FETs) were differentially amplified (10,000 times) and filtered (300 Hz to 5 kHz, notch at 50 Hz). The signal was then passed to a computer for automatic data collection. The acquisition software (DataWave Discovery, Longmont, CO) digitized and collected 32 voltage samples (from bundles of individual electrodes) or 128 voltage samples (from tetrodes) for each signal that crossed an experimenter-set threshold (sampling frequency ranged from 20 to 30 kHz). Single-unit activity was discriminated post hoc using "cluster-cutting" techniques based on at most eight different waveform parameters (maximum and minimum spike voltages, spike amplitude, time of occurrence of maximum and minimum spike voltages, spike duration, and 2 experimenter-defined voltage windows).

Prior to recordings, a support with two small lamps (10 cm separation) was mounted above the headstage. The positions of the two lamps were detected by a video camera mounted above the platform and a video tracking system (DataWave Technologies) that sampled at a rate of 60 Hz. After the end of the session, the heading direction of the animal in the horizontal plane was computed using the positions of the two lamps. C++ software (developed by M. B. Zugaro) scanned the position samples to automatically determine which lamp was rostral-most on the basis of displacement patterns (since the rats rarely walked backward). However, because tracking errors often produced ambiguous data, inversions of the lamps had to be further corrected with additional interactive software. Counter-clockwise rotations are considered positive here. Rotations of the platform were measured with a potentiometer and sampled by the acquisition system at 100 Hz.

Data analysis

HEAD DIRECTION. At each time step of data sampling, the orientation of the head of the rat was computed from the coordinates of the two head lamps sampled by the video tracking system. Because the arctangent operation required for this computation is sensitive to noise and jitter, before computing the heading directions the Cartesian coordinates of the two head lamps were smoothed by convolution with a Gaussian filter. Thus the smoothed abscissa of the front lamp was computed according to the following equation

$$X_{\text{front}}(t_i) = \frac{1}{N_i} \cdot \sum_{j=i-n/2}^{i+n/2} x_{\text{front}}(t_j) \cdot e^{-(t_j - t_i)^2/2\sigma^2}$$

where $X_{\text{front}}(t_i)$ is the smoothed abscissa of the front lamp at time t_i (in pixels), $x_{\text{front}}(t_j)$ is the raw abscissa of the front lamp at time t_j (in pixels), σ is the standard deviation of the Gaussian (in seconds), $(n + 1)$ is the range of the smoothing (in time steps of 1/60th of a second), and $N_i = \sum_{j=i-n/2}^{i+n/2} e^{-(t_j - t_i)^2/2\sigma^2}$ is a normalization factor. Here, we used $n = 10$ and $\sigma = nT/4 = 41.7$ ms (T is the sampling interval). This procedure was carried out independently for the abscissa and ordinate of the front and back lamps.

DIRECTIONAL RESPONSE CURVES. To determine the directional properties of the HD cells, the number of spikes was counted for each video sampling interval (1/60th of a second) and associated with the corresponding head orientation. This was used to compute a histogram wherein the magnitude of each 6° bin was the total number of action potentials divided by the time spent in that bin. A correction was made for the delay error of the data-acquisition system in the relative timing of video and cell discharge records.

For each HD cell in each recording session, an analytical approximation of the angular response curve was computed. This permitted reliable quantitative calculations of the preferred direction, peak firing rate, and angular range (a measure of the width of the directional response curve) for purposes of comparison. This curve fitting used a discretized adaptation of the Gaussian-like fit also used by Zhang (Johnson and Kotz 1970 as cited by Zhang 1996):

$$f(\theta) = A + B \cdot e^{K\cos(\theta - \theta_0)}$$

where $f(\theta)$ is the firing rate (in impulses/s), θ_0 is the preferred direction (in degrees), $B \cdot e^K$ is the peak firing rate (in impulses/s), $230°/\sqrt{K}$ is the angular range, and A is the baseline firing rate (in impulses/s). The angular range is computed as the distance between the two points at the intersection between the baseline firing rate line and the two tangent lines passing through the inflection points of the Gaussian-like curve (Zhang 1996). A best-fit (least-square distance) approximation to this curve was obtained with a Nelder-Mead type simplex search method via Matlab software (The MathWorks, Natick, MA).

ANGULAR AND LINEAR HEAD VELOCITIES. Angular head velocities were computed based on the general formula $\dot{\theta}(t) = X(t) \wedge X'(t)$. This describes the instantaneous angular velocity of a unit-length vector $X(t)$ as its vectorial product with its derivative vector. This method is preferable to the more intuitive differentiation of the instantaneous

heading angle because it overcomes the problem that instantaneous transitions from 0 to 360° are interpreted as very high angular velocities. Thus the vector series defined by the positions of the two lamps across time was smoothed (as described in the preceding text) and normalized as $X(t_i)$. Following classical numerical analysis methods, $X'(t_i)$ was approximated by filtering $X(t_i)$ with a Gaussian-derivative function (similar to the smoothing applied in the preceding text, except that the Gaussian function is replaced with its derivative and corrected with a minus sign). Angular head velocity was then computed as the vectorial product of $X(t_i)$ with $X'(t_i)$.

To compute linear head velocities, the Cartesian coordinates of the rostrally placed head lamp were differentiated (using the Gaussian-derivative smoothing explained above). This yielded linear velocity components along the *x* and *y* axes. The linear head velocities were then computed as the Euclidean norms of these velocity vectors. The latter analysis concerned only the position of the anterior lamp on the headstage since it was positioned directly over the head of the rat. If the anterior bulb was not in the central axis of rotation of the platform, this would give rise to measurements of lateral linear displacements. However, this is not likely to be a problem for the comparative analyses of passive and active rotations since this same ambiguity is present in both cases.

To avoid spurious results due to differences in the dynamics of active and passive rotations, analyses were also performed on subsets of data with comparable ranges of angular or linear head velocities. This reduced the number of samples taken into account, and sometimes the remaining data were suspected to be insufficient to compute reliable directional response curves. To determine whether the fit of the analytical approximation of the directional response curve was still adequate, an error function was computed

$$E = \frac{\sqrt{\sum (f(\theta_i) - f_i)^2}}{N \cdot \text{peak firing rate}}$$

where the numerator terms are the curve fit values and the actual measured values respectively (the sum is computed over the *N* bins falling within the angular range). Directional response data were discarded if this error was greater than 0.1 (this criterion was selected after subjective evaluation of a subset of the curves).

TEMPORAL PROPERTIES OF DISCHARGES. To investigate the temporal characteristics of the HD cell discharges, inter-spike interval histograms (ISIHs) were constructed (1 ms bins; range: 0–100 ms). To focus on discharge activity during maximal firing, this analysis

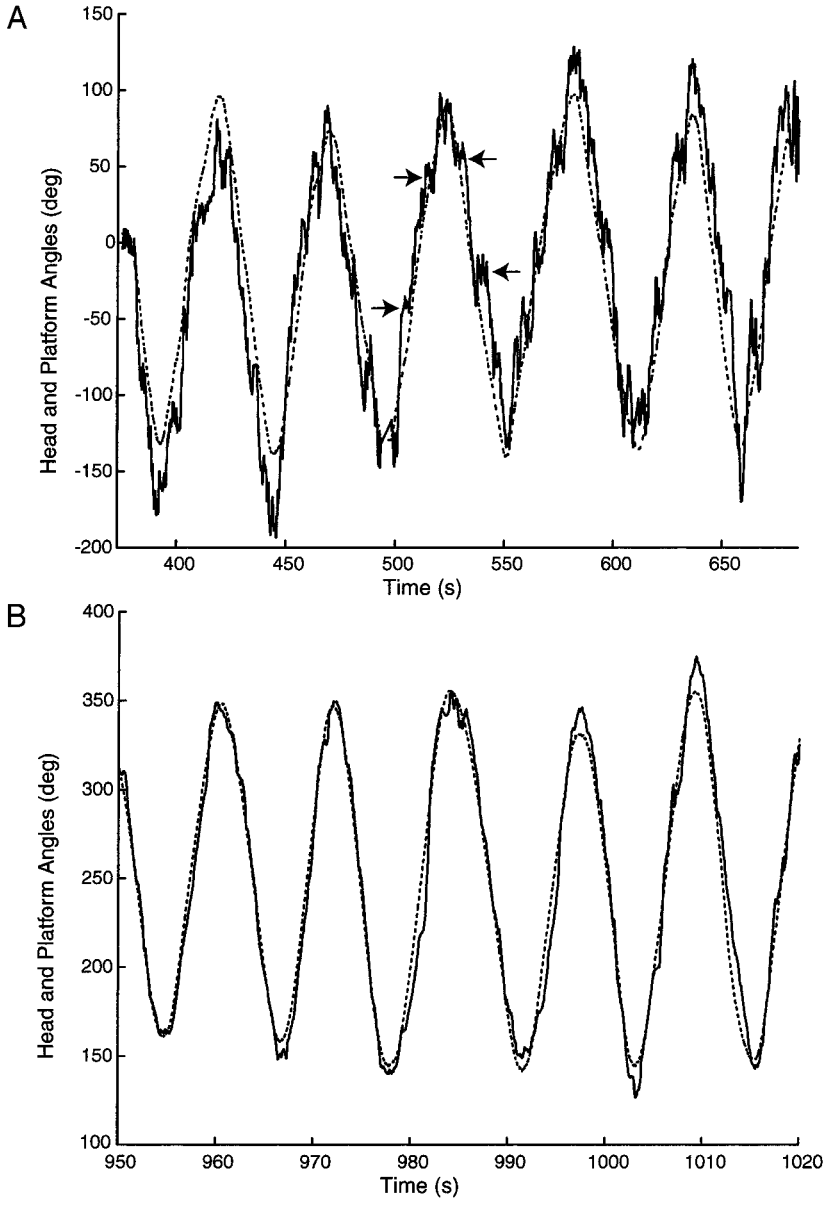

FIG. 2. Immobility of the rat during passive rotations. The angle of the platform relative to the room (- - -) as well as the angle of the head of the rat (—) are displayed in data from 2 different recording sessions with different time scales. *A*: slower rotations. The rat made a few active movements (→). *B*: more rapid rotations.

included only data recorded while the head of the rat was oriented in the preferred direction (± half a SD of the directional response curve $\approx 29°/\sqrt{K}$). The data collected when the rat was oriented in this range were not necessarily sufficient to compute reliable ISIHs because some HD cells had low firing rates and the number of discharges was insufficient to produce a smooth curve or because in some sessions where several HD cells were recorded, those with preferred directions near the limit of the angular oscillations of the platform were not recorded for sufficiently long periods of time. Analysis of temporal patterns of discharge was based on data that produced fairly continuous ISIH plots (readily discernible by visual inspection). Statistical tests were performed using Statistica (StatSoft, Tulsa, OK) software or Microsoft Excel.

All the preceding computations were done by C++/MATLAB programs.

Histology

At the end of the experiments, a small electrolytic lesion was made by passing a small cathodal DC current (30 μA, 10 s) through one of the recording electrodes to mark the location of its tip. The rats were then lethally anesthetized with pentobarbital. Intracardial perfusion with saline was followed by 10% formalin-saline. Histological sections were stained with cresyl violet. Recording sites were reconstructed by detecting the small lesion, taking into account the distance that the microelectrode driver had been advanced from the point of stereotaxic placement of the electrodes.

RESULTS

Behavior

During the passive rotations, the rats tended to remain stationary; that is, the heading direction of the rats reliably followed the changes in orientation of the platform (Fig. 2). In Fig. 2*A*, the notches (→) on the traces of head direction correspond to small active counter-rotation movements. Since the rats consistently maintained their muzzles above the centrally placed water source, these movements were counterrotations of the body rather than rotations of the neck about a stable trunk. Thus this would not correspond to the vestibulocollic reflex (or head nystagmus). In contrast, in some cases, rats rotated their body increasing neck flexion angle during the onset of rotations while maintaining the head fixed at the same position over the water reservoir. In some cases, the rats would maintain this flexion during subsequent passive rotations. However, trunk position was not tracked by the video system. To quantify the degree of head immobility of the rats throughout the passive rotation sessions, measures of instantaneous directions of the head of the animal were tested for correlation with concurrent orientation of the platform. The average value of r computed from a group of typical sessions ($n = 17$) was 0.94 ± 0.01 (mean ± SE; range: 0.87–0.98). All r values were significant ($P < 0.001$).

Figure 3 shows the ranges of computed linear and angular velocities of the head during passive rotations and active displacements in a typical session. Although in the active displacement sessions there were more movements at rapid linear and angular velocities, the velocity incidence curves for active displacements and passive rotations had a considerable degree of overlap. Of course, the range of values in such angular velocity incidence curves varied among the passive rotation sessions, depending on the force applied to rotate the platform. The apparently elevated values of velocities during passive rotations might be due to small amplitude movements of the

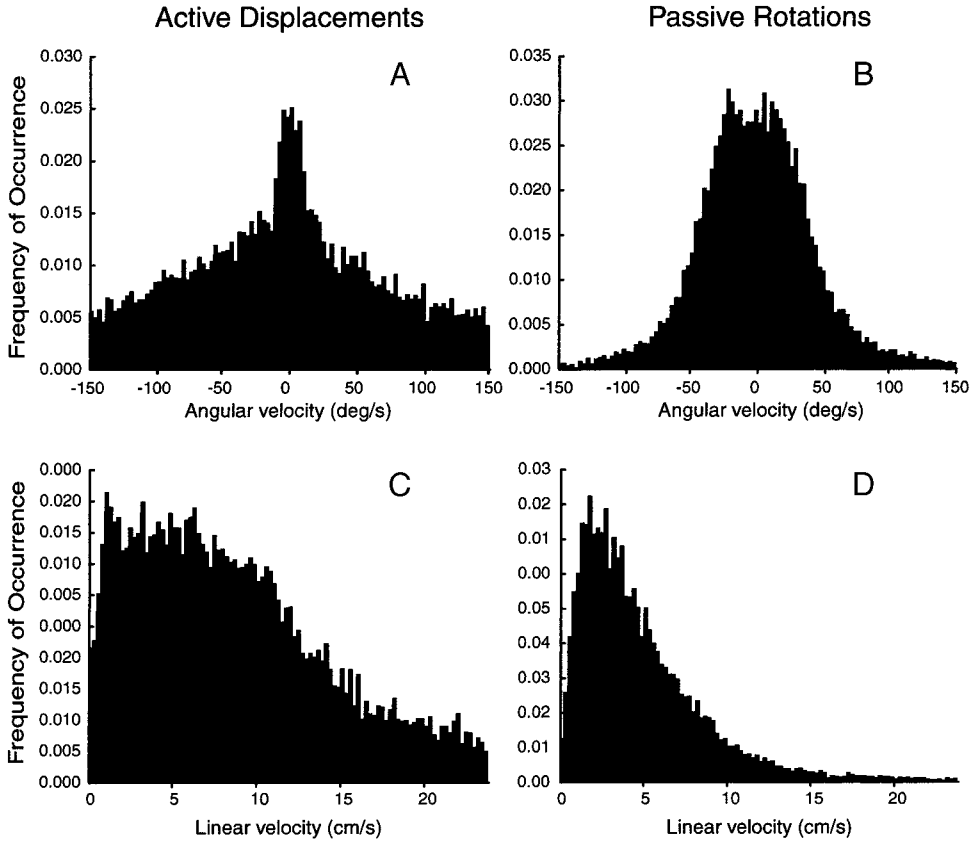

FIG. 3. Representative histograms of incidences of instantaneous angular head velocities during the active displacements (*A*) and passive rotations (*B*), all from 1 recording session (binwidth: 3°/s). Also shown are incidences of instantaneous linear velocities of the head during the active displacements (*C*) and passive rotations (*D*; binwidth: 0.24 cm/s).

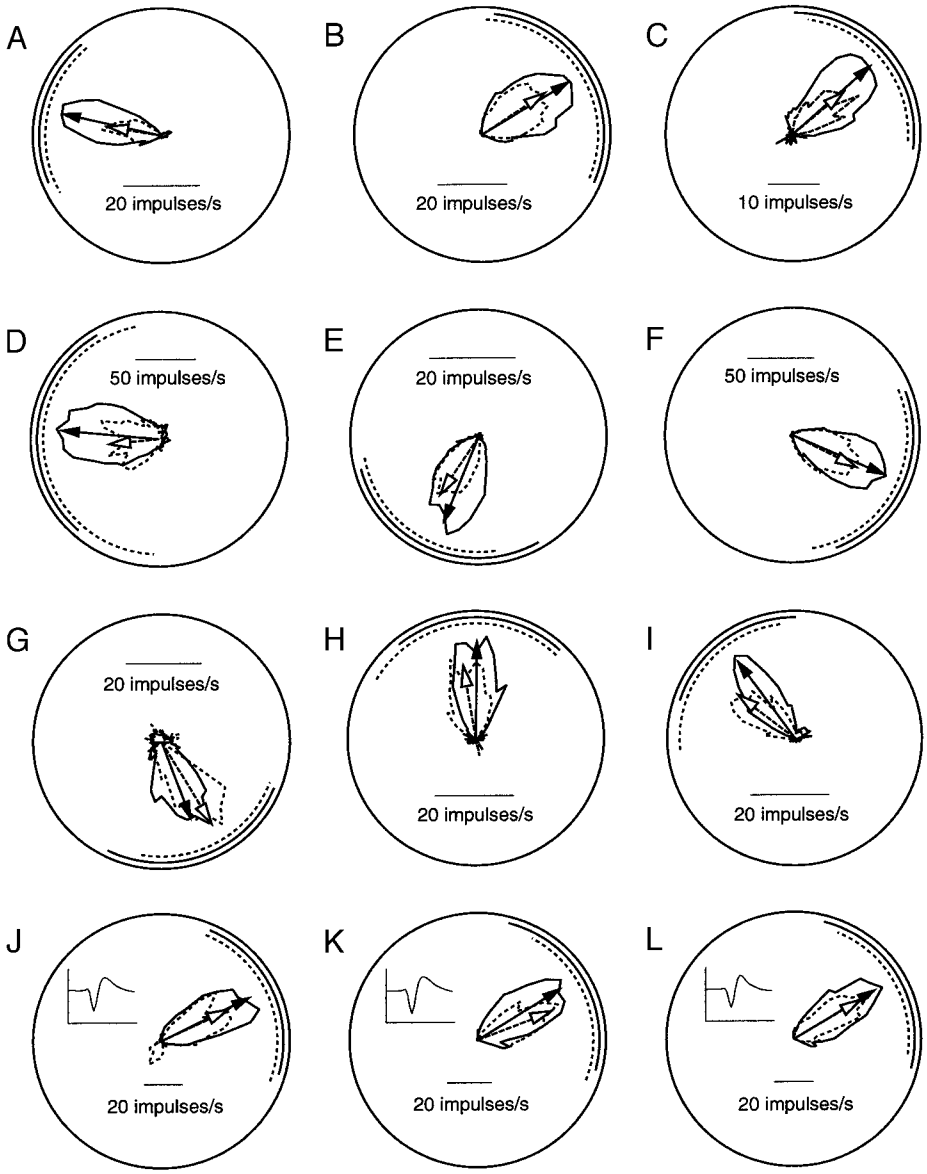

FIG. 4. Polar plots of directional response curves of 12 different HD cell recordings during active displacements (continuous lines) and passive rotations (dashed lines). The analytically computed preferred directions and peak firing rates are indicated by the directions and lengths of the arrows, respectively. Active displacements are indicated by continuous arrows and passive rotations by dashed arrows. Firing rate scales are shown in *insets* to each frame. The computed angular response ranges are represented as arcs (active displacements, continuous arcs; passive rotations, dashed arcs). In all cases the position of the cue card (not shown) was to the right as in Fig. 1. Cells shown in *G–I* were recorded simultaneously. Directional response curves *J–L* are from a single cell recorded on 3 different days (*insets*: waveforms are averages computed over 1,000 spikes; horizontal scale: 1 ms, vertical scale: 100 μV).

headstage lamps over very short time intervals or from slight head-bobbing movements observed while the rat was licking the water reservoir. Although these were small in amplitude, relatively high velocities would have been discriminated by the video detection system since the sampling rate was at 60 Hz. Jitter in video detection system could also have generated nonzero angular and linear velocities. Since each pixel corresponds to 0.3 cm, jumping one pixel in one sampling period would, for example, generate an instantaneous linear velocity of 18 cm/s. While this type of error was considerably reduced by the smoothing of the position data, it may not have been completely eliminated.

Overview of the cell response data

A total of 49 cells were recorded in the left (13 cells) and right AD (36 cells) of the six rats in 37 sessions. Eight cells were recorded in two or more sessions, yielding a total of 66 samples. Figure 4 shows 12 directional response curves computed for both active displacements (continuous lines) and passive rotations (dashed lines). The ovoid polar plots represent the actual response curves while arrows and concentric arcs concern parameters of the best fit analytic approximation. The peak firing rate (arrows) of most cells decreased markedly during passive rotations, but a few maintained the same value (e.g., Fig. 4*G*). In HD cells recorded in more than one session, similar decreases in firing rate were observed across sessions (Fig. 4, *J–L*). However, HD cells recorded simultaneously within a single session did not necessarily show the same reductions in peak firing rates during passive rotations. For example, Fig. 4, *G–I*, shows three cells recorded simultaneously: for two cells (Fig. 4, *H* and *I*), the peak firing rate decreased by 28 and 27%, respectively; but for the third cell (Fig. 4*G*), it increased by 11%. The ranges of the angular responses (dashed and continuous arcs) of the cells did not change consistently during passive rotations. In Fig. 4*D*, the angular response range increases; in Fig. 4*G*, it decreases. The HD cells generally maintained their preferred directions during passive rotations.

Peak firing rate reductions during passive rotations

The mean peak firing rate of the HD cells during the active displacements was 44 ± 3 (SE) impulses/s (range: 12–106 impulses/s) and 34 ± 2 impulses/s (range: 9–88 impulses/s) during the passive rotations. The peak firing rates were significantly reduced during the passive rotations (Wilcoxon matched pairs test, $n = 66$, $P < 0.001$).

To quantify the magnitude of this effect, Fig. 5 compares the peak firing rates measured during passive rotations and active displacements for each neuron. Previous results indicate that the discharge rate of the HD cells is higher when the rat moves at higher angular and linear velocities (Blair and Sharp 1995; Stackman and Taube 1997; Taube 1995; but see Taube and Muller 1998). To eliminate the risk that the reduced peak firing rates during passive rotations were due to the lower velocities in this condition, the data shown in Fig. 5 were computed based only on data where angular and linear head velocities were comparable in the two behavioral conditions ($\omega \leq 90°$/s and $v \leq 7.5$ cm/s). This did not affect the results: a linear regression analysis of the data in Fig. 5 showed that the firing rate of the HD cells decreased by 27% on average ($P < 0.001$) when the unrestrained rat was rotated passively. The magnitude of this reduction was not correlated with the value of the peak firing rate ($r = -0.12$, NS). During passive rotations, the peak firing rates decreased by more than 5% in 47/64 cases (73%), but increased by more than 5% in only 8 cases and remained constant for 9 cases (in 2 cases, there was insufficient data for this analysis; see METHODS).

VARIABLE RESPONSES OF SIMULTANEOUSLY RECORDED CELLS. Figures 4 and 5 show that there was some variability in the magnitude of the decreases in peak firing rates within the population of AD cells recorded. One possible reason for this might have been related to variations in the degree of immobility of the rats in the different sessions. As shown in Fig. 2, the rats tended to make active head movements slightly more frequently during passive rotations at lower velocities (Fig. 2*A*) than at higher velocities (Fig. 2*B*). We thus tested whether the change in peak firing rates was correlated with the degree of immobility of the rats during passive rotations in each recording session (measured by the correlation coefficient of the instantaneous head direction and instantaneous platform orientations; see *Behavior*). This showed no significant correlation ($r = -0.03$; NS).

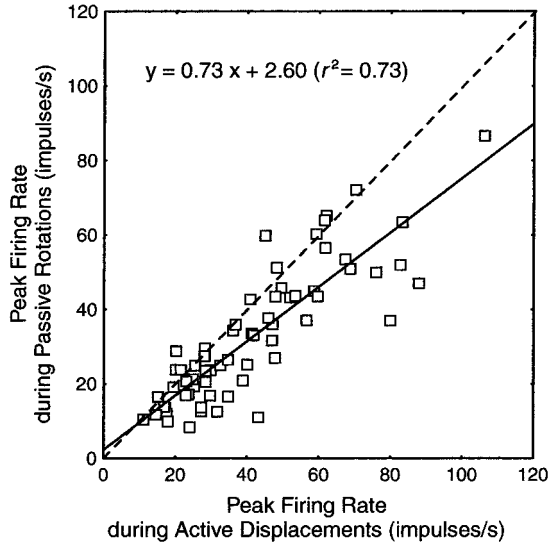

FIG. 5. Linear regression analysis of the peak firing rate of each neuron during passive rotations versus active displacements (slower movements). The equation of the regression line (continuous line) is shown *inset* above. Peak firing rates that remained the same during both conditions would fall on the dashed line.

Further evidence that inter-session variations in the behavioral parameters could not account for these fluctuations is that the magnitude of the decrease in peak firing rates varied among simultaneously recorded neurons (Fig. 4, *G–I*). This suggests that different HD cells may be affected differently by active locomotor signals. This is not likely to be simply due to random variation since, as reported below, in most cases when cells were recorded on successive days their responses did not vary. However, it is also possible that the differences in changes in peak firing rates were due to the fact that the oscillatory rotations of the platform oriented the head of the rat in the preferred directions of the cells at different phases of the cycle. Thus the activity of one cell may have been measured during movements with dynamics different from the others. To test for this, for each cell, the eccentricity of the preferred direction relative to the oscillatory rotations of the platform was determined. This was defined as the angular distance from the preferred direction to the center of the oscillations, divided by the half-amplitude of the oscillations. Thus a preferred direction near the center of the oscillations would yield an eccentricity close to 0, while a preferred direction near the edge would yield an eccentricity close to 1. A Pearson product-moment correlation failed to show a significant correlation between the eccentricities of preferred directions and reductions in peak firing rates of the HD cells ($r = 0.01$, $n = 66$; NS). This indicates that variations in movement dynamics cannot account for the different responses observed among simultaneously recorded cells.

RELIABILITY OF PEAK FIRING RATE REDUCTIONS. In several cases, the same HD cell was recorded from the same microelectrode during two or more consecutive sessions (2 sessions for 3 neurons; 3 sessions for 4 neurons, 1 of which is shown in Fig. 4, *J–L;* and 7 sessions for the remaining cell). Cell identification was based on visual inspection of waveforms (Fig. 4, *J–L*, *inset*) as well as the absence of marked differences in preferred direction and angular response range. Changes in peak firing rates during passive rotations were compared between successive recordings. This showed no significant difference between any of the sequential recordings (Wilcoxon matched pairs tests, $n = 17$; NS). Thus the responses were fairly consistent across recording sessions.

TEMPORAL CHARACTERISTICS OF CELL DISCHARGES DURING THE ACTIVE AND PASSIVE CONDITIONS. A possible basis for the peak firing rate decrease during passive rotations would be a lower overall level of excitation of the neurons leading to an increase in inter-spike intervals in this condition. Alternatively, changes in the temporal dynamics of the discharges could occur (e.g., due to changes in membrane properties of the neurons). To test for this, normalized inter-spike interval histograms (ISIHs) were constructed for those recordings with sufficient data (44 cases). As shown by the example in Fig. 6, there was little evidence for bursts in the discharges of the HD cells in either condition. The ISIHs shifted to the right (greater

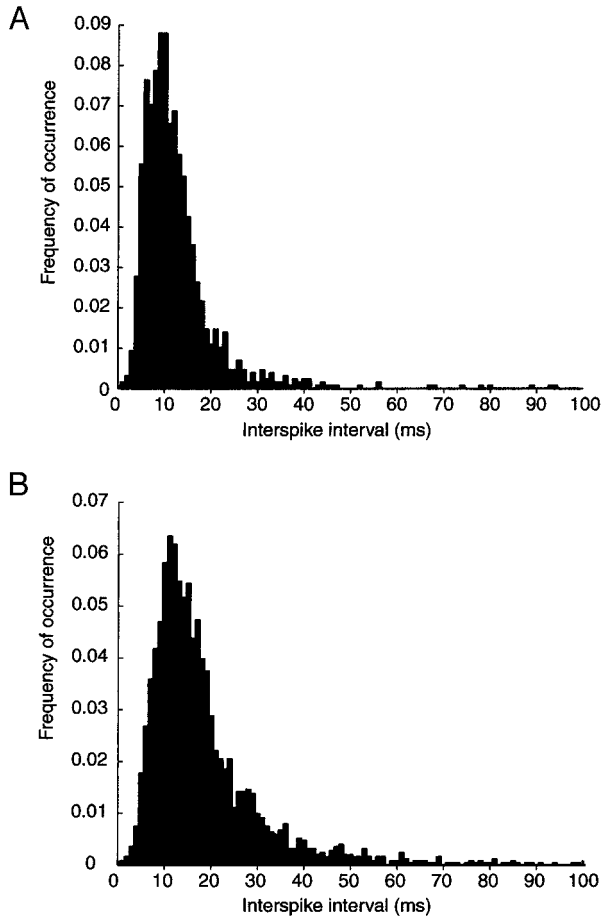

FIG. 6. Typical inter-spike interval histograms for a HD cell (shown in Fig. 4*F*) during active displacements (*A*) and passive rotations (*B*). The peak shifts to the right during passive rotations (the mean increases by 31%, coherent with the 34% reduction in peak firing rate). Bin widths are 1 ms; note that the *y* axes in *A* and *B* have different scales.

inter-spike intervals) during the passive rotations, resulting in greater medians (+29%), means (+25%), and modes (+25%) during the passive rotations. This shows that the observed decrease in peak firing rates is due to increased inter-spike intervals rather than to a change in temporal characteristics of the discharges.

ACTIVE LOCOMOTOR SIGNALS AND INERTIAL SIGNALS. As mentioned in the preceding text, several authors have reported an increase in firing rate during faster angular and linear head movements in freely moving rats (Blair and Sharp 1995; Stackman and Taube 1997; Taube 1995; but not Taube and Muller 1998). It is not known whether this results from stronger inertial (e.g., vestibular) signals, from active locomotor signals, or a combination of both. Because in our experiments the angular and linear head velocities and accelerations of the rats were more rapid during the active displacements (Fig. 3), it was necessary to determine whether this contributed to the difference in peak firing rates between active displacements and passive rotations.

To test for this, a repeated-measures ANOVA was conducted, where angular and linear head velocity levels were defined as independent factors. In addition, to compare data recorded during the active displacements and the passive rotations, movement type (active displacements vs. passive rotations) was considered a repeated measures factor. Angular velocity levels used for this analysis were $\omega \leq 30°/s$ and $30°/s < \omega \leq 90°/s$, while linear velocity levels were $v \leq 2.5$ cm/s, 2.5 cm/s $< v \leq 5$ cm/s, and 5 cm/s $< v \leq 7.5$ cm/s. Higher velocity data were discarded. The dependent variable was the increase in peak firing rate relative to the slowest movements ($\omega \leq 30°/s$ and $v \leq 2.5$ cm/s). The ANOVA showed a significant effect of movement type [$F(1,129) = 42.92$; $P < 0.001$]. All other factors, including interaction factors, were not significant. This indicates that, even for comparable angular and linear head velocity movements, the decrease in peak firing rate is not a secondary effect due to velocity dependence.

CONTROLLING FOR DIFFERENTIAL SHIFTS IN PREFERRED DIRECTIONS. Another possible explanation of the decrease in peak firing rate during passive rotations could have been that the preferred directions of the directional response curves had shifted by different angles during the clockwise and counterclockwise oscillations of the platform. In this case, the aggregate directional response curves computed in the preceding text would have lower peaks, although the individual clockwise or counterclockwise directional response curves would not show such a reduction. To test for this, data were separated into clockwise and counterclockwise oscillations during passive rotations, and peak firing rates were recomputed based on the new directional responses. This revealed that preferred directions were not significantly different between the clockwise and counterclockwise rotations (Wilcoxon matched pairs tests, $n = 66$, NS) Furthermore, peak firing rates during the clockwise and the counterclockwise passive rotations were each significantly lower than the peak rate computed for active displacements (Wilcoxon matched pairs tests, $n = 66$, $P < 0.001$). Therefore the decrease in peak firing rate during passive rotations is not due to the summation of offset response curves from the two directions of passive rotation.

TEST FOR RECORDING STABILITY. Small changes in the quality of isolation of extracellular recording signals can result in changes in measured firing rates. Because, in most sessions, active displacements were recorded before passive rotations, the decreases in peak firing rates observed here might have been due to electrode instability. Although this is an unlikely explanation for the systematic decreases in peak firing rates (cell isolation could also improve over time), an additional test was performed. Peak firing rates were compared between the first and second halves of the active displacements phase of the experiment. There was no significant difference between these measures (Wilcoxon matched-pairs test, $n = 66$, NS). Together with the fact that single cells recorded during successive days showed consistent decreases in peak firing rates across sessions (discussed in the preceding text), we conclude that variations in cell isolation do not account for the decrease in peak firing rates during passive rotations.

Preferred directions during the active displacements and passive rotations

The preferred direction of each HD cell was compared between active displacements and passive rotations. The mean absolute shift in preferred directions between the two conditions was 10 ± 1° (mean ± SE; range: −24 to +30°).

However, the preferred directions did not shift significantly clockwise or counterclockwise between the two conditions (Wilcoxon matched pairs test, $n = 66$; NS). This indicates that, on average, the HD cells maintained the same preferred directions when the animal was passively rotated (Fig. 7*A*).

Similar to the analysis conducted on peak firing rate decreases, the absolute shifts in preferred directions were tested for a correlation with the eccentricity of the preferred directions relative to the passive rotation oscillations. Again, this failed to show a significant correlation between the two variables (Pearson product-moment correlation, $r = 0.01$, $n = 66$; NS). This is consistent with the fact that the preferred directions of the HD cells are always updated in a coherent manner regardless of the dynamics of the passive movements.

Angular range of directional responses during the active displacements and passive rotations

The mean range of the directional responses of the HD cells during active displacements at all velocities was 98 ± 2° (range: 58–182°), while during passive rotations it was 107 ± 4° (range: 59–229°). The values measured during active displacements correspond to those of previous reports (Blair and Sharp 1996; Taube 1995). The angular ranges were not significantly different in the two conditions (Wilcoxon matched pairs tests, $n = 66$, NS; Fig. 7*B*).

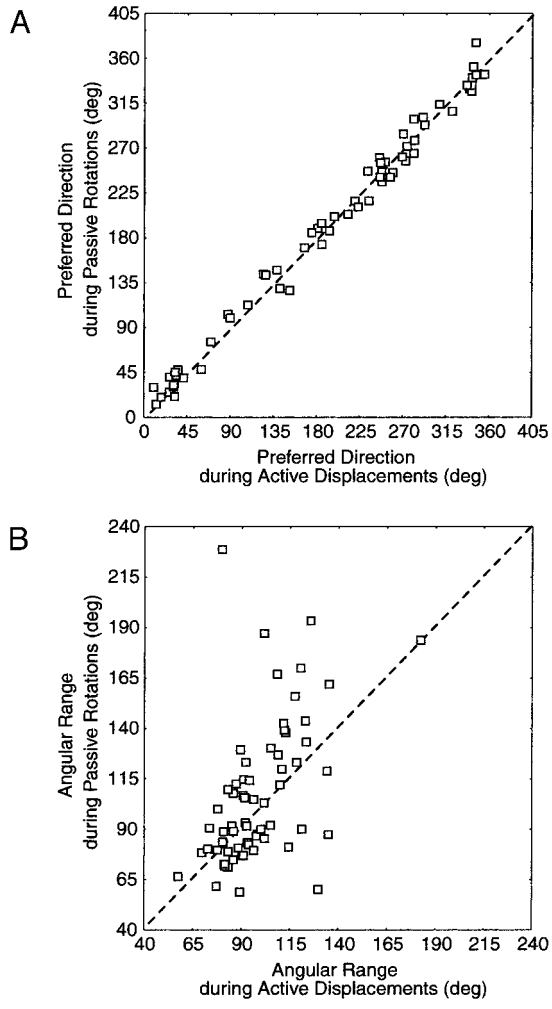

FIG. 7. Comparisons of the preferred directions (*A*) and angular response ranges (*B*) of the HD cells during passive rotations vs. active displacements. Dashed lines indicate values that remained the same during both conditions.

DISCUSSION

This study aimed to distinguish the respective contributions of active versus passive self-movement cues on directional signals in the AD. To do this, the directional responses of the same neurons were compared between active displacements and passive rotations in unrestrained animals. In the active displacement and the passive rotation phases of the present experiment, the preferred directions of the neurons did not change markedly. This indicates that the visual cues, as well as certain self-motion cues present in both conditions, were sufficient to establish and maintain this critical component of the directional signal. The 27% average decrease in peak firing rate during passive rotations is thus more likely to be due to those self-motion cues that were different in the passive and active conditions (discussed in the following text). In contrast, angular response ranges were not significantly different during the active displacements and the passive rotations. The implications of these results for understanding the generation and updating of thalamic head direction signals are discussed in the following sections.

Self-movement signals and AD HD cell activity

Several different self-motion cues could play a role in the reduction in peak firing rate from active displacements to passive rotations. Such cues could include the command signals for movement initiation, motor set (e.g., signals disinhibiting the subsequent activation of specific motor pathways), signals from efferent collaterals and corollary discharges of premotor and motor pathways proper, and the interaction of the latter with proprioceptive signals triggered by mechanical interactions with the substrate. Since the magnitude of the directional response increased when the rat made active movements, these results are consistent with the notion that the premotor and motor efferent collaterals (or corollary discharge) exert a state-dependent modulation of the AD HD signal. However, motor commands and motor set, while they were most likely different in the passive and active conditions, were still required in both cases. Remaining immobile in our passive condition also required the rats to exert forces to maintain postural equilibrium, resist rotational forces and inhibit movements of the head away from the water reservoir.

These observations suggesting that a state-dependent modulation of the AD HD signal is likely influenced by premotor and motor efferent collaterals, or corollary discharge, are consistent with the notion that head-direction information is critical during active locomotion and less so during nonlocomotor activities. The higher firing rates would thus convey more information to downstream structures (such as the hippocampus) during self-initiated movement than passive displacements.

Response suppression in HD cells and hippocampal place cells due to tight restraint

Taube (1995) found that when rats were tightly restrained, then rotated into the (previously determined) preferred direc-

tion, the directional responses were suppressed in 9 of 10 AD neurons, despite the continued presence of visual and inertial cues. In contrast, HD neurons of the postsubiculum, which is reciprocally connected to the AD (Van Groen and Wyss 1990, 1995), show decreases in firing rate by only 30% during tight restraint (Taube et al. 1990b). The degree of reduction in PoS HD cell discharges is proportional to the intensity of the restraint (E. J. Markus, personal communication) (cf. Markus et al. 1990). Chen et al. (1994) tested direction-selective neurons of retrosplenial cortical areas RSG and RSA in rats permitted to move freely, then passively rotated by 120–200° at 180–300°/s at regular intervals. For the latter, the rats were placed on a small elevated platform with 2 cm high barriers along the sides that restricted the movements, but not the view, of the animals. The majority of the neurons that showed significant direction selectivity during maze performance had little or no directional firing during the passive rotations.

Are peak firing rate reductions due to differences in vestibular inputs?

A recent electrophysiological study of the brain stem vestibular nuclei in monkeys (McCrea et al. 1999) showed that vestibular inputs are strongly attenuated during active head rotations. Vestibulo-spinal, and other non-eye-movement-related vestibular neurons that are sensitive to passive whole body rotations, showed firing suppression in most cases (73% of the 51 neurons recorded) during active head movements. In the remaining neurons, the discharge rate was attenuated by 20–75% during active head rotations. While the restraint and active movement conditions imposed on the monkeys were different from the present ones, these results suggest that vestibular neurons may have been more active in our rats during passive rotations than during the active displacements. Since the vestibular end organs are stimulated in both active and passive conditions, it is possible that movement initiation signals are responsible for the attenuation of vestibular neuron responses in the monkey experiments. However McCrea et al. (1999) suggest that the suppression of the vestibular signal would serve to inhibit the vestibulo-collic reflex during active movements. Thus during normal active turning movements, the head would turn with the body rather than reflexively turning toward the former direction. In our passively rotated rats, there was not convincing evidence for vestibulo-collic reflexes (Fig. 2), suggesting that such suppression was also present here (although it is not known whether the vestibular neurons with ascending projections are also inhibited during active movements). Thus following the above cited work, vestibular neuronal activity may have been attenuated both during the passive rotations and the active displacements of the rats in our experiment.

Can differences in motivational factors underlie peak firing rate reductions during passive rotations?

Because during the passive rotations the immobile animals were receiving droplets of water, while in the active displacements they received food, this difference may have contributed to the observed changes in peak firing rates. However, there is no evidence in previous studies for modulation of HD cell firings by ongoing behavior (for example, Dudchenko and Taube 1997). Furthermore, in both conditions the rats spent only a fraction of the time consuming rewards.

Are peak firing rate reductions during passive rotations associated with possible changes in hippocampal theta rhythmic slow activity (RSA)?

This question is motivated by the observation that place responses of hippocampal neurons are less specific during large-amplitude irregular (LIA) electroencephalogram than during theta RSA (Czurkó et al. 1999; Foster et al. 1989; Muller et al. 1987). However, there are indications that theta RSA was present during passive (as well as active) displacements. Theta RSA also occurs during passive rotations of restrained rats receiving periodic water rewards (Gavrilov et al. 1995, 1996). There was also no indication of rhythmic firing at theta frequencies in the inter-spike interval histograms, and there are no known direct projections from the theta-generating neurons of the nucleus of the diagonal band of Broca or from the hippocampus to the AD. In our view, it is more likely that other diffusely projecting neurotransmitter systems (perhaps also involved in the generation of theta RSA) might play a role in the firing rate reductions in the passive condition.

Serotonergic activity as a possible cause for firing reductions during passive rotations

The AD has one of the highest densities of 5-HT_7 receptor in the brain (Gustafson et al. 1996). In a review article, Jacobs and Fornal (1999) conclude that serotonergic neurons are activated in association with increased muscle tone and tonic motor activity. They interpreted this result within a theoretical framework where the serotonergic system plays an important role in facilitating motor output. In vitro, serotonin is known to regulate afterdepolarization of AD neurons (Chapin and Andrade 2000). Interestingly, AD receives serotonergic projections from the ventromedial and ventrolateral parts of the ipsilateral dorsal raphe, and to a lesser extent from the dorsomedial part of the nucleus, predominantly ipsilaterally, and the median raphe (Gonzalo-Ruiz et al. 1995). Altogether, this is consistent with the hypothesis that serotonergic mechanisms may be responsible for higher peak firing rates in AD neurons during active locomotion than passive displacements. If this is the case, such a mechanism could also mediate the suppression of place cell activity in hippocampal neurons of tightly restrained rats (Foster et al. 1989) since there is also a high 5-HT_7 receptor density there.

We thank Drs. R. Andrade, H. T. Blair, J. Droulez, P. E. Sharp, and J. S. Taube for valuable discussions; Dr. R. Lestienne for help in temporal analyses of neuronal discharges; Drs. N. Brunel and I. Israël for comments on the text; J. Cote for help in data analysis; M.-A. Thomas and N. Quenech'du for histology; A. Treffel, M. Ehrette, and S. Ilic for the construction of the behavioral apparatus; P. Leboucher for electronic equipment; F. Maloumian for illustrations; and S. Lemarchand and D. Raballand for animal care. E. Tabuchi was on leave from the Dept. of Physiology, Toyama Medical and Pharmacological University, Toyama, Japan.

This work was supported by Centre National de la Recherche Scientifique-National Science Foundation cooperation, Centre National d'Etudes Spatiales, Cogniseine, Groupement d'Intérêt Scientifique. M. B. Zugaro received a grant from the Fondation pour la Recherche Médicale.

REFERENCES

BLAIR HT, CHO J, AND SHARP PE. Role of the lateral mammillary nucleus in the rat head direction circuit: a combined single unit recording and lesion study. *Neuron* 21: 1387–1397, 1998.

BLAIR HT AND SHARP PE. Anticipatory head direction signals in anterior thalamus: evidence for a thalamocortical circuit that integrates angular head motion to compute head direction. *J Neurosci* 15: 6260–6270, 1995.

BLAIR HT AND SHARP PE. Visual and vestibular influences on head-direction cells in the anterior thalamus of the rat. *Behav Neurosci* 110: 643–660, 1996.

CHAPIN EM AND ANDRADE R. Calcium-independent afterdepolarization regulated by serotonin in anterior thalamus. *J Neurophysiol* 83: 3173–3176, 2000.

CHEN LL, LIN L-H, GREEN EJ, BARNES CA, AND MCNAUGHTON BL. Head-direction cells in the rat posterior cortex. I. Anatomical distribution and behavioral modulation. *Exp Brain Res* 101: 8–23, 1994.

CZURKÓ A, HIRASE H, CSICSVARI J, AND BUZSÁKI G. Sustained activation of hippocampal pyramidal cells by 'space clamping' in a running wheel. *Eur J Neurosci* 11: 4373–4380, 1999.

DUDCHENKO PA AND TAUBE JS. Correlation between head direction cell activity and spatial behavior on a radial arm maze. *Behav Neurosci* 111: 3–19, 1997.

FOSTER TC, CASTRO CA, AND MCNAUGHTON BL. Spatial selectivity of rat hippocampal neurons: dependence on preparedness for movement. *Science* 244: 1580–1582, 1989.

GAVRILOV V, WIENER SI, AND BERTHOZ A. Enhanced hippocampal theta EEG during whole body rotations in awake restrained rats. *Neurosci Lett* 197: 239–241, 1995.

GAVRILOV V, WIENER SI, AND BERTHOZ A. Whole-body rotations enhance hippocampal theta rhythmic slow activity in awake rats passively transported on a mobile robot. *Ann NY Acad Sci* 781: 385–398, 1996.

GONZALO-RUIZ A, LIEBERMAN AR, AND SANZ-ANQUELA JM. Organization of serotoninergic projections from the raphé nuclei to the anterior thalamic nuclei in the rat: a combined retrograde tracing and 5-HT immunohistochemical study. *J Chem Neuroanat* 8: 103–115, 1995.

GOODRIDGE JP AND TAUBE JS. Preferential use of the landmark navigational system by head direction cells in rats. *Behav Neurosci* 109: 1–12, 1995.

GUSTAFSON EL, DURKIN MM, BARD JA, ZGOMBICK J, AND BRANCHEK TA. A receptor autoradiographic and in situ hybridization analysis of the distribution of the 5-HT_7 receptor in rat brain. *Br J Pharmacol* 117: 657–666, 1996.

JACOBS BL AND FORNAL CA. Activity of serotonergic neurons in behaving animals. *Neuropsychopharmacology* 21: 9S–15S, 1999.

JOHNSON NL AND KOTZ S. *Continuous Univariate Distributions*. New York: Wiley, 1970, vol. 2.

KHABBAZ A, FEE MS, TSIEN JZ, AND TANK DW. A compact converging-electrode microdrive for recording head direction cells in mice. *Soc Neurosci Abstr* 26: 984, 2000.

KNIERIM JJ, KUDRIMOTI HS, AND MCNAUGHTON BL. Interactions between idiothetic cues and external landmarks in the control of place cells and head direction cells. *J Neurophysiol* 80: 425–446, 1998.

MARKUS EJ, MCNAUGHTON BL, BARNES CA, GREEN JC, AND MELTZER J. Head direction cells in the dorsal presubiculum integrate both visual and angular velocity information. *Soc Neurosci Abstr* 16: 441, 1990.

MCCREA RA, GDOWSKI GT, BOYLE R, AND BELTON T. Firing behavior of vestibular neurons during active and passive head movements: vestibulospinal and other non-eye-related neurons. *J Neurophysiol* 22: 3077–3099, 1999.

MIZUMORI SJY AND WILLIAMS JD. Directionally selective mnemonic properties of neurons in the lateral dorsal nucleus of the thalamus of rats. *J Neurosci* 13: 4015–4028, 1993.

MULLER RU, KUBIE JL, AND RANCK JB JR. Spatial firing patterns of hippocampal complex-spike cells in a fixed environment. *J Neurosci* 7: 1935–1950, 1987.

RANCK JB JR. Head-direction cells in the deep cell layers of dorsal presubiculum in freely moving rats. *Soc Neurosci Abstr* 10: 599, 1984.

RECCE M AND O'KEEFE J. The tetrode: a new technique for multi-unit extracellular recording. *Soc Neurosci Abstr* 19: 1250, 1989.

ROBERTSON RG, ROLLS ET, GEORGES-FRANÇOIS P, AND PANZERI S. Head direction cells in the primate pre-subiculum. *Hippocampus* 9: 206–219, 1999.

STACKMAN RW AND TAUBE JS. Firing properties of head direction cells in the rat anterior thalamic nucleus: dependance on vestibular input. *J Neurosci* 17: 4349–4358, 1997.

STACKMAN RW AND TAUBE JS. Firing properties of rat lateral mammillary single units: head direction, head pitch, and head angular velocity. *J Neurosci* 18: 9020–9037, 1998.

TAUBE JS. Head direction cells recorded in the anterior thalamic nuclei of freely moving rats. *J Neurosci* 15: 70–86, 1995.

TAUBE JS. Head direction cells and the neurophysiological basis for a sense of direction. *Prog Neurobiol* 55: 1–32, 1998.

TAUBE JS, GOODRIDGE JP, GOLOB EJ, DUDCHENKO PA, AND STACKMAN RW. Processing the head direction cell signal: a review and commentary. *Brain Res Bull* 40: 477–486, 1996.

TAUBE JS AND MULLER RU. Comparisons of head direction cell activity in the postsubiculum and anterior thalamus of freely moving rats. *Hippocampus* 8: 87–108, 1998.

TAUBE JS, MULLER RU, AND RANCK JB JR. Head-direction cells recorded from the postsubiculum in freely moving rats. II. Effects of environmental manipulations. *J Neurosci* 10: 436–447, 1990a.

TAUBE JS, MULLER RU, AND RANCK JB JR. Head-direction cells recorded from the postsubiculum in freely moving rats. I. Description and quantitative analysis. *J Neurosci* 10: 420–435, 1990b.

VAN GROEN T AND WYSS JM. The postsubicular cortex in the rat: characterization of the fourth region of the subicular cortex and its connections. *Brain Res* 529: 165–177, 1990.

VAN GROEN T AND WYSS JM. Projections of the anterodorsal and anteroventral nucleus of the thalamus to the limbic cortex in the rat. *J Comp Neurol* 358: 584–604, 1995.

WIENER SI. Spatial and behavioral correlates of striatal neurons in rats performing a self-initiated navigation task. *J Neurosci* 13: 3802–3817, 1993.

ZHANG K. Representation of spatial orientation by the intrinsic dynamics of the head-direction ensemble: a theory. *J Neurosci* 16: 2112–2126, 1996.

ZUGARO MB, BERTHOZ A, AND WIENER SI. Background, but not foreground, spatial cues are taken as references for head direction responses by rat anterodorsal thalamus neurons. *J Neurosci* 21: RC154(1–5), 2001.

ZUGARO MB, TABUCHI E, FOUQUIER CF, BERTHOZ A, AND WIENER SI. Peak firing rates of anterodorsal thalamic head direction cells decrease during passive rotations in rats trained to remain immobile while unrestrained. *Soc Neurosci Abstr* 26: 984, 2000a.

ZUGARO MB, TABUCHI E, AND WIENER SI. Influence of conflicting visual, inertial and substratal cues on head direction cell activity. *Exp Brain Res* 133: 198–208, 2000b.

Exp Brain Res (2000) 133:198–208
Digital Object Identifier (DOI) 10.1007/s002210000365

RESEARCH ARTICLE

Michaël B. Zugaro · Eiichi Tabuchi · Sidney I. Wiener

Influence of conflicting visual, inertial and substratal cues on head direction cell activity

Received: 20 July 1999 / Accepted: 28 January 2000 / Published online: 30 March 2000

Abstract In order to navigate efficiently, animals can benefit from internal representations of their moment-to-moment orientation. Head-direction (HD) cells are neurons that discharge maximally when the head of a rat is oriented in a specific ("preferred") direction in the horizontal plane, independently from position or ongoing behavior. This directional selectivity depends on environmental and inertial cues. However, the mechanisms by which these cues are integrated remain unknown. This study examines the relative influence of visual, inertial and substratal cues on the preferred directions of HD cells when cue conflicts are produced *in the presence of the rats*. Twenty-nine anterior dorsal thalamic (ATN) and 19 postsubicular (PoS) HD cells were recorded from 7 rats performing a foraging task in a cylinder (76 cm in diameter, 60 cm high) with a white card attached to its inner wall. Changes in preferred directions were measured after the wall or the floor of the cylinder was rotated separately or together in the same direction by 45°, 90° or 180°, either clockwise or counterclockwise. Linear regression analyses showed that the preferred directions of the HD cells in both structures shifted by ≈90% of the angle of rotation of the wall, whether rotated alone or together with the floor (r^2>0.87, P<0.001). Rotations of the floor alone did not trigger significant shifts in preferred directions. These results indicate that visual cues exerted a strong but incomplete control over the preferred directions of the neurons, while inertial cues had a small but significant influence, and substratal cues were of no consequence.

Eiichi Tabuchi is on leave from Toyama Medical and Pharmacological University, Toyama, Japan

M.B. Zugaro (✉) · E. Tabuchi · S.I. Wiener
CNRS-Collège de France,
Laboratoire de Physiologie de la Perception et de l'Action,
11 place Marcelin Berthelot, 75005 Paris, France
e-mail: michael.zugaro@college-de-france.fr
Tel: +33 1 44 27 16 21, Fax: +33 1 44 27 13 82

Key words Spatial orientation · Anterodorsal thalamic nucleus · Postsubiculum · Passive rotation · Multisensory integration

Introduction

In rats, head-direction (HD) cells are a possible substrate for an internal representation of the momentary orientation in the horizontal plane (Ranck 1984). These neurons have been found in many different areas of the rat brain, such as the postsubiculum (PoS) (Taube et al. 1990a), the anterodorsal thalamic nucleus (ATN) (Taube 1995), the dorsal striatum (Wiener 1993), the lateral dorsal thalamic nucleus (LDN) (Mizumori and Williams 1993), the lateral mammillary nucleus (LMN) (Stackman and Taube 1998; Blair et al. 1998), and certain areas of parietal and retrosplenial cerebral cortices (Chen et al. 1994). They discharge selectively when the head of the animal is oriented in a specific direction, the *preferred direction*, independently of position or ongoing behavior (Ranck 1984). Salient visual cues exert a strong influence on the preferred directions of the HD cells (Taube et al. 1990a; Goodridge and Taube 1995; Dudchenko et al. 1997), while olfactory and tactile cues exert a much smaller influence, and auditory cues do not appear to exert any influence at all (Goodridge et al. 1998). However, directional selectivity persists in total darkness (Chen et al. 1994; Mizumori and Williams 1993; Blair and Sharp 1996), and is abolished after lesions of the vestibular apparatus even when visual cues are available (Stackman and Taube 1997). Taken together, these results indicate that HD cells are influenced by a combination of environmental and self-movement cues.

It is of particular interest to understand how these diverse cues are integrated to produce HD cell responses, and this could shed light on the problem of multisensory fusion. However, in previous studies addressing this question, mixed results have been found (Goodridge and Taube 1995; Blair and Sharp 1996; Knierim et al. 1998). Although visual cues have been shown to exert a strong

influence on the preferred direction of ATN and PoS HD cells (Taube et al. 1990a; Taube 1995), this was found in conditions where the influences of inertial cues and substratal cues (such as tactile and olfactory cues on the floor) were minimized: between the control and test sessions, the rats were removed from the recording cylinder and disoriented, and paper on the floor was changed to remove potential cues. In a different study, Blair and Sharp (1996) addressed the question of the influence of inertial cues on the preferred direction of ATN HD cells directly by rotating the rats passively, but this was done in the absence of polarizing visual cues. Knierim and colleagues (1998) showed that the preferred directions of ATN HD cells follow the visual cues when the whole recording apparatus is rotated in the presence of the rat, except for fast rotations by a large angle (135° or 180°), for which the preferred directions shifted only half of the time. However, the respective influence of visual and substratal cues could not be distinguished under these conditions, because both wall and floor cues could have triggered the shifts.

Here, we examined the responses of ATN and PoS HD cells after experimental manipulations of visual, inertial and substratal cues *in the presence of the rats*. Since the animals remained in the cylinder and were not disoriented during cue manipulations, the influence of inertial cues could be tested directly. The experimental apparatus consisted of a black cylinder with a white card attached to its inner wall. The wall and floor of this cylinder could each be rotated independently (Blair and Sharp 1996). By rotating the wall or the floor separately, or both the wall and floor together in the same direction while the rat remained in the cylinder, we induced several types of conflicts between visual, inertial and substratal cues. By comparing the effects of these three types of manipulations, we were able to estimate the relative influence of the cues upon the preferred directions of the HD cells. Some of this work has been presented previously in abstract form (Zugaro et al. 1999).

Materials and methods

Experimental subjects

The subjects were seven male Long-Evans rats, weighing 200–250 g upon arrival (CERJ, Le Genest-St-Isle). They were housed in pairs until the time of surgery, and then kept in separate cages. After recovery they were placed on a food restriction diet keeping them at approximately 85% of their normal weight. Water was freely available. The animals were maintained on a 12 h light/12 h dark cycle. All animal care and experimental protocols were in accord with institutional and international standards and legal regulations ("Principles of laboratory animal care", NIH publication No. 86–23, revised 1985, as well as specific national laws where applicable).

Electrode implantation

Three rats were implanted with tetrodes – groups of four twisted nichrome wires (Recce and O'Keefe 1989), diameter 13 µm or 25 µm. Four rats were implanted with bundle electrodes. All electrodes had gold-plated tips (impedance 200–700 kΩ). Four rats were implanted both in ATN and PoS, and three rats received bilateral ATN implantation. Before surgery, the electrodes were inserted in 30-gauge stainless steel cannulas. Cannulas were mounted on two connectors that could be advanced independently via screws attached to a common base (Wiener 1993). For surgery, the animals were tranquillized with xylazine, then deeply anesthetized with pentobarbital (40 mg/kg). The tetrodes were implanted above the PoS (AP –6.5 mm to –7.3 mm, ML ±2.8 mm to ±3.5 mm relative to bregma) and above the ATN (AP –1.4 mm to –1.8 mm, ML ±1.2 mm to ±1.5 mm relative to bregma) using conventional surgical techniques. The headstage was permanently fixed to the skull with dental acrylic and seven tiny screws.

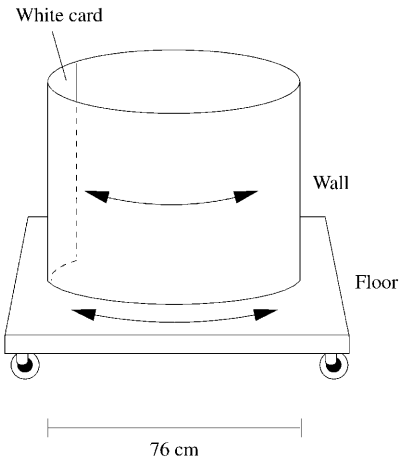

Fig. 1 The experimental apparatus. The cylinder wall and floor could be rotated independently

Behavioral apparatus

The square recording room was enclosed by black curtains suspended from the ceiling along four walls. Illumination was provided by a 40-W overhead lamp which diffused light evenly within the cylinder. The brightness of the lamp masked possible cues outside the cylinder. The experimental apparatus (Fig. 1) consisted of a black cylinder (60 cm high, 76 cm in diameter). A white card (50 cm wide, covering 75°) attached on the inner wall served as a salient visual landmark, referred to as the "cue card." The wall and the floor of the cylinder could be rotated independently (Blair and Sharp 1996). In order to ensure precise rotation angles, the floor was rotated manually with a pulley system calibrated for 45° steps. The wall had an angular graduation drawn on its outer side for calibration. All electronic instruments and computers were situated outside the curtains, and the entire experimental room was phonically isolated from the rest of the building.

Behavioral task

Before each recording session, the wall and floor were first rotated to a reference position, with the cue card center at 0°. The animals had been trained to retrieve small food pellets (5 mg chocolate sprinkles) thrown manually into the cylinder at pseudorandom locations (Muller et al. 1987). This kept the rats moving throughout the session, and resulted in visits to most of the floor surface and a fairly uniform distribution of head orientations over time. Each session lasted 20–25 min, and included three or four environmental manipulations (rotation of the wall, rotation of the floor, and rotation of both at ~10°/s) in the presence of the rat. These manipulations were made in a pseudorandom sequence. Wall and floor rotation angles included –180°, –90°, –45°, +45°, +90° and +180°.

The final configuration of the experimental apparatus was identical to the initial one. The following data compare preferred directions in recordings immediately prior to and after such manipulations.

Unit isolation and data collection

Animals were brought into the recording room in a transparent plastic cage; then the recording cable was attached to the electrode assembly, and the rat was placed in the cylinder without any attempt to disorient it. The electrode channels were screened while the rat performed the foraging task in the cylinder. If no suprathreshold HD cell activity was present, the electrodes were slightly advanced (50 µm, each pair of tetrodes being independently driveable), and the animal was checked again 4–96 h later. If cells were present, the floor was cleaned again (if necessary) and the curtains were closed before the recording session began. Note that since screening was conducted every working day, the rats were rather familiar with the environment.

During the recording sessions, electrode signals passed through FETs and were differentially amplified (×10,000) and filtered (300 Hz to 5 kHz, notch at 50 Hz). The signal was then passed to a computer for automatic data collection. The acquisition software (DataWave Discovery) digitized and collected 32 data points (at 20 kHz) for each signal that crossed a user-set threshold. In most cases, activity of individual neurons appeared on only one of the four twisted wires. Single unit activity was discriminated post hoc using "cluster cutting" techniques based on a maximum of eight different waveform parameters.

Prior to recordings, a support with two small lamps (10 cm separation) was mounted above the headstage. Reflectors were attached to the lamp in the rostral position to make it appear larger than the caudal lamp. The positions of the two lamps were detected by a video camera mounted above the platform (using the DataWave video tracking system) and sampled at a rate of 60 Hz. The heading direction of the animal was later computed using the positions of the two lamps. Inversions of the lamps due to tracking errors were corrected with our own interactive software. Counterclockwise rotations are considered positive here.

In order to build tuning curves for the HD cells, our software counted the number of spikes for each position sampling interval (16.6 ms), and associated the resulting frequency with the corresponding head angle. This was used to compute a histogram, for which each bin height was the average of all the frequencies associated with head angles within the range of the bin. Analyses were carried out on sessions where the rat spent a minimum of 2 s per 6° bin. Note that our software corrects for the delay between video and cell signal processing times.

To calculate HD cell parameters (preferred direction, peak firing rate, firing range, baseline firing rate), we used a discrete adaptation of the Gaussian-like fit employed by Zhang (1996):

$$f(\theta)=A+B.e^{K.\cos(\theta-\theta_0)}$$

where $f(\theta)$ is the firing rate, θ_0 the preferred direction, $B.e^K$ the peak firing rate, $230°/\sqrt{K}$ the firing range (width of the curve at the baseline level, computed using the two tangent lines at the inflexion points of the Gaussian curve), and A the baseline firing rate. A best-fit approximation to this curve was obtained via Matlab (The MathWorks, Natick, MA) software (least squares distance obtained with a Nelder-Mead type simplex search method).

Shifts in preferred directions were computed for the two successive preferred directions measured before and after each environmental manipulation. Statistics were performed using Statistica (StatSoft Inc., Tulsa, OK) software.

Histology

At the end of the experiments, a small electrolytic lesion was made by passing a small cathodal DC current (20 µA, 10 s) through one of the recording electrodes to mark the location of its tip. The rats were then deeply anesthetized with pentobarbital. Intracardial perfusion with saline was followed by 10% formalin-saline. Histological sections were stained with cresyl violet. Recording sites were reconstructed by detecting the small lesion and the track of the 30-gauge cannula, taking into account the distance that the microelectrode driver had been advanced from the point of stereotaxic placement of the electrodes. The recording sites were calculated by interpolation along the electrode track between the lesion site and the implantation site.

Experiment 1: rotation of the wall only

Manipulation

In this experiment, we recorded the HD cells for 5 min, rotated only the wall of the cylinder, and recorded for 5 more min (angles of rotation included –180°, –90°, –45°, +45°, +90°, and +180°).

Results

For this experiment, 29 ATN and 18 PoS HD cells were recorded in the 7 rats (in a total of 21 and 17 recording sessions respectively). The main characteristics of the directional tuning curves of these cells are displayed in the first two rows of Table 1.

The effect of rotating the wall of the cylinder upon the preferred directions of two HD cells is displayed in Fig. 2. The preferred directions of these HD cells shifted after the cylinder wall was rotated: they followed the wall cues, but shifted by a smaller angle. This will be referred to here as an "underrotation."

In order to examine the effect of wall rotations on the preferred directions, shifts in preferred directions were plotted against angles of rotation of the wall. This showed a linear relation (Fig. 3), except for two sessions (ATN cells recorded from the same animal, rotations of the wall

Table 1 HD cell firing properties for the three experiments. The same cells were often recorded in more than one experiment. These values are similar to those reported in previous studies (values are means ± standard errors of the mean)

Rotation	Structure	Peak firing rate (spikes/s)	Firing range (°)	Baseline firing rate (spikes/s)
Wall rotations	ATN	32.2±3.5	100.9±5.2	0.6±0.3
	PoS	20.7±3.1	105.3±11.0	5.5±1.6
Wall and floor rotations	ATN	31.1±3.4	98.1±5.0	0.8±0.3
	PoS	17.0±3.3	91.0±8.8	3.4±1.6
Floor rotations	ATN	32.9±3.4	94.1±4.0	0.5±0.3
	PoS	18.0±2.4	95.8±13.6	3.6±2.0

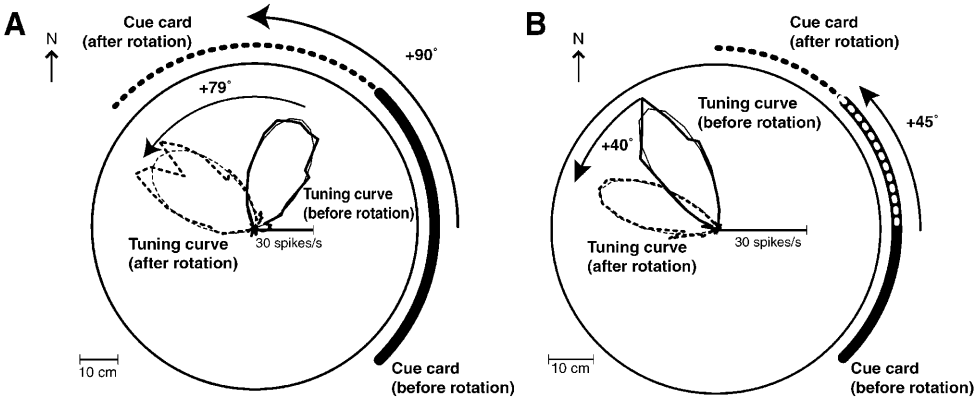

Fig. 2A,B Examples of underrotation of the preferred direction of two ATN HD cells after rotation of the cylinder wall only. The firing rate is plotted as a function of the head direction in polar coordinates (bin size: 6°). **A** While the cue card was centered at 0° (starting position, continuous arc), the preferred direction of this HD cell was 68° (*thick continuous line*; the pseudo-Gaussian approximation of this tuning curve is shown by *the thin continuous line*). After the cue card was rotated by 90° (*dotted arc*), the preferred direction rotated by only 79° (*thick dotted line*; the pseudo-Gaussian approximation of this tuning curve is shown by *the thin dotted line*). This is an underrotation of 12% (11°/90°). **B** After the cue card was rotated by 45°, the preferred direction of this cell rotated by only 40° (same conventions as in **A**). This is an underrotation of 11% (5°/45°)

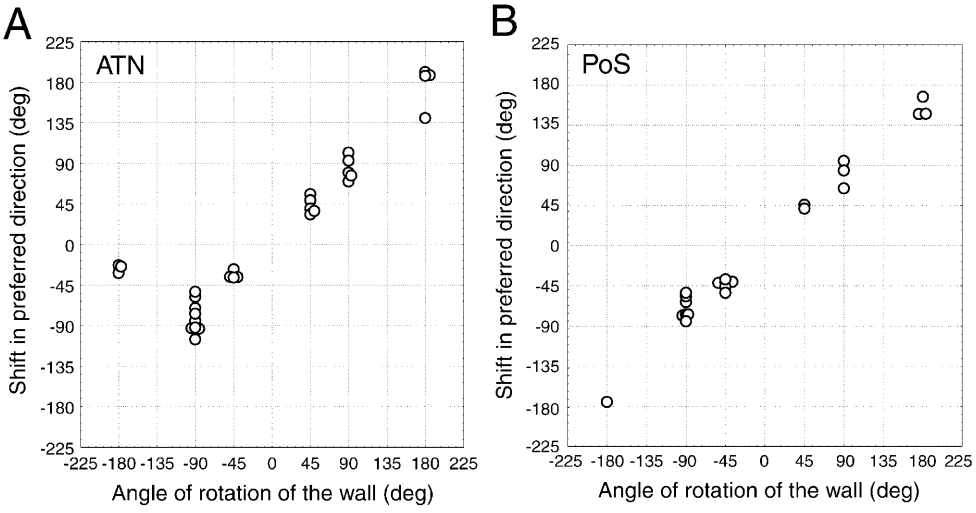

Fig. 3 The complete data set for shifts in preferred directions of all cells recorded after rotations of the wall only (**A** ATN cells, **B** PoS cells). Overlapping points are displaced laterally

by –180°) where the preferred directions shifted by a small angle. For these two sessions, however, the absence of preferred direction shift was obtained only after the rat had been trained in a different experiment conducted in the dark with asymmetrically distributed olfactory cues.

To quantify this linear relation, data for 180° rotations were excluded because it was not possible to determine whether the corresponding shifts in preferred direction were smaller or greater than wall rotations (for instance, a CW rotation of 170° is equivalent to a CCW rotation of 190°).

Linear regression analyses on the shifts in preferred directions ($\Delta\theta$) against the angles of rotation of the wall ($\Delta\alpha_{wall}$) yielded: $\Delta\theta=0.91\Delta\alpha_{wall}+2.51°$ ($r^2=0.97$) for ATN cells, and $\Delta\theta=0.85\Delta\alpha_{wall}+2.56°$ ($r^2=0.97$) for PoS cells. In both cases, the regression slope was highly significant ($P<0.001$), but the intercept value was not significantly different from zero ($P>0.1$).

From one to three neurons were recorded simultaneously in the sessions. Since the simultaneously recorded cells responded similarly to wall rotations, this could lead to overemphasis of the importance of such sessions, and bias the linear regression analysis (Goodridge et al. 1998). Therefore, in each recording where multiple HD cells were recorded simultaneously, the individual shifts in preferred directions were replaced by their mean. A second set of linear regression analyses confirmed the previous results (Fig. 4).

Blair et al. (1998) found differences in the responses of LMN HD cells during head turns depending on the hemisphere the cells were recorded from. To investigate possible differences between responses of neurons recorded in the left and right hemispheres to CW or CCW wall rotations, in Fig. 4 the data points are shown with different symbols. No obvious relation appears between lateralization and response properties.

In order to test for differences between responses to wall rotations in ATN and PoS recordings, we first conducted a linear regression analysis on the pooled data.

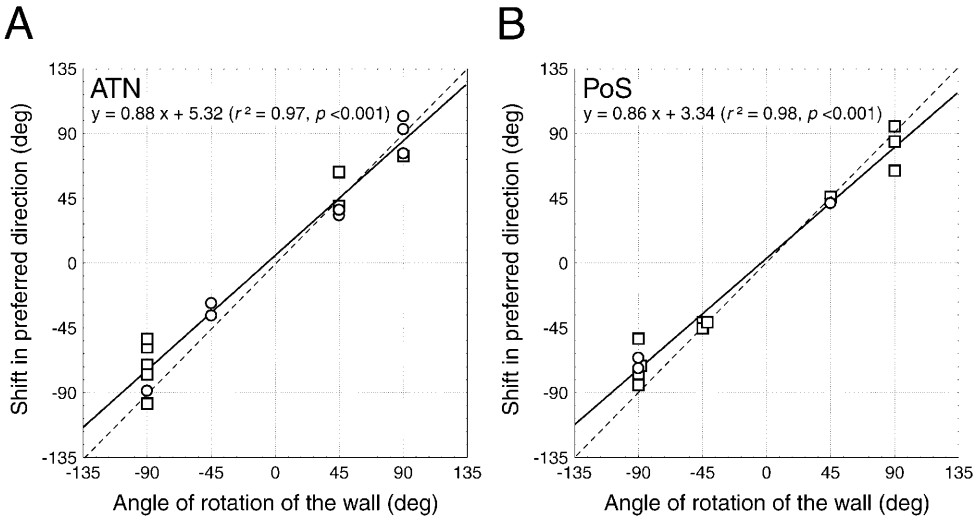

Fig. 4 Linear regression analysis of the effects of rotating only the wall of the cylinder upon the preferred directions of the HD cells (**A** ATN, **B** PoS). Each point is the average shift in the preferred direction of all cells recorded simultaneously in a given session. The data points are plotted along with the regression line (*continuous line; the dashed line* shows where the points would appear if the wall exerted complete control upon the preferred directions). The equations of the regression lines are indicated above. *Symbols* indicate the hemisphere from which the cells were recorded (*circles, left; squares, right*)

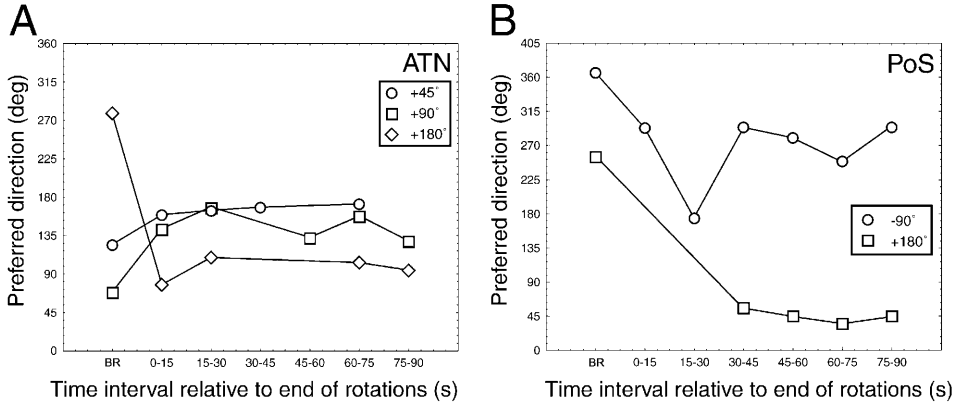

Fig. 5A,B Time course of preferred direction shifts after wall rotations for sessions with sufficient sampling. For each cell, *the first point* shows the preferred direction measured during the 5 min preceding the rotation (*BR* before rotation). Tuning curves are computed during successive 15-s blocks after rotations ended (**A** ATN cells, **B** PoS cells)

Then, residuals were computed for all the data points, and were separated into two groups corresponding to the respective structures. A *t*-test showed no significant difference between the two groups ($P>0.5$). This provides evidence that there was no significant difference between the results from ATN and PoS recordings in this experiment.

In summary, the preferred directions of the HD cells in both structures shifted in register with wall rotations, but by angles about 10% smaller. To test whether shifts in preferred directions were significantly smaller than wall rotation angles, the difference between complete (100%) and observed shifts in preferred directions was examined as a function of wall rotation angles. Linear regression analyses showed that the shifts in preferred directions are significantly different from wall rotation angles (ATN: $r^2=0.32$, $P<0.05$ for slope, $P>0.1$ for intercept offset; PoS: $r^2=0.56$, $P<0.01$ for slope, $P>0.1$ for intercept offset).

To investigate the time course of the shifts in preferred directions after wall rotations, tuning curves were made for six 15-s periods after the rotation ended. Since this reduced the data samples for each interval, recordings where the rat oriented its head a minimum of 100 ms in each 6° bin were selected (Fig. 5). Each tuning curve was treated as a histogram, and the preferred direction during each interval was computed as the mean of the histogram. Figure 5 shows that the preferred directions of the HD cells shifted to their new orientation as rapidly as 15–30 s after wall rotation and showed no apparent tendency for drift afterward.

In order to determine whether the degree of familiarity of the animals with the experiment affected the influence of the wall cues, the normalized shift in preferred directions (shift divided by wall rotation angle) was plotted against session number (Fig. 6). The absence of an obvious trend indicates that the control exerted by the wall cues did not depend on the previous experience of the rats with the wall rotations.

Discussion

The cues on the wall (the most salient of which was the cue card) exert a strong influence on the preferred directions of the HD cells in both structures. Furthermore,

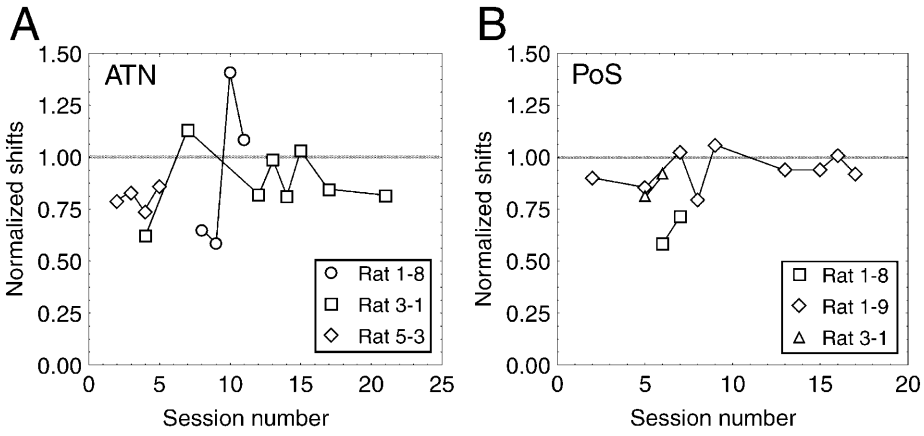

Fig. 6A,B Averaged preferred direction shifts after wall rotations in measurements from successive recording sessions. For each rat, normalized shifts in preferred directions (shifts divided by wall rotation angles) are plotted against session number. Sessions where no cells were isolated are counted. Data have been excluded for rats having only one recording session for a given structure (**A** ATN cells, **B** PoS cells)

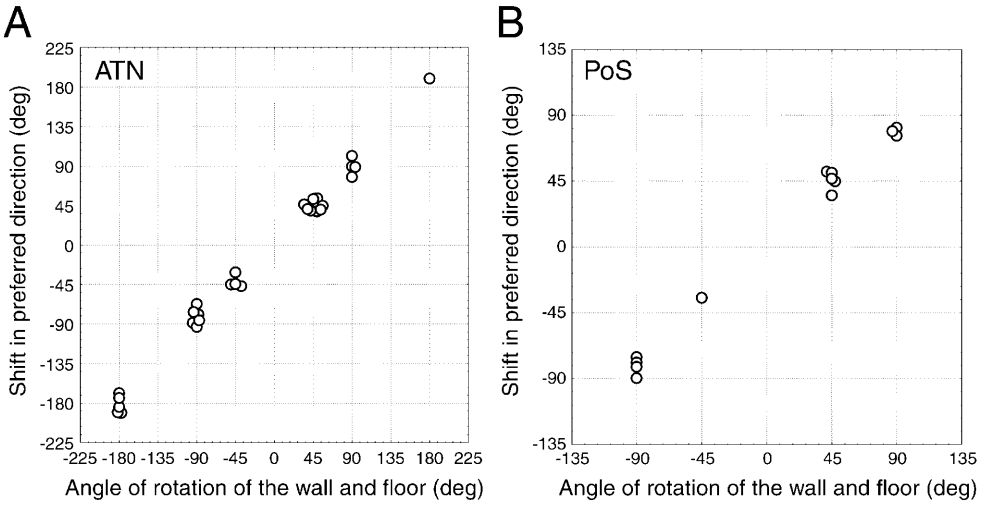

Fig. 7 The complete data set for shifts in preferred directions of all cells recorded after rotations of the wall and floor (**A** ATN cells, **B** PoS cells)

since the preferred directions tend to follow the cue card despite the lack of coherent inertial cues (under normal circumstances when the rat moves about, rotations of the visual cues are produced by self-rotations in the opposite direction), the results show that the visual cues dominate over the inertial cues under these conditions – our pilot experiments indicate that the olfactory cues on the wall exert no reliable effect on the preferred directions (Zugaro, Fouquier, Tabuchi, unpublished observations). However, the preferred directions rotate significantly less than the cue card: this trend to underrotation indicates that the cue card does not exert complete control upon the HD system.

Experiment 2: rotation of the wall and floor

Manipulation

In this experiment, we recorded the HD cells for 5 min, then rotated the wall and floor of the cylinder together, and recorded for 5 more min (angles of rotation included –180°, –90°, –45°, +45°, +90° and +180°).

Results

For this experiment, 28 ATN and 13 PoS HD cells were recorded in the 7 rats (in a total of 18 and 8 recording sessions, respectively). The main characteristics of the tuning curves of these cells are displayed in the middle two rows of Table 1.

The shifts in preferred directions ($\Delta\theta$) were plotted against the angles of rotation of the wall and floor ($\Delta\alpha_{both}$) (Fig. 7). All angles were measured relative to the fixed reference frame of the experimental room. Similar to experiment 1, there was a linear relation between shifts in preferred directions and angles of rotation of the wall and floor.

Linear regression analyses yielded: $\Delta\theta=0.95\Delta\alpha_{both}+2.47°$ ($r^2=0.99$) for ATN cells, and $\Delta\theta=0.91\Delta\alpha_{both}+1.85°$ ($r^2=0.99$) for PoS cells. In both cases, the regression slope was highly significant ($P<0.001$), while the intercept value was not ($P>0.1$). When replacing data obtained for simultaneously recorded cells by their mean, linear regression analyses were similar (Fig. 8).

Data points in Fig. 8 were represented differently depending on the hemisphere the cells were recorded from. This showed no obvious combined effect of sense of rotation and lateralization.

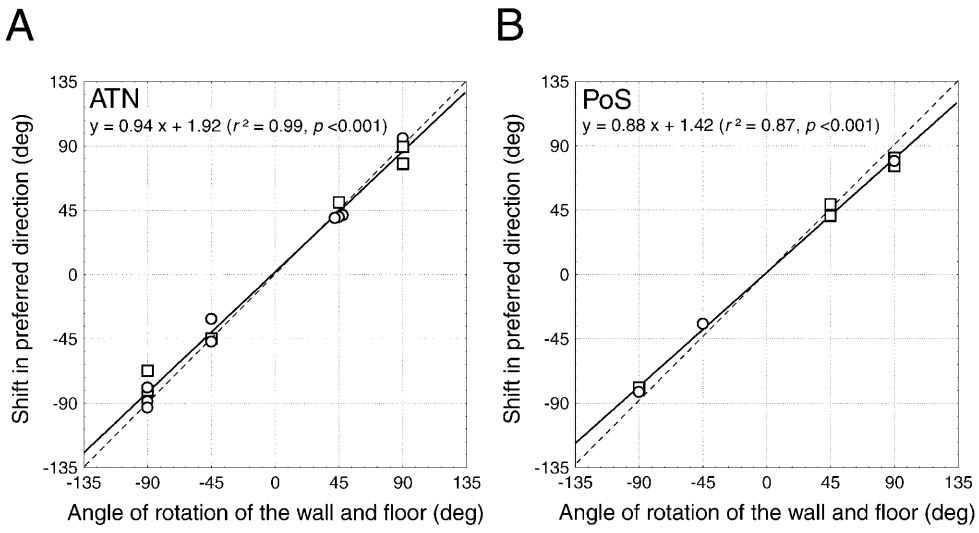

Fig. 8 Linear regression analysis of the effects of rotating the wall and floor of the cylinder upon the preferred directions of the HD cells (**A** ATN, **B** PoS). Each point is the average shift in the preferred directions of all cells recorded simultaneously in a given session. The data points are plotted along with the regression line (*continuous line; the dashed line* shows where the points would appear if the wall and floor exerted complete control upon the preferred directions). The equations of the regression lines are indicated above. *Symbols* indicate the hemisphere from which the cells were recorded (*circles, left; squares, right*)

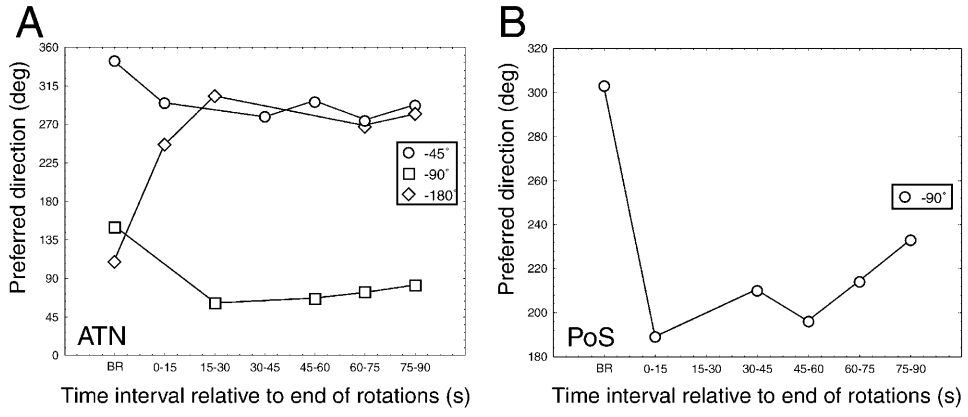

Fig. 9A,B Time course of preferred direction shifts after rotations of both wall and floor. Tuning curves are computed during successive 15-s blocks after rotations ended (**A** ATN cells, **B** PoS cells)

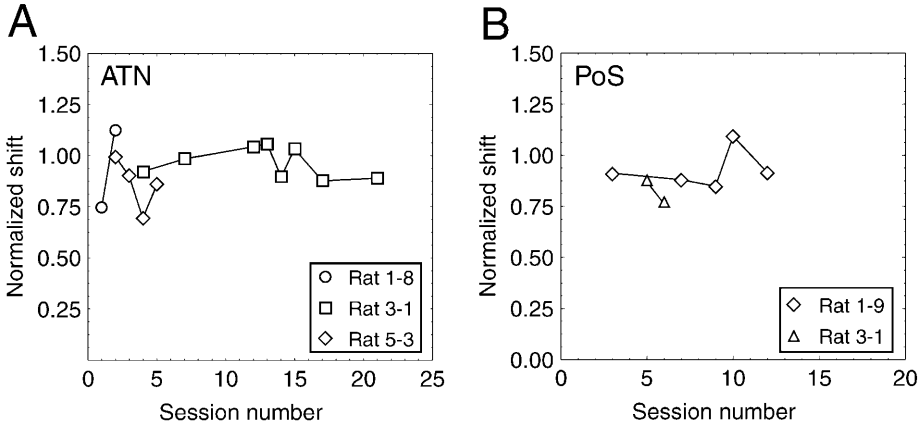

Fig. 10A,B Averaged preferred direction shifts after wall and floor rotations in successive recording sessions. For each rat, normalized shifts in preferred directions (shifts divided by wall rotation angles) are plotted against session number. Sessions where no cells were isolated are counted. Data have been excluded for rats having only one recording session for a given structure (**A** ATN cells, **B** PoS cells)

As in experiment 1, to test for differences between responses to wall and floor rotations in ATN and PoS recordings, linear regression analysis was conducted on the pooled data. A *t*-test on the two groups of residuals showed no significant difference between the two groups ($P>0.1$). This provides evidence that there was no significant difference between the results from ATN and PoS recordings in this experiment.

To test whether the preferred directions shifted significantly less than the wall and floor, the difference between complete (100%) and observed shifts in preferred directions was examined as a function of wall rotation angles. Linear regression analyses showed that the shifts in preferred directions are significantly different from rotation angles of the wall and floor (ATN: $r^2=0.28$, $P<0.05$ for slope, $P>0.1$ for intercept offset;

PoS: r^2=0.83, P<0.01 for slope, P>0.1 for intercept offset).

Similar to experiment 1, Fig. 9 shows that the preferred directions of the HD cells shifted to their new orientation within 15 s after wall and floor rotation and showed no apparent tendency for drift afterward. Similar to experiment 1, the control exerted by the wall and floor cues did not depend on the experience of the rats (Fig. 10).

In order to determine whether the effect of rotating both the wall and floor together was different from the effect of rotating the wall alone, we conducted a *t*-test on the residuals of a pooled regression (using the same methods as described above). This showed no significant difference between the two conditions (P>0.1 for ATN recordings, and P>0.1 for PoS recordings).

Discussion

The results indicate that the ensemble of cues within the cylinder exert a strong but incomplete influence on the preferred directions of both populations of HD cells. However, the shifts in preferred directions are not significantly different from those observed in the previous experiment. This suggests that the influences of wall and floor cues are not combined in a linear manner. Alternatively, floor cues may not exert any influence at all on the preferred directions of the HD cells under these experimental conditions.

Experiment 3: rotation of the floor only

Manipulation

In this experiment, we recorded the HD cells for 5 min, rotated the floor of the cylinder, and recorded for 5 more min (angles of rotation included –180°, –90°, –45°, +45°, +90° and +180°).

Results

A total of 28 ATN and 14 PoS HD cells were recorded in the 7 rats (in a total of 18 and 7 recording sessions, respectively). The main characteristics of the tuning curves of these cells are displayed in the last two rows of Table 1.

The shifts in the preferred directions ($\Delta\theta$) were plotted against the angles of rotation of the floor ($\Delta\alpha_{floor}$). All angles were measured in the fixed reference frame of the experimental room. Similar to previous experiments, there was a linear relation between shifts in preferred directions and floor rotation angles. Linear regression analyses yielded $\Delta\theta=0.04\Delta\alpha_{floor}–0.02°$ (r^2=0.16) for ATN cells, and $\Delta\theta=–0.001\Delta\alpha_{floor}+1.94°$ (r^2=0.002) for PoS cells. The regression slopes were not significant (P>0.05 for ATN and P>0.5 for PoS), and neither were the intercept values (P>0.1 in both cases).

The linear regression analyses for values averaged for each recording were similar (Fig. 11).

Similar to previous experiments, there was no significant difference between the results from ATN and PoS recordings (*t*-test on the two groups of residuals obtained from a linear regression analysis on the pooled data, P>0.5).

Discussion

The results indicate that substratal cues (such as odors or tactile cues on the floor) alone do not exert any significant influence on the preferred direction of the HD cells under these experimental conditions.

General discussion

In this study, we examined the influence of visual, inertial and substratal cues upon the HD cell system. The results show that, in this paradigm, visual cues have a

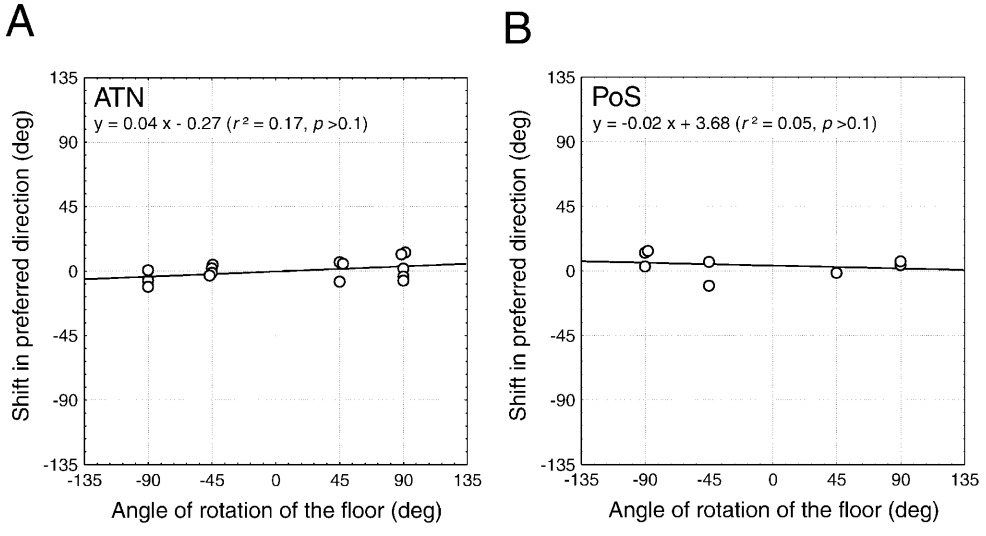

Fig. 11 Absence of effect of rotating only the floor of the cylinder upon the preferred directions of the HD cells (**A** ATN, **B** PoS). Each point is the average shift in the preferred direction of all cells recorded simultaneously in a given session. The data points are plotted along with the regression line (*continuous line*). The equations of the regression lines are indicated *above*

Table 2 Influences of the diverse cues on the preferred directions of the HD cells (measured relative to the experimental room) for the three experiments. As a reminder, the experimental (normalized) shift in preferred directions observed during the recordings is given in the last column. This indicates the relative influence of the cues

Type of rotation	Question 1	Question 2			Observed shift in preferred directions in ATN and PoS cells
	Does the HD change relative to the room?	Does this type of cue indicate that the HD has changed? A conflict with answer to question 1 would provoke a shift in preferred directions (indicated in parentheses)			
		Visual cues	Inertial cues	Substratal cues	
Wall	No	Yes (shift)	No (no shift)	No (no shift)	≈90%
Both	Yes	No (shift)	Yes (no shift)	No (shift)	≈90%
Floor	Yes	Yes (no shift)	Yes (no shift)	No (shift)	≈0%

strong but incomplete influence upon the updating of the preferred directions of the HD cells. In particular, although the preferred directions tend to recalibrate relative to the cue card when it is rotated, the angle of rotation is smaller than that of the cue card. In the following, we suggest that underrotation is due to the influence of inertial cues. Throughout this discussion, the preferred directions are measured in the fixed reference frame of the experimental room.

Resolving multisensory conflicts

In order to determine the respective influences of the diverse cues in our experiments, it will be helpful to answer the following two questions in each experiment for each type of cue: (1) after the cue rotation is performed, is the head of the rat oriented in a different direction *relative to the experimental room*? (2) does this cue indicate to the rat that its head has rotated *relative to its previous orientation*? If the answers to these two questions are different, this conflict could trigger a shift in the preferred directions of the HD cells (measured relative to the experimental room). Since all of our environmental manipulations induced conflicts between the diverse types of cues, the magnitudes of shifts in preferred directions observed above indicate the relative influence of each type of cue.

After rotation of only the wall of the cylinder, the head of the rat does not point to a different direction (relative to the experimental room). However, the new orientation of the cue card relative to the rat indicates that the head of the animal now points in a different direction. If the preferred directions of the HD cells depended solely on visual cues, they would shift after the rotation of the wall. On the other hand, since the rotation of the wall does not provide any inertial stimuli, the inertial cues indicate that the head of the animal has not moved. Similarly, since there is no movement of the floor relative to the rat, the substratal cues also indicate that the head has not moved. Hence, inertial and substratal cues would not tend to provoke a shift in preferred directions after rotation of the wall. This is summarized in the first row of Table 2.

After rotation of both the wall and floor of the cylinder together, the head of the rat points in a different direction (relative to the experimental room). However, the orientation of the cue card relative to the rat does not change, and this visual input indicates that there was no displacement of the head of the animal. Similarly, since the floor is not rotated relative to the rat, the substratal cues also indicate that the head has not moved. If the preferred directions of the HD cells depended solely on visual or substratal cues, they would shift after the rotation of the wall and floor. On the other hand, the inertial cues provided by this passive rotation indicate that the head of the animal now points in a different direction, and would not tend to provoke any shift in preferred directions after the rotation of the wall and floor. This is summarized in the second row of Table 2.

Finally, after rotation of only the floor of the cylinder, the head of the rat points in a different direction (relative to the experimental room). The new orientation of the cue card relative to the rat indicates that the head of the animal now points in a different direction. Similarly, the inertial stimuli provided by the passive rotation also indicate that the head of the animal now points in a different direction. If the preferred directions of the HD cells depended solely on visual or inertial cues, they would not shift after the rotation of the floor. On the other hand, since the floor is not rotated relative to the rat, the substratal cues indicate that the head of the animal points in the same direction, and would tend to provoke a shift in preferred directions after the rotation of the floor. This is summarized in the final row of Table 2.

The results showed that all shifts in preferred directions occurred rapidly and were consistent across recording sessions. This indicates that under these experimental conditions where manipulations were not abrupt (cue rotations typically lasted a few seconds), the HD cell system was able to resolve cue conflicts in an efficient manner.

Note that, during environmental manipulations, the rats often continue moving about, and associated sensorimotor activity also provides orienting cues. However, since there are no conflicts, the normal mechanisms called into play during active movement should make the HD system automatically compensate for these voluntary

movements. Therefore the self-initiated movements of the rats during the experimental manipulations should not affect the shifts in preferred directions.

Relation to previous studies

Our results are consistent with previous studies indicating the strong influence of visual cues on HD cell preferred directions. Taube et al. (1990b) recorded HD cells in the PoS and ATN (Taube 1995; Goodridge and Taube 1995) before and after rotating a cue card by 90°. They observed a similar shift in the preferred directions of the HD cells. This was interpreted as evidence for a control of the cue card over the preferred directions of the HD cells. The mean absolute difference between the angle of rotation of the cue card and the shift in preferred direction was approximately 13° for ATN cells and 20° for PoS cells (10/15 ATN cells underrotated and 3/15 overrotated, while 10/16 PoS cells underrotated and 6/16 overrotated). This was interpreted as indicating that the cue card exerts imperfect control on the preferred directions, but alternate influences could not be tested because, in these experiments, the rat was removed from the experimental cylinder during card rotations, and was disoriented. Also, the floor paper was changed before the rat was reintroduced into the cylinder. Note that in our experiments the mean difference between the angle of rotation of the wall and the shift in preferred direction was only 8° for both structures (data for rotations of the wall by 90°), *but* with a significant trend for underrotations. Such an influence of inertial cues could not be tested in previous experiments where the rat was intentionally disoriented before being returned to the cylinder (Taube et al. 1990b; Taube 1995).

To examine the interactions between visual and inertial cues, Knierim and colleagues (1998) recorded ATN HD cells before and after rotating the whole experimental apparatus (wall and floor). They observed a strong control of the visual cues for small rotation angles (+45°), but not for larger ones (+180°). In particular, three HD cells were tested under conditions comparable to those of our study (rotations of +45° in a familiar cylinder). The results for these cells are not consistent with those reported here: in all three cells, the preferred directions shifted more than the angle of rotation of the cylinder (range of overrotation: +3° to +15°). This may be due to differences in methods and analyses (Fisher-344 rats have poorer vision than the Long-Evans rats used here, the recordings lasted only 2–3 min, the rotations of the apparatus were almost instantaneous, the resolution of the tuning curves was 10°, each bin was averaged with the two closest bins, the preferred direction was defined as the bin with the highest firing rate, etc.), or the small sample of the latter study. Some of these differences may also explain why, contrary to our results, Knierim et al. observed that visual landmark control was delayed after large apparatus rotations (135° or 180°): the HD cells maintained their preferred directions immediately after the rotations, then slowly drifted over the course of a minute or two until they were realigned with the cue card. In our study, the shifts in preferred directions after rotations of the visual landmarks usually occurred in less than 15 s (for large as well as small angles). The model of Zhang (1996) actually predicts that the preferred directions should "jump" to their new orientation after large rotations, whereas transitions for smaller angles should be smooth. This is not inconsistent with our results, because the time course of such "jumps" or smooth transitions is predicted by the model to be on the order of 1 s, too rapid for detection with our techniques.

Blair and Sharp (1996) investigated the respective importance of dynamic visual cues and inertial cues in ATN HD cells: they applied passive rotations of the animal and visual field rotations separately or simultaneously. The visual cues consisted of a series of four vertical black and white stripes taped on the inner wall of the experimental cylinder, which ensured that the visual pattern remained the same after rotation of the wall by an angle of 90°. It must be emphasized that since the four cue cards were symmetrically placed, they did not polarize the environment like the cue cards in other studies, and they could not have served as a landmark cue. When the wall and the floor were rotated together (thus in the absence of any visual field flow), in most cases the preferred directions did not change relative to the room. Since the rat was actually rotated passively at perceptible velocities, and there was no optic flow, the stability of the preferred directions could be provoked only by inertial cues (see row 2, column 4 of Table 2). Moreover, when the wall alone was rotated by multiples of 90°, there were no shifts in the preferred directions (note that this provided no inertial stimulation, simply visual field motion – and, after the rotations, the environment appeared unchanged). This indicates that inertial cues dominate over visual motion cues, and points to the important distinction between optic field flow (not taken into account separately in our treatment above) versus visual landmark cues. This distinction explains why the results of Blair and Sharp (1996) are not inconsistent with those of Taube et al. (1990b; Taube 1995).

In the present study the effect of cue rotations upon the preferred directions of the HD cells did not vary across recording sessions as the rats became more experienced with the experimental conditions. In particular, the cue card continued to exert a strong control on the preferred directions even when the rats had experienced many wall rotations (more than 20 rotations each for 3 animals). Similarly, Knierim et al. (1995) found that the visual landmark cues, provided that they were stable from session to session during training, retained their strong influence on the preferred directions of ATN HD cells even when disorientation procedures repeatedly induced conflicts between visual and inertial cues. In our study, the rats had experienced the cylinder as stable for many days or even weeks before the first experiments were conducted. It is interesting that the influence of the cue card was not altered by the fact that the rats could see it being ro-

tated during the experiments. However, it is noteworthy that one of our rats also showed only a small shift in preferred directions after wall rotations by 180° in two recording sessions. This occurred only after the rat had been trained in the dark with asymmetrically placed olfactory cues. Although previous work suggests that the influence of visual landmark cues becomes stochastic after large rotations (Knierim et al. 1998), in our study this absence of shifts in preferred directions was not observed in the other rats. It is possible that the new experimental conditions trained the rat to use different strategies to orient itself within the cylinder, and this could have weakened the influence of visual cues observed here.

Finally, shifts in the preferred directions did not appear to depend on the hemisphere from which the HD cells were recorded, even when taking into account the sense of rotation of the cues. Together with the finding that the tuning curves of the HD cells in ATN, contrary to those of the HD cells in the lateral mammillary body (LMN), are not different during ipsiversive (toward the hemisphere of the cell) versus contraversive (in the opposite direction) head turns (Blair et al. 1998), this indicates that ATN and PoS HD cells may not have hemispherically lateralized properties. Alternatively, the effects could be very weak, and would require more data to appear.

In summary, under the present experimental conditions (where visual cues are salient), visual and inertial cues have unequal influences on HD signals. This is consistent with the notion that visual cues could be used to stabilize and realign directional responses continuously updated by self-motion cues (Mizumori and Williams 1993; McNaughton et al. 1993).

Acknowledgements We thank Prof. A. Berthoz for support in all aspects of this work; Profs. J.S. Taube and P. Sharp for critical reading and comments on earlier versions of the manuscript; C.F. Fouquier for help with data analysis; M.-A. Thomas and N. Quenech'du for the histology; Dr. J. Droulez for advice on the statistical tests; A. Treffel, M. Ehrette and S. Ilic for the construction of the behavioral apparatus; F. Maloumian for illustrations; and D. Raballand for animal care. This work was supported by CNES, Cogniseine, and GIS.

References

Blair HT, Sharp PE (1996) Visual and vestibular influences on head-direction cells in the anterior thalamus of the rat. Behav Neurosci 110:643–660

Blair HT, Cho J, Sharp PE (1998) Role of the lateral mammillary nucleus in the rat head direction circuit: a combined single unit recording and lesion study. Neuron 21:1387–1397

Chen LL, Lin L-H, Green EJ, Barnes CA, McNaughton BL (1994) Head-direction cells in the rat posterior cortex. I. Anatomical distribution and behavioral modulation. Exp Brain Res 101:8–23

Dudchenko PA, Goodridge JP, Taube JS (1997) The effects of disorientation on visual landmark control of head direction cell orientation. Exp Brain Res 115:375–380

Goodridge JP, Taube JS (1995) Preferential use of the landmark navigational system by head direction cells in rats. Behav Neurosci 109:1–12

Goodridge JP, Dudchenko PA, Worboys KA, Golob EJ, Taube JS (1998) Cue control and head direction cells. Behav Neurosci 112:749–761

Knierim JJ, Kudrimoti H, McNaughton BL (1995) Hippocampal place fields, the internal compass, and the learning of landmark stability. J Neurosci 15:1648–1659

Knierim JJ, Kudrimoti HS, McNaughton BL (1998) Interactions between idiothetic cues and external landmarks in the control of place cells and head direction cells. Am Physiol Soc 80:425–446

McNaughton BL, Markus EJ, Wilson MA, Knierim JJ (1993) Familiar landmarks can correct for cumulative error in the inertially based dead-reckoning system. Soc Neurosci Abstr 19:795

Mizumori SJY, Williams JD (1993) Directionally selective mnemonic properties of neurons in the lateral dorsal nucleus of the thalamus of rats. J Neurosci 13:4015–4028

Muller RU, Kubie JL, Ranck JB, Jr (1987) Spatial firing patterns of hippocampal complex-spike cells in a fixed environment. J Neurosci 7:1935–1950

Ranck JB, Jr (1984) Head-direction cells in the deep cell layers of dorsal presubiculum in freely moving rats. Soc Neurosci Abstr 10:599

Recce M, O'Keefe J (1989) The tetrode: a new technique for multi-unit extracellular recording. Soc Neurosci Abstr 1250

Stackman RW, Taube JS (1997) Firing properties of head direction cells in the rat anterior thalamic nucleus: dependance on vestibular input. J Neurosci 17:4349–4358

Stackman RW, Taube JS (1998) Firing properties of rat lateral mammillary single units: head direction, head pitch, and head angular velocity. J Neurosci 18:9020–9037

Taube JS (1995) Head direction cells recorded in the anterior thalamic nuclei of freely moving rats. J Neurosci 15:70–86

Taube JS, Muller RU, Ranck JB, Jr (1990a) Head-direction cells recorded from the postsubiculum in freely moving rats. II. Effects of environmental manipulations. J Neurosci 10:436–447

Taube JS, Muller RU, Ranck JB, Jr (1990b) Head-direction cells recorded from the postsubiculum in freely moving rats. I. Description and quantitative analysis. J Neurosci 10:420–435

Wiener SI (1993) Spatial and behavioral correlates of striatal neurons in rats performing a self-initiated navigation task. J Neurosci 13:3802–3817

Zhang K (1996) Representation of spatial orientation by the intrinsic dynamics of the head-direction ensemble: a theory. J Neurosci 16:2112–2126

Zugaro MB, Tabuchi E, Fouquier CF, Wiener SI (1999) In updating the preferred direction of head direction cells, visual cues dominate, but self-motion cues exert a significant influence. Soc Neurosci Abstr 25:1383

ELSEVIER

Behavioural Brain Research 117 (2000) 173–183

BEHAVIOURAL BRAIN RESEARCH

www.elsevier.com/locate/bbr

Research report

Lesions of the medial shell of the nucleus accumbens impair rats in finding larger rewards, but spare reward-seeking behavior

Sergey V. Albertin [1], Antonius B. Mulder [2], Eiichi Tabuchi [3], Michaël B. Zugaro, Sidney I. Wiener *

Laboratoire de Physiologie de la Perception et de l'Action, CNRS-Collège de France Laboratoire de Physiologie de la Perception et de l'Action, 11, place Marcelin Berthelot 75231 Paris Cedex 05 France

Received 25 April 2000; received in revised form 25 July 2000; accepted 25 July 2000

Abstract

The goal of this study was to help better understand the importance of the nucleus accumbens (Nacc) in the processing of position and reward value information for goal-directed orientation behaviors. Sixteen male Long–Evans rats, under partial water deprivation, were trained in a plus-maze to find water rewards in the respective arms which were lit in pseudo-random sequence (training trials). Each day one reward arm was selected to deliver six drops of water (at 1 s intervals) the others provided only one drop per visit. After 32 visits, probe trials were intermittently presented among training trials. Here, all four arms were lit and offered the previously assigned reward. The rats rapidly learned to go to the highly rewarded arm. Six trained rats were given bilateral electrolytic lesions in the Nacc shell, two others had unilateral lesions and eight had sham operations (with approved protocols). Field potentials evoked by fornix stimulation were recorded in lesion electrodes to guide placements. Only the lesioned rats showed significant impairments ($P < 0.05$) in selecting the greater reward on probe trials. However on training trials, lesioned (and sham-operated) rats made only rare errors. While the motivation to drink and the capacity for cue-guided goal-directed orientation behavior was spared, lesioned rats were impaired in learning the location of the larger reward. The accumbens lesions apparently impaired integration of position and reward value information, consistent with anatomical and electrophysiological data showing the convergence of hippocampal, amygdalar, ventral tegmental area (VTA) and prefrontal cortical inputs there.

Keywords: Ventral striatum; Motivation; Hippocampus; Amygdala; Spatial learning; Navigation

1. Introduction

Both anatomical [5,8,9,11] and neurophysiological data [12,16,17,23] indicate that the shell region of the nucleus accumbens (Nacc) is a site of integration of spatial (from ventral hippocampal CA1/subiculum) and reward information (from ventral tegmental area, that is, VTA, as well as amygdala). This convergence of afferents in the Nacc could provide the principal information required to accurately navigate in space, namely the relation between the present location of the animal, the environmental cues, the motivation to go to (or avoid) other locations and reward availability. Furthermore since the major projection areas of the Nacc consist of various motor, effector and activating regions such as the ventral pallidum, pedunculopontine nucleus, hypothalamus, substantia nigra and VTA, this suggests that the Nacc is involved in the initiation of goal directed behaviour.

* Corresponding author. Tel.: +33-1-44271621; fax: +33-1-44271382.

E-mail address: sidney.wiener@college-de-france.fr (S.I. Wiener).

[1] Present address: Pavlov Institute of Physiology, Russian Academy of Science, nab. Makarova 6, St. Petersburg 199034, Russia.

[2] Present address: Netherlands Institute for Brain Research, Meibergbreef 33, 1105 AZ Amsterdam, The Netherlands.

[3] Present address: Department of Physiology, Faculty of Medicine, Toyama Medical and Pharmaceutical University, 2630 Sugitani, Toyama 930-0194, Japan.

0166-4328/00/$ - see front matter
PII: S0166-4328(00)00303-X

However behavioral studies have revealed conflicting results following lesions of the Nacc. Electrolytic and neurochemical lesions of the Nacc induce impairments in alternation and reversal learning in the T-maze [2,24] and learning of a win/shift version of an eight-arm radial maze [22]. However Floresco, et al. [7] and Schacter, et al. [21] found no such impairments. Other studies have employed the T-maze that has been challenged as to whether it tests for spatial learning, or simply motor responses. In this task both Annett et al. [2] and Taghzouti et al. [24] concluded that the impairments demonstrated following Nacc lesions had no relation to spatial localization capacities in their rats.

Deficits in acquisition of the water maze task (with the submerged escape platform) are caused by Nacc lesions with ibotenic acid or intraccumbens haloperidol injections [20], but not by 6-OHDA dopamine depletion in Nacc and prefrontal cortex [10] or intra-accumbens lidocaine injections [7]. However the lesioned animals do eventually succeed at locating the platform [2]. This suggests that other brain systems can be involved in learning this task, albeit more slowly, perhaps by habit learning or simple guidance strategies rather than the use of configurational cues or 'mapping'. Thus successful performance in this task, at least with the analyses and criteria used by the latter authors, is possible with brain structures other than Nacc, and in this respect the water maze task lacks specificity.

In an attempt to surmount these difficulties in studying the specific role of the Nacc shell in orientation and displacement behaviors, we have developped a new behavioral task requiring rats on a daily basis to learn which maze arm is currently providing the largest rewards. Daily changes in the location of the largest reward prevents habit-learning from being employed successfully. Rather, the task permits analyses to discriminate several different types of strategies (motor response, place preference, or actual acquisition of a position-reward association). It also has low working memory demands. In addition, the frequent cue-guided trials provide a control for the level of motivation.

Possible reasons for the equivocal results concerning the role of Nacc (shell and core regions) in spatial behavior may be related to lesion-making methodology. Difficulties may arise from the fact that some studies include uncontrolled combinations of lesions to the shell and core regions of the Nacc, each of which have different anatomical connectivity and neurochemical properties. But even more anatomically selective lesions of the Nacc shell by micro-injections of lidocaine [22] or kynurenic acid (a glutamate antagonist) [21] have led to different results in rats performing the same win/shift version of the eight-arm radial maze. Perhaps this is caused by anatomical constraints: the thin Nacc shell extends along the medial and ventral surface of the Nacc core for its entire rostro-caudal extent. Small single injections might have inactivated different fractions of the Nacc shell, and risked nonetheless to have spread to the adjacent core. Furthermore fibres of passage would continue to innervate the spared portions of the Nacc shell.

Here we selected the electrolytic lesion technique. This permitted electrode placements under guidance of field potentials evoked by fornix stimulation. In this way, its position in the hippocampal projection zone could be directly verified. In addition, a massive destruction of afferent fibers from hippocampus was desirable since the shell region of nucleus accumbens is too widespread and narrow to conveniently permit a comprehensive but restricted series of microlesions. Since anatomical studies have shown that the hippocampal and amygdalar inputs to the nucleus accumbens enter through the dorsal part of the medial shell, medial to the anterior commissure [8], we directed lesions to this zone. Thus while no lesions were made to the ventral shell, the anatomical data indicate that these electrolytic lesions also likely interrupted its afferents from amygdala and hippocampus. Some of these results have previously been presented in abstract form [1].

2. Material and methods

2.1. Experimental animals

Sixteen male Long–Evans rats (320–350 g; CERJ, Le Genest-St-Isle, France) were water deprived during weekdays and maintained at not less than 85% body weight. Food was provided ad libitum. Animals were weighed and examined daily. In training and recording sessions the rats were permitted to acquire water until satiation, then supplemental water was provided as necessary to maintain body weight. Rats were permitted to rehydrate completely prior to weekends. All animal experimental protocols as well as housing conditions were in strict adherence with institutional, national and international standards and regulations. The animals were maintained in an animal care facility with lighting on a 12 h on/12 h off cycle.

2.2. Behavioral task and experimental design

In a square black curtained enclosure (3×3 m, see Fig. 1), a white poster board (180×60 cm) was mounted on the wall opposite the entrance. The poster board was lit up during training and experiments and served as the principal environmental cue. The experimenters and all equipment were outside the curtains. An elevated black platform (180 cm diameter) was situated at the center of the enclosure. Barriers in the form of outwardly inclined wall inserts (25 cm high) were positioned on the platform to form a plus maze

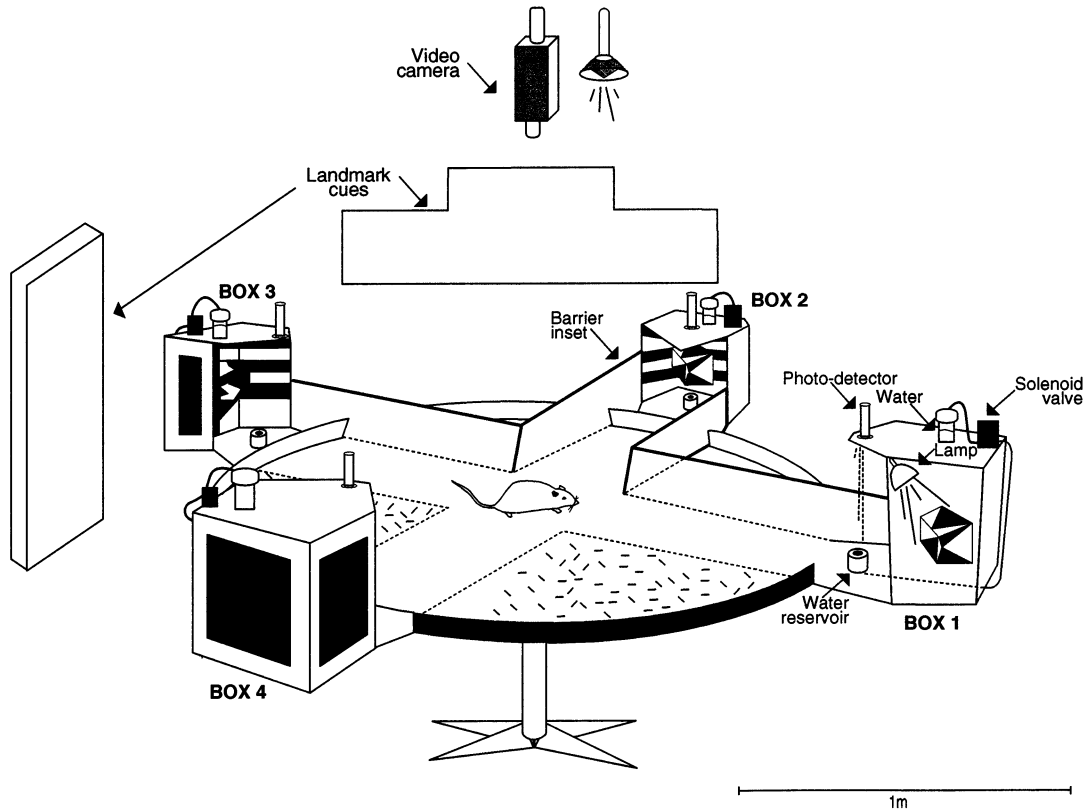

Fig. 1. The experimental plus maze was bordered by inclined walls and had four identical reward boxes. In the automated task under computer control, drops of water were delivered from water reservoirs through the respective solenoid valves when the rat blocked the photodetectors. There were two principal landmark cues on the walls outside the maze to aid the rat in orienting in the experimental environment.

with 30 cm wide arms. At the end of each arm were identical alcoves ('reward boxes'; $30 \times 30 \times 30$ cm). In each box, near the edge of the platform, was a short cylinder with a slight recess at the center of the top surface. A hole drilled from the bottom of this recess to the bottom of the cylinder transmitted water rewards which arrived via tubing connected to a solenoid valve and an elevated reservoir. Mounted in the back of the reward box was a highly contrasted, mobile polyhedron that served as a visual cue. The cues were identical in each reward box and could be illuminated independently under computer control. Delivery of water rewards in the respective boxes was automatically triggered after the rat arrived and tripped a photobeam mounted above the water reservoir.

2.3. The behavioral task (Fig. 2)

During training trials, reward boxes were illuminated one by one and water rewards were only available at the lit box. When the rat arrived at the center a photodetector automatically triggered the light to go on at the next reward box. There was no signal for error trials other than withholding water, and the box remained lit until the rat arrived there. The reward boxes were lit in a pseudo-random sequence that never pro-

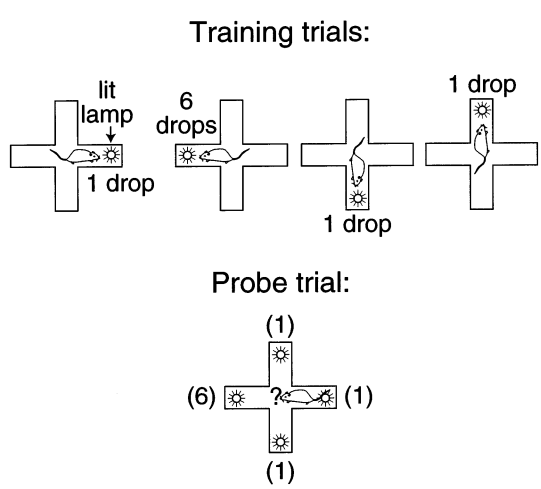

Fig. 2. The behavioral task. The rats were trained to get water rewards at the lit box (training trials). The boxes were lit in a random sequence. When the rat arrived at the center an automated system triggered the next light, and arrival at the lit box triggered the water reward. Each day a different box was selected to deliver six drops of water while the others delivered only one drop. After 32 visits, probe trials were intermittently presented: all four boxes were lit and armed. Although all boxes provided their ration of water on probe trials, the rats rapidly learned to go to the box delivering six drops of water.

vided more than two successive rewards at the same arm and also avoided requiring more than two successive repetitions of the same type of re-orienting movement upon returning to the maze center (turning left, right or by 180°, going straight ahead). Each day one of the alcoves was selected to deliver six drops of water at 1 s intervals while the others delivered only one drop (calibrated at 30 μl). When the rat arrived at this reward box, this triggered the delivery of the appropriate amount of water. After 32 training trial visits (including eight visits to the arm dispensing six drops of water), probe trials were presented at irregular intervals among the training trials. For probe trials all reward boxes were lit and enabled to deliver their assigned volume of water. Although on probe trials visits to any of the boxes successfully triggered water delivery, the rats rapidly learned to go to the box delivering six drops of water. Since this was the default behavior of all rats, visits to maze arms providing only one drop of water during probe trials will, for brevity, be referred to as 'error trials'. The timing of the blocking and unblocking of the photobeams as well as opening of solenoid valves were all coordinated by our own software (based on programs written by Dr O. Trullier), and executed and recorded by the DataWave data acquisition system (Longmont, CO, USA).

2.4. Performance measures

In each session at least ten probe trials were run, and the score was calculated as the percent of these trials performed correctly. Each rat was tested for 5 successive days prior to surgery, and five more after recovery from surgery. An analysis of variance examined repeated measures in the lesion and sham groups. Pairwise *t*-tests compared the pre-surgery and post-surgery scores measured for each animal. Analyses of response bias in error trials were conducted using the chi-square test. Statistical tests were performed with Statistica® (Tulsa, OK) or Microsoft® Excel.

Testing began about 1 week after the surgery and was repeated on 5 consecutive days. Rats in the lesion group were tested for 2 or 3 additional (and consecutive) days to allow for the possibility of slower relearning of the task. In these cases only data from the final 5 days of testing were analyzed statistically (to assure equal numbers of measures for the pair-wise *t*-tests).

2.5. Lesion surgery

After reaching plateau levels of performance, eight rats were operated surgically to make electrolytic lesions of the Nacc while eight others had sham lesion operations. Rats were returned to ad libatum water for at least 2 days prior to surgery. First they were tranquilized with 0.1 ml xylazine (Rompun®) intramuscularly then anesthetised with 40 mg/kg pentobarbital. The Nacc lesion electrode placement was made by recording from it field potentials evoked by hippocampal stimulation. A pair of 60 μm diameter insulated stainless steel stimulating electrodes separated by one mm were placed in the fornix/fimbria (AP −1.3 mm, ML 0.9 and 1.9 mm). The final depth of the placement of the stimulation electrodes was 3.7 mm, but they were first lowered to 4.0 mm, then raised to overcome possible indentation of the surface without penetration. The lesion electrode (an etched 200 μm acupuncture needle treated with insulating varnish) was placed ipsilaterally under stereotaxic control at AP 1.4 mm, ML 0.7 mm. Stimulus volleys (0.2 μs, bipolar, 0.4–0.6 mA) were delivered to the ipsilateral fornix via the bipolar electrodes. Signals in the lesion electrode were filtered (300–5000 Hz) and amplified with an A-M Systems model 1800 differential amplifier. Data were acquired on a PC hard disk with a Cambridge Electronic Design 1401 data acquisition system (Cambridge, UK) employing their SIGAVG® program which sampled at 5 kHz averaged over 16 stimuli with at least 7 s intervals between each pulse. Positive field potentials at delays 8 and 20 ms (characteristic of the fornix to accumbens pathway [3]) were searched for in recordings at 0.5 mm intervals at depths ranging from 4.5–8 mm (see Fig. 3). Two or three electrolytic lesions (typically 100 μAmp cathodal current for 20 s) were applied at points separated by 0.6–1.0 mm centered within this zone. Lesions were made only along one electrode track starting ventrally then progressing dorsally. If no satisfactory field potentials were evoked along the electrode track, responses were tested at a different electrode placement. Control animals were also operated using the same procedures except that (for six of the eight) only the stimulating electrode was implanted, and the same stimulation was applied 50 times, again respecting the minimum 7 s interval between successive pulse trains. The stimulation procedure was repeated on left and right sides in lesion and sham operated animals. The scalp was closed with suture and treated with Betadine®. The other two sham operated animals only had scalp incisions while under anesthesia.

2.6. Histology

At the end of the experiments, the rats were given full access to food and water. An overdose of pentobarbital was followed by transcardial perfusion with phosphate buffered saline followed by 4% formaldehyde solution in phosphate buffer. Histological sections were cut on a freezing microtome and stained with cresyl violet. The extent of the lesion site was identified as the zone with no remaining neurons.

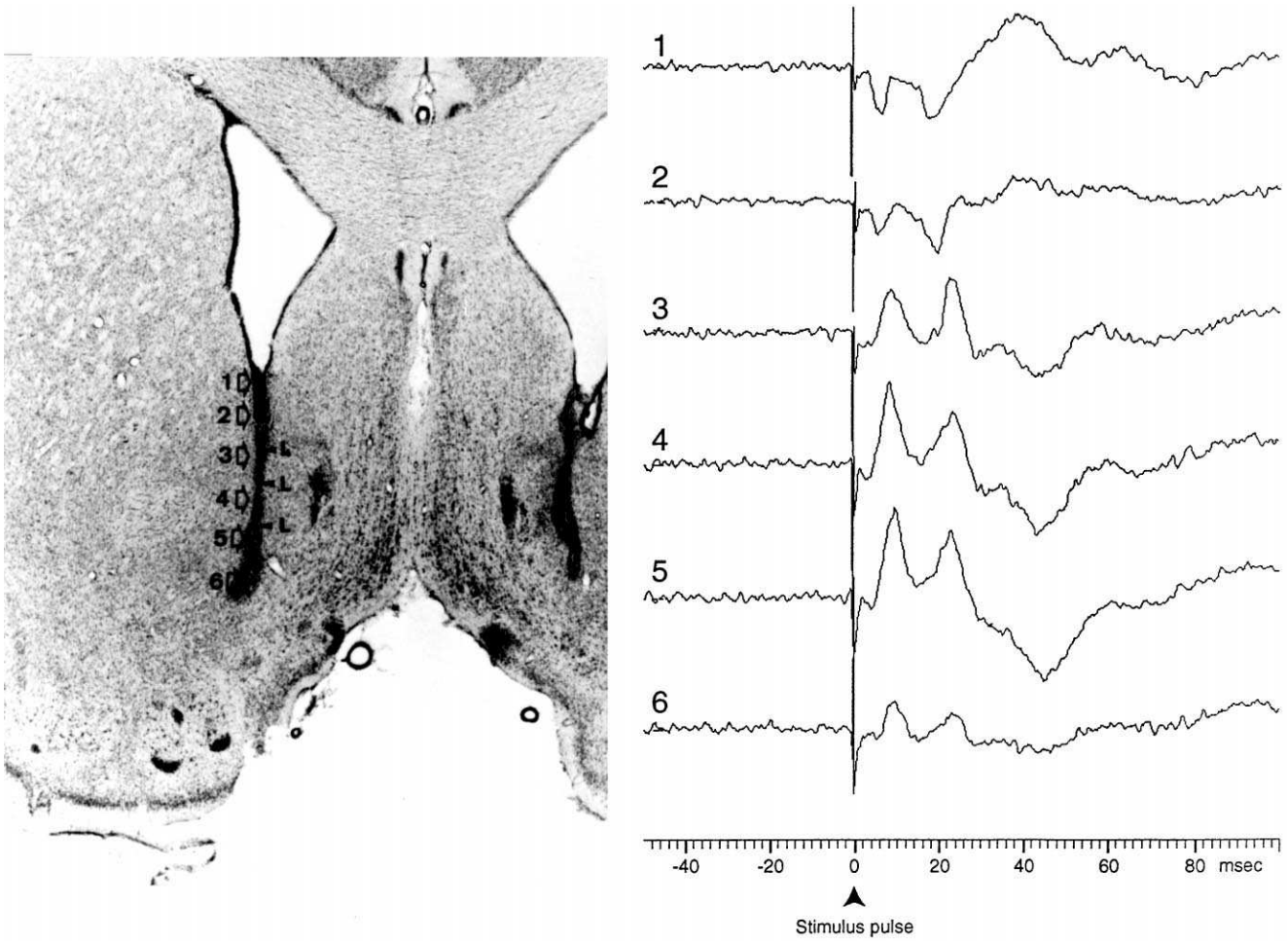

Fig. 3. To the left are the sites of electrolytic lesions. The placements were guided by field potentials evoked by fornix stimulation. Numbers correspond to recording sites; these are 0.5 mm apart. The evoked potentials for the respective sites 1-6 are shown to the right. The sites indicated 'L' correspond to where current was applied through the electrode. (Rat 2-1)

3. Results

The stereotaxic placement of the lesion electrode was confirmed by recording the characteristic positive potentials at latencies of 8 and 20 ms that were evoked by electrical stimulation of the fornix. Fig. 3 shows an example of the reconstruction of the lesion sites and the corresponding field potentials evoked in an electrode track in one of the rats. This corresponds to the coronal plane 1.0 mm anterior to bregma [19]. Recording sites 3, 4 and 5 show the prominent evoked potentials (averaged over ten sweeps), while responses were weaker at position 6. Note that the lesion extends deeper than the site of application of current.

The extent of the damage in each of the lesioned rats is shown in Fig. 4. In the lesion group, cell death in the Nacc was in general restricted to the medial shell region, rarely extended to the ventral shell and never spanned the entire rostro-caudal extent of the shell. In isolated cases damage extended to ventral pallidum, interstitial nucleus of Cajal, islands of Calleja, lateral septum, medial septum, nucleus of the vertical limb of the diagonal band, olfactory tubercle, anterior commissure as well as the medial part of the Nacc core. Usually lesions were in the form of vertically oriented cylinders of diameter 200–300 μm. Rats 2–2 and 2–3 had only unilateral lesions. Rat 1–5 had only a unilateral lesion in a zone medial to the Nacc shell and was excluded from further analysis. Rat 2–6 also had a lesion in the latter zone as well as a well-placed lesion along the medial shell/core border contralaterally — it was retained for analyses. Damage to the fornix (from stimulation electrodes) ranged from minor (track of electrode entry) to negligeable in control and lesion groups (not shown).

Rats were weighed each day. The average weight was computed for each animal for the weeks of pre-operation and post-operation testing. During both of these periods the rats were under water deprivation schedules. The overall average increase in weight was 6.6% for the sham lesion group and 3.0% for the Nacc lesion group. A *t*-test failed to show a significant difference

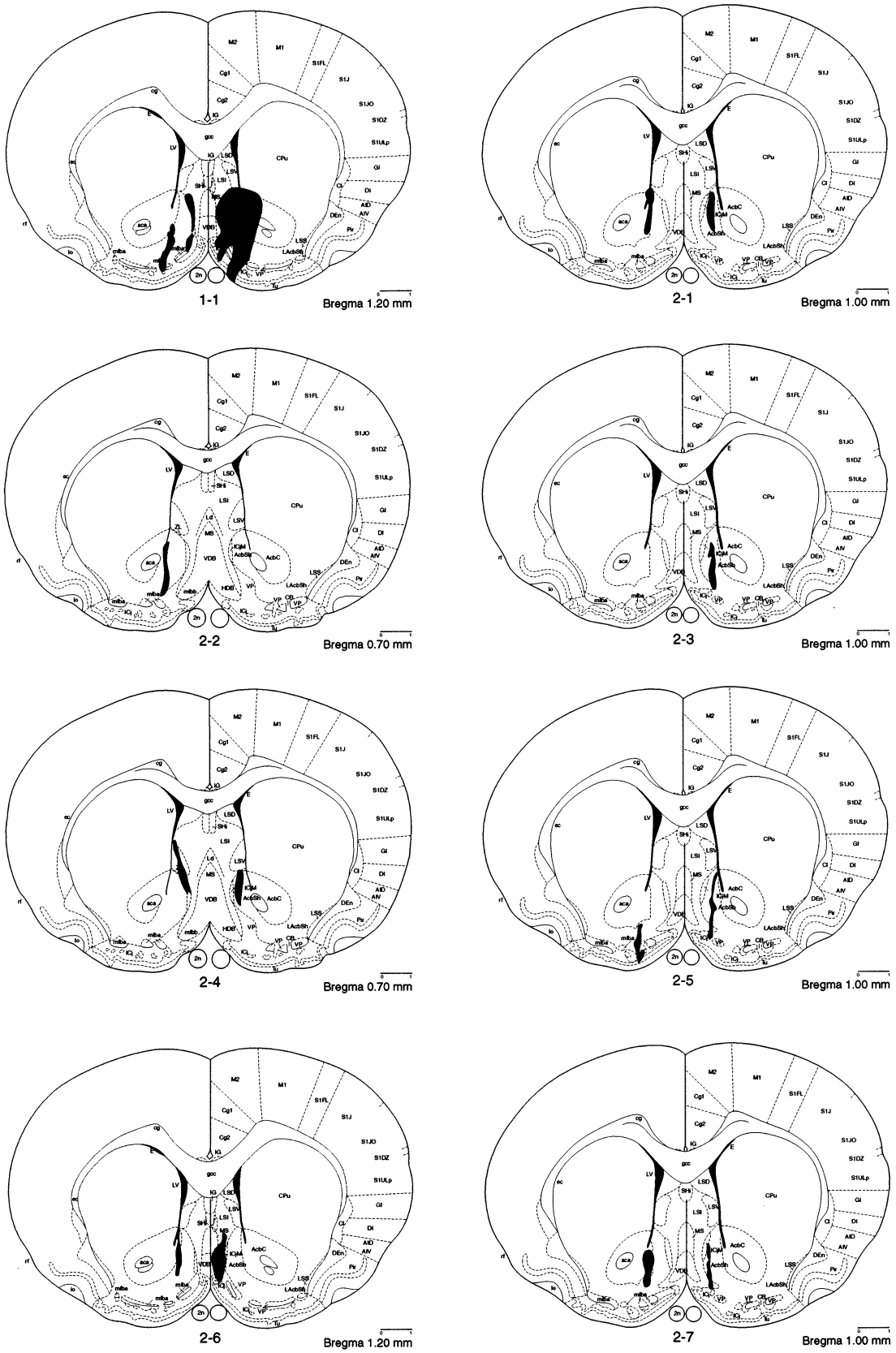

Fig. 4. The section with the maximal extent of the lesions in the coronal plane for each of the rats in the lesion group are indicated by the solid black regions ventral to the lateral ventricles. In general, the lesions were vertically oriented cylinders 200 to 300 μm in diameter. The numbers below each tracing identify the animal. The tracings of the lesions have been superimposed upon figures have been adapted from Paxinos and Watson [19] with permission. Scale bars are 1 mm.

between the weight increases of the two groups ($P = 0.072$).

3.1. Behavioral performance during recording sessions.

Rats of both groups performed almost perfectly on the (light-cued) training trials both prior to and after surgery. The repeated-measures analysis of variance showed significant differences between lesion and sham groups ($F(1, 14) = 21.78$, $P < 0.0004$), between pre- and post-surgery ($F(1, 14) = 498.06$, $P < < 0.0001$) as well as the interaction between these two factors ($F(1, 14) = 316.61$, $P < < 0.0001$). The overall mean score in the sham group diminished only slightly, from $77.3 \pm 2.4\%$ (SEM) prior to surgery to $73.0 \pm 2.9\%$ afterwards (t-test $P = 0.307$; Fig. 5). However in the lesion group the performance average on probe trials plummeted to $40.9 \pm 1.4\%$, from initial levels of $79.0 \pm 2.0\%$ (t-test $P < < 0.0001$). Furthermore dependent t-tests compared, for each individual rat, data measured in the respective weeks prior to and after recovery from surgery (Table 1). Each rat in the lesion group showed significant decreases in performance after surgery while no difference was observed in any of the sham lesioned rats. Even after 1 week of retraining, the best single session performance in the lesion group was 55%. Sham operated controls showed no significant differences in the level of accuracy as compared with pre-operation testing. There were no clear tendencies for performance improvement (or deterioration) over the course of the week of testing in either group. Thus in the group analyses above, the results were averaged for each rat for the pre- and post-surgery periods, respectively.

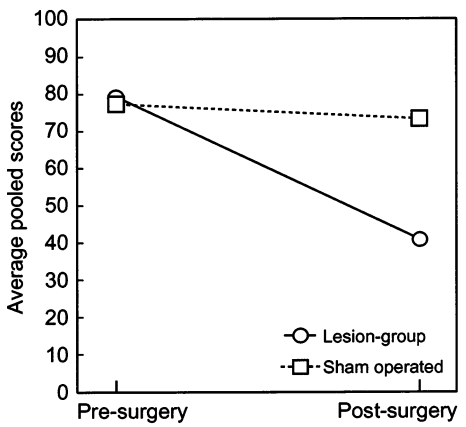

Fig. 5. Performance prior to and after surgery in the sham and lesion groups. Each rat was tested for 5 days prior to and after surgery. The weekly averages for each rat were then pooled for the respective groups.

Table 1
Comparisons of performance prior to and after surgery

	Mean % correct		t-test
Rat	Pre-surgery	Post-surgery	P values
Accumbens medial shell lesion			
2–1	68.6	37.2	0.0135
2–2	77.0	40.8	0.0021
2–3	81.6	45.6	0.0013
2–4	87.6	44.4	0.0000
2–5	79.0	35.0	0.0026
2–6	83.2	43.8	0.0001
2–7	82.2	43.8	0.0072
1–1	72.5	36.7	0.0051
Sham lesion			
3–1	73.8	65.7	0.4753
3–2	64.5	62.8	0.8149
3–3	78.5	77.2	0.8763
3–4	81.0	75.8	0.3893
3–5	78.5	69.3	0.3329
3–6	71.5	65.2	0.1056
1–2	82.5	80.0	0.7650
1–4	88.3	88.3	1.0000

In order to determine whether the errors made by the lesioned rats were random, or rather involved some types of stereotypy, further analyses were performed on their data. The errors on probe trials were analysed to test for two types of perseverance: place preferences or motor responses (turning left, right or going straight or turning 180° at the center). First the errors were examined to determine if the rats showed preferences for particular maze arms (see Table 2). The χ^2 statistic tested whether visits to maze arms on the error trials were disproportionately distributed. In analyses of data pooled from the 5 days of post-operative testing, four of the rats (1–1, 2–1, 2–3, 2–5) showed significant bias in error probe trials, that is, the rats tended to go to certain maze arms more than others (χ^2 test, $P < 0.05$). In analyses of the individual post-operative sessions for each of the eight lesioned rats (five sessions each), in the 'error' probe trials, visits were disproportionately distributed among the boxes in 13 (32%) of the sessions (χ^2 tests; $P < 0.05$). In rats 2–3 and 2–5 this preference for certain maze arms occurred in three of the five sessions, and in two of five sessions in rats 2–1 and 2–4. In all of these sessions, and three sessions in other rats with significant bias in cup selection, the majority of the error choices were for only two of the four maze arms (those opposite the wall with the large visual cue, in the foreground of Fig. 1). However the identities of the preferred arms varied from day to day and among the animals. In seven of the 13 sessions with visits unequally distributed among the low reward arms, a preferred arm was the highly rewarded arm of the previous day, despite the fact that performance on the previous day had been poor (40% correct) in all cases. In six of these seven sessions the preferred, rewarded arms of the previous day were those oriented toward the curtain opposite the large cue. (This curtain separated the experimenters and instrumentation from the

Table 2
Summary of error types in Nacb lesioned rats over 5 days of testing

Maze arms visited during error trials						Preferred re-orientation directions					
Rat number	Arm 1	Arm 2	Arm 3	Arm 4	P value of χ^2	Straight	Left	Right	reverse	P value of χ^2	Sum
1–1	3[a]	13	4	13	0.035	11	14	5	3	0.023	33
2–1	23	10	2[a]	11	0.001	10	8	15	13	0.471	44
2–2	18	12	6[a]	19	0.187	20	25	7	3	0.000	55
2–3	15	4	7	20[a]	0.000	10	13	13	10	0.854	26
2–4	19	13	4[a]	16	0.101	18	8	18	8	0.052	48
2–5	16[a]	6	4	25	0.000	14	21	9	7	0.027	35
2–6	13	8[a]	10	19	0.290	24	14	10	2	0.000	42
2–7	9	19	10	13[a]	0.136	13	30	2	6	0.000	38

[a] This arm was the correct choice on 2 testing days while the others were correct only once. Fewer errors would be expected here.

experimental apparatus.) Thus these error types are partially confounded: the tendencies toward errors at these reward boxes might be related to latent or implicit learning of the reward distribution of the previous day, perhaps in association with some other factors concerning these maze arms. Nonetheless these animals maintained a clear capacity for place preferences. In contrast the same analyses of error trials in the sham lesioned rats showed no significant preference for particular reward boxes or for the box most highly rewarded in the previous session. However the small number of errors in this group may have obscured possible minor tendencies for place preferences.

Secondly, the error trials were studied with respect to the movement that the rat made at the center when re-orienting from the previously visited arm toward the (incorrect) arm providing only one drop of water. This compared the incidence of left turns, right turns, proceeding forward or going in reverse, assuming that these would be equally distributed among the low reward arms. The analyses showed that the re-orienting movements of the rats at the maze center were not equally distributed on error trials in 30% of the sessions. These same sessions only rarely (two out of 40) also showed disproportionate distributions of error visits to particular maze arms in the analyses of the preceding paragraph. In order to determine whether individual rats tended to turn in a particular direction (or go straight ahead) during error trials, the total number of incidences of each type of movement was accumulated for the 5 day testing period (Table 2). χ^2 analyses of these data showed significantly disproportionate distributions of these orientation movements in error probe trials in rats 1–1, 2–2, 2–5, 2–6 and 2–7. In four of these rats, during error trials there were from 2.5 to 15 times fewer turns by 90° to the right (and straight ahead) than to the left, and few 180° turns. In rat 2–4, the result of the χ^2 test missed significance ($P = 0.052$) but there were over twice as many errors involving turning to the right and straight ahead as there were for turning 90° to the left as well as by 180°. The two rats with unilateral lesions showed performance levels and error patterns indistinguishable from those of bilaterally lesioned animals, an observation to be replicated with a larger data set. All but two of the sham lesioned rats also showed significant preferences for certain movement types in their error trials. Interestingly, in all of the latter rats with sufficient data, most errors also involved left turns at the choice point, while 180° turns were least common.

Note that in the analyses of data pooled over all post-operative trials, lesioned rats 1–1 and 2–5 both had significant arm preferences and re-orientation preferences during error trials. These two effects do not appear to be confounded (for example, left turns and visits to cup 1 always occurring together on error trials). In the error analyses of individual sessions from these two rats, only one (of ten) showed significance for both types of bias (χ^2 test). The remaining rats showed either arm preferences or dominant re-orientation movements within a given session. These data indicate that arm preference and movement preference were alternate and unrelated strategies.

4. Discussion

The principal findings of this study are that electrolytic lesions of the medial shell of the Nacc impair learning to go to the maze arm providing the largest rewards, but preserve reward-seeking behaviour that is guided by a visual cue. The latter result, and the fact that the weights of the lesioned animals remained normal, confirms that they were capable of being motivated to execute orienting behaviours toward reward sites [13,22]. Thus the failure in probe trials to seek out the greatest reward was not due to a lack of motivation. In the first part of each session when only training trials were presented, the rats had at least eight trials at the arm providing the largest reward. There rats always

remained until the sixth drop of water was delivered and the cue light was turned off. This and the fact that the six water drops were distributed at 1 s intervals provided the rats ample opportunities to register that greater quantities of water were being given there. In addition, the probe trials were presented intermittently among cue-guided training trials that continued to include visits to the arm providing large rewards.

In the animals with accumbens lesions, reward box choices did not become completely random. Rather, most of the rats tended to show preferred error types, albeit not in a completely consistent manner over all sessions. Two strategies were detected: repeated visits to certain arms, and repetition of the same turning (or continuing straight ahead) responses at the maze center. Both of these could be considered as examples of types of perseverative or habit-like behaviors that have been shown to be preserved after lesions of the hippocampal system. The lesioned rats did show a tendency to visit certain arms more than others in probe trials in 30% of the sessions. This shows that these rats were able to distinguish, to some degree, among the respective arms. However preferences were for two among the four maze arms, indicating more a generalized taxis-like response in relation to cues rather than a precise map-like representation or accurate utilisation of cue configurations in these accumbens lesioned animals. While the rats were able to discriminate cues distinguishing the maze arms, there was an impairment in the ability to associate these cues with the position of the highly rewarded arm or the movements necessary to orient towards it.

A particularly intriguing observation was that the preferred maze arms during error trials often corresponded to the arm providing the large reward on the previous day. This was surprising since performance on the previous day was poor in comparison with pre-operation scores. This suggests that the rats might have been gradually acquiring information on the previous day that they were unable to express until the following day, when the information was no longer valid. If this can be confirmed, it would be consistent with the notion that, in the case of dysfunction in the hippocampal-accumbens system, alternate pathways such as dorsal striatum [6,14,18] persist in mediating other types of learning. However the delay in acquiring the previous day's correct response observed here indicates that the time course of these types of learning is slower, and in our paradigm the daily change in the highly rewarded location foiled their effectiveness. While rats with accumbens lesions have slower acquisition in the Morris water maze (with the submerged platform), they do eventually reach normal levels of performance, typically after several days [2,20]. It must be recalled that in these studies the platform location remains constant, and there are a limited number of departure points. Our results suggest that these accumbens lesioned animals had eventually learned taxis-like habits to approach the platform from each of the (typically four) departure points in the water maze.

The principal difficulty for the lesioned rats during the probe trials then was more likely related to an inability to register or recall the location of the arm with the greatest reward. There are several possible processes which could underlie this. Since the arms of the maze were identical, on probe trials when all four reward boxes were lit, there remained only room cues to guide the rat to orient to the box with the greater reward. This could have been accomplished in several different ways, as discussed by Trullier et al. [25]. In one scenario, the rats could have associated the subsequent large reward with (a) the view experienced when arriving at the choice point at the center of the maze from each of the three respective arms, and (b) the appropriate orienting movement to enter into the highly rewarded arm. Another way would be for the rat to form a map-like representation of the position of the highly rewarded box in the room, and to compare its current position and orientation with this representation to determine the appropriate orienting behavior. Of course if there were perceptible differences between the arms these too could, hypothetically, be employed as well. But such a strategy (guidance by local cues) was preserved in our accumbens lesioned rats in training trials, and the poor performance of these animals in the probe trials indicates that if this strategy was employed then, it was not done effectively.

On about 30% of the error probe trials the rats made non-random choices of orienting movements at the choice point at the center of the maze. This was observed in five of the eight lesioned rats. While the movements were inappropriate, this nonetheless shows that in these sessions, these rats were capable of programming specific orienting movements. This may be interpreted as a simple motor response strategy, which has also been shown to be preserved after hippocampal system lesions in numerous studies. All but two of the sham lesioned rats also made particular orienting movements on error trials. Thus this strategy is not completely suppressed in animals showing normal performance levels. Even in the presence of intact hippocampal-accumbal pathways there appears to be a dynamic competition among the pathways involved in the choice of goals for orientation and displacement behaviors.

Taking into account the relatively small size of the lesions, and the sparing of large parts of the Nacc shell, the performance impairments are remarkably consistent and severe. The efficacy of these small lesions may also be explained by neuroanatomical findings. The tract-tracing study of Groenewegen et al. [8] showed that afferent fibers from the hippocampus as well as magno-

cellular basal amygdala enter the accumbens dorsally through the medial shell region at locations corresponding to where our lesions were placed. Thus the behavioral changes brought on by these electrolytic lesions could well be due to destruction in these afferent pathways, as well as of the cell bodies in these regions. While in some cases the lesions also spread to other nuclei, impairment in probe trials and spared capacities in the light-guided trials were always present if there was Nacc shell damage. Even unilateral lesions had profound effects on behavioral performance (rats 2–2 and 2–3). Unilateral lesions of the dorsal striatum have also been shown to be effective in disrupting behavior [4].

The evoked potential technique proved quite useful in locating a small, elusive brain structure. A useful pilot experiment is to map in a grid of electrode penetrations the evoked potentials corresponding to respective brain structures in the region of interest. These profiles can then be used to determine and correct the lesion electrode position in trained experimental animals.

The present task should prove to be valuable for future studies in rats, and possibly in mice. It requires the animal each day to learn a new reward-place association and permits continuous dissociation of cue-guided and memory guided goal seeking. Error analyses permit the assessment of place preference and of motor habit strategies. The animals learn the task easily. Once installed, the maze is easy to operate under automatic control. Data analyses can also be carried out automatically by appropriate software analysing the timing of the rat blocking the various photodetectors. Future studies might also benefit from analyses comparing the latencies of running from the center to high and low reward arms to determine the time course of learning.

Overall our results show that the ability to acquire new knowledge about the spatial distribution of rewards requires an intact accumbens system. While rats with Nacc shell lesions are capable of retrieving rewards indicated by a visual cue, and thus they retain motivation and sensorimotor capacities. However they are impaired in locating a larger reward when the local cues are ambiguous. The choices made on error trials showed the ability to distinguish among arms in the maze, and to program specific types of reorientation movements. The deficit then seems to be in linking together information concerning reward values, information about locations and the appropriate orienting movements required to reach specific locations. This is consistent with the notion that there is convergence of location information (from hippocampus) with reward information (VTA and amygdala) in the Nacc shell, which would serve as a limbic-motor interface [15].

Acknowledgements

This work was supported by GIS, Cogniscience, a Human Frontier Scientific Program individual fellowship grant to A.B.M., a French MENRT grant to S.V.A. Thanks to F. Maloumian for preparing figures, S. Doutremer and N. Quenech'du for histology and A. Grantyn for advice for fabricating the lesion electrodes.

References

[1] Albertin S, Mulder AB, Tabuchi E, Zugaro M, Wiener SI. Accumbens medial shell lesions impair performance in rats performing in a differentially rewarded plus maze. Soc Neurosci Abs 1998;24:1909.

[2] Annett LE, McGregor A, Robbins TW. The effects of ibotenic acid lesions of the nucleus accumbens on spatial learning and extinction in the rat. Behav Brain Res 1989;31:231–42.

[3] Boeijinga PH, Pennartz CMA, Lopes da Silva FH. Paired-pulse facilitation in the nucleus accumbens following stimulation of subicular inputs in the rat. Neuroscience 1990;35:301–11.

[4] Brasted PJ, Humby T, Dunnett SB, Robbins TW. Unilateral lesions of the dorsal striatum in rats disrupt responding in egocentric space. J Neurosci 1997;17:8919–26.

[5] Brog JS, Salyapongse A, Deutch AY, Zahm DS. The patterns of afferent innervation of the core and shell in the 'accumbens' part of the rat ventral striatum: immunohistochemical detection of retrogradely transported fluoro-gold. J Comp Neurol 1993;338:255–78.

[6] Carr GD, White NM. Conditioned place preference from intra-accumbens but not intra-caudate amphetamine injections. Life Sci 1983;33:2551–7.

[7] Floresco SB, Seamans JK, Phillips AG. Differential effects of lidocaine infusions into the ventral CA1/subiculum or the nucleus accumbens on the acquisition and retention of spatial information. Behav Brain Res 1996;81:163–71.

[8] Groenewegen HJ, Mulder AB, Beijer AVJ, Wright CG, Lopes da Silva FH, Pennartz CMA. Hippocampal and amygdaloid interaction in the nucleus accumbens. Psychobiology 1999;27:149–64.

[9] Groenewegen HJ, Vermeulen-VanderZee E, TeKortschot A, Witter MP. Organization of the projections from the subiculum to the ventral striatum in the rat: a study using anterograde transport of *Phaseolus vulgaris* leucoagglutinin. Neuroscience 1987;23:103–20.

[10] Hagan JJ, Alpert JE, Morris RGM, Iversen SD. The effects of central catecholamine depletions on spatial learning in rats. Behav Brain Res 1983;9:83–104.

[11] Kelley AE, Domesick VB. The distribution of the projection from the hippocampal formation to the nucleus accumbens in the rat: an anterograde- and retrograde-horseradish peroxidase study. Neuroscience 1982;7:2321–35.

[12] Lavoie AM, Mizumori SJY. Spatial, movement- and reward-sensitive discharge by medial ventral striatum neurons of rats. Brain Res 1994;638:157–68.

[13] Maldonado-Irizarry CS, Kelley AE. Excitotoxic lesions of the core and shell subregions of the nucleus accumbens differentially disrupt body weight regulation and motor activity in rat. Brain Res Bull 1995;38:551–9.

[14] McDonald RJ, White NM. Parallel information processing in the water maze: evidence for independent memory systems involving dorsal striatum and hippocampus. Behav Neur Biol 1994;61:260–70.

[15] Mogenson GJ, Brudzynski SM, Wu M, Yang CR, Yim CY. From motivation to action: a review of dopaminergic regulation of limbic-nucleus accumbens-ventral pallidum-pedunculopontine nucleus circuitries involved with limbic-motor integration. In: Kalivas PW, et al., editors. Limbic-Motor Circuits and Neuropsychiatry. Boca Raton: CRC Press, 1993:193–263.

[16] Mulder AB, Gijsberti Hodenpijl M, Lopes da Silva FH. Electrophysiology of the hippocampal and amygdaloid projections to the nucleus accumbens of the rat: convergence, segregation and interaction of inputs. J Neurosci 1998;18:5095–102.

[17] O'Donnell P, Grace AA. Synaptic interactions among excitatory afferents to nucleus accumbens neurons: hippocampal gating of prefrontal cortical input. J Neurosci 1995;15:3622–39.

[18] Packard MG, McGaugh JL. Inactivation of hippocampus or caudate nucleus with lidocaine differentially affects expression of place and response learning. Neurobiol Learn Mem 1996;65:65–72.

[19] Paxinos G, Watson C. The Rat Brain in Stereotaxic Coordinates (CD-ROM Version), 4th edition. San Diego: Academic Press, 1998.

[20] Ploeger GE, Spruijt BM, Cools AR. Spatial localization in the Morris water maze in rats: acquisition is affected by intra-accumbens injections of the dopaminergic antagonist haloperidol. Behav Neurosci 1994;108:927–34.

[21] Schacter GB, Yang CR, Innis NK, Mogenson GJ. The role of the hippocampal-nucleus accumbens pathway in radial-arm maze performance. Brain Res 1989;494:339–49.

[22] Seamans JK, Phillips AG. Selective memory impairments produced by transient lidocaine-induced lesions of the nucleus accumbens in rats. Behav Neurosci 1994;108:456–68.

[23] Shibata R, Trullier O, Raballand D, Mulder AB, Berthoz A, Wiener SI. Behavioral correlates of nucleus accumbens neurons in rats performing a water search task in an open field. Soc Neurosci Abstcts 1996;22:911.

[24] Taghzouti K, Louilot A, Herman JP, LeMoal M, Simon H. Alternation behavior, spatial discrimination, and reversal disturbances following 6-hydroxydopamine lesions in the nucleus accumbens of the rat. Behav Neurosci Biol 1985;44:354–63.

[25] Trullier O, Wiener SI, Berthoz A, Meyer J-A. Biologically based artificial navigation systems: review and prospects. Prog Neurobiol 1997;51:483–544.